

# Environmental Assessment of the Alaskan Continental Shelf

Annual Reports of Principal Investigators  
for the year ending March 1980

Volume VI: Transport

3 4982 00033945 6



U.S. FISH & WILDLIFE SERVICE--ALASKA



**U.S. DEPARTMENT OF COMMERCE**  
**National Oceanic & Atmospheric Administration**  
**Office of Marine Pollution Assessment**

**On Reserve**

**U.S. DEPARTMENT OF INTERIOR**  
**Bureau of Land Management**



GC  
85.2  
.A4  
E57  
1980  
v.6

# Environmental Assessment of the Alaskan Continental Shelf

**Annual Reports of Principal Investigators  
for the year ending March 1980  
Volume VI: Transport**

## **ARLIS**

Alaska Resources  
Library & Information Services  
Ancient Alaska



**U.S. DEPARTMENT OF COMMERCE**  
**National Oceanic & Atmospheric Administration**  
**Office of Marine Pollution Assessment**



**U.S. DEPARTMENT OF INTERIOR**  
**Bureau of Land Management**

The facts, conclusions and issues appearing in these reports are based on interim results of an Alaskan environmental studies program managed by the Outer Continental Shelf Environmental Assessment Program (OCSEAP) of the National Oceanic and Atmospheric Administration (NOAA), U.S. Department of Commerce, and primarily funded by the Bureau of Land Management (BLM), U.S. Department of Interior, through interagency agreement.

#### DISCLAIMER

Mention of a commercial company or product does not constitute an endorsement by National Oceanic and Atmospheric Administration. Use for publicity or advertising purposes of information from this publication concerning proprietary products or the tests of such products is not authorized.

TABLE OF CONTENTS

VOLUME VI: TRANSPORT

<u>RU#</u>	<u>PI - Agency</u>	<u>Title</u>	<u>Page</u>
87	Martin, Seelye - University of Washington Seattle, WA	The Interaction of Oil with Sea Ice in the Arctic Ocean	1
88	Kovacs, A and W.F. Weeks - Cold Regions Lab Hanover, NH	Dynamics of Near-Shore Ice	9
91	Aagaard, Knut - University of Washington Seattle, WA	Current Measurements in Possible Dispersal Regions of the Beaufort Sea	29
138	Schumacher, J.D. and C.A. Pearson - PMEL, Seattle, WA	Gulf of Alaska Study of Mesoscale Oceanographic Processes (GAS-MOP)	51
289	Royer, Thomas C. - University of Alaska Fairbanks, AK	Circulation and Water Masses in the Gulf of Alaska	223
367	Overland, James E. and Carol H. Pease - PMEL, Seattle, WA	Coastal Meteorology (Synoptic Climatology Component)	307
435	Leendertse, J.J. and S.K. Liu - Rand Corporation Santa Monica, CA	Modeling of Tides and Circulations of the Bering Sea	559
526/77	Matthews, J.B. - University of Alaska Fairbanks, AK	Characterization of the Nearshore Hydrodynamics of an Arctic Barrier Island - Lagoon System	577



ANNUAL REPORT

Contract #03-5-022-67  
Research Unit #87  
Reporting Period:  
1 April 1979-1 April 1980  
Number of Pages: 7

THE INTERACTION OF OIL WITH SEA ICE IN THE ARCTIC OCEAN

Seelye Martin  
Department of Oceanography  
University of Washington  
Seattle, Washington 98195

27 March 1980

I. Summary of Objectives:

Our purpose is to understand from laboratory experiments and field traverses how oil and sea ice would interact in an arctic oil spill.

II. Introduction:

A. General Nature and Scope of Study:

To understand how spilled oil might interact with the various kinds of ice in the Beaufort, Bering and Chukchi Seas, we have done field traverses in these regions, with particular emphasis on ice types which have previously not been studied. These include grease and pancake ice in Norton and Kotzebue Sound, and most recently a field investigation of the ice bands which form at the pack ice edge in the Bering Sea. In the laboratory, we have carried out experiments on how spilled oil interacts with grease ice, pancake ice, and simulated multi-year ice.

B. Specific Objectives:

1. To understand how first-year sea ice entrains petroleum;
2. To understand from laboratory experiments the interaction of petroleum with grease and pancake ice;
3. To understand from field observations the behavior of the Bering Sea ice edge and the relevance of this behavior to oil entrainment from industrial development.

C. Relevance to Problems of Petroleum Development:

The above specific objectives have an obvious application to the impact and problems of oil spills in sea ice.

III. Current State of Knowledge:

Our work over the past year has been written up in five papers and reports.

- A. Martin, S., P. Kauffman, 1979. Data report on the ice cores taken during the March 1979 Bering Sea ice edge field cruise on the NOAA ship SURVEYOR. (Data report submitted to BLM/NOAA, 14 September 1979.)
- B. Martin, S., 1979. Anticipated oil-ice interactions in the Bering Sea. (Chapter 8 in the proposed Bering Sea ice behavior book. Submitted to Don Hood, 21 December 1979.)
- C. Martin, S., J. Bauer, 1979. Bering Sea ice edge phenomena. (Chapter 5 in the proposed Bering Sea ice behavior book. Submitted to Don Hood, 21 December 1979.)

- D. Bauer, B., S. Martin, 1980. Field observations of the Bering Sea ice edge during March 1979. Monthly Weather Review (submitted). (Revised version of C, above).
- E. Squire, V.A., S.C. Moore, 1980. Direct measurement of the attenuation of ocean waves by pack ice. Nature, 283: 365-68. (See Auxiliary Material for copy).

#### IV. Study Areas:

We have worked in the Beaufort, Bering and Chukchi Seas. In the Beaufort, we worked on the ice over the Alaskan continental shelf, with particular emphasis on the Prudhoe Bay region. In the Bering and Chukchi, we concentrated on Norton and Kotzebue Sound, and most recently on the Bering Sea ice edge.

#### V. Methods:

In the field we rely on working from helicopters, taking ice cores, then analyzing the cores for their salinity and temperature profiles as well as their crystal structures. During the past year, we also worked cooperatively with Dr. Vernon Squire of the Scott Polar Research Institute in Cambridge, England, who carried out measurements of wave attenuation by pack ice and the flexure of floes in a wave field from the NOAA ship SURVEYOR. We have also recently concluded our laboratory program on oil spills in sea ice.

#### VI. Results:

Our formal results are contained in the papers and reports cited in Section III. The first report gives the ice core data which we took from the cruise. The second report, which is intended as a chapter in the BLM/NOAA book on the Bering Sea, summarizes all of our work on oil spills and pack ice. The third and fourth report and paper on the list, which will also go into the Bering Sea book, interpret the field ice core observations in the field report, and summarize our observations on the formation and movement of the bands of ice which form at the ice edge. Finally, the fifth paper on the list is the analysis of some of the wave decay data gathered on SURVEYOR cruise.

#### VII. Discussion:

I feel that the problem of the small-scale interaction of oil with first-year ice is now sufficiently well understood from the field and laboratory experiments described in Martin (1979) above. Also, our laboratory experiments give consistent results with field spills such as the Buzzards Bay spill, for example, on the behavior of oil spilled in grease and pancake ice. Two major problems remain: First, the interaction of oil with the grease ice-Langmuir roll circulation which form in the large lee-shore polynyas as exist south of Port Clarence and St. Lawrence Island; second, the interaction of oil with the ice edge bands and the broken ice floes near the ice edge. As Martin (1979) discusses, in both the bands and ice edge case, the ice is heavily deformed and strongly worked by swell and winds. Addition of oil to this ice might create a rapidly-moving, difficult-to-clean up oil-ice mixture. From the analysis of our existing cruise data, we hope to obtain more information on these ice edge processes.

### VIII. Conclusions:

These are summarized in the two chapters submitted to the BLM/NOAA book.

### IX. Needs for Further Study:

We need to address the problem of how the ice edge in the Bering Sea and Chukchi Seas behave during periods of rapid southward advancement, and periods of retreat during spring and summer. Second, we need more information on how wave and tide absorption at the ice edge contribute to relative ice motion and to the formation of currents parallel to the ice edge. Third, we need more research into the formation, movement and decay of the ice edge bands. Our work on the bands from the 1979 SURVEYOR cruise show that they move more rapidly than an oil slick; and satellite photographs suggest that they move distances of 60 km in two days. These bands may play an important role in redistributing and transporting oil over large distances. Fourth, we need to verify a numerical model of the generation of ocean swell by storm for the Bering Sea with field measurements of swell. Such a model will play an important role in the future determination of both ice edge properties and oil slick trajectories.

### X. Summary of January-March Quarter:

Dr. Vernon Squire arrived in Seattle on 1 February 1980, and continued his work on the analysis of the Bering Sea data. Since his arrival, he has worked on the problem of the response of a single floe to ocean swell.

Specifically, he has interpreted the heave and strain records from instruments mounted on the floes, using spectral analysis in the light of the measured open water ocean wave forcing. From these records, he has computed the approximate directionality and spread of the ocean wave energy. Most important, his statistical calculations have enabled him to estimate the strain necessary to fracture a Bering Sea ice floe. This work should be written up by the time of his departure in July.

Second, he is presently visiting the NASA Langley center to obtain the laser imagery gathered from an overflight during the cruise. From this data, we plan to compute the wave attenuation by the pack ice along a flight line parallel to the swell. Because we also have simultaneous aerial photography for this run, we also plan to look at the floe size distribution, then use this data to calculate the theoretical wave attenuation.

Also during the past quarter, S. Martin worked with J. Bauer on the writing up of our ice edge data for publication in Monthly Weather Review. S. Martin has also been working with NASA Goddard on the Scanning Multichannel Microwave Radiometer (SMMR) data for the Bering Sea for March 1979. The period 1-15 March 1979 has just been released; in the coming months beginning during a visit to Goddard 30 March - 3 April we plan to analyze this data and compare it with our existing surface truth data and our ice charts. If our analysis is successful, we also plan to work on the period March 16-31. Our long-range plan is to see if the SMMR data can be used to analyze the ice properties during periods of heavy cloud cover and darkness. We also plan to incorporate this SMMR data into a general report on the ice properties in the Bering Sea during March 1979.

XI. Auxiliary Material:

- A. Papers in Print or Submitted: See Section III.
- B. The paper, "Direct measurement of the attenuation of ocean waves by pack ice" by Squire and Moore, is attached below.

## Direct measurement of the attenuation of ocean waves by pack ice

Vernon A. Squire & Stuart C. Moore

Scott Polar Research Institute, University of Cambridge, UK

Early experimental work in the Antarctic<sup>1</sup> using a ship-borne wave recorder has shown that pack ice can significantly attenuate incoming ocean waves, particularly those of shorter period. Wadhams<sup>2,3</sup> has subsequently reported similar wave decay through Arctic ice in data obtained remotely by means of airborne laser profiling and inverted echo sounding from a submarine. The two predominant mechanisms by which the decay can occur—scattering by individual ice floes and energy loss by creep within each flexing floe—have been studied theoretically by Wadhams<sup>4,5</sup>, Squire<sup>6,7</sup>, and Squire and Allan<sup>8</sup>. We present here the results of further experiments to measure wave decay which took place in the Bering Sea during spring 1979 from the research ship *Surveyor* of the National Oceanic and Atmospheric Administration<sup>9</sup>. During the cruise, oceanographic, meteorological and remote sensing data were also collected<sup>10,11</sup>. The results show the energy decay of waves in pack ice to be exponential with an attenuation coefficient which increases with decreasing wave period.

The attenuation experiment comprised eight floe stations of similar size and thickness, which lay along a line parallel to the direction of the observed principal swell (the attenuation line). They were chosen so that their separation increased away from the ice edge (Fig. 1). The seven floes within the ice pack were visited using the ship's Bell 206 helicopter equipped with a GNS-500A global navigation system which had been pre-programmed from Loran-C on *Surveyor*. Distances calculated from position fixes should therefore be good to within 0.2 km (Table 1). The first floe, situated on the ice edge itself ~1 km from *Surveyor*, was reached using the ship's whaleboat. The heaving motion of each floe was measured using a Schaevitz-EM vertical accelerometer. For logistic reasons we were not able to instrument floes simultaneously so that the complete experiment lasted about eight hours. Ideally such an experiment should take place over a very short time so that waves incident on the ice cover may be assumed to be statistically stationary. To overcome this problem a Waverider buoy was deployed from *Surveyor* to monitor the open-water wave spectrum.

Routine ice observations were carried out during each helicopter flight. The ice margin was diffuse with an average

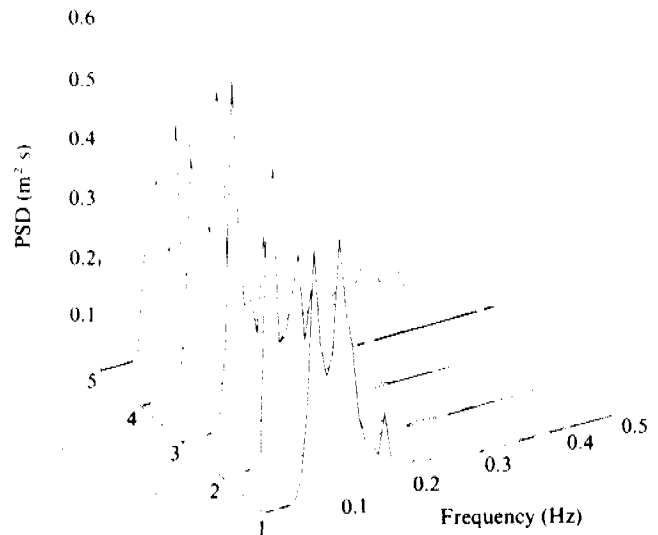


Fig. 2 Three-dimensional graph showing evolution of power spectra from Waverider buoy during the experiment.

concentration of four Oktas for tens of kilometres into the ice cover with occasional isolated bands of higher concentration. Floe diameter increased gradually from 10 m at the ice edge to 40 m some 30 km in. At 30 km, the floe size increased abruptly to more than 100 m in diameter, the typical size thereafter. From the air the ice cover could be divided into three distinct zones made up of floes of quite different character: the edge zone, which stretched from the ice edge some 5 km into the pack; the transition zone, which stretched a further 25 km; and the interior zone. This zonal structure had been observed earlier in the field trip and was the reason behind our choice of floe separation. The edge zone was made up of floes which had been buffeted together in waves of sufficient intensity to ridge, raft and fracture the ice. Floes were typically 10 m across, of uneven thickness, with heavily rafted perimeters. Floes within the transition zone were much smoother since the incoming waves had lost much of their energy in the extremely active edge zone. The penetrating waves were still able to fracture the ice, however, and the average floe diameter remained 10 m. Further into the ice cover, the incoming swell had been attenuated to such an extent that little or no fracturing took place and floes in the interior zone were typically smooth and >100 m across.

All the floes visited were between 10 and 20 m across, less than 0.5 m thick and relatively smooth. CTD casts had shown the underlying seawater to be well-mixed and well above the

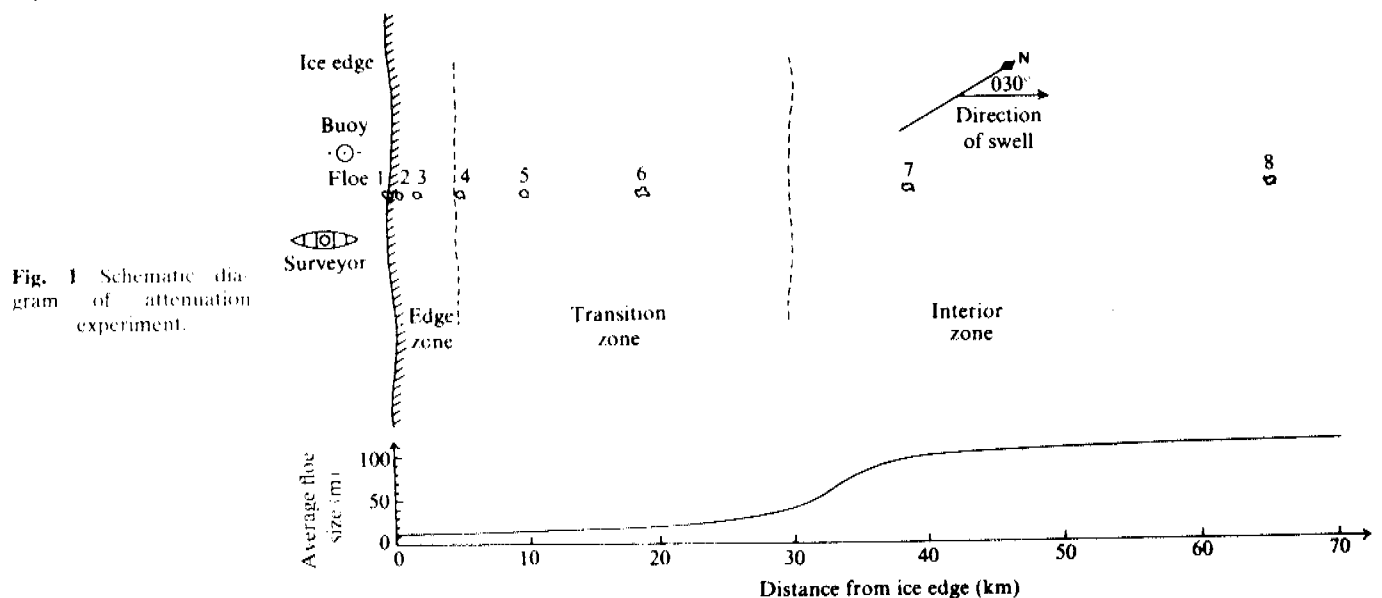


Fig. 1 Schematic diagram of attenuation experiment.

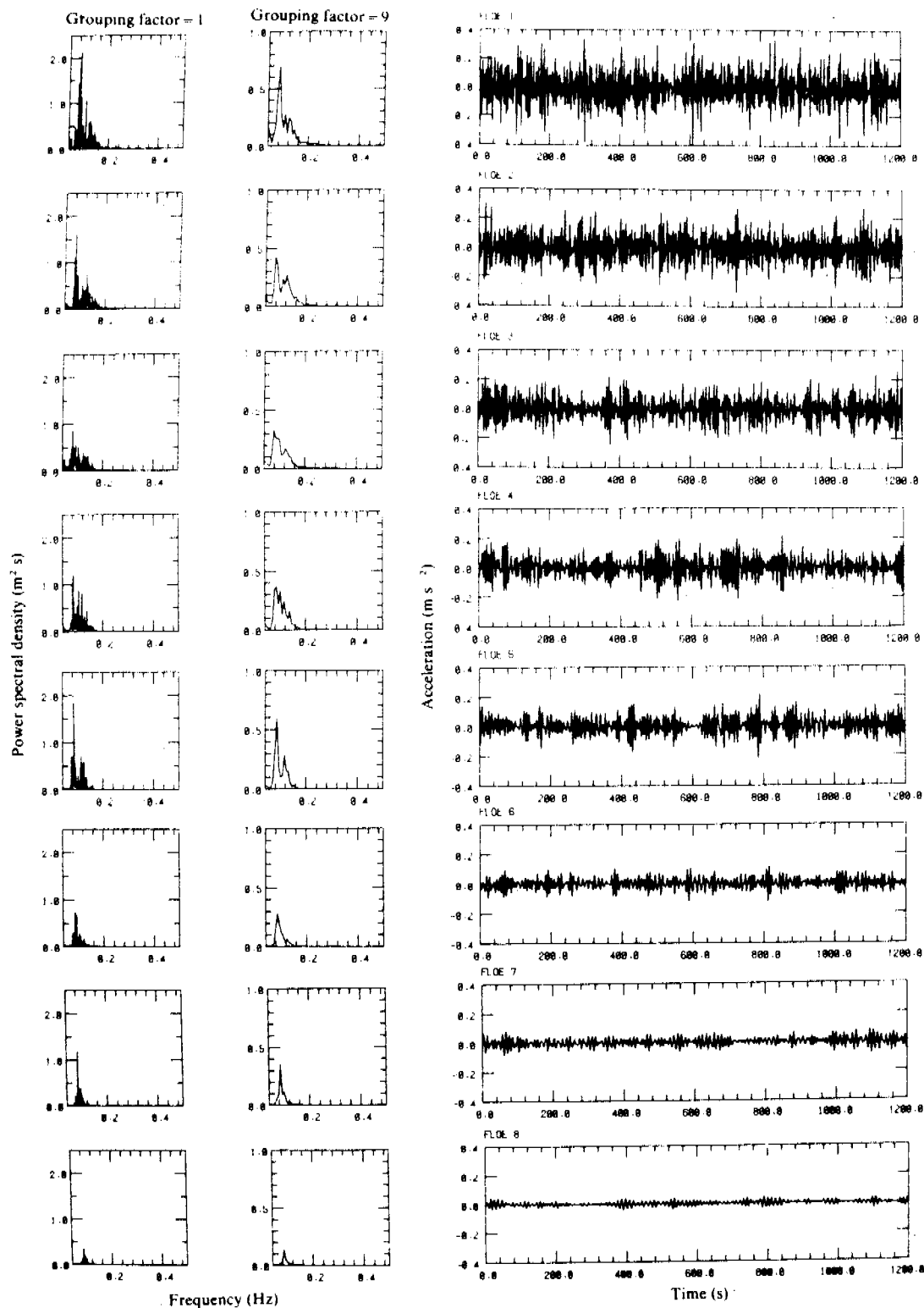


Fig. 3 The attenuation run showing time series at each floe and corresponding power spectra.

freezing point, and this together with several days of warm weather, had left the ice in a mushy and decaying condition. Twenty minutes of wave data were collected on each of the floe stations and it was noted that there were at least two components of swell present. There seemed to be a noticeable attenuation between floes but at this stage we could not be sure that the change in amplitude was not due to a decline in the open-water wave forcing. The wave records obtained at each site were digitised and, together with the Waverider buoy data, were calibrated and transferred to IBM digital tape for further analy-

sis. All data processing was carried out on the IBM 370 at Cambridge University using the FFT/graphics package developed by the Sea Ice Group at the Scott Polar Research Institute (SPRI).

The Waverider buoy data are presented in Fig. 2. Each power spectrum represents a 20-min sample of the open-sea wave conditions during the experiment. Records are between 1 and 2 h apart. Within the statistical errors generated by a frequency domain analysis<sup>12</sup>, the smoothed power spectra show the wave conditions off the ice edge to be stable throughout the day. This

**Table 1** Position of ice floes along attenuation line

Floe station	1	2	3	4	5	6	7	8
Distance from ice edge (km)	0	0.7	2.2	5.3	10.3	18.9	38.6	65.1

being so, the wave forcing for the attenuation run may be assumed stationary and any comparison between wave data from individual ice floes is valid.

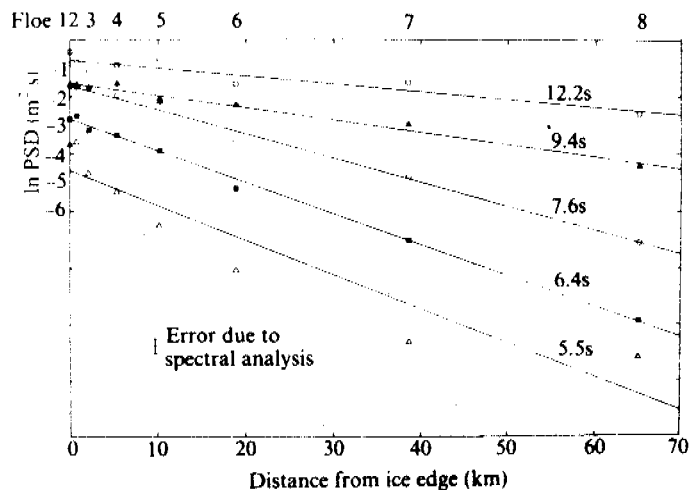
Figure 3 shows the time series and the unsmoothed and smoothed power spectra for the wave data recorded at each floe station. All records are 20 min (1,200 s) long and are plotted to the same scale so that a direct comparison may be made. Each time series represents the vertical acceleration at a point along the attenuation line. There is a clear attenuation with distance from the ice edge together with a noticeable filtering of the incoming waves in favour of longer wavelengths. The power spectra confirm these observations. Each pair of spectra, derived from the corresponding time series and corrected for acceleration, shows the power spectral density (PSD) as a function of frequency. The first spectrum of the pair is unsmoothed and is presented for completeness. The second has been frequency smoothed with a grouping factor of nine. There is a striking decay in the available wave energy as the reader proceeds from floe to floe. Furthermore,

**Table 2** The attenuation coefficients for energy decay at various central wave periods

Central period (s)	Attenuation coefficient ( $m^{-1} \times 10^{-4}$ )
12.2	$0.272 \pm 0.054$
9.4	$0.438 \pm 0.036$
7.6	$0.855 \pm 0.049$
6.4	$1.087 \pm 0.037$
5.5	$1.214 \pm 0.192$

waves of shorter period are attenuated more rapidly than long waves.

From the smoothed spectra, five central wave periods were selected at which significant wave energy was present. Figure 4 shows these wave energies plotted against distance from the ice edge. The energy decay is seen to be approximately exponential with the attenuation coefficient a function of wave period (Table 2). The line corresponding to a period of 5.5 s shows the most scatter. This is believed to be due to an increase in energy at shorter periods occurring late in the day (see Fig. 2). If the 5.5 s point for floe 8 is assumed to be an overestimate and is neglected, the best straight line between the remaining seven stations gives an attenuation coefficient of  $(1.824 \pm 0.183) \times 10^{-4} m^{-1}$ . With this revised value for the energy decay at 5.5 s, the data fit the empirical inverse square relationship between attenuation

**Fig. 4** Energy decay as a function of wave period.

coefficient and wave period found by Wadhams<sup>2</sup>. Similar studies carried out off the coast of East Greenland<sup>1,3</sup> by SPRI, the Cavendish Laboratory at the University of Cambridge, and the Technical University of Denmark promise attenuation runs for thicker floes and longer wave periods.

We thank Dr Seelye Martin who was chief scientist for the cruise, Dr David Halpern of the Pacific Marine Environmental Laboratory for the loan of the Waverider buoy, Ms Jane Bauer for preliminary analysis of the Waverider tapes, and the officers and crew of Surveyor. We thank the Office of Naval Research (contracts N00014-78-G-0003 and N00014-76-C-0234) and BP Co. Ltd for support. This study was part of a program managed by the Outer Continental Shelf Environmental Assessment Program Office, and was supported by the Bureau of Land Management through the National Oceanic and Atmospheric Administration.

Received 22 October; accepted 29 November 1979.

1. Robin, G. de Q. *Phil. Trans. R. Soc. A* **255**, 313-339 (1963).
2. Wadhams, P. *Deep Sea Res.* **25**, 23-40 (1978).
3. Wadhams, P. *J. geophys. Res.* **80**, 4520-4528 (1975).
4. Wadhams, P. *J. geophys. Res.* **78**, 3552-3563 (1973).
5. Wadhams, P. thesis, Univ. Cambridge (1973).
6. Squire, V. A. *J. Glaciol.* **29**, 425-431 (1978).
7. Squire, V. A. thesis, Univ. Cambridge (1978).
8. Squire, V. A. & Allan, A. J. *Proc. Symp. Sea Ice Processes and Models*, Seattle (in the press).
9. Squire, V. A. *Tech. Rep. 79-2*, (Scott Polar Research Institute, Cambridge, 1979).
10. Martin, S. *Surveyor S132 Cruise Rep.* (NOAA, 1979).
11. Martin, S. & Kauffman, P. *Special Report No. 89* (Department of Oceanography, University of Washington, Seattle, 1979).
12. Bendat, J. S. & Piersol, A. G. *Random Data: Analysis and Measurement Procedures* (Wiley-Interscience, New York, 1971).
13. Wadhams, P. *Polar Rec.* **19**, 373-376 (1979).



Annual Report  
April 1979-March 1980  
Research Unit # 88  
Number of Pages: 19

DYNAMICS OF NEAR-SHORE ICE

Principal Investigators: A. Kovacs and W. F. Weeks  
Cold Regions Research and Engineering Laboratory

20 March 1980

## I. SUMMARY OF OBJECTIVES, CONCLUSIONS, AND IMPLICATIONS

R.U. #88 investigates the movement, deformation and structure of sea ice along the coasts of the Beaufort, Chukchi, and Bering Seas. New results reported during FY80 include further documentation of coastal ice pileup and over-ride events, the statistical aspects of ice-induced seafloor gouging, the crystal alignment characteristics of sea ice as determined by direct petrographic and indirect radar observations and radar studies of near-shore lakes on the North Slope that may serve as year-round sources of fresh water.

## II. INTRODUCTION

### A. General Nature and Scope of Study

There are several principal thrusts to the present proposal. These are concerned with

1) studies of the nature of ice morphology, pressure ridging and ice gouging along the coast of the Beaufort and Chukchi Seas and in Norton Sound,

2) studies of the deformation and movement of shore-fast ice, including ice pile-ups and override of beaches,

3) studies of the crystal orientation of sea ice and the relation between this orientation, the physical properties of the ice, and the current under the ice.

4) radar measurements of the movement and deformation of the pack ice in the vicinity of the Bering Strait,

5) SLAR determination of near-shore lakes on the Beaufort Coast that contain fresh water during the late winter.

### B. Specific Objectives

Our five research thrusts can be broken into eight sub-programs as follows:

A. Statistical Studies of Ridging and Ice Gouging Via the Use of Remote Sensing Techniques (Weeks and Tucker) [Thrust #1] - Our previous studies of coastal ridging via the use of laser profilometry have produced quite significant results. To be specific, that the average ridge height changes as a function of season but not as a function of location, that the number of ridges show large systematic variations both normal to and parallel to the coast and that it is possible to estimate the occurrence of rare large ridges. The problem is that these conclusions were based on a very limited data set in a time sense.

We are currently expanding this temporal sampling base by analyzing laser data collected in 1978 by NASA (Beaufort Sea and Norton Sound), 1980 by Canadian AES and in addition collecting new data ourselves during 1979 and 1980. This study will allow statements to be made concerning the year-to-year variations in ridging intensity and ridging patterns. We will also be able to make greatly improved estimates of rare ridging events. We will also complete a study of the statistics of ice gouging along selected profiles off the Beaufort Coast. This is a cooperative program with P. Barnes and E. Reimnitz of the U.S. Geological Survey.

B. Interrelations between Pressure Ridge Characteristics and Ice Thickness- (Tucker) [Thrust #1] - Previous studies of nearshore ridging have shown little spatial variation in mean ridge height. However, there was a significant variation in mean height with season. This suggests that the ridge height may be related to the thickness of the ice being deformed. Such considerations also pose the question "Are stresses in the nearshore ice zone sufficiently large to cause the complete thickness of the winter ice cover to fail or is deformation in this region almost completely limited to thin, new ice formed in cracks and leads?" No study has been made in which a statistically designed sampling scheme was used to select ridge sites for study and then block thickness and geometry and ridge height were measured. We plan to undertake such a study.

C. Ice Morphology Within the State-Federal Lease Area (Kovacs) [Thrusts 1 and 2]. Here we will attempt to acquire sea ice morphology information within the Alaska Beaufort Sea federal-state lease area which can be used in the assessment of ice forces against and ice pile-up and ride-up on offshore structures. We have collected a limited body of data to date and any additional data will greatly help in expanding the existing data base. Our studies will include recon flights along the barrier islands for the purpose of recording ice pile-ups and over rides. We will also investigate major deformation features found

along the fast ice edge and any unique features, e.g. ice islands, which may be found.

D. Net-Winter Fast Ice Motions Along the Beaufort Coast (Kovacs) [Thrust #2]. Our study of fast ice movement will center on making measurements of past ice displacement events. This will be accomplished by measuring the offset of geophysical survey roads. The measurements in past years have allowed us to record the largest fast ice displacements which have been measured inside the 15 m depth contour.

E. Petrographic Studies of Crystal Orientations in Sea Ice (Weeks, Gow) [Thrust #3]-During the 1977 and 1978 winter field seasons we collected information on the occurrence and characteristics of horizontal c-axis alignments along the northern coast of Alaska. The sampling sites are scattered between Shishmaref and Camden Bay covering almost the complete coasts of the Chukchi and Beaufort Seas. We also did fabric studies in support of physical property measurements on sea ice undertaken by several different groups of investigators at locations off Barrow. We plan to complete the final editorial work necessary to produce two papers on this general subject.

F. Radar Studies of Crystal Orientations in Sea Ice (Kovacs) [Thrust #3]-In our previous work we have investigated the c-axis orientation phenomena by visual core analysis and with the use of impulse radar. The results have shown that when the antenna E field is parallel to the ice c-axis direction we receive a strong reflected signal from the ice bottom. However, when the E field is orientated perpendicular to the ice c-axis direction a very weak reflection is received from the ice bottom. In the spring of 1979 we began a study to determine if we could detect this effect from the air by mounting our radar system on the NOAA helicopter. Our results indicate that we were successful. Inasmuch as the c-axis alignment is controlled by current direction under

the ice we should be able to use our radar to rapidly collect under-ice current direction data for areas where such data does not exist. This spring we plan to undertake further tests to further evaluate this remote detection technique.

G. Radar Measurements of the Movement and Deformation of the Pack Ice Near the Bering Strait (Weeks, Frank) [Thrust #4]-We have been attempting to measure the time-lapse photography of the PPI display a 50KW X-band radar unit which we have installed on top of Cape Mountain at Tin City. Until this last spring the program had been largely unsuccessful because of a string of equipment problems ultimately related to a power surge that occurred soon after we installed the radar unit. It is intended to continue to operate the radar unit until the spring of 1980.

H. Radar Determination of the Presence of Fresh Water Beneath the Ice Cover on North Slope Lakes (Weeks, Gow). [Thrust #5]-Although the North Slope is covered with lakes, the vast majority of these are very shallow and freeze completely to the bottom during the late winter. Therefore, they cannot be used as water supply during the complete year. When offshore development is considered it is very useful to know the location of the nearest "deep" lake where fresh water can be obtained on a year-round basis. This information can be obtained through the analysis of SLAR imagery in that the radar return from lakes frozen to the bottom is significantly less than the return from lakes with water under the ice cover. During the late winter of 1979 we were able to obtain SLAR data over a wide swath of the near coastal area of the Beaufort Sea (a cooperative effort with NASA Lewis Research Center). We were also able to complete extensive field observations (ground-truth) to verify the interpretation of the imagery. We plan to complete the final analysis of this data which will result in a map giving the location of the deep water sites.

### C. Relevance to Problems of Petroleum Development

The specific relevance of these programs to problems of petroleum development is as follows:

A. The studies of ridging and ice morphology contribute directly to estimating the magnitude of the design ice events that will impact offshore structures.

B. The studies of ice gouging are essential to estimating safe burial depths for offshore pipelines.

C. The studies of winter fast and pack ice motions are essential input to adequate design of offshore structures.

D. As crystal orientation has a pronounced effect on ice strength, studies of the nature of such orientations contribute to our knowledge of the directional nature of ice forces in the near-shore environment.

E. As direct measurements of crystal orientation are time consuming, the ability to measure these orientations indirectly via radar would allow the regional mapping of such orientations. This in turn would contribute to our knowledge of ice forces and offshore current directions.

F. As most North Slope lakes freeze to the bottom during the winter, sources of fresh water for coastal operations are hard to find. The identification of potential sites would be most useful in locating adequate water sources.

### III. CURRENT STATE OF KNOWLEDGE

The majority of the work on near-shore ice motions and ice properties relative to offshore development that is currently available in the non-proprietary literature has been produced by this project. A listing of these papers is given under results.

#### IV. STUDY AREAS

Areas of field study for this program include Norton Sound and the coastal areas of the Chukchi and Beaufort Seas.

#### V. RESULTS

Our results are documented in the following reports:

1. Published reports (DB indicates availability in the OCS Data Bank)
  - a) Kovacs, A. (1976) Grounded ice in the fast ice zone along the Beaufort Sea Coast of Alaska. *CRREL Report 76-32*, 21 pp. (DB).
  - b) Kovacs, A. and Gow, A.J. (1976) Some characteristics of grounded floebergs near Prudhoe Bay Alaska. *CRREL Report 76-34*, 10 pp.; also available in *Arctic* 29 (3), 169-73 (1976).
  - c) Weeks, W.F., Kovacs, A., Mock, S.H., Tucker, W.B., Hibler, W.D. and Gow, A.J. (1977) Studies of the movement of coastal sea ice near Prudhoe Bay, Alaska. *Journal of Glaciology*, Vol. 19, No. 81, p. 533-46 (DB).
  - d) Kovacs, A. (1977) Sea ice thickness profiling and under-ice oil entrapment. *Offshore Technology Conference Paper OTC 29-49*, (DB).
  - e) Schwarz, J. and Weeks, W.F. (1977) Engineering properties of sea ice. *Journal of Glaciology*, Vol. 19, No. 81, p. 499-531 (DB).
  - f) Gow, A.J. and Weeks, W.F. (1977) The internal structure of fast ice near Narwhal Island, Beaufort Sea, Alaska. *CRREL Report 77-29*, 9 pp. (DB).
  - g) Sodhi, D.S. (1977) Ice arching and the drift of pack ice through restricted channels. *CRREL Report 77-18*, 14 p. (DB); also published by Sodhi, D.S. and Weeks, W.F. in *Proceed. Part 2 IAHR Sympos. on Ice Problems*, Lulea, Sweden, p. 415-32.



- h) Kovacs, A. (1977) Iceberg thickness profiling. In "Conference on Port and Ocean Engineering under Arctic Conditions" Memorial University of Newfoundland, St. Johns. (DB).
- i) Kovacs, A. (1978) Iceberg thickness and crack detection. *Iceberg Utilization* (A.A. Husseiny, ed.) Pergamon Press, p. 131-145.
- j) Weeks, W.F. and Gow, A.J. (1978). Preferred crystal orientations in the fast ice along the margins of the Arctic Ocean. *CRREL Report* 78-13, 24 pp; also published in *Journ. Geophys. Res.*, 83 (c 10), p. 5105-21 (1978).
- k) Weeks, W.F. (1978). Environmental hazards to offshore operations. In "Environmental Assessment of the Alaskan Continental Shelf; Interim Synthesis: Beaufort/Chukchi," NOAA/ERL Boulder CO., p. 335-348.
- l) Tucker, W.B., Weeks, W.F., and Frank, M. (1979). Sea ice ridging over the Alaskan continental shelf. *Journal of Geophysical Research*, 84 (C 8), p. 4885-97; also published as *CRREL Report* 79-8, 24 pp.
- m) Weller, G. and Weeks, W.F. (1979). Problems of offshore oil drilling in the Beaufort Sea. *The Northern Engineer* 10 (4), p. 4-11.
- n) Weeks, W.F. and Gow, A.J. (1979). Crystal alignments in the fast ice of Arctic Alaska. *CRREL Report* 79-22, 21 pp.
- o) Kovacs, A. and R.M. Morey (1979) Anisotropic properties of sea ice in the 50-150MHz range. *Jl. Geophys. Res.*, Vol. 84, C9: also given at Int. Workshop on Remote Estimation Sea Ice Thickness, Memorial University of Newfoundland, St. Johns, Newfoundland.
- p) Kovacs, A. (1979) Recent ice observations in the Alaskan Beaufort Sea federal-state lease area, *Northern Engineer*, Vol. 10, No. 3.

2. Completed reports currently in press

- a) Kovacs, A. Radar profile of a multiyear pressure ridge. *Arctic*.
- b) Tucker, W.B., III, Weeks, W.F., Kovacs, A., and Gow, A.J., (1980) Near-shore ice motion at Prudhoe Bay, Alaska. *AIDJEX Sea Ice Symposium*. Univ. of Washington Press.
- c) Weeks, W.F., Tucker, W.B. III, Frank, M., and Fungcharoen, S. (1980) Characterization of the surface roughness and floe geometry of the sea ice over the continental shelves of the Beaufort and Chukchi Seas. *AIDJEX Sea Ice Symposium*. Univ. of Washington Press.
- d) Weeks, W.F. and Russer, J. (1980) Ice related environmental problems: Appendix VIII. In "Environmental Exposure and Design Criteria for Offshore Oil and Gas Structures" Report of the Committee on Offshore Energy Technology of the Marine Board, Assembly of Engineering, National Research Council, Washington, DC.
- e) Kovacs, A., and D.S. Sodhi (1980) Shore ice pile-up and ride-up; field observations, models, theoretical analyses. In "The Seasonal Sea Ice Zone" *Cold Regions Science and Technology*.
- f) Kovacs, A. Some problems associated with radar sea ice profiling. *Cold Regions Research and Engineering Laboratory Technical Note*, 6 p.
- g) Kovacs, A. Remote detection of water under ice covered lakes on the North Slope. *Cold Regions Research and Engineering Laboratory Report*.
- h) Weeks, W.F. (1980). The seasonal Sea Ice Zone: An Overview. In "Workshop on Problems of the Seasonal Sea Ice Zone." *Cold Regions Science and Technology*.
- i) Kovacs, A. and D.S. Sodhi (1979) Ice pile-up and ride-up on arctic and subarctic beaches, 5th Int. Conf. on Portland Ocean Engineering Under Arctic Conditions, Trondheim, Norway.

3. Reports currently in preparation

- a) Gow, A.J., Weeks, W.F., Olheoft, G., Kohnen, H. Shapiro, L., Onstott, R., Moore, R., Noguchi, Y., Aota, M., and Tabata, T. (1980). Interrelations between the internal structure and the physical properties of fast ice at Barrow, Alaska."
- b) Weeks, W.F., Gow, A.J., Schertler, R.J., and Gedney, R.T. (1980). The radar return from ice-covered North Slope lakes. *Cold Regions Research and Engineering Laboratory Report*.
- c) Weeks, W.F., Barnes, P. and Reimnitz, E., (1980). Statistical aspects of ice gouging on the shelf of the Beaufort Sea.

VI. DISCUSSION

Some specific comments on each of our eight sub-programs are as follows:

A. Statistical Studies of Ridging and Ice Gouging.

Frank completed a series of laser flights during early January. All sample lines were completed except the line off Lonely (the aircraft blew an engine). We have arranged to obtain the NASA laser data for March 1979 which includes runs in Norton Sound and the Beaufort Sea. We are also being supplied with data in the Beaufort Sea for March 1980 by the Canadian AES. We plan to re-fly our lines in April 1980. That will give us 3 sets of laser lines off Cross and Barter Islands for the winter of 1979-80. The analysis of the ice gouging data is nearing completion (see Section VII). A paper was published in the *Journal of Geophysical Research* on the analysis of the laser results.

B. Interrelations Between Pressure Ridge Characteristics and Ice Thicknesses.

Tucker is planning to initiate data collection during late March 1980.

C. Ice Morphology Within the State-Federal Lease Area.

Kovacs will start field studies in Norton Sound and the Beaufort Sea during March 1980. Two papers were published on the results of this work (in *Arctic* and in *The Northern Engineer*). Specific results are given in Section VII.

D. Net-Winter Fast Ice Motions Along the Beaufort Coast.

Field studies are being started in March 1980.

E. Petrographic Studies of Crystal Orientations in Sea Ice.

A CRREL Report was published and a shorter version is in press in the *Journal of Geophysical Research*.

F. Radar Studies of Crystal Orientations in Sea Ice.

A report has been published in the *Journal of Geophysical Research* and further field studies will start in March 1980.

G. Radar Measurements of the Movement and Deformation of the Pack Ice Near the Bering Strait.

This project continues to be bothered by equipment failures. Termination of this program is planned for the end of the present field season.

H. Radar Determination of the Presence of Fresh Water Beneath the Ice Cover on North Slope Lakes.

NASA Lewis has completed initial data processing. A report is now in preparation.

## VII. CONCLUSIONS

Recent results that are not as yet documented in published reports are as follows:

1. Coastal Ice Pile-ups and Ride-ups. (Kovacs). Field observations of shore ice pile-up and ride-up were made in November 1979 along the arctic coast of Alaska from Tigvariak Island to the barrier islands north of Dease Inlet. The only significant shore ice pile-up observed was west of Cape Halkett at about 152°35'W. The pile-up extended along the coast for approximately 1 km, and was up to 3.5 m high. The pile-up rested along the top edge of a bluff which appeared to be something over 2 m above sea level. Ice block measurements revealed that the ice was 25-30 cm thick at the time it was driven ashore.

Minor shore ice pile-up or ride-up was observed on the north side of an island at 152°42'W, 70°55'N, on the north and south side of Argo Island, on the north side of Cross Island and four other unnamed islands of the McClure Islands. On two of the eastern islands of the Stockton Island group, ice ride-up appeared to extend up to 15 m onto the low lying beaches.

We have continued our literature search on observations of shore ice pile-up and ride-up and have translated a very interesting 1930 German paper "Ice pressure ridges" by Kraus on this subject. This work is available as a CRREL Draft Translation and from the OCS data bank.

Recently, we have learned of a major ice over-ride and pile-up (9 m high) on a dredge spoil island inside McKinley Bay on Tuktoyaktuk Peninsula. The event occurred about 15 December 1979. We are awaiting further documentation of it.

From Tom Kuglar of Muckluck it was learned that in the spring of 1970 ice piled up on the storage and work pad near the Prudhoe Bay East Dock. This pad is about 4 m above sea level. It was reported that the event occurred in the early morning on a day at the end of May or very early June. The ice offshore had melt pools on the surface and a light breeze was coming from the east at the time. Bob Garrett of Catco confirmed the above event during another interview. Apparently, fuel bladders were stored on the pad but were not contacted by the ice.

2. Statistical Aspects of Ice Gouging (Weeks, Barnes, Reimnitz, Rearic- A joint CRREL-USGS project). Of all the aspects of the gouges it is the variation in the depths of the gouges that arouse the most interest from the engineering community. The reason for this interest is the need to know for any given offshore location the burial depth required to prevent pipelines from being regularly plowed up during gouging events.

We initially prepared several histograms showing the frequency of different depths of gouges for different regions. The nature of graphs was clearly a decreasing exponential with a rapid fall-off in the frequency of occurrence of the larger gouges. A similar tendency has been noted by both Lewis (1978) and Wahlgren (1979) for the gouges occurring north of the Mackenzie Delta. However, an examination of their data (Lewis, in press, 1978) shows that the number of small gouges are consistently less than would occur in an exponential model suggesting that a log normal distribution might also be a possibility.

Figure 1 shows a semilog plot of gouge frequency vs gouge depth for three representative areas of our study region, a) all the data from the lagoons and sounds, b) all the data from the 4 profiles (7-39, 40, 41, 42) off of Lonely and all the data from the profiles seaward of the barrier islands and east of Harrison Bay (2-17 and east). Other groupings of the data and data from other areas gave similar plots. Note that all three plots are effectively linear over their complete range of 4 decades. There is no decrease in the observed frequency of shallow gouge depths as compared to the exponential fit (this suggests that the utilization of an exponential distribution in the Mackenzie studies were correct and the "missing" small gouges were possibly infilled by more rapid sedimentation near the river mouth).

Fortunately, the exponential distribution is a simple, well studied distribution (see among others Benjamin and Cornell, 1970 and Miller and Freund, 1977). If the simple frequency distribution is a negative exponential, then the probability density function (PDF) of X where X is the gouge depth will also be of a similar form

$$f_X(x) = ke^{-\lambda x} \quad X \geq 0$$

[Here  $x$  represents the values that the random variable  $X$  may acquire].

Inasmuch as the integral of  $f_X(x)$  from 0 to  $\infty$  must equal 1 as it contains all the sample points with nonzero probabilities

$$\int_0^{\infty} k e^{-\lambda x} dx = \frac{-k}{\lambda} e^{-\lambda x} \Big|_0^{\infty} = \frac{k}{\lambda} = 1$$

or

$$k = \lambda$$

This gives the following PDF

$$f_X(x) = \lambda e^{-\lambda x} \quad x \geq 0$$

Here the free parameter  $\lambda$  is simply the reciprocal of the sample mean

$$\lambda = \frac{1}{\bar{X}}$$

The probability that a random variable will assume a value in the interval

$(x_1, x_2)$  is then

$$P[x_1 \leq X \leq x_2] = \int_{x_1}^{x_2} f_X(x) dx = \lambda \int_{x_1}^{x_2} e^{-\lambda x} dx$$

The cumulative distribution function (CDF) is, in turn, found by integration

$$\begin{aligned} F_X(x) &= P[X \leq x] = \int_0^x f_X(u) du = \int_0^x \lambda e^{-\lambda u} du \\ &= -e^{-\lambda u} \Big|_0^x = 1 - e^{-\lambda x} \quad x \geq 0 \end{aligned}$$

Finally because we will be interested in the probability of occurrence of gouges that have depths greater than or equal to some specified value, we will largely be concerned with the value of the complementary distribution function  $G_X(x)$ .

$$G_X(x) = P[X \geq x] = 1 - F_X(x) = e^{-\lambda x}$$

$G_X(x)$  is a particularly simple function to graph as it is a straight line on semi-log paper and has a value of 1 at  $x = 0$ . Figure 2 shows this type of presentation for the 3 data sets presented in Figure 1. Also on each line we

have indicated the range of  $G_X(x)$  values encountered within each class interval by using  $G_X(x^{(i)}) = 1 - (i/n)$  where  $x^{(i)}$  is the  $i^{\text{th}}$  value in an ordered increasing list of the observed values and  $n$  is the total number of values in the sample.

Therefore we can use the simple relation

$$P[X \geq x] = \frac{n[X \geq x]}{N} = e^{-\lambda x}$$

where  $N$  is the number of gouges that have occurred to estimate  $n[X \geq x]$ , the expected number of gouges with depths greater or equal to  $x$ . We currently propose to estimate  $N$  from the product of the number of years of projected pipeline operation, the length of the buried pipeline and the average number of new ridges per km per year. This latter figure will in turn be estimated as a percentage of the number of gouges/km that are visible on the sea floor at a given time. We currently are attempting to find a satisfactory PDF for this latter parameter.

#### VIII. NEED FOR FURTHER STUDY

Here the letters indicate the specific sub-programs. A number of years of data are needed in Programs A, C, D, and F to determine the intra-annual variability of these characteristics. In Program A repeat measurements of the number of new gouges in the variety of identified areas are essential to making adequate probalistic estimates of the frequency at which ice will plow up buried pipelines. Laboratory studies are essential in Program E in order to understand exactly how crystal alignments originate. Detailed experimental studies and model calculations are also needed in Program F to advance our understanding of sea ice.



IX. SUMMARY OF JAN-MAR QUARTER

Project personnel were primarily involved in data analysis, report writing and preparation for field studies.

Frank completed laser flights on Sub-Program A over the northern Bering Sea, the Chukchi Sea, and the Beaufort Sea in January 1980.

Kovacs and Tucker leave for field programs on Sub-Programs B, C, D, and F in late March 1980.

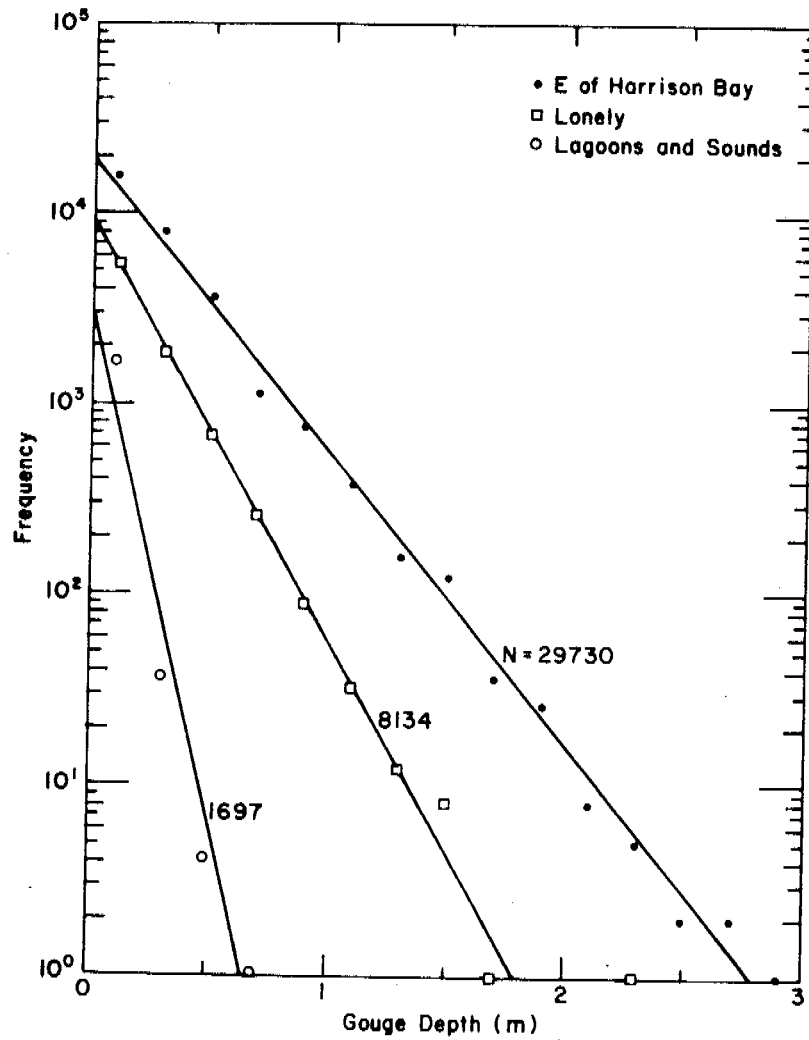


Figure 1. Semilog plot of the frequency of gouges of different depths from 3 different areas along the coast of the Beaufort Sea.

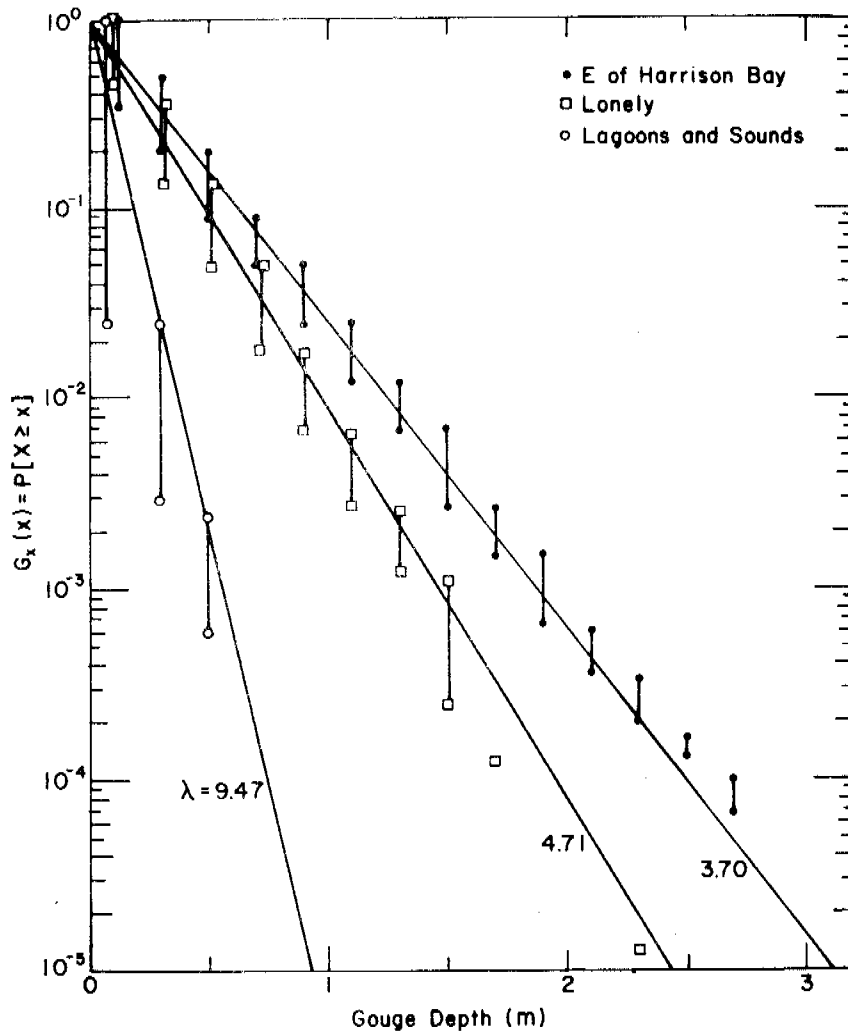


Figure 2. Semilog plot of  $G_X(x)$  versus gouge depth for 3 different areas along the coast of the Beaufort Sea.

X. AUXILIARY MATERIAL

1. Bibliography

- Benjamin, J.R. and Cornell, C.A., (1970). *Probability, Statistics, and Decision for Civil Engineers*. McGraw-Hill.
- Lewis, C.F.M. (1978). The frequency and magnitude of drift-ice groundings from ice-scour tracks in the Canadian Beaufort Sea. POAC 77 Proceedings, Vol. 1, 568-79.
- Lewis, C.F.M. (in press). Bottom scour by sea ice in the southern Beaufort Sea. Beaufort Sea Project Tech. Report. 23, Department of the Environment, Victoria, B.C.
- Miller, I. and Freund, J.E. (1977). *Probability and Statistics for Engineers*, Prentice-Hall.
- Wahlgren, R.V. (1979). Ice-scour tracks in eastern Mackenzie Bay and north of Pullen Island, Beaufort Sea. In "Current Research, Part B, Geol. Surv. Canada, Paper 79-1B, 51-62.

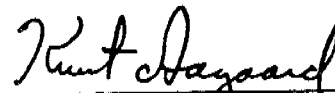
ANNUAL REPORT

Contract No.: 03-5-022-67, T.O.3  
Research Unit No.: 91  
Reporting Period: 1 April 1979-  
31 March 1980  
Number of Pages: 21

Current Measurements in Possible Dispersal  
Regions of the Beaufort Sea

Knut Aagaard  
Department of Oceanography  
University of Washington  
Seattle, Washington 98195

31 March 1980



---

Knut Aagaard, Research Professor  
Principal Investigator

Ref. A80-16



---

George C. Anderson, Professor  
Associate Chairman for Research

## I. Summary

The outer shelf regime extends landward of the 60 m isobath. This regime is characterized year-round by relatively fast flow parallel to the isobaths. Speeds exceeding  $25 \text{ cm sec}^{-1}$  are common. The long-term set is eastward, but frequent pulse-like flow reversals toward the west can last from 1-10 days or more. At a new mooring site 60 m deep north of Oliktok there was no indication of a change in this flow regime, either in speed or direction. However, at another site in the same depth north of Flaxman Island, the current speeds were reduced by 50% or more. Furthermore, flow events directed offshore with typical speeds of  $5 \text{ cm sec}^{-1}$  were relatively common at the latter site and may possibly be of significance to cross-shelf transport. So far, only one instance of deep upwelling, such as is common further offshore, has been found at these two more shallow mooring sites, although one instrument record is yet to be analyzed.

The significance of these results to the dispersion of various materials seaward of the 50-60 m contours is as follows:

(1) Material trajectories will nearly follow isobaths. (2) Over a period anywhere from 1-10 days, displacement may be either eastward or westward, and the magnitude of such displacement can exceed 40 km over 24 hours. (3) On time scales exceeding about one month, the net displacement will be eastward, with mean speeds corresponding to typical monthly displacements in the range of 100-250 km. (4) Materials can also move on- and offshore on time scales of a few days. Some of these movements represent a deep onshore upwelling originating over the continental slope and affecting large stretches of the shelf, while others appear to be offshore movements, possibly more local, through the mid-shelf zone.

## II. Introduction

The objective of this work has been to obtain long-term Eulerian time series of currents at selected locations on the outer shelf of the Beaufort Sea. Such measurements are necessary to describe and understand the circulation on the shelf and the exchange between the shelf and the deep Arctic Ocean. It is this circulation and exchange which transports and disperses the plankton, substances of biological and geological consequence, and pollutants. The water motion also influences the ice distribution and drift. The current time series must be long enough to define the important temporal scales of motion.

## III. Current State of Knowledge

Some of what is known about the circulation on the Beaufort shelf has been inferred from the hydrography, and these conclusions have been discussed in past reports (e.g., cf. the annual report for RU151 for 1977-78).

Direct current measurements were extremely sparse prior to the work done under the present RU91. The measurements made under RU91 began in March 1976. Since then about 2330 days of current measurements have been accumulated seaward of the 25 m isobath, extending from 146°-152°W.

Prior to the present contract year, current measurements seaward of the land-fast ice had been restricted to water depths greater than about 100 m because of anticipated danger to the moorings from drifting ice. Based on these measurements, we concluded that an energetic current regime over the outer shelf extends landward to at least the 100 m isobath. The flow is characterized by a series of pulses, in which the water alternately

moves eastward or westward along the isobaths in a reciprocating fashion. The strength of these pulses is typically about  $20 \text{ cm sec}^{-1}$ , but can on occasion exceed  $65 \text{ cm sec}^{-1}$ , and their duration varies from a day to several weeks. The eastward pulses are generally stronger and longer-lasting. The long-term mean flow is therefore eastward (along the isobaths) and in the range of  $5\text{--}10 \text{ cm sec}^{-1}$ . There does not appear to be any seasonal cycle in the flow. These remarks apply to the motion below about 60 m; above this depth, the velocity field is unknown, as the drifting ice makes moored measurements at lesser depths extremely hazardous.

The thermal regime down to at least 65 m is largely advectively controlled, with the water bearing the mark of the freezing process until mid-summer. At that time, warm water is advected into the region, probably largely from the Bering Sea, and there are strong horizontal temperature differences. Under these circumstances, waters of different origin being advected past a given point cause a highly variable local temperature regime. Closer to the bottom there is a frequent invasion of warm and saline Atlantic water, occurring in a pulse-like manner and extending over large portions of the shelf. During such events the temperature increases to  $1\text{--}2^\circ\text{C}$  or more above the freezing point. The pulses occur at all times of the year and have time scales similar to the reciprocating along-shelf motion discussed above. These are in effect upwelling events from 350 m or deeper offshore, and they must bring relatively large amounts of salt and sensible heat onto the shelf.

On the inner shelf, under landfast ice, the flow in winter appears to be extremely slow. This contrasts with the summer situation, when the wind can drive a vigorous circulation in these same waters.



#### IV. Study Area

The area of interest extends eastward from Point Barrow along the entire northern Alaska coast, i.e., from about 156° 30'W to 141°W, a lateral distance of 600 km. The shelf is narrow, with the shelf break typically 80-90 km offshore. The total runoff is small and highly seasonal. Tidal amplitudes are also small; they are mixed, predominantly semi-diurnal. Meteorological tides can exceed the astronomic tide by a factor of ten. The prevailing winds are from the ENE and are generally light. The entire area is covered by sea ice, both first- and multi-year, through all but two to three months. Even during the height of summer, ice is usually found well onto the shelf.

#### V. Data collection

The methods and rationale of data collection have been discussed at some length in earlier reports, both annual and quarterly.

#### VI. Results

The field work accomplished during this reporting period includes the recovery of two moorings, one north of Flaxman Island and one north of Oliktok, both in about 60 m of water. The Flaxman recovery was described in the quarterly report dated 30 September 1979. The first attempt to recover the Oliktok mooring was described in the quarterly report dated 31 December 1979, and the final successful attempt is described in the preliminary report (Ref. M80-9) appended to this annual report.

Table 1 summarizes the four current meter records from these recoveries, for which there are 25,400 hours of clear data. Figure 1

Table 1

<u>Current meter</u>	<u>Flaxman 1 upper</u>	<u>Flaxman 1 lower</u>	<u>Oliktok 1 upper</u>	<u>Oliktok 1 lower</u>
Latitude	70° 43.6'N	70° 43.6'N	71° 10.0'N	71° 10.0'N
Longitude	146° 00'W	146° 00'W	148° 52.7'W	148° 52.7'W
Sounding	59 m	59 m	60 m	60 m
Depth of meter	39 m	49 m	40 m	50 m
Date deployed	22 Feb 1979	22 Feb 1979	21 Feb 1979	21 Feb 1979
Date recovered	22 July 1979	22 July 1979	6 March 1980	6 March 1980
Start of record (GMT)	2205 22 Feb 79	2206 22 Feb 79	0332 21 Feb 79	0033 21 Feb 79
End of record (GMT)	0405 22 July 79	0406 22 July 79	2032 6 Mar 80	2033 6 Mar 80
Recording interval	60 mins.	60 mins.	60 mins.	60 mins.
No. of records	3583	3583	9114	9117

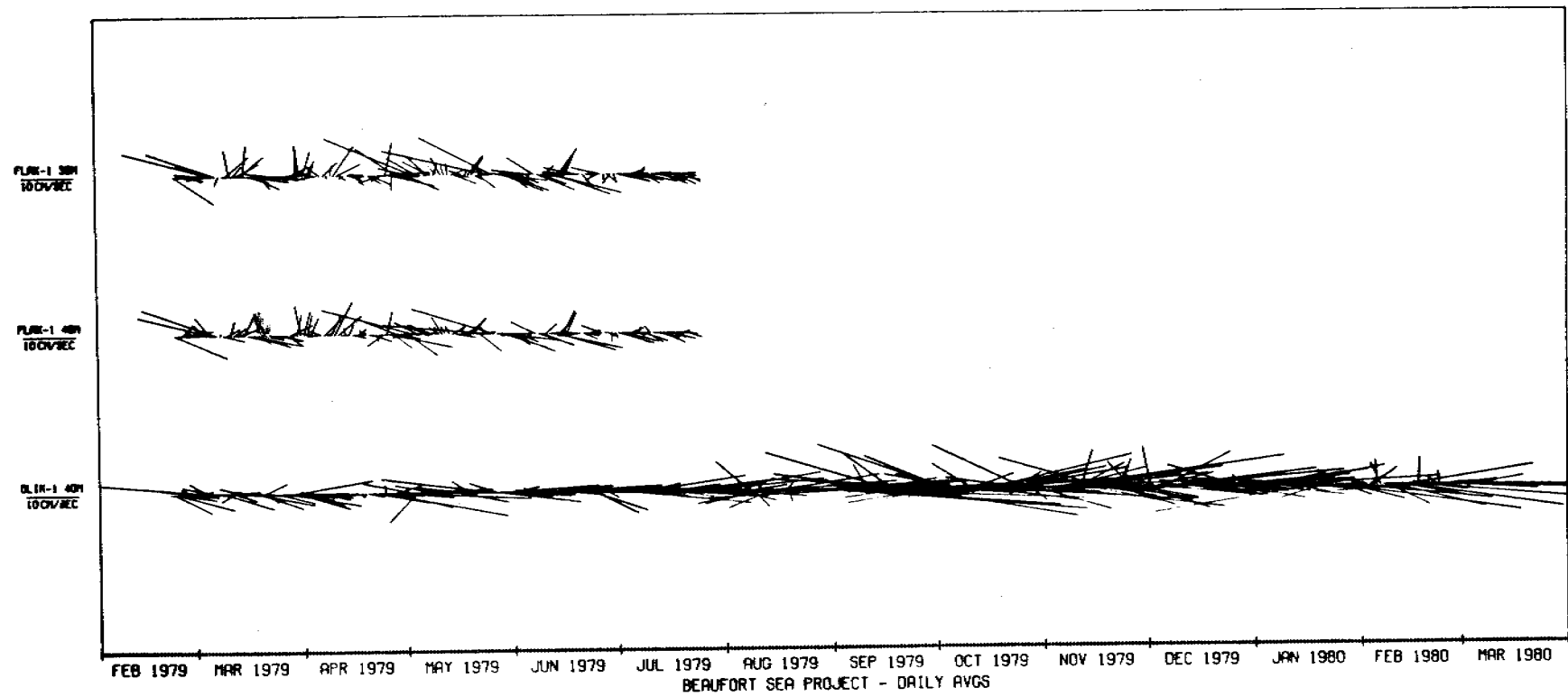


Figure 1

shows the daily mean velocities for the two Flaxman 1 instruments and the upper Oliktok 1 meter. Geographic north is toward the top of the figure. The lower meter at Oliktok 1 has not yet been processed to this stage.

## VII. Discussion

Figure 2 shows the current roses for all time series obtained under our RU91 work, including the two Oliktok 1 instruments; and Table 2 shows the time span covered by the 13 separate records. The current roses represent the mean speed and the frequency of occurrence of the current in each sector of angular measure 20 degrees arc. For example, at L0-5 which recorded from 13 March to 7 October 1978 the current was predominantly toward  $100 \pm 10^\circ$  (occurring 43% of the time) with a mean speed over the nearly 7 months of about  $15 \text{ cm sec}^{-1}$ . At the same location the next most commonly observed current was in the reciprocal direction and in the mean about  $2 \text{ cm sec}^{-1}$  slower. The still relatively high occurrence rates in the sectors  $120 \pm 10^\circ$  and its reciprocal (11 and 9%) are due to the method of computation, which places the vectors into discrete directional intervals. That is, the predominant current at L0-5 is not distributed uniformly over the interval  $100 \pm 10^\circ$ , but is actually directed somewhat south of  $100^\circ$ ; in fact, a vector mean calculation yields  $112^\circ$ . It is important to note that this figure by itself provides no information on observational time spans and may therefore be misleading. It must be examined together with Table 2. For example, at site L0-1 the rather round current rose represents just over a week of measurements, whereas the elongated elliptical rose represents nearly seven months and is therefore in a probabilistic sense far more representative of the current conditions.

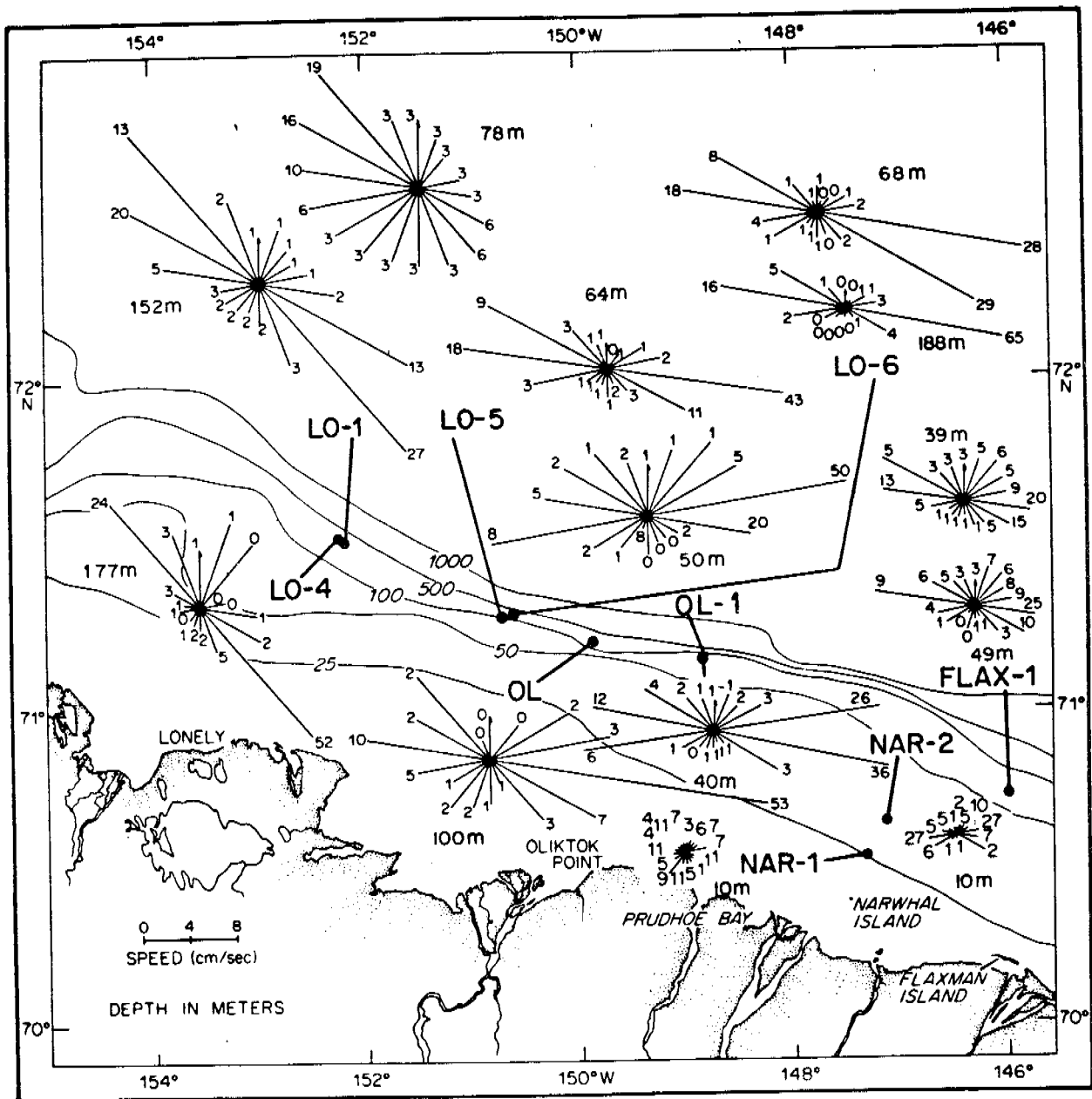


Figure 2

Table 2

<u>Current meter (depth)</u>	<u>1976</u>	<u>1977</u>	<u>1978</u>	<u>1979</u>	<u>1980</u>
NAR-1 (10 m)	28/3 - 22/4				
NAR-2 (10 m)	28/3 - 19/4				
OL (100 m)	27/5 - 1/9				
LO-1 (78 m)		29/3 - 6/4			
LO-1 (152 m)		29/3 - 20/10			
LO-4 (177 m)		13/11 ———— 30/10			
LO-5 (64 m)			13/3 - 7/10		
LO-6 (68 m)			11/3 - 4/9		
LO-6 (188 m)			11/3 - 14/9		
FLAX-1 (39 m)				22/2 - 22/7	
FLAX-1 (49 m)				22/2 - 22/7	
OL-1 (40 m)				21/2 ———— 6/3	
OL-1 (50 m)				21/2 ———— 6/3	

Figure 2 shows that except at the two Narwhal sites, where the measurements were taken under fast ice during winter, the flow is strongly influenced by the bathymetry, tending to align with it, whether the motion is generally eastward or westward. Furthermore, Figure 2 shows that the long-term mean flow is eastward, contrary to the westward flow traditionally attributed to the Beaufort gyre. A third flow characteristic apparent from the current roses is that the predominant flow directions are reciprocal, as was shown above for LO-5. This of course corresponds to the pulse-like nature of the flow, which was discussed in Section III: the flow is characterized by a series of pulses, in which the water alternately moves eastward or westward along the isobaths in a reciprocating fashion. Finally, it is clear from Figure 2 that the mean speeds are relatively high, typically 15-20 cm sec<sup>-1</sup> for the dominant mode. This is true even for OL-1, in 60 m of water; the only exception to these general characteristics is at FLAX-1, in 59 m, where the mean speed for the dominant mode is reduced to about 5 cm sec<sup>-1</sup>. The lower speeds at FLAX-1 compared to OL-1 are also apparent in Figure 1.

The conclusion therefore is that the outer shelf regime of relatively fast flow parallel to the isobaths, generally eastward but with frequent reversals lasting for days, extends landward past the 60 m contour. At OL-1 there was no indication of a change in the flow characteristics, but at FLAX-1 the currents were slower, indicating a possible transition. There is also another difference between the FLAX-1 and the other records: at the former site there is an asymmetry between offshore and onshore flow, with offshore flow being common. That is, Figure 2 shows that flow in directions other than the two principal modes and their reciprocals occurs

relatively frequently, and that 70 to 80% of such flow is offshore. Furthermore, the offshore flow is stronger. In this part of the shelf, therefore, we're beginning to see a tendency for offshore transport. Conceivably, of course, this could be a local phenomenon, and in fact bottom slopes appear to be less at the FLAX-1 site than at OL-1 (cf. Fig. 2), so that the topography is less effective in trapping the motion. The offshore flow events are apparent in Figure 1, where on the average they appear about once a month and last from a day to a week, with typical speeds in the vicinity of  $5 \text{ cm sec}^{-1}$ . A few events with similar signature can also be seen in the OL-1 record (Fig. 1) later in the year, for example in November.

It's important to note that all of the above discussion pertains to motion below about 40 m; motion in the upper part of the water column has not been measured.

The temperature record suggests that both the OL-1 and FLAX-1 sites are landward of the area frequently invaded by Atlantic water (cf. Section III), although we have not yet processed the temperature record for current meter OL-1 lower, where such signals would seem most likely to occur. No large temperature excursions identifiable with deep upwelling were seen at either of the FLAX-1 meters, and only one such event occurred at OL-1, in January 1980. At that time the temperature rose to about  $1^\circ\text{C}$  above freezing. The anomaly lasted about one day and was preceded by strong ( $\sim 35 \text{ cm sec}^{-1}$ ) flow toward WSW, i.e., with an onshore component.

#### VIII. Conclusions

The outer shelf regime extends landward of the 60 m isobath. This regime is characterized year-round by relatively fast flow parallel to the



isobaths. Speeds exceeding  $25 \text{ cm sec}^{-1}$  are common. The long-term set is eastward, but frequent pulse-like flow reversals toward the west can last from 1-10 days or more. At a new mooring site 60 m deep north of Oliktok, there was no indication of a change in this flow regime, either in speed or direction. However, at another site in the same depth north of Flaxman Island, the current speeds were reduced by 50% or more. Furthermore, flow events directed offshore with typical speeds of  $5 \text{ cm sec}^{-1}$  were relatively common at the latter site and may possibly be of significance to cross-shelf transport. So far, only one instance of deep upwelling, such as is common further offshore, has been found at these two more shallow mooring sites, although one record is yet to be analyzed.

#### IX. Needs for Further Study

The primary immediate need would appear to be to further analyze the rather considerable body of data that now exists. Of particular interest is the correlation between atmospheric and oceanographic events. We have just recently received some of the necessary atmospheric time series, which must be formatted and bridged before correlation routines can be run.

It's likely that future studies will be rather site- and/or process-specific, and their design should be guided by a more complete analysis of data in hand.

#### X. Summary of January-March Quarter

##### A. Field operations

See appended report.

B. Estimate of funds expended to February 29, 1980

Allocation 10/1/79 - 9/30/80		\$60,000
1. Salaries, faculty and staff	\$ 11,731	
2. Benefits	1,832	
3. Indirect costs	6,826	
4. Supplies and other direct costs	14,630	
5. Equipment	0	
6. Travel	<u>4,584</u>	
Total expenditures	\$ 39,603	
BALANCE		<u>\$20,397</u>

XI. Auxiliary material

A paper is in press after review:

L.K. Coachman and K. Aagaard. Reevaluation of water transports in the vicinity of Bering Strait. In Oceanography of the Bering Sea Shelf, D. Hood, ed.

A paper was presented at the Fall 1979 AGU meeting:

K. Aagaard and L.K. Coachman. Time-dependent transports through the Chukchi Sea, 1976-77. EOS, 60(46), 848.

University of Washington  
Department of Oceanography  
Seattle, Washington 98195

Preliminary Report  
University of Washington Participation in  
NOAA Recovery Phase of Cruise W-34

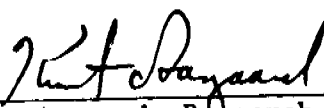
Current Measurements in Possible Dispersal Regions  
of the Beaufort Sea  
28 February - 7 March 1980

by

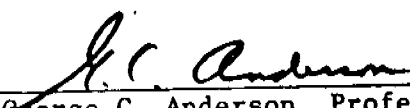
Clark H. Darnall

NOAA Contract 03-5-022-67, TO-3

Approved by:

  
Knut Aagaard, Research Professor  
Principal Investigator

Ref. M80-9

  
George C. Anderson, Professor  
Associate Chairman for Research

1. Objective

To look at the time-dependent circulation and dynamics of the outer continental shelf of the Beaufort Sea, by means of long-term Eulerian time-series current studies at selected locations, where the ice cover is not seasonally removed. Cruise W-34 was a recovery phase of the current meter studies.

2. Narrative

*Mooring recovery phase*

One mooring (designated Oliktok #1) was to be recovered.

(a) General area relocation (within 7-8 km) by use of the helicopters GNC 500A, VLF navigation equipment.

(b) Precise mooring relocation by ranging and bearing on the mooring's acoustic transponder/release. Upon satisfactory relocation, the mooring would be released, allowing the flotation to lie against the underside of the ice cover.

(c) After further acoustic pinpointing of the mooring (within 50 m), a diving hole would be cut through the ice and scuba divers would secure a retrieval line to the mooring. The mooring would then be recovered through the same hole.

For location of the mooring and a map of the search area, see Appendix.

The report of events is as follows.

28 Feb 1980. Dale Ripley and Stephen Harding arrived in Deadhorse.

When they checked with ERA Helicopter Service, they learned that there was no helicopter with VHF homing capability available.

29 Feb 1980. S. Harding notified me in Seattle of the VHF homer problem. I contacted Dan Brooks, OCS coordinator in Fairbanks, and began assembling a

VHF homer/antenna system. The rest of the equipment at Mukluk Camp was allright.

3 Mar 1980. I arrived in Deadhorse and began setting up a JMR satellite navigator. This would be the back-up navigation as the helicopter was not equipped with a VLF navigation system.

We would first try to locate the mooring by dead reckoning out of Oliktok DEW site.

4 Mar 1980. We installed the VHF homer antenna and receiver/indicator head on NOAA helicopter N56RF. The pilot was Lt. Gary Vanderberg, and mechanic was our old friend Roy DeHart.

In the afternoon, we set up the VHF beacon, and Lt. Vanderberg and I flew out to check the operation of the homer system. We made several approaches (from as far out as 15 nm) and everything worked fine.

The satellite navigator was also working well with many accurate fixes.

5 Mar 1980. Weather: high thin stratus, temperature  $-18^{\circ}\text{C}$ , wind  $040^{\circ}\text{T}$  at 8 kts. We loaded up.

0750 AST. Ripley, Harding and Darnall departed Mukluk in N56RF (Vanderberg). We would fly to Oliktok and then take a radial bearing of  $21^{\circ}\text{T}$  ( $350^{\circ}\text{M}$ ) and go out 43.5 nm. The radar transponder in N56RF was not operating, and the DEW site was unable to get a fix on us. We used the NDB at Oliktok and the VOR at Deadhorse to get cross bearings. They corresponded with our dead reckoning at the estimated mooring site.

0852 AST. We landed at site #1. The ice was approximately 5 ft. thick. We received a transponder reply giving a range of 4.3 km at  $315^{\circ}\text{M}$ . We also got a timed ping reply, 1 pulse/2 sec. The output of the AMF 301 power amplifier was very weak,  $<.2$  amp. We moved.

0933 AST. We landed at site #2. The transponder reply was range 1.02 km at 145°M. We moved.

1001 AST. We landed at site #3. The transponder reply was range 480 m.

1012 AST. We sent the release command. The reply was 1 pulse/sec for 60 sec. The transponder range was 470 m. We paced off the distance and moved the helicopter.

1027 AST. We landed at site #4. The transponder range was 100 m. We used the APL pinger directional receiver to get a cross bearing. We moved the helicopter to this final site.

1130 AST. We started digging the diving recovery hole. The ice was approximately 5 ft. thick. We heard the pinger many times.

1430 AST. We finished the hole, leaving the center plug and slush to be removed after it had refrozen. All hands were tired and diving would not be a good idea. We set up the VHF beacon and marked the ice.

1440 AST. We took off, flew out about 8-10 nm and then homed back in on the site. All worked well. As we returned to Deadhorse, we lost audio on the beacon at about 30 nm (at 2300 ft).

1600 AST. After refueling, we landed at Mukluk Camp. The satellite navigator was not working, and the program had been dumped. I spent some time reprogramming and setting up with the satellite navigator, to no avail.

6 Mar 1980. Weather: clear, temperature -20°C, wind 050°T at 11 kts.

It was a bit brisker than the previous day.

0836 AST. Harding, Ripley and Darnall departed Mukluk in N56RF (Vanderberg and DeHart). We got needle heading indication on the VHF homer as soon as we picked up some altitude. At about 30 nm away, we picked up audio.

0920 AST. We landed at the mooring site. We cleaned out the hole and used the helicopter to pull the center plug (all very smooth and easy).

1020 AST. Harding and Darnall begin suiting up.

1040 AST. Divers in the water. The mooring was about 10-15 m away right on the bearing received from the APL pinger directional receiver.

1055 AST. Divers out.

1105 AST. Current meters, release and entire mooring out. We packed up and Ripley joined the P.B. club.

1212 AST. We departed the ice for Mukluk.

1300 AST. We landed at Mukluk, unloaded, removed the VHF homer antenna, and began packing for shipment home.

1430 AST. The current meters were opened. Equal amounts of tape had been recorded (about 80-90%) and the batteries were up. The main batteries were the exact same unloaded voltage as when deployed.

1432/36 AST. Each meter cycled through.

1532/36 AST. Last recorded cycle was recorded.

1900 AST. Darnall returned to Seattle.

7 Mar 1980. Harding and Ripley returned to Seattle.

### 3. Methods

#### *Recovery*

An AMF (now EG & G) model 301 ranging and bearing command system was used for precise relocation of the AMF model 322 transponder/releases. Additional cross bearings were acquired using an APL pinger directional receiver.

The divers used Unisuits (a variable volume dry suit), double 80 cu.ft. aluminum tanks with independent Poseidon regulators on each tank. Each diver was connected to a common tether line and used U.S. Navy Diving procedures and line signals.

4. Personnel

Stephen Harding	Research Aide	Dept. of Oceanography University of Washington
Dale Ripley	Research Aide	"
Clark Darnall	Oceanographer	"
Lt. Gary Vanderberg	Pilot	NOAA
Roy DeHart	Mechanic	"

Acknowledgement

Lt. Vanderberg's and Mr. DeHart's assistance in completing this project was greatly appreciated.



Appendix

Mooring location

Oliktok #1            71° 11.0'N, 149° 2.5'W

Flight time

NOAA UH-1H    N56RF            5 hrs., 20 min.



SIXTH ANNUAL REPORT

Research Unit # 138  
Reporting Period: 1 April 1979 -  
31 March 1980

GULF OF ALASKA STUDY OF MESOSCALE OCEANOGRAPHIC PROCESSES  
(GAS-MOP)

J.D. Schumacher  
C.A. Pearson

Pacific Marine Environmental Laboratory  
3711-15th Avenue, N.E.  
Seattle, Washington 98105

31 March 1980

## TABLE OF CONTENTS

I.	Summary . . . . .	53
II.	Introduction . . . . .	53
III.	Current State of Knowledge . . . . .	54
IV.	Study Area . . . . .	54
V.	Sources, Methods and Rationale of Data Collections . . . . .	54
VI.	Present Status	
	A. Some observations of physical oceanographic conditions in the northeast Gulf of Alaska . . . . .	55
	B. Very low frequency variations in current near the northeast Gulf of Alaska shelf break . . . . .	58
	C. Sea level variations in relation to coastal flow around the Gulf of Alaska . . . . .	88
	D. On baroclinic transport of the Alaskan Stream near Kodiak Island . . . . .	89
	E. Coastal flow in the northwest Gulf of Alaska: The Kenai Current . . . . .	118
	F. Direct measurement of recirculation in the Alaskan Stream . . . . .	150
	G. Physical and meteorological conditions in the northwest Gulf of Alaska . . . . .	163
	H. Preliminary results from WIST experiment . . . . .	166
	I. A one-pass processing system for Aanderaa current meter data . . . . .	168
	J. R2D2: An interactive graphics program for rapid retrieval and display of oceanographic data . . . . .	184
	K. A microprocessor-based transcriber. . . . .	203
VII.	Cooperation . . . . .	214
VIII.	Publications . . . . .	214
IX.	Needs for further study . . . . .	220
X.	Conclusions . . . . .	221

## I. Summary

Field investigations, begun in Autumn 1974, have and continue to provide data which aid our understanding of hydrographic and current regimes in the northern Gulf of Alaska. Important results include:

- . Delineation of baroclinic transport in the Alaskan Stream
- . Identification of a coastal current system extending from Copper River delta through Shelikof Strait: the Kenai Current.
- . Description of mean flow in lower Cook Inlet and verification of the flow using new field data.
- . Description of circulation and hydrography over the continental shelf of the northwest Gulf of Alaska during fall, winter and spring.

Further analysis of the field data collected during the past year will focus on explaining driving mechanisms for mean and fluctuating flow components and evaluating their importance.

## II. Introduction

### A. General Nature and Scope of Study

The general objective of this work unit is to relate oceanic advective and diffusive processes to potential pollution problems due to OCS petroleum development. This is being accomplished through field activities including moored current measurements and water mass analysis using temperature and salinity observations. The region being considered includes the northwest Gulf of Alaska continental shelf west from about the longitude of Seward, Alaska to Unimak Pass and extends offshore to the outer boundary of the Alaskan Stream some 100 km off Kodiak Island.

### B. Specific Objectives

#### 1. Shelf region around Kodiak Island

- a) Examine flow over the troughs and banks off Kodiak Island and on the shelf downstream from Shelikof Strait using current meters, drift cards and hydrographic data.
- b) Characterize temporal and spatial variability in the flow field as a function of season.
- c) Relate observed and computed geostrophic surface winds to observed currents.
- d) Determine spatial variability of tidal currents.
- e) Characterize seasonal hydrographic distributions.

## 2. Lower Cook Inlet

- a) Relate observed and computed over-the-water winds to observed currents.
- b) Correlate surface currents obtained by Lagrangian techniques with subsurface Eulerian observations.
- c) Relate surface currents obtained by Doppler radar techniques to Lagrangian surface current measurements.
- d) Characterize temporal and spatial variability in the flow field including flows through the Barren Islands and upper Shelikof Strait as a function of season.

## C. Relevance to Problems of Petroleum Development

Two distinct environmental problems can accompany petroleum development in a marine region; catastrophic spills and chronic or long-term leakage. This research unit addresses both of these problems. The eventual effect of a catastrophic spill depends upon where the spilled oil goes, i.e., its trajectory, how long it takes to get there, and how much diffusion of oil occurs along the trajectory. This study will provide estimates of the fields of water motion which exert primary control over such trajectories and over diffusion processes along the trajectories. Oil introduced into the environment via long-term or chronic leakage is more likely to be dispersed throughout the water column and, possibly, scavenged by suspended particulate matter. The problem then becomes one of understanding net transport of suspended matter, a process related to advective and diffusive fields within the water column. Understanding of these processes requires an analysis of the velocity field and its driving mechanisms. This study addresses these latter points.

## III. Current State of Knowledge

The first annual report (31 March 1975) summarized the state of knowledge prior to commencing this study. That report, subsequent reports and publications and Sections VI-VIII of this report update the initial summary.

## IV. Study Area

Upon completion of the Final Report for the Northeast Gulf of Alaska Continental Shelf program (1 October 1978), this study has been concerned with the northwestern Gulf of Alaska continental shelf from Portlock Bank east of Kodiak Island (about the longitude of Seward, Alaska) westward to Unimak Pass. Detailed physical descriptions of this region have been presented in previous annual reports, in manuscripts and in prior publications.

## V. Sources, Methods and Rationale of Data Collection

Instrumentation, field and processing methods are identical to those used in the past and are documented in previous reports from this series. Where deviations from standardized methods are significant, they are discussed within the context of the appropriate subregional study.

A. The following is from an amended Final Report: RU 138 (Northeast Gulf) which has been reviewed and is being sent to Boulder for publication as an ERL/PMEL Technical Memo:

SOME OBSERVATIONS OF PHYSICAL  
OCEANOGRAPHIC CONDITIONS ON THE  
NORTHEAST GULF OF ALASKA  
CONTINENTAL SHELF

Contributors: R. D. Muench<sup>1</sup>  
J. D. Schumacher  
S. P. Hayes  
R. L. Charnell<sup>2</sup>  
G. Lagerloef  
C. A. Pearson

Pacific Marine Environmental Laboratory  
National Oceanic and Atmospheric Administration  
3711 - 15th Avenue N E.  
Seattle, Washington 98105

<sup>1</sup>Now at SAI/Northwest, 13400B Northrup Way, Bellevue, WA 98005.

<sup>2</sup>Deceased.

## PREFACE

Commencing in 1974, the Pacific Marine Environmental Laboratory, NOAA, has been investigating physical oceanographic processes on the continental shelf in the northern Gulf of Alaska. The work has been funded by the Bureau of Land Management as part of the Alaskan Outer Continental Shelf Environmental Assessment Program. The initial phases of this effort addressed processes in the northeastern gulf, in particular the shelf region adjacent to Icy and Yakutat Bays. Geographical emphasis has shifted westward with time; the program currently emphasizes the northwest Gulf of Alaska with stress on the region surrounding Kodiak Island. Initially, the program was concerned primarily with obtaining moored current and bottom pressure measurements with only minor attention to coincident conductivity and temperatures versus depth (CTD) and other data. More recently, the program has shifted emphasis to include collection of CTD data along with ancillary information such as that obtained from satellite-tracked drifters, drift cards and environmental buoys.

The field program in the northeastern gulf was completed in summer 1977 while that in the western section is continuing. However, based on our observations, it is evident that the Gulf of Alaska continental shelf can be divided geographically at Middleton Island into an eastern and western regime. The northeastern gulf is a region of relatively broad, diffuse westerly flow. The western gulf, particularly the region off Kodiak Island is characterized by a narrow, high-speed boundary flow, the Alaskan Stream. In addition to the difference in major current regimes, the shelf is narrower off Yakutat and Icy Bays than off Kodiak Island and bottom topography is somewhat more irregular, though considerable topographic irregularities also exist off Kodiak Island. We would a priori expect shelf circulation off Kodiak Island to be more heavily influenced by shelf break circulation than in the northeastern gulf because of the more intense shelf break current in the former location. Conversely, local meteorological effects and freshwater input might be expected to have relatively greater effect on shelf circulation in the northeastern gulf.

In view of the oceanographic differences between the two regions, we can present in this final report an independent synopsis of the results of the northeast Gulf of Alaska field program without loss of understanding. The stress will be measured currents and bottom pressures, consistent with the major thrust of our field effort. These will be related to regional circulation where possible, and to coincident temperature, salinity and weather data where appropriate. It is hoped that the end product will provide a useful working document both for environmental planning and for future, more focused, scientific endeavors in the region.



## TABLE OF CONTENTS

### PREFACE

### TABLE OF CONTENTS

1. INTRODUCTION
  - 1.1 History of Oceanographic Research
  - 1.2 Geographical Setting
  - 1.3 Oceanographic and Meteorological Setting
    - 1.3.1 Regional Oceanographic Processes
    - 1.3.2 Local or Shelf Oceanographic Processes
    - 1.3.3 Meteorological Conditions
2. OBSERVATIONAL PROGRAM
  - 2.1 The Overall Mooring Program
  - 2.2 Icy Bay Experiment
  - 2.3 Kayak Island Experiment
  - 2.4 Current Observations
3. LONG PERIOD TIME VARIATION IN CURRENTS
4. EXTREME VALUE ANALYSIS APPLIED TO CURRENT DATA
  - 4.1 Introduction
  - 4.2 Extreme Speed Analysis
  - 4.3 Summary
5. CURRENT, BOTTOM PRESSURE AND WIND CORRELATIONS OFF ICY BAY
  - 5.1 Introduction
  - 5.2 Observation
    - 5.2.1 Hydrographic Observations
    - 5.2.2 Wind Observations
    - 5.2.3 Bottom Pressure Observations
  - 5.3 Analysis
    - 5.3.1 Current Time Series, Vertical and Cross-Shelf Structure
    - 5.3.2 Pressure Time Series, Spectra and Correlations
    - 5.3.3 Velocity-Pressure Correlations
    - 5.3.4 Wind Correlations
  - 5.4 Discussion and Summary
6. CURRENTS WEST OF KAYAK ISLAND
  - 6.1 Introduction
  - 6.2 Observation
  - 6.3 Conclusion
7. DISCUSSION AND SUMMARY
  - 7.1 Spatial Variability
  - 7.2 Time Variations
  - 7.3 Summary
8. ACKNOWLEDGEMENTS
9. REFERENCES

B. The following manuscript is in preparation:

VERY LOW FREQUENCY VARIATIONS IN CURRENTS  
NEAR THE NORTHEAST GULF OF ALASKA SHELF BREAK

Gary Lagerloef

Robin Muench<sup>1</sup>

James Schumacher

Pacific Marine Environmental Laboratory  
Environmental Research Laboratories  
National Oceanic and Atmospheric Administration  
Seattle, Washington 98105

<sup>1</sup>Now at SAI/Northwest, 13400B Northrup Way, Bellvue, wa 98005.

## ABSTRACT

We present current observations from 20, 50, 100 and 175 m depths obtained over a three year period near the northeast Gulf of Alaska shelf break. These records, some with continuous segments of over two years, indicated a moderate ( $\sim 16$  cm  $\bar{s}^{-1}$  at 50 m) mean flow directed, at all depths, alongshelf toward the northwest. The typical seasonal alongshelf mean speed varied from  $\sim 12$  cm  $\bar{s}^{-1}$  in summer to  $\sim 20$  cm  $\bar{s}^{-1}$  in winter due to intensification of winter southeasterly winds over the Gulf. Very low frequency ( $< 0.1$  cpd) current fluctuations were prominent flow factors and were coupled vertically to 100 meters depth. Fluctuating kinetic energy contained in these very low frequencies was a significant fraction of the total and displayed an inter-year increase with no seasonal trend. Although correlation between alongshelf local wind and current increased with the averaging time scale, the majority ( $\sim 70\%$ ) of the very low frequency kinetic energy was not accounted for by wind forcing. We suggest that these fluctuations were related to oceanic scale features such as eddies or meanders in the Alaskan Current.

## 1. INTRODUCTION

Past current observations on continental shelves have generally yielded records of one-year duration or less (e.g. Smith 1978; Hayes, 1979). These investigations have been concerned primarily with such phenomena as tidal and inertial motions, continental shelf waves and responses to atmospheric forcing, generally characterized by frequencies higher than 0.1 cpd.

An exception to this was reported by Mayer *et al.* (1979), who analyzed long-term, current measurements from the Middle Atlantic Shelf. They noted that seasonal variations in monthly mean current were obscured by transient events, that seasonal shifts in spectral patterns were present, and that low frequency variability in alongshelf currents was not well correlated with local wind forcing. In this paper, we investigate long term flow features using a three-year long composite time series of current observations obtained from a shelf break location in the northeastern Gulf of Alaska.

The mooring site, referred to herein as 62, was located in 185 m of water some 50 km southwest of Icy Bay, Alaska (Fig. 1). This is a shelf region of complex bathymetry, with ridges and troughs transecting the shelf normal to the coast. The moorings were located adjacent to a trough-like feature, which results in a local shoreward trend in the isobaths. Southeast of the mooring the bathymetry is nearly aligned along 310°T, the direction used to define the alongshore flow axis. Relief of adjacent coastline is abrupt, consisting of 4000-5000 m mountains cut by deep, transverse glaciated valleys. This vertical relief affects the local wind field to 20-30 km out from the coastline (R.M. Reynolds,

PMEL/NOAA, personal communication). Flow blockage by the mountains causes crowding of atmospheric isobars near the coastline and consequent acceleration of the near-coastal winds, which are also constrained to follow the trend of the local coastline.

Regional oceanic circulation in the northern Gulf of Alaska is dominated by the Pacific subarctic gyre; a cyclonic wind-driven gyre which occupies the Gulf of Alaska and which results in a northwestward shelf break flow, the Alaska current, in the vicinity of 62. About 500 km downstream from 62, the westward flow intensifies to form a western boundary current, the Alaskan Stream, off Kodiak Island due to the southward trend in the coastline at that location (Favorite and Ingraham, 1977; Reed et al., 1980). Circulation in the gyre, hence in the Alaskan Stream, would be expected to fluctuate seasonally consequent to an order of magnitude seasonal variation in wind-stress curl over the Gulf of Alaska due to winter intensification of the Aleutian Low atmospheric pressure system (Royer, 1975). A recent investigation of baroclinic flow along the shelf break off Kodiak Island by Reed et al. (1980) suggests, however, that seasonal baroclinic fluctuations in transport are negligible. There is not yet sufficient current meter data from the Alaskan Stream to resolve the seasonal variations in flow.

On the shelf in the vicinity of 62, winter intensification of the Aleutian Low leads to strong southeasterly winds and, concurrently, a tendency toward onshore Ekman transport and downwelling (Royer, 1975). In summer, the North Pacific High pressure system dominates, bringing lighter, more variable winds and a relaxation of coastal convergence. Inner and outer shelf dynamic processes appear to be decoupled in the vicinity of 62. Fluctuations in subtidal flow at the shelf break were not well correlated with cross shelf bottom pressure fluctuations and did not propagate onto

the shelf (Hayes, 1979; Hayes and Schumacher, 1976). Hayes (1979) suggested anticyclonic shelf break fluctuations were associated with eddies in the Alaskan current. Complex eddy-like features have been identified along the shelf break using surface water temperatures as a tracer (Royer and Muench, 1977) and from dynamic heights and drogue trajectories (Royer et al., 1979). In this paper we describe long term behavior in shelf break flow and kinetic energy; in particular seasonal, inter-year and other very low frequency ( $<0.1$  cpd) fluctuations are addressed.

## 2. OBSERVATIONAL PROGRAM      Currents:

The current data for 62 were obtained from 12 sequential moorings, each of about three months average duration. The mean location was  $50^{\circ} 36'N$ ,  $142^{\circ}11'W$ , with a deviation of about 2 km. This position variability is inconsequential for our purposes; it is less than either the local topographic scales (20-30 km) or the internal Rossby radius of deformation ( $>15$  km). Each mooring consisted of four Aanderaa RCM-4 current meters emplaced 20, 50, 100 and 175 m below the surface in a taut-wire configuration having subsurface flotation at about 17 meters.

Unedited data from the current meters were processed according to Charnell and Krancus (1976). Each record was then filtered using a Lanczos two-sided filter (-6 db at periods shorter than 2.86 hours). With the highest frequencies thus removed, each data set was interpolated to an hourly sample to provide a common time base for the entire set of records. A linear interpolator was used which removed less than 1% of the total variance. The mean gap between successive mooring deployments was about 17 hours and a weighted Fourier series of a small portion of the records

adjacent to the gap was used as a bridge. Extended gaps (>120 hours) spanning periods of no data due to instrument failure were zero filled. The results were composite three year continuous time series of hourly sampled data at 20, 50, 100 and 175 m depths. These included continuous (i.e. no zero filled gaps) series from 50 m and 100 m depths spanning more than two years of observations (Fig. 2). Extended gaps precluded continuous series of this length from the other depths, but these data nevertheless were useful as supporting observations. These series were subsequently low pass filtered (-6db) at 35 hours and 240 hours.

Subsurface moorings can have increased mean speeds due to surface wave-induced rotor pumping (Halpern and Pillsbury, 1976). Hayes (1979) has shown that high frequency motions (>5.0 cpd) at 62 at 50 m depth were more energetic during high winds than those observed at nearby moorings having subsurface flotation 45 m below the surface. Mayer et al. (1979) found consistent increases in energy in the semidiurnal tidal band at shallower moorings on the Middle Atlantic shelf during winter. To test whether our records were contaminated in this manner we performed a sequence of 29-day harmonic analyses of the 50 m record. No significant seasonal variability was evident in the M2 component. We show below moreover, that the variance energy at frequencies below 0.1 cpd at 62 reveals no seasonal trend (Fig. 7). We conclude that contamination of the current records at 62 due to rotor pumping is confined primarily to the higher frequencies (> 5.0 cpd) and has no significant effects upon the low frequencies addressed here.

b. Winds:

Two sources of wind data were available. A NOAA environmental buoy,

EB-70, measured surface wind in the vicinity of 62 during a six month portion of the experiment (Figure 2). In addition, geostrophic wind data spanning the entire period of current records were supplied by Fleet Numerical Weather Central (FNWC). These winds are computed from atmospheric pressure using the geostrophic relation, and an assumed frictional parameter (Bakun, 1973). Since EB-70 data did not span the entire current observation period, it was necessary to use the FNWC computed winds in our analyses. Correlations between the two data sets have been computed by R.M. Reynolds (PMEL/NOAA, personal communication). His results show better correlation in speed than in direction. The EB-70 winds had greater east-west symmetry, whereas the FNWC winds were more omnidirectional. His comparisons with a buoy inshore from 62, EB-43, suggested that there may have been short-term mesoscale features, such as flow reversals, that were not resolved on the synoptic scale of the FNWC model. Our computed correlation coefficients between FNWC and measured (EB-70) alongshore wind components after 35-hr and 240-hr low pass filters were  $r = .83$  and  $r = .89$ , respectively. These high values may have been somewhat biased by the input of EB-70 data to the FNWC model. However we feel this effect was small and that use of the FNWC winds for long term analysis was justified.

c. Hydrographic Data:

Cross shelf hydrographic transects adjacent to 62 were occupied intermittantly during the study. Data were recorded with a Plessey CTD system, signal processer and data logger. The data processing included despiking and 1-m depth averaging before being used to compute dynamic heights.



### 3. DISCUSSION

#### a. Mean Flow:

The progressive vector diagrams (PVD's) depict the mean flow for the composite records (Figure 4). The flow was northwestward (alongshelf) for both the wind and currents at all depths. Current directional shear was insignificant.

From the continuous two year segments (Figure 2), linear cross correlations were made between the 50 m and 100 m depth series. The 240-hr. low pass filtered data yielded coefficients of  $r^2 = 0.86$  (cross shelf),  $r = 0.95$  (alongshelf) and  $r = 0.94$  (speed). These results imply that the currents were vertically coupled between these depths for time scales longer than 10 days.

The 50 m current record was assumed to represent flow conditions at 62 and was used for the following analyses. The mean current for this series was  $16.3 \text{ cm sec}^{-1}$  at  $307^\circ$ . Using the alongshelf axis of  $310^\circ$  yielded a mean alongshelf speed,  $v$ , of  $16.3 \text{ cm sec}^{-1}$  and cross-shelf speed,  $u$ , of  $-0.8 \text{ cm sec}^{-1}$ . Variances about those means decreased sharply as the cutoff period of the low pass filters was increased. Figure 4 depicts the distribution functions of the  $u$  and  $v$  components for the two filtered series. Both components showed nearly normal distributions; variances and confidence limits are given in Table 1. The ratio of the alongshelf standard deviation to the alongshelf mean was 0.69 for the 240 hr filtered series, indicating considerable variability with periods longer than 10 days. Variation about the cross-shelf axis was nearly random, and there was no evidence of a net long term cross-shelf flow at this depth.

With the degree of variance measured, mean flow was clearly not representative of short term conditions. To assess the time scale required to compute a mean with reasonable certainty, autocorrelation functions were generated (Figure 5). We note that the auto-correlation function for  $v$  does not converge on the abscissa due to long term trends or non-stationarity in this component. The area under the curve (from  $-\infty$  to  $+\infty$  since the auto correlation is symmetrical about zero, assuming stationarity) represents the integral time scale  $T$  for independent measurements. Keeping in mind the lack of stationarity, we estimated  $T$  from  $-15$  to  $+15$  days of lag and obtained the results shown in Table 1. The rms error,  $\epsilon$ , of the mean velocity components was estimated using  $\epsilon = \sigma \left(\frac{T}{\tau}\right)^{\frac{1}{2}}$  (Kundu and Allen 1975); where  $\tau$  is the series length and  $\sigma$  is the series standard deviation. These rms errors are also given in Table 1. The error indicates the reliability of the estimate of the true mean since it decreases as the averaging time ( $\tau$ ) increases. The equation for  $\epsilon$  can be used to estimate the minimum averaging time,  $\tau$ , needed to gain a maximum acceptable error (Monin and Yaglom, 1965). Table 2 shows the estimated rms errors for various averaging time. The ratio  $\tau/T$  represents the number of independent observations that can be formed by taking means over the sequence of subsets of length  $T$ . Using a  $T$  of 10 days from the alongshelf component, a series of 10-day means was generated from the two-year data set. The rms errors (i.e. standard deviations) for this set of observations were  $3.7 \text{ cm s}^{-1}$  and  $9.9 \text{ cm s}^{-1}$  for  $u$  and  $v$  respectively. These values were slightly smaller than the rms estimates for 10 days in Table 2, which indicates that the time scale  $T$  is somewhat overestimated. This is attributed to the aforementioned trends in the series which increased the autocorrelation function at large lags. Referring again to

Table 2 with a 95% confidence limit estimated by  $2\epsilon$ , a 30 day mean has a positive  $v$  as its lower 95% limit. The series of 30 day mean current vectors is shown in Figure 6a. Only one of 24 or  $\sim 4\%$  of the mean observations had a direction other than northwest. The foregoing calculations and observations lead us to conclude that 30 days is a minimum sampling time required to obtain a reliable estimate of the mean flow at 62.

b. Kinetic Energy Distribution of Wind and Current

Temporal behavior and frequency distribution of kinetic energy were investigated to determine forcing mechanisms for the current.

The total kinetic energy is defined by  $KE_{tot} = KE + \overline{KE'}$ , where  $\overline{KE}$  and  $KE'$  are the mean and fluctuating kinetic energies defined in turn by  $KE = \frac{1}{2}(\overline{u^2 + v^2})$  and  $KE' = \frac{1}{2}(\sigma_u^2 + \sigma_v^2)$  where  $\overline{u}$  and  $\overline{v}$  are the component means  $\sigma_u^2$  and  $\sigma_v^2$  are the component variances. The ratio of  $\overline{KE'}/\overline{KE}$  was used to assess the changes in the degree of flow variability. For monthly mean kinetic energy computations the ratio showed no seasonality, indicating that the flow was no more uniform in one season than another. The seasonal variability in  $KE_{tot}$  is apparent in the monthly means (Figure 6b). This result contrasts with that by Mayer et al. (1979) from the middle Atlantic shelf where seasonal trends were apparently masked by long term transient events. The wind data exhibited high winter and low summer kinetic energy levels with high and low energy divisible into consecutive 6 month periods. Partly based upon this observation and partly upon the timing of the recovered current meter data, analyses to follow used six month "seasons" defined as March - August and September - February.

A least squares cosine fit was used on the 240 hour low pass filtered data to measure and remove the annual signal. The resultant cosine had an amplitude of 6.2 cm/sec and removed 22% of the variance. Figure 6c shows the monthly mean data before and after the annual signal was subtracted, along with a plot of the computed cosine. Those results show that subtracting a 365 day cosine was insufficient to completely detrend the series. There are fluctuations both shorter and longer than one year that remain.

The distribution of variance by frequency bands was approximated by computing the energy removed by each filter. The ratio,  $\alpha$ , of the speed variance to the sum of the component variances was also computed ( $\alpha = \sigma_s^2 / (\sigma_u^2 + \sigma_v^2)$ ). The limits of this ratio are  $0 \leq \alpha \leq 1$ , being 1 if the variations were purely rectilinear and zero if purely directional. The results (Table 3) show that tidal and inertial bands contained 41% of the variance, and this was nearly all directional, ( $\alpha = .04$ ) and that the lowest frequency band was the second most energetic (34%) and its variance was primarily rectilinear ( $\alpha = .58$ ).

The seasonal and longer-term behavior in the distribution of kinetic energy with frequency is shown in (Figure 7). The currents during the second year were more energetic than during the first year and the energy increase was greatest in the very low frequencies ( $<0.1$  cpd). The mean kinetic energy did not change appreciably. Segmenting the two-year series into six-month "seasons" brought out some interesting features. Like seasons had different characteristics from one year to the next in the two lower frequency bands. In the very low frequencies, there was an inter-year trend of steadily increasing kinetic energy over the continuous two-year observation period. Subtracting the annual signal damped some of

the summer-winter behavior but did not affect the interyear trend. The tidal band became nearly stationary, and the stationarity of the middle band was improved. However, both energy at the very low frequencies and the mean kinetic energy remained highly non-stationary. These band distributions for the FNWC winds and the 50 m current did not show good agreement except in the band conventionally attributed to wind forcing (35 to 240 hour periods). It did display similar seasonality with increases in current coincident with increases in wind. In the very low frequency band the wind exhibited a seasonal fluctuation where the current had the aforementioned increasing trend.

With this long-term trend in mind, it was of interest to investigate whether there were dominant frequencies in the lowest band, what relationship these may have had to the trend and what role the wind played. Given the bottom depth and proximity to the coast of station 62, an alongshore wind induced slope current should, by Ekman's theory, take 5 - 10 days to become steady (Neumann and Pearson, 1966). We therefore expected a correlation between alongshore wind and alongshore interior geostrophic current (represented by the 50 m data) longer than 10 days. Figure 8a is a periodogram of the very low frequency band generated from the two-year alongshore component current and wind series. There was no significant peak in these spectra. This suggests that wind and current fluctuations either were aperiodic or perhaps occurred in unevenly spaced trains of periodic fluctuations. The alongshore current spectra for two one-year subsets and four six-month subsets show an increase in total energy for the second year and the absence of any significant peak (Figures. 8b and 8c) The six-month subsets also show that there was no consistent spectral signature between seasons or from year to year. The

lack of a dominant frequency or consistent spectral signature suggests that the very low frequency fluctuations were random in spacing and duration. The wind-current cross and rotary spectra (not shown) for these subsets also did not show a consistent peak. However, this does not rule out a relationship, because covariance energy would also have been distributed across the spectrum of aperiodic fluctuations.

Linear correlations, on the other hand, are not dependent on periodic components. The cross-correlation coefficients between alongshore winds and currents were  $r = 0.45$  (at a lag of .5 days) for the 35 hr low pass data and  $r = .56$  (at a lag of 3 days) for the 240-h low pass data. The linear correlation of the monthly mean longshore components was  $r = 0.75$ . These correlations indicate that the response of currents to wind increased with the length of the time considered. Nevertheless, most of the overall current variability was not correlated with wind. The square of the correlation coefficient provides an estimate of the percentage of variance in one series due to the variance in the other. In the case of the 240 hour filtered data  $r^2 = 0.31$ , which meant that about 70% of the current variance was not accounted for by winds.

c. Baroclinic Effects:

Figure 9 shows a section of the 240 hr filtered series at 20, 50 and 100 m depths. Several events, apparently not related to the concurrent wind activity, are evident during which the current vector rotated through a large arc. A possible explanation is that these events reflect advection of meanders and/or eddies past the mooring. Figure 10 depicts the current record which would result from advection of a hypothetical eddy past the mooring. This hypothetical pattern bears strong similarities to several events depicted on the time series.

As mentioned above, eddy-like structures have been identified in this region. Additional evidence is available in the form of 0-100 db dynamic topographies (Figure. 11). Though contouring is subject to individual interpretation, we find credibility in the April 1976 0-100 db contour presented by Royer et al. (1979), which agrees closely with our yet was contoured independantly from the same data set. Since the dynamic height only represents the baroclinic shear between two depths, we did not attribute total flow to this source. Nevertheless, these illustrations show that the baroclinic field in this region was complex, with meanders and eddies. Comparison of the dynamic contours with the current time series showed a reasonable correspondence between baroclinic eddy-like structures and fluctuations in the current meter record. Though there were not enough dynamic height data to sufficiently corroborate all of the fluctuations in current, it appears that variability in the baroclinic field was an important factor affecting the very lowest frequency fluctuations.

The baroclinic structure presented here indicates the degree of structure and variability in the Alaska Current in this region. Hayes (1979) suggested that the shelf break flow was associated with eddies in the Alaska current. Smith (1978) also attributes fluctuations of 10 to 30 day periods to off shore forcing at the Nova Scotian shelf break. Our results support the foregoing in attributing very low frequency fluctuations in the shelf break flow to oceanic foring in the form of eddies and meanders incident upon the shelf break

4. CONCLUSIONS This analysis of our three-year composite of current records from the shelf break in the northeast Gulf of Alaska has yielded the following results:

1. The flow was alongshelf at all depths, with negligible vertical directional shear;
2. The cross-shelf current component had essentially a zero mean and was normally distributed;
3. Wind and current kinetic energy increased significantly during winter;
4. An interyear trend of increasing kinetic current energy was detected. The increase came primarily from the very low frequency (<0.1 cpd) fluctuations and was not well correlated with wind forcing;
5. The very low frequency fluctuations exhibited no dominant periodic components; and
6. These fluctuations are attributed to larger scale non-local aperiodic features such as mesoscale oceanic eddies or meanders.

5. ACKNOWLEDGMENTS:

We wish especially to express our appreciation for the efforts of Robert Charnell who supervised this project since its inception and to N. Patrick Laird who was responsible for instrumentation and data processing until their untimely loss with the RU HOLO HOLO in December 1978. We also thank David Pashinski, James Haslett and William Parker for their preparation of instrumentation and Richard Sillcox and Mona Janopaul for their processing efforts. Carl Pearson's assistance in programming data retrieval and analysis routines was indispensable. Lastly, we wish to commend the crews of the many ships that participated in the field program. These included the NOAA Ships SURVEYOR, DISCOVERER, MILLER FREEMAN, RAINIER, and McARTHUR and the R.V. MOANA WAVE. This study was supported in part by the Bureau of Land Management through interagency agreement



with the National Oceanic and Atmospheric Administration, under which a multiyear program responding to needs of petroleum development of the Alaskan continental shelf is managed by the Outer Continental Shelf Environmental Assessment Program office.

Table 1. Statistical parameters for  
alongshelf and cross-shelf currents at 62.

See text for definition of parameters.

	<u>35 hr</u>	<u>240 hr</u>
$\sigma$	70.7 cm <sup>2</sup> /sec <sup>2</sup>	22.3 cm <sup>2</sup> /sec <sup>2</sup>
$\sigma_v^2$	187.1 cm <sup>2</sup> /sec <sup>2</sup>	125.9 cm <sup>2</sup> /sec <sup>2</sup>
±75%(u)	±16.48 cm/sec	±9.26 cm/sec
±75%(v)	±26.81 cm/sec	±21.99 cm/sec
Tu	2.90 days	
Tv	9.89 days	
$\epsilon_u$	0.53 cm/sec	
$\epsilon_v$	1.59 cm/sec	

Table 2. Estimated rms errors  $\epsilon$  for alongshelf and cross-shelf current components u and v at 50 m for averaging times  $\tau$ .

$\tau(\text{days})$	$\epsilon u(\text{cm/sec})$	$\epsilon v(\text{cm/sec})$
10	4.5	13.7
20	3.2	9.7
30	2.6	7.9
60	1.8	5.6
90	1.5	4.6
180	1.1	3.2
365	.7	2.3
730	.5	1.6

Table 3. Values for component and speed variance at different frequency bands.

<u>Band</u>	<u><math>\sigma_u^2 + \sigma_v^2</math></u>	<u><math>\sigma_s^2</math></u>	<u><math>\sigma_s^2 / (\sigma_u^2 + \sigma_v^2)</math></u>
1	183.0 cm <sup>2</sup> /sec <sup>2</sup>	7.9 cm <sup>2</sup> /sec <sup>2</sup>	.04
2	110.0 cm <sup>2</sup> /sec <sup>2</sup>	31.9 cm <sup>2</sup> /sec <sup>2</sup>	.27
3	148.2 cm <sup>2</sup> /sec <sup>2</sup>	86.5 cm <sup>2</sup> /sec <sup>2</sup>	.58

Band:

- 1 35 hr > T > 2.9 hr
- 2 250 hr > T > 35 hr
- 3 T > 240 hr

FIGURE 1: Showing the location of Station 62.

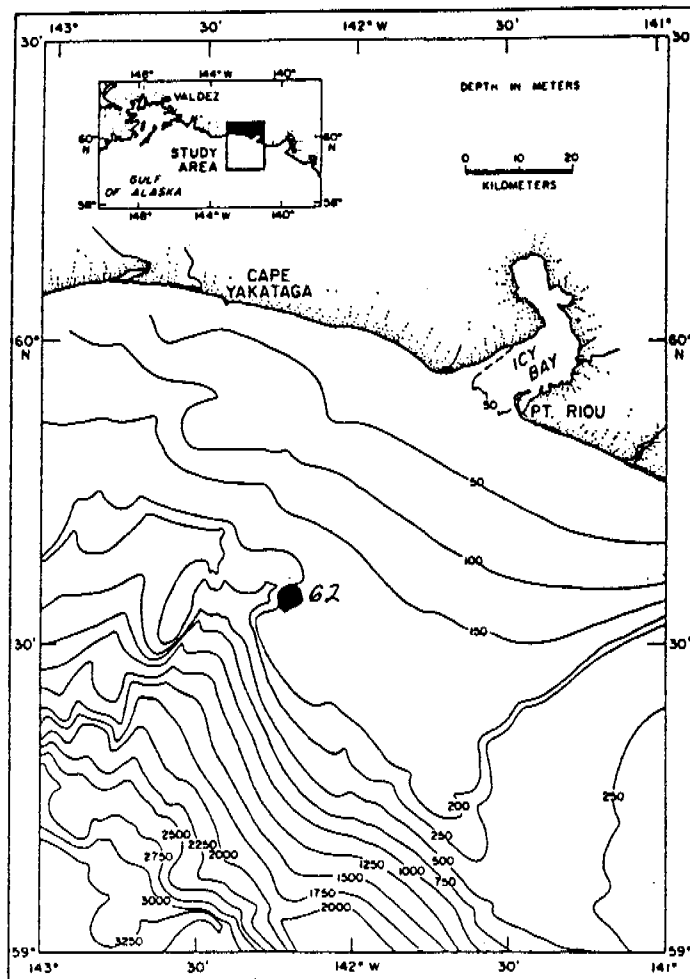
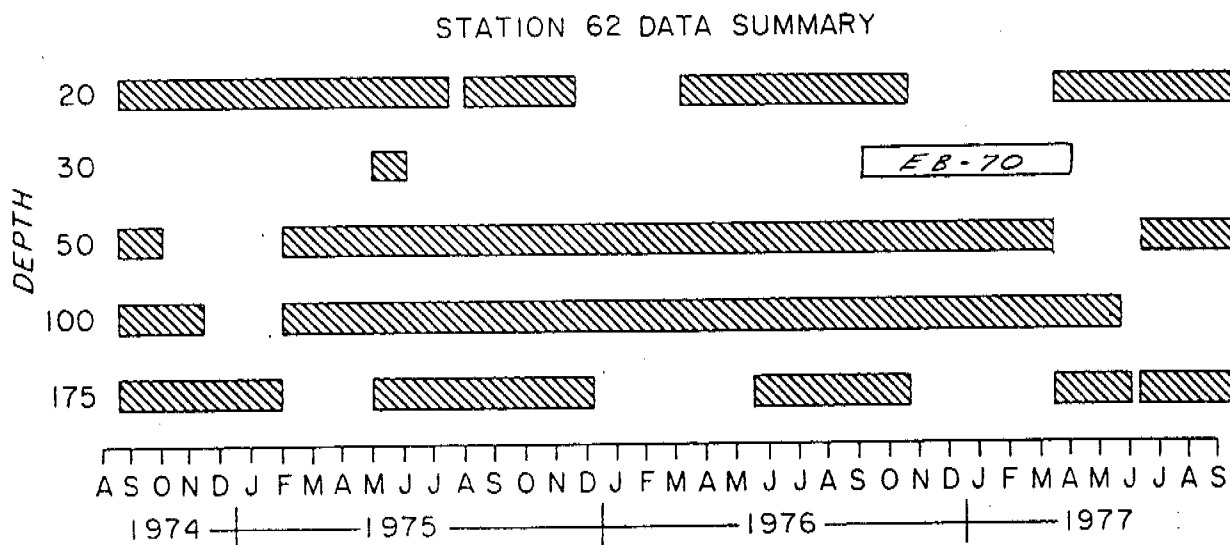
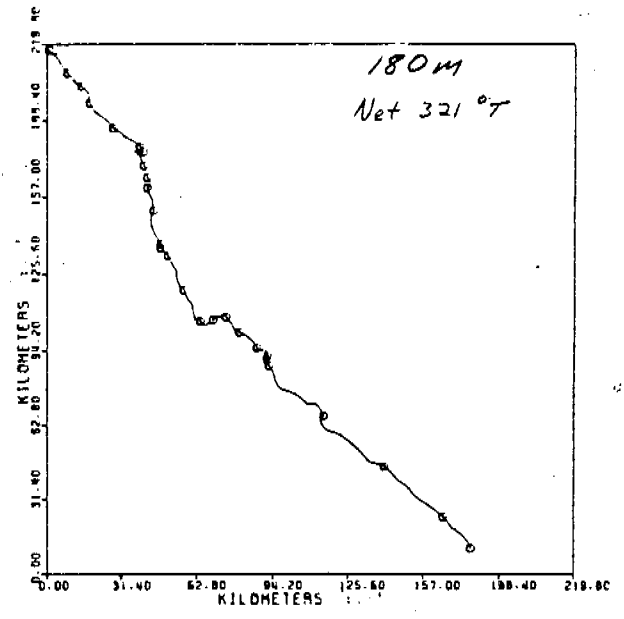
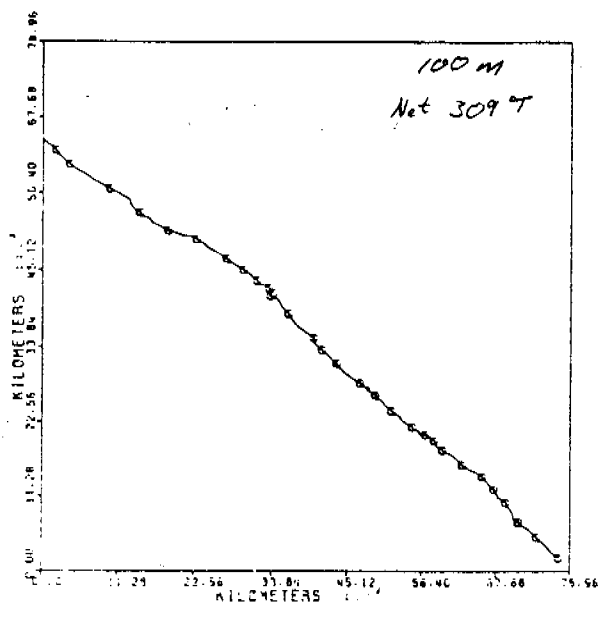
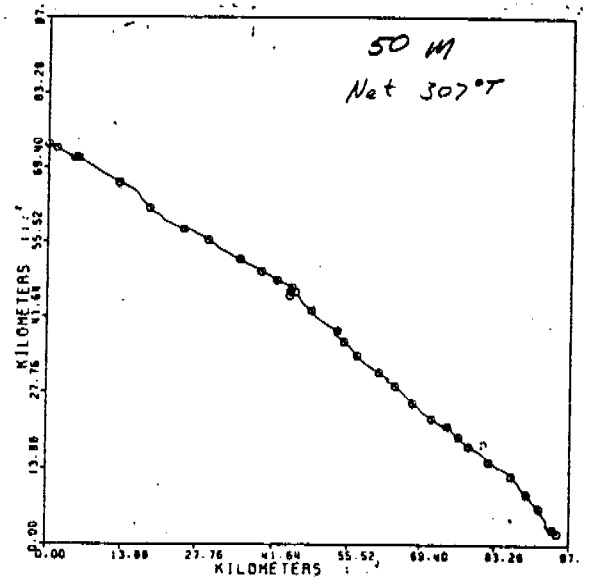
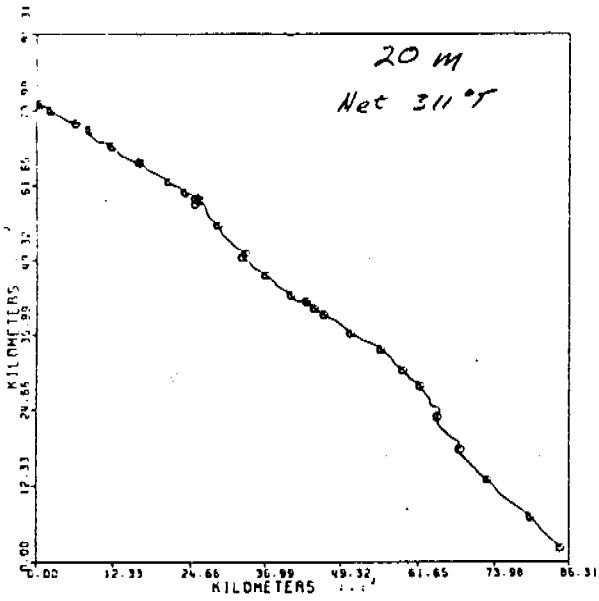


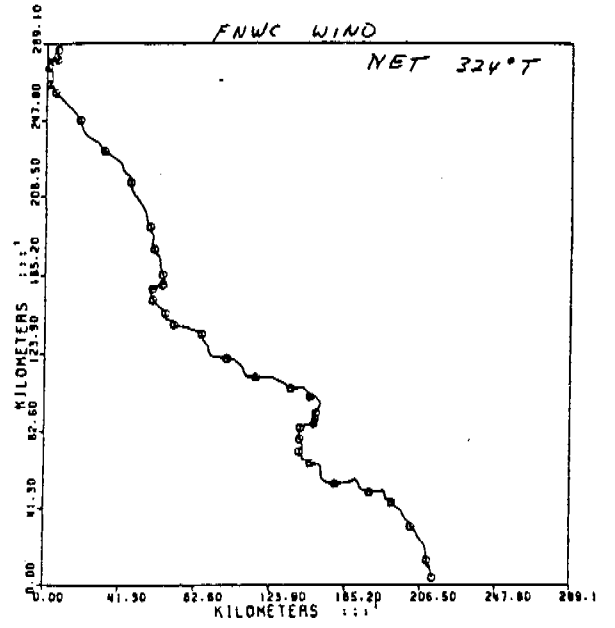
FIGURE 2: Summary of current meter data recovered and of the deployment of EB-70.





○ EVERY 30 DAYS

FIGURE 3: Progressive Vector Diagrams of current and wind computed over the entire three year mooring deployment.



DISTRIBUTION OF VELOCITY COMPONENTS

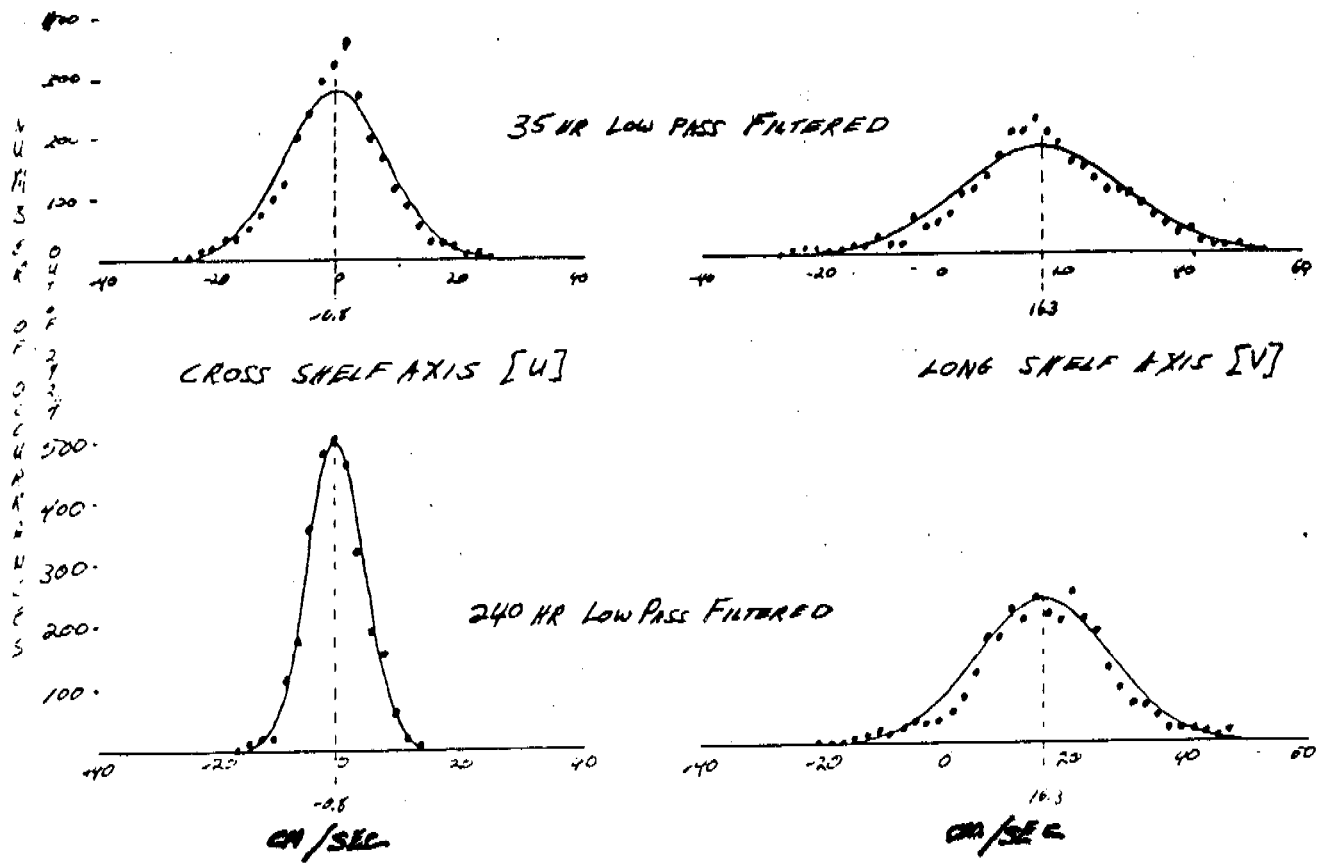


FIGURE 4 (above): Distributions of velocity components shown with true normal distributions (solid curves).

FIGURE 5 (below):

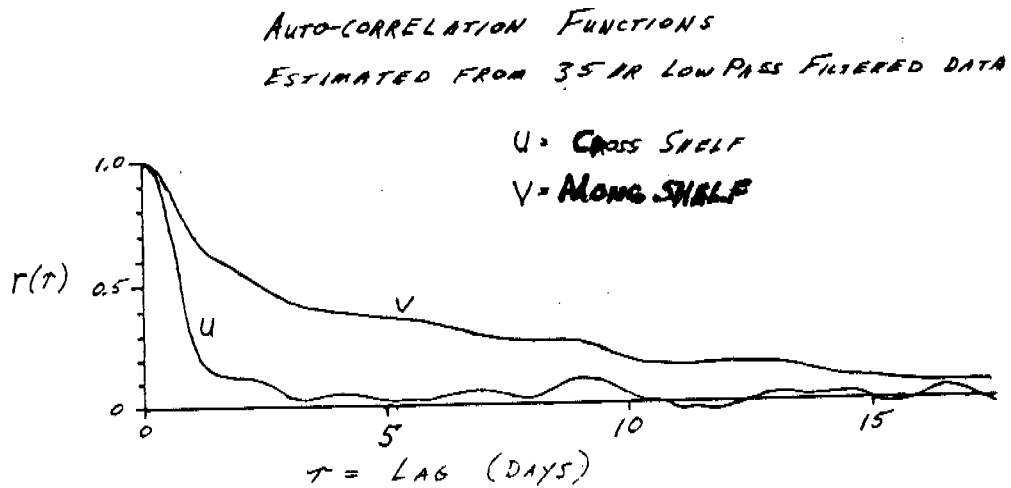
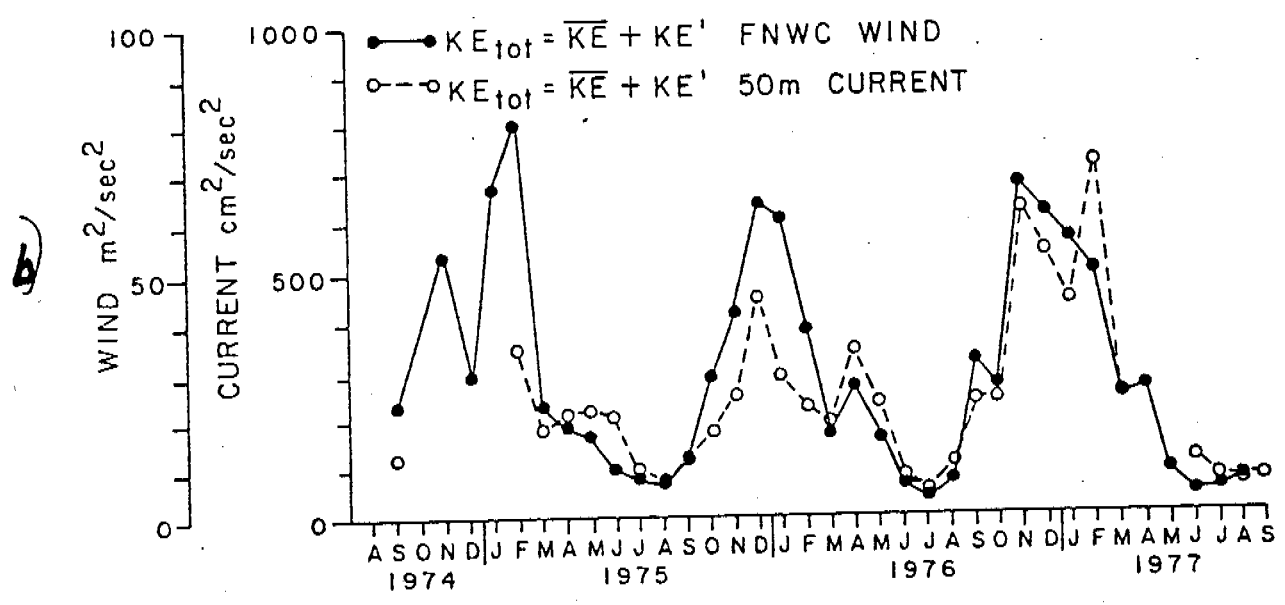
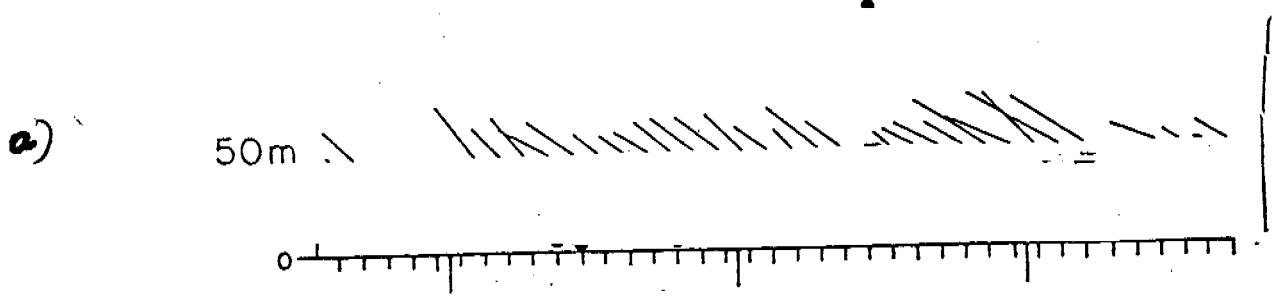
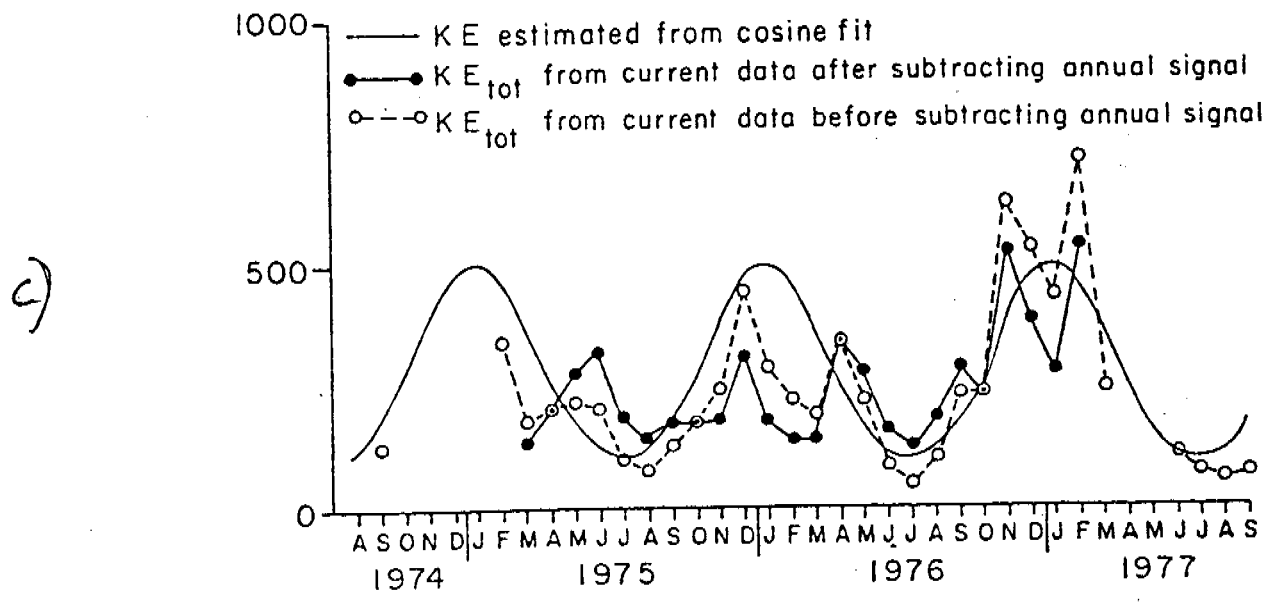


FIGURE 6

**CURRENT**  
MONTHLY MEAN ~~KINETIC ENERGY~~

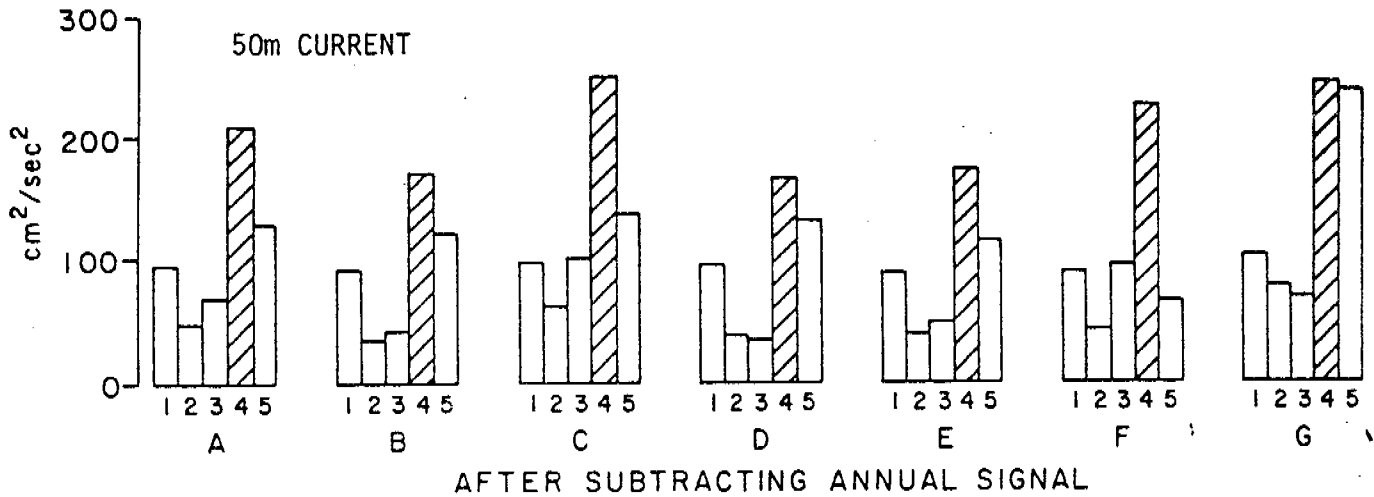
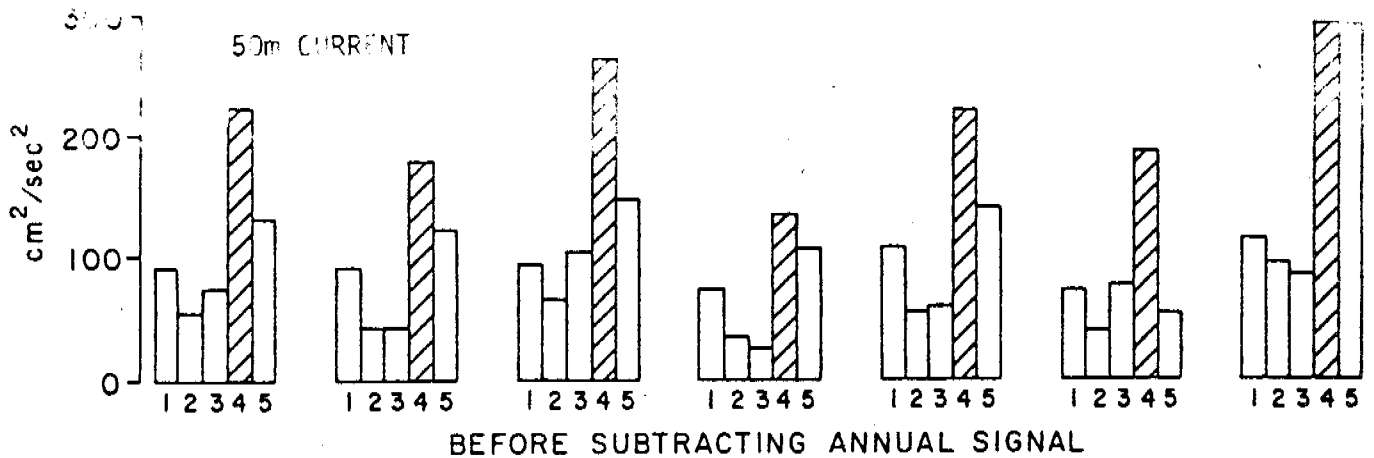


~~MONTHLY MEAN KINETIC ENERGY~~





# HISTOGRAMS OF KINETIC-ENERGY DISTRIBUTION



## WIND KINETIC-ENERGY DISTRIBUTION

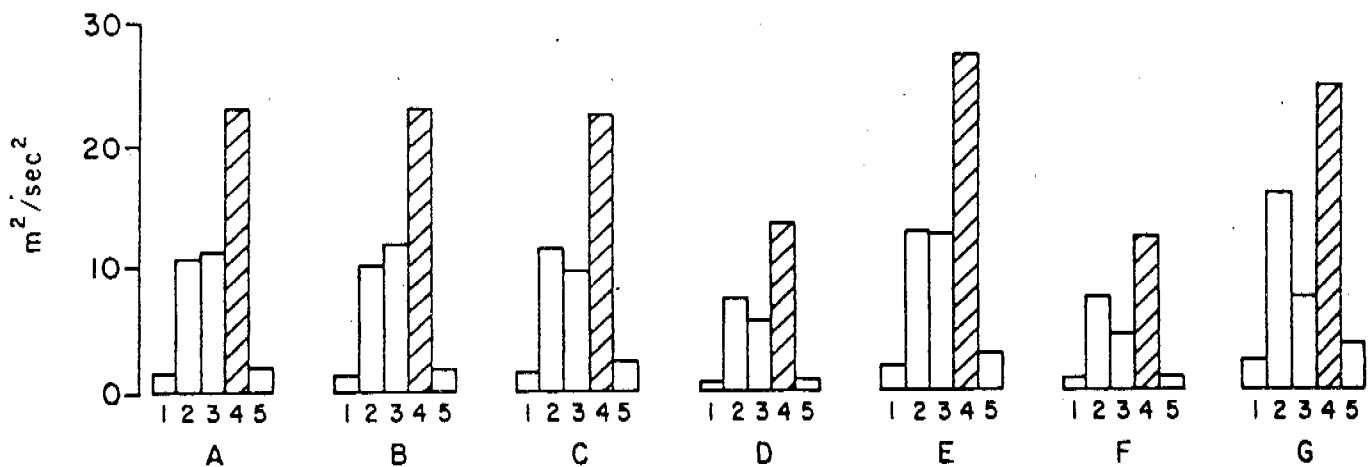


FIGURE 7: A= Two years 3/75-2/77  
 B= One year 3/75-2/76  
 C= One year 3/76-2/77  
 D= Six months 3/75-8/75  
 E= Six months 9/75-2/76  
 F= Six months 3/76-8/76  
 G= Six months 9/76-2/77

BAND: 1= KE' between 2.9 and 35hrs  
 2= KE' between 35 and 240hrs  
 3= KE' greater than 240hrs  
 4= Sum of bands 1,2 and 3  
 5=  $\overline{KE}$

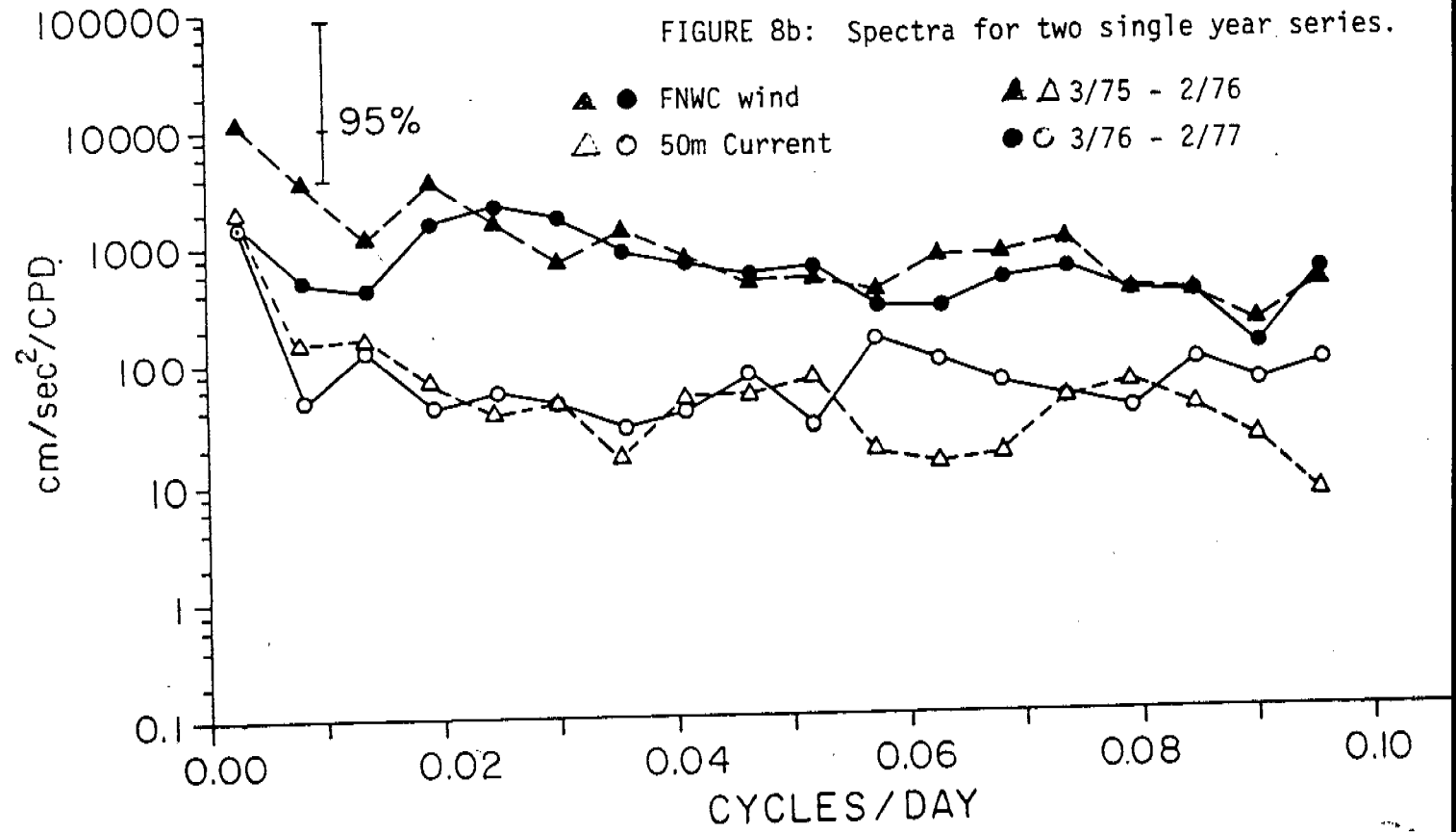
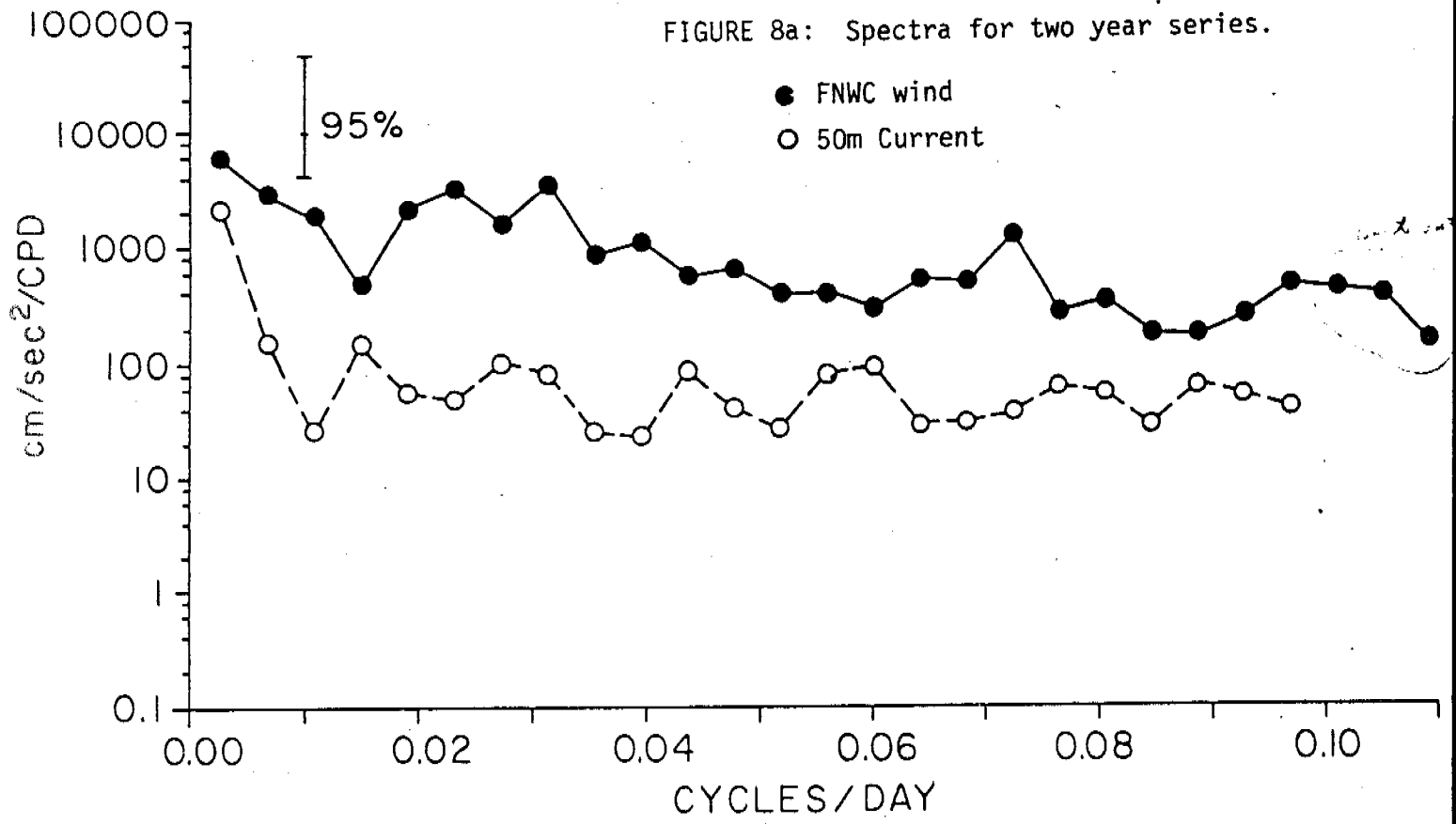


FIGURE 8c: Kinetic energy spectra for four six-month subsets; 50m current.

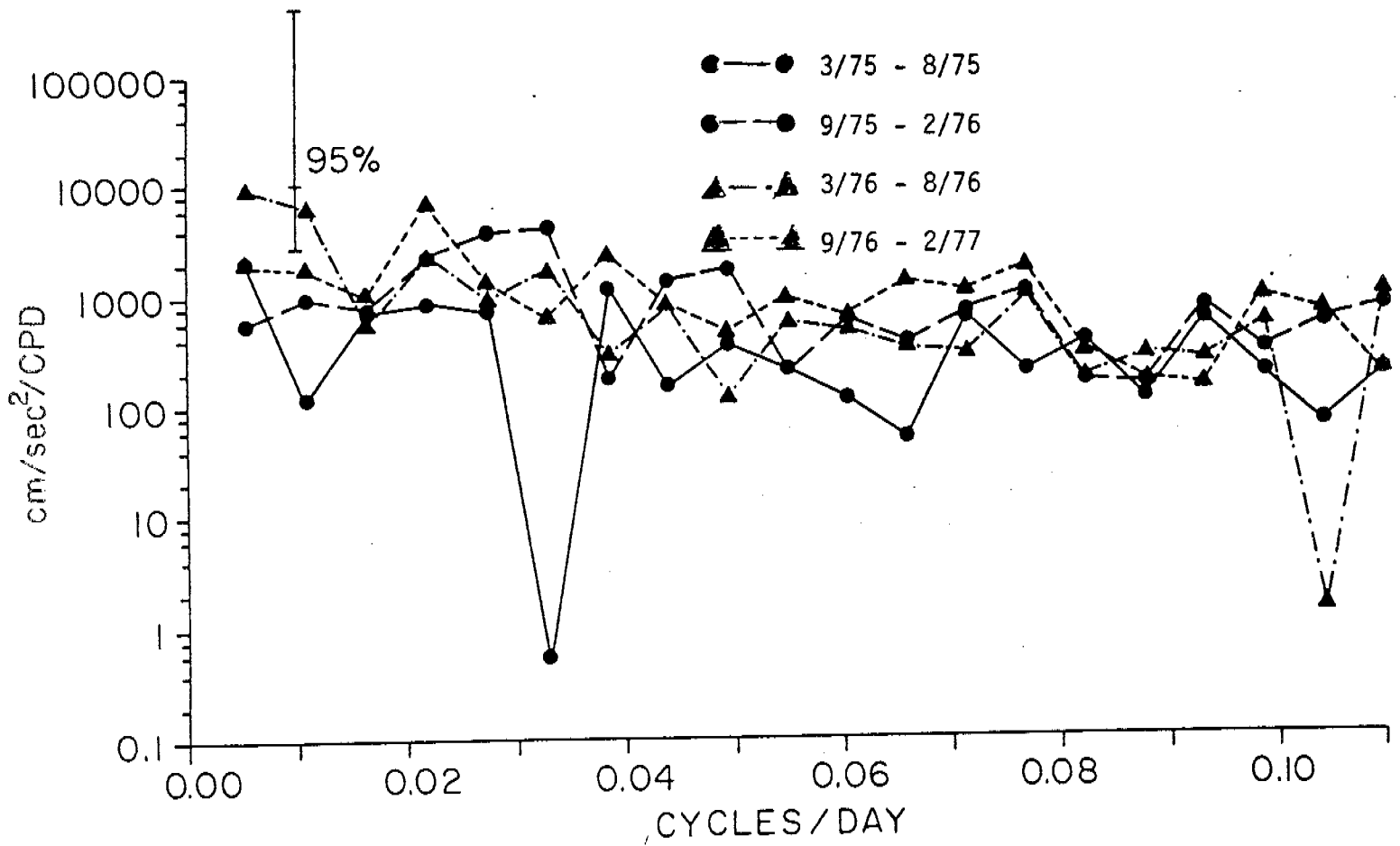


FIGURE 9: 240 hour filtered current meter data segment.

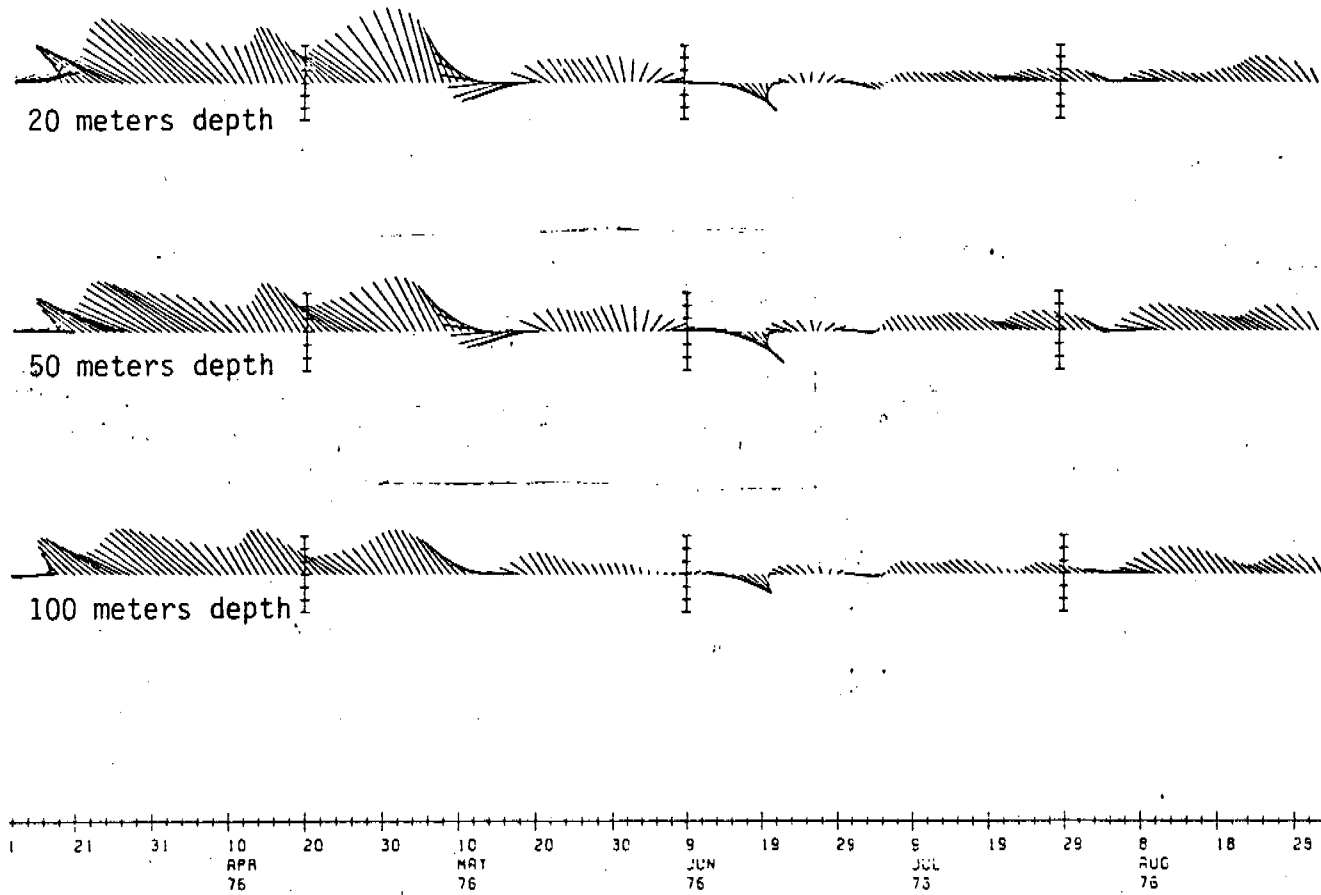
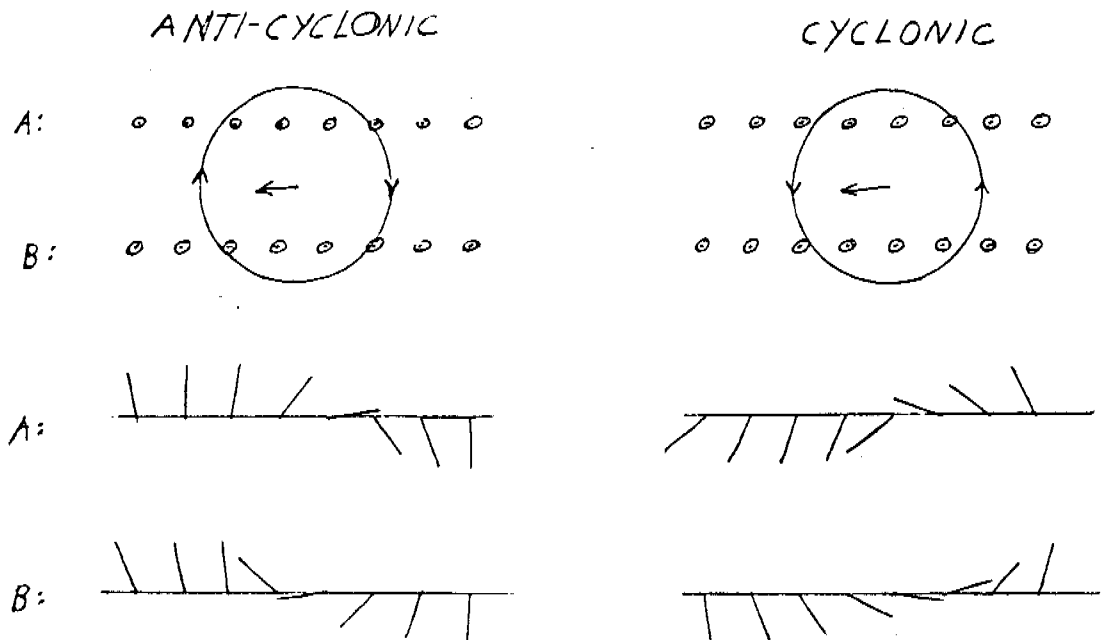


FIGURE 10: Hypothetical currents resultant from a transiting eddy.



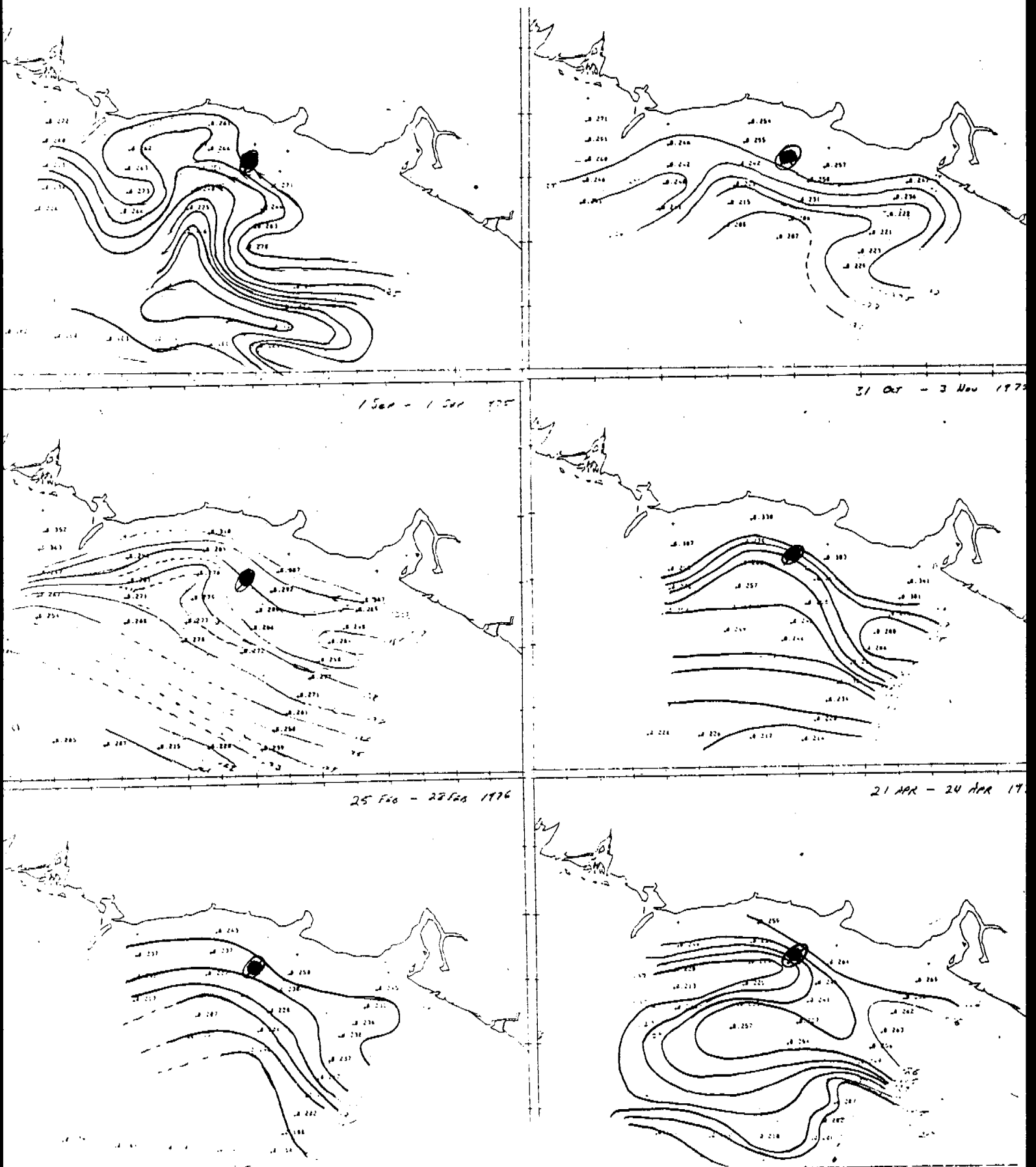


FIGURE-11: 0 - 100db dynamic contours.

## REFERENCES

- Bakun, A., 1975: Wind driven convergence-divergence of surface waters in the Gulf of Alaska. Eos, Trans AGU, 56, 1008.
- Charnell, R.L., and G.A. Krancus, 1976: A processing system for Aanderaa current meter data. NOAA Tech. Memo. ERL PMEL-6, Nat. Oceanic and Atmos. Admin., Seattle, Wash., 50 pp.
- Favorite, F., and W.J. Ingraham, 1977: On the flow in the northwestern Gulf of Alaska, May 1972. J. Oceanogr. Soc. Japan, 33, 67-81.
- Halpern, D., and R.D. Pillsbury, 1976: Influence of surface waves on subsurface current measurements in shallow water. Limnol. and Oceanogr., 21, 611-616.
- Hayes, S.P., 1979: Variability of current and bottom pressure across the continental shelf in the northeast Gulf of Alaska. J. Phys. Oceanogr., 9, 88-103.
- Hayes, S.P., and J.D. Schumacher, 1976: Description of wind, current and bottom pressure variations on the continental shelf in the northeast Gulf of Alaska from February to May 1975. J. Geophys. Res., 81, 6411-6419.
- Ingraham, W.J., A. Bakun, and F. Favorite, 1976: Physical oceanography of the Gulf of Alaska. Final Report, RU-357, Northwest Fish. Center, NMFS/NOAA, Seattle, Wash.
- Kroll, J., 1979: The kinetic energy on a continental shelf from topographic Rossby waves generated off the shelf. J. Phys. Oceanogr., 9, 712-723.
- Kundu, P.K., and J.S. Allen, 1976: Some three-dimensional characteristics of low-frequency current fluctuations near the Oregon coast. J. Phys. Oceanogr., 6, 181-199.
- Mayer, D.A., D.V. Hansen, and D.A. Ortman, 1979: Long-term current and temperature observations on the Middle Atlantic Shelf. J. Geophys. Res., 84, 1776-1792.
- Monin, A.S., and A.M. Yaglom: Statistical Fluid Mechanics. MIT Press, Cambridge, Mass., 251-252.
- Neumann, G., and W.J. Pearson, 1966: Principles of Physical Oceanography. Prentice-Hall, N.J., 208.
- Reed, R.K., R.D. Muench, and J.D. Schumacher, 1980: On baroclinic transport of the Alaskan Stream near Kodiak Island. Deep-Sea Res., 27, in press.
- Royer, T.C., 1975: Seasonal variations of waters in the northern Gulf of Alaska. Deep-Sea Res., 22, 403-416.

Royer, T.C., D.V. Hansen, and D.J. Pashinski, 1979: Coastal flow in the northern Gulf of Alaska as observed by dynamic topography and satellite-tracked drogued drift buoys. J. Phys. Oceanogr., 9, 785-801.

Royer, T.C., and R.D. Muench, 1977: On the ocean temperature distribution in the Gulf of Alaska, 1974-75. J. Phys. Oceanogr., 7, 92-99.

Smith, P.C., 1978: Low frequency fluxes of momentum, heat, salt and nutrients at the edge of the Scotian shelf. J. Geophys. Res., 85, 4079-4096.

C. The following manuscript is in preparation:

SEA LEVEL VARIATIONS IN RELATION TO  
COASTAL FLOW AROUND THE GULF OF ALASKA

R.K. Reed and J.D. Schumacher

ABSTRACT

Adjusted sea level deviations at six tide stations around the Gulf of Alaska were examined in light of our recent knowledge of the flow regime. On the east side of the Gulf, a maximum in the deviations seems to be caused by winter barotropic flow on the shelf. On the north side of the Gulf, the maximum in fall is apparently produced by a marked increase in flow of the baroclinic coastal current. Farther west the seasonal sea level signal is greatly reduced.



D. The following manuscript has been accepted for publication in Deep-Sea Res.

ON BAROCLINIC TRANSPORT OF THE ALASKAN STREAM  
NEAR KODIAK ISLAND\*

R. K. Reed<sup>1</sup>, R. D. Muench<sup>1,2</sup>, and J. D. Schumacher<sup>1</sup>

<sup>1</sup>National Oceanic and Atmospheric Administration  
Environmental Research Laboratories  
Pacific Marine Environmental Laboratory  
Seattle, Washington 98105

<sup>2</sup>Now at SAI/Northwest, 13400B Northrup Way #36  
Bellevue, Washington 98005

\*Contribution No. 405 from the NOAA/ERL Pacific Marine Environmental Laboratory

## ABSTRACT

Near Kodiak Island the Alaskan Stream, a southwestward-flowing boundary current, exhibits no significant alongshore variability in volume transport; hence data in this region are suitable for examination of temporal changes in flow. Seventeen CTD sections occupied during 1975-79 were used to compute baroclinic transport by two methods: (1) referred to 1500 dbar or the deepest common level; and (2) adjusted to 1500 dbar by the method of Jacobsen and Jensen. The second method gave larger values and less variability than the first. The mean adjusted volume transport was  $12 \times 10^6 \text{m}^3/\text{sec}$ , and maximum and minimum values were  $17$  and  $8 \times 10^6 \text{m}^3/\text{sec}$ , respectively.

Baroclinic transport computed from the CTD data did not reveal a seasonal signal, even though wind-stress curl in the Gulf of Alaska increases by an order of magnitude from summer to winter. A combination of changes in location of the Stream along the continental slope and failure to adjust the transport to 1500 dbar seems to have caused some of the previously inferred variability. It appears that the baroclinic flow does not consistently spin up or down seasonally because of insufficient response time at these high latitudes.

## INTRODUCTION

The eastern limb of the North Pacific subarctic gyre is a broad, variable flow northward into the Gulf of Alaska; this flow narrows and intensifies near the head of the Gulf and then moves westward along the Alaska Peninsula and Aleutian Islands (DODIMEAD, FAVORITE, AND HIRANO, 1963; see Fig. 1). FAVORITE (1967) concluded that the northern limb of the subarctic gyre, the Alaskan Stream, is a return flow for the wind-driven transport in the northeast Pacific and that its characteristics (narrow, deep, asymmetric velocity profile) are a result of vorticity conservation. Peak surface speeds in the Alaskan Stream are of the order of 100 cm/sec, and there is some evidence that the flow is in geostrophic balance (REED and TAYLOR, 1965).

Wind stress in the Gulf of Alaska displays a strong annual cycle. Long-term integrated total wind-driven transports into the Gulf vary from about  $20 \times 10^6 \text{m}^3/\text{sec}$  in winter to less than  $5 \times 10^6 \text{m}^3/\text{sec}$  in spring and summer (INGRAHAM, BAKUN, and FAVORITE, 1976), although there are considerable year-to-year variations. One would intuitively expect such variations to be accompanied by changes in the volume transport of the Alaskan Stream. OHTANI (1970) and FAVORITE (1974), however, concluded that baroclinic transports were fairly constant. Later, REID and MANTYLA (1976) suggested that winter intensification of the subarctic gyre occurred. The present study is an attempt to ascertain if changes in baroclinic transport of the Stream do occur and if there is evidence of a seasonal cycle in the variations.

## THE DATA

From September 1975 through February 1979, oceanographic observations were made in the vicinity of Kodiak Island as part of the Outer Continental

Environmental Assessment Program (OCSEAP) of the Bureau of Land Management and the National Oceanic and Atmospheric Administration. The emphasis of this work was to provide information about continental shelf circulation, but a number of oceanographic sections did extend far enough seaward to allow computation of the baroclinic transport of the Alaskan Stream. The observations were obtained on cruises aboard the NOAA ships Discoverer and Surveyor by the Pacific Marine Environmental Laboratory (PMEL) and on the R. V. Acona and R. V. Moana Wave by the University of Alaska's Institute of Marine Science (IMS). Both the PMEL and IMS data are used in this study. The hydrocasts were made with Plessey model 9040 CTD units, and the data were recorded every 0.2 sec on Plessey model 8400 data loggers. Calibration samples were obtained on almost every cast. The digital data were processed by computer; various routines eliminated spurious scans to derive 1-m averages of temperature and salinity from which density and other parameters were computed. All of these data are on file at the National Oceanographic Data Center.

#### HYDROGRAPHY

Before discussing the computations of transport and the resulting values, we will discuss the rationale for using data near Kodiak Island and will describe some features of the Alaskan Stream. If one is to examine temporal changes in transport, regions with large spatial changes should be avoided. It has been known for decades that spatial changes in transport of the Stream do occur (FAVORITE, DODIMEAD, and NASU, 1976). This happens in three major ways: (1) loss of water to the south or by recirculation around the Alaska gyre; (2) gain of water from the south (Subarctic Current), usually west of 175°W; and (3) loss of water to the north through some passes in the western Aleutians (see Fig. 1). We are mainly concerned here with loss by southward recircula-

tion, which may occur in one or more places and seems to vary in intensity (FAVORITE et al., 1976). The large body of available data suggests, however, that this recirculation rarely if ever occurs east of about 155°W; thus, observations in the vicinity of Kodiak Island should be suitable for an examination of temporal changes in transport.

The PMEL cruises in March 1978 and May-June 1978 had the best offshore coverage. Station locations, geopotential topography, surface salinity, and subsurface maximum temperature are shown in Figures 2 and 3. Only casts which reached (or were extrapolated to) 1000 m are used here, although numerous casts were made at lesser depths. DODIMEAD et al. (1963) used the horizontal distribution of surface salinity and subsurface maximum temperature to infer the path and continuity of the Alaskan Stream, which is characterized by dilute, relatively warm water. (In summer the sub-surface maximum temperature nearly always underlies a subsurface minimum, but in winter the minimum is frequently at the surface.) The distributions of surface salinity and subsurface maximum temperature from our data in Figures 2 and 3 show that the warmest, most dilute water is inshore, in agreement with DODIMEAD et al., (1963), and there is no evidence of any large-scale offshore movement of this water.

As expected, the property distributions in Figures 2 and 3 are closely paralleled by the geopotential topography. As we will discuss later, 1000 dbar is not an adequate reference level for computation of transport, but the proper direction of flow is nevertheless shown. The March data show a continuous, southwestward flow with no major perturbations. Such "unperturbed" flow was also present in May 1972 (FAVORITE and INGRAHAM, 1977) and in September 1977 and October-November 1977 (PMEL data, not shown). On the other hand, a major perturbation was present in May-June 1978; in the north-east part of the area the flow turned south, then veered north, and a clock-wise eddy was present

inshore. The flow was again "unperturbed" to the southwest. Although the data are inadequate to indicate what caused the perturbation, the northward turn and movement after the flow moved south into deep water is in agreement with conservation of potential vorticity. The data for stations 610-613 (just west of stations 571-772) were not used in the map of geopotential topography because it appeared that marked temporal changes had occurred in the eight days since occupation of stations 571-772. A clockwise eddy also appeared to be present; its geopotential anomalies were almost 0.1 dyn m greater than eight days before, however, and isopleths had deepened by almost 100 m. It is tempting to speculate that this feature may have been a cut-off eddy that migrated westward and intensified in some unknown manner.

Representative vertical sections of temperature, salinity, and density for stations 693-776 (see Figures 2 and 3 for location) for March and June 1978 are shown in Figures 4 and 5 to acquaint the reader with the cross-stream distribution of these properties and hence flow. All of the sections show steeply sloping (downward) isolines along the inner portion of the continental slope in agreement with the westward baroclinic flow. The slopes decrease offshore in concert with weaker flow, and the last station pair (weak flow to the east) is seaward of the Alaskan Stream. Over the continental shelf, the slopes also indicate a flow reversal or zones of negligible baroclinicity.

Two reviewers pointed out that there was a noticeable difference between the deep density structures in March and June 1978 (Figures 4 and 5); in March the isopleths below 200 m were deeper and more steeply sloping than in June. These were the two most extreme cases we encountered of this variability in subsurface structure, and they were accompanied by appreciable changes in baroclinic speed (Figure 6). Horizontal density gradients throughout the baroclinic layer were smaller in June than in March and may reflect a geo-

strophic readjustment as found by REID (1973) off Kamchatka. The lower speeds in June occurred during a time with relatively small volume transport (Table 1), which was also the period of perturbed flow with the eddy shown in Figure 3. In general, however, maximum surface speeds were not well correlated with variations in volume transport in this data set, in agreement with the results obtained by FAVORITE et al. (1976) off Adak Island in the western Aleutians.

#### METHODS

The baroclinic mode in the subarctic gyre extends to relatively great depths, but sampling frequently did not. Horizontal gradients of geopotential do not vanish until depths of about 3000 m (REED, 1970; REID and ARTHUR, 1975); flow computations, however, were usually referred to depths of 1000 or 1500 m. Consideration of the deep geopotential topography would indicate that computations of volume transport referred to 1500 dbar are deficient by perhaps  $5 \times 10^6 \text{m}^3/\text{sec}$ ; speeds are not appreciably in error, however, and temporal and spatial variations in transport are believed to be properly shown (REED, 1970), although small temporal changes may occur as deep as 1500 m as suggested by the data in Figures 4 and 5. It should be stressed that we are not attempting to quantify the barotropic mode, even though its transport could be significant.

Computations of the baroclinic volume transport of an ocean current are often less straightforward than the frequent quotation of values would imply. Currents such as the Gulf Stream often have complex counterflows, and determination of what is the "Gulf Stream", especially on the seaward side, is not always a simple matter (WARREN and VOLKMANN, 1968). The situation may be further complicated by a sloping surface of no motion. Also, some current systems impinge on the continental slope or shelf and are flowing in water depths shoaler than a realistic reference level, which suggests the need for

some adjustment to the transports. This latter factor is the major complicating feature in computing transports of the Alaskan Stream.

It is apparent that it is inappropriate to ignore sloping isopycnals near the bottom and refer flow to the deepest common reference level between stations. FOMIN (1964) describes in some detail three methods for adjusting the geopotential in water depths less than the reference level; the three methods are generally attributed to (1) Helland-Hansen, (2) Jacobsen and Jensen, and (3) Groen, although MONTGOMERY (1941) seems to have first used this last method. Helland-Hansen's method was not seriously considered because it involves graphical construction and seems to have no particular advantage over the simpler method of Jacobsen and Jensen. Intuitively, one might expect that the Montgomery-Groen method would give the most realistic results because it does not assume, as the first two methods do, that the horizontal pressure gradient along the bottom is zero. Recently, REID and MANTYLA (1976) used this method, and we also attempted to use it with the PMEL data. Our results were inconsistent, however; some values were implausible, and transports for nearby sections were not in good general agreement. We suspect that the problem lies in the fact that in this region isopycnals near the bottom have steep and often varying slopes; the method of step-wise extrapolation up the slope causes any uncertainties to be additive as one proceeds inshore, unlike in the method of Jacobsen and Jensen.

Hence we used the method of Jacobsen and Jensen. The difference in geopotential anomaly, referred to the deepest level common to two stations, was corrected by:

$$\Delta = h/2(\delta_1 - \delta_2), \quad (1)$$

where  $h$  is the depth difference between the deepest level common to two stations and 1500 dbar, and  $\delta_1$  and  $\delta_2$  are the specific volume anomalies at the deepest



common level for the two stations. These corrections were then incorporated into the computations of transport.

The locations of the PMEL CTD sections used to compute transport are shown in Figure 7. The most seaward station on each line is shown even if it was beyond the offshore edge of the Alaskan Stream. Although the sections extended across the continental shelf, the most northerly station shown is the station that was considered to define the inshore boundary of the Stream as discussed below. The location of the IMS sections is shown in Figure 8; except for 8(b), all of the IMS lines were occupations of sections A or B and will be so identified when the values are listed. The most northerly stations in 8(a) are the farthest inshore locations of the Stream found in the IMS data.

In computing transport, only those sections which met one of the following criteria were used: (1) if seaward stations showed a flow reversal, the station with minimum geopotential anomaly was used as the offshore boundary of the Stream; and (2) if there was no clearly defined minimum anomaly, the most seaward station was used as the boundary provided that values of geopotential and physical properties clearly showed the station to be near the center of the subarctic gyre. The inshore boundary of the Stream was in all cases unambiguously defined by a flow reversal or by a zone of very weak flow which made virtually no contribution to the transport. Transports were first computed relative to 1500 dbar or the deepest common reference level in depths less than 1500 m, and these "unadjusted" transports were then "adjusted" by the corrections computed by the Jacobsen and Jensen method. Although "unadjusted" transport was computed, corrections were not applied to station data in water depths less than 300 m. Water properties near the bottom on the continental shelf tend to vary considerably, probably mainly as a result of mixing over the complex topography, and these local features create unrepresentative isopycnal slopes

which lead to erroneous corrections. A calculation using plausible speeds from shelf-edge current-meter records (SHUMACHER, SILLCOX, DREVES, and MUENCH, 1978) suggests that transport inshore of 300 m is not likely to be greater than  $1 \times 10^6 \text{m}^3/\text{sec}$ . Finally, the inshore edge of the Stream, as indicated by a flow reversal, was frequently in water deeper than 300 m.

## RESULTS

### Transport Values

Both the unadjusted and adjusted transport values for the 17 PMEL-IMS sections are given in Table 1. Two features are immediately apparent; the unadjusted values are less than the adjusted values, and there is greater variability between the values for individual sections on a single cruise (sections A and B in September 1975), for example) in the unadjusted than the adjusted values. (The one exception to this trend occurred in the three sections for April-May 1976; the large adjusted transport for section B though is strongly influenced by a computed correction of  $4.4 \times 10^6 \text{m}^3/\text{sec}$  between two stations with the inshore cast in 400 m depth, near the limit, 300 m, of where we consider the method reliable.) The general lack of variability between adjacent sections on the same cruise is logical because we would not expect large alongshore changes in transport in this region as the unadjusted values would imply.

The adjusted values in Table 1 indicate that the mean transport of the Stream is about  $12 \times 10^6 \text{m}^3/\text{sec}$ . As discussed previously, this value would be increased by perhaps  $5 \times 10^6 \text{m}^3/\text{sec}$  if the baroclinicity at 1500 dbar and below were not neglected. Most values were close to  $12 \times 10^6 \text{m}^3/\text{sec}$ , but the maximum and minimum values were  $17 \times 10^6 \text{m}^3/\text{sec}$  (July 1976) and  $8 \times 10^6 \text{m}^3/\text{sec}$  (June 1978), respectively. Also, these latter values were not strongly influenced by

corrections to the unadjusted transport. The data in Table 1 do not support the existence of any significant seasonal variation in baroclinic transport which could be associated with the large seasonal changes in wind stress over the Gulf of Alaska. The winter values in March 1978 and February 1979 were near the mean, and the maximum and minimum transports both occurred in summer, the period of minimum wind-stress curl. Although rather large changes in transport do occasionally occur, they do not appear to be of a seasonal nature.

#### Wind-Stress Transport

It is of interest to compare the observed volume transport of the Stream with transport computed from wind stress. Various components of wind-stress transport are routinely prepared by the National Marine Fisheries Service from monthly average pressure data on a  $3^{\circ} \times 3^{\circ}$  grid (see BAKUN, 1973 for discussion of methods). INGRAHAM *et al.* (1976) used the total transport integrated along a latitude circle from the coast line at  $55^{\circ}$  N as an index of the westward outflow of the Alaskan Stream. We have determined the integrated total transport at  $55^{\circ}$ N,  $149^{\circ}$ W from the monthly wind-stress transport listings, provided by A. Bakun, for comparison with the observed transports near Kodiak Island (Figure 9). The observed volume transports in Figure 9 are shown as averages when more than one section was occupied on a cruise.

The most striking feature about the wind stress transport is the order-of-magnitude change from winter to spring and summer. Large values usually occur as early as October and persist through February or March. An exception to this general trend occurred in winter 1976-1977; however, except for February, values were generally much lower than for the other winters shown here. We noted that the observed volume transports in March 1978 and February 1979 were very close to the mean value. Wind-stress transports for these winters were not abnormally low, INGRAHAM *et al.*, 1976), however, so this

cannot explain the lack of a winter increase in baroclinic transport. The maximum observed Stream transport was in July 1976, and the minimum was in June 1978; again, computed wind-stress transports near these times were not unusual for the season. Thus there is no apparent relationship between integrated total transport calculated from the wind stress and observed baroclinic volume transport. In fact, the correlation coefficient between the mean wind-stress transports (averaged for the two months prior to the cruises) and the observed transports was only 0.04. An attempt was also made to compare observed values with other components of wind-stress transport (meridional total and Ekman transport), but no clear relationships were apparent.

#### DISCUSSION

Obviously, it would be desirable to have more data than presented here; the fact remains, however, that normal baroclinic transports occurred in two winters with above normal wind-stress transport, and the largest baroclinic transport appeared in a summer with typically weak wind stress. Earlier, REED (1968) suggested that the Alaskan Stream intensified in winter, and REID and MANTYLA (1976) attributed an increase in coastal sea levels to intensification of the subarctic gyre. On the other hand, OHTANI (1970) discounted the concept of large winter-summer differences in Stream transport, and FAVORITE (1974) also concluded that baroclinic transports lacked a clear seasonal signal. Furthermore, INGRAHAM *et al.* (1976) cast doubt on the existence of large winter-summer differences in the northward flow into the Gulf of Alaska. Finally, S. Tabata (Institute of Ocean Sciences, Canada, personal communication) has not found clear-cut seasonal differences in northward flow across the hydrographic line between Vancouver Island and ocean weather station P.

FAVORITE et al. (1976) presented data which at first glance would appear to refute our conclusions from the observations off Kodiak but on closer examination are in agreement with them. They list 24 transport values between 155°W and 178°E during 1965-1970. Because of these variable locations west of Kodiak, they are subject to much more uncertainty because of alongshore changes than are transports in the area which we have studied. Twelve sections, however, were near the same location off Adak Island. Except for one winter and one spring transport, there does appear to be a trend of relatively large values in winter-spring and small values in summer-fall. (One would expect maxima and minima to occur later near Adak Island than in the Gulf of Alaska because of the downstream location of the former area.) The values reported by FAVORITE et al. (1976) were computed relative to 1500 dbar or the deepest common level between stations, but the transport in depths less than 1500 m was not adjusted as in this study. FAVORITE et al. (1976) concluded, however, that the Stream was generally well offshore in winter but closer inshore in summer. A more inshore location in summer than winter would result in appreciable Stream water in depths less than 1500 m; lack of an adjustment inshore would result in transport being deficient by generally  $2-4 \times 10^6 \text{ m}^3/\text{sec}$ , as seen in our Table 1. The winter values though should need little if any correction because of the offshore location of the Stream. Thus the contrast seen between winter and summer values would be greatly reduced. This same problem of location of the Stream and the method used led REED (1968) to the erroneous conclusion of a winter enhancement of transport. Furthermore, REID and MANTYLA (1976) suggested that the subarctic gyre intensifies in winter, but their departures in coastal sea levels may be related to changes in coastal currents rather than the offshore Alaskan Stream (HAYES, 1979). We must conclude then that none of the available

data provide convincing evidence of a significant seasonal cycle in baroclinic transport of the Alaskan Stream.

Why does the baroclinic transport seem to be unaffected by the order of magnitude increase of wind-stress curl in winter? One reason may be that  $\beta$ , the planetary divergence, becomes relatively small at high latitudes, and thus the response dictated by the Sverdrup balance of mass transport to the imposed curl is also small. VERONIS and STOMMEL (1956), using the  $\beta$ -plane approximation with a two-layer ocean but ignoring bathymetry, predicted baroclinic response times on the order of a year for high latitudes. (One would expect that the barotropic mode, if significant, could undergo relatively rapid perturbations, but we have no confirmation of this.) LIGHTHILL (1969) used a linear, stratified model to demonstrate a relatively rapid response of the ocean circulation to time-varying winds near the equator, but a response time of order ten years for the latitudes in the Gulf of Alaska was indicated. In his model, baroclinic response is limited primarily to the upper oceanic layers, which is at variance with our finding that baroclinic structure may vary to appreciable depths. This apparent disagreement is not surprising; Lighthill has pointed out that at high latitudes the problem becomes nonlinear and, moreover, that topography should be allowed for in any theoretical model. Variations in density gradients may occur which are unrelated to changes in volume transport but rather result from other influences such as interaction of the stream with bathymetry along its inshore boundary. In order to explain the observed variability and adequately account for baroclinic response to variable winds, a model should include nonlinear and topographic effects in addition to stratification and  $\beta$ -effects. Such a model would clearly be a major undertaking and is beyond the scope of this effort.

### Acknowledgements

This study is dedicated to R. L. Charnell and N. P. Laird, our colleagues who were lost at sea aboard the Holo Holo off Hawaii in mid-December 1978. R. L. Charnell was particularly interested in transport variations in this region, and he encourages us to pursue this topic. We are also indebted to the anonymous reviewers whose suggestions have improved the quality of the manuscript.

This study was supported in part by the Bureau of Land Management through interagency agreement with the National Oceanic and Atmospheric Administration under which a multi-year program responding to needs of petroleum development of the Alaskan continental shelf is managed by the Outer Continental Shelf Environmental Assessment Program (OCSEAP) office.

## REFERENCES

- BAKUN, A. (1973) Coastal upwelling indices, west coast of North America, 1946-1971. NOAA Technical Report NMFS SSRF-671, 103 pp.
- DODIMEAN, A. J., F. FAVORITE and T. HIRANO (1963) Review of oceanography of the Subarctic Pacific region. International North Pacific Fisheries Commission, Bulletin 13, 195 pp.
- FAVORITE, F. (1967) The Alaskan Stream. International North Pacific Fisheries Commission, Bulletin 21, 20 pp.
- FAVORITE, F. (1974) Flow into the Bering Sea through Aleutian Island passes. In: Oceanography of the Bering Sea with emphasis on renewable resources. D. W. HOOD and E. J. KELLY, editors, University of Alaska, Occasional publication 2, pp. 3-37.
- FAVORITE, F., A. J. DODIMEAD and K. NASU (1976) Oceanography of the Subarctic Pacific region, 1960-1971. International North Pacific Fisheries Commission, Bulletin 33, 187 pp.
- FAVORITE, F. and W. J. INGRAHAM (1977) On flow in the northwestern Gulf of Alaska, May 1972. Journal of the Oceanographical Society of Japan, 33, 67-81.
- FOMIN, L. M. (1964) The dynamic method in oceanography. Elsevier, 212 pp.
- HAYES, S. P. (1979) Variability of current and bottom pressure across the continental shelf in the northeast Gulf of Alaska. Journal of Physical Oceanography, 9, 88-103.
- INGRAHAM, W. J., A. BAKUN AND F. FAVORITE (1976) Physical oceanography of the Gulf of Alaska. Final Report, RU-357, Northwest Fisheries Center, National Marine Fisheries Service, Seattle, 132 pp. (Unpublished document.)



- LIGHTHILL, M. J. (1969) Unsteady wind-driven ocean currents. Quarterly Journal of the Royal Meteorological Society, 95, 675-688.
- MONTGOMERY, R. B. (1941) Transport of the Florida Current off Habana. Journal of Marine Research, 4, 198-219.
- OHTANI, K. (1970) Relative transport in the Alaskan Stream in winter. Journal of the Oceanographical Society of Japan, 26, 271-282.
- REED, R. K. and N. E. TAYLOR (1965) Some measurements of the Alaska Stream with parachute drouges. Deep-Sea Research, 12, 777-784.
- REED, R. K. (1968) Transport of the Alaskan Stream. Nature, 220, 681-682.
- REED, R. K. (1970) Geopotential topography of deep levels in the Pacific Ocean. Journal of the Oceanographical Society of Japan, 26, 331-339.
- REID, J. L. (1963) Northwest Pacific Ocean waters in winter. The Johns Hopkins Oceanographic Studies, No. 5, 96 pp.
- REID, J. L. and R. S. ARTHUR (1975) Interpretation of maps of geopotential anomaly for the deep Pacific Ocean. Journal of Marine Research, Supplement, 33, 37-52.
- REID, J. L. and A. W. MANTYLA (1976) The effect of geostrophic flow upon coastal sea elevations in the northern North Pacific Ocean. Journal of Geophysical Research, 81, 3100-3110.
- SCHUMACHER, J. D., R. SILLCOX, D. DREVES and R. D. MUENCH (1978) Winter circulation and hydrography over the continental shelf of the northwest Gulf of Alaska. NOAA Technical Report ERL 404-PMEL 31, 16 pp.
- VERONIS, G. and H. STOMMEL (1956) The action of variable wind stresses on a stratified ocean. Journal of Marine Research, 15, 43-75.
- WARREN, B. A. and G. H. VOLKMANN (1968) Measurement of volume transport of the Gulf Stream south of New England. Journal of Marine Research, 26, 110-126.

TABLE 1. Summary of Alaskan Stream volume transport near Kodiak Island.

The unadjusted transports were computed relative to 1500 dbar or the deepest common level. Adjusted transports were computed by the method of Jacobsen and Jensen in water depths between 1500 and 300 m.

Stations or section	Dates	Unadjusted Transport ( $10^6\text{m}^3/\text{sec}$ )	Adjusted Transport ( $10^6\text{m}^3/\text{sec}$ )
2989-2996	21-22 Sept. 75	5.8	10.4
A			
2968-2976	18-19 Sept. 75	8.7	10.6
B			
A	6-10 Nov. 75	5.1	8.6
B	4-5 Nov. 75	10.7	10.7
A	30 Apr. - 1 May 76	12.2	12.2
B	29 Apr. 76	10.8	15.9
3049-3053	10-11 May 76	9.1	12.5
A	27 July 76	13.5	16.8
192-279.2	29-30 Oct. 77	8.4	11.6
231-235	2 Nov. 77	9.4	11.4
A	9-10 Nov. 77	10.8	12.3
568-769	7-8 Mar. 78	9.5	11.0
697-774	16 Mar. 78	12.0	12.4
696-775	3-4 June 78	7.1	8.0
19-25	6-7 Oct. 78	9.6	10.4
87-79	11 Oct. 78	8.0	11.3
B	15-16 Feb. 79	9.7	12.3
Mean		9.4	11.7

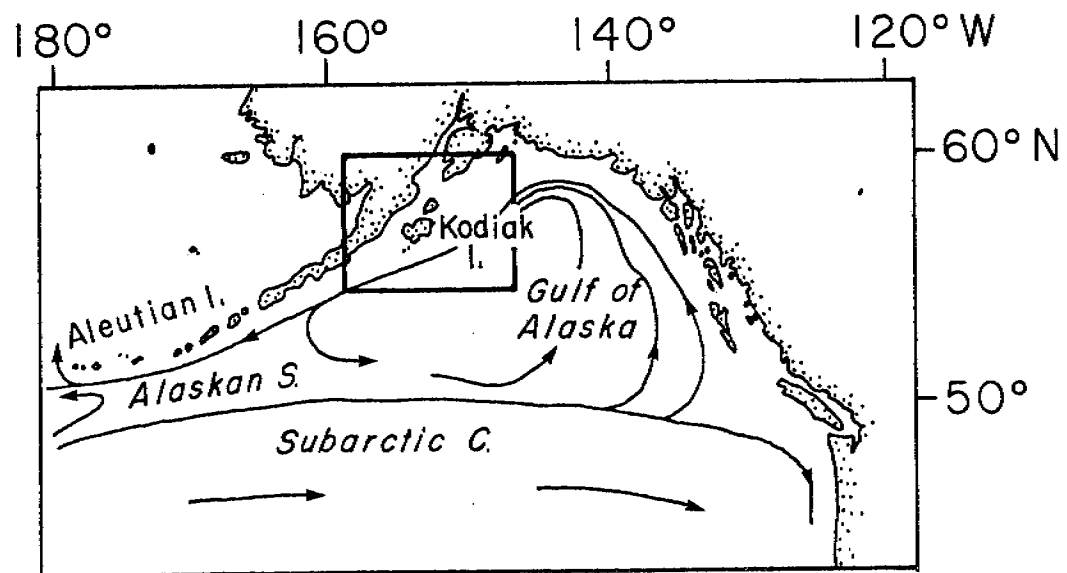
## LIST OF FIGURES

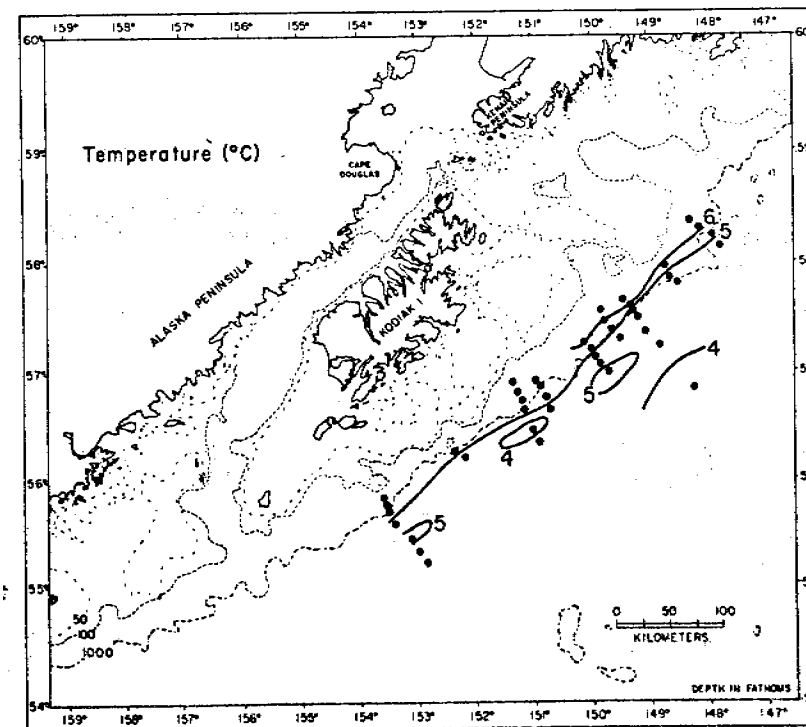
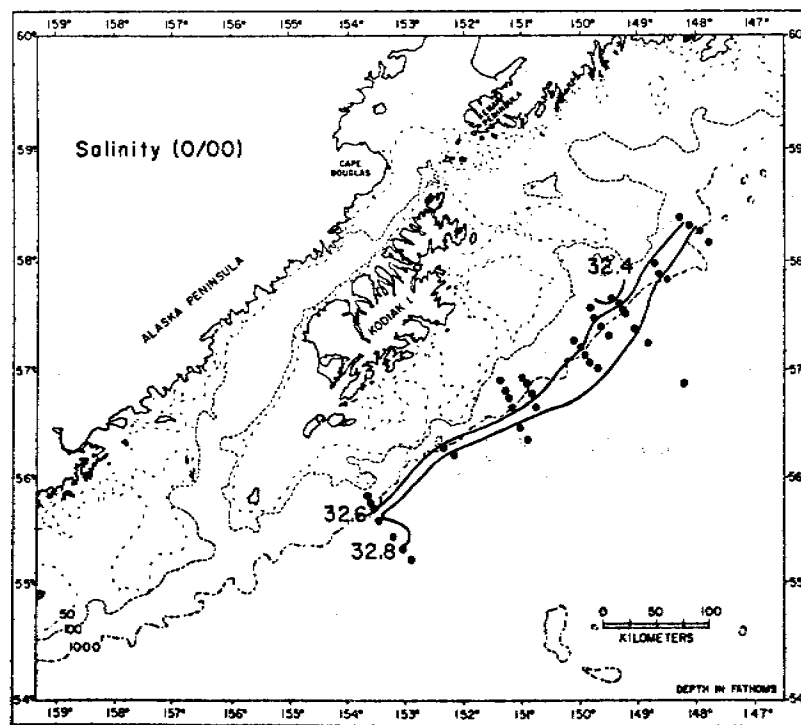
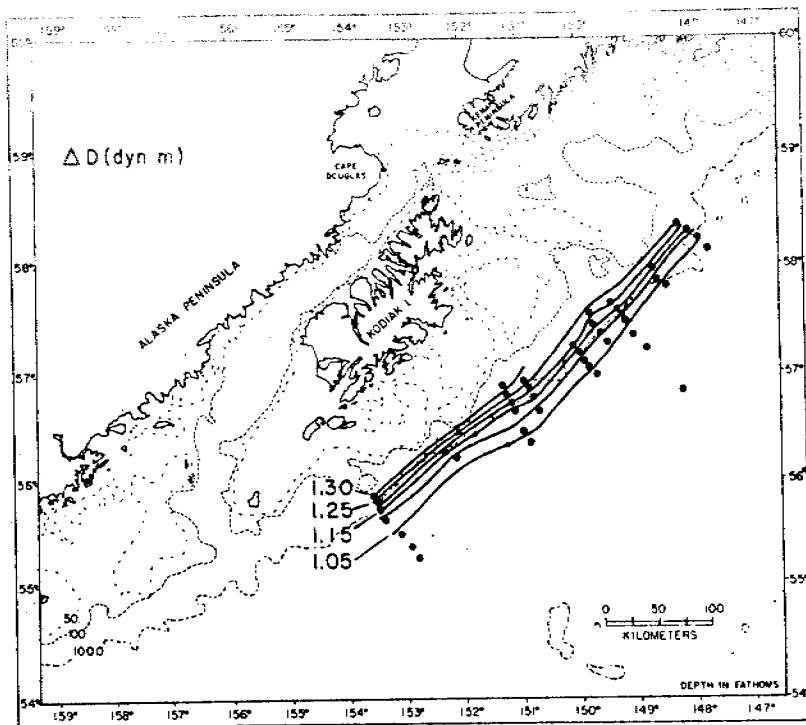
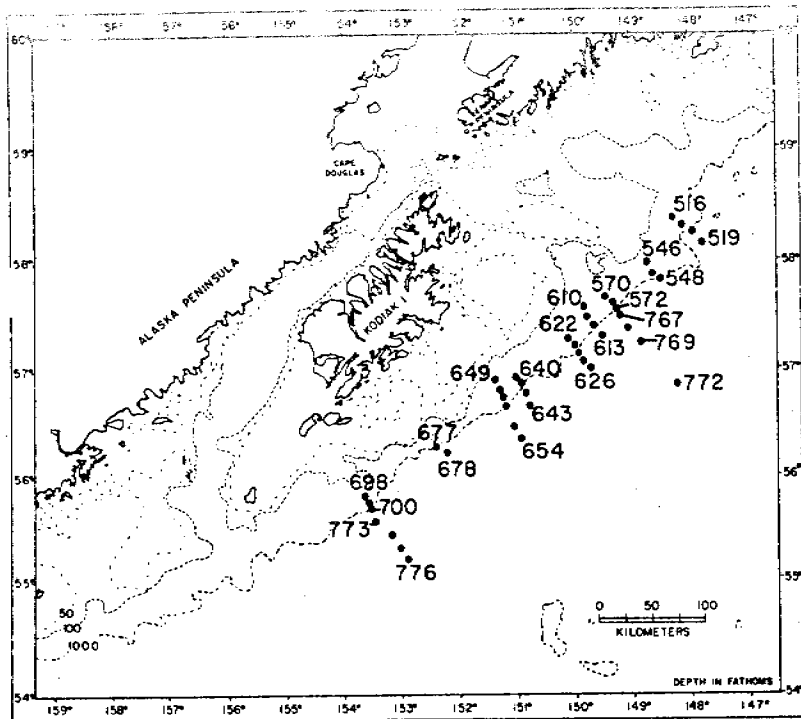
- Figure 1. Schematic diagram of surface circulation in the subarctic Pacific. The area near Kodiak Island shown on subsequent maps is indicated by the rectangle with a thick border.
- Figure 2. Observations during 4-16 March 1978. (a) Location of CTD casts that reached 1000 m; (b) geopotential topography (in dyn m) of the sea surface referred to 1000 dbar; (c) surface salinity ( $^{\circ}/\text{oo}$ ); and (d) subsurface maximum temperature ( $^{\circ}\text{C}$ ).
- Figure 3. Observations during 26 May - 6 June 1978. (a) Location of CTD casts that reached 1000 m; (b) geopotential topography (in dyn m) of the sea surface referred to 1000 dbar; (c) surface salinity ( $^{\circ}/\text{oo}$ ); and (d) subsurface maximum temperature ( $^{\circ}\text{C}$ ).
- Figure 4. Vertical sections of (a) temperature ( $^{\circ}\text{C}$ ), (b) salinity ( $^{\circ}/\text{oo}$ ), and (c) density ( $\sigma\text{-t}$ ) near  $153^{\circ}\text{W}$ , 15-16 March 1978.
- Figure 5. Vertical sections of (a) temperature ( $^{\circ}\text{C}$ ), (b) salinity ( $^{\circ}/\text{oo}$ ), and density ( $\sigma\text{-t}$ ) near  $153^{\circ}\text{W}$ , 3-4 June 1978.
- Figure 6. Vertical profiles of maximum geostrophic velocity (cm/sec) computed from the density data shown in Figures 4 and 5, March and June 1978. The velocity profile for June 1978 was adjusted to a reference level of 1500 dbar by the method of Jacobsen and Jensen.

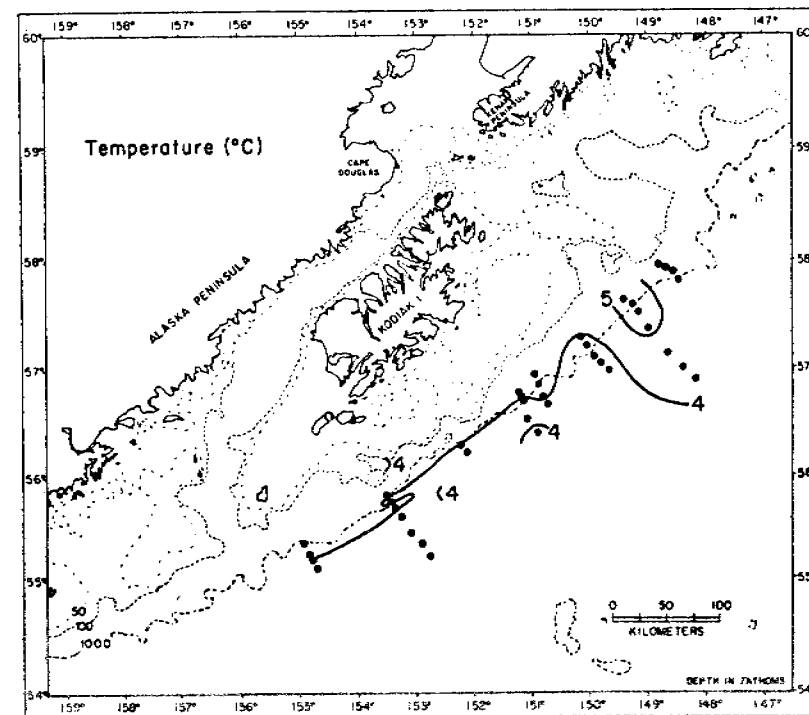
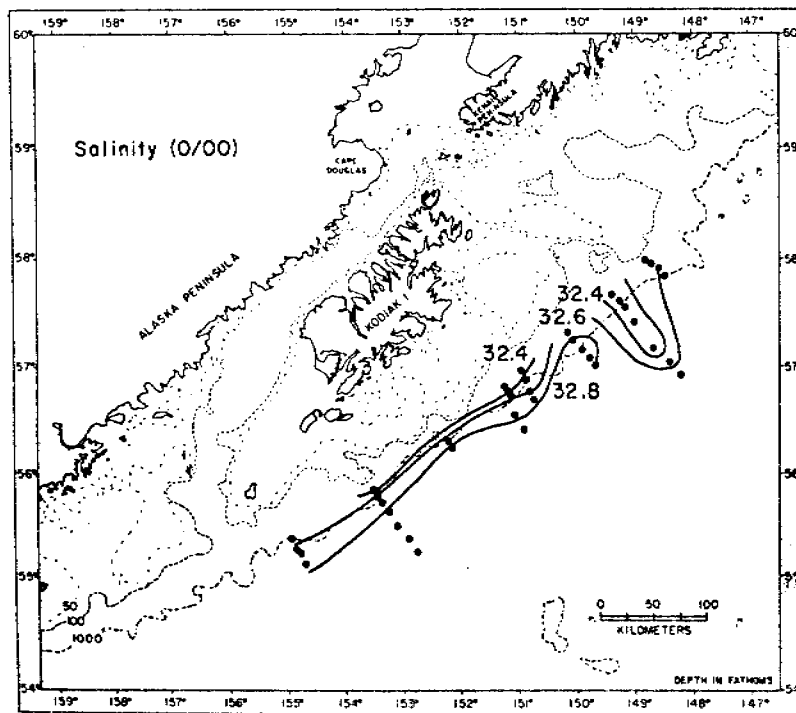
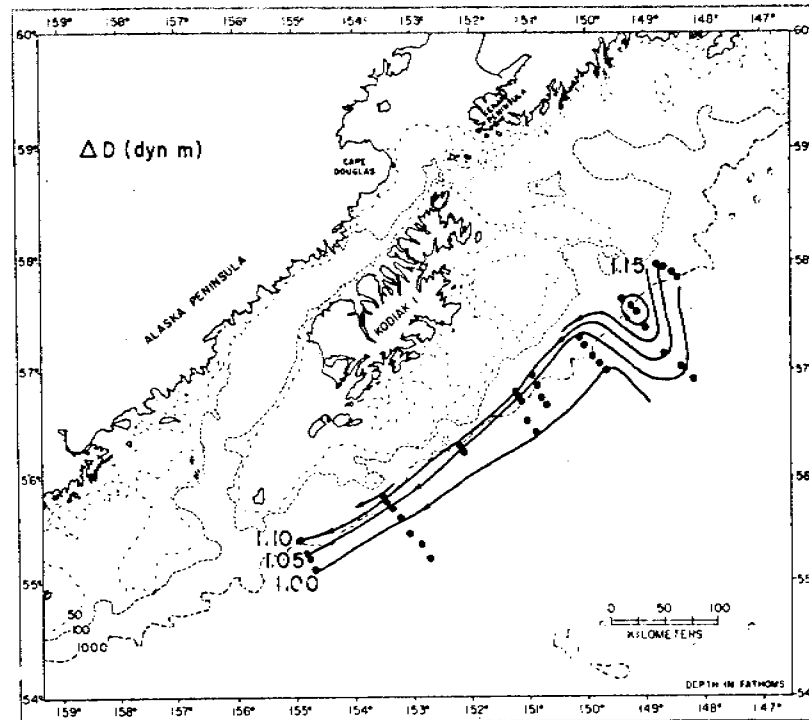
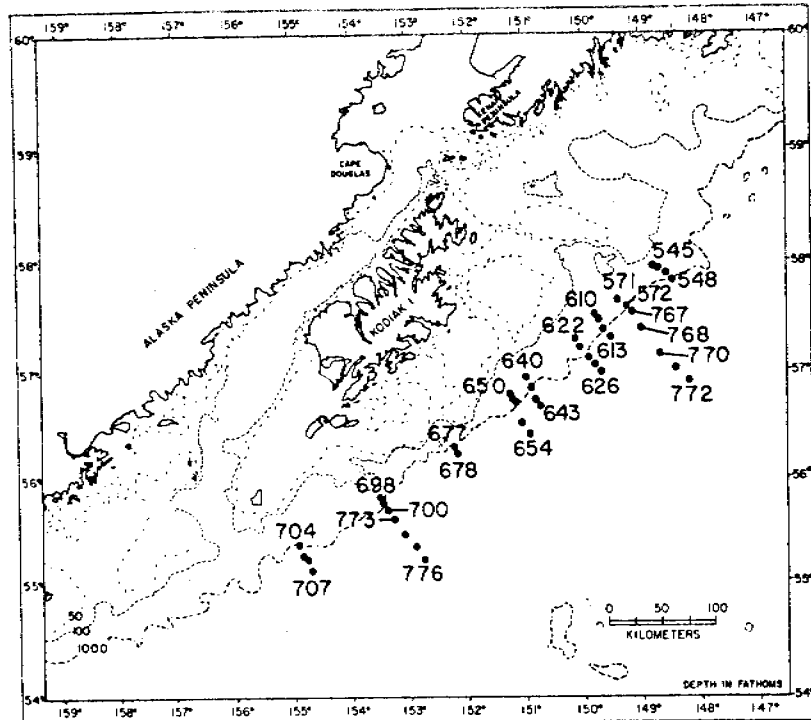
Figure 7. Location of the PMEL CTD sections used to compute volume transport;  
(a) 29 October - 2 November 1977, (b) 7-16 March 1978, (c) 3-4  
June 1978, and (d) 6-11 October 1978.

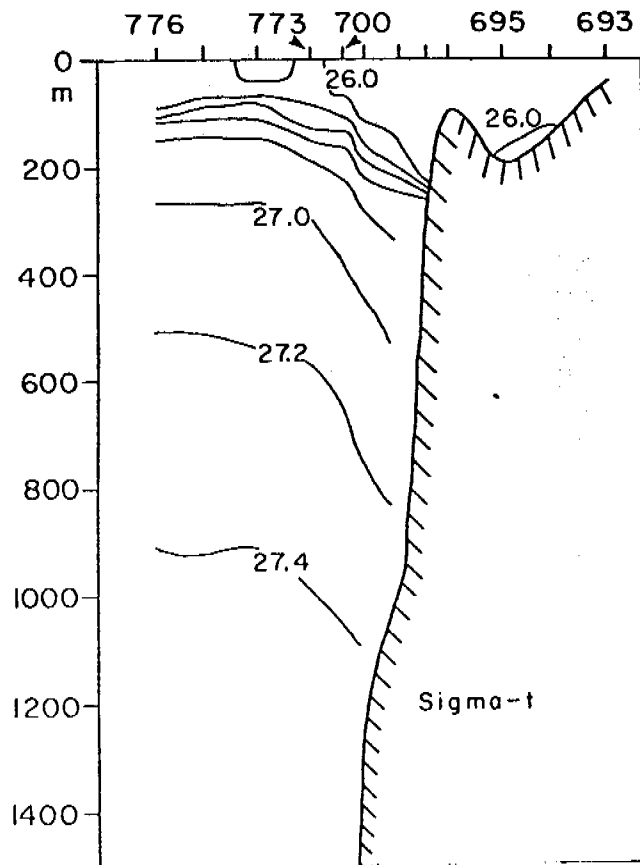
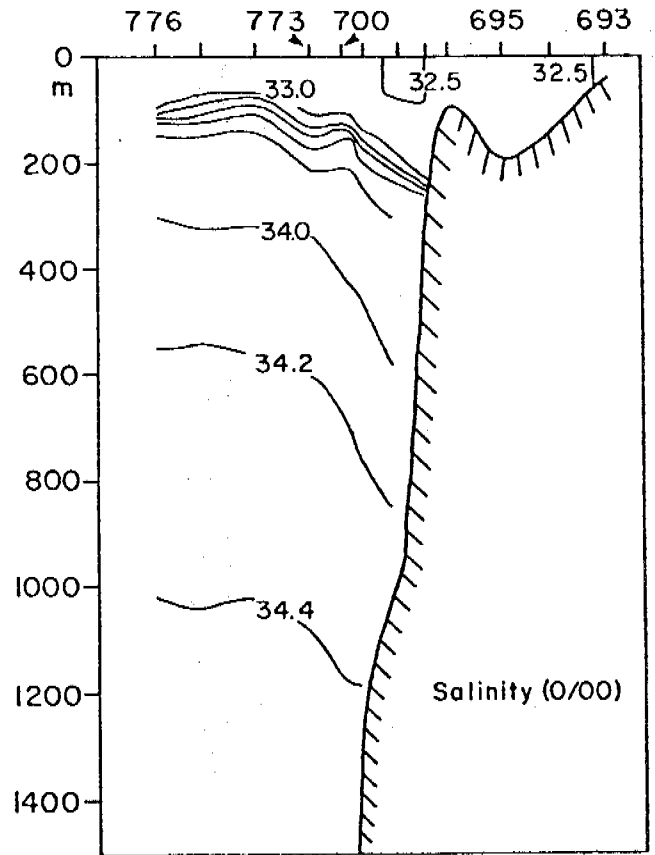
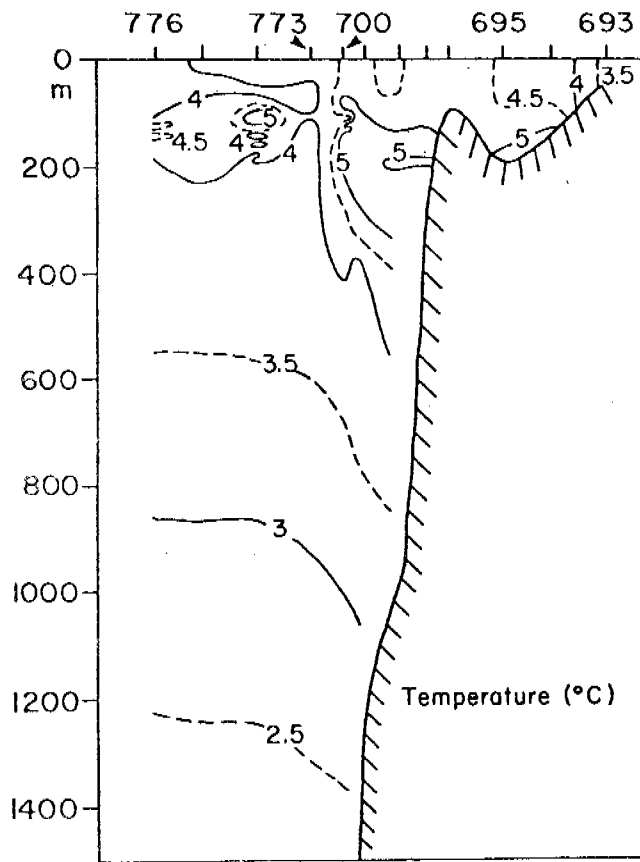
Figure 8. Location of IMS CTD sections used to compute volume transport;  
(a) 18-22 September 1975 and (b) 10-11 May 1976. The other IMS  
sections were occupations of section A or B as in (a).

Figure 9. Time series of the integrated total transport ( $10^6\text{m}^3/\text{sec}$ ) computed  
from wind-stress curl and the observed volume transport ( $10^6\text{m}^3/\text{sec}$ )  
of the Alaskan Stream, 1975-1979. Observed transports for more than  
one section on a cruise were averaged.

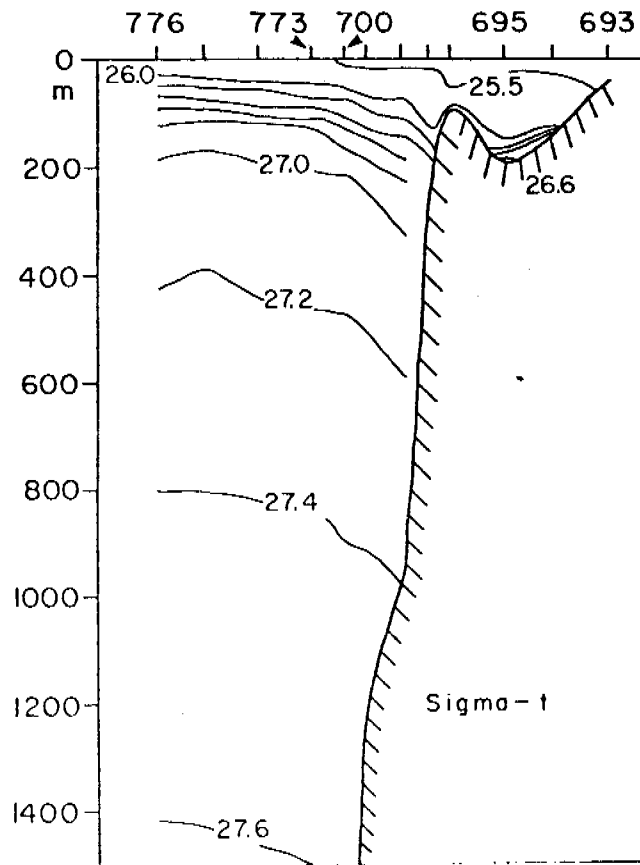
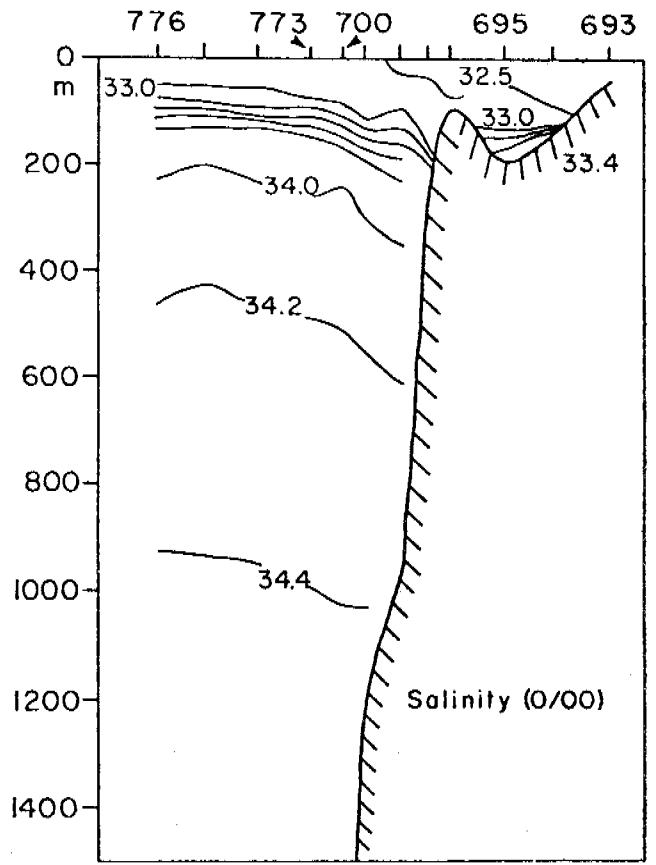
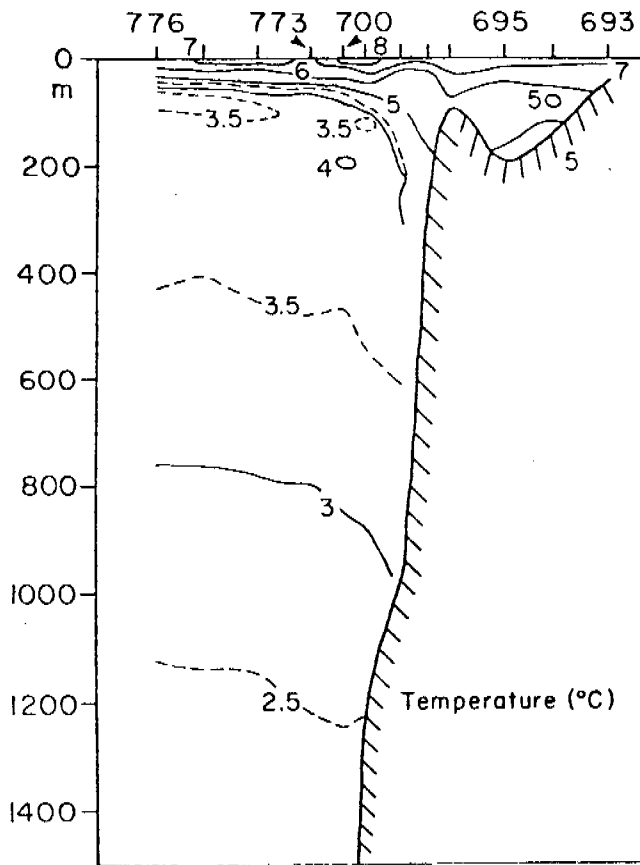


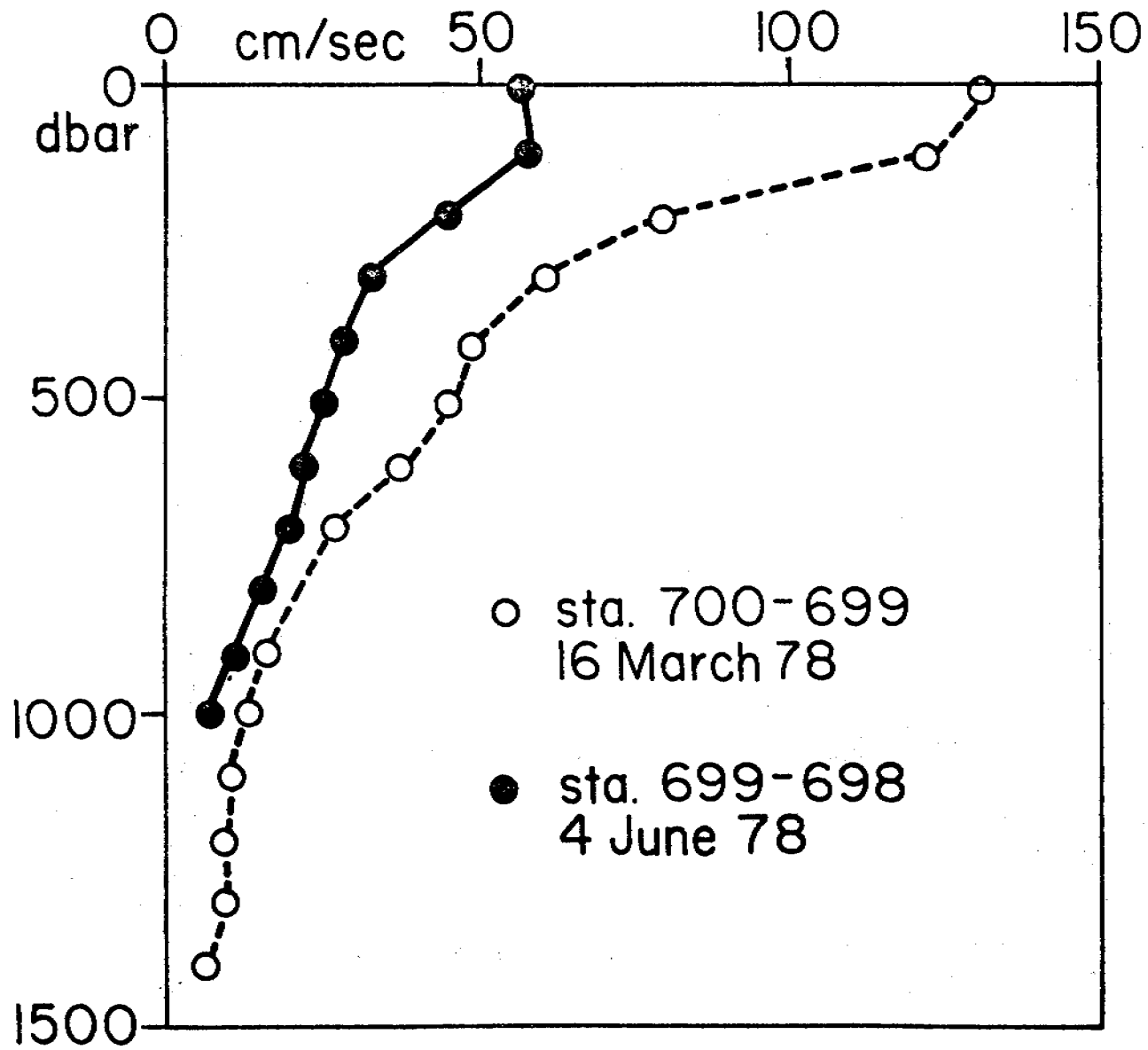


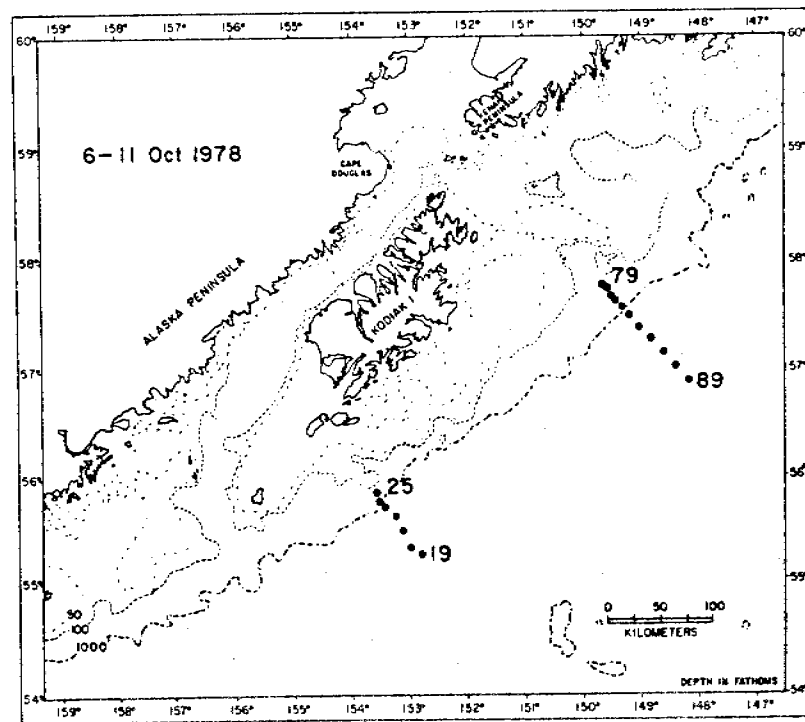
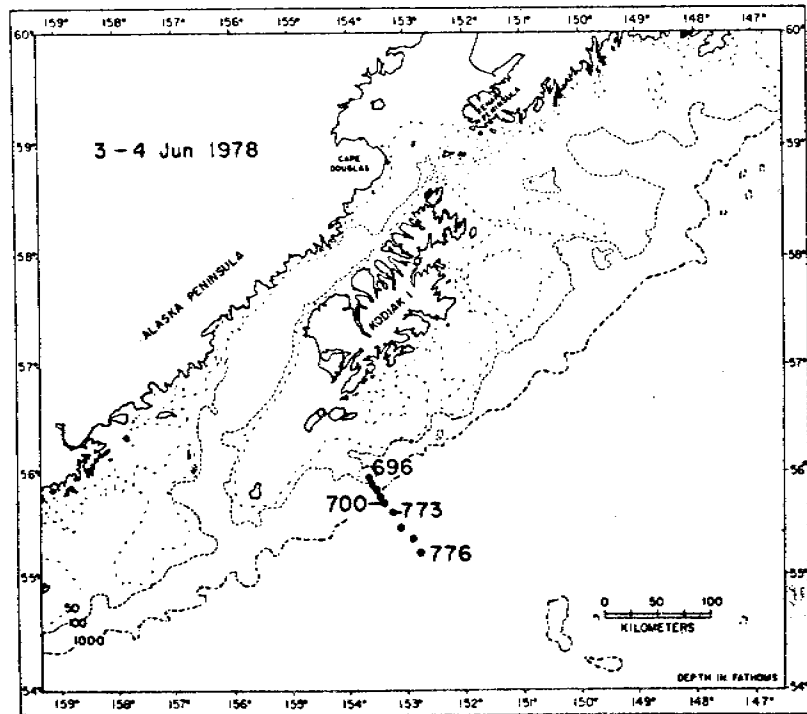
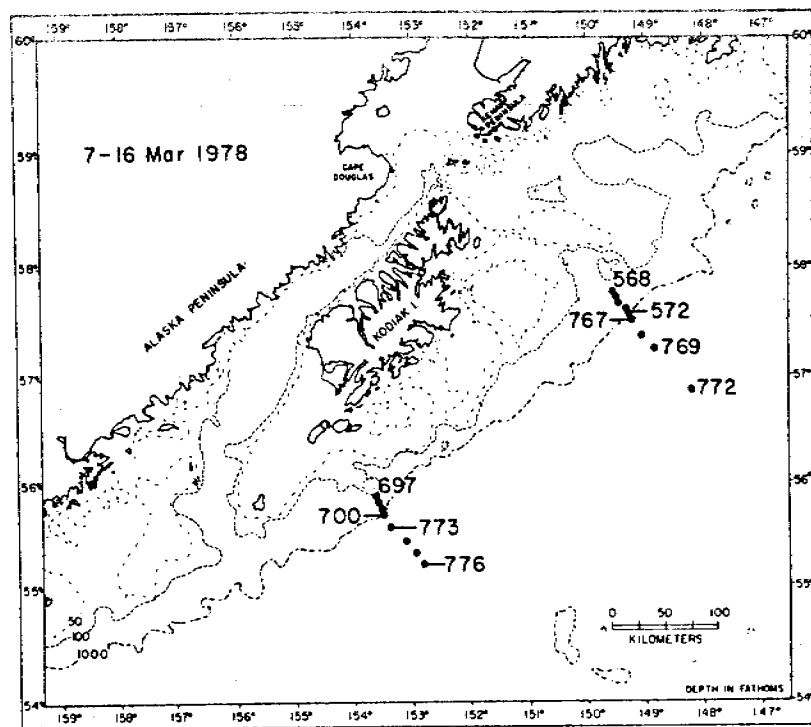
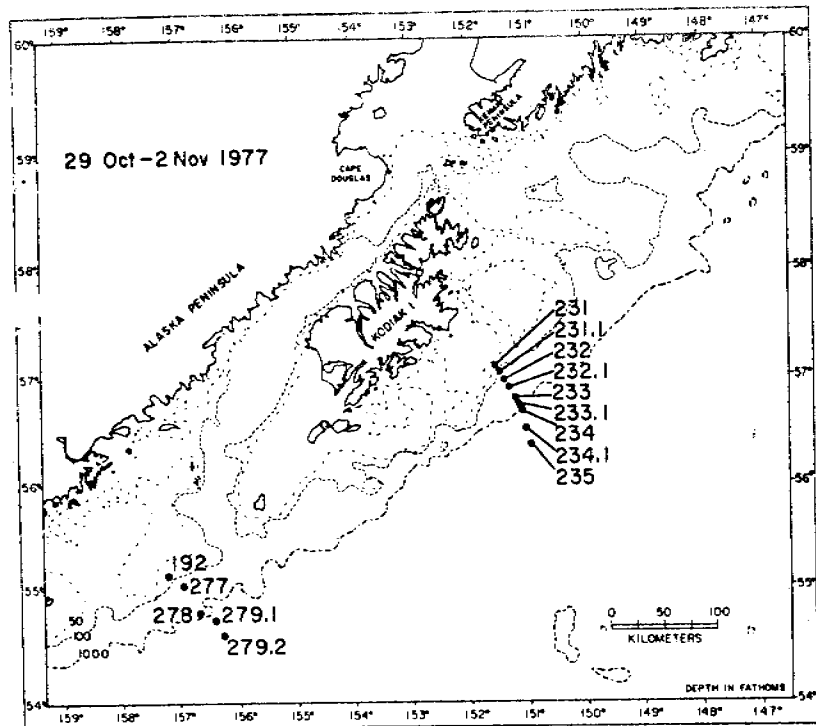


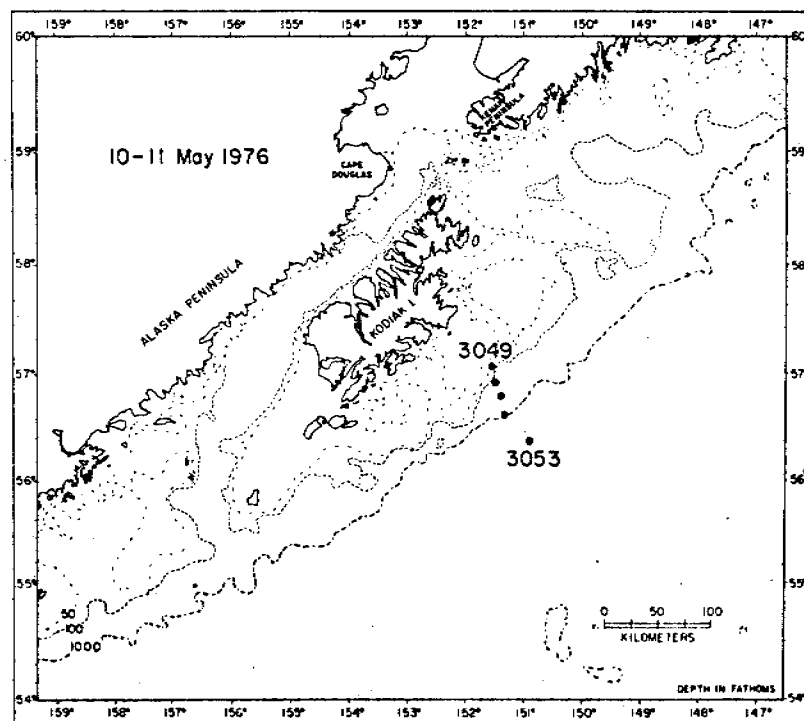
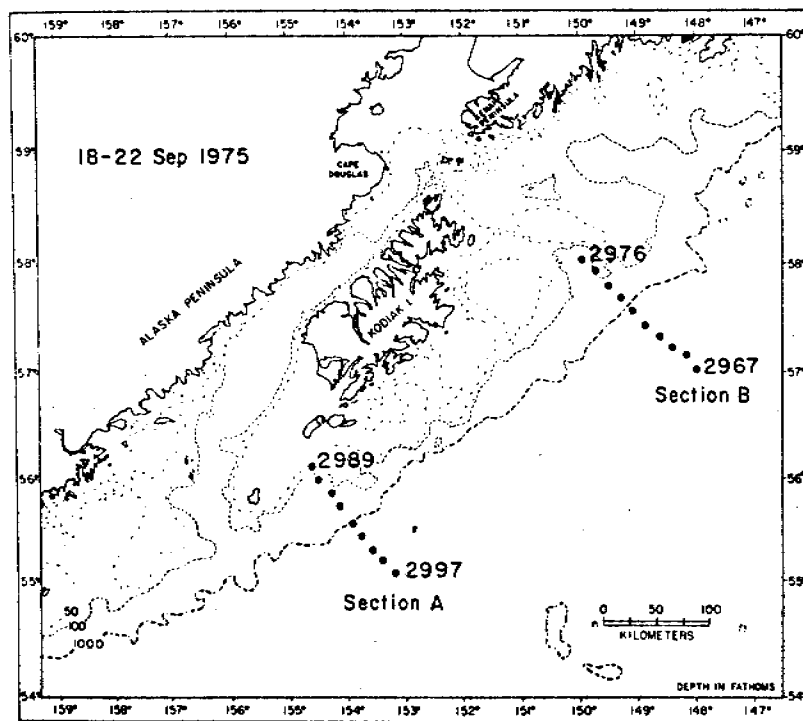


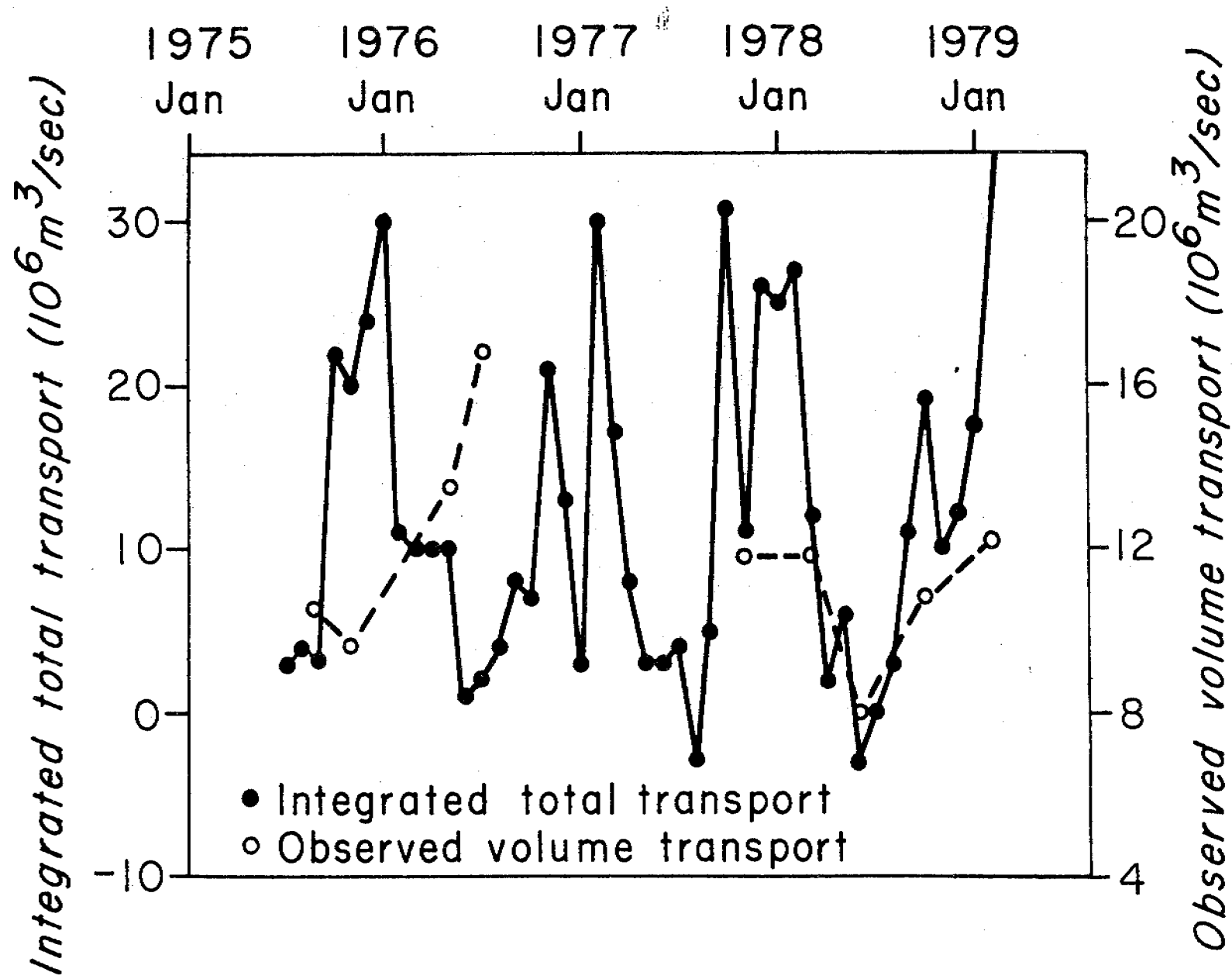












E. The following manuscript has been submitted to the J. Geophys. Res. :

COASTAL FLOW IN THE NORTHWEST

GULF OF ALASKA: THE KENAI CURRENT\*

J. D. SCHUMACHER<sup>1</sup>

AND

R. K. REED<sup>1</sup>

<sup>1</sup> National Oceanic and Atmospheric Administration  
Environmental Research Laboratories  
Pacific Marine Environmental Laboratory  
Seattle, WA 98105

\*Contribution No. 427 from the NOAA/ERL Pacific Marine Environmental Laboratory

## INTRODUCTION

With increasing concern for the environmental impact of petroleum development and management of food resources, interest is being focused on the continental shelf environment. Although shelf circulation patterns vary regionally, there are general classes of forcing mechanisms for shelf flow. As noted by Smith [1978], over an outer continental shelf region, dominant energy sources are atmospheric variability caused by passing storm systems and fluctuating ocean currents. On the shelf, the main driving forces for "first-order" flow are winds and tides [Csanady, 1976]. Seasonally varying wind stress and ensuing mass redistribution result in coastal flow off the Oregon coast [Smith, 1974; Huyer et al., 1975; Kundu and Allen, 1976]. Over the southeast Bering Sea shelf, tides dominate horizontal kinetic energy [Reed, 1978; Schumacher et al., 1979a]. Model results [Semtner and Mintz, 1977] and momentum considerations [Csanady, 1978; Beardsley and Winant, 1979] suggest that oceanic circulation results in the observed residual flow off the east coast of the United States, and runoff appears to be only locally important [Beardsley and Hart, 1978]. A model of winter circulation for the Adriatic Sea [Hendershott and Rizzoli, 1976], however, suggests that river runoff is a significant driving force, and a recent shelf circulation model [Pietrafesa and Janowitz, 1979] indicates that, in the absence of wind stress, a reasonable value of surface buoyancy flux results in alongshore velocities of about 20 cm/sec.

Historically, little information is available on properties, flow, or dynamics of shelf waters in the northwest Gulf of Alaska. Most investigations were confined to studies of the offshore boundary current, the Alaskan Stream, and the subarctic gyre in general [Dodimead et al., 1963; Roden,

1969; Thomson, 1972; and Favorite et al., 1976]. The Alaskan Stream is the northern boundary of the subarctic gyre and acts as a return flow for wind-curl driven Sverdrup transport northward into the Gulf of Alaska [Favorite et al., 1976]. An estimate of mean baroclinic transport for the Stream off Kodiak Island is  $12 \times 10^6 \text{ m}^3/\text{sec}$ ; however, variations do not reflect the large seasonal signal of wind-stress curl [Reed et al., 1980].

Recent studies of coastal circulation in the northeast Gulf of Alaska [Hayes and Schumacher, 1976] suggest that, while oceanic forcing is dominant at the shelf edge, the inner shelf or coastal circulation differs from the shelf-break flow. Further, Royer et al. [1979] provide evidence for a coastal flow which extends from Yakutat to Prince William Sound, a distance of approximately 500 km. Royer [1979] discussed the impact that extensive precipitation and runoff have on dynamic height and sea level along the Gulf of Alaska coast; at high latitudes, and consequent low temperature, salinity primarily controls density. Royer estimated that maximum monthly freshwater addition is about  $20 \times 10^3 \text{ m}^3/\text{sec}$ .

Preliminary results from part of the Outer Continental Shelf Environmental Assessment Program (OCSEAP) of the Bureau of Land Management and the National Oceanic and Atmospheric Administration [Schumacher et al., 1978, 1979b] indicate that in the northwest gulf, the Alaskan Stream is an offshore feature whose typically high velocities do not extend onto the shelf. Hydrographic data, however, indicate that there is a shoreward flux of heat and salt. In this paper we present further evidence that a well-defined coastal flow exists over the inner shelf from at least as far east as the Copper River to southern Shelikof Strait. This flow, which we call the Kenai Current, has a transport up to  $1 \times 10^6 \text{ m}^3/\text{sec}$  toward the west and is primarily driven by the baroclinic component of a cross-shelf pressure gradient.



## SETTING

This investigation is concerned with a region of the western Gulf of Alaska in the vicinity of the Kenai Peninsula, Kodiak Island, and Shelikof Strait (Figure 1). The area is characterized by extremely complex bottom topography shoreward of the 1830-m isobath, and the continental shelf is excised by several deep troughs which alternate with prominent banks. The northernmost of these features is Amatuli Trough, which is a broad, deep (>200-m) cleft in the shelf as indicated by the 183-m isobath. Water depths in excess of 150 m occur within 10 km of the Kenai Peninsula. Two passages, Kennedy and Stevenson entrances, enter Shelikof Strait between the Kenai Peninsula and Afognak Island. Depths in Kennedy Entrance are as great as 200 m, but east and west of this passage sill depths are about 150 m. Stevenson Entrance has an average depth of about 120 m. The combined cross-sectional area for these passages is about  $5 \times 10^6 \text{ m}^2$ . Shelikof Strait lies between the Alaska Peninsula to the northwest and Kodiak and Afognak islands to the southeast. To the north, the Strait connects with lower Cook Inlet. Maximum depths in the upper Strait are generally 175 m, and the cross-sectional area is about  $6 \times 10^6 \text{ m}^2$ . To the south of Amatuli Trough lies Portlock Bank, which is an extensive region with depths between 45 and 60 m. The trough separating it from North Albatross Bank is indicated by a marked inshore trend of the 183-m isobath. The rugged undersea topography is similar to features above sea level; the coastline is ringed by coastal mountains (typically 1-km relief with numerous peaks in excess of 3 km within 60 km of the coast) and valleys. These features have major effects on winds and precipitation (mean annual value of about 2.3 m for 1931-1960).

## DATA ACQUISITION AND PROCESSING

Conductivity and temperature versus depth (CTD) data were obtained during seven cruises (see Table 1) conducted by NOAA's Pacific Marine Environmental Laboratory from March 1977 through October 1978. CTD data were collected using Plessey model 9040 systems with model 8400 data loggers. These systems sampled five times per second for values of temperature, conductivity, and pressure. Data were recorded only during the down-cast using a lowering rate of 30 m/min. Nansen bottle samples were taken at most stations to provide temperature and salinity calibration. Data were despiked and averaged over 1-m intervals to yield temperature and salinity values from which density and geopotential anomaly were computed.

Current-meter station locations are shown in Figure 1. Aanderaa model RCM-4 current meters were used on taut wire moorings with an anchor and acoustic release at the bottom and a subsurface buoyant float just above the top current meter. The taut-wire mooring tends to minimize surface wave-induced noise on the meter's rotor. A summary of current records is given in Table 2.

Two time-series were produced from edited observations using a Lanczos filter [cf. Charnell and Krancus, 1976]. The first series was filtered so that over 99% of the amplitude was passed at periods greater than 5 hr, 50% at 2.9 hr, and less than 0.5% at 2.0 hr. The second series was filtered to remove most of the tidal energy; it passed 99% of the amplitude at periods over 55 hr, 50% at 35 hr, and less than 0.5% at periods less than 25 hr. This series was resampled at 6-hr intervals for use in examining subtidal circulation.

During summer 1978 a number of satellite-tracked drifting buoys were also deployed as part of the OCSEAP work. These drifters had "windowshade"

drogues centered at about 10 m, and they were interrogated several times a day by the Nimbus 6 satellite. A program was written to derive valid daily positions, and the data through September 1978 were reported by Hansen [1978].

Wind measurements from Middle Albatross Bank were provided by NOAA's data buoy EB 46008 (formerly EB 72) located at  $57^{\circ}06'N$ ,  $151^{\circ}45'W$  (Figure 1), approximately 60 km offshore. This buoy was installed in August 1977 and provided data from 1 November 1977 until February 1979. Winds were sampled every three hours by satellite transmission link and were averaged for eight minutes prior to transmission. Data gaps less than 6 hr were filled by linear interpolation, and results from a sea-level pressure analysis by Fleet Numerical Weather Central (U.S. Navy) were used for longer gaps.

#### ANALYSIS OF HYDROGRAPHIC DATA

Geopotential Topography. Limited evidence was presented [Schumacher et al., 1978] that net flow from current records agreed with that inferred from the 0/100-dbar geopotential topography. The paths of drogued buoys tracked by satellite also support the circulation patterns deduced from the geostrophic relation; Royer et al. [1979] found reasonable agreement between the two methods over the shelf east of this area, and summer 1978 drogued buoy data [Hansen, 1978] around Kodiak Island showed paths that support flow inferred from the 0/100-dbar geopotential topography. The geopotential patterns presented here are in good agreement with additional direct current measurements and with various physical property distributions.

We summarize features of geopotential topography from Schumacher et al. [1978, 1979b] which are relevant to this study. During March, September, and October 1977, two flow regimes existed: 1) the southwestward flowing Alaskan Stream over the slope accompanied by inshore counterflows east of Portlock

Bank and 2) a well-defined coastal flow along the Kenai Peninsula. Weak, variable circulation occurred between the two more organized flows. During September and October a southward extension of the coastal flow appeared east of Afognak and Kodiak Islands and may have been important in initiating a well-developed (relief of  $\approx 0.04$  dyn m) gyre-like feature between Portlock and North Albatross banks. The coastal flow appeared to be strongly influenced by fresh water as indicated by very low surface salinities. Relief across the coastal flow was about 0.05 dyn m in March and September but increased three-fold in October. In the vicinity of the entrances to Shelikof Strait, geostrophic patterns for April-May 1972 also suggested westward baroclinic flow [Favorite and Ingraham, 1977].

Coastal flow off the Kenai Peninsula had important effects on circulation in Shelikof Strait [Schumacher et al., 1978]. Two cruises listed in Table 1 (March 1978, NOAA Ship DISCOVERER; October 1978) had adequate coverage to examine concurrent conditions off the Kenai Peninsula and in Shelikof Strait. We present these data to summarize coastal conditions. The 0/100-dbar geopotential topography in March 1978 is shown in Figure 2A. The coastal flow was present, and its relief was about 0.06 dyn m. It entered Shelikof Strait through both passages and turned south off Cape Douglas. Conditions in October 1978 (Figure 2B) showed a more clearly defined coastal flow like that in October 1977. The relief across the flow in October 1978 was about 0.20 dyn m, and a portion of the flow appeared to turn south near Afognak Island. The remainder of the coastal flow, however, entered Shelikof Strait through Kennedy Entrance and turned south as a well-defined flow off Cape Douglas. A relatively strong, southward flow off Cape Douglas seems to be a permanent feature, as suggested by Muench et al. [1978].

We emphasize that the coastal flow off the Kenai Peninsula is distinct from the Alaskan Stream. This is especially apparent from CTD data extending east of this area [SAI (1979), Royer et al. (1979)], which we summarize as follows: the Stream is present seaward of the shelf break, inshore there is very weak flow (often with reversals), but a continuous flow is present along the coast. This coastal flow had an alongshore extent of over 500 km - that is, east to the Copper River - and had high velocities and transport. We call it the Kenai Current; it is a major feature of shelf circulation in the Gulf of Alaska.

Physical Property Distributions. The distribution of surface salinity, salinity at 50 m, and the sigma-t difference between 50 m and the surface in October 1978 are shown in Figure 3A, B, and C, respectively. The surface salinity distribution is similar to the geopotential topography, but there are significant differences. Along the easternmost CTD section, low-salinity water ( $<32.0$  g/kg) is confined quite close to shore and does not reflect the rather broad flow indicated in Figure 2B. The salinity pattern near Shelikof Strait is quite similar to the flow, however, even suggesting a counterflow on the north side of Kennedy Entrance as in Figure 2B. A new feature shown by surface salinity is an intrusion of low-salinity water from the north on the western side of Shelikof Strait; this could not really be shown by the geopotential topography because most of the northwest side of Shelikof Strait is shoaler than the reference level (100 dbar). The salinity distribution at 50 m (Figure 3B) is also similar to the geostrophic flow pattern, and estuarine outflow (salinity  $<31.0$  g/kg) from Lower Cook Inlet is apparent as in the surface salinity distribution. The zone of high-salinity water outlined by the 32.5-g/kg isohaline south of the Kenai Peninsula coincides with the low in geopotential anomaly on the seaward side of the coastal flow.

The distribution of the sigma-t difference between 50 m and the surface (Figure 3C) indicates that greatest stratification is associated with the coastal flow. This is caused primarily by dilute (low-density) near-surface water, and values are reduced somewhat by enhanced tidal mixing through the entrances and near shore. Relatively large differences ( 0.5) occur in waters off Cape Douglas, but the water column is homogeneous over Portlock Bank and over a shoal area stretching west of the Kenai Peninsula. This distribution supports geopotential features previously described and also depicts zones of vertical mixing which are strongly influenced by the effect of topography on tidal-power density per unit mass,  $V^3/H$  [Fearnhead, 1975], where V is mean tidal speed and H is water depth. Tidal mixing affects the lower part of the water column, and winds mix the upper layer; thus over banks water may become homogeneous, especially when initial stratification and/or positive bouyancy flux are small.

The geopotential topography in March 1978 (Figure 2A) indicated an appreciably reduced flow into Shelikof Strait compared to that in October 1978. The patterns during the two seasons were similar, however. The surface salinity distribution pattern in March 1978 (not shown) is similar to that in October 1978 (Figure 3A), but the lowest values in Shelikof Strait were about 1 g/kg greater in March than in the fall. Differences in the salinity at 50 m during the two seasons were less marked, however. The surface temperature distribution in March 1978 (not shown) shows that the coldest water is associated with the southerly flow on the western side of Shelikof Strait, and waters in the Kenai Current are somewhat cooler than to the south. During October 1978, coastal waters at the surface and at 50 m were warmer than those in other regions. Coastal waters affected by land drainage tend to be cooled more rapidly in winter (but warmed more rapidly in summer) than waters of oceanic origin.

Vertical sections of temperature, salinity, and sigma-t along the CTD sections off the Kenai Peninsula (stations 59-68, 70-73 in October 1978, see Figure 2B; stations 119-134 in March 1978, see Figure 2A) are presented in Figures 4 and 5. The sections in October display a narrow band (20 km) of warm, dilute, low-density water adjacent to the Kenai Peninsula; this strong baroclinicity is in agreement with the westward coastal flow that enters Shelikof Strait. Indications of weak westward flow, however, extend well south of this band to the northern flank of Portlock Bank. The three stations (67, 68, and 70) over Portlock Bank exhibit weak stratification, and the water at station 68 (63-m depth) is completely mixed. South of Portlock Bank, the varying density slopes suggest that peak speeds in the Alaskan Stream were offshore of station 73. In March (Figure 5) the gradients across the coastal flow were much weaker than in fall, and there are no indications of significant baroclinicity elsewhere. Minimum temperatures were near the surface (rather than the bottom as in March), and there was much less stratification everywhere than that measured in fall. The homogeneous water atop Portlock Bank extended about 15 m deeper than in October, which suggests that total mixing (presumably a combination of wind mixing near the surface and tidal mixing near the bottom) was more efficient in winter than in summer through fall. Another feature shown by these data is that the intermediate and deeper parts of the water column were more saline in October than in March, while the coastal flow near the Kenai Peninsula was much more dilute during fall. This pattern of decreased surface salinity and increased intermediate and deep salinity during fall is consistent in our data set (Table 1); the results suggest that the saline water is "drawn up" during periods of peak transport in the Kenai Current, perhaps as an interior upwelling in conjunction with buoyancy flux [Pietrefesa and Janowitz, 1979].

Baroclinic Transport and Speed Variations. The data presented thus far have indicated that coastal flow was more intense in October 1978 than during March of that year. The CTD section used to prepare Figures 4 and 5 was occupied on all of the PMEL cruises (Table 1). These data were used to compute baroclinic volume transport and maximum surface speed (both referred to the deepest common level) of the Kenai Current (Table 3). (A CTD section slightly west of this one was used for March 1977 because the former did not contain adequate data.) The data from four cruises in March, May, and September all indicate volume transport of  $0.4 \times 10^6 \text{ m}^3/\text{sec}$  or less and surface speeds not greater than 30 cm/sec. In October of 1977 and 1978, however, transport was 1.0 and  $1.2 \times 10^6 \text{ m}^3/\text{sec}$  with maximum speeds of 89 and 133 cm/sec. This marked increase in transport is in agreement with Royer's [1979] conclusions that geopotential anomaly and alongshore flow respond to an annual hydrological cycle which has a fall maximum.

Precipitation often deviates considerably from the long-term mean, but these variations do not seem to have marked effects on the Kenai Current. Figure 6 shows the observed precipitation averaged for the National Weather Service stations at Cordova, Seward, and Kodiak during 1977 and 1978 and the long-term mean for these stations (NOAA National Climatic Center, 1977, 1978). During four months prior to the March 1977 cruise, precipitation averaged over twice that of the long-term mean, but the March transport ( $0.4 \times 10^6 \text{ m}^3/\text{sec}$ ) and surface salinity were not unusual for the season. Royer [1979] concluded that accumulated land drainage over a large area was the major factor in producing variations in dynamic height. Hence monthly variations in precipitation, especially in winter when much of it is frozen, probably do not seriously alter the apparent seasonal pattern of large transport in fall and reduced values at other times. It seems likely, especially



after considering Royer's [1979] analysis of geopotential, sea level, and runoff, that the material presented provides a reasonable estimate of mean conditions. Thus we expect the Kenai Current to normally have a transport of about  $0.3 \times 10^6 \text{ m}^3/\text{sec}$  and peak surface speeds of perhaps 20 to 30 cm/sec; in October and November, however, transport rapidly increases to over  $1 \times 10^6 \text{ m}^3/\text{sec}$ , and peak surface speeds may exceed 100 cm/sec. These extreme seasonal changes and very high velocities make the Kenai Current atypical of coastal flows [Winant, 1979] that are separate from major, oceanic boundary currents.

#### ANALYSIS OF CURRENT OBSERVATIONS

Lagrangian Measurements. Ten satellite-tracked drifting buoys were deployed during May-July 1978 as part of OCSEAP studies [Hansen, 1978]. Four of these drifters showed features of the Kenai Current, and we summarize relevant trajectories from Hansen [1978] as follows. Drifter number 1473 moved westward in the southern part of the Kenai Current and turned south off Afognak Island as suggested by some of the property distributions and plots of geopotential topography (see e.g. Figures 2B and 3B). Number 1775 moved west along the Kenai Peninsula and passed through Kennedy Entrance at net speeds of about 25 cm/sec. It then moved eastward at very low speeds into Stevenson Entrance, where it eventually turned west and moved south through Shelikof Strait. Number 1450 moved westward at low speeds for five days and then ceased transmission. Number 1421 was deployed on Portlock Bank, moved northwest into Shelikof Strait, and exhibited weak rotary motion before grounding on Cape Douglas. In addition, a drifting buoy released as part of another project [Reed, 1979] entered the coastal flow at the head of the Gulf in December 1978, moved westward along the Kenai Peninsula into Shelikof Strait, and

grounded on Cape Douglas in January 1979. Net speed for the 10-day portion of the track near the Kenai Peninsula was about 40 cm/sec.

These data do provide direct evidence of an organized flow along the Kenai Peninsula with speeds comparable to those determined by the geostrophic relation. The westward movement into Shelikof Strait also agrees with the geopotential topography, but the apparent eastward movement out of Stevenson Entrance does not. We suspect that this may reflect a relatively brief flow "event", because similar features are suggested in some of the current meter records to be discussed.

Eulerian Measurements. Current records were low-pass filtered and then averaged over seven days on rotated coordinates which correspond to the geographical boundaries. The coordinate systems are: U positive  $300^{\circ}$ , V positive  $030^{\circ}$  for both entrances; U positive  $225^{\circ}$ , V positive  $315^{\circ}$  for Shelikof Strait; and for wind stress, U positive  $240^{\circ}$ , V positive  $330^{\circ}$ . Wind stress was calculated following Meyer et al. [1979], where the drag coefficient is a function of wind speed for winds less than 15 m/sec. The resulting net speeds through (toward the southwest) Shelikof Strait, net speeds into the entrances, and the alongshore and cross-shelf net wind stress are shown in Figure 7. Since the bulk of the Kenai Current flows through Shelikof Strait and local contributions to flow are minimal [Muench et al., 1978; Schumacher et al., 1978], current records should be characteristic of flow along the coast.

During the winter observation period, flow in Shelikof Strait was always toward the southwest with typical speeds of 20 to 30 cm/sec; during mid-October and early November, however, speeds were much higher, with a maximum of 70 cm/sec. Similar characteristics were observed during the previous winter [Schumacher et al., 1978]. During the peak flow period, shear between the two meters at 25 and 72 m was about five times greater than the shear over

the remaining observation period. When baroclinic transport in the Kenai Current attains a maximum, baroclinic shear is not eliminated by mixing, although tidal speeds in Kennedy Entrance are strong ( $\approx 65$  cm/sec). It is apparent that neither the long-shore nor cross-shelf wind stress was acting in a manner to contribute appreciably to the Kenai Current during October or early November. During late December through February, alongshore wind stress averaged  $1.2 \text{ dyne/cm}^2$  and was directed such that barotropic set-up should occur along the Kenai Peninsula; observed currents also generally increased during this period. x

Flow through Shelikof Strait over the summer observation period indicated a single flow reversal in early June. A few reversals were also noted in Stevenson Entrance but not in Kennedy Entrance. The records for Kennedy and Stevenson entrances suggest a pattern noted from the CTD data; flow is stronger and more persistent through Kennedy Entrance, and Stevenson Entrance should be more responsive to forcing from wind "events". Over the summer observation period though, neither alongshore nor cross-shelf wind stress are of proper direction or sufficient magnitude to significantly augment flow of the Kenai Current.

#### DISCUSSION

Hydrographic and current observations presented above indicate that the Kenai Current is a continuous feature which extends for about 200 km along the Kenai Peninsula and in northern Shelikof Strait. Results from previous studies allow us to extend the horizontal scale of the Kenai Current. Schumacher et al. [1978] presented current and hydrographic data which indicated that the Kenai Current is evident throughout Shelikof Strait and probably follows

the 183-m depth contours across the shelf southwest of Kodiak Island. Royer et al. [1979] provided data which showed strong baroclinic relief along the coast about 100 km east of the present study area (see his Figures 4 and 8). Feely and Massoth [1980] indicated that suspended material (aluminosilicate) derived from the Copper River is found in northern Shelikof Strait. Synthesizing these results, we identify the coastal flow which exists from the Copper River westward through Shelikof Strait (about 1000 km) as the Kenai Current. We note that coastal flow east of the Copper River may also contribute to the Kenai Current.

Although the impact of wind forcing on coastal flow cannot be quantified with the present data, wind observations support the concept of set-up due to alongshore wind stress during winter. Royer [1979] showed strong correlation ( $r=0.93$ ) between dynamic height anomaly (0/200-dbar) and adjusted sea level at Seward and noted that the small difference between sea level and dynamic height cycles implied that annual changes in the barotropic current are small. The largest differences between sea level and dynamic height anomaly (see his Figure 2) occurred in January through March, which is in agreement with our suggestion that barotropic set-up is important only from December through February.

We can estimate the magnitude of baroclinic and barotropic gradients using data from this and other shelf studies. The observed geopotential topography has a relief of 0.04 to 0.20 dyn m, which indicates an elevation of coastal sea-level of 4 to 20 cm, over a cross-shelf length scale of about 25 km. Estimates of sea-level changes in response to an alongshore wind stress of  $1 \text{ dyne/cm}^2$  range from 9 to 17 cm; [Noble and Butman, 1979] the barotropic length scale, however, is likely to be larger than the baroclinic scale here [Hayes and Schumacher 1976]. Using March dynamic topography, as

representing winter, the baroclinic gradient is about  $10^{-6}$ . If the barotropic scale were the shelf width (about 150 km), and there is a 20-cm set up from the observed stress of  $1.2 \text{ dyne/cm}^2$ , the barotropic and baroclinic gradients of sea surface elevation might be approximately equal in winter. During summer and fall the baroclinic gradient increases while the barotropic gradient decreases and may become negative.

Recent hypotheses for the residual flow off the east coast of the United States [Csanady, 1978; Beardsley and Winant, 1979] suggest that an alongshelf pressure gradient is generated by oceanic circulation, and a barotropic along-shelf flow results from this feature. The Alaskan Stream, however, is separated from the Kenai Current by a zone of very weak baroclinic flow or counter flow; hence it cannot be a major driving force for the Kenai Current. Water properties, of course, may be affected by transfer of stream water shoreward by eddies or an onshelf flux through the deep troughs. Royer et al. [1979] suggested that cross-shelf ageostrophic flow resulted from a combination of off-shelf Ekman flow in the upper layer and entrainment of water from below; this may be valid during summer but cannot apply under typical winter wind-stress conditions. Further experiments are required to determine the magnitude of the barotropic component of the Kenai Current and the mechanisms involved in generating the observed on-shelf flux of shelf-edge waters.

#### CONCLUSIONS

The organized coastal flow in the northwest Gulf of Alaska is a continuous, westward flowing current, the Kenai Current, which exists from the Copper River/Prince William Sound area through Shelikof Strait. This feature is clearly defined in geopotential topography as a narrow (15- to 30-km) band whose mean salinity is generally 0.5 g/kg less than that of adjacent shelf

water. During October–November, when the integrated effect of precipitation, river discharge, and melt water attains a maximum, the mean salinity of coastal flow is about 1.5 g/kg less than that of the seaward shelf waters. At such times, baroclinic transport is about  $1.0 \times 10^6 \text{ m}^3/\text{sec}$ . Baroclinic transport at other times is reduced, but still indicates a substantial ( $\approx 0.3 \times 10^6 \text{ m}^3/\text{sec}$ ) westward flow. The magnitude of mean baroclinic transport ( $0.6 \times 10^6 \text{ m}^3/\text{sec}$ ) is about twice that observed over the Scotian shelf [Drinkwater et al., 1979] or in the Adriatic Sea [Hendershott and Rizzoli, 1976], where cross-shelf density gradients resulting from freshwater addition also appear to be the main driving mechanism.

The Kenai Current is driven by a cross-shelf pressure gradient whose baroclinic component responds to an annual freshwater flux. The barotropic pressure gradient component responds to seasonally varying wind stress; due to the characteristics of this forcing, however, the barotropic component augments flow only in winter. During winter, it may be of equal magnitude to the baroclinic gradient, but at other times it typically does not strengthen Kenai Current flow. Pressure gradients from oceanic currents do not seem to have a significant impact on the flow. This factor plays a major role in recent theories of coastal circulation, but our results suggest that "coastal dynamics" cannot be unified so simply. The Kenai Current has an uncommon driving mechanism, and its speeds and transports are unusually large, particularly during the fall maximum.

#### ACKNOWLEDGEMENTS

We thank all those who helped in field operations, data processing, drafting, typing, and editing; in particular, W. Parker, L. Long, J. Golly, P. Hutchens, and S. C. Dong. We also appreciate useful comments from and

discussions with R. D. Muench, G. Lagerloef, and R2D2. The complements of the NOAA ships DISCOVERER and SURVEYOR are thanked for their efforts in obtaining the data at sea. "This study was supported in part by the Bureau of Land Management through interagency agreement with the National Oceanic and Atmospheric Administration, under which a multi-year program responding to needs of petroleum development of the Alaskan continental shelf is managed by the Outer Continental Shelf Environmental Assessment Program (OCSEAP) office."

## REFERENCES

- Beardsley, R. C., and J. Hart, A simple theoretical model for the flow of an estuary onto a continental shelf, J. Geophys. Res., 83, 873-883, 1978.
- Beardsley, R. C., and C. D. Winant, On the mean circulation in the mid-Atlantic bight, J. Phys. Oceanogr., 9, 612-619, 1979.
- Charnell, R. L., and G. A. Krancus, A processing system for Aanderaa current meter data, NOAA Tech. Memo. ERL-PMEL 6, Nat. Oceanic and Atmos. Admin., Boulder, Colo., 1976.
- Csanady, G. T., Mean circulation in shallow seas, J. Geophys. Res., 81, 5389-5400, 1976.
- Csanady, G. T., The arrested topographic wave, J. Phys. Oceanogr., 8, 47-62, 1978.
- Dodimead, A.J., F. Favorite, and T. Hirano, Review of oceanography of the subarctic Pacific region, Bull. Int. N. Pac. Fish. Comm., 13 1-195, 1963.
- Drinkwater, K., B. Petrie, and W. H. Sutcliffe, Jr., Seasonal geostrophic transports along the Scotian shelf, Estuarine and Coastal Marine Sci., 9, 17-27, 1979.
- Favorite, F., A. J. Dodimead, and K. Nasu, Oceanography of the subarctic Pacific region, 1960-1972, Bull. Int. N. Pac. Fish. Comm., 33, 1-187, 1976.
- Favorite, F., and W. J. Ingraham, Jr., On flow in northwestern Gulf of Alaska, May 1972, J. Oceanogr. Soc. Japan, 33, 67-81, 1977.



- Fearnhead, P. G., On the formation of fronts by tidal mixing around the British Isles, Deep-Sea Res., 22, 311-322, 1975.
- Feely, R. A., and G. J. Massoth, Sources, compositions, and transport of suspended particulate matter in lower Cook Inlet and northwestern Shelikof Strait, Alaska, U.S. Geol. Survey Prof.Pap., (submitted), 1980.
- Hansen, D.V., OCSEAP Quarterly Report (1 April - 30 Sept 1978) for RU 217, available from OCSEAP Juneau Project Office, Juneau, Alaska, (unpublished manuscript), 1978.
- Hayes, S. P., and J. D. Schumacher, Description of wind, current, and bottom pressure variations on the continental shelf in the northeast Gulf of Alaska from February to May 1975, J. Geophys. Res., 81, 6411-6419, 1976.
- Hendershott, M. C., and P. Rizzoli, The winter circulation of the Adriatic Sea, Deep-Sea Res., 23, 353-370, 1976.
- Huyer, A., B. M. Hickey, J. D. Smith, R. L. Smith, and R. D. Pillsbury, Alongshore coherence at low frequencies in currents observed over the continental shelf off Oregon and Washington, J. Geophys. Res., 80, 3495-3505, 1975.
- Kundu, J., and J. S. Allen, Three dimensional structure of low frequency current fluctuations near the Oregon coast, J. Phys. Oceanogr., 6, 181-199, 1976.
- Mayer, D. A., D. V. Hansen, and D. A. Ortman, Long-term current and temperature observations on the Middle Atlantic Shelf, J. Geophys. Res., 84, 1776-1792, 1979.

- Muench, R. D., H. O. Mofjeld, and R. L. Charnell, Oceanographic conditions in Lower Cook Inlet: spring and summer 1973, J. Geophys. Res., 83, 5090-5098, 1978.
- NOAA National Climatic Center, Climatological data, national summary, January 1977-December 1977, Asheville, N.C., 1977.
- NOAA National Climatic Center, Climatological data, national summary, January 1977-December 1978, Asheville, N.C., 1978.
- Noble, M, and B. Butman, Low-frequency wind-induced sea level oscillations along the east coast of North America, J. Geophys. Res., 84, 3227-3236, 1979.
- Pietrafesa, L. J., and G. S. Janowitz, On the effects of buoyancy flux on continental shelf circulation, J. Phys. Oceanogr., 9, 911-918, 1979.
- Reed, R. K., Lagrangian measurement of recirculation in the Alaskan Stream, EOS Trans. Amer. Geophys. Un., 60, 290, 1979.
- Reed, R. K., The heat budget in the eastern Bering Sea, summer 1976, J. Geophys-Res., 83, 3635-3645, 1978.
- Reed, R. K., R. D. Muench, and J. D. Schumacher, On baroclinic transport of the Alaskan Stream near Kodiak Island, Deep-Sea Res., (in press), 1980.
- Roden, G. I., Winter circulation in the Gulf of Alaska, J. Geophys. Res., 74, 4523-4534, 1969.
- Royer, T. C., On the effects of precipitation and runoff on coastal circulation in the Gulf of Alaska, J. Phys. Oceanogr., 9, 785-801, 1979.
- Royer, T. C., D. V. Hansen, and D. J. Pashinski, Coastal flow in the northern Gulf of Alaska as observed by dynamic topography and satellite-tracked drogued drift buoys, J. Phys. Oceanogr., 9, 785-801, 1979.
- SAI, Kodiak interim synthesis report, Science Applications, Inc., Boulder, Colo., (unpublished report), 215 pp, 1979.

- Schumacher, J. D., R. Silcox, D. Dreves, and R. D. Muench, Winter circulation and hydrography over the continental shelf of the northwest Gulf of Alaska, NOAA Tech. Rep. ERL 404-PMEL 31, Nat. Oceanic and Atmos. Admin., Boulder, Colo., 1978.
- Schumacher, J. D., T. H. Kinder, D. Pashinski, and R. L. Charnell, A structure front over the continental shelf of the eastern Bering Sea, J. Phys. Oceanogr., 9, 79-87, 1979a.
- Schumacher, J. D., R. K. Reed, M. Grigsby, and D. Dreves, Circulation and hydrography near Kodiak Island, September to November 1977. NOAA Tech. Memo. ERL PMEL-13, Nat. Oceanic and Atmos. Admin., Seattle, Wash., 1979b.
- Semtner, A. J., and Y. Mintz, Numerical simulation of the Gulf Stream and mid-ocean eddies, J. Phys. Oceanogr., 7, 208-230, 1977.
- Smith, P. C., Low-frequency fluxes of momentum, heat, salt and nutrients at the edge of the Scotian shelf, J. Geophys. Res., 83, 4079-4096, 1978.
- Smith, R. L. A description of current, wind and sea level variations during coastal upwelling off the Oregon coast, July-August 1972, J. Geophys. Res., 79, 435-443, 1974.
- Thomson R. E., On the Alaskan Stream, J. Phys. Oceanogr., 2, 363-371, 1972.
- Winant, C.D., Coastal current observations, Rev. Geophys. Space Phys., 17, 89-98, 1979.

TABLE 1. - Dates of observations in the vicinity of Kodiak Island and Shelikof Strait used in this study.

---

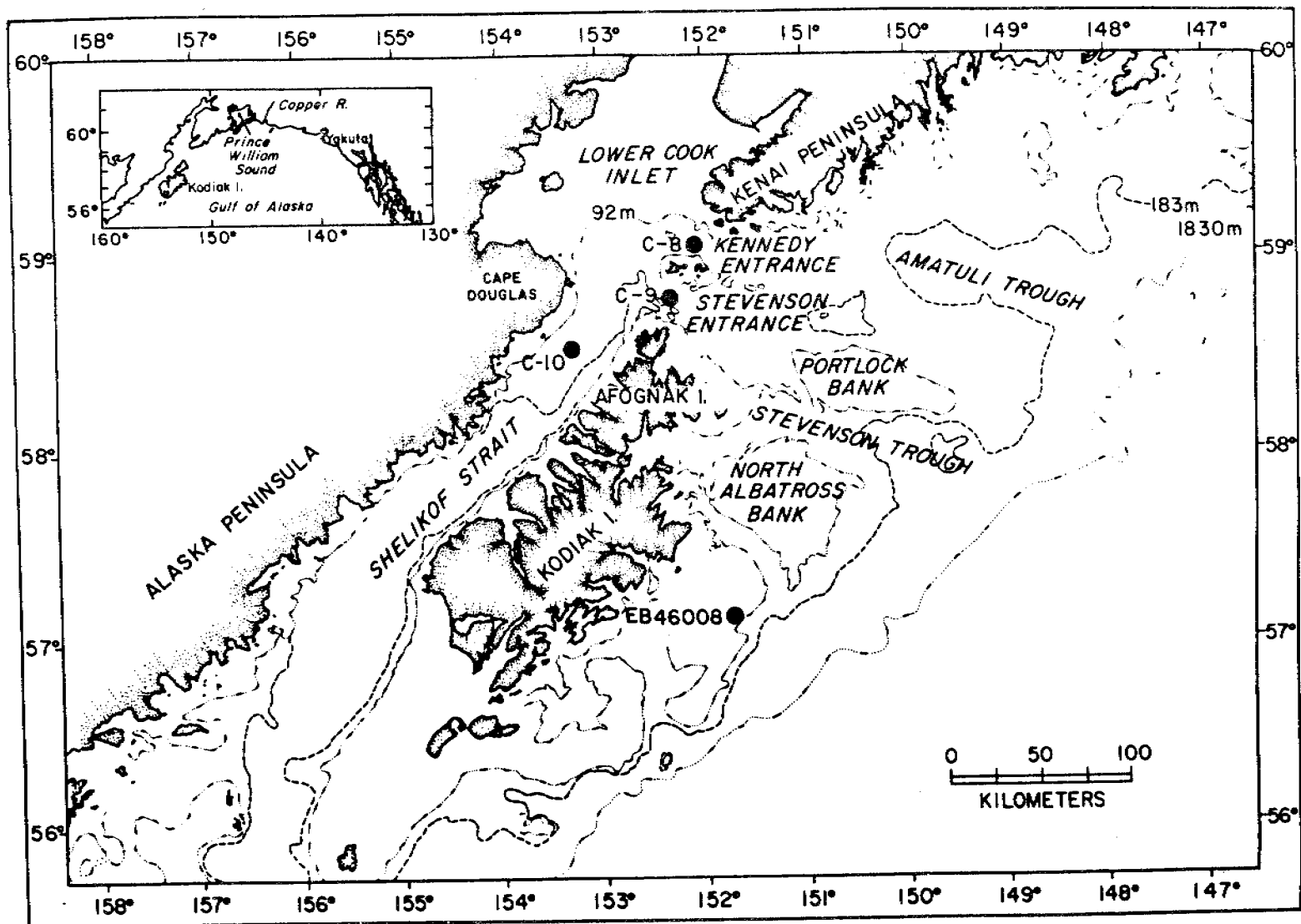
Date	Ship
2-10 March 1977	NOAA Ship DISCOVERER
5-11 September 1977	NOAA Ship SURVEYOR
13-22 October 1977	NOAA Ship DISCOVERER
4-17 March 1978	NOAA Ship SURVEYOR
6-24 March 1978	NOAA Ship DISCOVERER
26 May - 7 June 1978	NOAA Ship DISCOVERER
3-22 October 1978	NOAA Ship DISCOVERER

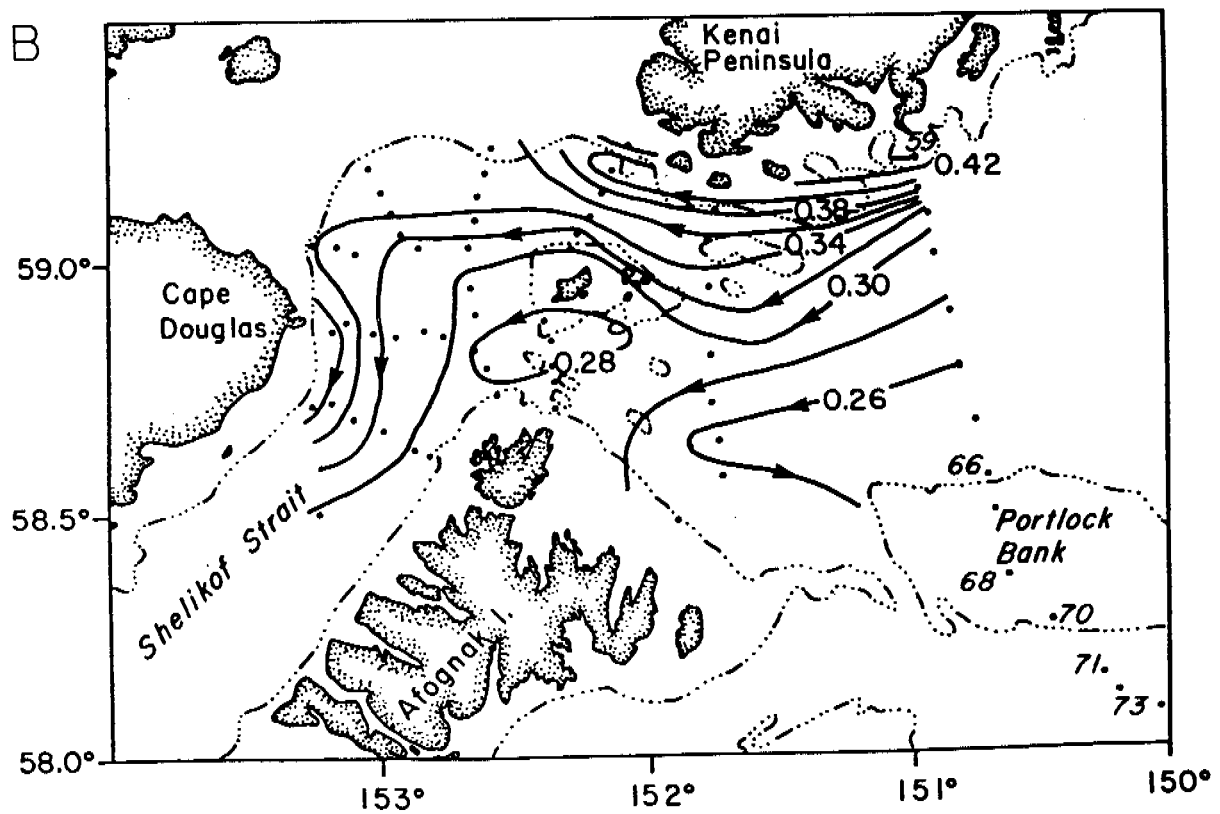
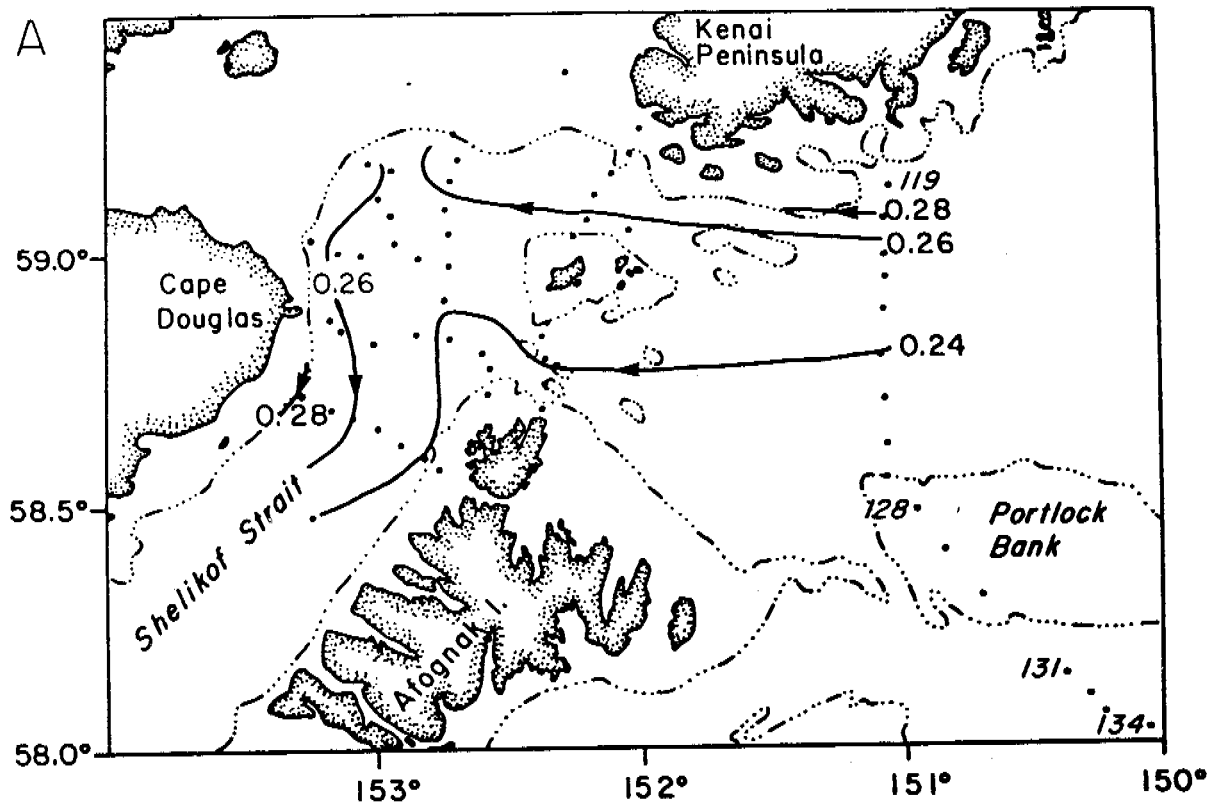
TABLE 3 - Variations in baroclinic volume transport and maximum surface speed of the westward coastal flow off the Kenai Peninsula.

Date	Volume Transport ( $10^6 \text{ m}^3/\text{sec}$ )	Maximum Speed (cm/sec)
March 4, 1977	0.4	15
September 10, 1977	0.4	30
October 19, 1977	1.0	89
March 6, 1978	0.3	14
May 29, 1978	0.1	13
October 10, 1978	1.2	133

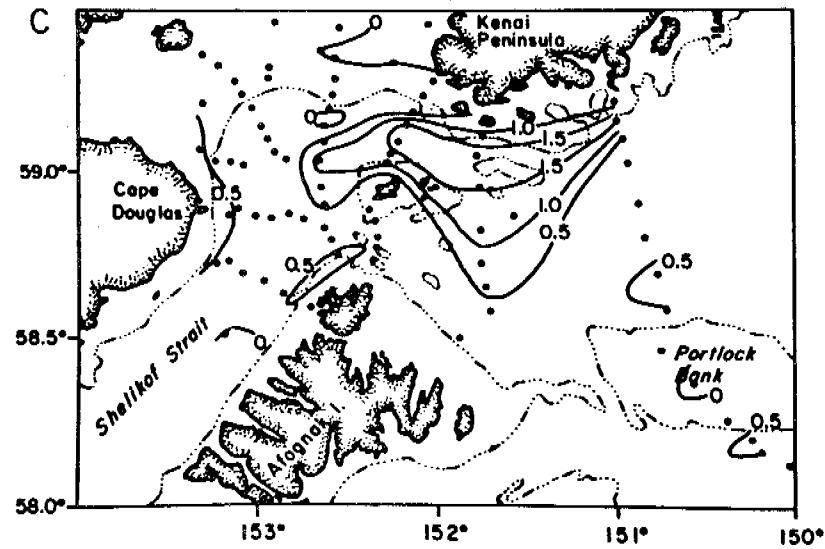
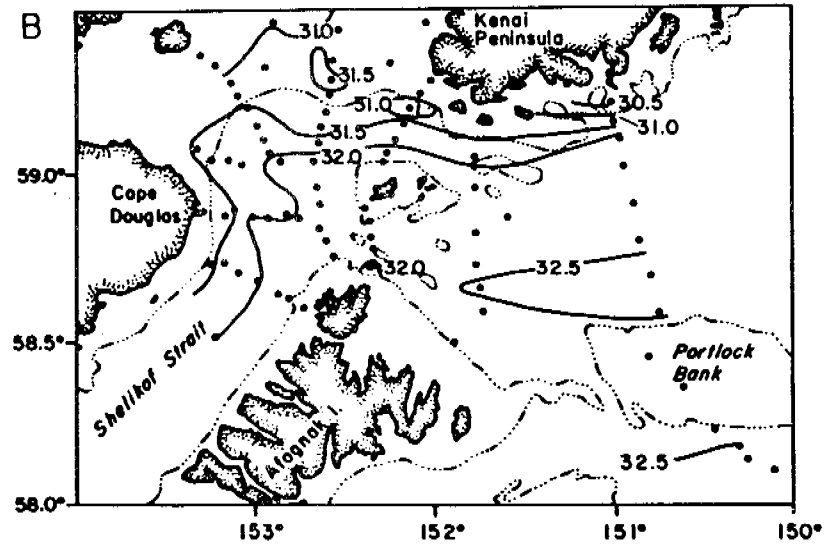
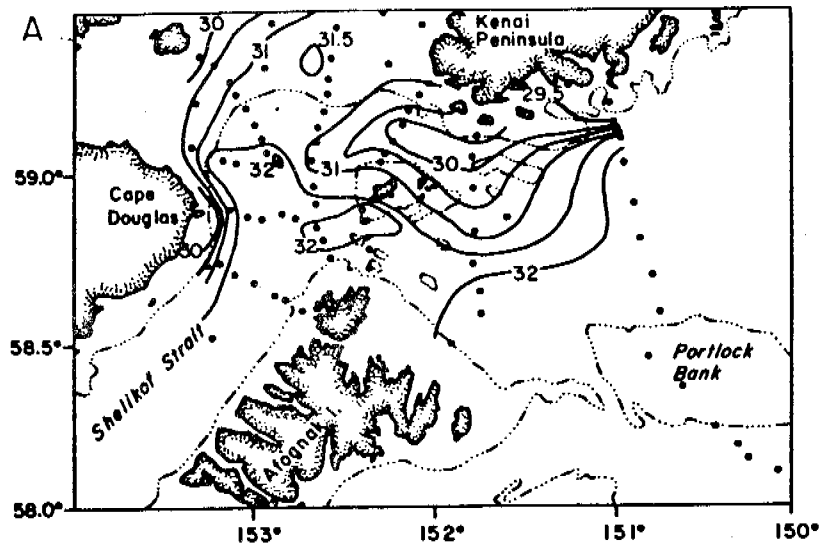
## FIGURES

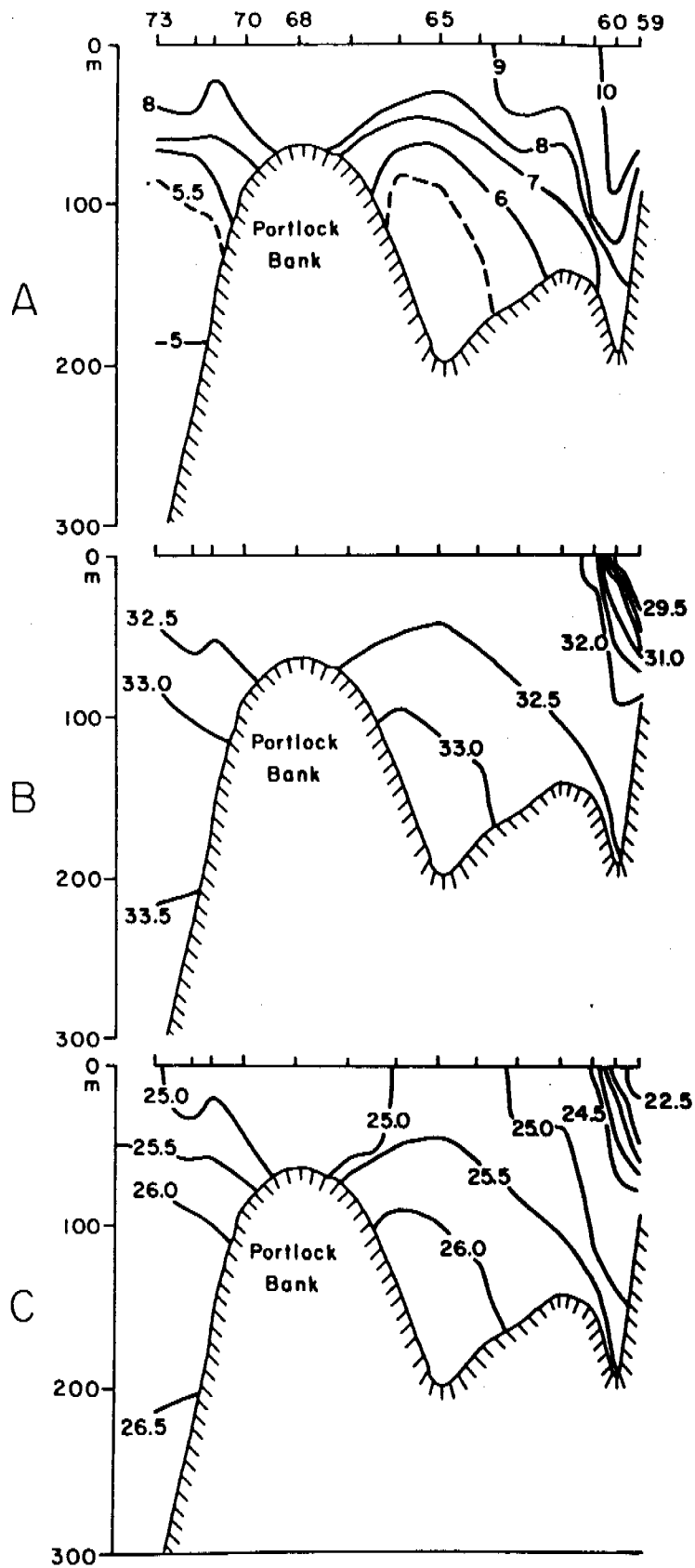
- Figure 1. Northwest Gulf of Alaska setting with prominent features and place names. The location of current meter stations and the NOAA data buoy are indicated.
- Figure 2. Geopotential topography (0/100 dbar, in dyn m) observed during A) 13-21 March 1978 and B) 9-22 October 1978. Some CTD station locations are shown in italics.
- Figure 3 Horizontal sections of A) Surface salinity (0.5 g/kg contour interval), B) salinity at 50 m (0.5 g/kg contour interval), and C) sigma-t difference between 50 m and the surface (0.5 sigma-t unit contour interval), 9-22 October 1978.
- Figure 4. Vertical sections of A) temperature in  $^{\circ}\text{C}$ , B) salinity in g/kg, and C) sigma-t, 10 October 1978.
- Figure 5. Vertical sections of A) temperature in  $^{\circ}\text{C}$ , B) salinity in g/kg, and C) sigma-t, 20 March 1978. Additional contours have been included to emphasize features.
- Figure 6. Observed averaged precipitation (cm) at Cordova, Seward, and Kodiak during 1977 and 1978 and the long-term mean.
- Figure 7. Seven-day averaged net current and wind stress from A) Shelikof Strait, B) EB 46008, and C) Kennedy and Stevenson entrances.

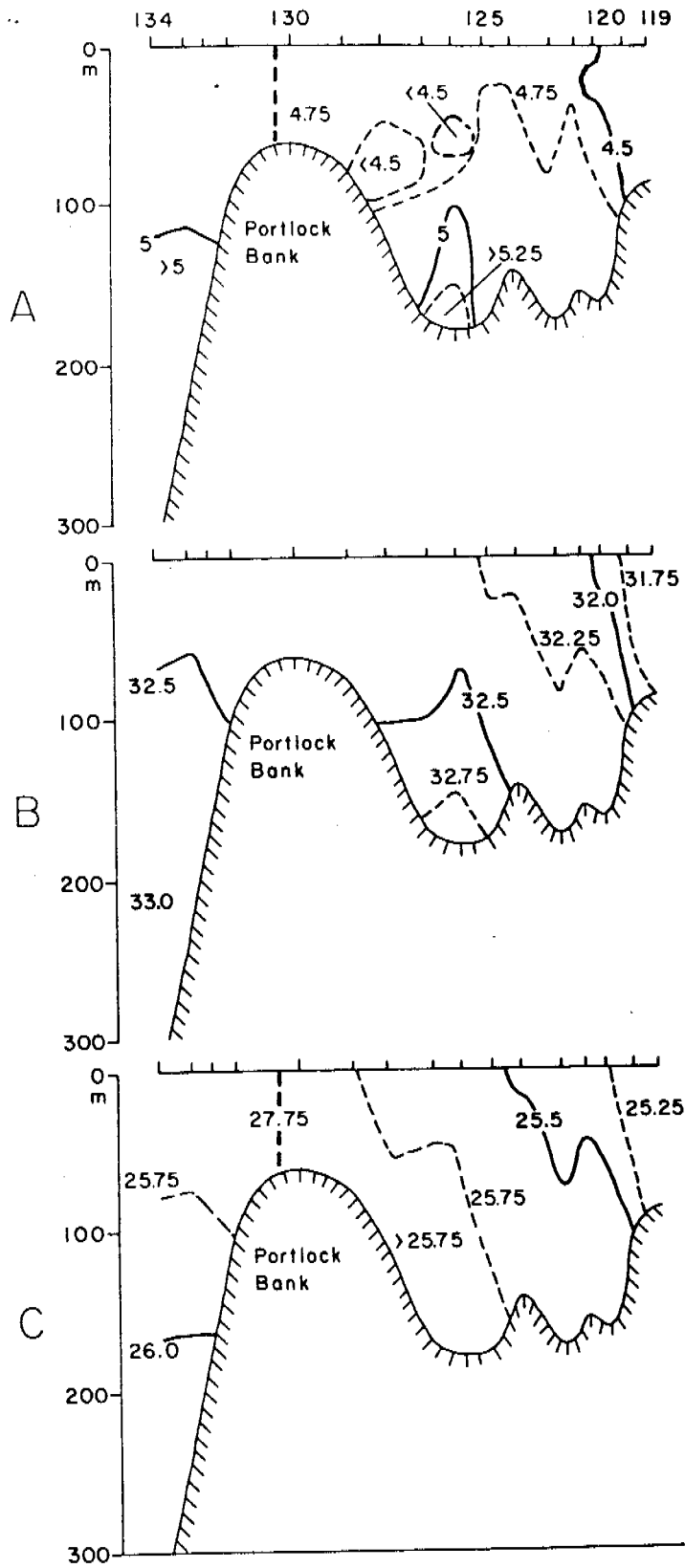


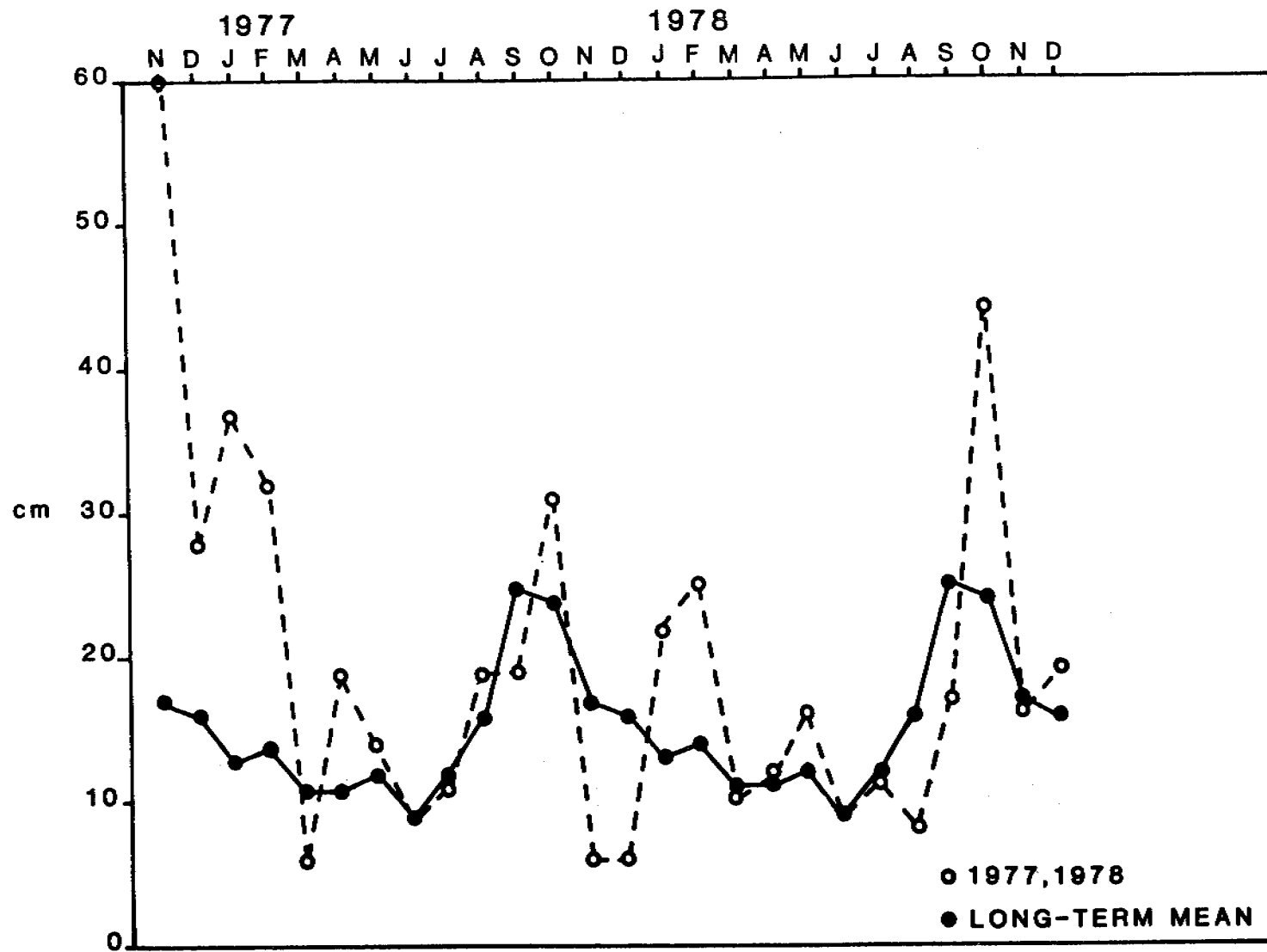


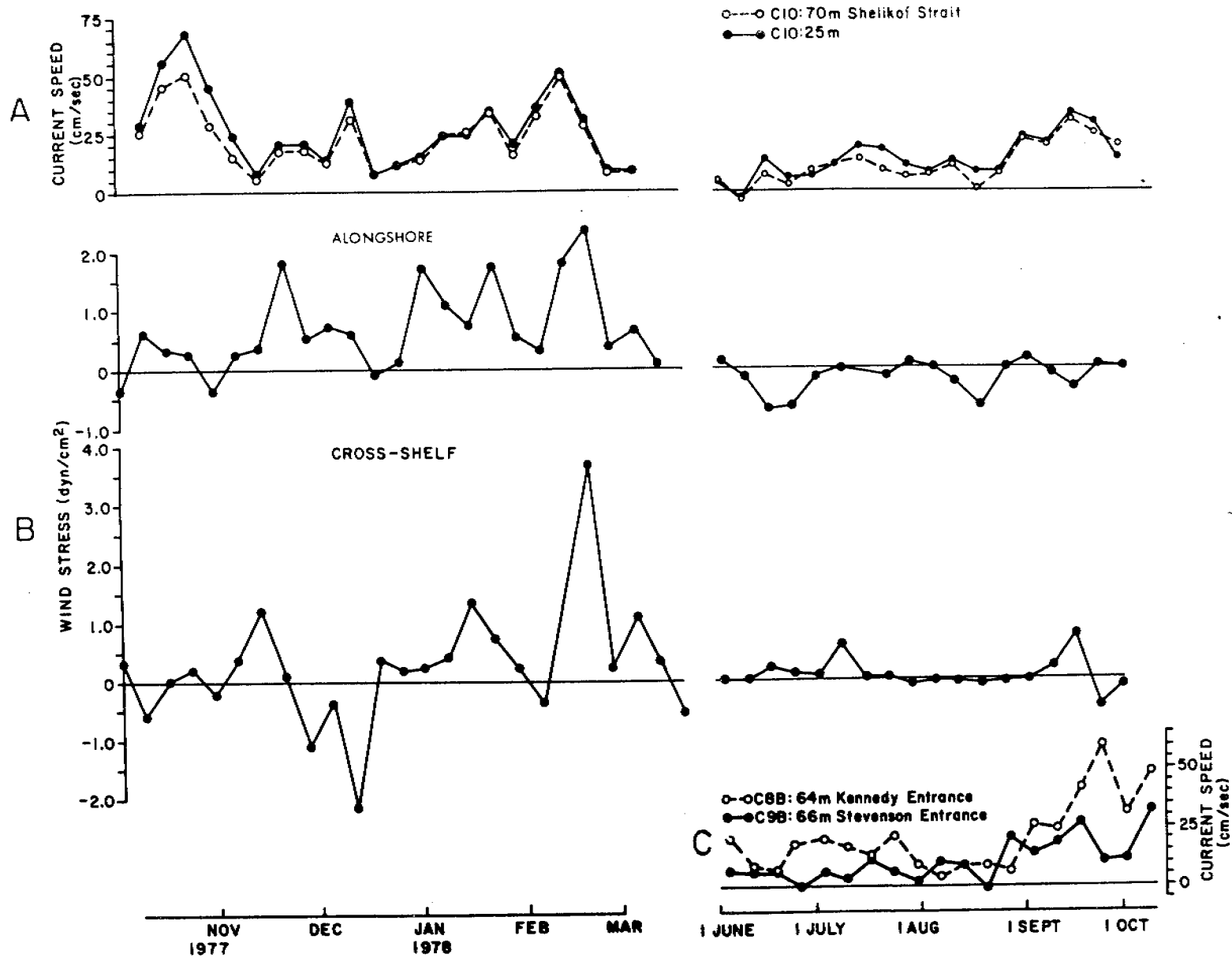












- F. The following manuscript has been accepted for publication in the J. Phys. Oceanogr., although this work was not funded by OCSEAP, it is relevant to our understanding of the Gulf of Alaska oceanography:

Direct Measurement of Recirculation in  
the Alaskan Stream

R. K. Reed

Pacific Marine Environmental Laboratory  
Environmental Research Laboratories  
National Oceanic and Atmospheric Administration  
Seattle, Washington 98105

\*Contribution No. 438 from the NOAA/ERL Marine Environmental Laboratory

## ABSTRACT

Three drifting buoys were deployed off Kodiak Island and tracked by satellite in summer 1978; all three veered out of the south-westward flowing Alaskan Stream and moved to the east and northeast around the Gulf of Alaska gyre. This is the first direct measurement of recirculation around the gyre, but the pattern is strikingly similar to what was inferred two-three decades ago from property distributions and has been predicted theoretically.

## 1. Introduction

The arcuate Gulf of Alaska coastline forces the northern boundary of the Pacific subarctic gyre into a westward outflow of water from the Gulf of Alaska. This narrow, deep, intense flow (the Alaskan Stream) appears to be continuous from the head of the Gulf to the western Aleutian Islands, but losses or gains of water across its southern boundary seem to occur (Favorite *et al.*, 1976). A loss of Stream water to the southeast is indicated frequently in the vicinity of 160°W (Favorite *et al.*, 1976); this water is presumably entrained into the eastward flowing Subarctic Current and recirculates around the Gulf of Alaska gyre. Most of the evidence for this type of circulation is based on physical property distributions, but theoretical studies also support such a pattern. Munk's (1950) pioneering study, for example, suggested southward outflows from the northern boundary of the subarctic gyre, and Thomson's (1972) model of the Alaskan Stream indicated one or more zones of eastward recirculation well east of the western portion of the subarctic gyre.

The salinity pattern in Figure 1 (summer 1959; Dodimead *et al.*, 1963) is suggestive of a southeastward recirculation of dilute Stream water near 160°W, but the data do not provide conclusive evidence that a significant part of the water column was actually flowing to the east in a quasi-steady manner. This note presents data from drogued, drifting buoys, however, which do indicate the existence of a large-scale recirculation around the Gulf of Alaska gyre that supports the classical concept of the flow regime.



## 2. Data and methods

Three drogued buoys were deployed off Kodiak Island in July 1978 as part of NOAA's Seasat-A verification project. The buoys were manufactured by the Polar Research Laboratories; they consisted of cylindrical aluminum spars with a flotation collar and ballast and "windowshade" drogues ( $\sim 2\text{m} \times 10\text{m}$ ) centered at a depth of about 20m. The buoy locations were determined by the Random Access Measurements System of the Nimbus 6 satellite, and they were provided by Sperry Support Services at NOAA's Data Buoy Office. Additional details on this system are contained in Royer et al. (1979). For about the first six weeks after deployment, several locations were obtained each day, but the number of fixes thereafter rapidly declined, mainly because the receiving stations were being used with a new satellite system. The drifters were equipped with tension devices to determine if the windowshade drogues were intact; the data received by the satellite could not be used unambiguously for this purpose, but it seems likely that the drogues remained intact during the trajectories and that the paths were not strongly affected by windage as indicated by the results of Kirwan et al. (1978). The location data were subjectively evaluated, and the resulting positions probably have reliabilities comparable to the rms position error ( $\sim 4$  km).

## 3. Drifter paths and circulation

Reed (1979) analyzed the July-August 1978 data from two of these drifters; mean daily positions were used, and some evidence was found

for changes in speed associated with inshore-offshore migrations near the Stream edge. The drifter paths, from deployment until the last positions were received, are shown in Figure 2. Representative positions are given rather than locations at fixed intervals; this was necessitated by the very irregular nature of the data received after August. All three drogued buoys moved southwest in the Alaskan Stream, all turned southeast, and they all moved northeast toward the Gulf of Alaska. Drifter numbers 400 and 561 moved in very similar paths until both buoys approached the head of the Gulf of Alaska, when number 561 became entrained in the coastal Kenai Current (Schumacher and Reed, 1980) but number 400 did not. Drifter number 753 was deployed between numbers 400 and 561; after early August, however, it moved inshore of the other two buoys and did not turn offshore until almost 500 km west of where they departed the continental slope. The eastward movement of number 753 was subsequently to the south of the other two drifters. Its more easterly course may have been affected by the smaller northward total wind-stress transport at this latitude than to the north near the other two drifters (wind-stress data provided by A. Bakun, National Marine Fisheries Service; see also Reed et al., 1980).

Table 1 compares the net speeds determined for various positions of the drifter tracks. (Southeast flow is the initial part of the recirculation, and northeast flow is presumably the movement of the Subarctic Current.) Speeds within the Alaskan Stream were greatest, except for the one drifter in the Kenai Current, and the southeast flow was slightly less than the northeast flow toward the Gulf. The net speed in the Kenai Current is similar to values in Royer et al.

(1979). Although flow perturbations are present, the large-scale movement during the period is quite orderly.

#### 4. Discussion

Maximum velocities in the Alaskan Stream (Favorite et al., 1976) are generally at least twice as great as the larger values here, so it is likely that the peak Stream speeds were inshore of where the drifters were deployed. We expect recirculation to occur on the southern side of the Stream, of course, as these data would suggest; the offshore movement though occurred in at least two distinct locations (near 158 and 166°W). Eastward velocities in the Subarctic Current are roughly twice those obtained from the geostrophic relation as was found by Kirwan et al. (1978), who attributed the differences largely to an Ekman component from the westerly winds. Unfortunately, there are not adequate data during these observations to map the large-scale geopotential topography for comparison with the observed flow.

Perhaps the most striking impression from Figure 2 is that the large-scale flow is quite smooth. The flow does not seem chaotic or disorganized, although there is evidence for some "events" (little movement during 22-30 September for example). These results provide additional evidence that Lagrangian methods can yield very useful descriptions of the flow field (see also Kirwan et al., 1978 and Grundlingh, 1978). It is difficult to envision how a large-scale feature such as recirculation in the Alaskan Stream could have been so unambiguously and easily determined from Eulerian data.

These are the first data to conclusively demonstrate recirculation around the Gulf of Alaska gyre. This modern method substantiates the early inferences about circulation based on property distributions (Dodimead et al., 1963), and it is heartening to see that these classical interpretations appear to be essentially correct.

Acknowledgments. Funding for this work was partially provided by NOAA's Seasat-A Project. D. J. Pashinski of PMEL prepared the drifting buoys for deployment. Various personnel at NOAA's Data Buoy Office gave assistance, and James Person of Sperry Support Services provided invaluable help in obtaining the position data. This presentation has benefited considerably from the ideas and comments of R. D. Muench of SAI/Northwest.

## REFERENCES

- Dodimead, A. J., F. Favorite and T. Hirano, 1963: Review of oceanography of the subarctic Pacific region. Int. N. Pac. Fish. Comm., Bull. 13, 1-195.
- Favorite, F., A. J. Dodimead and K. Nasu, 1976: Oceanography of the subarctic Pacific region, 1960-1971. Int. N. Pac. Fish. Comm., Bull. 33, 1-187.
- Grundlingh, M. L., 1978: Drift of a satellite-tracked buoy in the southern Agulhas Return Current. Deep-Sea Res., 25, 1209-1224.
- Kirwan, A. D., Jr., G. J. McNally, E. Reyna and W. L. Merrell, Jr., 1978: The near-surface circulation of the eastern North Pacific. J. Phys. Oceanogr., 8, 937-945.
- Munk, W. H., 1950: On the wind driven ocean circulation. J. Meteor., 8, 79-93.
- Reed, R. K., 1979: Lagrangian measurement of recirculation in the Alaskan Stream (abstract). Trans. Amer. Geophys. Union, 60, 290-291.
- Reed, R. K., R. D. Muench and J. D. Schumacher, 1980: On baroclinic transport of the Alaskan Stream near Kodiak Island. Deep-Sea Res. (in press).

Royer, T. C., D. V. Hansen and D. J. Pashinski, 1979: Coastal flow in the northern Gulf of Alaska as observed by dynamic topography and satellite-tracked drogued drift buoys. J. Phys. Oceanogr., 9, 785-801.

Schumacher, J. D. and R. K. Reed, 1980: Coastal flow in the northwest Gulf of Alaska: The Kenai Current. J. Geophys. Res. (submitted).

Thomson, R. E., 1972: On the Alaskan Stream, J. Phys. Oceanogr., 2, 363-371.

Table 1. Net speeds (cm/sec) during various portions of the drifter tracks, July 1978-January 1979.

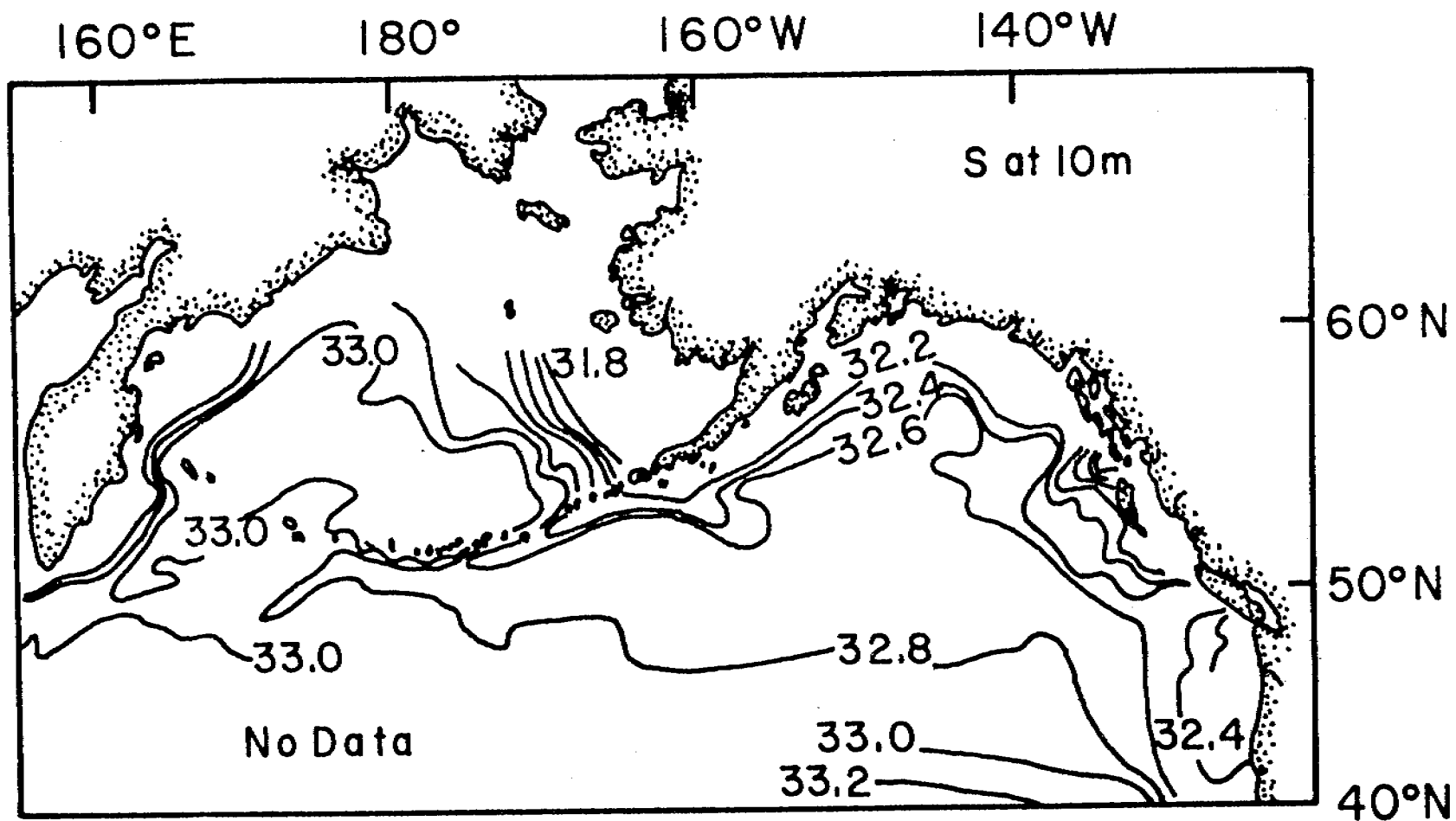
Drifter number	Alaskan Stream	Southeast flow	Northeast flow	Coastal (Kenai) Current
400	29	13	15	--
561	15	10	17	43
753	27	11	14	--

## LIST OF FIGURES

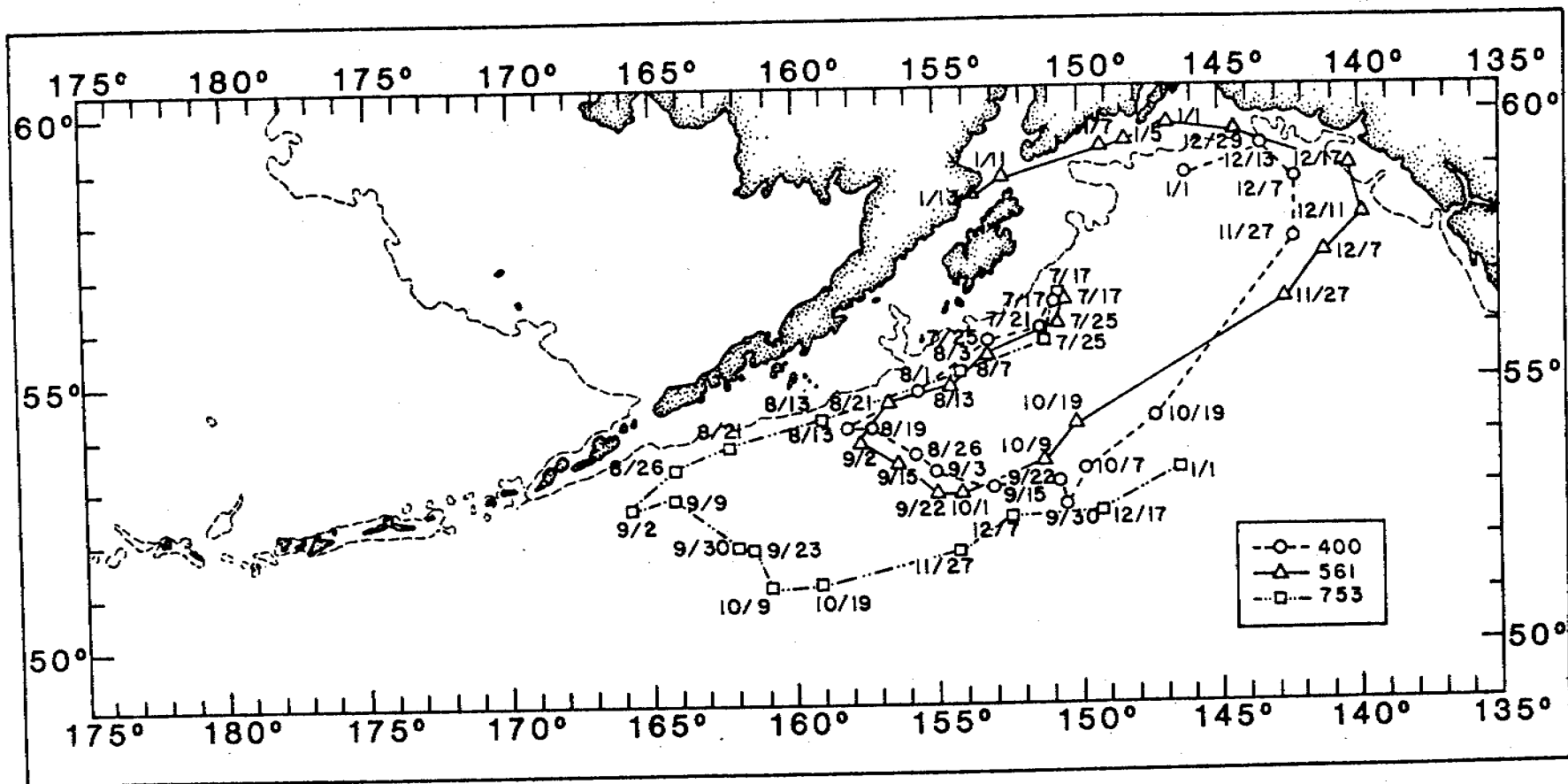
Figure 1. Horizontal distribution of salinity ( $^{\circ}/\text{oo}$ ) at 10 m during summer 1959, from Dodimead et al. (1963).

Figure 2. Paths of drogued drifting buoys (numbers 400, 561, and 753), 17 July 1978-13 January 1979. The dashed line on the map is the 100-fathom 183-m) isobath.





162



G. The following is from the Final Report: RU138 (Northwest Gulf of Alaska), and in amended form is to be published as an ERL/PMEL Technical Report.

PHYSICAL OCEANOGRAPHIC AND METEOROLOGICAL CONDITIONS  
IN THE NORTHWEST GULF OF ALASKA

Robin D. Muench<sup>1</sup>

James D. Schumacher<sup>2</sup>

Contributors:

C. A. Pearson

R. M. Reynolds

J. A. Galt

G. Watabayashi

C. Rauw

R. Overstreet

M. Pelto

<sup>1</sup>SAI/Northwest, 13400B Northrup Way #36, Bellevue, WA 98005

<sup>2</sup>NOAA/PMEL, 3711 - 15th Ave., NE, Seattle, WA 98105

## TABLE OF CONTENTS

### Preface

#### 1. INTRODUCTION

- 1.1 Statement of Purpose
- 1.2 Geographical Setting
- 1.3 History of Past Research
- 1.4 Oceanographic and Meteorological Setting

#### 2. OBSERVATIONAL PROGRAM

- 2.1 Program Rationale
- 2.2 Current Observation Program
  - 2.2.1 Taut-wire Moorings
  - 2.2.2 Drift Card Studies
  - 2.2.3 Satellite Tracked Buoys
  - 2.2.4 Wave Radar (CODAR) Observations
- 2.3 Temperature and Salinity Observations
- 2.4 Meteorological Observations

#### 3. RESULTS AND DISCUSSION

- 3.1 Mean Currents, Seasonal Variability and the Temperature, Salinity and Density Fields
  - 3.1.1 Introduction
  - 3.1.2 The General Northwestern Gulf Region
  - 3.1.3 The Kenai Current
  - 3.1.4 Shelikof Strait and Lower Cook Inlet
  - 3.1.5 The Bank and Trough Region
- 3.2 Behaviour of Low Frequency Current Fluctuations
  - 3.2.1 Introduction

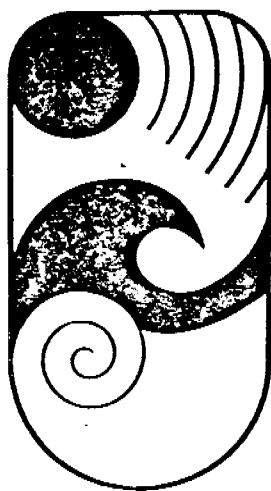
- 3.2.2 The Bank-Trough Region
- 3.2.3 Shelikof Strait
- 3.2.4 Lower Cook Inlet
- 3.3 Tidal Currents
- 3.4 Partitioning of Current Energy with Frequency
- 3.5 Wind Observations in Lower Cook Inlet
  - 3.5.1 Orographic Channeling
  - 3.5.2 Pressure Gradient Forcing
  - 3.5.3 Drainage Winds
  - 3.5.4 Wake Effects
  - 3.5.5 Summary
- 4. SUMMARY
- 5. ACKNOWLEDGEMENTS
- 6. REFERENCES
- 7. APPENDICES

H. Preliminary results from WIST experiment: The following is an initial abstract of National Research Council funded analysis and interpretation of OCSEAP data by J. Blaha.

From March to June 1977, currents were measured near the bottom at two sites off Icy Bay in depths of 55 and 108 m (10 and 25 km offshore). Simultaneous winds were measured at 2 environmental buoys, ~20 and ~50 km offshore. These data are being used to study the development of oceanic bottom boundary layers on the shelf and their importance to the wind-driven circulation, and to study the influence of bottom friction on the tides. The tidal currents are ~10 cm/sec in amplitude at the bottom and ~15 cm/sec above. Ekman veering at the 108 m mooring is toward the left looking downstream and from above; total veering is estimated to be  $18^{\circ}$ . Present estimates for bottom mixed layer thickness based on CTD data taken for this region are ~15 m leading to bottom friction estimates  $<.05$  dynes/cm<sup>2</sup>. Over 3-day periods wind stress at the surface is estimated to be at least an order of magnitude greater. The average veering at the shallow mooring, and the presence of bottom mixed layers in the Aanderaa temperature and conductivity data are still being determined. In addition, attempts are being made to apply a one dimensional, eddy viscosity model recently described by Long and Smith at the University of Washington.

The three following manuscripts, I., J. and K appear in:

# Second Working Conference On Oceanographic Data Systems Proceedings 1978



Editor:  
C.D. Tollios  
Assoc. Editor:  
M.K. McElroy

WOODS HOLE OCEANOGRAPHIC INSTITUTION

I.

## A ONE-PASS PROCESSING SYSTEM FOR AANDERAA

### CURRENT METER DATA\*

G. A. Krancus\*\*

C. A. Pearson\*\*

R. L. Charnell\*\*\*

#### Abstract

Several projects being conducted by the Pacific Marine Environmental Laboratory (PMEL) of NOAA involve the direct measurement of current using the Aanderaa RCM-4 current meter, equipped with conductivity, temperature, and pressure sensors. At present, PMEL has over 100 RCM-4's and obtains 300-400 months of current meter data per year. To cope with this volume of data, a system has been developed to rapidly process raw data and produce several routine products in one computer run.

A significant feature of this system is that a single program unpacks the data, converts it into scientific units, establishes a correct time base if possible, and produces a clean time series. This time-base check is accomplished by looking for a coded signal in certain channels (pressure, conductivity, etc.) after the data have been converted. If the time base is correct or can be reconciled, three other programs are executed in the same computer job to produce a summary printout, a filtered data set, and various plots. But if a time base can not be rectified, the program aborts and the data processor manually corrects the time base before restarting the system.

#### Introduction

The main objective of the PMEL Aanderaa current meter processing system is to minimize the human resources (time and expertise) normally required to process field measurements while maintaining high data quality. Because of a high current meter use rate, it is imperative that data from the field be examined rapidly to ensure proper operation prior to redeployment of the instruments. One result is that more man hours may be committed to scientific analysis instead of data processing.

The system is composed of a microprocessor-based transcriber and four computer programs. Processing consists of seven phases: 1) translation, 2) conversion of coded data to scientific units, 3) time base verification, 4) editing, 5) summarizing, 6) filtering, and 7) plotting. The programs, which accomplish all but the translation phase, are linked together by job control cards in such a way that they appear to be one large program. This is shown in Figure 1 together with all intermediate and final outputs.

\*Contribution number 379 from the NOAA/ERL Pacific Marine Environmental Laboratory.

\*\*National Ocean Survey, assigned to the Pacific Marine Environmental Laboratory.

\*\*\*Coastal Physics Group, Pacific Marine Environmental Laboratory.



FIGURE 1  
SYSTEM FLOW

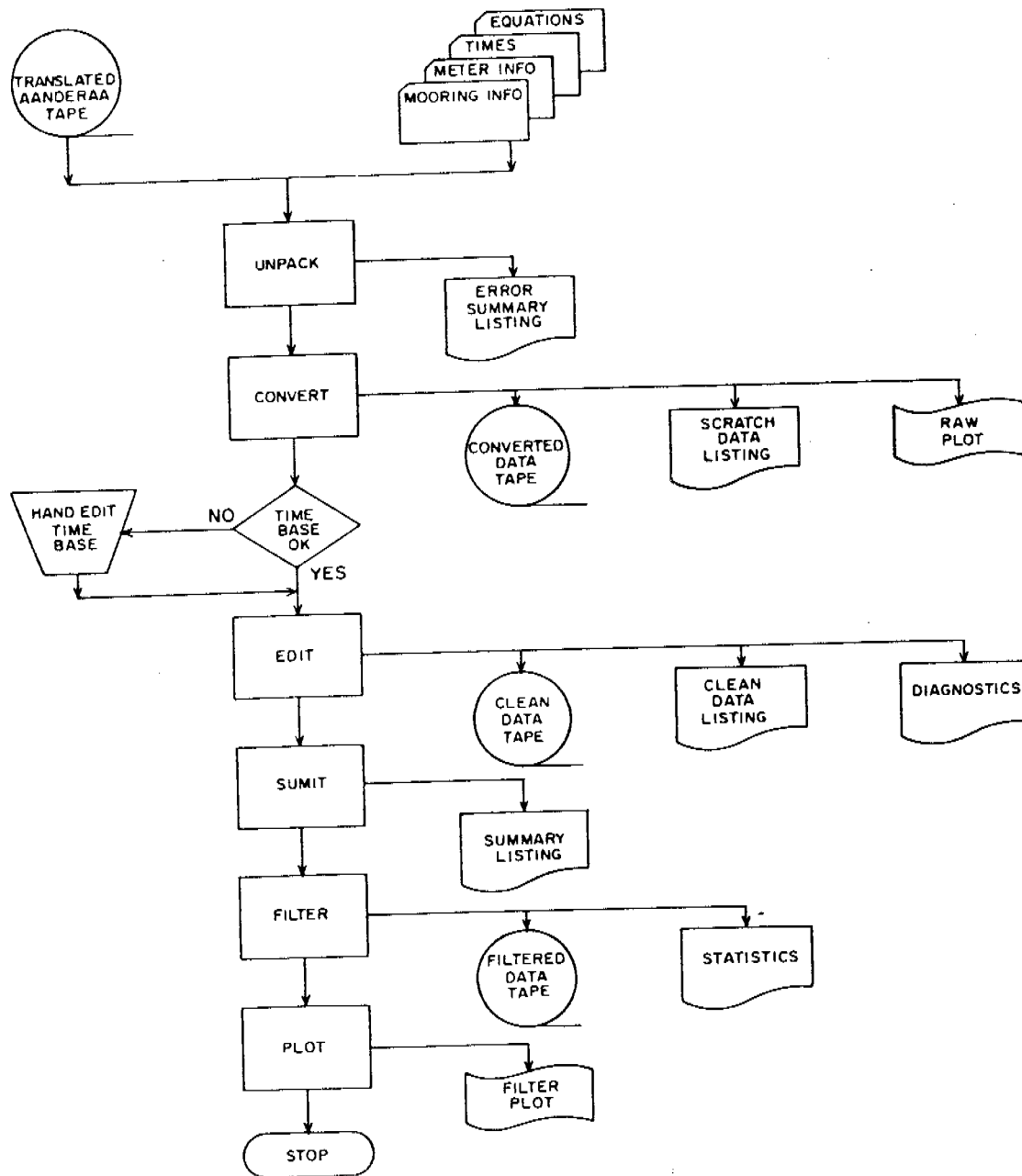


FIGURE 2  
 ERROR SUMMARY LISTING FROM UNPACK

ERROR LEGEND:

- A - MISSING REFERENCE WORD
- B - ZERO FILLED FRAM
- C - BIT COUNT ERROR
- D - MISSING SYNC BIT
- E - PULSE WIDTH ERROR(ND OP)
- F - WORD 6
- G - WORD 5
- H - WORD 4
- I - WORD 3
- J - WORD 2

RECORD	REF	TEMP	COND	PRESS	DIR	SPEED	ARCD EFGHIJ
106	699	689	509	56	245	0	10000011
192	698	777	9	177	244	0	1011000100
193	992	0	0	0	0	0	1000000000
507	698	236	500	783	426	925	100000110
508	698	236	490	104	418	427	1001000000
509	676	236	493	104	453	536	1000000000
512	698	236	489	105	434	38	1001000000
513	224	940	235	490	105	419	1101100001
514	880	0	0	0	0	0	1000000000
521	698	233	438	943	564	1	10000110
622	722	470	489	99	592	615	1011000001
673	992	0	0	0	0	0	1000000000
711	698	221	487	104	407	738	10000010
930	698	212	486	101	588	191	1001000000
931	992	297	485	101	589	237	10000001
1213	698	206	478	101	767	205	1011001000
1214	992	478	100	414	667	0	100001000
1276	698	216	480	105	361	719	10000000
1750	698	202	431	99	62	608	10000010
1821	698	181	470	1015	508	0	110001100
1948	698	173	477	105	634	603	1001000000
1949	224	375	478	105	780	555	1011000001
1950	32	0	0	0	0	0	100000000
2101	698	169	466	105	367	713	10000001
2123	698	180	468	106	436	629	10000000
2181	698	179	472	97	509	372	10000010
2182	693	174	464	97	561	282	10000000
2267	698	164	458	105	404	270	10000010
2382	698	154	462	99	199	144	10001000
2472	698	156	464	102	479	482	10001000
2640	698	154	464	106	362	698	10000000
2641	992	154	451	106	408	174	10000010
3020	698	130	457	104	491	606	10000001
3044	687	131	456	102	439	509	10000000
3066	698	131	922	104	511	182	10000010

3127 RECORDS PASSED  
 35 ARE BAD  
 4 WERE DELETED  
 0 PARITY ERRORS

## Translation

The current meter data tape translator was designed and built at PMEL (reference McLain, A Microprocessor-Based Transcriber, this volume). It is microprocessor controlled with 2K of Read-Only-Memory. It produces a 7-track medium density computer-compatible magnetic tape and a 6-channel strip chart used for early detection of current meter malfunction and evaluation of data quality.

The translator is programmed to make extensive use of the Aanderaa record structure. Every record should have 6 10-bit data words followed by a sync bit. The first data word is a reference word which is a unique number assigned to each meter. The PMEL translator is distinguishable from other translators in that it uses both the reference word and the sync bit to delineate data records.

Each 10-bit Aanderaa word is examined and expanded to 12 bits by inserting zeros in the 6th and 12th positions. When the sync bit is encountered, 6 words have been processed, or a reference word is found after a missing sync bit, the translator sets the 12th bit of the 6th word to 1 and encodes a 12-bit error word (with bits 6 and 12 set to 1) that is appended to the record. This error word, an essential part of the system, carries information about the record as a whole and each word in it (i.e. missing reference word, bit count not equal to 10, etc.), so that appropriate action may be taken to maintain both high data quality and a good time base.

## Data Unpacking and Conversion

The first computer function applied to the translated data is to remove the 6th and 12th bit put on by the translator to get back the original counts recorded by the RCM-4 or any diagnostics the translator may have encoded in the error word. Records that have errors are listed in the Error Summary Listing (Fig. 2). During this process, a record may be deleted if it fails to meet certain criteria determined by careful analysis of the outputs from several test runs. For example, a record in which the translator zero-filled all words except the reference word would appear in the Error Summary Listing followed by "deleted", but it would not be passed to the data conversion routine and hence would not be written on the Converted Data Tape. This is the most important action taken to reconstruct a good time base.

The next step in processing is the conversion of raw counts to scientific units. The program converts pressure, expressed in pounds per square inch, to decibars. Salinity is computed from conductivity, temperature, and the pressure entered on the first data card (the design depth). The salinity routine being used was developed by Crease and Sankey at IOS, Wormly, England. As individual records are converted, both the raw counts and the scientific units are printed on OUTPUT (Fig. 3). In addition, a plot is made of velocity components U and V, speed, direction, temperature, conductivity, pressure, and salinity versus record number (Fig. 4) to aid in quality control.

## Time-Base Verification and Recovery

The unique feature of this system is its ability to evaluate, verify, and reconcile a time base. This is done in the subroutine TBCHK which gives diagnostics on nine specific events. These are the first-in-water record, the first full on-bottom record, the last full on-bottom record, the first out-of-water record, 4 spin marks, and the last recorded record.

FIGURE 3

SCRATCH DATA LISTING FROM CONVERT

RECORD	U	V	SPEED	DIR	TEMP	COND	PRESS	SALIN	REF	TEMP	COND	PRESS	DIR	SPEED	MSPD	ABCDEFGHIJ	RECORD
241	.00	.00	.00	209.65	21.45	-21	.83	-21	93	1023	4	76	542	0	0	241	
242	.00	.00	.00	209.65	21.45	-21	.83	-21	93	1023	4	76	542	0	0	242	
243	.00	.00	.00	209.65	21.45	-21	.83	-21	93	1023	4	76	542	0	0	243	
244	.00	.00	.00	209.65	21.45	-29	.83	-25	93	1023	3	76	542	0	0	244	
245	.00	.00	.00	209.65	21.45	-21	.83	-21	93	1023	4	76	542	0	0	245	
246	.00	.00	.00	209.65	21.45	-21	.83	-21	93	1023	4	76	542	0	0	246	
247	.00	.00	.00	209.65	21.45	-29	.83	-25	93	1023	3	76	643	0	0	247	
248	.00	.00	.00	177.54	17.03	-29	.83	-27	93	848	3	76	643	0	0	248	
249	.00	.00	.00	176.50	17.03	-29	.83	-31	92	529	3	76	446	0	0	249	
250	12.64	-23.60	26.55	153.71	6.30	34.15	36.40	32.49	93	476	465	177	380	0	0	250	
251	9.91	20.68	22.94	25.61	7.89	34.37	70.39	33.11	93	450	468	177	9	0	0	251	
252	10.42	17.49	20.36	30.79	7.87	34.30	70.39	33.05	92	457	467	263	24	0	0	252	
253	8.54	14.54	16.86	30.44	7.92	34.30	70.39	33.01	92	459	467	263	23	0	0	253	
254	16.76	6.98	18.15	67.39	7.89	34.37	70.39	33.11	92	458	468	263	130	0	0	254	
255	7.93	11.21	13.74	35.28	7.87	34.30	70.39	33.05	92	457	467	263	37	0	0	255	
256	8.88	-5.10	10.24	119.87	7.94	34.37	70.39	33.07	92	460	468	263	282	0	0	256	
257	6.08	-7.51	9.50	140.25	7.96	34.37	70.39	33.04	92	461	468	263	341	0	0	257	
258	4.39	-9.76	10.70	155.79	7.98	34.37	70.02	33.02	92	462	468	262	386	0	0	258	
259	3.16	-12.80	13.18	166.14	8.10	34.44	70.02	32.95	92	467	469	262	416	0	0	259	
260	3.80	-16.24	16.68	166.84	8.14	34.44	70.02	32.91	92	471	469	261	455	0	0	260	
261	-1.54	-23.53	23.58	183.76	8.26	34.52	69.27	32.93	92	474	470	260	467	0	0	261	
262	-5.92	-24.82	25.51	193.42	8.28	34.44	68.90	32.90	92	479	471	259	495	0	0	262	
263	-11.29	-23.27	25.88	205.85	8.37	34.59	68.90	32.86	92	481	471	259	531	0	0	263	
264	-13.72	-23.77	27.44	210.00	8.41	34.59	68.90	32.86	92	484	472	259	546	0	0	264	
265	-16.43	-27.30	31.86	211.03	8.46	34.67	68.90	32.85	92	485	472	259	563	0	0	265	
266	-20.79	-27.68	34.62	216.90	8.51	34.67	68.90	32.85	92	486	472	259	589	0	0	266	
267	-24.89	-25.45	35.45	225.88	8.30	34.67	68.90	32.96	92	480	472	259	589	0	0	267	
268	-24.89	-25.45	35.45	225.88	8.39	34.67	68.90	32.96	92	480	472	259	589	0	0	268	
269	-26.13	-17.36	33.06	236.31	8.37	34.67	68.90	32.96	92	479	472	259	618	0	0	269	
270	-25.24	-17.09	30.48	235.90	8.37	34.67	68.90	32.98	92	479	472	259	618	0	0	270	
271	-25.07	-11.39	27.54	245.56	8.37	34.67	68.90	32.98	92	479	472	259	618	0	0	271	
272	-20.89	-10.74	23.49	242.80	8.39	34.67	68.90	32.96	92	480	472	259	618	0	0	272	
273	-19.46	-5.26	20.18	254.89	8.39	34.67	68.90	32.96	92	479	472	259	618	0	0	273	
274	-15.98	-1.33	16.04	265.25	8.37	34.67	69.27	32.98	92	479	472	259	618	0	0	274	
275	-16.64	-3.39	15.02	266.96	8.32	34.59	69.27	32.94	92	477	471	260	619	0	0	275	
276	-18.84	-11	14.84	270.43	8.23	34.59	69.27	33.03	92	473	471	260	619	0	0	276	
277	-15.41	-1.56	15.48	276.64	8.19	34.59	69.64	33.07	92	471	471	260	619	0	0	277	
278	-17.03	1.98	17.14	276.64	8.10	34.52	69.64	33.12	92	465	470	261	736	0	0	278	
279	-13.51	6.78	15.12	296.67	8.03	34.52	69.64	33.14	92	464	470	261	794	0	0	279	
280	-9.49	10.51	13.83	319.46	7.98	34.52	69.64	33.10	92	462	469	261	860	0	0	280	
281	-8.99	11.47	12.72	334.31	7.98	34.44	69.64	33.10	92	458	469	260	973	0	0	281	
282	-5.52	17.59	17.60	358.48	7.98	34.37	69.64	33.19	92	454	468	261	1013	0	0	282	
283	-4.47	12.44	12.45	1.58	7.94	34.44	69.64	33.14	92	460	469	261	1013	0	0	283	
284	1.34	10.63	10.88	12.29	7.94	34.44	69.64	33.14	92	467	469	261	60	0	0	284	
285	2.32	9.88	13.55	43.22	8.10	34.44	69.64	32.99	92	472	470	261	187	0	0	285	
286	9.28	9.88	12.72	87.07	8.21	34.52	69.64	32.85	92	474	469	261	212	0	0	286	
287	15.04	-1.50	15.12	95.70	8.26	34.44	69.64	33.17	92	455	468	261	842	0	0	287	
288	6.57	9.60	313.24	313.24	7.83	34.37	69.64	33.22	92	449	467	261	885	0	0	288	
289	-7.69	11.50	13.55	328.09	7.69	34.30	69.64	33.29	92	449	467	261	885	0	0	289	
290	-6.99	6.57	14.93	264.90	8.10	34.44	69.64	33.29	92	467	469	261	702	0	0	290	
291	-11.48	1.02	11.93	330.51	8.10	34.44	69.64	33.29	92	446	467	261	902	0	0	291	
292	-7.35	13.00	13.92	333.96	7.58	34.30	69.64	33.23	92	444	467	261	902	0	0	292	
293	-6.11	12.51	13.92	344.66	7.60	34.30	69.64	33.23	92	445	466	261	924	0	0	293	
294	-4.41	16.09	16.68	344.66	7.60	34.22	69.64	33.23	92	445	466	261	924	0	0	294	
295	-5.22	15.65	16.50	341.56	7.60	34.22	69.64	33.23	92	439	465	261	924	0	0	295	
296	-4.50	15.68	16.31	343.97	7.83	34.30	69.64	33.28	92	439	465	261	924	0	0	296	
297	-1.60	14.98	15.67	342.94	7.46	34.15	69.27	33.28	92	439	465	261	924	0	0	297	
298	-1.40	17.27	17.32	353.37	7.46	34.22	69.64	33.36	92	439	466	261	924	0	0	298	
299	-1.79	17.58	17.60	357.44	7.46	34.22	69.64	33.36	92	439	466	261	924	0	0	299	
300																300	

STATION-K7A  
PROJECT-KISS  
LATITUDE-57 03.40N  
LONGITUDE-152 18.00W  
DEPTH- 80.00 METERS

METER-1984  
DEPTH-70.0 METERS

FULL SPEED- 95.62 CM/SEC

RUN DATE-09/13/78  
VERSION- 78255

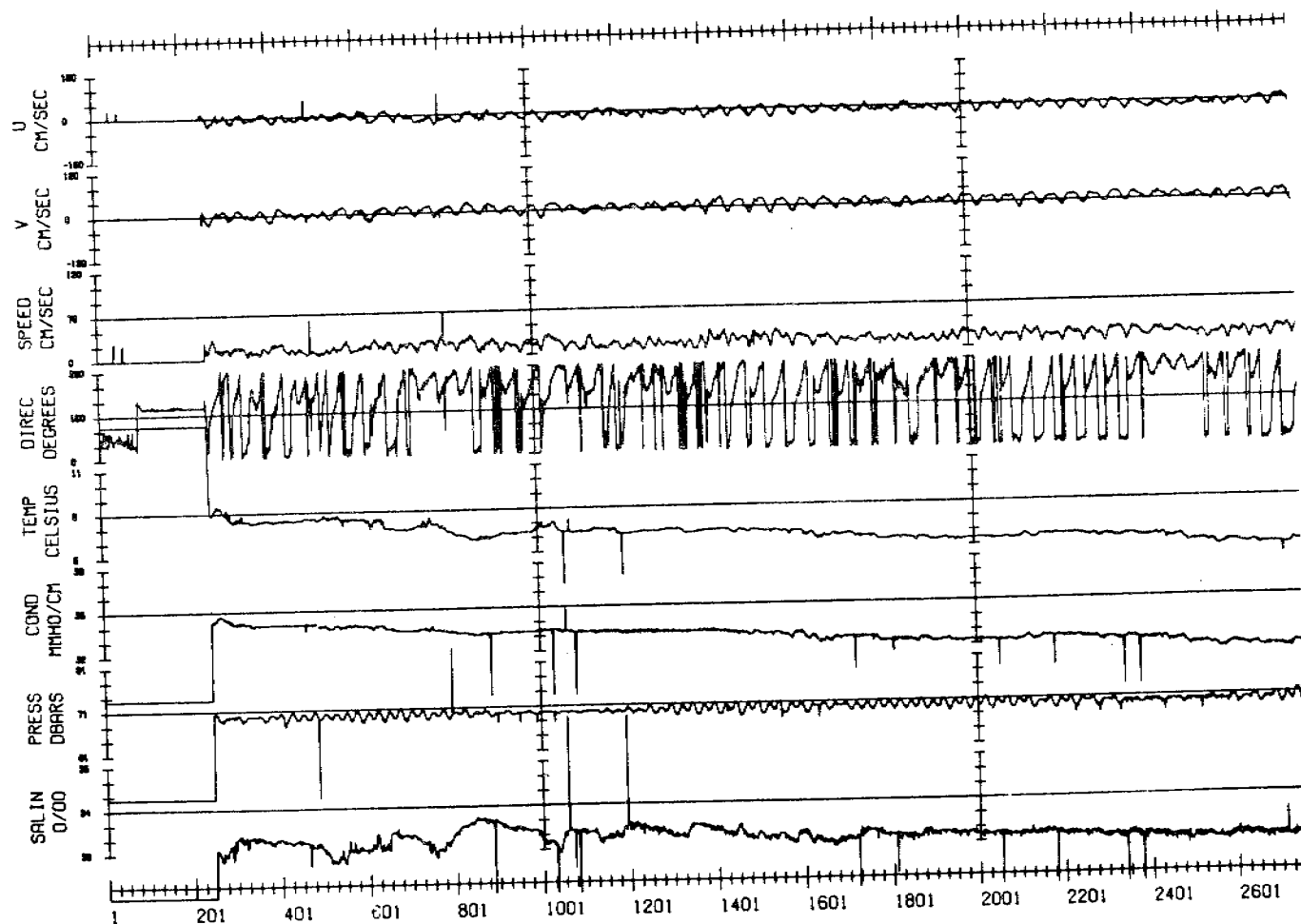


FIGURE 4  
SCRATCH DATA PLOT FROM CONVERT

FIGURE 5  
 TIME BASE DIAGNOSTICS FROM TBCHK

TIME BASE CHECK			
TOTAL	COMPUTED= 7176	ACTUAL= 7176	DIFFERENCE= 0
SPIN 1 (1536 287 77)	COMPUTED= 39	ACTUAL= 39	DIFFERENCE= 0
SPIN 2 ( 136 288 77)	COMPUTED= 59	ACTUAL= 59	DIFFERENCE= 0
IN ( 106 292 77)	COMPUTED= 250	ACTUAL= 250	DIFFERENCE= 0
FIRST 1 ( 206 292 77)	COMPUTED= 252	ACTUAL= 252	DIFFERENCE= 0
LAST 1 (1806 69 78)	COMPUTED= 7100	ACTUAL= 7100	DIFFERENCE= 0
OUT (1906 69 78)	COMPUTED= 7102	ACTUAL= 7102	DIFFERENCE= 0
SPIN 3 ( 606 70 78)	COMPUTED= 7124	ACTUAL= 7124	DIFFERENCE= 0
SPIN 4 ( 506 71 78)	COMPUTED= 7170	ACTUAL= 7170	DIFFERENCE= 0
IN-OUT	COMPUTED= 6853	ACTUAL= 6853	DIFFERENCE= 0
ON-OFF	COMPUTED= 6849	ACTUAL= 6849	DIFFERENCE= 0
FIRST RECORD IS	252	LAST RECORD IS	7100

The spin marks are spikes in the speed channel of at least 5 units entered manually by spinning the rotor. Two are put on before the meter is deployed and two after it is recovered.

For all events a computed record number is determined from the times fed into the program, and an attempt is made to locate the actual record by searching a difference array for predetermined jumps. The resultant diagnostics are printed on OUTPUT (Fig. 5) and used to assure that the decisions made by the program are correct.

The first test by TBCHK is a comparison of the total number of records processed versus the computed number. This is followed by a search for the first two predeployment spin marks. The next four tests are critical to establishing the time base, whereas the others are only informative. These four are the in-water, first full on-bottom, last full on-bottom, and out-of-water tests. To qualify as either an in- or out-of-water record, there must be a jump of 20 or more units in the conductivity channel. The first full on-bottom record must not vary by more than 1 pressure unit from the preceding record, which must show an increase in pressure of 2 units. To uniquely identify the last full on-bottom record, the sum of the pressure drops across the following two records must be greater than 10 pressure units with the first drop being at least 5 units. Finally, the last two spin marks entered after recovery of the meter are evaluated in the same way as the first two.

To verify the time base, TBCHK computes the elapsed time between the in- and out-of-water records, if they were found, and compares this with the real elapsed time. This process is repeated with the first and last full on-bottom records. As depicted in Figure 6, if the program found these last two events and the difference between the real and observed elapsed time is zero, the time base is considered "good" and TBCHK passes control to the editing routines.

If this test fails, a series of additional computations and comparisons are made to try to recover the time base. For example, if the program could not find the first full on-bottom record, an estimate is made using the observed in-water record and the computed number of records between the times of the in-water and full on-bottom records. Again the test is made to see if the new observed time interval is equal to the real elapsed time.

If TBCHK exits normally, it will pass the first and last good record numbers to the editing routine described in the next section. If it cannot accurately establish a time base the program is terminated and the converted data are saved. If the data processor can figure out the problem, then a very simple restart program is executed to correct the time base, which then passes control to the editing routines.

### Data Editing and Summary Listing

CMCLEAN is the subroutine that identifies and interpolates across erroneous points in the observed data. It operates on blocks of 1020 records checking all 6 data channels except direction. First it flags any values that fall outside of preselected ranges. Then the squared first difference series is computed for each channel and large jumps are flagged. If more than 3 "spikes" in a row are found, it is assumed that this jump is real and the flags are reset. Next, standard deviation is computed for the original and squared first difference series using only those points that are not flagged. A third pass is then made over both series, flagging those points that exceed 6 standard deviations from the

FIGURE 6  
TIME BASE VERIFICATION FLOW

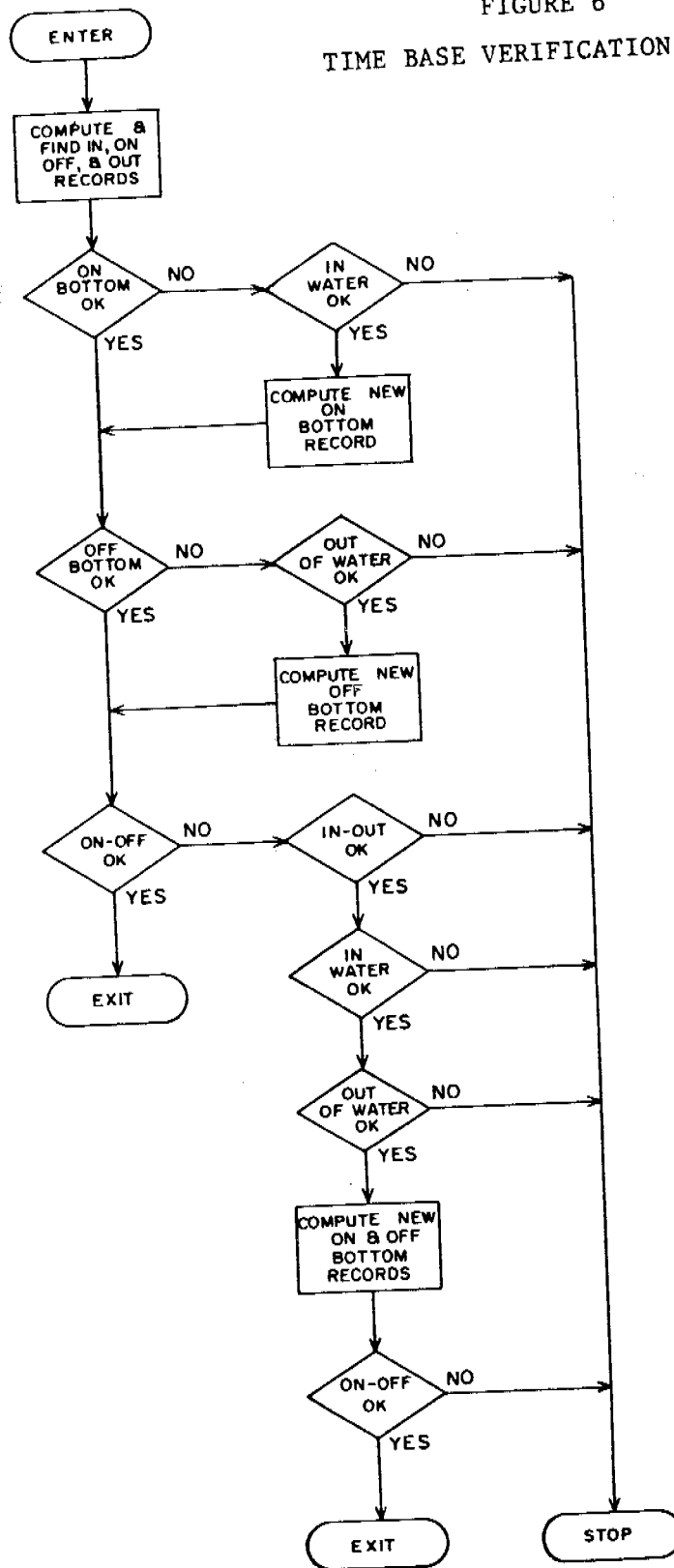




FIGURE 7  
EDITING DIAGNOSTICS FROM EDIT

CMCLEAN VERSION OF MAR 17, 78. (ADDS DLCLEAN)

CORRECTIONS FOR 1019 RECORDS STARTING AT 252

U LIMIT ERRORS = 1  
 U MEAN = -6.30  
 V LIMIT ERRORS = 0  
 V MEAN = 5.28  
 V MEAN TEST FOR MEAN = 1.32819E+02; FOR DIF = 1.23325E+03  
 SPEED LIMIT ERRORS = 1  
 SPEED MEAN = 16.67  
 SPEED MEAN TEST FOR MEAN = 1.44012E+02; FOR DIF = 3.32500E+02  
 TEMP LIMIT ERRORS = 2  
 TEMP MEAN = 6.87  
 TEMP MEAN TEST FOR MEAN = 1.11971E+02; FOR DIF = 1.13522E+03  
 CONDO LIMIT ERRORS = 5  
 CONDO MEAN = 33.63  
 CONDO MEAN TEST FOR MEAN = 4.48304E+00; FOR DIF = 2.44845E-01  
 PRES LIMIT ERRORS = 2  
 PRES MEAN = 69.55  
 PRES MEAN TEST FOR MEAN = 3.26711E+00; FOR DIF = 7.93475E-02  
 SALIN LIMIT ERRORS = 6  
 SALIN MEAN = 33.29  
 SALIN MEAN TEST FOR MEAN = 5.23486E+00; FOR DIF = 2.56125E+00  
 SALIN MEAN TEST FOR MEAN = 2.24878E+00; FOR DIF = 2.26530E-01

OLD/NEW=>	REC NO.	U	V	SPEED	TEMP	CONDO	PRES	SALIN
465	214	.00	.00	.00	.00	33.62	.00	32.69
490	239	59.99	-23.74	-7.82	64.52	9.78	.00	.00
629	378	16.00	-1.05	-1.11	-16.00	.00	.00	.00
797	546	73.48	-21.43	-15.97	10.48	23.86	.00	.00
889	638	.00	.00	.00	.00	.00	.00	.00
902	651	.00	.00	.00	.00	.00	.00	.00
953	702	.00	.00	.00	.00	.00	.00	.00
991	740	.00	.00	.00	.00	.00	.00	.00
1031	780	.00	.00	.00	.00	.00	.00	.00
1060	809	.00	.00	.00	.00	.00	.00	.00
1073	822	.00	.00	.00	.00	.00	.00	.00
1083	832	.00	.00	.00	.00	.00	.00	.00
1084	833	.00	.00	.00	.00	.00	.00	.00
1195	944	.00	.00	.00	.00	.00	.00	.00

CORRECTIONS FOR 1019 RECORDS STARTING AT 1252

U LIMIT ERRORS = 0  
 U MEAN = -6.38  
 V LIMIT ERRORS = 0  
 V MEAN = 7.53  
 V MEAN TEST FOR MEAN = 1.28709E+02; FOR DIF = 1.94551E+02  
 SPEED LIMIT ERRORS = 0  
 SPEED MEAN = 17.59  
 SPEED MEAN TEST FOR MEAN = 1.46110E+02; FOR DIF = 2.28491E+02  
 TEMP LIMIT ERRORS = 0  
 TEMP MEAN = 5.81  
 TEMP MEAN TEST FOR MEAN = 1.08338E+02; FOR DIF = 2.19301E+02  
 CONDO LIMIT ERRORS = 3  
 CONDO MEAN = 32.64  
 CONDO MEAN TEST FOR MEAN = 3.12376E+00; FOR DIF = 2.09643E-02  
 PRES LIMIT ERRORS = 0  
 PRES MEAN = 69.83  
 PRES MEAN TEST FOR MEAN = 6.41872E+00; FOR DIF = 1.76256E-01  
 SALIN LIMIT ERRORS = 3  
 SALIN MEAN = 33.22  
 SALIN MEAN TEST FOR MEAN = 1.65297E+00; FOR DIF = 2.22437E-01

OLD/NEW=>	REC NO.	U	V	SPEED	TEMP	CONDO	PRES	SALIN
1509	1258	-5.83	-23.64	-5.52	-22.44	8.03	32.60	.00
1551	1300	.00	.00	.00	.00	.00	.00	.00
1636	1385	.00	.00	.00	.00	.00	.00	.00
1722	1471	.00	.00	.00	.00	.00	.00	.00
1766	1535	-6.75	-3.68	-9.34	10.03	.00	.00	.00
1810	1559	.00	.00	.00	.00	.00	.00	.00
2033	1802	.00	.00	.00	.00	.00	.00	.00
2181	1930	.00	.00	.00	.00	.00	.00	.00

FIGURE 8  
CLEAN DATA PRINTOUT FROM EDIT

REC. NO.	DATE	TIME	U-VEL. CM/SFC	V-VEL. CM/SEC	SPEED CM/SEC	COMPASS DEGREES	TEMP DEG.C	PPFS DRARS	CMND. MMD/FCM	SALINITY (PPT)
1	19 OCT 77	0206	10.421	-17.491	20.360	30.787	7.871	70.388	34.294	33.050
2	19 OCT 77	0236	6.544	14.539	16.864	30.442	7.916	70.388	34.296	33.007
3	19 OCT 77	0306	16.757	6.979	18.152	67.389	7.893	70.388	34.370	33.108
4	19 OCT 77	0336	7.933	11.214	13.736	35.276	7.871	70.388	34.296	33.050
5	19 OCT 77	0406	8.870	-5.101	10.250	119.875	7.939	70.388	34.370	33.065
6	19 OCT 77	0436	6.078	-7.307	9.504	140.247	7.961	70.388	34.370	33.044
7	19 OCT 77	0506	4.389	-9.759	10.700	155.786	7.984	70.016	34.370	33.022
8	19 OCT 77	0536	3.157	-12.600	13.184	166.145	8.097	70.016	34.445	32.995
9	19 OCT 77	0606	3.799	-16.262	16.880	166.835	8.142	70.016	34.445	32.952
10	19 OCT 77	0636	1.122	-17.988	17.968	179.611	8.188	69.644	34.445	32.910
11	19 OCT 77	0706	-1.544	-23.529	23.580	183.755	8.256	69.272	34.519	32.925
12	19 OCT 77	0736	-5.923	-24.815	25.512	193.423	8.278	66.900	34.445	32.825
13	19 OCT 77	0806	-11.286	-23.290	25.880	205.854	8.369	66.900	34.594	32.698
14	19 OCT 77	0836	-13.721	-23.768	27.444	209.998	8.415	68.900	34.594	32.656
15	19 OCT 77	0906	-16.425	-27.300	31.800	211.034	8.483	68.900	34.668	32.871
16	19 OCT 77	0936	-20.788	-27.684	34.620	216.904	8.505	68.900	34.668	32.850
17	19 OCT 77	1006	-25.448	-24.677	35.448	225.882	8.301	68.000	34.668	33.041
18	19 OCT 77	1036	-24.880	-22.447	33.516	227.953	8.392	68.900	34.668	32.956
19	19 OCT 77	1106	-28.128	-17.364	33.056	238.312	8.392	68.900	34.668	32.956
20	19 OCT 77	1136	-25.238	-17.090	30.480	235.895	8.369	68.528	34.668	32.977
21	19 OCT 77	1206	-25.069	-11.391	27.536	245.564	8.369	68.900	34.668	32.977
22	19 OCT 77	1236	-20.891	-10.736	23.488	242.801	8.369	68.900	34.668	32.956
23	19 OCT 77	1306	-19.478	-5.260	20.176	258.887	8.392	68.900	34.668	32.977
24	19 OCT 77	1336	-15.981	-1.329	16.036	265.246	8.369	69.272	34.594	32.940
25	19 OCT 77	1406	-14.636	-3.390	15.024	256.959	8.324	69.272	34.594	32.940
26	19 OCT 77	1436	-14.840	1.110	14.840	270.625	8.233	69.272	34.594	33.026
27	19 OCT 77	1506	-15.405	-1.562	15.484	264.210	8.188	69.644	34.594	33.068
28	19 OCT 77	1536	-17.025	1.982	17.140	276.641	8.097	69.644	34.519	33.074
29	19 OCT 77	1606	-13.508	6.784	15.116	296.668	8.052	69.644	34.519	33.117
30	19 OCT 77	1636	-9.489	8.198	12.540	310.825	8.029	69.644	34.519	33.139
31	19 OCT 77	1706	-8.968	10.508	13.828	319.458	7.984	69.644	34.519	33.191
32	19 OCT 77	1736	-5.517	11.466	12.724	334.306	7.984	69.644	34.445	33.102
33	19 OCT 77	1806	-4.468	17.594	17.600	358.677	7.893	69.272	34.445	33.182
34	19 OCT 77	1836	3.344	12.443	12.448	1.295	7.803	69.644	34.370	33.184
35	19 OCT 77	1906	2.317	10.635	10.884	12.289	7.939	69.644	34.445	33.145
36	19 OCT 77	1936	9.280	9.876	13.552	43.218	8.037	60.644	34.519	32.995
37	19 OCT 77	2006	12.707	6.50	12.774	87.071	8.210	69.644	34.519	32.968
38	19 OCT 77	2036	15.041	-1.502	15.116	95.704	8.256	69.644	34.445	32.846
39	19 OCT 77	2066	-6.990	6.574	9.596	313.243	7.826	69.644	34.370	33.172
40	19 OCT 77	2136	-7.183	11.504	13.552	378.090	7.690	60.644	34.296	33.222
41	19 OCT 77	2206	-11.482	-1.025	11.528	264.901	8.097	69.644	34.445	32.995
42	19 OCT 77	2236	-7.351	12.997	14.932	330.508	7.622	69.644	34.296	33.286
43	19 OCT 77	2306	-6.111	12.507	13.920	333.961	7.577	69.644	34.296	33.330
44	19 OCT 77	2336	-5.219	16.086	16.680	364.665	7.599	69.644	34.221	33.228
45	20 OCT 77	0006	-4.503	15.678	16.496	341.557	7.599	69.644	34.221	33.228
46	20 OCT 77	0036	-4.597	14.978	16.312	343.974	7.826	69.644	34.296	33.277
47	20 OCT 77	0106	-1.399	17.267	17.324	355.369	7.464	69.644	34.221	33.358
48	20 OCT 77	0136	-0.786	17.582	17.600	357.641	7.464	69.644	34.221	33.358
49	20 OCT 77	0206	-2.634	17.043	17.416	348.118	7.374	69.644	34.146	33.364
50	20 OCT 77	0236	-3.586	17.774	17.968	351.571	7.351	70.016	34.146	33.385
51	20 OCT 77	0306	0.767	16.754	16.772	2.620	7.328	68.644	34.146	33.407
52	20 OCT 77	0336	7.077	15.127	16.680	24.917	7.328	68.644	34.146	33.407
53	20 OCT 77	0406	8.174	10.578	13.568	37.693	7.328	69.644	34.144	33.298
54	20 OCT 77	0436	10.653	5.696	12.080	61.864	7.441	70.016	34.146	33.336
55	20 OCT 77	0506	9.673	-1.440	9.780	98.466	7.441	70.016	34.146	33.298
56	20 OCT 77	0536	7.735	-4.506	8.952	120.720	7.441	70.016	34.146	33.306
57	20 OCT 77	0606	1.468	7.616	7.756	10.908	7.328	70.016	34.146	33.407
58	20 OCT 77	0636	1.564	-8.343	8.492	169.252	7.351	70.016	34.146	33.385
59	20 OCT 77	0706	0.511	-11.885	11.896	177.540	7.374	69.644	34.146	33.364

mean. Up to this point no corrections have been made, only flags have been set. If more than 400 values in any channel are flagged, editing for that parameter is aborted and processing on the next parameter begins.

CMCLEAN then makes a fourth pass checking for combinations of flags. For example, if conductivity and temperature are flagged but salinity is not, then the flags are turned off, since spikes in both of these channels imply a real temperature variation. Similarly U, V, and speed are reviewed and changes to the flags are made to ensure continuity in all channels including direction. Hence, direction is edited indirectly. Finally, the last pass is made and the flagged values are corrected by doing a straight line interpolation between adjacent values, computing new salinities when necessary.

When editing has been completed on a block of data (1020 records), CMCLEAN keeps the last 20 of these records and gets the next 1000 records. Hence a 20-record overlap exists between the blocks of data to ensure continuity in the editing. During this process, information about the criteria used in editing and which values were changed is printed on OUTPUT (Fig. 7). In addition, the clean time series is written on both a mass storage device and OUTPUT (Fig. 8).

The clean data set is then passed to a program called SUMIT. This produces a listing that is a short, concise summary of the data (Fig. 9). Hourly, daily, and 7-day mean values are given for temperature, salinity, and density plus the vector-averaged speed and direction. In addition daily and 7-day mean speed and depth are computed and displayed.

### Filtering and Spectra

The filter program, FILTR, runs the data through 2 separate filters, calculates total spectral energy, and determines extrema of the U and V excursions for a Progressive Vector Diagram (PVD). Two separate two-sided Lanczos filters are used on the data. The first is a low-pass filter designed to remove high-frequency noise with a half-amplitude response at a period of 2.86 hrs; less than 0.1% of the amplitude is passed at periods of 2 hrs and more than 99% of the amplitude is passed at periods greater than 5 hrs (see Fig. 10). U, V, temperature, pressure, and salinity are all passed through this filter, which resamples the data set once per hour with 4-hr starting and stopping transients removed from each end.

A second filter, applied only to the U and V components, removes most of the tidal energy with a half-amplitude response at a period of 35 hrs with 0.1% of the amplitude being passed at periods of 25 hrs while 99% is passed at periods of 55 hrs (see Fig. 10). The resultant time series is resampled at a 6-hr interval with 60-hr starting and stopping transients removed from each end. The output from each filter is copied to tape and saved for subsequent analyses.

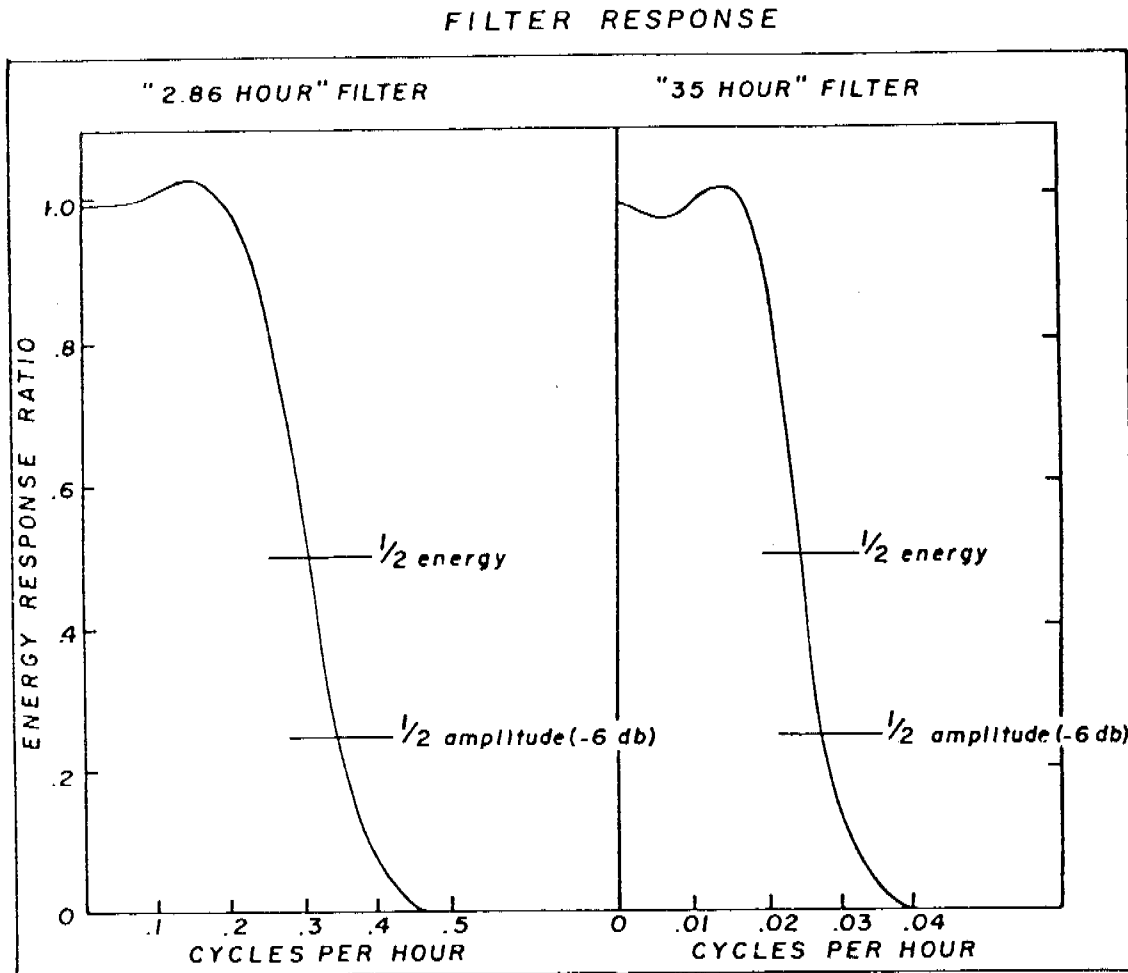
The total-energy spectra is calculated using both the 2.86-hr and 35-hr filtered U and V components. The complete operation is performed in 4 steps. The first two use the 35-hr filtered data, which has been demeaned and cosine tapered, to compute Fourier coefficients for frequencies up to 0.4 cycles per day. Raw spectral estimates are given for frequencies less than 1 cycle per month if the series is no longer than 1 month. Between 1 cycle per month and 0.4 cycles per day, 3 adjacent frequencies are averaged with the result that each point has 6 degrees of freedom.

For frequencies between 0.4 and 4.8 cycles per day, the spectrum is computed from the demeaned 2.86-hr filtered data set by dividing the series into 15-day segments. If there are less than 10 days of data in the last segment, it is not used, otherwise it is zero-filled

FIGURE 9  
CLEAN DATA SUMMARY FROM SUMIT

DAYHR	TEMP	SALI	SIGMA	SPED	DIR	DAYHR	TEMP	SALI	SIGMA	SPED	DIR	DAYHR	TEMP	SALI	SIGMA	SPED	DIR
29200	7.9	33.1	25.78	9.7	130	29200	7.9	33.0	25.76	18.6	31	29203	7.9	33.1	25.81	15.3	34
29204	8.4	32.9	25.57	26.6	208	29206	8.2	32.9	25.65	17.2	173	29207	8.3	32.9	25.59	24.3	189
29208	8.4	33.0	25.65	25.5	244	29210	8.3	33.0	25.67	34.5	227	29211	8.4	33.0	25.64	31.8	237
29212	8.4	33.1	25.82	13.7	303	29214	8.3	33.0	25.67	14.8	264	29215	8.1	33.1	25.76	16.2	271
29216	8.0	33.1	25.82	13.7	303	29218	7.8	33.2	25.90	15.0	360	29219	8.0	33.1	25.78	11.8	29
29220	8.2	32.9	25.62	13.9	92	29222	7.9	33.1	25.86	11.2	302	29223	7.6	33.3	26.00	15.2	340
FOR 19 OCT 77 TEMP= 6.11 SALINITY=33.03 SIGMAT=25.74 NET SPEED= 7.26 AT 245 MEAN SPEED= 18.53 DEPTH= 69.52																	
29300	7.7	33.2	25.89	16.4	343	29302	7.4	33.4	26.09	17.3	353	29303	7.3	33.4	26.13	17.3	357
29304	7.3	33.4	26.14	14.9	31	29306	7.4	33.4	26.09	4.9	71	29307	7.4	33.4	26.11	10.2	174
29308	7.5	33.3	26.01	14.8	700	29310	7.5	33.3	26.02	17.3	245	29311	7.5	33.4	26.09	18.9	263
29312	7.4	33.3	26.06	18.5	249	29314	7.4	33.2	25.97	19.1	287	29315	7.4	33.4	26.09	18.7	306
29316	7.4	33.3	26.08	17.6	339	29318	7.4	33.4	26.09	20.1	12	29319	7.4	33.4	26.10	17.4	24
29320	7.4	33.4	26.09	19.3	23	29322	7.4	33.3	26.04	16.4	41	29323	7.3	33.3	26.07	16.5	59
FOR 20 OCT 77 TEMP= 7.44 SALINITY=33.32 SIGMAT=26.05 NET SPEED= 7.75 AT 341 MEAN SPEED= 16.72 DEPTH= 69.47																	
29400	7.3	33.3	26.10	11.2	68	29402	7.3	33.3	26.08	4.6	213	29403	7.3	33.4	26.11	9.9	235
29404	7.3	33.3	26.09	13.3	264	29406	7.3	33.3	26.08	14.9	287	29407	7.3	33.3	26.04	8.7	246
29408	7.3	33.3	26.08	9.6	230	29410	7.4	33.3	26.04	10.2	202	29411	7.4	33.3	26.04	9.9	207
29412	7.4	33.3	26.05	11.2	221	29414	7.4	33.3	26.05	9.0	258	29415	7.4	33.3	26.02	8.0	296
29416	7.4	33.2	26.00	6.5	330	29418	7.4	33.2	25.98	11.2	350	29419	7.4	33.2	26.00	17.2	355
29420	7.4	33.2	25.98	18.2	6	29422	7.4	33.3	26.05	16.7	39	29423	7.4	33.3	26.05	14.8	47
FOR 21 OCT 77 TEMP= 7.35 SALINITY=33.29 SIGMAT=26.05 NET SPEED= 3.82 AT 305 MEAN SPEED= 11.58 DEPTH= 69.54																	
29500	7.4	33.3	26.06	13.0	38	29502	7.3	33.3	26.08	11.4	112	29503	7.3	33.3	26.08	13.6	129
29504	7.3	33.3	26.07	16.1	177	29506	7.4	33.3	26.03	24.5	160	29507	7.4	33.3	26.02	19.0	190
29508	7.4	33.3	26.04	20.1	198	29510	7.4	33.3	26.01	22.7	728	29511	7.4	33.3	26.02	21.6	248
29512	7.4	33.3	26.02	20.6	268	29514	7.4	33.2	26.00	23.6	307	29515	7.4	33.2	25.98	22.8	332
29516	7.4	33.2	25.98	23.7	332	29518	7.4	33.2	25.98	24.7	14	29519	7.4	33.2	26.00	21.0	8
29520	7.4	33.3	26.01	16.1	5	29522	7.4	33.3	26.02	12.5	10	29523	7.4	33.3	26.03	11.7	13
FOR 22 OCT 77 TEMP= 7.39 SALINITY=33.26 SIGMAT=26.02 NET SPEED= 3.94 AT 296 MEAN SPEED= 19.16 DEPTH= 69.48																	
29600	7.4	33.3	26.04	11.0	44	29602	7.4	33.3	26.04	7.9	247	29603	7.4	33.3	26.02	13.3	255
29604	7.4	33.3	26.02	15.2	280	29606	7.4	33.2	26.00	15.0	299	29607	7.4	33.2	26.00	12.0	314
29608	7.4	33.2	26.00	7.8	303	29610	7.4	33.2	25.98	11.3	230	29611	7.5	33.2	25.97	13.8	224
29612	7.5	33.2	25.96	13.7	226	29614	7.5	33.2	25.95	16.3	258	29615	7.5	33.1	25.90	12.7	254
29616	7.5	33.1	25.90	13.3	278	29618	7.5	33.1	25.90	10.6	298	29619	7.5	33.2	25.93	10.6	324
29620	7.5	33.1	25.91	9.7	19	29622	7.5	33.2	25.95	5.4	265	29623	7.5	33.2	25.95	6.5	226
FOR 23 OCT 77 TEMP= 7.47 SALINITY=33.21 SIGMAT=25.96 NET SPEED= 7.67 AT 276 MEAN SPEED= 11.53 DEPTH= 69.54																	
29700	7.5	33.2	25.93	7.7	210	29702	7.5	33.1	25.90	10.9	245	29703	7.4	33.1	25.86	9.9	235
29704	7.4	33.1	25.86	12.5	234	29706	7.4	33.1	25.86	11.3	273	29707	7.3	33.0	25.81	9.4	319
29708	7.5	33.0	25.77	8.2	330	29710	7.6	32.9	25.75	6.3	34	29711	7.7	32.9	25.68	6.9	66
29712	7.7	32.8	25.60	5.3	115	29714	7.6	32.8	25.66	9.1	210	29715	7.6	32.8	25.62	8.7	233
29716	7.5	32.8	25.65	6.5	264	29718	7.6	32.8	25.60	8.6	315	29719	7.5	32.8	25.64	11.8	354
29720	7.5	32.8	25.64	13.6	6	29722	7.6	32.9	25.71	10.6	56	29723	7.6	32.9	25.69	8.1	104
FOR 24 OCT 77 TEMP= 7.55 SALINITY=32.99 SIGMAT=25.74 NET SPEED= 2.73 AT 288 MEAN SPEED= 9.57 DEPTH= 69.53																	
29800	7.6	33.0	25.76	9.9	142	29802	7.6	32.9	25.67	12.3	176	29803	7.7	32.8	25.61	15.2	197
29804	7.6	32.8	25.61	17.9	203	29806	7.5	32.9	25.75	16.4	230	29807	7.4	33.0	25.79	10.0	257
29808	7.4	33.1	25.86	11.7	288	29810	7.3	33.1	25.89	14.2	326	29811	7.4	33.1	25.85	13.9	342
29812	7.5	33.0	25.84	12.2	2	29814	7.5	33.1	25.85	16.3	355	29815	7.4	33.1	25.92	20.2	348
29816	7.5	33.1	25.82	23.4	16	29818	7.4	33.0	25.82	25.8	28	29819	7.5	33.0	25.83	28.0	20
29820	7.5	33.1	25.85	23.4	21	29822	7.5	33.1	25.89	21.1	16	29823	7.5	33.1	25.88	11.6	67
FOR 25 OCT 77 TEMP= 7.47 SALINITY=33.01 SIGMAT=25.81 NET SPEED= 6.66 AT 358 MEAN SPEED= 17.22 DEPTH= 69.55																	
FOR 7 DAYS TEMP= 7.53 SALINITY=33.15 SIGMAT=25.91 NET SPEED= 4.46 AT 303 MEAN SPEED= 14.86 DEPTH= 69.52																	

FIGURE 10  
RESPONSE CURVES OF FILTER

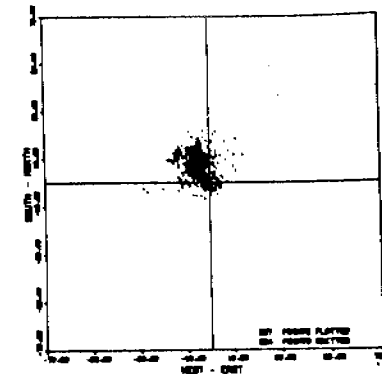
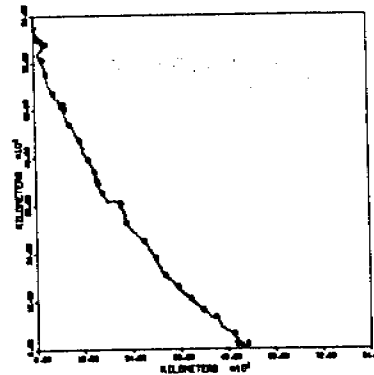
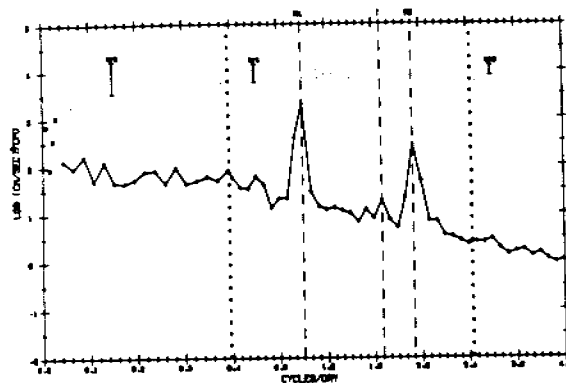


STATION-K7R  
 PROJECT-MISS  
 LATITUDE=87 03.40N  
 LONGITUDE=152 18.00W  
 DEPTH= 80.00 METERS

METER-1984  
 DEPTH=70.0 METERS

MEAN PRESSURE= 70.14 METERS  
 U-VARIANCE= 104.1  
 V-VARIANCE= 158.5  
 RECORD LENGTH= 142.36 DAYS  
 NET DRIFT= 7.72 CM/SEC. 326°T  
 MEAN SPEED= 16.58 CM/SEC

RUN DATE= 09/13/78  
 VERSION= 77300



182

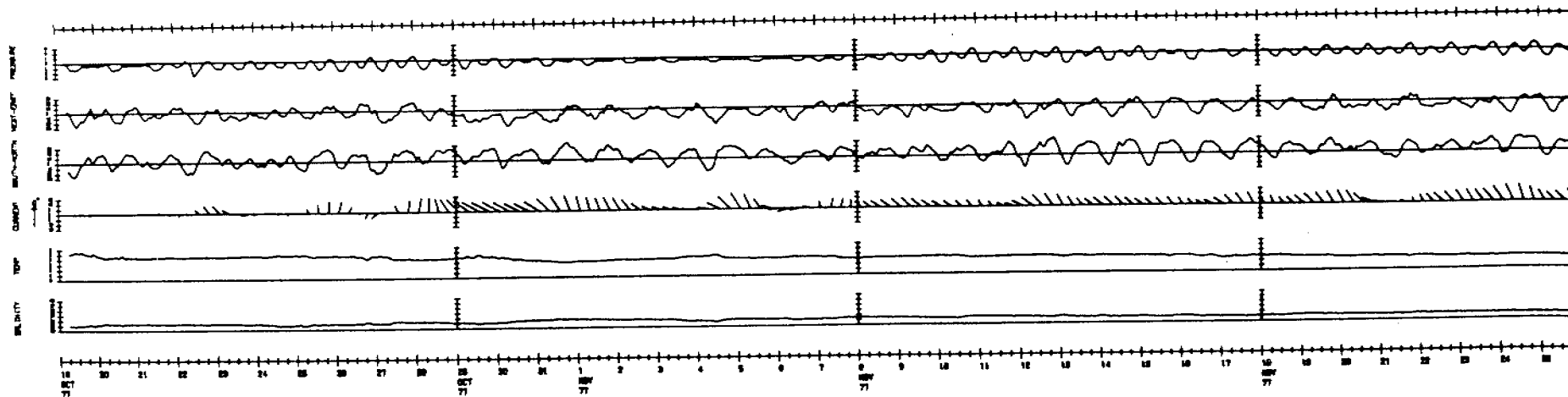


FIGURE 11  
 FILTERED DATA PLOT FROM PLOT

and the resultant energy values are prorated. Ensemble averages are then computed for each frequency from 0.4 to 2.4 cycles per day such that each point has a number of degrees of freedom equal to 2 times the number of 15-day segments. In the region from 2.4 to 4.8 cycles per day, 3 adjacent frequencies are averaged to yield 12 values that have a number of degrees of freedom equal to 6 times the number of segments.

All four of these steps are performed on U and V separately and the corresponding components are summed. The spectra and PVD information are written on OUTPUT and also at the end of the filtered time series.

### Filtered Data Plot

The program CMPLOT uses both of the filtered time series to produce plots of the various components versus time. The minimum standard plot has pertinent mooring information, some statistics, a progressive vector diagram (PVD), a spectral plot, a scatter plot, U and V versus time line plot, and a U-V versus time stick plot (see Fig. 11). Any combination of the 2.86-hr filtered temperature, pressure, and salinity data may be plotted versus time by using the appropriate input card. Additional features include the ability to scale the entire plot up or down and to rotate the vector time series axis to improve visual resolution. The program was designed to be used with the filtered data set, and hence it is somewhat more difficult to use on other types of data. This plot is used by the scientist as a "first look" at the data from which subsequent analyses may be planned.

### Summary

This system has been up and running at PMEL for about 1 year. Seventy percent of the data sets are being processed in one pass. The advantages of this are many: the time normally required to process the data has been greatly reduced, the scientist receives his data in a much more timely fashion, and data quality is both higher and more consistent. The extensive set of output products simplifies the task of quality control and gives the scientist the essential information in such a concise format that plans for further analysis can be readily made. The net effect is that resources may be more fully utilized and applied to meet overall project goals and commitments.

R2D2: AN INTERACTIVE GRAPHICS PROGRAM  
FOR RAPID RETRIEVAL AND DISPLAY OF OCEANOGRAPHIC DATA\*

Carl A. Pearson\*\*  
Gary A. Krancus\*\*  
Robert L. Charneil\*\*\*

ABSTRACT

The Coastal Physics group of the Pacific Marine Environmental Laboratory (NOAA) has collected a large amount of physical oceanographic data over the past few years, including an estimated 7500 STD casts and 1000 months of current meter and pressure gage data. To allow our researchers fast and easy access to this data, a computer program called R2D2 (Rapid Retrieval Data Display) was developed. Data and programs are stored on disk in a CDC 6600 computer. The data are divided by type (STD or current meter/pressure gage) and geographical area. Each data set is further divided into a random access header file (which includes a unique reference number, date, time, position, cruise and station name, comments, and basic statistics); and a random access data file linked to the header file by the reference number. The researcher, working at a remote data terminal, executes a procedure file which loads the appropriate data and programs and begins program execution. Using interrogative interaction the user can sort the header file by any of several criteria (such as area, time period, cruise name, etc.), and then manipulate and display the selected data in a variety of formats. Output includes maps of physical properties, vertical profiles, time series plots, statistical summaries, and standard "data reports". Plotting and output may be done either on the terminal or at a central site. The program is designed as a research tool for the user with no programming experience, provides feedback and checking to prevent user mistakes, and is self-documenting.

INTRODUCTION

Since 1975 the Coastal Physics group of NOAA's Pacific Marine Environmental Laboratory has collected extensive sets of physical oceanographic data as part of its involvement in projects such as the Outer Continental Shelf Environmental Assessment Program (OCSEAP) and Marine Ecosystems Analysis (MESA) program. To date this includes approximately 7500 CTD/STD casts and over 1000 months of current meter and pressure gage data from Alaskan continental shelf waters and the Puget Sound region. As this collection of data grew, it became increasingly difficult and time-consuming to determine what data existed, the status of data, and to locate tapes and printouts. An efficient data retrieval system was needed to allow the researcher fast and easy access to his data; the best tool for accomplishing this was the computer.

\* Contribution No. 376 from the NOAA/ERL Pacific Marine Environmental Laboratory.

\*\* National Ocean Survey, assigned to Pacific Marine Environmental Laboratory, NOAA, Seattle, Washington.

\*\*\* Pacific Marine Environmental Laboratory, NOAA, Seattle, Washington.



The main requirements of such a system were: 1) that data be readily accessible and capable of being sorted to the user's specification; 2) that no programming experience be required of the user; 3) that the program be interactive and be as "user-proof" as possible; and 4) that a wide variety of graphical and printed output products be available for analysis. This system was named Rapid Retrieval Data Display, or R2D2.

#### DATA STRUCTURE

The first requirement, rapid access, was met by storing data as random access files on a mass storage device with a large mainframe computer. During periods of low usage, files may be stored on tape, and copied to disk as needed. Our extensive data base, about 6 million words, would be unmanageable on one file. Data are therefore divided by type (STD or current meter) and geographical area: Puget Sound-Strait of Juan de Fuca, Gulf of Alaska, and Bering Sea. The six data sets are further subdivided into header and data files. Each STD cast or current meter station in a set has been assigned a unique reference number which serves as the key to the random access storage location. The header file contains station information such as cruise and station name, latitude and longitude, time and date, basic statistics, and comments. STD data files contain 1-m average temperature and salinity arrays. Corresponding scan depth is computed from the depth of the first scan and the array subscript. Densities and dynamic height anomalies are computed as needed. Current meter data files contain 2.86-hr low-pass filtered hourly values of U (east) and V (north) velocity components, temperature, salinity and pressure, as well as 35-hr low-pass filtered six-hourly U and V components.

The separation of header information from the detail data is an important feature of the R2D2 system; it allows for rapid sorting without bringing large data files into core and saves considerable time and mass storage transfer. The Gulf of Alaska STD file, for example, contains over 3200 casts and may be sorted for time period, area and cruise name in about 1.5 seconds of CPU time and at a cost of less than a dollar. Restricting the sort to a smaller range of stations shortens processing time proportionately.

#### PROGRAM STRUCTURE

The user accesses the R2D2 system by remote terminal and executes a procedure file called R2D2. The procedure file is a series of control language commands which attach and load the subroutine libraries and execute the programs (Fig. 1). Registers set from within the programs control flow through the procedure file. Like the data files, programs have been divided by type to keep program size reasonable, i.e., less than 100K octal central memory.

R2D2 communicates with the user by asking questions or requesting input parameters, and the user types the appropriate response on the terminal. Questions are answered with a "Y" for yes or "N" for no, while numerical parameters are entered free-form with commas as separators. Responses are checked for "correctness" before proceeding. For instance, a reply of "X" to a yes or no question would bring a response of "please answer yes or no". In other cases entries are printed out in an understandable format with the question, "is this O.K.?" If only a "carriage return" is entered, an end-of-file condition is detected on input, causing instructions to be printed.

Programs are written in Fortran, and compiled versions are stored on disk as libraries or core images. The main programs are fairly short, and serve chiefly to set up buffers and call the main subroutines. Program structure is modular, so that new routines for data manipulation and display may be added as the need arises with minimal change to the calling routines. Many routines are common to both the STD and current meter programs; others serve more specialized functions. The higher level routines call utility subroutines for specific tasks, such as on-screen plotting, listing control, mercator map projection, coastline sorting, and answer-checking.

Plotting may be done on a Tektronics graphics terminal or an offline plotter. The plot routines use Calcomp calls, which write a file of pen coordinates that may be saved and converted for any type of plotter. For terminal plotting, the file is read and converted using Tektronix PLOT10 calls, and automatically scaled to fit onto the screen.

#### PROGRAM FLOW

R2START, the first program executed, greets the user, determines which data type and area are desired, and attaches the selected header, data and coastline files. Then R2D2 branches to the appropriate main program.

Figure 2 illustrates the important features of flow in the STD program. The main program calls subroutines SORTSTA (to sort the stations), and DATLOOK (to access the selected data). In SORTSTA, the user is first asked to enter a sort option number. Options are available for sorting by area, time period, cruise name, and reference numbers, as well as for a summary listing of file contents by cruise. Subroutines are called for each option selected which simply verify and set the sort parameters. Any combination of options may be used. When the desired options have been chosen, option 0 is entered to initiate actual sorting. As each station header is read in, the appropriate information is checked against the sort parameters. For instance, if time period sort has been selected, the station date is tested against the specified start and end dates. If it falls within these dates, the next option is checked. If not, the next station is tested. When the reference range option has been selected, only that range of stations is sorted; otherwise, all stations are sorted. As a station is selected, the reference number and other pertinent information is stored on a scratch file for later use in accessing and displaying the data.

When sorting has been completed, the number of stations selected is printed. The researcher then has the option of doing nothing more, listing stations selected, plotting stations on a map, re-sorting, going on to the data display options, or saving the selected casts on a new file for later use outside the program. The listing option gives one the choice of listing the header information of all or a portion of the selected stations, either on the terminal or at the central site. Maps are plotted on a mercator projection within any desired latitude and longitude boundaries. Chart scale may be either user-specified for overlaying on a nautical chart, or computed by the program from user-supplied latitude boundaries and plot height. Coastline resolution is about 5 km for Alaska and 1 km for Puget Sound.

The DATLOOK routine has options for displaying areal distributions of physical properties, vertical transections, profiles, T-S (temperature-

salinity) diagrams or full data listing for the selected stations. Option one, distributions, has 13 further options; the resulting values may be listed and/or plotted on a map. The options include temperature, salinity, or sigma-t at a specified depth; vertical differences, averages or dynamic topography between specified depths; or depth, temperature or salinity in a specified sigma-t surface.

Transections may be plotted for temperature, salinity or sigma-t on any desired size plot to user-specified depth and data resolution. Profiles are automatically scaled for depth, temperature, salinity and sigma-t ranges to fit 8" x 10" page size, or user may specify depth range.

T-S diagrams may be done on a default 6" x 9" diagram for temperatures -2°C to 16°C and salinities of 24‰ to 36‰; or, if preferred, any temperature and salinity range may be selected and plotted on any size page. Lines of equal sigma-t are plotted as a standard feature. Options include depth ticks, selected stations on individual plots or all on the same plot.

The current meter program contains similar sort options and data display options including time series plots, histograms, current roses, scatter plots, spectral energy diagrams, progressive vector diagrams, maps of mean current distribution, as well as performance history of each meter.

#### EXAMPLE

As an illustration of the flexibility and some of the capabilities of R2D2, let's assume we're interested in hydrographic cast data in an area of the Gulf of Alaska during early March 1977, specifically the continental shelf region east of Kodiak Island.

We begin by logging into the computer at our graphics terminal, getting procedure file R2D2, and starting execution by entering "R2D2". Figure 3 shows the first screen-full of output from the start program. After the logo, greetings and messages, R2D2 asks whether we are novice users. If we reply "yes", a switch is set to automatically print out instructions before each subsequent question. Whether we are novice or experienced, instructions may be obtained at any time by entering just a "carriage return" in reply to a question. The next requests are for data type and geographical area. We enter "S" for STD data and "GA" for Gulf of Alaska area. Files are attached from within the program. If they have been attached without error, we are told so, and then R2D2 moves on to the STD program.

Our first task is to have R2D2 sort through the data to obtain the desired subset (Fig. 4). Since we want a particular area, we type in option 2 and then enter boundaries of 57° to 60° latitude and 148° to 154° longitude. These are repeated and, if correct, we select another sort option. We now use option 4 and enter a time period of 1 to 5 March 1977. After ascertaining that the dates are correct, we select option 0 to initiate sorting.

The approximately 3200 stations in the file are tested for the area and time period, and we are soon informed that 30 of them meet our criteria (Fig. 5). To see which they are, we list a sample of every 5th station and find that they are all from the same cruise, RP4-D177A2.

Next we want to plot the station positions on a map. The program needs to know scale or plot height, so we enter 0 for scale, which tells R2D2 to compute scale itself, and 6" for plot height. Before doing the first plot, we are asked if we are using a graphics terminal and if so, to enter the baud rate. This enables initialization of the PLOT10 routines. The resulting plot (Fig. 6) shows the distribution of stations in the area, with optional station reference numbers. If desired, this plot may be saved for later plotting on a Calcomp plotter.

We are now ready to look at data from these stations. Figure 7 shows the range of options available. We enter "4" to get to the DATLOOK routine, then "1" for area distributions, followed by "2" under area options to plot salinities at a given depth. We select surface salinity by entering "-1" for depth, and then obtain a plot of surface salinities for the selected stations (Fig. 8). The plot shows an area of low salinity water near the coast, probably due to local runoff, and another tongue of low salinity water near the shelf break, possibly due to runoff from the Copper River to the east.

Next we might want to examine a vertical transection of one of the lines of stations, for instance stations 607 to 610 and 613. We enter "-1" to re-sort and use sort option 7 to select individual stations; then select salinity under data option 2, asking for a 5" x 5" plot with a maximum depth of 250 m, and a salinity interval of 0.5‰. The resulting plot (Fig. 9) shows the salinity transection, looking toward the west with the coastal water to the right. Bottom depth is indicated by a star (the shallow area to the south is due to the proximity to Kodiak Island). The dotted contour lines were added later for easier viewing. Here again we see the relatively fresh coastal water to the north.

To look at a particular station, say 613, in more detail, we again re-sort and then use data option 3, which produces a standard profile for that station (Fig. 10). Station depth was 142 m, so the depth range was scaled 0-200 m. The water here is two-layered, with coastal run-off overlying a warmer, more saline layer advected from the Alaskan Stream. Option 4 produces a T-S diagram (Fig. 11). In this case we have selected a relatively narrow range of temperature, 4°C to 7°C and salinity, 30‰ to 33‰, to provide greater detail. The dotted lines are contours of equal sigma-t. Finally, we may obtain a full data printout with option 5 (Fig. 12), and list either on the terminal or to an output file for later printing at a central site.

## SUMMARY AND CONCLUSIONS

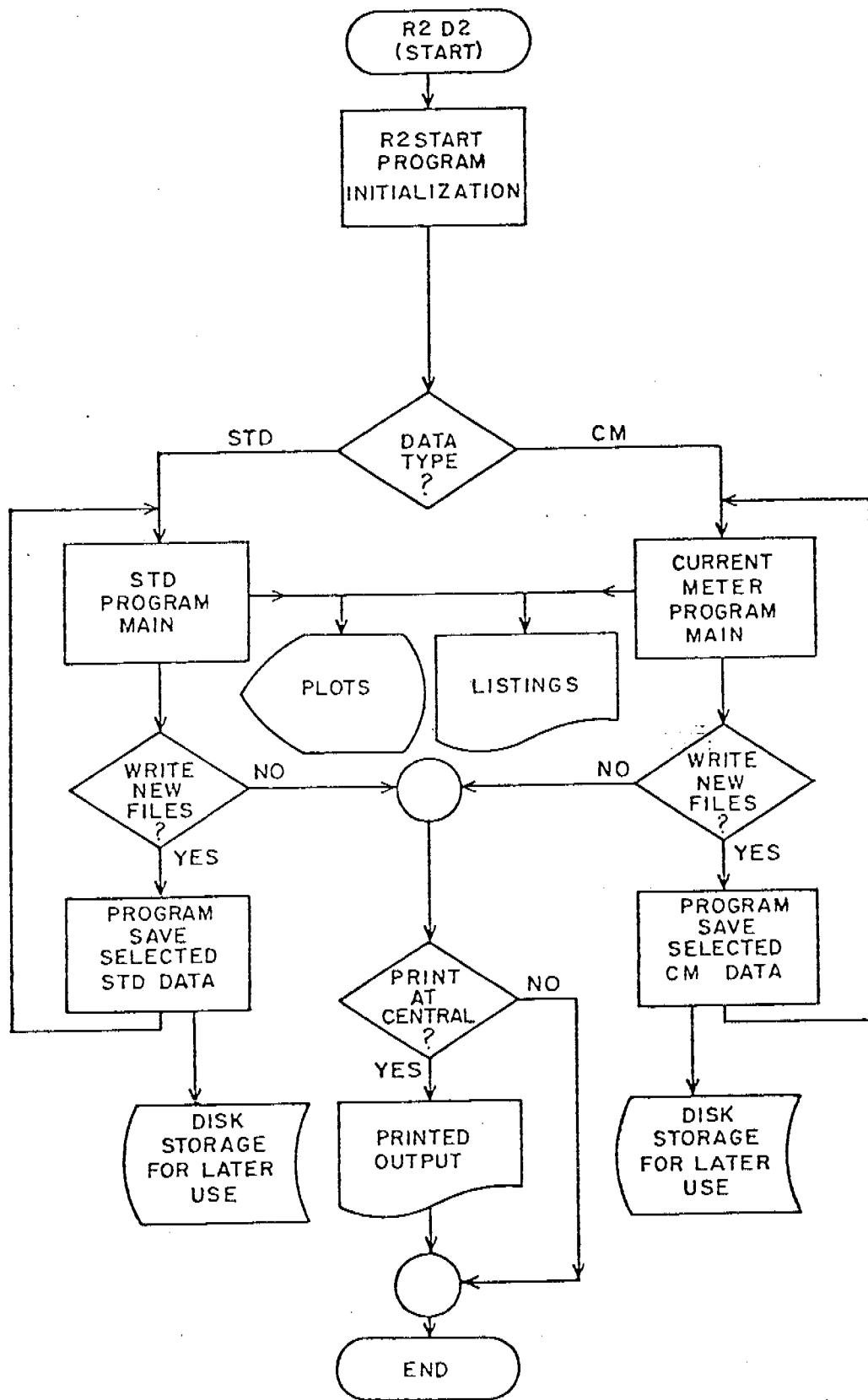
Total cost of the preceding example was about \$5.00 and took approximately half an hour at the terminal. In comparison, it might have taken as long as a week to complete the same task without the R2D2 system. One would have had to locate the printouts for the appropriate cruise, trace a chart and plot station positions, construct the transections, and graph the data on a T-S diagram. R2D2 allowed the researcher almost immediate access to the desired data, quickly and accurately did the required computations, and produced a manuscript-quality output in about the time it would take to explain the task to a graduate student.

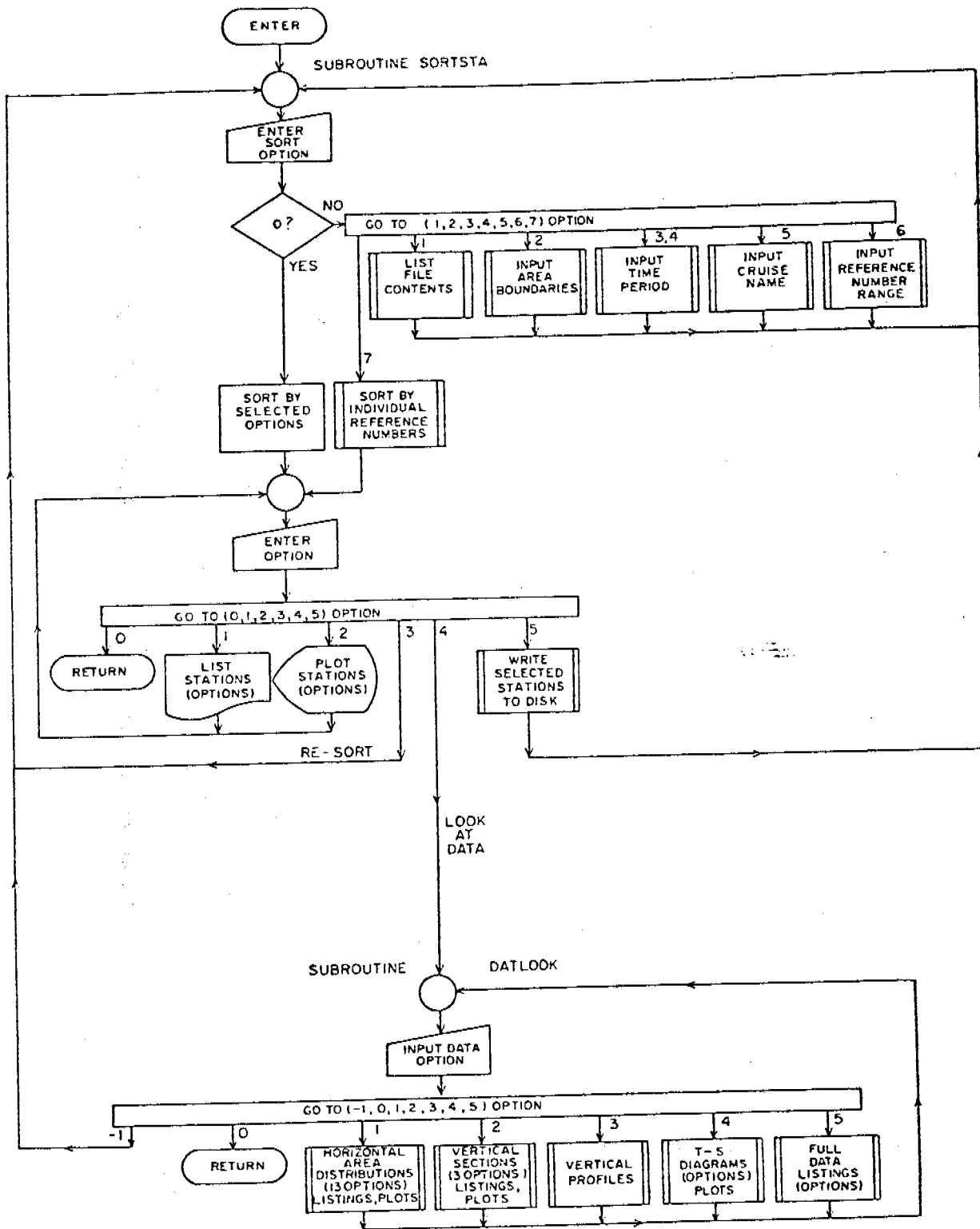
The interrogative, interactive nature of R2D2 enables the user with no programming experience to begin using the system without having to consult a manual (although one is available). Extensive error checking vir-

tually eliminates chances that the program will "bomb out" due to user error. Separation of header information from the data files greatly facilitates sorting while random access storage keyed to the header reference number allows efficient retrieval of selected data. As a research tool, R2D2 has significantly enhanced project efficiency by providing rapid and easy access to any of the data and to a large variety of products oriented toward data interpretation.

## FIGURE CAPTIONS

- Figure 1. Flow diagram of R2D2 control language procedure file.
- Figure 2. Flow diagram of STD data sort and display program.
- Figure 3. Output from R2START program.
- Figure 4. Setting sort parameters in subroutine SORTSTA.
- Figure 5. Sample listing of stations selected.
- Figure 6. Plot of station locations.
- Figure 7. Selecting data display options in subroutine DATLOOK.
- Figure 8. Plot of surface salinities.
- Figure 9. Salinity transection, stations 607-610, 613.
- Figure 10. Profile of temperature, salinity and sigma-t versus depth for station 613.
- Figure 11. Temperature versus salinity (T-S) diagram for station 613, with lines of equal sigma-t.
- Figure 12. Portion of full data listing for station 613.







THE COASTAL PHYSICS GROUP

PRESENTS

	DATA	WARS
R	RAPID	RRDD
		RR DD
2	RETRIEVAL	RR DD
		RRDDRRDD
D	DATA	RRDDRRDD
		RRDDRRDD
2	DISPLAY	RR DD RR

BUILT A LONG TIME AGO  
...ON A DATA BASE FAR FAR AWAY

GOOD AFTERNOON CARL  
R2D2 AT YOUR SERVICE

==> A NEW OPTION, DATA REPORT, HAS BEEN ADDED  
ARE YOU A NOVICE USER ? Y  
NOTE: FOR INSTRUCTIONS TO QUESTIONS, PRESS RETURN KEY  
ENTER: S FOR STD  
C FOR CURRENT METERS, PRESSURE GAGES  
DATA TYPE ? S  
TYPE IN AREA OF INTEREST  
GA = GULF OF ALASKA  
BS = BERING SEA  
PS = PUGET SOUND  
AREA? GA  
GA STD FILES HAVE BEEN ATTACHED  
PLEASE STAND BY WHILE THE STD PROGRAMS ARE LOADED

YOU MAY NOW SORT  
OPTION

-99 CLEAR PREVIOUS OPTIONS  
0 SORT WITH OPTIONS SELECTED  
(IF NONE SELECTED, NO SORTING WILL BE DONE)  
1 CONTENTS OF FILE: CRUISE NO., DATES, NO. OF CASTS  
2 SORT BY AREA  
3 " " TIME (JULIAN DATE)  
4 " " TIME (DAY, MONTH)  
5 " " CRUISE NAME  
6 " " REFERENCE NUMBER RANGE  
7 SELECT INDIVIDUAL REFERENCE NUMBERS (ALSO PRINTS  
TEMP, SALIN, SIGMA T RANGES. . . USE FOR SECTIONS

AND MANY MORE TO COME

ENTER SORT OPTION ? 2

LAT1 AND LAT2 ARE LATITUDE BOUNDARIES

LOH1 AND LOH2 ARE LONGITUDE BOUNDARIES

ENTER: LAT1, LAT2, LOH1, LOH2

? 57, 60, 148, 154

AREA IS BOUNDED BY:

LATITUDES 57.00 TO 60.00

LONGITUDES 148.00 TO 154.00

IS THIS CORRECT ? Y

ENTER SORT OPTION ? 4

SORT IS BY TIME PERIOD

(DAY, MON, YEAR. . . USE NUMBER FOR MON)

ENTER: STARTDAY, MON, YEAR, ENDDAY, MON, YEAR

? 1, 3, 77, 5, 3, 77

TIME PERIOD IS:

FROM 1 MAR 77 TO 5 MAR 77

IS THIS OK?

? Y

ENTER SORT OPTION ? 0

30 STATIONS WERE SELECTED

ENTER:

- 0 TO DO NOTHING MORE
- 1 TO LIST STATIONS SELECTED
- 2 TO PLOT STATIONS SELECTED
- 3 TO RE-SORT
- 4 TO LOOK AT DATA FOR STATIONS SELECTED
- 5 TO WRITE DATA ON PERMANENT FILE
- 6 FOR DATA REPORT

WHAT WOULD YOU LIKE TO DO ? 1

YOU MAY PRINT ALL OR SOME OF THE STATIONS  
SELECTED, ON YOUR TERMINAL. REGARDLESS OF WHICH YOU  
PRINT NOW, ALL WILL BE AVAILABLE FOR PRINTING LATER  
AT A CENTRAL SITE (I.E. PMEL)

DO YOU WANT TO PRINT ALL OF THEM? N

TYPE IN NUMBERS I, J, K TO LIST EVERY K-TH STATION  
FROM I THRU J

? 1,30,5

REF	CRUISE	CAST	STA	LAT	LONG	GMT	DAY	MON	JD	YR	DEP
587	RP4-DI77A2	1	1	57.54	149.03	927	2	MAR	61	77	2580.
592	RP4-DI77A2	6	7	58.73	150.09	2157	2	MAR	61	77	168.
597	RP4-DI77A2	11	12	58.58	150.57	5 3	3	MAR	62	77	181.
602	RP4-DI77A2	16	16	57.91	150.09	1223	3	MAR	62	77	237.
607	RP4-DI77A2	21	38	58.33	151.66	511	4	MAR	63	77	64.
612	RP4-DI77A2	26	33	59.02	151.95	1410	4	MAR	63	77	196.

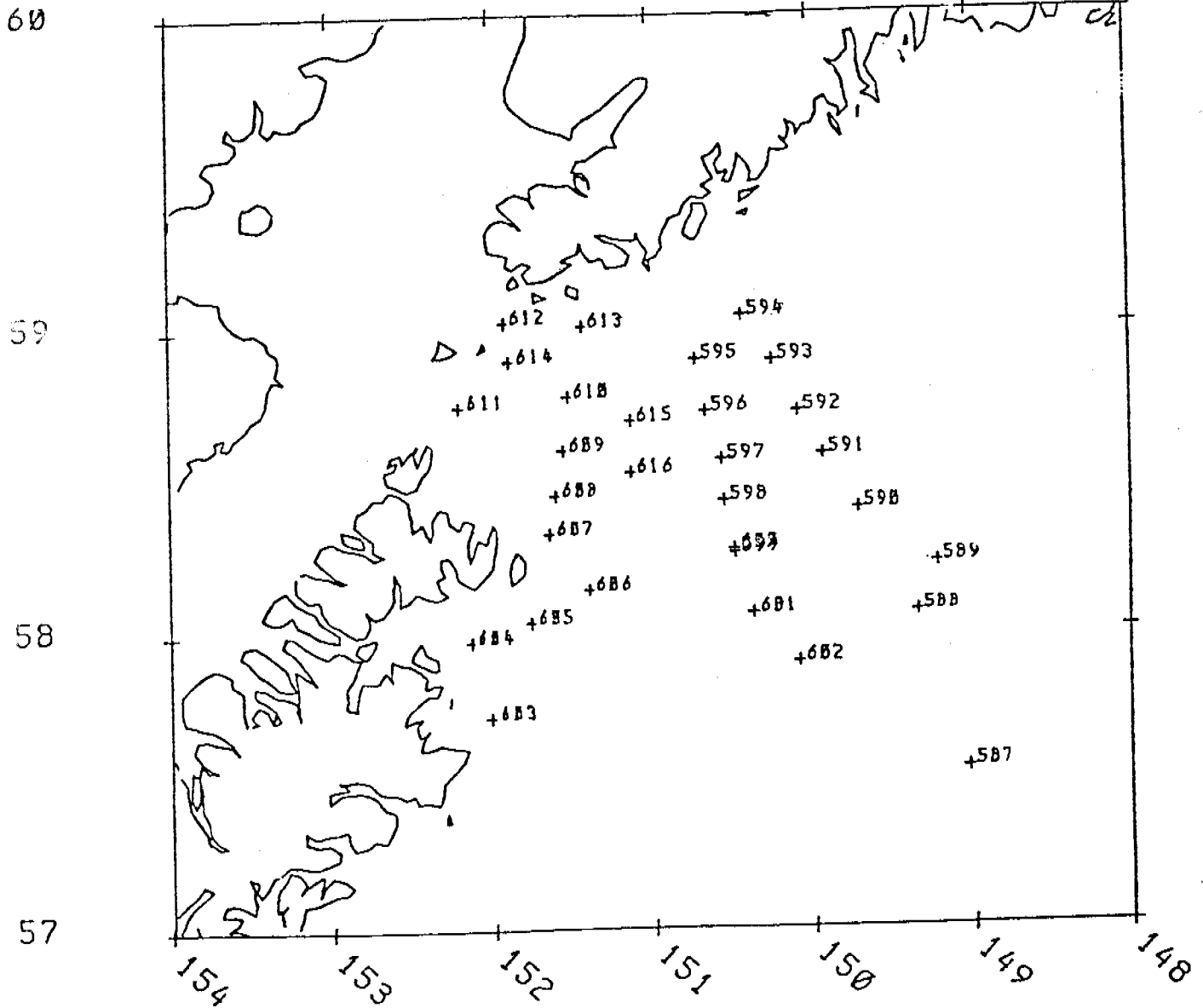
ENTER:

- 0 TO DO NOTHING MORE
- 1 TO LIST STATIONS SELECTED
- 2 TO PLOT STATIONS SELECTED
- 3 TO RE-SORT
- 4 TO LOOK AT DATA FOR STATIONS SELECTED
- 5 TO WRITE DATA ON PERMANENT FILE
- 6 FOR DATA REPORT

WHAT WOULD YOU LIKE TO DO ? 2

SCALE 2194271  
AT LAT. 58.500

STATION REF. NO.  
1MAR 77 TO 5MAR 77



FOR TYPE OF DATA OUTPUT, ENTER:

-1 TO RE-SORT FIRST

0 FOR NONE

1 FOR AREA DISTRIBUTIONS (MAPS OF PHYSICAL PROPERTIES)

2 FOR VERTICAL SECTIONS

3 FOR PROFILES

4 FOR T-S DIAGRAMS

5 FOR FULL DATA PRINTOUTS

NOTE: TO RE-SORT FIRST, ENTER A NEGATIVE OPTION NUMBER

TYPE OF DATA OUTPUT ? 1

FOR THE STATIONS SELECTED ABOVE, YOU MAY SELECT  
ANY ONE OF 13 OPTIONS LISTED BELOW:

1 TEMPERATURE AT DEPTH D

2 SALINITY AT DEPTH D

3 SIGMA T AT DEPTH D

4 TEMP DIFFERENCE BETWEEN DEPTHS D1 & D2

5 SALIN DIFFERENCE BETWEEN D1 & D2

6 SIGMA T DIFFERENCE BETWEEN D1 & D2

7 TEMP AVERAGE BETWEEN D1 & D2

8 SALIN AVERAGE BETWEEN D1 & D2

9 SIGMA T AVERAGE BETWEEN D1 & D2

10 DYNAMIC HEIGHT BETWEEN D1 & D2

11 DEPTH OF A SIGMA-T SURFACE

12 TEMPERATURE OF A SIGMA-T SURFACE

13 SALINITY OF A SIGMA-T SURFACE

NOTE: DEPTH OF -1. MEANS TOPMOST DEPTH, -2. BOTTOM  
OUTPUT LISTING WILL GIVE REFERENCE NUMBER OF THE STATION  
VALUE COMPUTED, AND DEPTH(S). A -99 MEANS NO VALID DATA.

ENTER OPTION DESIRED

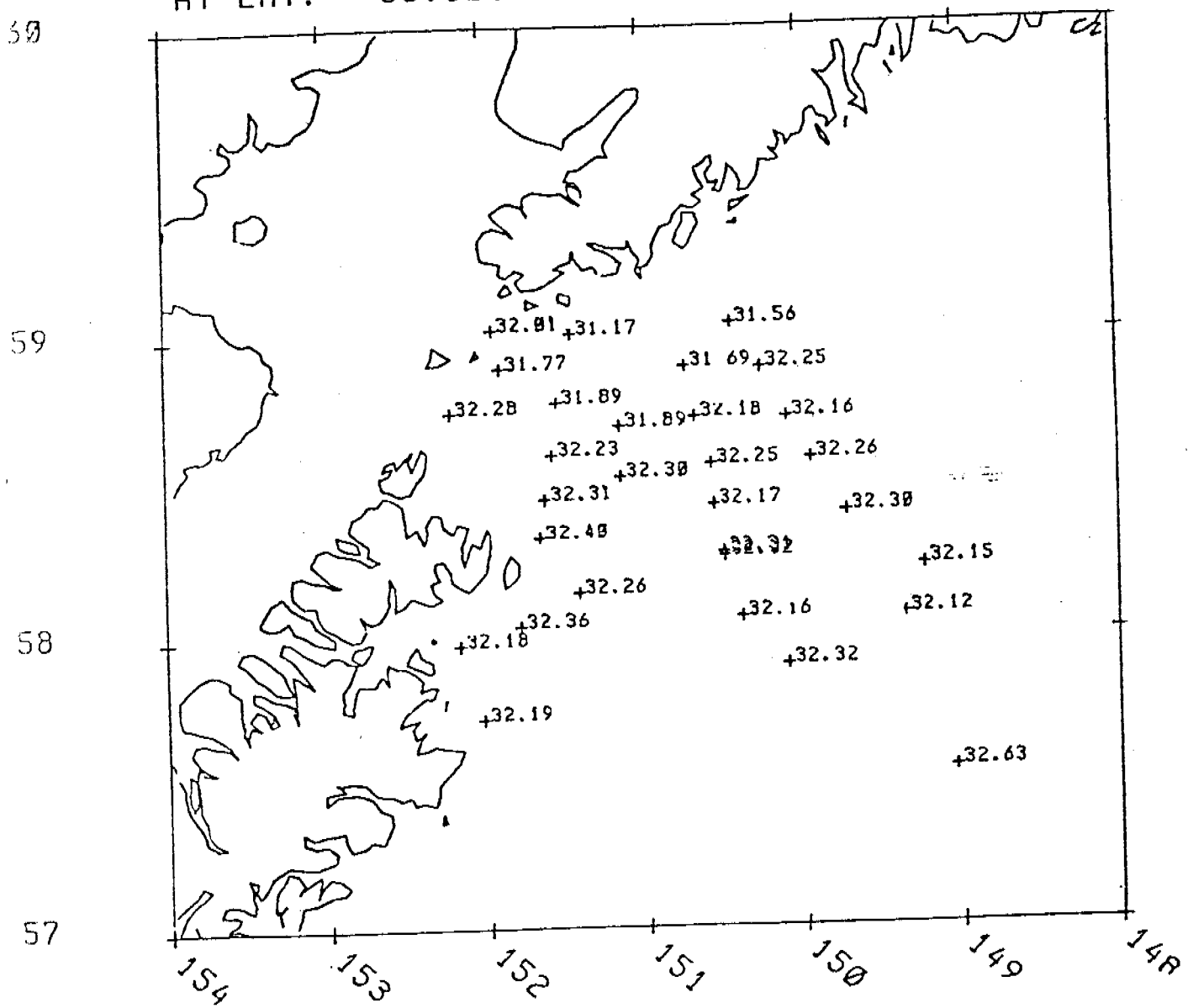
? 2

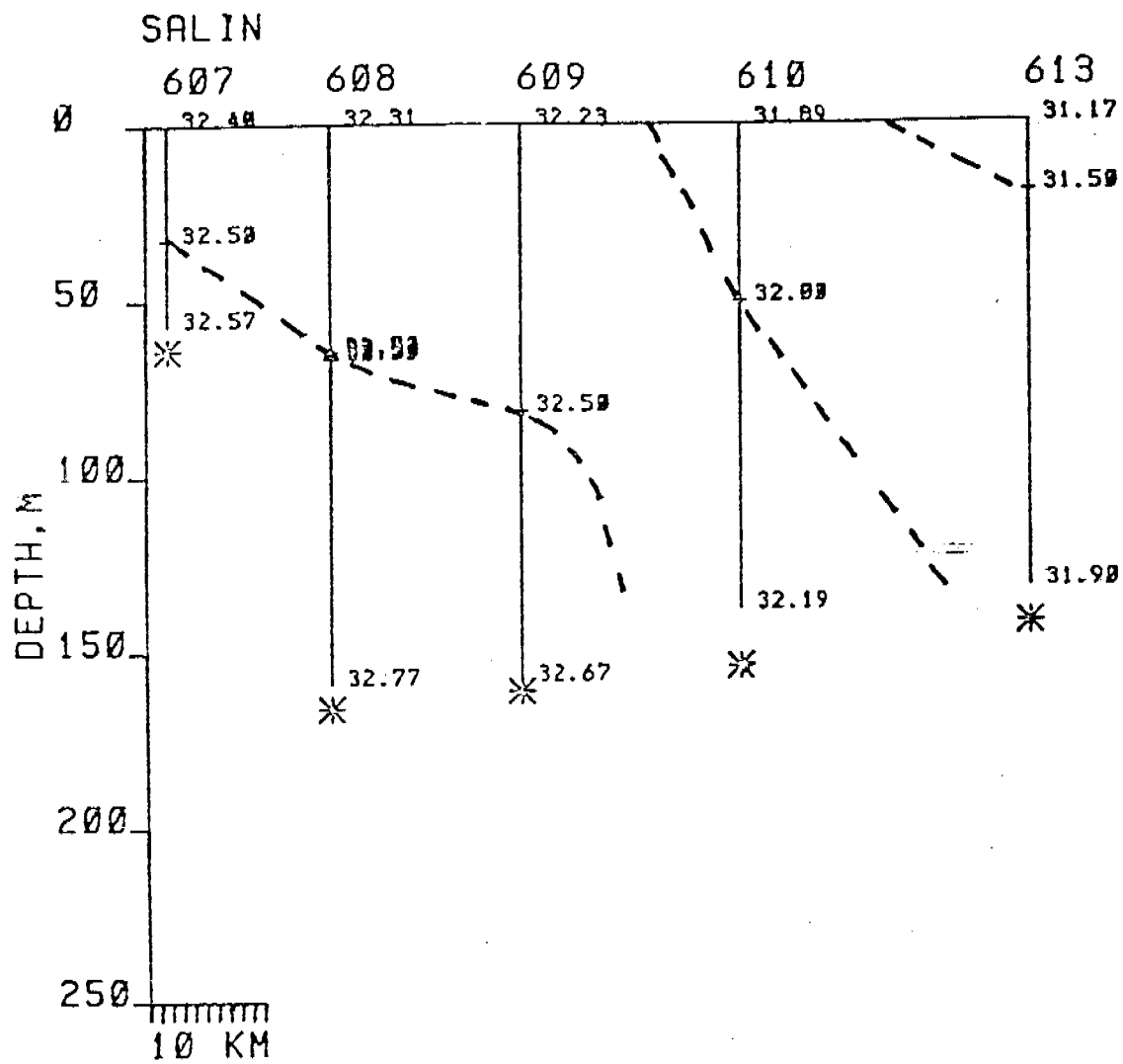
ENTER DEPTH D

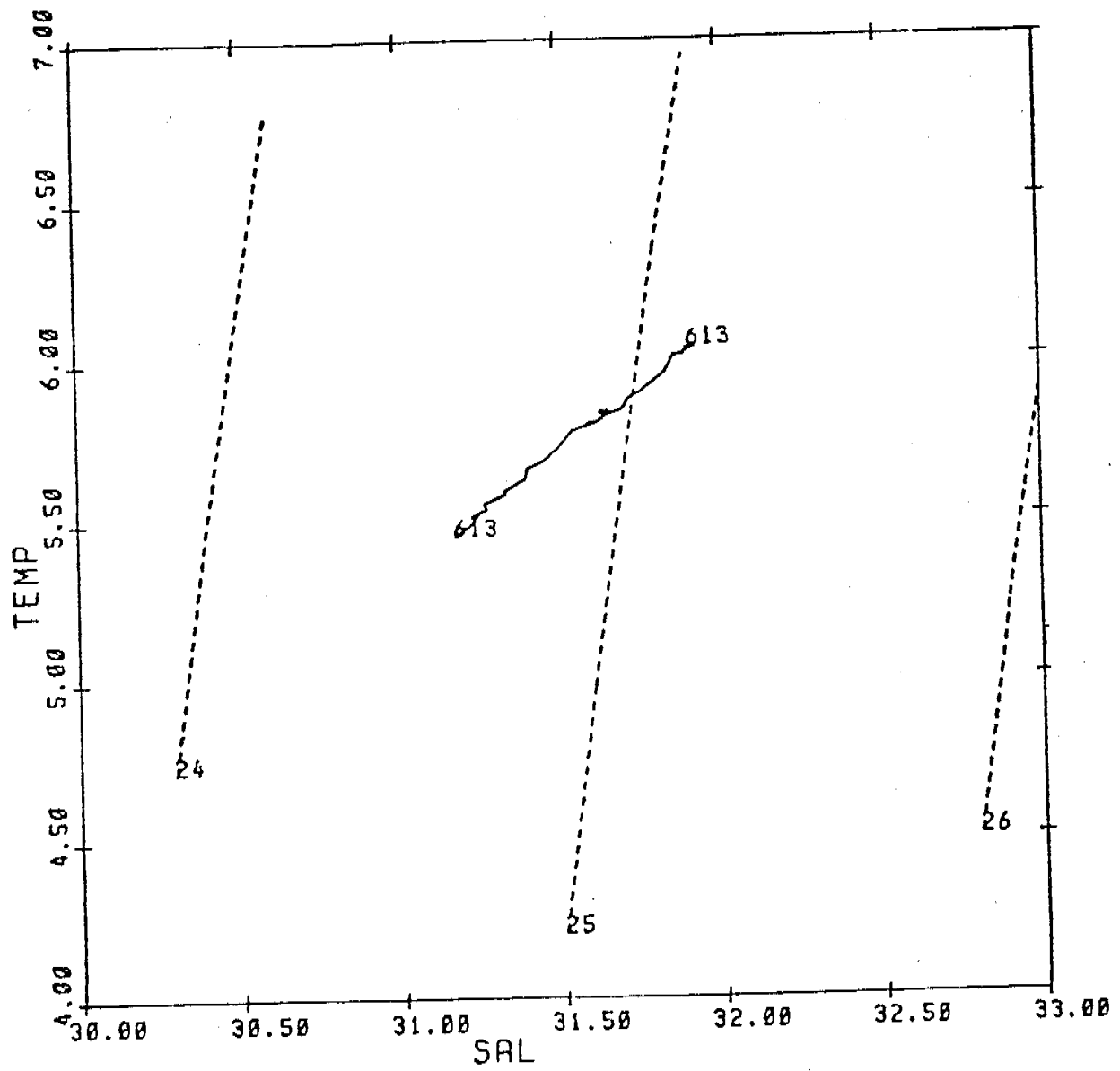
? -1

SCALE 2194271  
AT LAT. 58.500

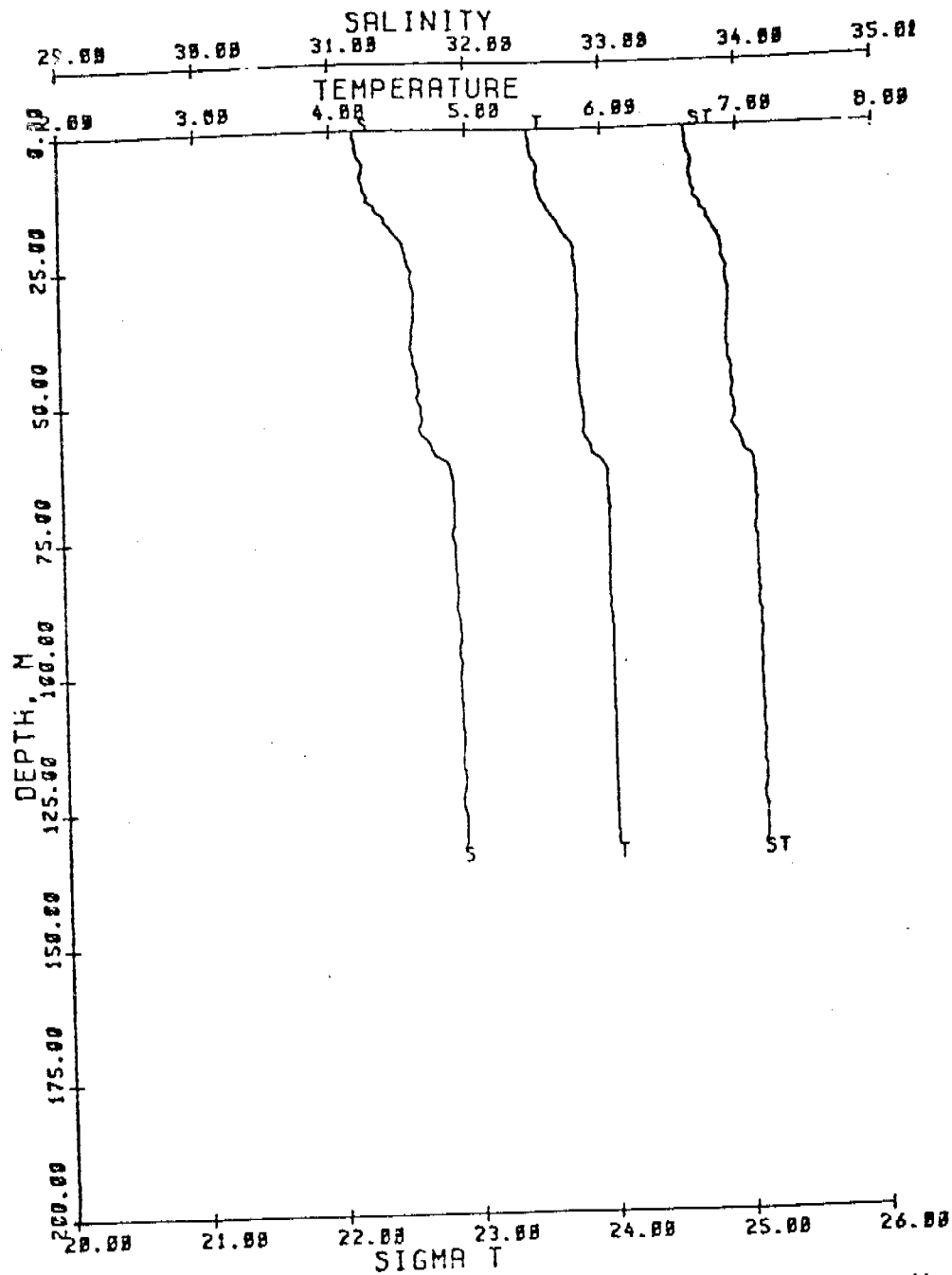
SALINITY SURFACE  
1MAR 77 TO 5MAR 77











REF. NO. 613

4 MAR 77 16 0 GMT

STA. 32

RP4-DI77A2-27

59.01 N

151.45 W

REF CRUISE CAST STA LAT, N LON, W GHT DAY MON JD YR DEP  
 613 RP4-DI77A2 27 32 59.01 151.45 16 0 4 MAR 63 77 142

DEP	TEMP	SAL	SIG-T	DYN M	DEP	TEMP	SAL	SIG-T	DYN M
0	5.45	31.17	24.62	0.000	1	5.46	31.18	24.62	.003
2	5.47	31.19	24.63	.007	3	5.47	31.19	24.63	.010
4	5.48	31.20	24.64	.013	5	5.48	31.21	24.65	.017
6	5.51	31.24	24.67	.020	7	5.52	31.24	24.67	.023
8	5.52	31.22	24.65	.026	9	5.51	31.22	24.65	.030
10	5.51	31.24	24.67	.033	11	5.52	31.25	24.67	.036
12	5.53	31.27	24.69	.040	13	5.55	31.26	24.68	.043
14	5.58	31.33	24.73	.046	15	5.59	31.33	24.73	.049
16	5.63	31.39	24.77	.053	17	5.66	31.40	24.77	.056
18	5.68	31.44	24.80	.059	19	5.70	31.47	24.82	.062
20	5.73	31.50	24.85	.065	21	5.77	31.53	24.87	.068
22	5.78	31.54	24.87	.071	23	5.78	31.55	24.88	.074
24	5.78	31.56	24.88	.078	25	5.79	31.57	24.89	.081
26	5.79	31.60	24.91	.084	27	5.80	31.58	24.90	.087
28	5.80	31.58	24.91	.090	29	5.80	31.60	24.91	.093
30	5.80	31.61	24.92	.096	31	5.81	31.61	24.92	.099
32	5.81	31.61	24.92	.102	33	5.81	31.60	24.92	.105
34	5.80	31.60	24.92	.108	35	5.80	31.60	24.92	.111
36	5.80	31.59	24.91	.114	37	5.80	31.58	24.90	.117
38	5.79	31.59	24.91	.120	39	5.79	31.58	24.90	.123
40	5.79	31.58	24.90	.126	41	5.79	31.59	24.91	.129
42	5.79	31.60	24.92	.133	43	5.80	31.60	24.91	.136
44	5.80	31.62	24.93	.139	45	5.81	31.62	24.93	.142
46	5.81	31.62	24.93	.145	47	5.81	31.63	24.94	.148
48	5.81	31.64	24.95	.151	49	5.81	31.62	24.93	.154
50	5.82	31.62	24.93	.157	51	5.82	31.65	24.95	.160

K.

## A Microprocessor-Based Transcriber\*

Patrick D. McLain

NOAA/ERL Pacific Marine Environmental Laboratory

### Abstract

A data transcriber that would accept several data formats as inputs and produce a computer tape with a standard format as an output would help to optimize both the transcription process and subsequent data analysis. The application of microcomputer-based technology is seen as a possible method of developing such a system.

In this paper, the development of a microprocessor-based Aanderaa Transcriber is discussed. In addition, characteristics of a more sophisticated transcribing system are explored.

### Introduction

The retrieval and subsequent analysis of oceanographic data plays a major role in oceanographic research. Currently, most data is entered into a computer where it can be subjected to sophisticated mathematical analysis techniques. Thus, the process of transferring large quantities of data from the data-gathering instrument into the computer is a very crucial step. A transcriber is needed to accept data from the instrument as an input and produce the same data in a computer-compatible form as the output.

NOAA's Pacific Marine Environmental Laboratory deploys many instruments of various kinds and consequently processes much data. Each instrument manufacturer has his own format in which data is recorded. Furthermore, several types of magnetic tape devices are used as the storage medium. This variety of formats and storage media encourages a corresponding variety of data processing software; different software is developed for each individual data format. Both the data transcription process and the data analysis process would be improved by development of a transcriber capable of accepting several data formats as inputs and producing a standard format computer tape as an output.

In addition, an intelligent transcribing system could be assigned some initial data clean-up chores, which are currently either done by hand or on a main-frame computer. At the present state-of-the-art, microcomputer systems are a logical choice as a method of developing the proposed data transcriber. Micro-based systems are well suited to a dedicated control- and decision-making process. They have enough power to support a fairly sophisticated system, yet their cost is considerably less than that of a traditional minicomputer. An opportunity arose to apply microcomputer technology to the data transcription process at PMEL when an old Aanderaa transcriber began losing its reliability.

In order to keep this first transcribing system as simple and inexpensive as possible, it was decided that it would only handle Aanderaa-format input data. Furthermore, the format of the output should retain as much compatibility as possible with the processing software developed for the previous translator. For this reason, the output is recorded on 7-track digital tapes.

\* Contribution No. 380 from the NOAA/ERL Pacific Marine Environmental Laboratory.

## Data Format Analysis

For the sake of simplicity, the following discussion will use as its model the Aanderaa current meter data format. This data has six 10-bit words per frame, the first word of which is the reference word. Each meter is assigned its own unique reference word value, which ideally stays constant throughout the entire data tape. Appended onto the end of a frame of data is a sync bit. When the data tape is played at  $7\frac{1}{2}$  i.p.s., the data has the following characteristics:

1. Bit pulses have a duration of approximately  $450 \mu\text{s}$  if they are "0" bits, and  $250 \mu\text{s}$  if they are "1" bits or the sync bit.
2. There are approximately  $667 \mu\text{s}$  between the leading edges of successive bits.
3. There are approximately 4 ms between the end of one data word and the beginning of the next data word.
4. The sync bit occurs approximately 1.5 ms after the end of the last bit of word 6.

The first step in analyzing the data is to determine whether a pulse on the input is "1" or "0". The pulse duration is detected by using the input signal to gate on the clock input to a counter. As long as the data pulse is high, the counter counts the clock pulses. The contents of the counter can then be read by the microcomputer and compared against preset values to determine whether it is "1" or "0". By this technique the data is buffered into the microcomputer's memory 1 bit at a time and stored in units of 5 bits per 8-bit byte of memory.

A count of the number of bits in the current word is kept, along with a count of the number of words buffered in during the current data frame. At every word gap, one of five possible conditions is checked:

1. If there are less than 6 words detected in the current frame, and the present word has 10 bits, then this is the desired format.
2. Similarly, if there are 6 words in the current frame, and the current word had a bit count of 11 (10 plus the sync bit) then again this is the desired format. The data frame is written to the selected recorder (digital or strip-chart). We assume here that if an 11th bit occurs on the 6th word, it is the sync bit. The attempt to look for the sync bit is not limited to a certain time interval. This technique eliminates any dependence on the temporal stability of either the device playing the input data tape or the timing circuit responsible for opening the "sync window".
3. If there are less than 6 words and less than 10 bits, then a bit-count error has occurred. This is one of the 5 error types that the translator checks.
4. If there are less than 6 words, but more than 10 bits, then it is possible that a sync bit was generated. This situation could occur if the translator got out of sync with the incoming data, or if some words of incoming data were lost. In order to determine whether the extra bit is a sync bit or a meter malfunction, the translator does a reference word check routine. The current data buffer is retained,

and the next word is read from the input. This word is then compared to the reference word. If it is not the reference word, then the 11-bit word merely has a bit-count error. If it is the reference word, however, then the 11th bit must have been a sync bit. In this event, the partial frame is filled out to a complete 6-word frame with zeros. The frame is then written to the appropriate recorders. A zero-filled frame is another of the error types for which the translator looks.

5. If there are 6 words in the current frame but less than 11 bits in the last word, the transcriber must again do a reference word check. As before, the current data buffer is retained; the next word is obtained from the input and compared to the reference word. If it is the reference word, then there is a missing sync bit. If it is not the reference word, then the translator has gotten out of sync with the data, since both the sync bit and the reference word are missing. In either case, after flagging the appropriate errors, the frame is written to the recorders.

### Error Types

While performing the preceding data format checks, the translator looks for and keeps a running total of 5 possible error types: bit-count error, missing sync bit, missing reference word, zero-filled frame, and pulse-width error. The bit count and missing sync-bit error types are self-explanatory. The missing reference word error is flagged only if an 11th (sync) bit is not found on the 6th data word, and the reference word check routine does not detect the presence of the reference word. The translator does not check the value of the reference word on every frame. A zero-filled frame error implies that a frame with less than 6 words has been detected. The pulse-width error type is one which was carried over from the old translator; it is not being used currently.

### Output Data Format

The output data format is as follows (see Fig. 1). Each 10-bit data word is separated into two 5-bit bytes; the high byte of a word is recorded first, followed by the low byte. The translator appends a 6th bit to each byte. On the first (n-1) words, where n is the number of words per data frame, the 6th bit is set to zero. On the nth word, the 6th bit is "0" on the high byte, and "1" on the low byte. The 6th bit on both bytes of the error word is "1". This flag bit helps the processing software identify the end of a data frame. The 7th bit on every 7-bit character is the parity bit added by the tape recorder.

This data format is exactly the same as that used by the previous translator. Thus, all the bit manipulation and data word recognition routines used on data from the old transcriber are applicable to data from the new one. The only exception is the software that interprets the error word. As there are 5 error types detected by the new translator as opposed to 3 for the old translator, an entirely new error word encoding scheme was devised.

### Error Word Encoding

A 10-bit error word is appended to each data frame. This word is divided into two 5-bit bytes. The bits in the high byte are used to flag the occurrence of a particular error type during the data frame. The bits in the low byte are

used to show which words in the frame had errors. See Figure 2 for the significance of each bit in the error word.

### Front Panel Controls

As mentioned earlier, the preceding discussion used the Aanderaa current meter data format as its model for ease of description. Through the use of various front panel controls, the operator can configure the transcriber so that it will accept data from other Aanderaa-format instruments, such as tide gages and Plessey current meters. Several other operational mode options are also available through the front panel controls (refer to Fig. 3).

The Total Records display tells how many records have been written to the recorders. The Errors display is controlled by the Error Type thumb switch. With the thumb switch set on "0", the total number of errors is displayed. A setting of "1" displays pulse-width errors; "2" displays missing sync errors; "3" displays bit-count errors; "4" displays zero-filled frame errors; and "5" displays missing reference word errors. The Error Type thumb switch may be changed at any time during or after tape transcription.

The Words/Sync thumb switch is used to select how many words there are per data frame on a given tape to be transcribed. The Records/IRG switch determines how many data frames are to be grouped into 1 record on the Digital tape drive. The Run/Test switch, when in test position, operates in conjunction with the Zero/One switch to cause either zero- or full-scale deflection on the strip-chart recorder channels, thus allowing them to be properly calibrated.

The Reference Number/Range thumb switches are used to determine the range of values that will be considered acceptable reference numbers. The value on the Range thumb switch is added to and subtracted from the value on the Reference Number switch to determine the acceptable range of reference number values. A range of values is necessary here, as the reference number is not always stable. Obviously, the larger the range setting, the higher the probability that a data word will fall within the range of accepted reference word values. If all of these thumb switches are set to zero, then the transcriber bypasses all reference word check routines. An 11th bit is automatically assumed to be a sync bit. Similarly, if the number of words in a data frame specified by the Words/Sync switch have been buffered in, then they are written to the recorders, regardless of the presence or absence of a sync bit.

### Data Quality

The transcriber has not been in use long enough to have made any in-depth studies of data quality. According to those who work with the data, its quality has improved considerably over that of the previous translating system. However, a problem has been encountered: the zero-filled frames occasionally increase the number of data records. Determining the data time-base can be difficult as a result. Some modifications in the processing software are necessary to correct this situation.

The development of this transcriber gave the necessary experience with microprocessors to begin development of a more sophisticated system. Following are some characteristics that such a system should possess:

1. The transcribing system should have the ability to input data from a variety of types of data.
2. The transcriber should produce computer-compatible tapes with a standardized data format.

3. The transcriber should be capable of doing some simple data reduction chores.

By accepting a variety of types of data as inputs, all data tapes generated by a particular laboratory group could be read on the same transcriber. When an instrument is selected for use that has a new data format, a new interface would need to be developed for that type of data. This interface would involve both hardware and software (see Fig. 4). The various interfaces would supply binary data to a high-speed controller, such as a bit-slice processor. This processor would then check for word framing and produce data words with a standard length, blanking high-order bits where necessary. A microcomputer could then assess the data, do further error and format checking, and produce the digital tapes.

Lack of a standard format on the computer-compatible data tapes encourages the development of separate software routines, often causing expensive redundancy. This is especially true if a laboratory or institution grows rapidly without a coordinated plan for software development. The easiest and most obvious place to attempt to bring different types of data tapes together to allow common processing techniques is in the transcribing process. If the data on the computer tape has a standard format, then it can be buffered into the computer's memory using the same routine, regardless of the original format of the data. Further processing, which would look for words, frames, etc., could be configured by the individual user for his particular application.

Consider the following example. Suppose that only 4 bits in every 9-track character are to be filled with data. The next 3 are to be zeros, and the last one is to be a flag bit, used to signal the end of a frame. Every Aanderaa word would then occupy 3 characters. Since this implies 12 data bits, the 2 most significant bits would be zeros (see Fig. 5). All data word boundaries would occur at integral multiples of 4 bits. In the above example, all Aanderaa words would occupy 12 bits. This technique would cause a certain amount of tape overhead, and there are surely many others that could be considered. Yet a standardized format on computer tape would encourage the use of common data analysis routines, thus reducing the expense of software development.

Finally, an intelligent transcriber could be used to do some of the initial reduction. The intelligence of such a device offers the flexibility to perform many of the routine and time-consuming chores in an efficient and often cost-effective manner.

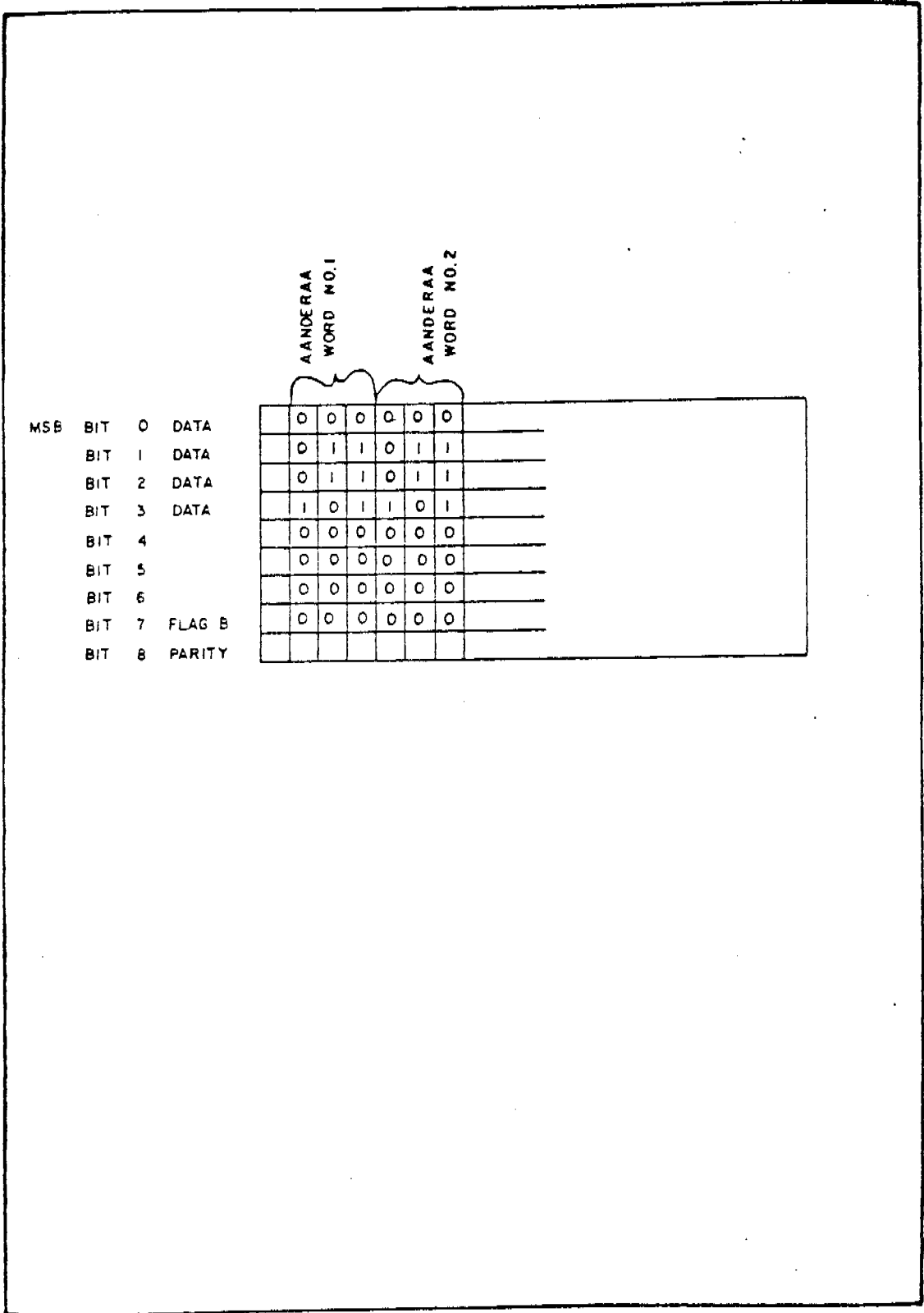
### Summary

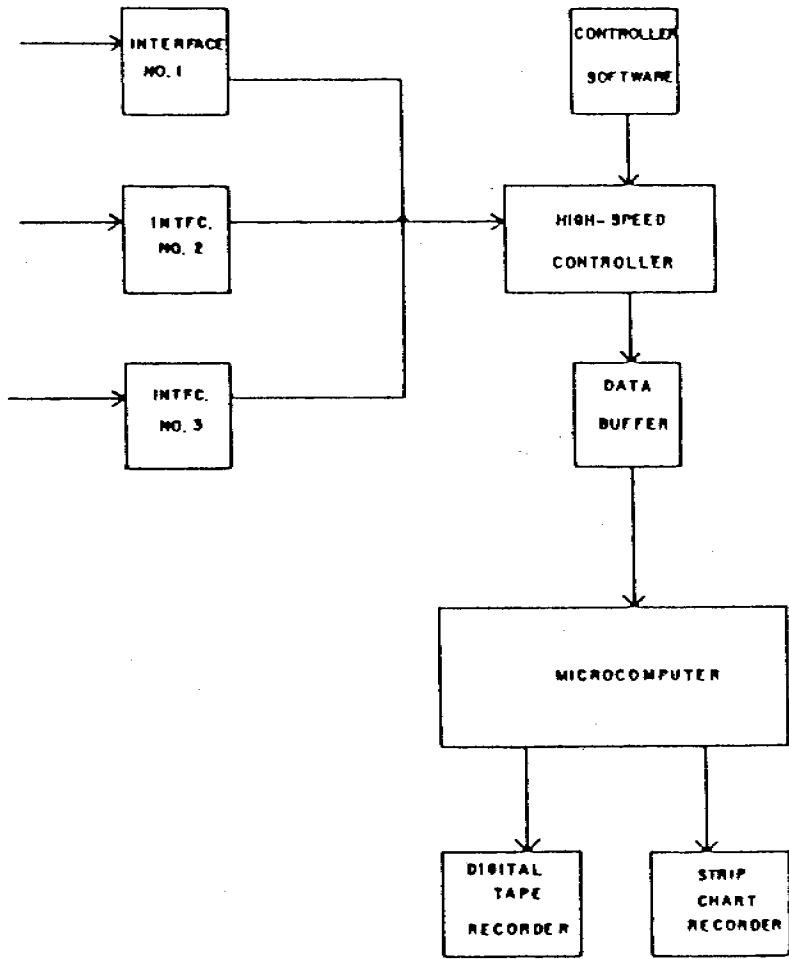
The successful operation of the microprocessor-based Aanderaa transcriber is an encouraging first step toward a standardized transcribing system. Future efforts will be directed toward expanding the system as outlined above.

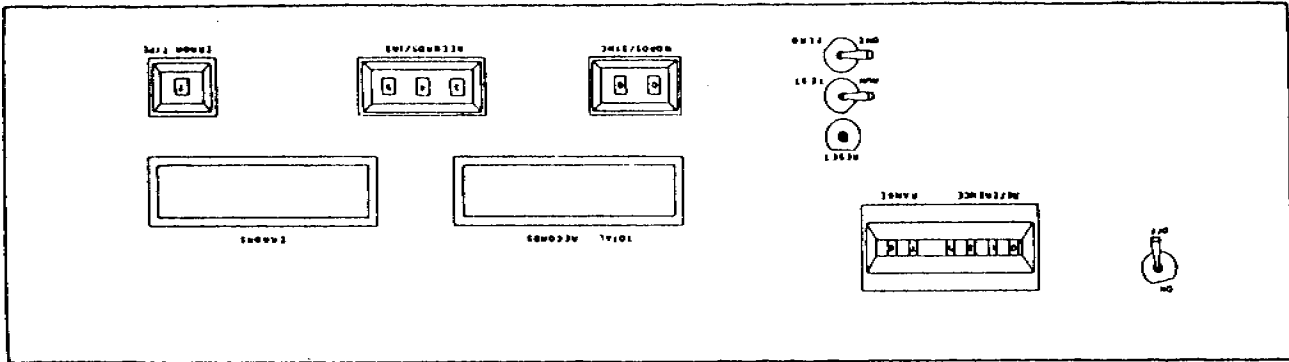
### Figure Captions

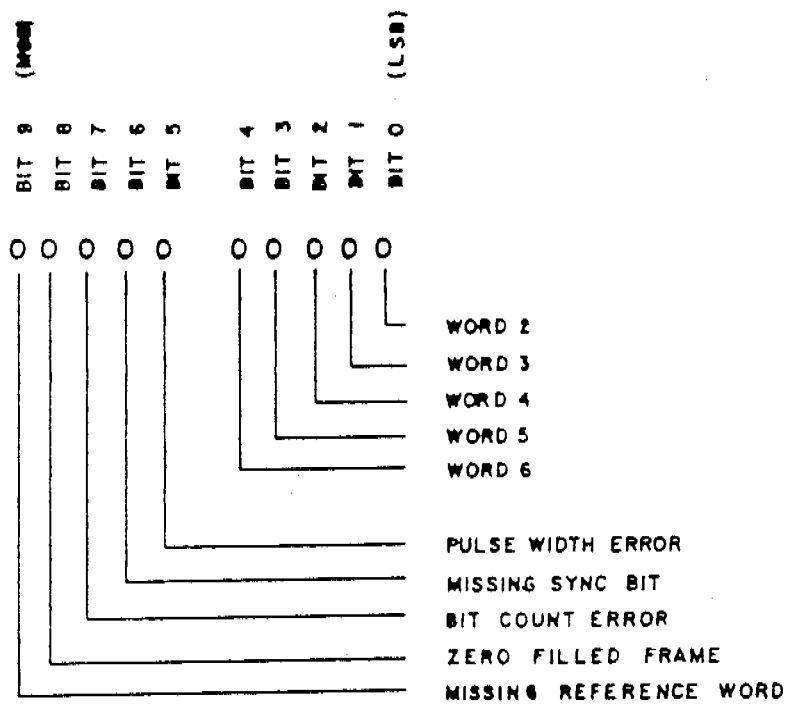
- Figure 1. Output data format of the Aanderaa transcriber. Bits 0 through 4 are data bits; bit 5 is a flag bit.
- Figure 2. Aanderaa error word encoding. An error word is generated for each Aanderaa data frame.
- Figure 3. Front panel controls of the Aanderaa translator.
- Figure 4. Block diagram of a multi-input transcribing system.
- Figure 5. Example of a standardized computer tape format.

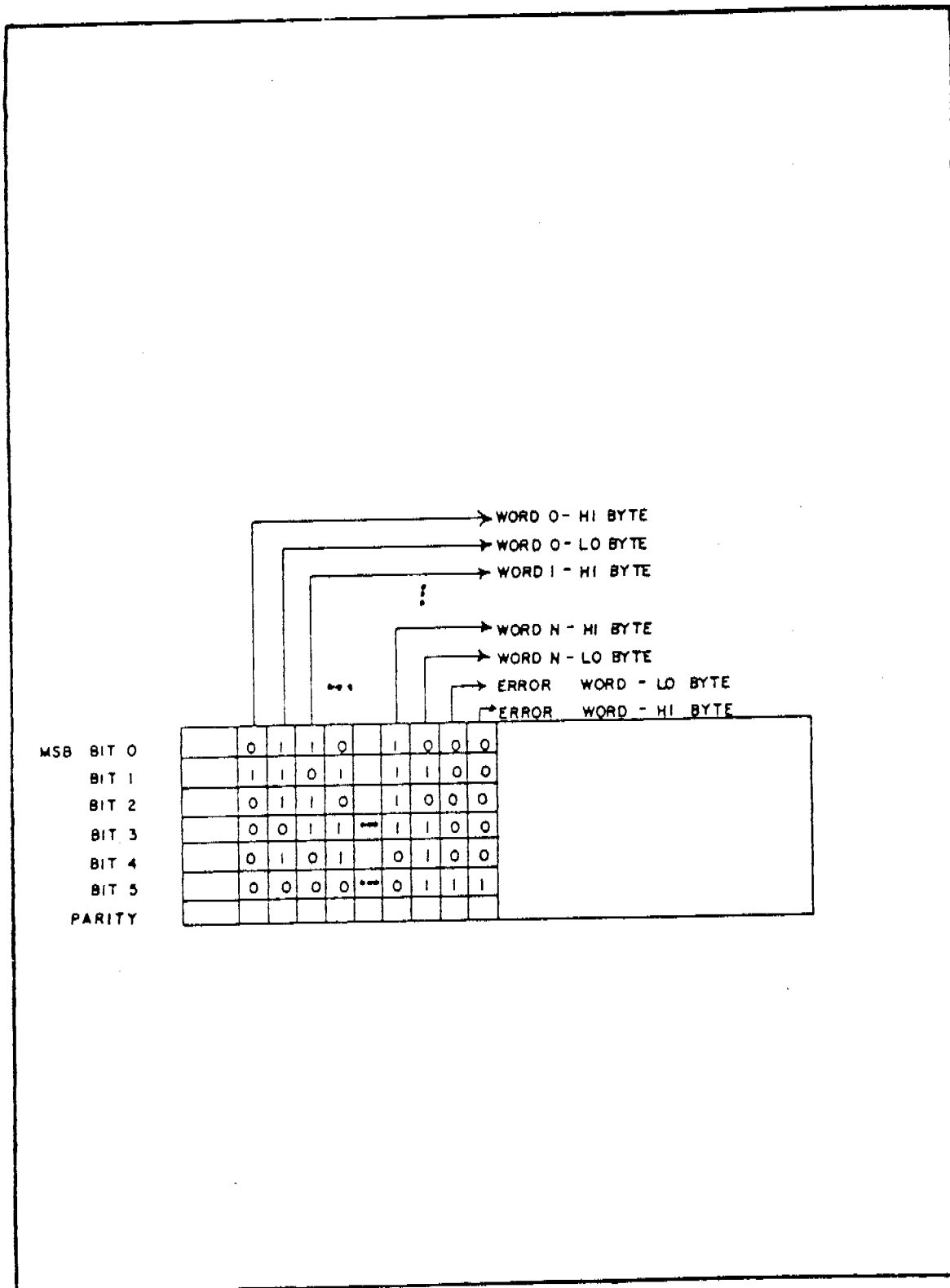












## VII. Cooperation

During the past year, extensive cooperation has occurred with the following RU's: 289 (Royer), 217 (Hansen), 367 (Reynolds), 140 (Galt) 348 (Barrick), 551/552/553 (Kodiak Island Food Web Study) and 436 (Rauw). Such coordination has resulted in a draft synthesis report for the Northwest Gulf of Alaska. This report is presently under revision and is to be, on amended form, published as a NOAA/ERL/PMEL Technical Report (see Section VI.G).

## VIII. Publications

The following list of publications was compiled in March 1980 and does not include other than "in print" manuscripts:

Reviewer's Name J.D. Schumacher  
Affiliation PMEL/COASTAL PHYSICS

### 1. CITATION: (INCLUDING TITLE, DATE, PLACE OF PUBLICATION)

Schumacher, J.D., R.L. Charnell, S.P. Hayes, H. Mofjeld and R. D. Muench, 1978. GULF OF ALASKA STUDY OF MESOSCALE OCEANOGRAPHIC PROCESSES. In Envir. Assessment of the Alaskan Continental Shelf, Vol. IX, Transport: 61-213.

RU # : 138

	<u>CODE WORD(S)</u>	<u>CODE NUMBER(S)</u>
REGION:	GOA	8
LEASE AREA:	Kodiak, Lower Cook Inlet, NE GOA	19, 20, 21
RESEARCH AREA:	Oceanography	30

Reviewer's Name J. D. SCHUMACHER  
Affiliation PMEL/COASTAL PHYSICS

1. CITATION: (INCLUDING TITLE, DATE, PLACE OF PUBLICATION)

Galt, J.A. 1977. GULF OF ALASKA STUDY OF MESOSCALE OCEANOGRAPHIC PROCESSES (GAS-MOP). In Envir. Assessment of the Alaskan Continental Shelf, Annual Rep. Summary for the year ending 1975: 238-258

RU # : 138/140

	<u>CODE WORD(S)</u>	<u>CODE NUMBER(S)</u>
REGION:	GOA	8
LEASE AREA:	NE GOA	21
RESEARCH AREA:	Oceanography	30

2. CITATION: (INCLUDING TITLE, DATE, PLACE OF PUBLICATION)

Hayes, S.P. and J.D. Schumacher, 1976. GULF OF ALASKA STUDY OF MESOSCALE OCEANOGRAPHIC PROCESSES (GAS-MOP). In Envir. Assessment of the Alaskan Continental Shelf, Vol. II: 75-106.

RU # : 138

	<u>CODE WORD(S)</u>	<u>CODE NUMBER(S)</u>
REGION:	GOA	8
LEASE AREA:	NE GOA, Kodiak	21,19
RESEARCH AREA:	Oceanography	30

3. CITATION: (INCLUDING TITLE, DATE, PLACE OF PUBLICATION)

Royer, T.C. and R.D. Muench, 1977. ON THE OCEAN TEMPERATURE DISTRIBUTION IN THE GULF OF ALASKA, 1974-1975. J. Phys. Oceanogr., 7: 92-99.

RU #: 138/289

	<u>CODE WORD(S)</u>	<u>CODE NUMBER(S)</u>
REGION:	GOA	8
LEASE AREA:	Non-site	25
RESEARCH AREA:	Oceanography <u>2/5</u>	30

Reviewer's Name J. D. SCHUMACHER  
Affiliation PMEL/COASTAL PHYSICS

1. CITATION: (INCLUDING TITLE, DATE, PLACE OF PUBLICATION)

Holbrook, J.R. and D.Halpern, 1977. A COMPILATION OF WIND, CURRENT, BOTTOM-PRESSURE AND STD/CTD MEASUREMENTS IN THE NORTHEAST GULF OF ALASKA, FEBRUARY - MAY 1975. NOAA Tech, Memo ERL-PMEL 10: 119 pp.

RU # : 138

	<u>CODE WORD(S)</u>	<u>CODE NUMBER(S)</u>
REGION:	GOA	8
LEASE AREA:	NE GOA	21
RESEARCH AREA:	Oceanography	30

2. CITATION: (INCLUDING TITLE, DATE, PLACE OF PUBLICATION)

Muench, R.D., H. Mofjeld and R.L. Charnell, 1978. OCEANOGRAPHIC CONDITIONS IN LOWER COOK INLET, SPRING AND SUMMER 1973. J. Geophys. Res. 83: 5090-5098.

RU # : 138

	<u>CODE WORD(S)</u>	<u>CODE NUMBER(S)</u>
REGION:	GOA	8
LEASE AREA:	Lower Cook Inlet	20
RESEARCH AREA:	Oceanography	30

3. CITATION: (INCLUDING TITLE, DATE, PLACE OF PUBLICATION)

Feely, R.A., E.T. Baker, J.D. Schumacher, G.J. Massoth and W.M. Landing, 1979, PROCESSES AFFECTING THE DISTRIBUTION AND TRANSPORT OF SUSPENDED MATTER IN THE NORTHEAST GULF OF ALASKA. Deep-Sea Res. 26; 445-464.

RU #: 138/152

	<u>CODE WORD(S)</u>	<u>CODE NUMBER(S)</u>
REGION:	Gulf of Alaska (GOA)	8
LEASE AREA:	NE GOA	21
RESEARCH AREA:	Oceanography	30

216



Reviewer's Name J.D. Schumacher  
Affiliation PMEL/COASTAL PHYSICS

1. CITATION: (INCLUDING TITLE, DATE, PLACE OF PUBLICATION)

Galt, J.A., 1976, CIRCULATION STUDIES ON THE ALASKAN CONTINENTAL SHELF OFF THE COPPER RIVER. U.S. Dept. of Comm./NOAA (ERL Report: 36 pp.

RU #: 138/140

	<u>CODE WORD(S)</u>	<u>CODE NUMBER(S)</u>
REGION:	GOA	8
LEASE AREA:	NE GOA	21
RESEARCH AREA:	Oceanography	30

2. CITATION: (INCLUDING TITLE, DATE, PLACE OF PUBLICATION)

Hayes, S.P., 1979. VARIABILITY OF CURRENT AND BOTTOM PRESSURE ACROSS THE CONTINENTAL SHELF IN THE NORTHEAST GULF OF ALASKA. J. Phys. Oceanogr. 9: 88-103

RU #: 138

	<u>CODE WORD(S)</u>	<u>CODE NUMBER(S)</u>
REGION:	GOA	8
LEASE AREA:	NE GOA	21
RESEARCH AREA:	Oceanography	30

3. CITATION: (INCLUDING TITLE, DATE, PLACE OF PUBLICATION)

Royer, T.C., D.V. Hansen and D.J. Pashinski, 1979. COASTAL FLOW IN THE NORTHERN GULF OF ALASKA AS OBSERVED BY DYNAMIC TOPOGRAPHY AND SATELLITE-TRACKED DROGUED DRIFT BUOYS. J. Phys. Oceanogr. 9(4): 785-801.

RU #: 138/217#289

	<u>CODE WORD(S)</u>	<u>CODE NUMBER(S)</u>
REGION:	GOA	8
LEASE AREA:	NE GOA	21
RESEARCH AREA:	Oceanography 217	30

Reviewer's Name J. D. Schumacher  
Affiliation PMEL/COASTAL PHYSICS

1. CITATION: (INCLUDING TITLE, DATE, PLACE OF PUBLICATION)

Schumacher, J.D., R. Silcox, D. Dreves and R.D. Muench, 1978. WINTER CIRCULATION AND HYDROGRAPHY OVER THE CONTINENTAL SHELF OF THE NORTHWEST GULF OF ALASKA. NOAA/ERL Tech. Rep., ERL 404-PMEL 31: 16 pp.

RU # : 138

	<u>CODE WORD(S)</u>	<u>CODE NUMBER(S)</u>
REGION:	GOA	8
LEASE AREA:	Kodiak, Lower Cook Inlet	19,20
RESEARCH AREA:	Oceanography	30

2. CITATION: (INCLUDING TITLE, DATE, PLACE OF PUBLICATION)

Schumacher, J.D., R.K. Reed, M. Grigsby and D.Dreves, 1979. CIRCULATION AND HYDROGRAPHY NEAR KODIAK ISLAND, SEPTEMBER TO NOVEMBER 1977. NOAA Tech. Memo ERL PMEL-13: 49 pp.

RU # : 138

	<u>CODE WORD(S)</u>	<u>CODE NUMBER(S)</u>
REGION:	GOA	8
LEASE AREA:	Kodiak, Lower Cook Inlet	19, 20
RESEARCH AREA:	Oceanography	30

3. CITATION: (INCLUDING TITLE, DATE, PLACE OF PUBLICATION)

Hayes, S.P. and J.D. Schumacher, 1977. GULF OF ALASKA STUDY OF MESOSCALE OCEANOGRAPHIC PROCESSES (GAS-MOP). In Envir. Assessment of the Alaskan Continental Shelf, Vol. XIV, Transport: 251-328.

RU #: 138

	<u>CODE WORD(S)</u>	<u>CODE NUMBER(S)</u>
REGION:	GOA	8
LEASE AREA:	Kodiak, NE GOA	19, 21
RESEARCH AREA:	Oceanography 218	30

2. CITATION: (INCLUDING TITLE, DATE, PLACE OF PUBLICATION)

Reynolds, R.M. and B. Walter, 1975. CURRENT METER MEASUREMENTS IN THE GULF OF ALASKA - PART 1 RESULTS FROM NEGOA MOORINGS 60, 61, 62A. NOAA Tech. Memo. ERL PMEL-3: 290 pp.

RU # : 138

	<u>CODE WORD(S)</u>	<u>CODE NUMBER(S)</u>
REGION:	GOA	8
LEASE AREA:	NE GOA	21
RESEARCH AREA:	Oceanography	30

3. CITATION: (INCLUDING TITLE, DATE, PLACE OF PUBLICATION)

Hayes, S.P. and J.D. Schumacher, 1976. DESCRIPTION OF WIND, CURRENT AND BOTTOM PRESSURE VARIATIONS ON THE CONTINENTAL SHELF IN THE NORTHEAST GULF OF ALASKA FROM FEBRUARY TO MAY 1975. J. Geophys. Res., 81: 6411-6419.

RU #: 138

	<u>CODE WORD(S)</u>	<u>CODE NUMBER(S)</u>
REGION:	GOA	8
LEASE AREA:	NE GOA	21
RESEARCH AREA:	Oceanography	30

## IX. Needs for Further Study

Based on our present understanding of the physical oceanography of this study area, we suggest the following programs. The order of priority is:

- a) first, contribute to our knowledge and be of use in trajectory analyses/modelling effects.
- b) second, increase validity of present knowledge through further documentation of important advective and diffusive processes.
- c) third, contribute to science primarily from further analysis of existing data.

1. Detailed study of processes on a bank: Bathymetric features such as Portlock or North Abatross bank can result in complex circulation. For example, recent studies on Georges Bank (Loder, Scarlet, Magnell, Frye, Flagg and Andrews; and several other abstracts in EOS, Trans, Am. Geophys. Union, Vol 60(18): pp 278-279) indicate that enhanced tidal mixing, rectification of tidal currents and episodic events (including eddies) play significant roles in residence time of water over this bank. To evaluate the nature of such processes over lease area banks would require a substantial field program, requiring hydrographic, bottom pressure, current and wind measurements of at least one year duration. Imbedded within such an experiment should be a well defined examination of vertical shear and stability, such as that proposed for the north Aleutian lease area. The use of a surface mooring would permit measurement of local wind, near-surface (~4 m) current, vertical density and current structure, tidal energy dissipation and local sea-level perturbations. This program would address priorities a) and b).

2. Detailed study of the Kenai Current: Acquire along and across flow density, current and bottom pressure measurements to define low frequency behavior, width and integral time scale and to elucidate processes by which warm saline bottom waters transit from the shelf edge into the coastal current. Recent work by P. Poole (NWS, Anchorage, AK) suggests that the relatively warm Kenai

Current waters may delay ice formation and impact extent and distribution of ice cover in Cook Inlet. This observational program would address a) and b).

3. Detailed study of Kamashak Bay: Further field work in the bay and adjacent Lower Cook Inlet waters using current meters, radar tracked drifting buoys and CTD data to address a) and b).

4. Further analysis of existing CTD data and the temperature and conductivity data collected from current meters to establish statistical characteristics of the mass field and its seasonal behavior: Such information would be useful in evaluating the validity of a "mean" density field in a diagnostic model. Such analysis, coupled with a moderate field program including current meter moorings and model grid CTD data points, would serve as model verification and would address all priorities.

5. Further analysis of meso-scale meteorological features (as compiled from surface atmospheric pressure charts) and existing current and bottom pressure records. Such an effort would require no new field work and would address a) and c).

#### X. Conclusions

With completion of Physical and meteorological conditions in the northwest Gulf of Alaska, RU138 will have produced Final Reports for both the northeast and northwest Gulf of Alaska programs. Many conclusions regarding regional circulation, dynamics and hydrography have resulted from the Gulf of Alaska Study of Meso-scale Oceanographic Processes and these appear in published literature (see Section VI and VIII of this report). We take this opportunity to thank BLM and the Juneau Project Office for their support. May any future programs be as fruitful and contribute as well to OCSEAP needs.

The first part of the document discusses the importance of maintaining accurate records of all transactions. It emphasizes that every entry, no matter how small, should be recorded to ensure the integrity of the financial statements. This includes not only sales and purchases but also expenses and income. The document provides a detailed list of items that should be tracked, such as inventory levels, accounts payable, and accounts receivable. It also outlines the procedures for recording these transactions, including the use of double-entry bookkeeping to ensure that the debits equal the credits.

The second part of the document focuses on the analysis of the recorded data. It explains how to calculate key financial ratios and metrics, such as the gross profit margin, operating profit, and return on investment. These calculations are essential for understanding the company's financial performance and identifying areas for improvement. The document also discusses the importance of comparing the company's performance against industry benchmarks and historical data to provide context for the results.

The final part of the document addresses the reporting requirements for the financial statements. It details the format and content of the income statement, balance sheet, and cash flow statement, as well as the accompanying notes and disclosures. It emphasizes the need for transparency and accuracy in the reporting process, as well as the importance of obtaining external audits to verify the reliability of the financial data.

ANNUAL REPORT

Contract: #03-5-022-56  
Research Unit: #289  
Task Order: #19  
Reporting Period: 04/01/79-  
03/31/80  
Number of Pages: 84

CIRCULATION AND WATER MASSES IN THE GULF OF ALASKA

Thomas C. Royer

Institute of Marine Science  
University of Alaska  
Fairbanks, Alaska 99701

March 1980

## TABLE OF CONTENTS

I.	SUMMARY . . . . .	225
II.	INTRODUCTION. . . . .	225
III.	CURRENT STATE OF KNOWLEDGE. . . . .	226
IV.	STUDY AREA. . . . .	227
V.	SERVICES, METHODS AND RATIONALE OF DATA COLLECTION. . . . .	228
VI.	RESULTS AND DISCUSSION. . . . .	228
	Remote Sensing Activities . . . . .	228
	Gulf of Alaska Review . . . . .	230
	Northwest Gulf of Alaska Synthesis. . . . .	231
	Currents at IMS 9 . . . . .	232
	Transport Variations in the Alaskan Current . . . . .	232
	Transport Variations in the Alaskan Coastal Current . . . . .	232
	Prince William Sound. . . . .	233
VII.	CONCLUSIONS AND OUTLOOK . . . . .	234
VIII.	SUMMARY OF FOURTH QUARTER OPERATIONS. . . . .	236
	Task Objectives . . . . .	236
	Field Operations. . . . .	236
	Results . . . . .	236
	Problems Encountered. . . . .	237
	APPENDIX I - Review of the Physical Oceanography of the Northeast Gulf of Alaska, with Emphasis on its Implications to Oil and Gas Development. . . . .	238



## I. SUMMARY

The understanding and interpretation of the data acquired during the past five years in the Gulf of Alaska has continued in the past year along with the acquisition of data from a few selected sites. The analysis is allowing us to return to our previously acquired data and refine our interpretations. For example, last year we concluded that small or mesoscale eddies are frequently located over the outer shelf near the continental slope. This year, we are using this knowledge of eddies to help analyze previous hydrographic data. Perturbations in numerical models near Kodiak support this existence of these eddies.

The focus of this year's research has continued to be on mesoscale driving mechanisms. The mechanisms for driving the shelf circulation, such as wind stress, precipitation, runoff, and offshore circulation have been more clearly identified. A more detailed analysis of Alaska Current and Alaskan Coastal Current responses to these forcing mechanisms has been accomplished this year.

A review of the physical oceanography for the Northeast Gulf of Alaska (NEGOA) has been completed. The latest draft of this review is contained in this report as an appendix.

## II. INTRODUCTION

The emphasis of RU #289 this year has continued to be on the analysis of data gathered in previous years under OCSEAP support. A transition has occurred from data gathering to data analysis and interpretation. Limited field work under OCSEAP support has continued with project personnel participating in three cruises. All

current meter moorings from the entrances of Prince William Sound have been recovered. The purpose of the continued field effort is to better define the circulation and its driving mechanisms in Prince William Sound. The hydrography program and current measurements were terminated in September 1979.

A progression of ideas on the circulation of the shelf area of the Gulf of Alaska has lead us from an initial concept of generalized cyclonic flow to highly localized flow patterns. We have identified flow regimes and delineated their driving mechanisms. We now have the annual cycle in the baroclinic circulation quite well-defined and attention is now being directed to the smaller scale temporal and spatial perturbations. At the same time we are able to adjust our focus and address processes which influence the circulation over the continental shelf of the entire Gulf of Alaska.

### III. CURRENT STATE OF KNOWLEDGE

Since the inception of the OCSEAP-NEGOA program, the knowledge of the physical oceanography, in particular circulation and water masses, has evolved from the point where the annual cycle was marginally described to where we now understand some of the physical mechanisms which control the annual cycle. This progress follows the traditional scientific method where initial observations lead to the development of a hypothesis which is then tested. After testing, the hypothesis should be modified and retested until a satisfactory refinement is attained. The work of this research unit remains somewhere between the development and initial testing of hypothesis. The practical

implications of this evolution are obvious in the case of OCSEAP: we will be better able to predict the shelf circulation and hence the possible trajectories that oil spills would follow. The improved understanding of the physical mechanisms which control the circulation allow predictions to be made for times outside our observational periods. Therefore, from measureable or easily predicted functions, such as the meteorological parameters, we might imply the response of those parameters which are more difficult to measure in real time, such as currents.

As stated above, the hypothesis development from observations is presently underway. The next stage, the experiment to test the hypothesis, apparently will never be a part of the OCS program. For this reason, many scientists involved with the program now must look elsewhere to fund their academic growth.

#### IV. STUDY AREA

Field work under this research unit has ranged over the continental shelf of the southern Alaska coastline from Yakutat to Umiak Pass from the coastline to tens of kilometers beyond the shelf break. The satellite data archived for OSCEAP by this unit covers the entire Alaskan coastline from the Beaufort Sea to Southeast. The analysis portion of the past year's work has addressed the entire Gulf of Alaska region, while the field work has been limited to the area between the Copper River and Seward including Prince William Sound.

## V. SERVICES, METHODS AND RATIONALE OF DATA COLLECTION

As in previous years, the primary data collection method used by this research unit was the CTD/STD (salinity - temperature - depth) profile. Some current meter and bottom pressure gauge deployments have also been undertaken to supplement the hydrographic data. From the CTD/STD data, contour maps of salinity, temperature, density and dynamic height were constructed. The contours provide information on the direction and intensity of the flow. The current meter measurements provide a means of "calibrating" the currents obtained from the density fields. The sea level as measured at the coastline by NOS (National Ocean Survey) stations was used in conjunction with the bottom pressure data to determine changes in the slope of sea level between the positions and hence a measure of current changes.

The CTD/STD station positions were determined by 1) a knowledge of the spatial scales of the features to be measured and 2) requirements to continue a time history of oceanographic parameters at a particular location. The objective has been an improved understanding of changes in the oceanographic parameters, spatially and temporally.

## VI. RESULTS AND DISCUSSION

### Remote Sensing Activities

The incoming NOAA-AVHRR satellite imagery has been monitored through transparencies sent to the Geophysical Institute Remote Sensing Library from the NOAA-NESS CDA Satellite Station at Gilmore. After it was noticed that the Gulf of Alaska was poorly covered in the transparencies, all negatives produced by the TIROS-N and NOAA-6 satellites have also been

screened at the tracking station since October 1979. From March 1979 through February 1980 a total of 1323 prints including 317 photographic enlargements and 37 temperature enhancements have been produced by the tracking station for archiving. Requests from other users total 292 prints including 59 enlargements. In addition to the temperature enhancements made specifically for this RU, copies of enhancements and computer enlargements requested by the NESS-Satellite Field Service Station in Anchorage since November have also been ordered by this RU. The new prints are contained in 9 ring binders which increases the total collection to 37 binders.

Enlargements of Norton Sound and the polynyas near Nome and St. Laurence Island, have been made since December for studies of ice movement. These enlargements extend to the Bering Strait. So far, no indication of ice export from the Chukchi Sea has been observed this season. However, the problem of ice export was addressed at presentations given in Tokyo, Japan and Trondheim, Norway.

During the past year the satellite facility has provided imagery to other users in support of research along the Bering Sea ice edge, upwelling around the Pribilofs, break-up along the Beaufort Sea coast, bird migration and nesting in Chukchi Sea in relation to the ice edge and sea-surface temperatures from 1974 to present, suspended sediments from the Yukon and the Anadyr Rivers and eddies east of Kamchatka (request from USSR). In addition, advice and reprints when applicable, have been given to people inquiring about herring and crab harvesting in relation to the ice edge in the Bering Sea, Karman vortices off the Aleutians, migration of arctic fox to the far western Aleutians and availability of

satellite imagery from NW Greenland for walrus studies (inquiry from Denmark).

Due to the necessity to move the satellite facility twice during the past year, including the dismantling and re-creation of exhibits and planning of new space, some disruptions in the work have been inevitable.

#### Gulf of Alaska Review

The synthesis of the physical oceanography for the Northwest Gulf of Alaska which was reported in the 1979 annual report was not completed. Problems of principal investigator participation in the synthesis made this effort impossible. Additional analysis and write-up of the archived data by the principal investigators did not occur due to monetary and time constraints. Therefore, the synthesis report was abandoned and replaced by a single authored review paper. This review does not necessarily represent the views of the individual investigators, but instead it attempts to tie all the physical oceanography studies into a common document.

The review represents this principal investigator's thoughts over the last year on the processes in the northern Gulf of Alaska. It is used as the main body of this report in the form of an appendix. I acknowledge the assistance of the other P.I.'s who gratefully provided reviews of this review, especially R. D. Muench and J. D. Schumacher. Comments by M. Pelto and R. Overstreet were also appreciated and incorporated into the text.

This review should be treated as an interim document only. Numerous publications dealing with the physical oceanography in the Gulf of Alaska are either in preparation or in press. While I hope that the general conclusions in the review remain valid, I expect that they will be refined and some outdated. After the publication of this initial round of papers, it is appropriate that a bibliography or collected reprints be published to summarize the vast OCS effort. This collection should include papers from all disciplines.

#### Northwest Gulf of Alaska Synthesis

The participation of this research unit in the synthesis of the physical oceanography of the Kodiak region was primarily of an editorial nature. The manuscript was reviewed and input was provided during the synthesis meetings. The most important conclusion about work in that area is that it appears that the data were undersampled horizontally. This somewhat discouraging conclusion suggests that small scale features (on the order of kilometers) are present on the shelf in this region and possibly elsewhere. Because a 2-5 kilometer sampling interval is beyond most navigational capabilities, new sampling schemes should be devised. This undersampling seriously affects the current velocities determined from the numerical mode. However, since a surface trajectory integrates horizontally, the predicted pollutant paths are probably still valid.

### Currents at IMS 9

A paper discussing the currents as measured at IMS 9 (see 1979 Annual Report) is in the final stages of preparation. The presence of eddies in those data strengthen the assumption that small or mesoscale effects are important on this shelf. A seasonal shift in the Alaska Current is also observed (we believe) in those current meter data. This manuscript will be forwarded to the Juneau Project Office in April 1980.

### Transport Variations in the Alaskan Current

As discussed in the 1979 Annual Report, seasonal variations in the baroclinic transport of the Alaska Current have been determined using historical and OCSEAP data. The maximum transport of the annual cycle occurs between March and June. The mean transport is about  $9.2 \times 10^6 \text{ m}^3 \text{ s}^{-1}$  with an annual amplitude of  $1.2 \times 10^6 \text{ m}^3 \text{ s}^{-1}$ . The confidence interval for this estimate is greater than 90% according to F statistics. This seasonal response is expected from the seasonal variation in the wind stress and wind stress curl. The phase shift of the ocean's response is in accord with theoretical considerations. This manuscript will be forwarded to the Juneau Project Office in April 1980.

### Transport Variations in the Alaskan Coastal Current

Analysis of the alongshore baroclinic transport over the continental shelf of the Gulf of Alaska has revealed a very strong annual cycle which is controlled by fresh water discharge and winds. These effects were discussed in the 1979 Annual Report. This year, statistical techniques indicate that the transport response is in phase with the fresh water



discharge, but lags the winds by one month. Evidently, this is the response time required for a coastal convergence and downwelling.

This program has established the existence of the westward flowing alongshore Alaskan Coastal Current throughout the northern Gulf of Alaska. The current is primarily controlled by fresh water discharge and secondarily by wind stress. Peak flows (greater than  $1 \times 10^6 \text{ m}^3 \text{ s}^{-1}$ ) occur in fall concurrent with maximum fresh water discharge. Anomalies of fresh water discharge and wind stress are associated with anomalies in the baroclinic transport. The exact mechanisms by which wind stress and fresh water interact to produce this current are presently unknown.

An important result of this year's field effort and analysis is that the width of this coastal jet is apparently much narrower than previously thought. Instead of being 20 km wide, in September 1979 it was 5-10 km wide. Previously computed baroclinic transports are still correct, but the speeds are about twice those determined previously. This means that alongshore flow might be 2-3 knots for a 5-10 km wide coastal band. Even this might be an underestimate, since we have not included the barotropic response. It is very desirable to place current meters within this coastal jet.

#### Prince William Sound

We now have nearly two years of current meter and hydrographic data for Prince William Sound. Other than calibrating and listing these data, little analysis has been done due to financial constraints. Using the watershed area and the hydrology model from the alongshore current study, the annual input of fresh water has been computed to be more

than seven meters. The tidal flushing time for Prince William Sound has been computed to be between 40 and 80 days.

More analysis of Prince William Sound is expected to take place in the final six months of this contract after completion of the baroclinic flow papers. This analysis will be contained in the final report.

## VII. CONCLUSIONS AND OUTLOOK

Relevant scientific conclusions from this research unit are contained in the previous sections and the appendix. Emphasis needs to be placed on the possibility that our horizontal cross-shelf sampling grid was inadequate to properly resolve important features.

The Alaskan OCS program is an interesting mixture of government, business and science. The TDP's, RFP's, DEIS's, and EIS's will continue to come and go. Quarterly, annual and final reports will be filed or hopefully find some higher purpose such as heating homes. Lease areas will be bid on, drilled on and passed on. However, the scientific knowledge that has been developed from this program will also be passed on, but in another sense it will remain to build the base for future endeavors in these areas. The enduring nature of this research has been generally ignored as a valuable product of this program.

In this same light, it is disturbing that the aging of the OCS program has produced aspects that hamper the scientific merits of future programs. Originally, the OCS program was guided by input from the scientific community. In the first years many principal investigators used the program to continue scientific inquiries into problems not directly related to the mission of the OCS program. This unfocused approach

was gradually altered as the bureaucratic structure within NOAA and BLM increased. This change involved less scientific and more bureaucratic input to the direction of the program. At this stage the program was the "best" mixture of scientific inquiry and practical problem answering (Science:2; Administration:2). OCS has now entered the age where the questions which guide the program are being posed by the administrators with little scientific input. The proposed work is now extremely narrow and too often does not involve science. It is overfocused. Its thrust is to provide information on a particular lease area by a particular date. The OCS policy is similar to employing six men to describe an elephant in the dark whereas one man with a light could do a more integrated description. That is, investigations of lease areas to meet the leasing schedules do provide data for the area but do not necessarily provide the insight or knowledge which is essential to good overall planning (Science:3; Administration:6).

From the inception of the OCS program, the administrators seem to have viewed data submission and annual report writing as the highest scientific goals of OCSEAP. Actually, the data submission should be only the first step in a very long process of analysis. The complete analysis should include descriptions, formulation of hypotheses, the testing of these hypotheses, their reformulation, retesting, and so on. With this program, we have just emerged from the descriptive phase. In this age of instant coffee, instant soup, instant pictures and other instant gratification, motherhood and scientific inquiry must still be given time to run their course. Under the present OCSEAP, a farmer might

be expected to gather his harvest as soon as the sprouts pierce the soil. Fortunately, some cultivation of scientific knowledge has already taken place in OCSEAP, but unfortunately, this nurturing was not taken into account by the National Academy of Science report on OCSEAP.

In summary, while the OCS research continues, the overfocused nature and the unscientific direction could lead to undesirable results, with the exception of providing fragmentary data for impact statements. This is unfortunate for the same effort and funds could be used in a manner to benefit both science and OCS.

#### VIII. SUMMARY OF FOURTH QUARTER OPERATIONS

##### Task Objectives

To gather and analyze hydrographic and current meter data in the northern Gulf of Alaska for the purpose of describing possible flow trajectories; to describe the physical environment and to understand its driving mechanisms; to continue to monitor NOAA satellite data for use by this project and other OCSEAP investigators; to prepare a review of the physical oceanography for NEGOA.

##### Field Operations

None

##### Results

The third draft of a review of the OCS physical oceanography was completed. The NWGOA synthesis report was reviewed and the synthesis meeting attended.

Studies of the physical oceanography of Prince William Sound were organized and some initial analysis has begun. A freshwater estimate of greater than 7 meters enter the sound each year from runoff and precipitation. The significance of this discharge is being investigated. Other work illustrates the importance of shelf waves on the circulation of Prince William Sound.

#### Problems Encountered

As of this date, we have not received our FY80 funds!

APPENDIX

REVIEW OF THE PHYSICAL OCEANOGRAPHY OF THE NORTHEAST  
GULF OF ALASKA, WITH EMPHASIS ON ITS IMPLICATIONS  
TO OIL AND GAS DEVELOPMENT

REVIEW OF THE PHYSICAL OCEANOGRAPHY OF THE NORTHEAST  
GULF OF ALASKA, WITH EMPHASIS ON ITS IMPLICATIONS  
TO OIL AND GAS DEVELOPMENT

Thomas C. Royer

Institute of Marine Science  
University of Alaska  
Fairbanks, Alaska 99701

Third Draft

March 1980

The satellite photo of the Gulf of Alaska, NOAA infrared imagery, 1 March 1978, was not included in this publication since the copy supplied was not of sufficient quality for reproduction.



TABLE OF CONTENTS

LIST OF TABLES . . . . .	242
LIST OF FIGURES . . . . .	243
I. INTRODUCTION . . . . .	244
II. HISTORICAL BACKGROUND . . . . .	245
III. CIRCULATION OF THE ALASKA CURRENT . . . . .	247
IV. OUTER SHELF CIRCULATION . . . . .	253
V. ALASKAN COASTAL JET . . . . .	267
VI. SHELF CIRCULATION FORCING MECHANISMS. . . . .	274
A. Winds and Wind Stress. . . . .	274
B. Freshwater Discharge . . . . .	282
C. Alaska Current Forcing . . . . .	283
D. Bathymetry . . . . .	284
VII. ESTUARY CIRCULATION . . . . .	284
VIII. NUMERICAL MODEL RESULTS . . . . .	286
IX. DEVELOPMENT OF A PROCEDURE TO PREDICT THE TRAJECTORY OF AN ACTUAL OIL SPILL . . . . .	299
X. RECOMMENDATIONS FOR FUTURE STUDIES. . . . .	300
XI. CONCLUSIONS . . . . .	302
XII. REFERENCES. . . . .	304

LIST OF TABLES

Table I.	Kinetic energy for flow at stations 9 (April-July 1976) and 62 (May-August 1976). . . . .	259
Table II.	Weather types for Gulf of Alaska. . . . .	275
Table III.	Transitions from initial weather type to following type .	277

LIST OF FIGURES

Figure 1. Historical hydrographic stations, up to 1974. . . . . 246

Figure 2. OCSEAP station locations. . . . . 248

Figure 3. Schematic diagram of surface currents in the northern Gulf of Alaska (both real and imaginary parts). . . . . 252

Figure 4a-f. Satellite-tracked drifting buoy trajectories (Royer *et al.*, 1979). . . . . 256

Figure 5. Geostrophic flow for Seward Line. . . . . 261

Figure 6. Current vectors for IMS 9 current meter array . . . . . 262

Figure 7. Current vectors for Station 62 current meter array (Muench *et al.*, 1978) . . . . . 263

Figure 8. Seward line phasing, depth and baroclinic transports. . . . . 268

Figure 9a-c. Cross-section of a) temperature, b) salinity and c) sigma-t. . . . . 271

Figure 10. NEG OA winds showing high katabatic conditions (Galt *et al.*, 1978) . . . . . 279

Figure 11. NEG OA winds under influence of Aleutian Low (Galt *et al.*, 1978) . . . . . 280

Figure 12a-k. Calculated trajectories at surface in NEG OA (Galt *et al.*, 1978) . . . . . 288

## I. INTRODUCTION

The harsh climate over the Gulf of Alaska plays a dominant role in the control of the ocean's circulation there. In concert with the climate, the orographic and bathymetric features in the Gulf of Alaska significantly influence the coastal and shelf circulation. The coastal waters in the northeast Gulf of Alaska are bounded to the north by a mountainous coastline (Fig. 1). Their southern boundary is the westward flowing Alaska Current, located along the continental slope. The Gulf of Alaska's coastline contains numerous embayments and fjords, including Prince William Sound. Moving from the coast onto the shelf, the depth increases rapidly offshore: depths in excess of several hundred meters within 10 km of the shore are common. The width of the shelf in the northern Gulf of Alaska varies from tens of kilometers to several hundred kilometers. The shelf bottom contains numerous canyons and ridges, with vertical scales up to several hundred meters. Two prominent islands, Kayak and Middleton, are found on the shelf and they have significant effects on the circulation of the shelf. The central Gulf of Alaska adjacent to the shelf has water depths in excess of 3 km, punctuated with seamounts.

## II. HISTORICAL BACKGROUND

The first modern oceanographic work in the northern Gulf of Alaska occurred in the late 1920's with the purpose of determining the expected trajectories of halibut eggs and larvae (Thompson, McEwen and Van Cleve, 1936). The physical oceanography portion of that work consisted of hydrographic sections over the continental shelf. A general westward flow was established by these studies, however eastward flow appeared occasionally. With the exception of a single cruise into the region in 1949 by Scripps Institution of Oceanography, no oceanographic cruises were carried out in the region until 1955, when the International North Pacific Fisheries Commission began a major oceanographic study of the region (Dodimead, Favorite and Hirano, 1963). Cruises from 1955 to 1960 form the bulk of historical data available for the northern Gulf of Alaska prior to the establishment in 1974 of the Outer Continental Shelf Environmental Assessment Program (OCSEAP). The distribution of the available hydrographic station data is somewhat misleading (Fig. 1), since most of these data were taken in summer, August being the most popular month for cruises. (This is reasonable for the weather is best in August with high temperatures and low winds.) While more hydrographic surveys occurred in the subarctic Pacific after 1955, the sampling of waters of the continental shelf of the northern Gulf of Alaska did not substantially increase until 1970 when a seasonal field program began in the northwestern gulf (Royer, 1975). Though many of the conclusions of seasonal studies conducted off the Washington-British Columbia coasts (Doe, 1955; Dodimead, Favorite and Hirano, 1963; Tabata, 1965, Tully and Barber, 1960; Bennett, 1959) apply to this region, many differences are to be expected for regions 1000 km apart.

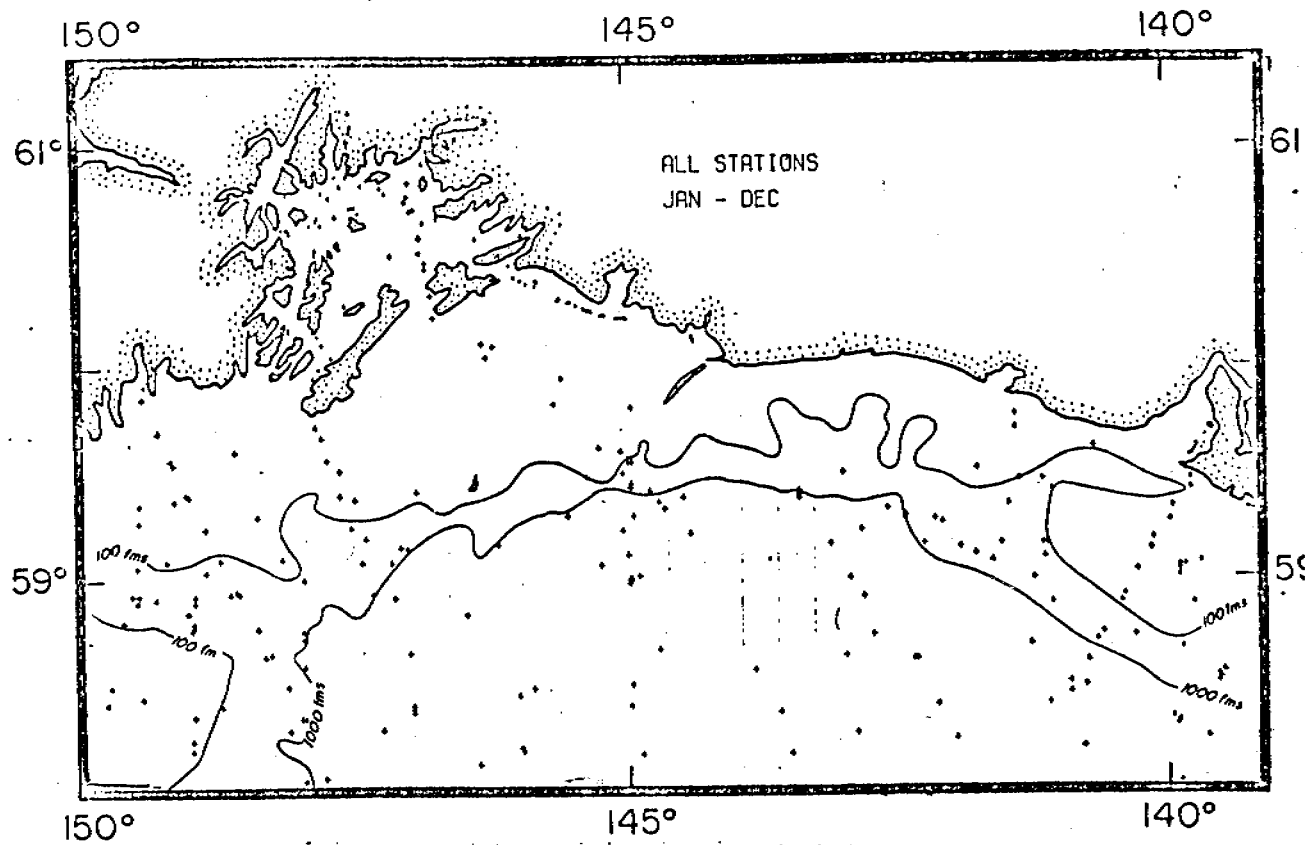


Figure 1. Historical hydrographic stations, up to 1974.

A vast, multidisciplinary oceanographic program was initiated in 1974 by the Bureau of Land Management, under the direction of NOAA to describe features of this continental shelf and to assess potential impacts of oil and gas exploration and development. Phenomena occurring on a short temporal and spatial scales were to be investigated for the first time in this region (Fig. 2). The only previous seasonal study in the northern Gulf of Alaska (Royer, 1975) was to the west of the OCS study region, so these investigations began with no time series and only widely spaced (in time and space) hydrographic stations. No current meter moorings had been deployed prior to 1974, and only a few Lagrangian drifter measurements had been made. Based on this background, several years of hydrographic surveys and current meter measurements were necessary prior to a significant improvement in the description and understanding of the oceanographic processes of this region.

### III. CIRCULATION OF THE ALASKA CURRENT

The North Pacific Current, an extension of the Kuroshio, impinges on the coast of North America and separates into the relatively cold California Current and the relatively warm Alaska Current. The former flows south along the Oregon-California coast, whereas the latter flows northward into the Gulf of Alaska. The volume transport in these two currents is about the same,  $10\text{--}15 \times 10^6 \text{ m}^3 \text{ s}^{-1}$  (Sverdrup, Johnson and Fleming, 1941) and could be dependent on the transport in the North Pacific Current and local forcing at the point of separation. The local forcing includes wind stress, wind stress curl and bathymetry.

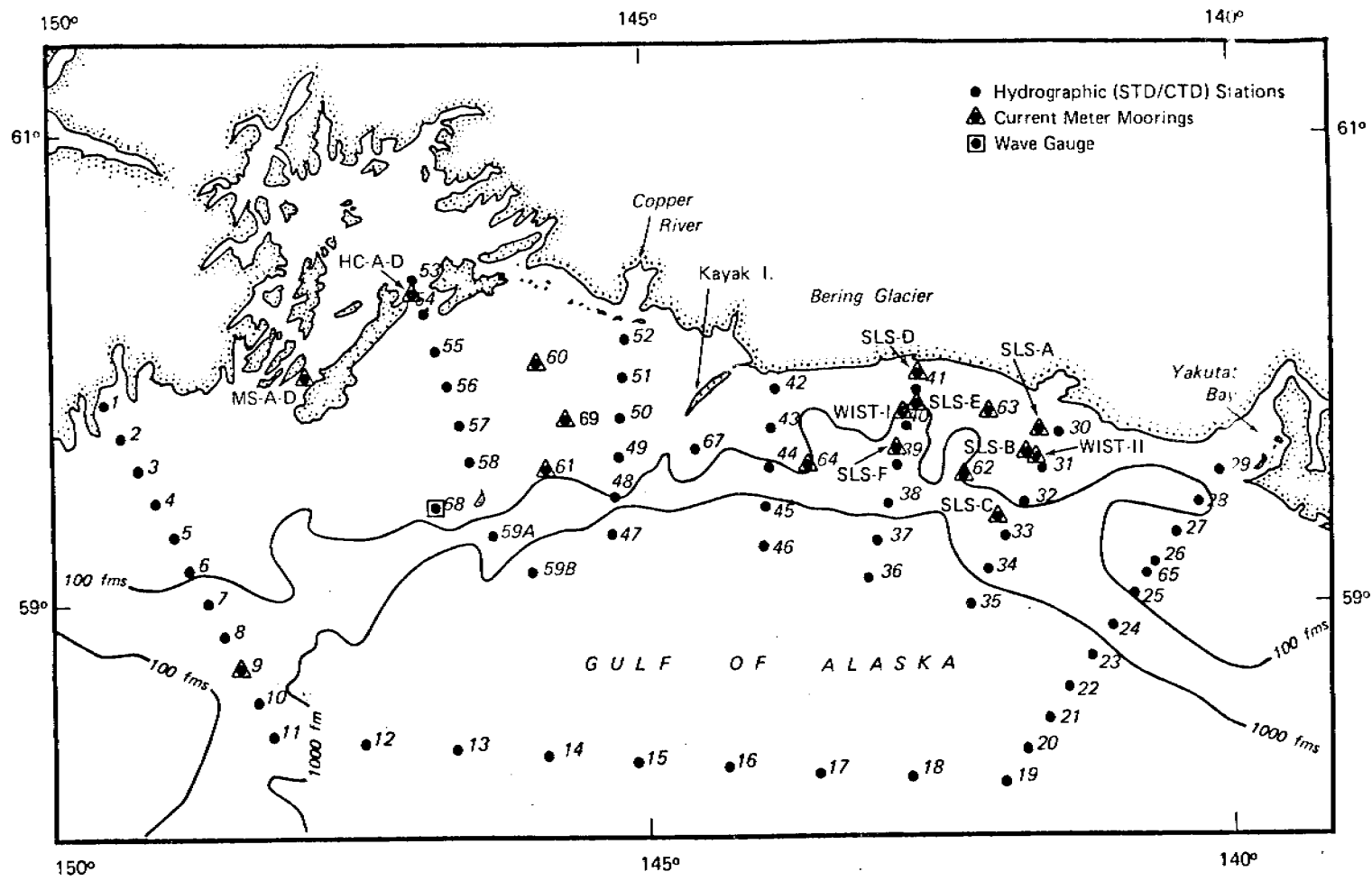


Figure 2. OCSEAP station locations.



The broad northward flow along the British Columbia and Alaskan coasts is forced to turn westward as it approaches the head of the Gulf of Alaska (Dodimead, Favorite and Hirano, 1963). This current intensifies toward the western side of the gulf due to western intensification (Stommel, 1964). The flow is concentrated along the continental shelf break with the majority of flow occurring within 50 km of the shelf break near Kodiak (Favorite and Ingraham, 1977; Royer, 1979a). Because this is a narrow, intense flow, previous computations of geostrophic velocity in the Alaska Current by earlier studies have been underestimated, though the transports are close to the presently observed values. The transport is directly dependent on the geostrophic velocity and distance between hydrographic stations, but the velocity is inversely dependent on the distance between stations. This makes the transport independent of the distance between hydrographic stations. For example, Roden (1969) estimates the maximum winter geostrophic current at less than  $30 \text{ cm s}^{-1}$ ; while more recent closely spaced hydrographic stations within the Alaska Current routinely yield speeds in excess of  $60 \text{ cm s}^{-1}$  and occasionally in the range of  $80\text{-}100 \text{ cm s}^{-1}$  along the shelf break. Speeds in excess of  $120 \text{ cm s}^{-1}$  have been measured directly by current meters near the shelf break.

As mentioned above, the baroclinic transport estimates do not suffer from inadequate station spacing and hence can be compared with our more recent estimates. A mean transport of  $9.5 \times 10^6 \text{ m}^3 \text{ s}^{-1}$  relative to 1000 db agrees with Favorite, Dodimead and Nasu (1976) and the hydrographic data gathered under OCSEAP (Royer, 1979a; Reed, Muench and Schumacher, 1980). The amplitude of the annual signal in the baroclinic transport is about

$1.4 \times 10^6 \text{ m}^3 \text{ s}^{-1}$  for Favorite, Dodimead and Nasu (1976) and Royer (1979a). (Reed, Muench and Schumacher (1980) indicate that there is not a significant seasonal signal in transports in the Gulf of Alaska off Kodiak, but their data set is a subset of that used by Royer (1979a) and has a larger standard deviation than that of the complete data set.) The phasing of the annual transport signal is different than that assumed by Reid and Mantyla (1976) and Favorite (1974) who suggest a maximum flow in winter. Instead, the maximum flow occurs in either February, based on data from Favorite, Dodimead and Nasu (1976) or in June, based on data from Royer (1979a). If major driving is accomplished by wind stress or wind stress curl, which have maxima in December-January, then a delay could be expected in the response of the ocean to this forcing. Therefore a maximum transport is expected in the Alaska Current in late spring. However, the change in the amplitude of this transport is about the same as the error, meaning that while a seasonal signal might occur, it is often swamped or masked by a variation of shorter or longer period. The transport at any given time can be expected to range from 13.9 to  $5.1 \times 10^6 \text{ m}^3 \text{ s}^{-1}$ , which are the maximum and minimum observed.

A seasonal signal of the baroclinic, geostrophic velocities was not established because the velocities are dependent on the station spacings, which were frequently inconsistent. Since the transport represents a depth integration, it does not necessarily follow that maximum currents at a particular depth are associated with the maximum transport in the water column. For example, a highly stratified water column might have high surface currents but a low transport due to large vertical velocity shear. Direct measurements of the Alaska Current would solve this problem but up

to this time these measurements have not been carried out. The moorings for the OCSEAP work were on the continental shelf and not necessarily within the Alaska Current. The seasonal change in the position of the Alaska Current can appear in these moored current meter records as a current acceleration or deceleration, whereas it might actually be due to the position change. Therefore, any comments about velocity changes based on OCSEAP data must be questioned. Currents observed in the northeast Gulf of Alaska at 20 m were typically 25-35  $\text{cm s}^{-1}$  in winter (October-April) and 10-15  $\text{cm s}^{-1}$  in summer (Muench, Schumacher, Hayes and Charnell, 1978). The average currents near the shelf break at 20 m in the northwest Gulf of Alaska (Station 9) are 45  $\text{cm s}^{-1}$  for April-June and 42  $\text{cm s}^{-1}$  for July-November (Niebauer, Roberts and Royer, 1979). (A schematic current diagram for the northern Gulf of Alaska is presented in Fig. 3. The information used to compose this figure include current meter, CTD/STD, diagnostic model, Lagrangian drifter, bathymetry and satellite images.)

Spatial variations of the Alaska Current are more easily described than the temporal variations due to the synoptic nature of the observations. Near Kodiak Island the Alaska Current is very narrow (< 75 km) and generally follows the shelf break (Fig. 3) (Favorite and Ingraham, 1977; Royer, 1979a). A low salinity surface layer and subsurface temperature maximum core of about 5.5°C characterize this flow. The current appears to become more organized in the western portion of the Gulf of Alaska. East of Middleton Island this current is a broad, weak westward flow (Muench, Schumacher, Hayes and Charnell, 1978). Satellite IR images depict the surface conditions as similar to a reverse-diffusive flow, with the wide, unorganized flow at the head of the gulf and a narrowing toward Kodiak

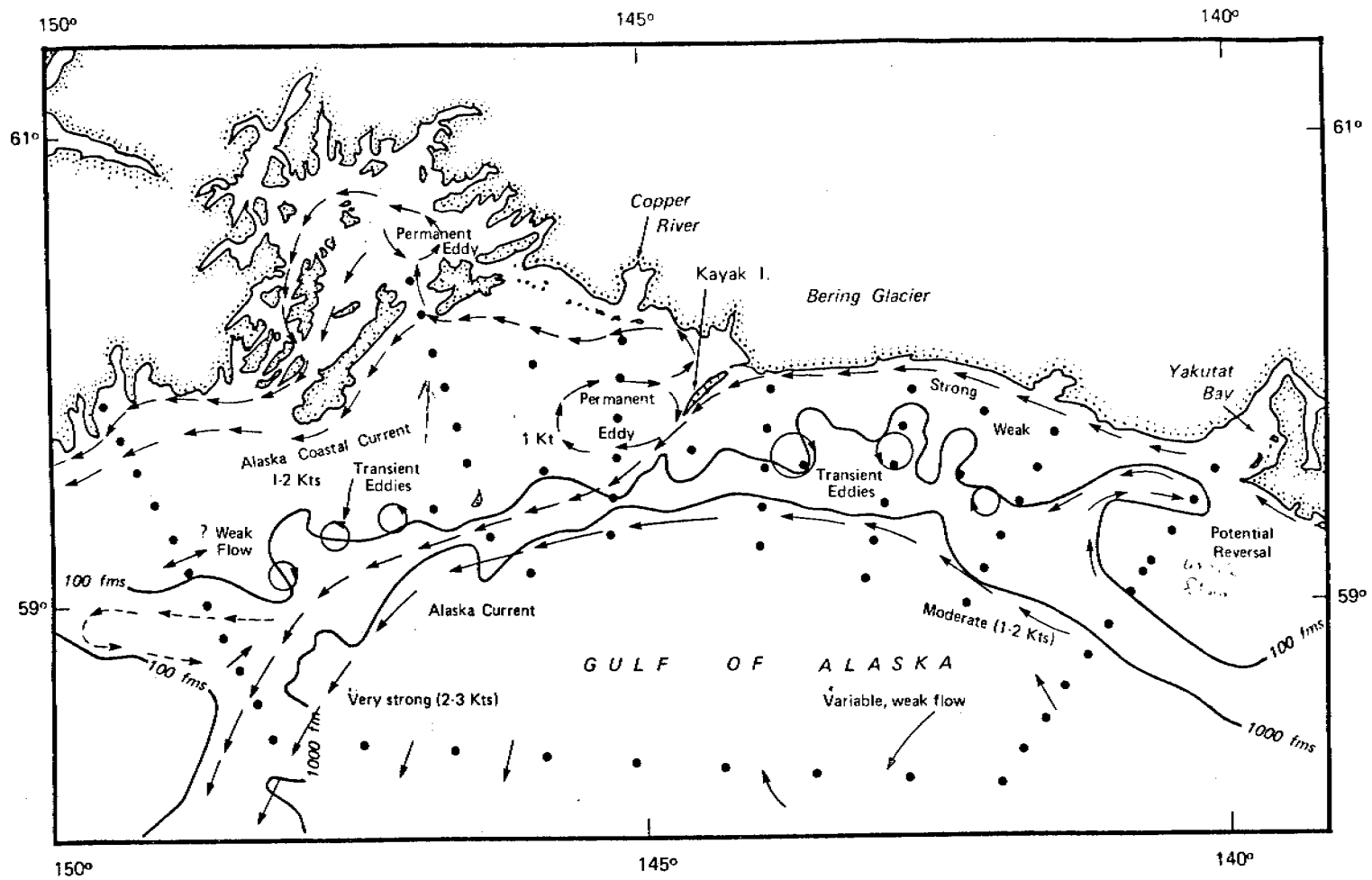


Figure 3. Schematic diagram of surface currents in the northern Gulf of Alaska (both real and imaginary parts).

Island. Although repeated attempts were made to place drifting buoys in the Alaska Current, they generally pass through the current without displaying any tendency to remain in it. However, surface waters remain cohesive in the Alaska Current for hundreds or possibly thousands of miles.

The Alaskan Gyre might be thought of as similar to the North Atlantic circulation where the Gulf Stream corresponds to the Alaska Current off Kodiak Island and the North Atlantic Drift Current corresponds to return flow in the North Pacific Current. This part of the analogue is particularly vague as evidence for the return flow in the Gulf of Alaska is not clear at this time. Dodimead, Favorite and Hirano (1963) indicate for both types of flow; that is, a multiple gyre system and single gyre system. Reed and Muench (1979) present evidence of a recirculation within the Gulf of Alaska proper, indicating a multiple gyre configuration. In either case, the poleward flow in the eastern Gulf of Alaska corresponds to the eastern boundary currents in the North Atlantic (Veronis, 1973) and the equatorial currents correspond to the westward flow in the northern gulf. The surface heating and density decrease in the equatorial current is similar to the surface dilution and subsequent density decrease in the northern Gulf of Alaska. Both systems are believed to be driven by wind stress and its curl, though the direct evidence for this coupling in the Gulf of Alaska has not been developed.

#### IV. OUTER SHELF CIRCULATION

Progressing shoreward from the Alaska Current, there is a shelf region of very high horizontal current shear (see Fig. 3). Because of this shear, the lateral momentum transfer across the shelf reaches a maximum here

(Muench, Schumacher, Hayes and Charnell, 1978) and might be a significant controller of circulation on the shelf. This outer shelf region is a location of many of the OCSEAP current meter deployments; both Station 62 in the eastern gulf and Station 9 in the western gulf (Fig. 2). These meters can sometimes be within the Alaska Current, while at other times they can measure the shelf circulation depending on the position of the current. As mentioned in the previous section, temporal changes in the flow at these current meter sites can be either local or field accelerations. A local acceleration is a change in the flow with respect to time. A field acceleration is a change in the flow due to a shift in the current position. A shift of the flow away from the meter position will appear as a deceleration.

In a mean sense, the currents over the shelf tend to follow bathymetry in both the eastern and western gulf (Fig. 3). The vertical current shear is greater ( $20 \text{ cm s}^{-1}/100 \text{ m}$ ) in the western Gulf of Alaska (Station 9) than at Station 62 in the eastern gulf where it is about  $6 \text{ cm s}^{-1}/100 \text{ m}$ . At both locations the directional current shear was small, except for the bottom or near bottom meter which was generally directed offshore. This offshore flow is consistent with downwelling and/or a bottom Ekman layer associated with westward currents along the continental shelf bottom. At one location (Station C in the eastern gulf near the shelf break) there was onshore flow at all depths, suggesting that downwelling might not be a shelf-wide phenomenon. The mean flow was small ( $5\text{-}10 \text{ cm s}^{-1}$ ) and generally directed along isobaths, with the above exceptions. Even these exceptions represent very slight deflections from bathymetric flow. An important conclusion of these studies is that flow is generally along isobaths.

The satellite-tracked Lagrangian drifters released in the northeast Gulf of Alaska in late spring 1976 appear to contradict this concept of isobathic flow. Drifters released near the shelf break (Fig. 4) generally moved westward and shoreward. They also described a few perturbations identified as eddies (Royer, Hansen and Pashinski, 1979). In this drifter study, buoys were drogued at 35 m depth and released "upstream" of Kayak Island over the outer shelf or deep water. In addition to describing eddies on the shelf and near the shelf break, the drogues generally moved shoreward until they came within 5-10 km of the coast. At that point, they followed the coastal flow, through the Kayak Island gyre and into Prince William Sound. The drifters appear to "stabilize" on the coastal jet. This jet will be discussed in detail later in this paper and is driven by very high rates of coastal fresh water discharge. The stabilization of the drifters is readily explained by a fresh water entrainment process, similar to that occurring in estuaries. The fresh water discharge at the coastline moves offshore but friction requires that this offshore moving upper layer take some of the water beneath it offshore. This in turn requires a subsurface replenishment, causing an onshore movement of subsurface water. The fresh water lens becomes deeper toward shore. Therefore, while well offshore the drifter drogues are within the shoreward moving lower layer. As they near the coastline, the offshore moving upper layer becomes thicker until finally the drogues at 35 m encounter this upper layer. They then move offshore in this upper layer until they encounter the shoreward moving lower layer. Through this mechanism they stabilize on the sloping interface between the shoreward moving lower layer and the offshore moving upper layer. They remain on this interface until the interface

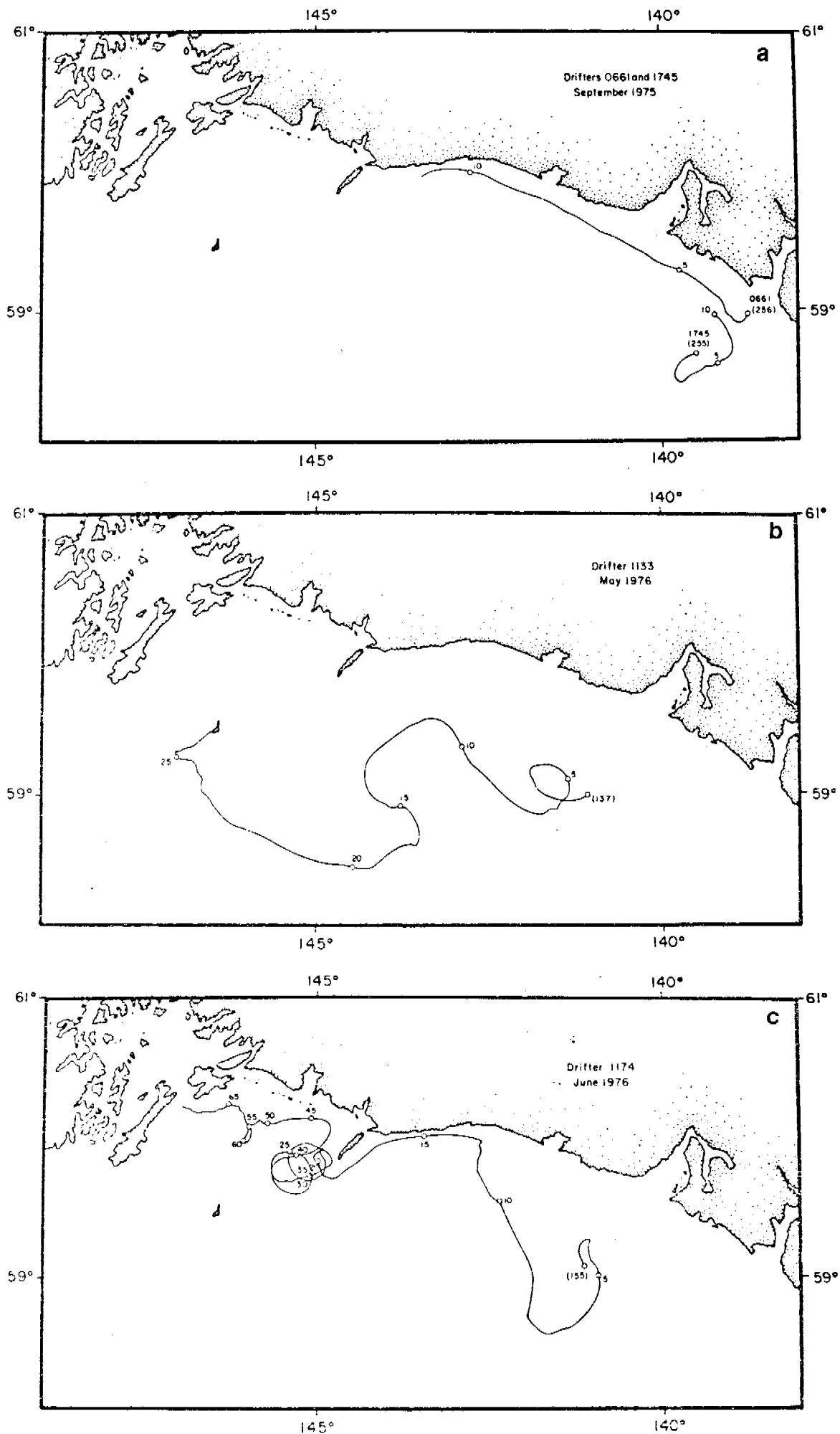
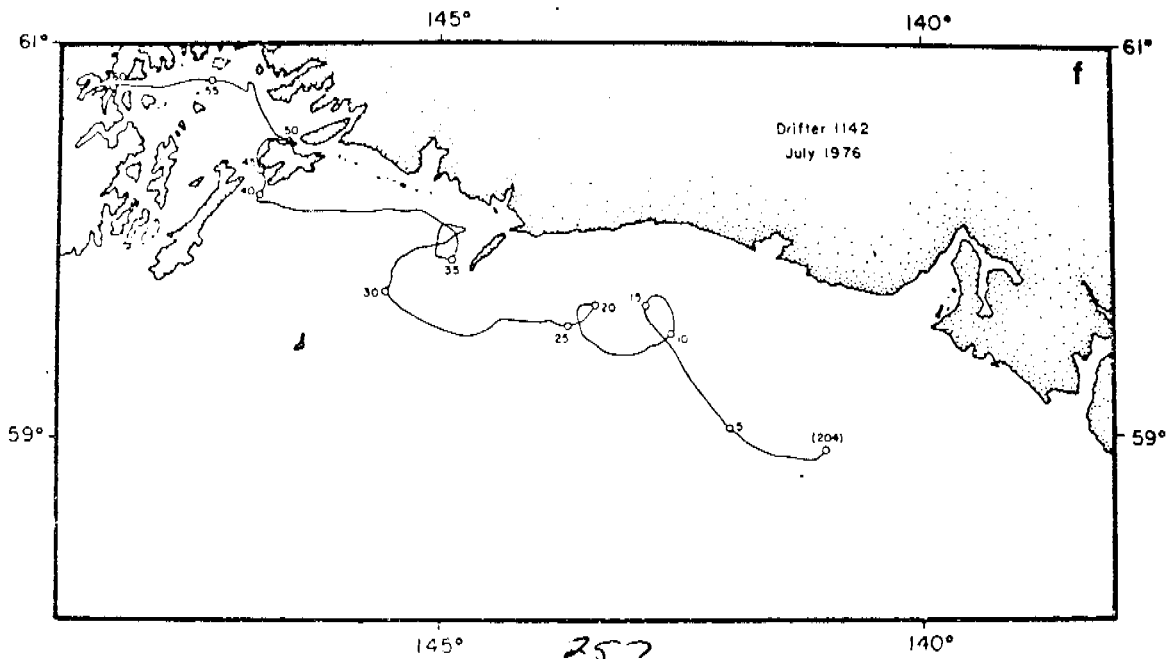
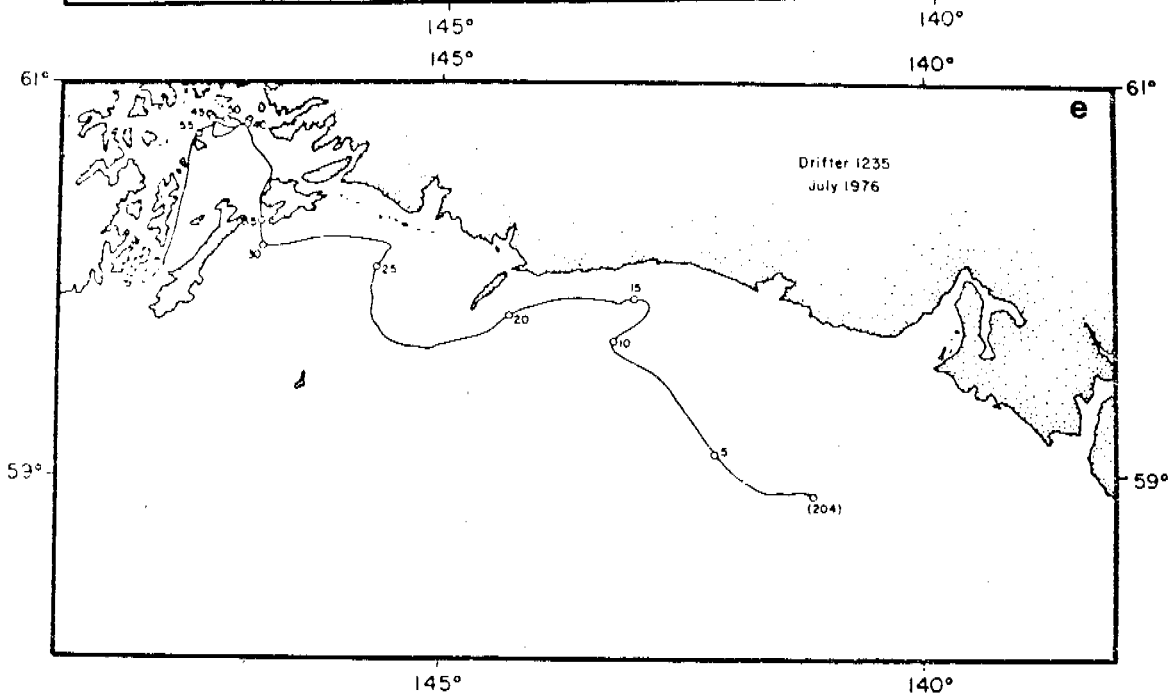
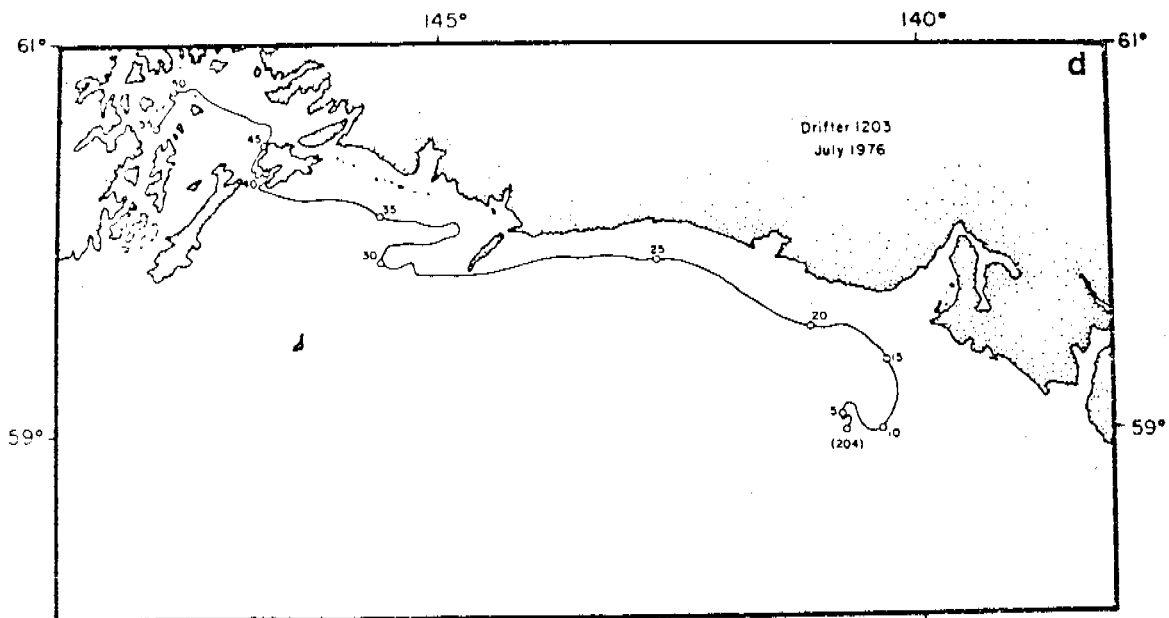


Figure 4 a-f. Satellite-tracked drifting buoy trajectories (Royer *et al.*, 1979). 256





is destroyed, the bottom is encountered or other forces remove them from the interface. Therefore, once the drogues enter the coastal jet, they are poor direct indicators of onshore-offshore motion. The consequence of this mechanism is that fresh water might keep surface pollutants offshore especially at the time of peak runoff - autumn.

Returning to a discussion of currents near the shelf break, there is a distinct difference between the kinetic energy of the mean flow at Station 62 and Station 9. (Since these stations are not located on the same isobath, these differences could be spatially longshore or cross-shelf.) For comparable time periods, the mean kinetic energy in the western Gulf of Alaska (Station 9) is more than an order of magnitude greater than for the eastern portion (Station 62) (Table I). This could be the greater influence of the Alaska Current at this location. Also note that the vertical shear in the energy is greater at Station 9. The fluctuations from this mean flow have been used to determine the eddy kinetic energy. While the eddy kinetic energy is still much greater in the western region than the eastern, the ratio of mean to eddy kinetic energy is greater in the eastern Gulf of Alaska. The weaker flow has a higher amount of energy in current fluctuations. This conclusion was also reached in the section dealing with the Alaska Current. The model results of Galt (1979) show an organizing of flow in the western Gulf of Alaska. The eddy kinetic energy near Icy Bay decreases in the shoreward direction while the mean kinetic energy increases (Muench, Schumacher, Hayes and Charnell, 1978). Therefore eddies play an important role in the dynamics near the shelf break throughout the Gulf of Alaska with their relative energy being greatest in the northeast.

TABLE I

KINETIC ENERGY FOR FLOW AT STATIONS 9 (APRIL-JULY 1976)  
AND 62 (MAY-AUGUST 1976)

[Source: Niebauer, Roberts and Royer (1980) for 9; Hayes (1979) for 62]

Depth	Mean Kinetic Energy/ Unit Mass ( $\text{cm}^2 \text{s}^{-2}$ )		Eddy Kinetic Energy/ Unit Mass ( $\text{cm}^2 \text{s}^{-2}$ )	
	9	62	9	62
13	329		445	
20		7		62
22	213		363	
49	189		285	
50		14		72
97	161		124	
100		9		36
273	9		33	

Direct observations of these eddies (or meanders) were made at Stations 9 and 62 where fluctuations in speed and direction were superimposed on the mean flow. The rotational speed in these eddies varies from 10 to 50 cm s<sup>-1</sup>. The satellite tracked drifters also displayed the presence of these eddies and Galt's (1979) model also demonstrates them. Rossby dynamics require that these relatively small eddies (< 200 km) propagate eastward against the mean flow. A possible scenario is that the eddies (or meanders) are formed in the western Gulf of Alaska through the interaction of Alaska Current with bathymetry. These eddies propagate eastward on the shoreward side of the Alaska Current, impinging on the continental shelf as they move. This impingement will cause a distortion of the eddy (Galt, 1979) and possibly the eddy could be trapped. Such trapping was observed in the dynamic topography associated with the satellite tracked drifter studies (Royer, Hansen and Pashinski, 1979).

Additional evidence for this region of low net flow shoreward of the Alaska Current is present in the baroclinic, geostrophic computations for the Seward line (see Figs. 2, 5). High flow variability north of the strong westward flowing Alaska Current suggests eddies or meanders.

Short-term fluctuations and occasional current reversals were observed in the current measurements taken at both Stations 9 and 62 (Figs. 6, 7). The majority of the variance at Station 62 occurred in the 1.5-7.5 day period, with similar periods found in the records for Station 9.

Circulation near the shelf break can be depicted as generally following isobaths with frequent fluctuations in direction and magnitude due to eddies and meanders (Fig. 3). These fluctuations represent a larger portion of the total kinetic energy per unit mass in the eastern portion than

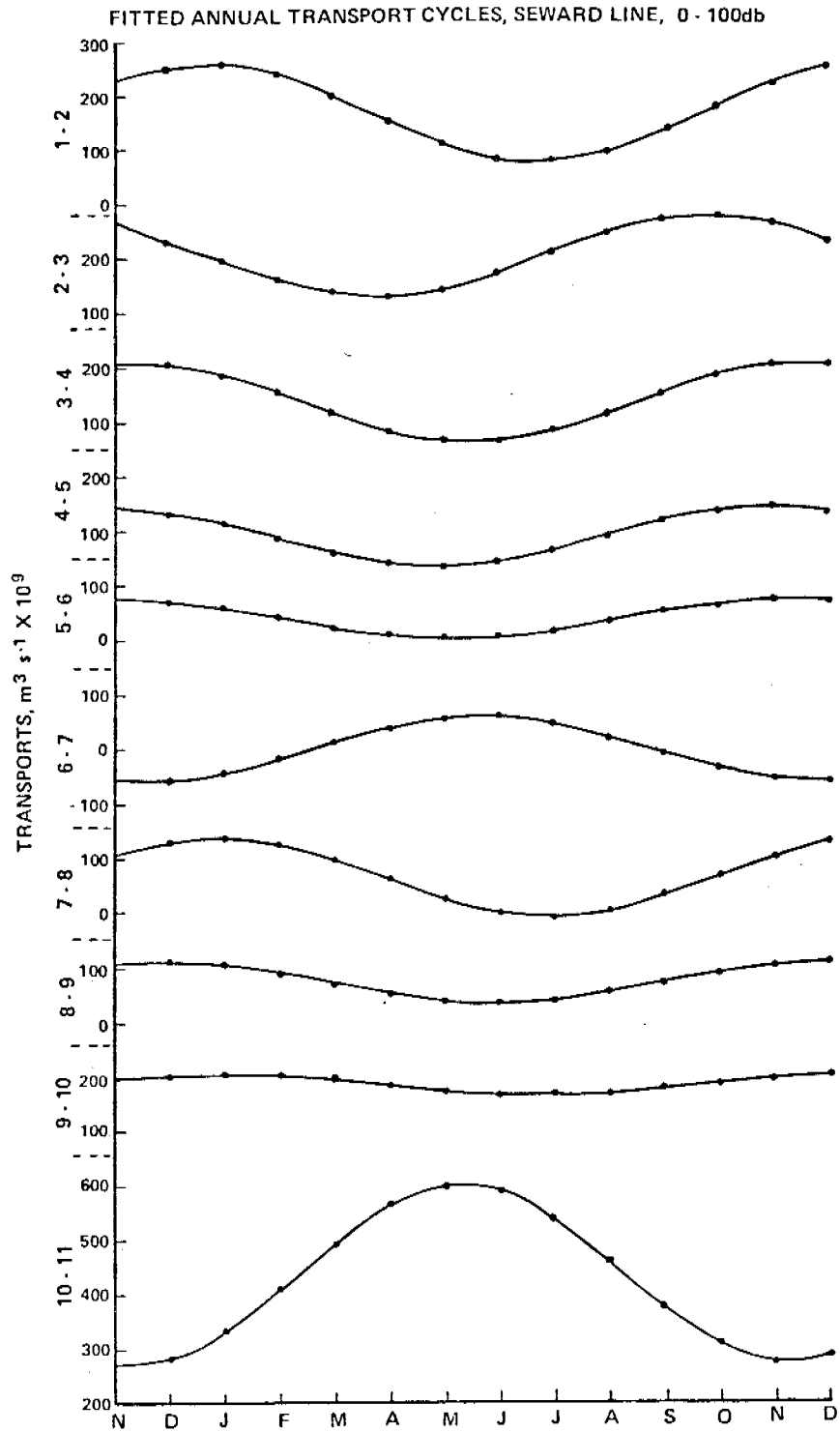


Figure 5. Geostrophic flow for Seward Line.

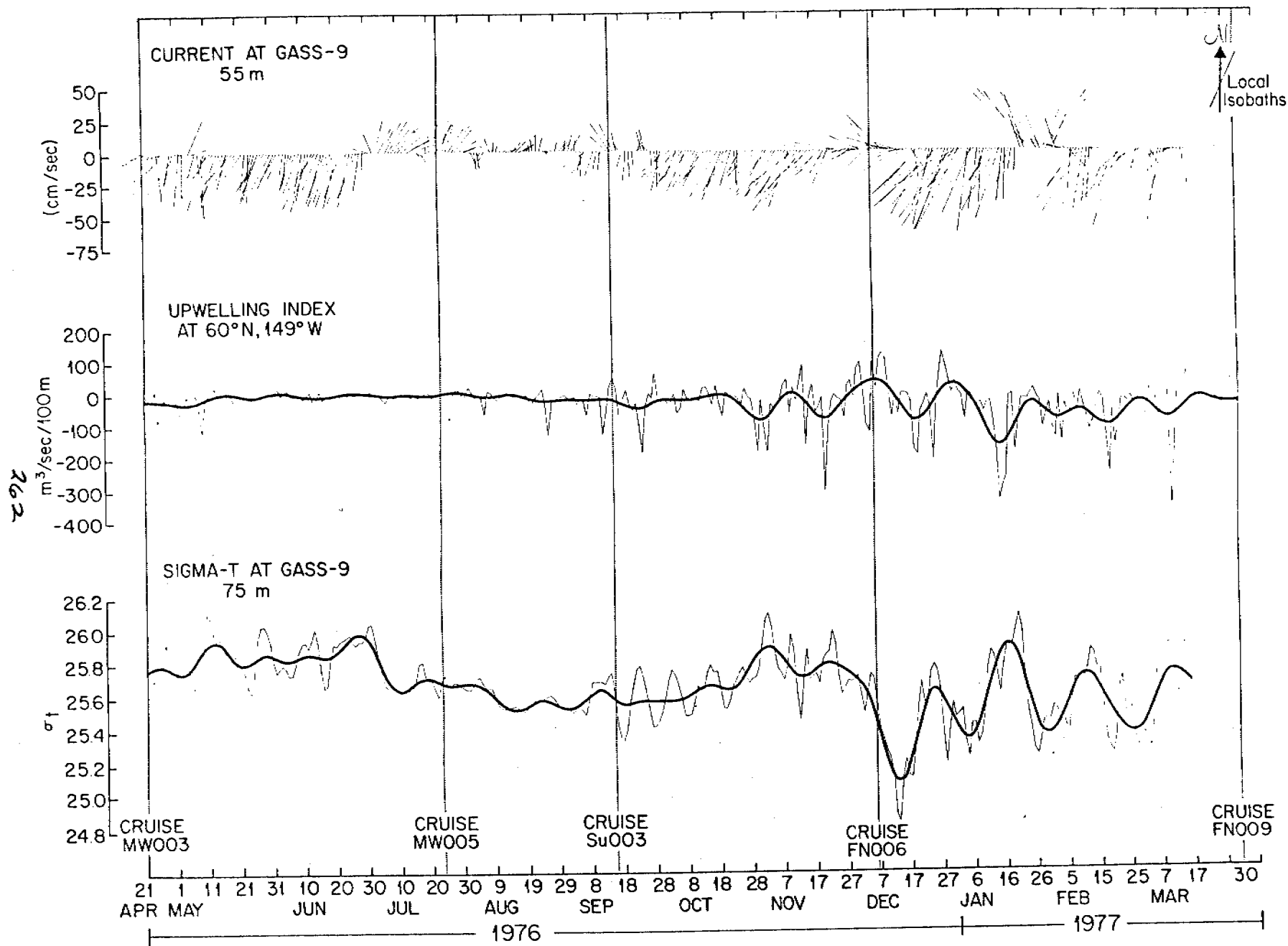


Figure 6. Current vectors for IMS 9 current meter array.

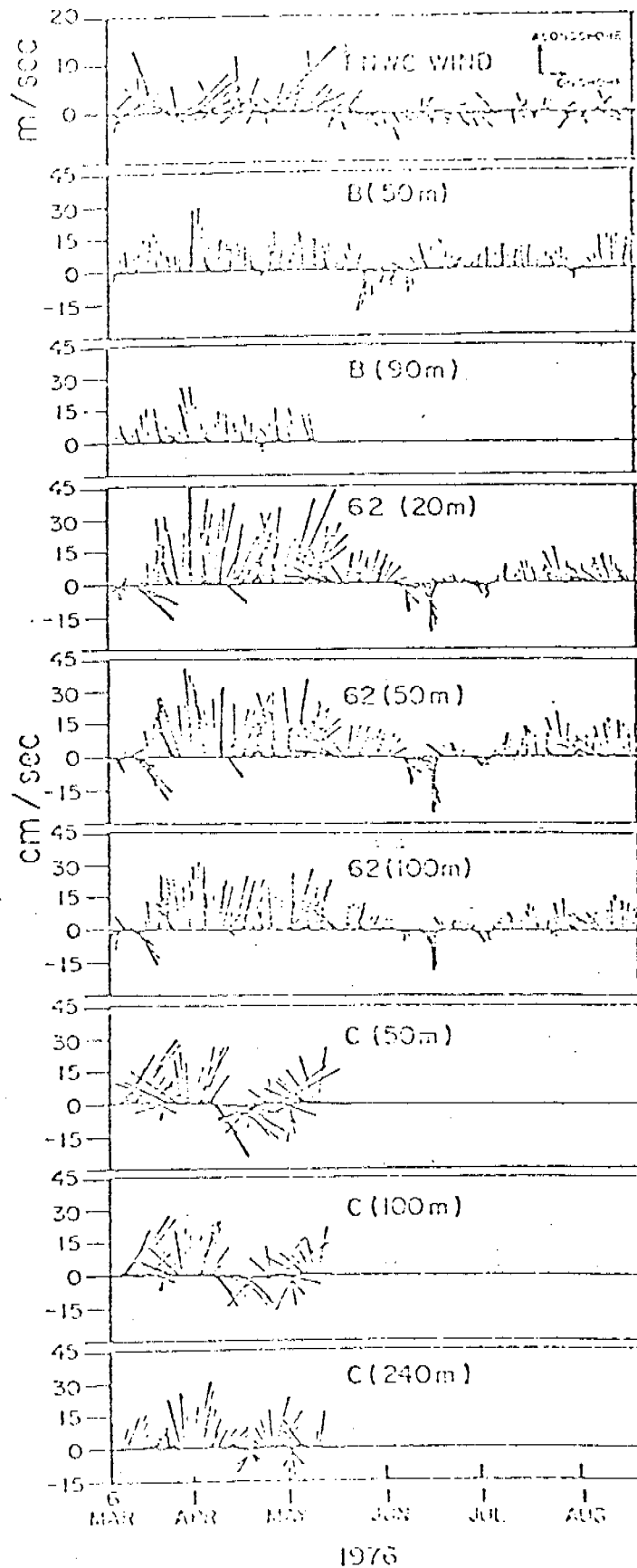


Figure 7. Current vectors for Station 62 current meter array. (Muench *et al.*, 1978)

in the western section, though the total kinetic energy is much larger in the west. Offshore, in the Alaska Current itself, the total kinetic energy should be greater than at the shelf break and the relative percentage of the eddy kinetic energy should be less, although no direct observations are available. Similarly, the eddy kinetic energy decreases significantly shoreward of the shelf break. The stratification or vertical geostrophic current shear is greater in the western Gulf of Alaska, with average upper layer speeds of the order of  $40-50 \text{ cm s}^{-1}$ .

Toward the coast from the shelf break, the circulation decreases in magnitude (Fig. 3). The vertical density stratification is a minimum over the shelf and mid-shelf upwelling is possible. The boundary between this region and the eddy infested region closer to the shelf break is not distinct. It is likely that many of the eddies and/or meanders can temporarily enter this region. This mid-shelf region was where some current meter moorings were located (Fig. 2) in the northeastern Gulf of Alaska. Off Icy Bay, the mean current speed at Station B, near the mid-shelf, is less than that at the shelf break, with the relative eddy kinetic energy still smaller (Muench, Schumacher, Hayes and Charnell, 1978). The mid-shelf contains many bathymetric features, such as Kayak and Middleton Island and troughs, which can direct the flow. The currents are expected to have less fluctuations due to eddies and tend to follow the bottom topography to a great extent. Currents in this transition might also respond to fluctuations of flow elsewhere, in the nearshore currents or Alaska Current. In the surface layers, local winds could have a significant influence here.

Near Yakutat and Icy Bay, a trough which extends from the shelf break to within tens of kilometers of the shore (Fig. 2), causes the flow to be



diverted shoreward with easterly flow occurring occasionally. Similar diversions take place with the other troughs between Yakutat and Kayak Island. For example, the currents at Station 62 are not directed along-shore, but are instead shoreward, though parallel to the local bathymetry. This strong bathymetric control requires the incorporation of bathymetry whenever a numerical modelling approach is attempted.

Proceeding westward along the mid-shelf region, Kayak Island protrudes from the coast (Fig. 2). A mechanism is provided by this island, to enhance cross-shelf movement of water. The mid-shelf region disappears abruptly here and all that remains is coastal and shelf break currents. To the west of Kayak Island, the mid-shelf region appears again. Now, it is in the "lee" of Kayak Island with a large circular trough. Further westward lies Middleton Island (Fig. 2) with a vast shoal area surrounding it, which is much larger than the island itself. These shoals block the flow, forcing it into a nearshore and offshelf circulation (Fig. 3). Immediately west of Middleton Island is another trough or canyon extending from the shelf break into Prince William Sound. Several other small troughs accentuate the shelf between Middleton and Kodiak Islands. These topographic features are important to the shelf circulation.

Returning to the Kayak Island area, an eddy-like feature dominates the region to the west of Kayak Island. This eddy was described by Galt (1976) using hydrographic station data and infrared satellite derived sea surface temperature images. This eddy was also observed in suspended sediment distributions from the Earth Resources Technology Satellite (ERTS) by Muench and Schmidt (1975). Lagrangian drifters passing through the region became entrapped in this eddy occasionally. At other times the eddy only

deflected slightly the drifter direction (Royer, Hansen and Pashinski, 1979). There is a seasonal cycle in the strength of the eddy, but at no time is there evidence in the hydrographic data that the eddy disappears. Of course, occasionally, it is not visible in the satellite or IR images. The inability of the eddy to capture all the drogues as they passed by was due to the drogue configuration, not because the eddy had disappeared. This anticyclonic (clockwise) gyre typically has speeds of  $15-30 \text{ cm s}^{-1}$  at the surface, based on baroclinic, geostrophic current computations relative to 100 m. Apparently the coastal jet, to be described later, which is directed southward by Kayak Island, supplies the low density water found in the core of the eddy. As the low density flow passes the island it becomes trapped by the bathymetry, in this case a semi-circular configuration about the size of the eddy. It is hypothesized that the bathymetry controls the direction of the flow, trapping the coastal flow. Transport out of the gyre can occur across the subsurface lateral boundaries with the eddy representing a surface convergence. Strongest convergence should occur in early fall when the freshwater discharge is a maximum. This eddy has been identified as a potential site for surface pollutant accumulation (Galt, 1976). Whether the residence time here is greater than other mid-shelf regions on this continental shelf has not been clearly resolved. While the speeds within the gyre are fairly high ( $> 20 \text{ cm s}^{-1}$ ), the net transport is still low; in contrast, other mid-shelf regions have very low mean speeds ( $< 5 \text{ cm s}^{-1}$ ).

Inshore of the Kayak Island eddy, the outflow of the Copper River creates a longshore (westward) transport toward Prince William Sound. Some of this flow might recirculate into the Kayak Island eddy as is indicated

by the numerical model of Galt (1979), but this recirculation could be a manifestation of the station transect not extending into the coastal freshwater flow.

To the west of Middleton Island, the mid-shelf circulation is characterized by cross-shelf flow, that is both onshore and offshore apparently depending on local conditions. This trough is an avenue for deep water exchange between the central gulf and Prince William Sound.

#### V. ALASKAN COASTAL JET

Adjacent to the coastline, throughout the northern Gulf of Alaska, there is a coastal current or jet formed from wind stress and freshwater discharge. This current is about 20-30 km wide and intensifies in fall or early winter. The baroclinic flow in this jet ranges from 15-70  $\text{cm s}^{-1}$  relative to the bottom which is often 200 m. Even higher current speeds are expected with a smaller sampling grid, probably speeds are 100-150  $\text{cm s}^{-1}$ . The annual maximum in this transport occurs in January for the Seward line (Fig. 8). Over this section the baroclinic transport is a maximum between Stations 2 and 3, so that the coastal jet could be considered as having a width of 20 nm (37 km). The maximum transport in the second segment of the Seward coastal jet (Stations 2-3) occurs in October and this transport is slightly larger than that for the part of the jet adjacent to the coastline. It must be remembered that these computations pertain only to the baroclinic portion of the current and it is expected that the barotropic and Ekman portions would serve to increase the transport in this coastal jet.

The abrupt change in the phasing of the maximum transport at Stations 6-7 on the Seward line from the other maximum transports over this line

S  
O  
N  
D  
J  
F  
M  
A  
M  
J  
J  
A

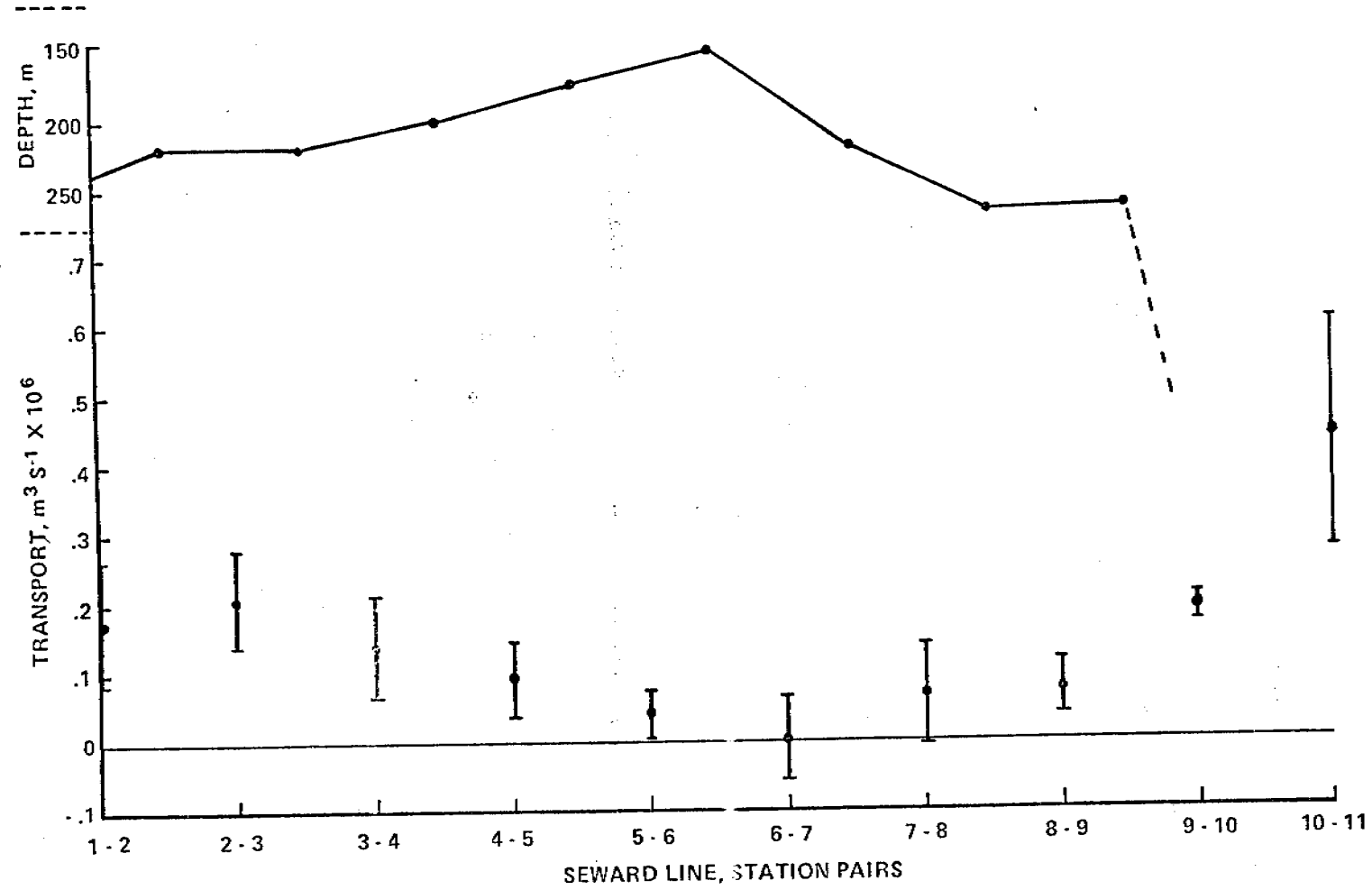


(Fig. 8) is hypothesized to be a consequence of the coastal jet being deflected offshore by Kayak Island. The coastal jet is then forced by bathymetry to flow south of Middleton Island and ultimately intersects the Seward line slightly offshore of Station 7. The reverse phasing for Stations 6-7 represents the inner boundary of this baroclinic flow. It is a maximum eastward flow at that time of the year with maximum westward flow on the outer boundary. While a baroclinic current reversal is possible for Stations 6-7, the westward barotropic current and/or a deeper reference level will probably cause a net westward flow here.

The freshwater coastal jet is continuous throughout this region, though most hydrographic sections do not include it because of the station positioning. This jet begins somewhere along the British Columbia - Southeast Alaska coast, where there are significant sources of freshwater. For example, some satellite tracked drifting buoys released in the North Pacific entered the coastal jet at about Sitka and followed it to the entrance of Icy Bay with a brief excursion over the Fairweather Grounds (Kirwan, personal communication). The various freshwater sources such as Yakutat Bay, Icy Bay, Copper River and Prince William Sound introduce only part of the freshwater into the coastal jet. A significant portion enters by way of short, small rivers which are common in the region. West of Seward, the annual rainfall rate decreases dramatically and relatively little additional freshwater enters the system with the exception of sources from Cook Inlet.

The freshwater portion of this coastal jet is confined to the upper 100 m. During the period of maximum discharge it penetrates to less than 50 m. Beneath this upper layer, the cross-shelf density is affected by

the seasonal cycle in the wind stress (Royer, 1975) which will be discussed later. This same wind stress effectively confines the freshwater to the nearshore region, so that, indirectly the wind stress increases the baroclinic flow in the coastal jet. With regard to wind stress and the coastal jet, during most of the year downwelling and onshore surface transport takes place. This is especially true in fall and winter. This onshore movement of surface water is opposed by an offshore displacement of the fresh surface water. The offshore displacement is implied by entrainment used to explain the onshore movement by the satellite tracked drifting buoys. Thus the lower layers have an onshore displacement while the surface layers move offshore. Surface pollutants released offshore beyond the coastal jet have several possible fates. A possible consequence of the onshore upwelling and offshore entrainment is that surface contaminants might be confined to move parallel to the coast at some distance dependent on: 1) rate of freshwater discharge, and 2) the intensity of the longshore winds. No direct measurements of this possible configuration have been made, though the hydrographic cross-section data do support it (Fig. 9). The low density surface layer extends to about 25 km and the downwelling due to the wind stress is evident inshore of this region.

The addition of freshwater at the coast throughout this region causes surface features such as sediment plumes to disappear downstream. For example, the distinctive sedimentation from the Copper River is often observed between the shore and Middleton Island in satellite images, but does not appear at the surface to the west of Prince William Sound. It is hypothesized that those waters which contain the surface sediments, are covered by the fresher outflowing surface water. The sediment is

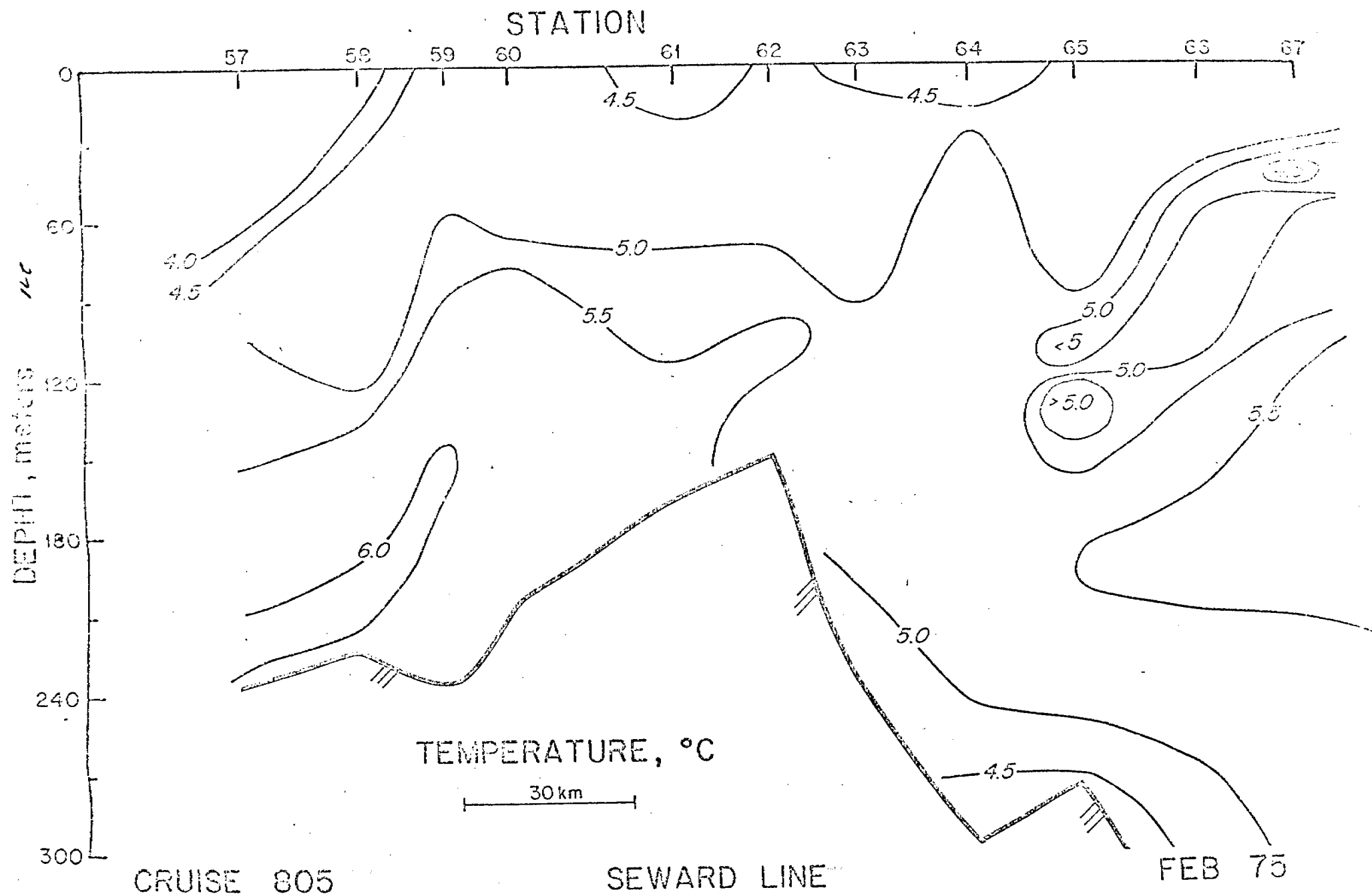


Figure 9a. Cross-section of temperature.

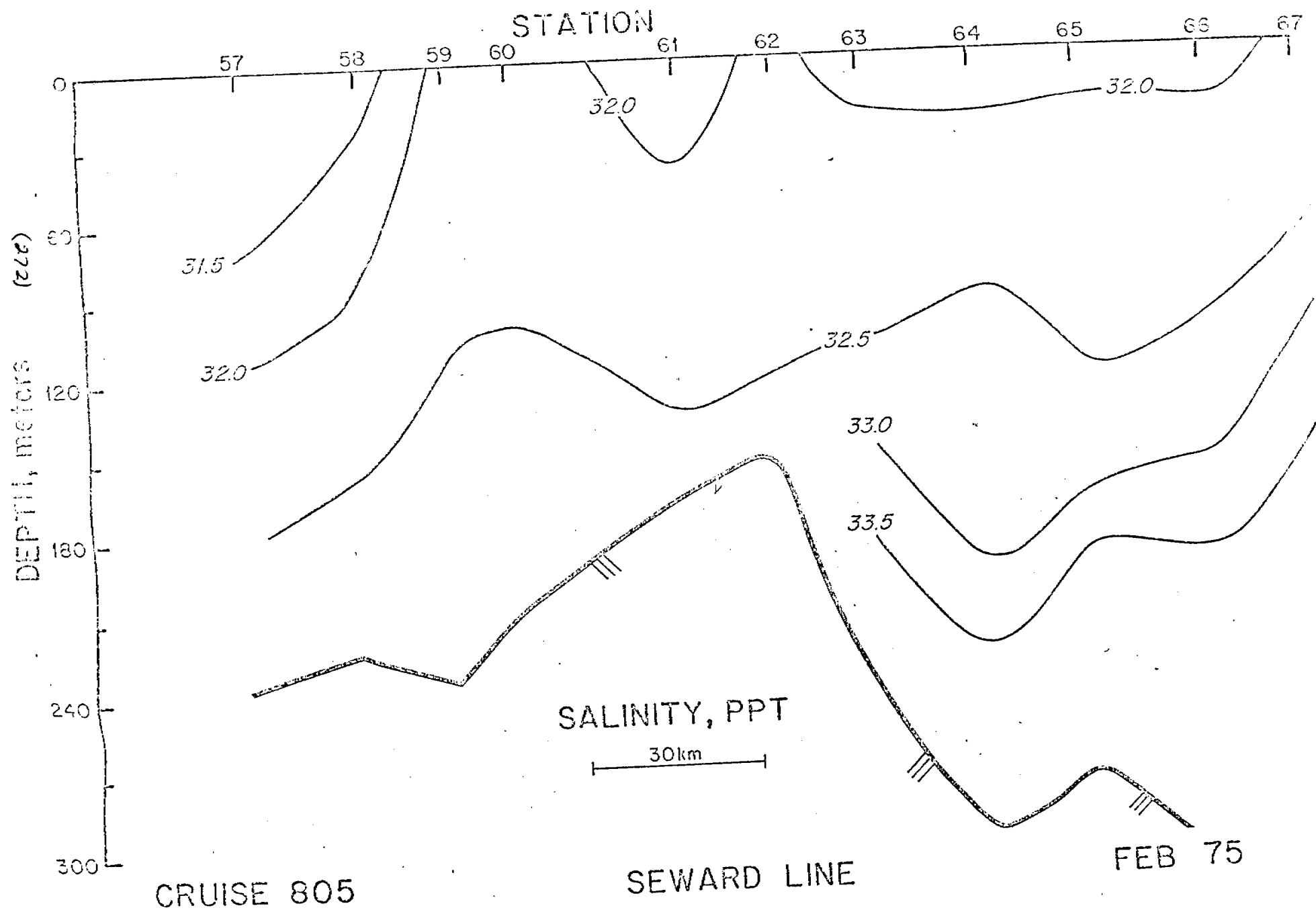


Figure 9b. Cross-section of salinity.



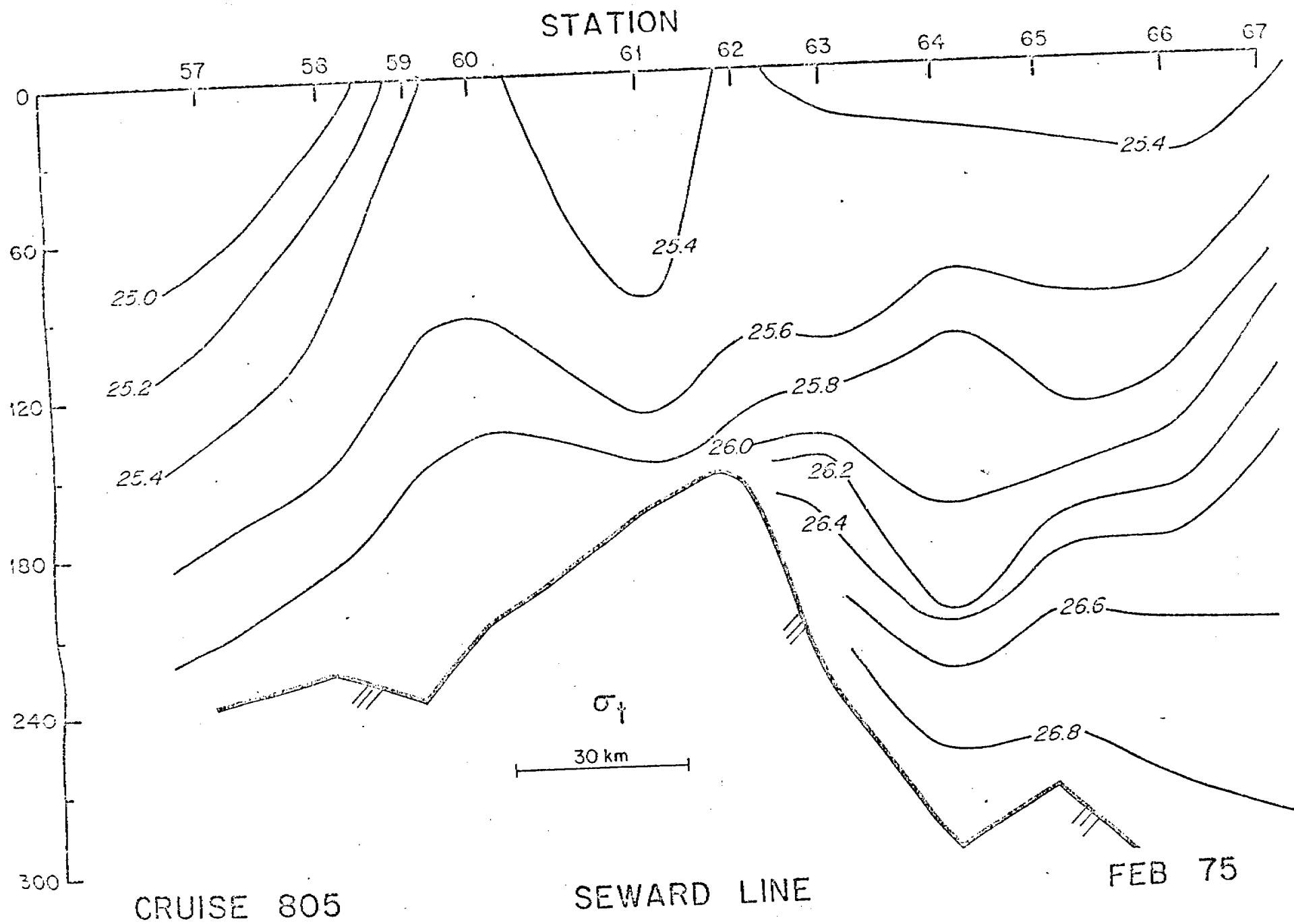


Figure 9c. Cross-section of sigma t.

advected in the coastal jet beneath the surface layer. Copper River sediments have been found in the eastern portion of Cook Inlet (Bouma, personal communication) where they have been deposited after being carried by the coastal jet.

To the west of Kayak Island, the coastal jet splits into a nearshore portion which flows into Prince William Sound and an offshore portion flowing to the south of Middleton Island. The nearshore jet is renewed with additional fresh water whereas the offshore jet is not.

## VI. SHELF CIRCULATION FORCING MECHANISMS

The most significant effects on the circulation over the continental shelf in the northern Gulf of Alaska are: 1) wind and wind stress, 2) runoff (and other possible thermohaline effects), 3) forcing by Alaska Current and 4) bathymetry. The last does not act in an active manner, but steers or directs the flow.

### A. Winds and Wind Stress

The annual cycle in wind stress over the Gulf of Alaska dominates all the forcing parameters. The monthly mean winds change by a factor of two from summer ( $\sim 4 \text{ ms}^{-1}$ ) to winter ( $\sim 8 \text{ ms}^{-1}$ ) (Livingstone and Royer, 1979). Depending whether data from Bakun's (1973) large scale wind field or local observations are used, the upwelling index goes from a maximum negative value (downwelling) in December or January to a small negative or over slight positive number in June-July.

The wind fields over the Gulf of Alaska can be classified into six types (Galt *et al.*, 1978). The winds in Table II have been used as input

TABLE II

WEATHER TYPES FOR GULF OF ALASKA (GALT *et al.*, 1978)

Type	Description	Dominant Season
I	Low in Gulf of Alaska	Winter
II	Aleutian Low	Winter, Spring, Fall
III	High pressure in Alaska interior	Winter
IV	Low pressure center over central Alaska	Summer
V	Pacific Anticyclone	Summer
VI	Stagnating low off off Queen Charlotte Islands	Spring, Fall

for numerical models and were determined using a pattern correlation technique on digital daily weather maps and sea level pressure grids. Actual surface winds are not necessarily well represented by calculated geostrophic winds. The real wind field is subjected to coastal blocking, extensive air mass modification and other mesoscale features induced by coastal topography (Galt *et al.*, 1978). For a particular weather type, the transition to another weather type is predicted in Table III. Thus a temporal sequence of weather types can be achieved.

There are few observations of the actual winds over the Gulf of Alaska. Of these observations, however, those at Middleton Island are the most numerous. Other observations include NOAA data buoys EB-03 (east of Kodiak) and EB-33 (near Icy Bay). An evaluation of the surface winds using Middleton Island observations and Bakun's (1973) calculated geostrophic winds reveals a large discrepancy between the two sets especially in winter (Livingstone and Royer, 1979). In summer, Bakun's computations contain a brief period of upwelling (or eastward winds) for 60°N, 146°W. The actual observed winds at nearby Middleton Island do not indicate this tendency of summer upwelling. The actual wind stress in winter is 3-4 times less than that determined by Bakun using his 3° x 3° surface atmospheric pressure grid. The differences in the actual versus calculated winds could be due to small scale effects such as mountain blockage and local heating. Since one of the grid locations for his calculated winds is in the Alaskan interior, the effect of high pressure atmospheric systems inland is incorporated in this computation. The greater persistence of the calculated winds is also due to the long residence time of this high (Livingstone and Royer, 1979). Muench *et al.* (1978) disagree with these results. They conclude that the winds calculated

TABLE III

TRANSITIONS FROM INITIAL WEATHER TYPE TO FOLLOWING TYPE (GALT *et al.*, 1978)  
Based on 12 hourly analyses 1968-1974

Initial Type		% Occurrence of Initial Type	% of Initial Type Followed by Following Type					
			1	2	3	4	5	6
Y E A R	1	16	47	17	6	13	2	15
	2	31	12	71	6	7	3	1
	3	9	14	15	56	1	1	13
	4	18	8	11	20	60	16	5
	5	12	20	24	1	15	59	1
	6	14	15	3	9	8	3	62
W I N T E R	1	23	57	15	6	6	1	15
	2	26	13	71	8	6	1	1
	3	19	10	10	70	20	1	9
	4	7	19	14	1	42	13	11
	5	4	0	29	5	14	52	0
	6	21	14	2	9	4	1	70
S P R I N G	1	16	43	17	6	16	1	17
	2	37	11	73	6	7	2	1
	3	8	16	21	47	0	0	16
	4	16	8	14	1	54	16	7
	5	9	0	35	2	10	52	1
	6	14	16	4	8	10	4	58
S U M M E R	1	8	34	20	4	27	5	10
	2	30	8	68	5	9	8	2
	3	3	27	20	29	2	7	15
	4	26	4	7	0	67	20	2
	5	27	20	19	0	12	68	1
	6	6	14	7	4	15	7	52
F A L L	1	18	45	18	6	14	1	16
	2	30	15	68	6	8	2	1
	3	8	16	18	43	3	1	19
	4	22	9	12	20	60	13	6
	5	7	1	27	0	34	37	1
	6	15	15	2	10	9	3	61

from the large scale atmospheric pressure grid underestimate the actual winds due to the packing of isobars by the coastal mountain range. Both of these studies (Livingstone and Royer, 1979, and Muench *et al.*, 1978) believe that the coastal mountains affect the offshore winds significantly but in opposite manners.

Near the coast, the topography will have a large effect on the local winds and katabatic winds become very important in the nearshore region (< 30 km) and estuaries (Fig. 10) (Reynolds *et al.*, 1978). However, with the Aleutian Low dominating the atmospheric pressure system, the winds become oriented alongshore, especially in the nearshore region (Fig. 11). Katabatic winds are most important between Yakutat and Icy Bay and in the vicinity of the Copper River.

Winds drive the ocean circulation as a surface wind drift, a redistribution of density within the water column (baroclinic currents) and by imposing a slope to the sea surface (barotropic currents). The direct response, actual movement of the surface water, is the most easily determined, yet even these determinations are somewhat doubtful. The generally accepted method is to assume that the surface water movement from wind occurs at a rate of 3% of the wind speed and in that same direction as the wind speed. The baroclinic response can be determined indirectly from the mass field. It is difficult to separate the wind effects on this field from the other influences such as advection and vertical mixing. The barotropic response can be determined from sea level pressure measurements after these measurements have been corrected for tidal fluctuations.

In early 1977, a detailed observational program of currents and bottom pressure was carried out near Icy Bay (see Fig. 2). The sampling

SAME SURFACE PRESSURES AS 3.0 BUT HIGH (>50KTS) KATABATIC WINDS

PAGE 3.4

279

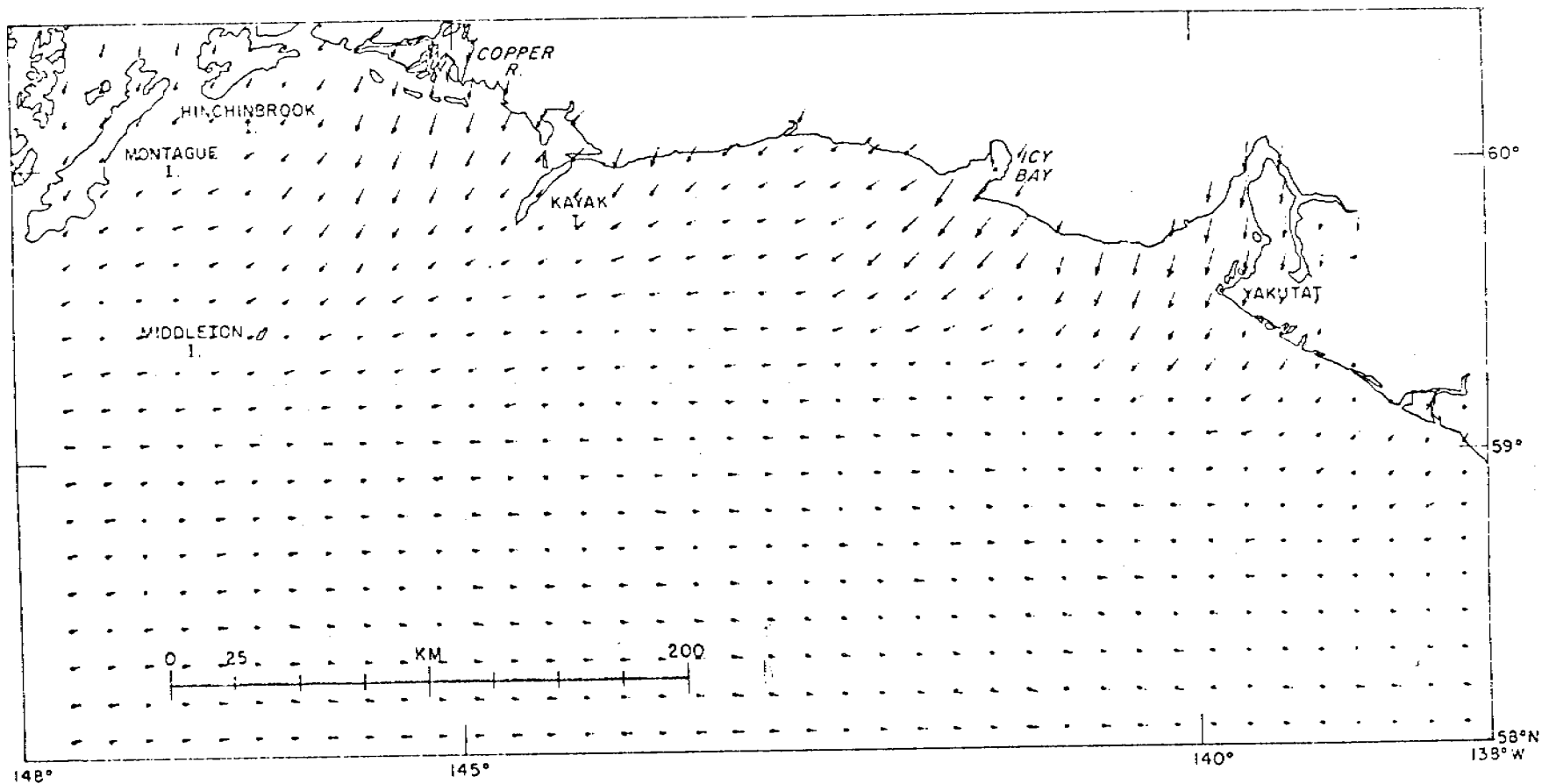


Figure 10. NEGOA winds showing high katabatic conditions (Galt *et al.*, 1978).

ALEUTIAN LOW

CASE 2.0

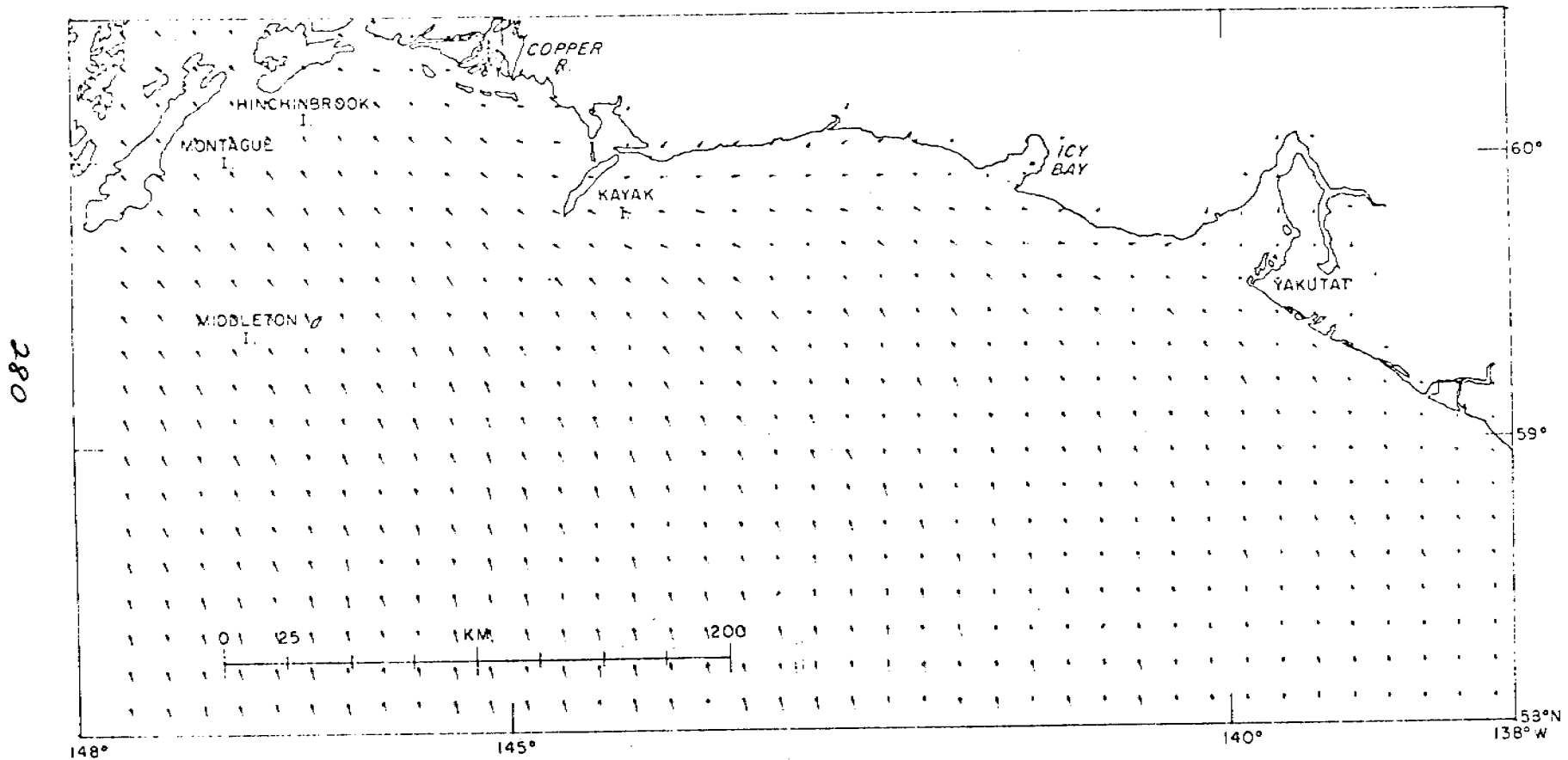


Figure 11. NEGOA winds under influence of Aleutian Low (Galt *et al.*, 1978).



took place from March through August at most of the moorings (SLS-A-F, WIST I, II). The important results of that experiment are that the flow on the shelf differed from that at the shelf break and that small scale waves (< 50 km) or eddies are reflected at the shelf break (Muench *et al.*, 1978). It was also concluded that the bottom pressure across the shelf was more coherent than the velocity and that a simple geostrophic barotropic model would be sufficient to describe the flow. However, the shortcomings of this experiment are that the current meters were at depths greater than 20 m, their records were short, not allowing seasonal coverage and there were no currents measured in the Alaskan coastal jet. It is not surprising then, that the barotropic current component overshadowed the baroclinic component. Also, this experiment did not have good measurements of the offshore Alaska Current.

Studies near Icy Bay showed that nearshore the pressure field responded to onshore winds whereas the offshore response was primarily to alongshore winds (Hayes, 1979). This depth dependent response to the winds can yield nearshore coastal currents that differ from currents over the mid- and outer shelf regions. The scale length of the shelf baroclinic response is of the order of the internal Rossby radius of deformation which in our case is about 30 km. Coastal upwelling and downwelling should occur within a coastal band of this width. This is also the width of the observed coastal jet. The response of the ocean to the winds at this short distance from shore is nearly instantaneous, that is, of the order of hours. The nearshore response to winds here has not yet been measured directly because the current meters have been installed only outside this coastal boundary. Based on the strong barotropic response found by Hayes (1979), the coastal

jet can be expected to be a maximum in winter when the alongshore winds are a maximum, and least in summer.

#### B. Freshwater Discharge

The coastal current is also strongly influenced by the coastal freshwater discharge which peaks in autumn about in phase with the annual precipitation maximum (Royer, 1979). The freshwater also has an unknown effect on the circulation on the shelf and throughout the Alaskan gyre. The addition of freshwater at the coastal boundary will increase the dynamic height there and, when in geostrophic equilibrium, will drive a westward flow. The alongshore wind will keep this freshwater lens along the coast through downwelling in the winter months. These two processes should act together to intensify this coastal jet especially in winter. No direct current measurements have been made of this jet, however.

The freshwater discharge has been approximated using a very simple hydrology model with two different drainage areas (Royer, 1979b). The amount of discharge was determined from the average annual precipitation rate is measured at a few coastal stations. The orogenic effect on precipitation will cause these measurements to underestimate the actual average precipitation over the region. The amount of water stored as snow and ice was also considered though actual measurements were not used. (The freshwater discharge will be dependent on the air temperature and insolation, neither of which have been considered up to this point.)

### C. Alaska Current Forcing

On the outer reaches of the continental shelf, the Alaska Current will influence circulation patterns. Apparently, the generation of eddies along this boundary is an important mechanism by which the momentum of this current is distributed onto the shelf. This type of behavior is expected, in retrospect, from vorticity considerations. Decreasing depth to the right of the flow in conjunction with the potential vorticity, will force an impinging meander to turn to the right and to propagate onto the continental shelf. Most other boundary currents have deeper water to the right, hence, the propagation is offshore into deeper water where it turns onshore thus stabilizing itself along an isobath.

The Alaska Current might also be thought of as a boundary between the warm high salinity water of the North Pacific and the cold, low salinity water of the coastal region. With this concept, the renewal of the fresh-water along the outer shelf becomes very important since it would play a major role in maintaining the Alaska Current. For example, the horizontal density gradient which drives the baroclinic portion of the Alaska Current, is due more to horizontal salinity gradients than the horizontal temperature gradients. Thus, mechanisms are necessary for the maintenance of both of these horizontal gradients.

An evaluation of the temporal and spatial changes in the Alaska Current is impossible based upon the current meter data and hydrographic sections in the northeast Gulf of Alaska. First, the hydrographic sections did not extend far enough offshore to always intersect the Alaska Current. This problem was not known when the original sections were established. Second, the Alaska Current can shift position in a manner that makes it impossible

to distinguish a spatial acceleration from a temporal one. In summary, it was impossible to "capture" and "measure" the Alaska Current on anything other than as a synoptic snapshot or as it passed by the current meter arrays.

#### D. Bathymetry

A conclusion agreed upon by the investigators undertaking these various studies is that "in general the flow follows isobaths". The Alaska Current follows the shelf break contour with the exception of occasional eddies. Flow over the shelf outlines submerged canyons and ridges. The coastal current, of course, is constrained to follow the shoreline. All of these flows as measured by infrared images from satellites indicate that sea surface temperature distributions have closely reproduced the bottom contours. That is, a map of sea surface temperature often resembles a chart of bottom topography. The most notable exceptions to this isobathic flow are the eddies and cross-shelf wind-driven flow.

#### VII. ESTUARY CIRCULATION

The coastline of the northern Gulf of Alaska contains numerous fjords, embayments and other estuaries, including Prince William Sound. Water in each of these embayments is diluted at the surface by runoff and precipitation and has salt added through exchanges with the waters of the Gulf of Alaska. These exchanges are mechanisms by which pollutants released on the shelf can enter the estuaries, or by which pollutants released in the estuaries can be flushed onto the shelf.

The trajectories described by satellite-tracked, drogued-drifting buoys indicate a flow of shelf water into Prince William Sound (Fig. 4) (Royer *et al.*, 1979). Taken without additional considerations, these trajectories imply that pollutants released over the continental shelf in the eastern Gulf of Alaska have a high probability of entering Prince William Sound. However, the drogues of these buoys were 35 m deep and therefore do not represent surface flow. It has been hypothesized that the drogues actually describe a subsurface counterflow from upper layer entrainment by the fresh, offshore moving surface layer (see Section VI). To the contrary, this offshore moving surface layer implies that surface pollutants would be forced to remain away from the coastline in the absence of wind or wave effects. Under the conditions described above, protection for the coastline would be greatest in fall and least in spring.

Hydrography and current meter observations point to a classification of Prince William Sound as an inland sea, with inflow at Hinchinbrook Entrance and outflow through Montague Strait. Within the sound there is a cyclonic sense to the circulation and considerable surface dilution from runoff, since the drainage area is large. The extent to which waters are modified during their passage through the sound is not clear, although data have been collected but not analyzed to answer this question. Short term current reversals can take place at Hinchinbrook Entrance but none have been noted in the current meter data from Montague Strait. Current meter records for Prince William Sound and Valdez Arm indicate that large scale events occur in this region which appear to be related to changes in the atmospheric pressure system (J. Colonell, personal communication).

The other estuaries in this region which have been studied in this region are Resurrection Bay (in the western gulf) and Russell Fjord (in the eastern gulf). Heggie *et al.* (1977) report an annual deep water renewal in Resurrection Bay coincident with the minimum downwelling or maximum upwelling. Muench and Heggie (1978) discuss similar deep water renewal for other fjords on the Alaskan coastline and conclude that the exchange of deep water is very dependent on the sill depth. Reeburgh, Muench and Cooney (1976) find that the exchange of water with adjacent marine sources occurred on a discontinuous basis.

#### VIII. NUMERICAL MODEL RESULTS

The description of surface flow patterns using numerical modeling techniques shows that baroclinic currents dominate the flow at the shelf break while barotropic currents and surface wind drift dominate the response on the shelf (Galt *et al.*, 1978). The input fields for this model are synoptic meteorological data which drive local wind fields, hydrographic observations, current meter observations and bottom topography. The density (baroclinic) and wind driven components are separable, allowing studies of the responses to the individual forcing mechanisms. The model represents an extension of charts of dynamic topography, which describe the baroclinic currents and the surface wind field describing the wind response.

The numerical model developed by Galt *et al.* (1979) assumes, in addition to the ability to separate the density and wind driven current components, that there is a uniform cross-shelf slope to the sea surface over the entire shelf, that the wind stress curl is negligible and that the

level of no motion is 1200 m. The model assumes no tidal or inertial currents and cannot resolve meso-scale eddies since it assumes that the baroclinic field is constant. The weakest assumptions are the invariant nature of the baroclinic field, the independence of the density driven and wind driven current components and the uniform response of the shelf waters to the wind stress. Observations indicate that the majority of the shelf circulation occurs in the coastal jet, less than 30 km offshore and near the shelf break and not uniformly over the shelf. The winds interact with the density driven flow, generally intensifying it here. The actual current speeds will be much higher than those predicted by this model.

Trajectories, representing possible oil spill motion, are generated by the numerical model. These trajectories (Figs. 12a-k) project an on-shore movement of spilled oil, for summer (s) and winter (w) conditions, with nearshore movement in either direction. Most commonly it moves westward however. There are, of course, some exceptions to this motion especially near the shelf break where eddies are common. There is also a tendency for the oil to enter the eddy to the west of Kayak Island and remain there (Fig. 12). The model does not give evidence of the strong coastal current suggested by studies near Seward. However, the hydrographic station positions did not extend into the coastal current on most of the section lines. Also, these stations near the coast were often in shallow water, which did not allow a deep reference level to be used. Therefore, currents here could be much less than the real currents.

Another deficiency of the model is its inability to include a time dependent wind or density fields. Obviously, the winds, density structure

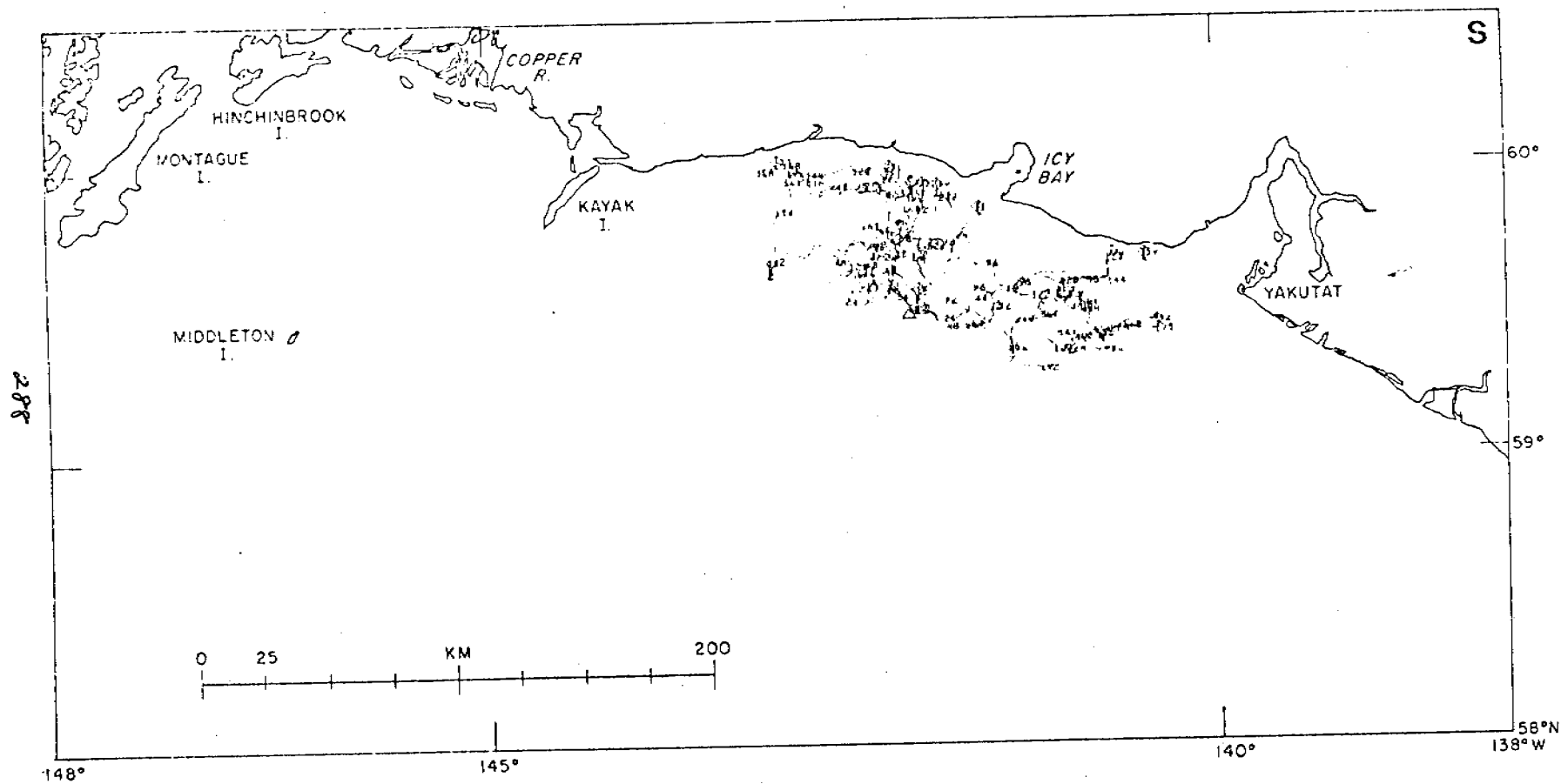


Figure 12a. Calculated trajectories at surface in NEGOA (Galt *et al.*, 1978).



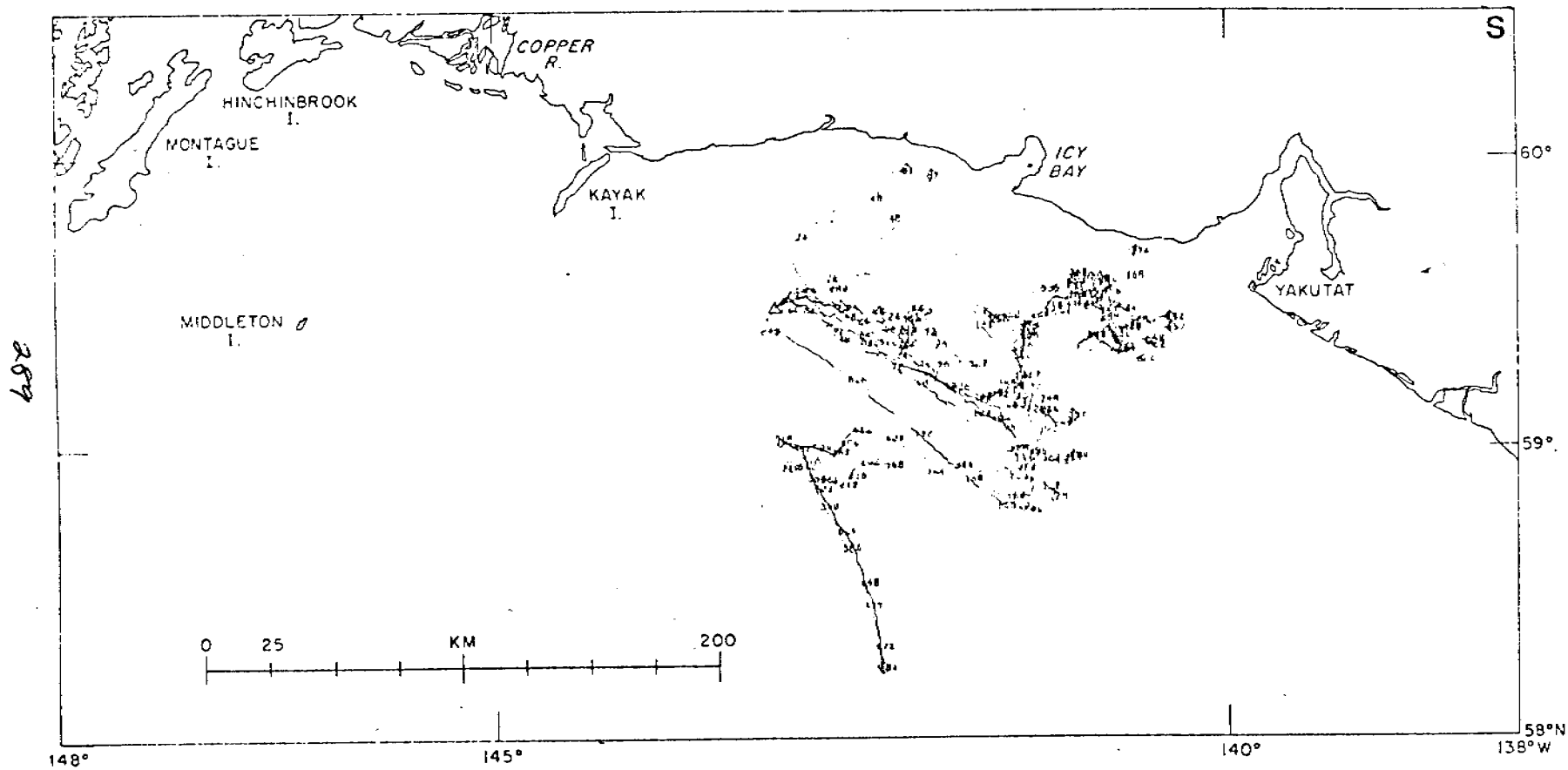


Figure 12b. Calculated trajectories at surface in NEGOA (Galt *et al.*, 1978).

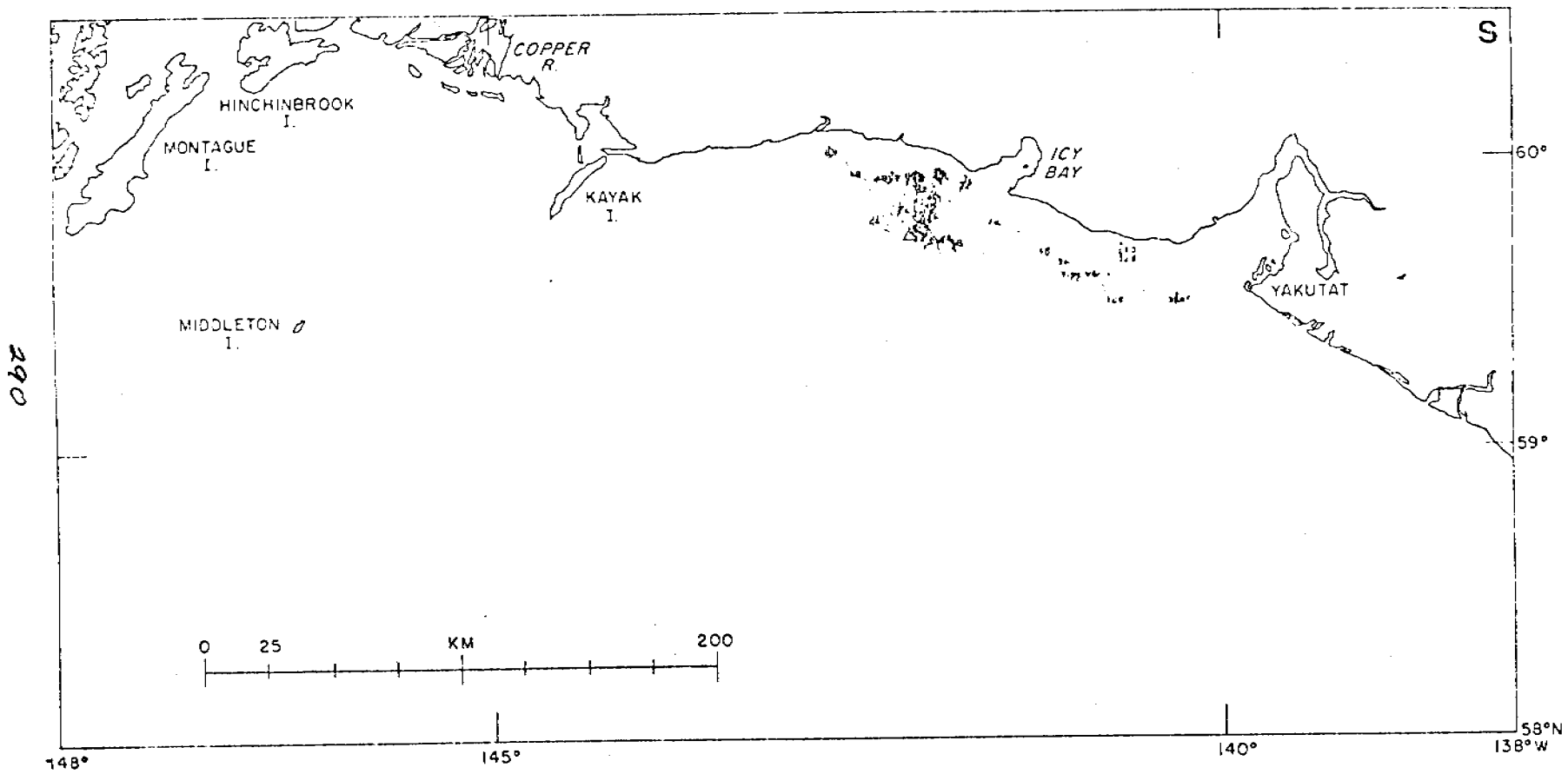


Figure 12c. Calculated trajectories at surface in NEGOA (Galt *et al.*, 1978).

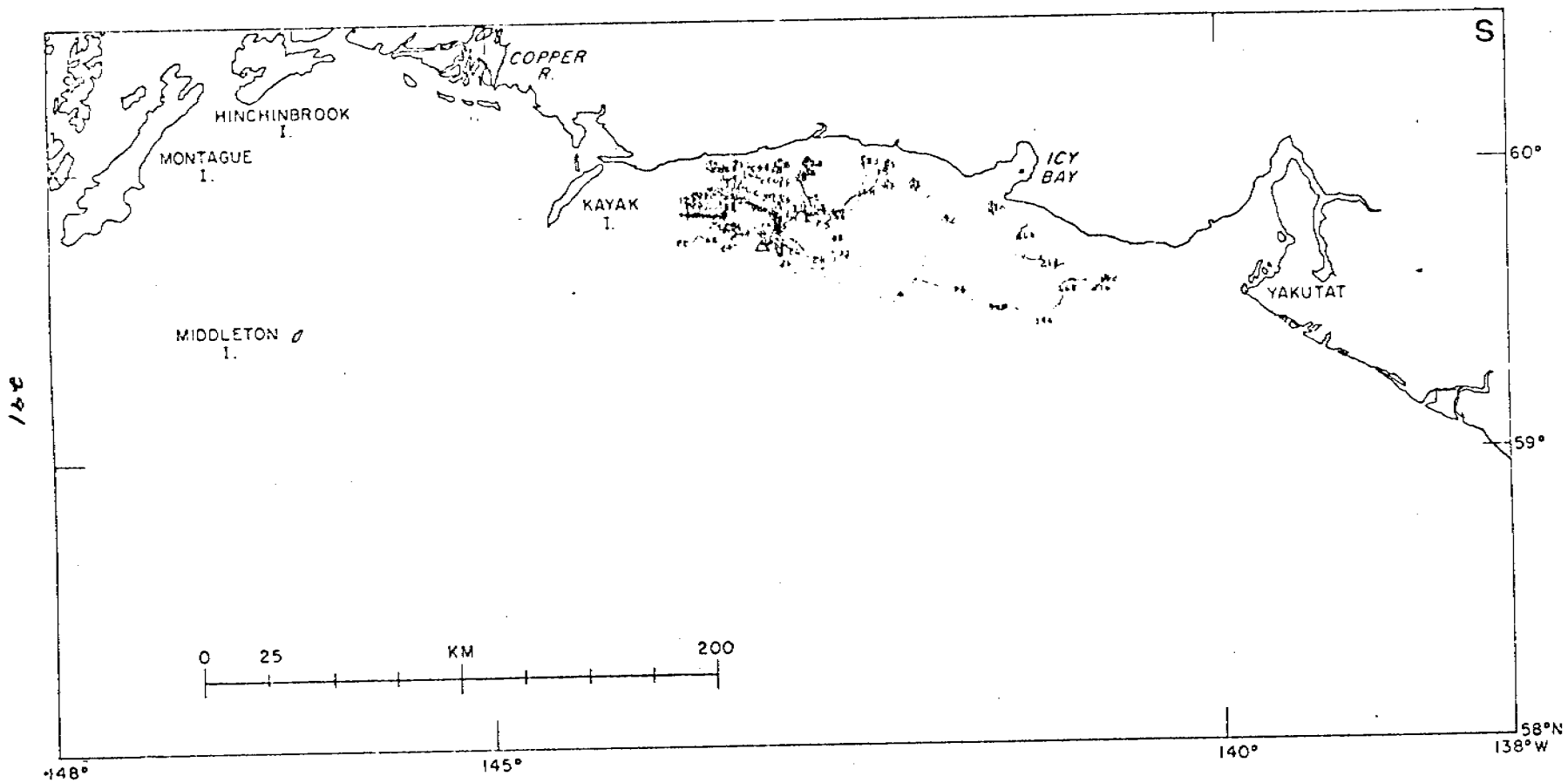


Figure 12d. Calculated trajectories at surface in NEGOA (Galt *et al.*, 1978).

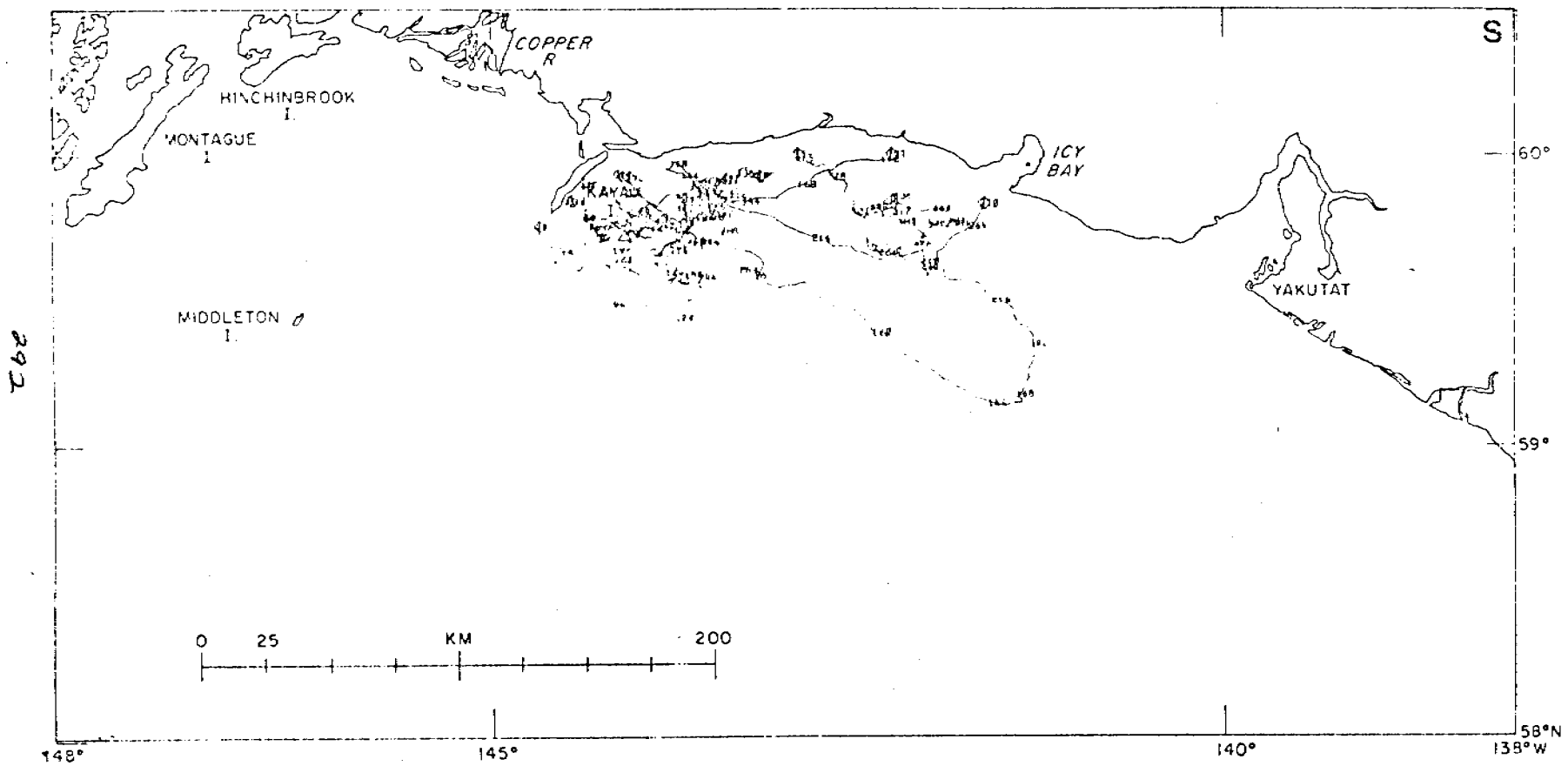


Figure 12e. Calculated trajectories at surface in NEGOA (Galt *et al.*, 1978).

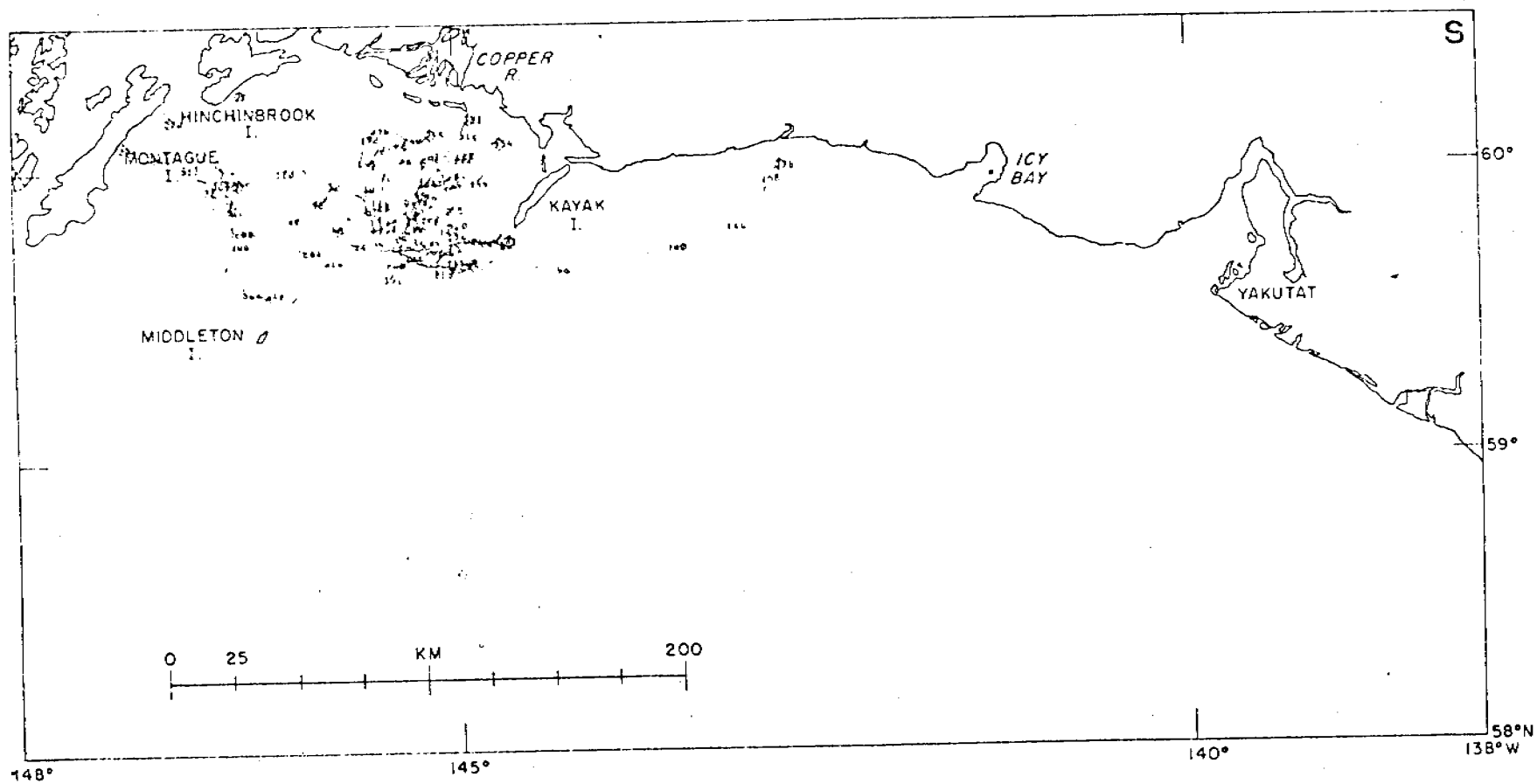


Figure 12f. Calculated trajectories at surface in NEGOA (Galt *et al.*, 1978).

294

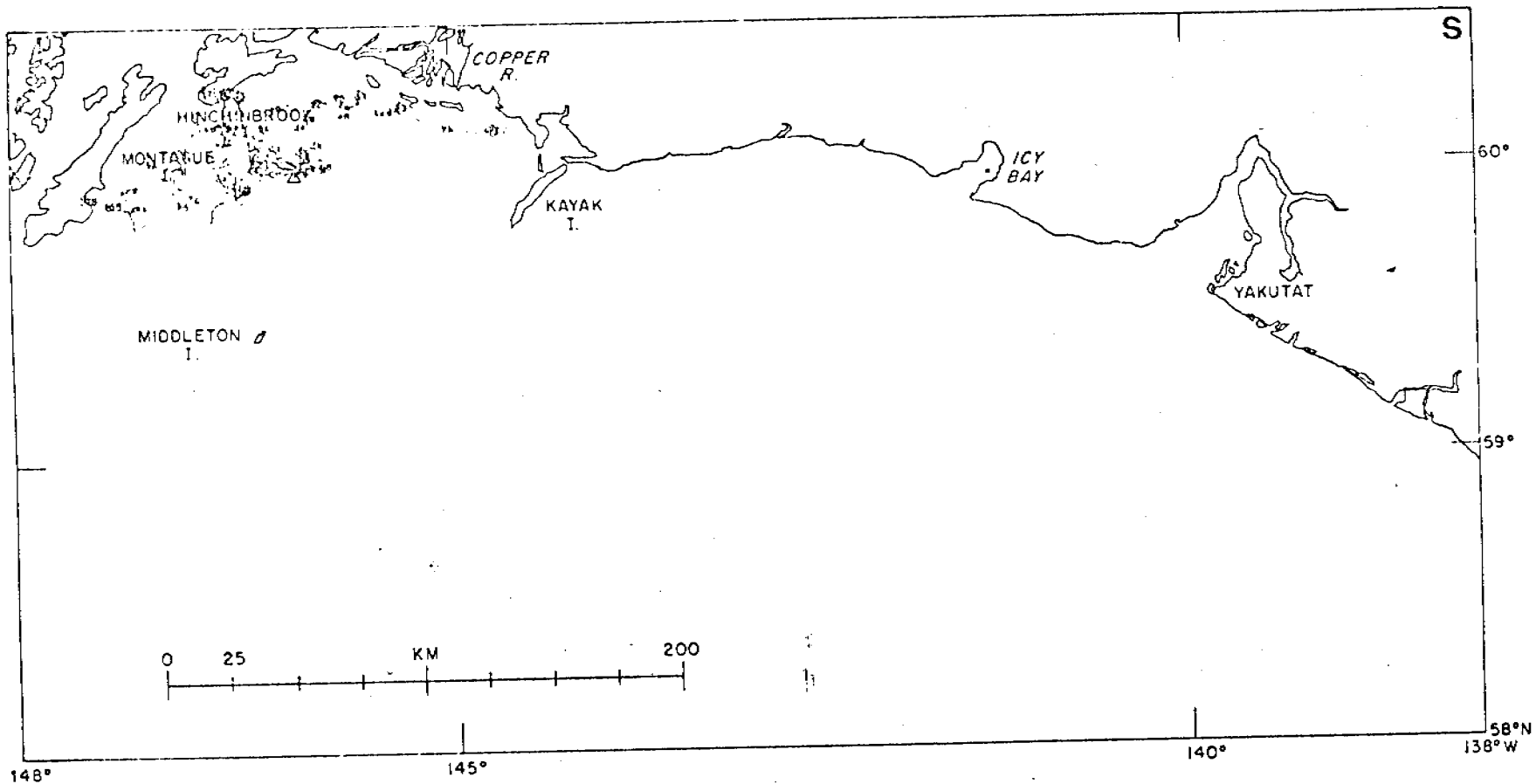


Figure 12g. Calculated trajectories at surface in NEGOA (Galt *et al.*, 1978).

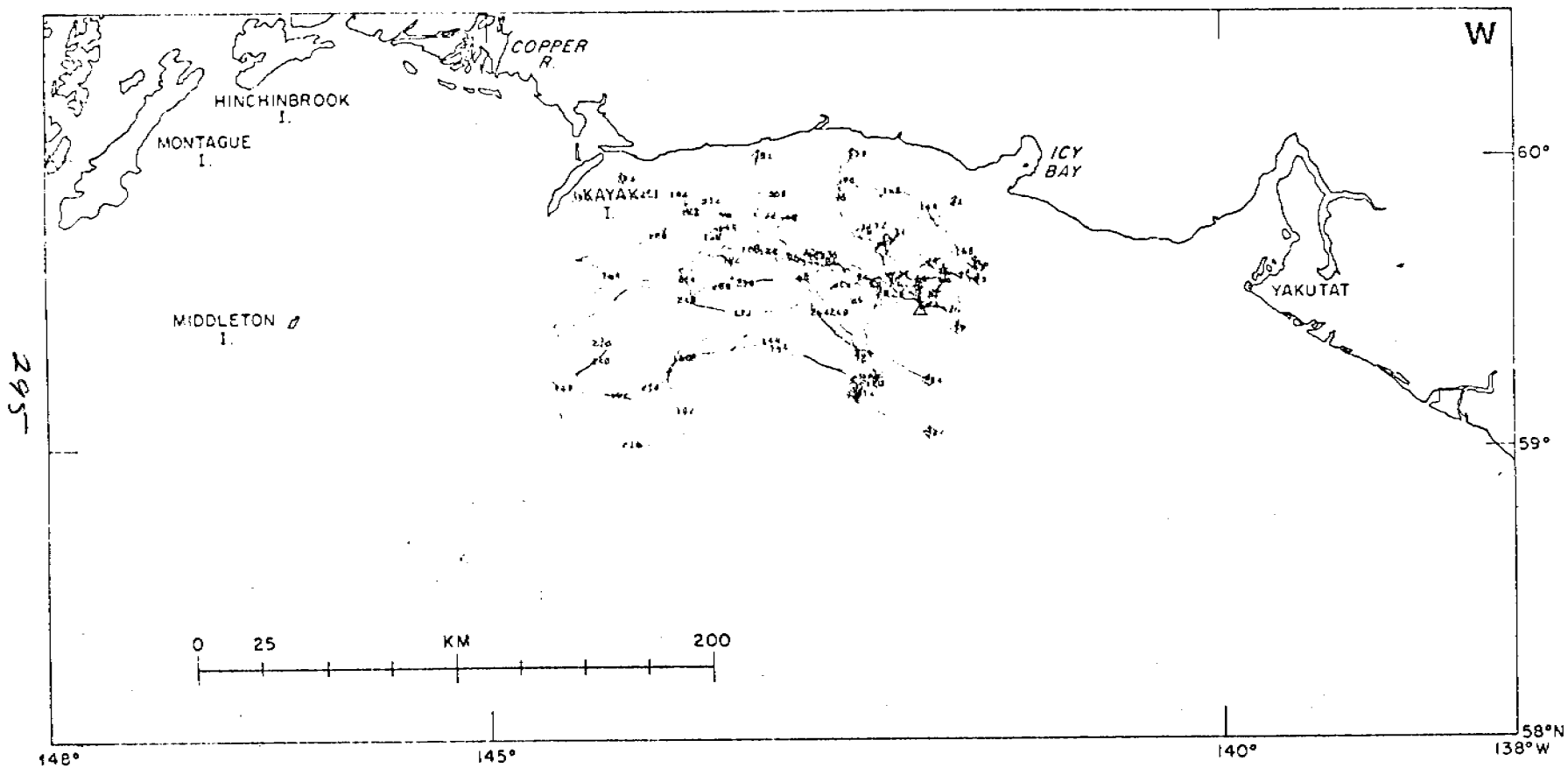


Figure 12h. Calculated trajectories at surface in NEGOA (Galt *et al.*, 1978).

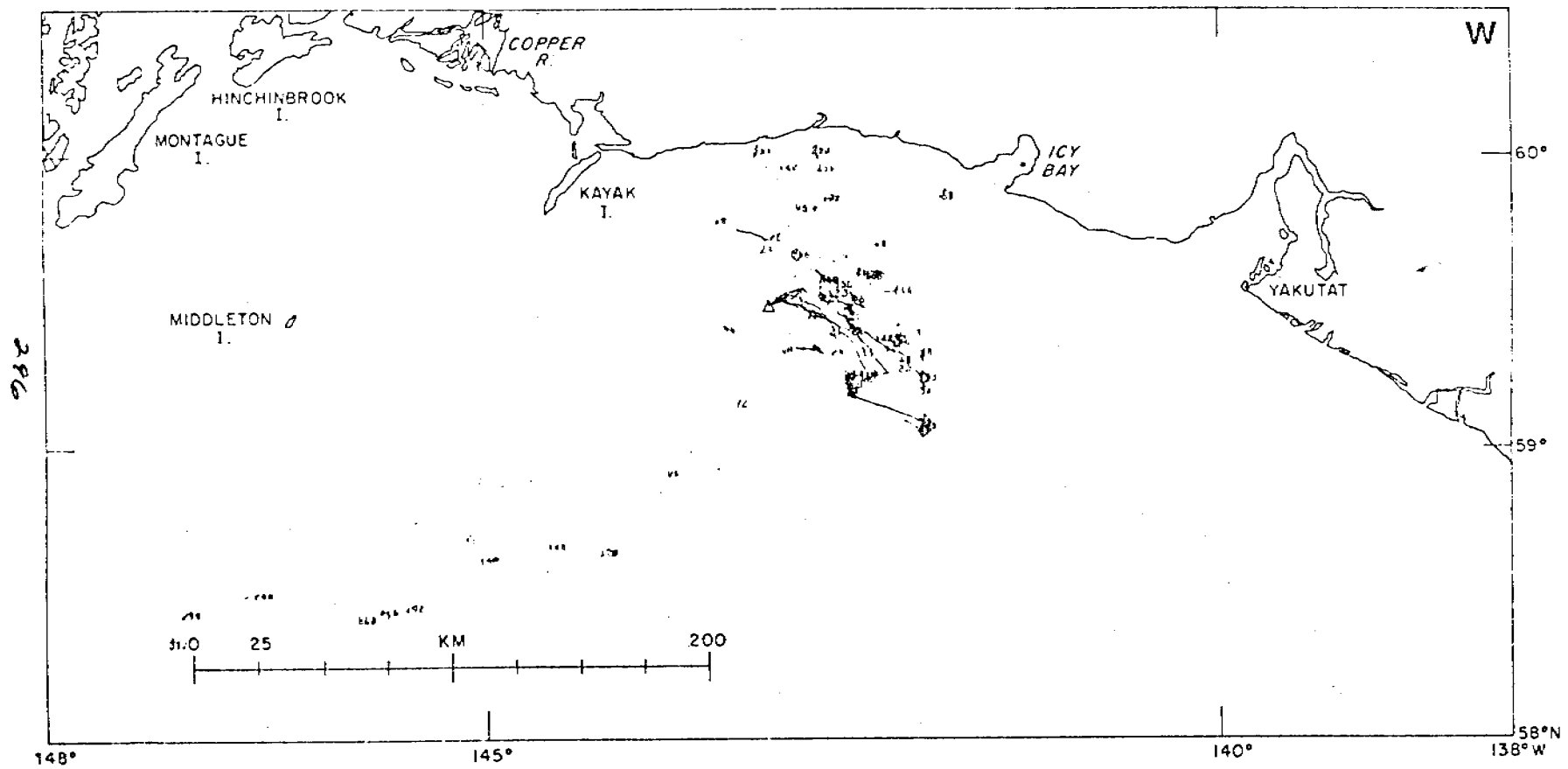


Figure 12i. Calculated trajectories at surface in NEGOA (Galt *et al.*, 1978).



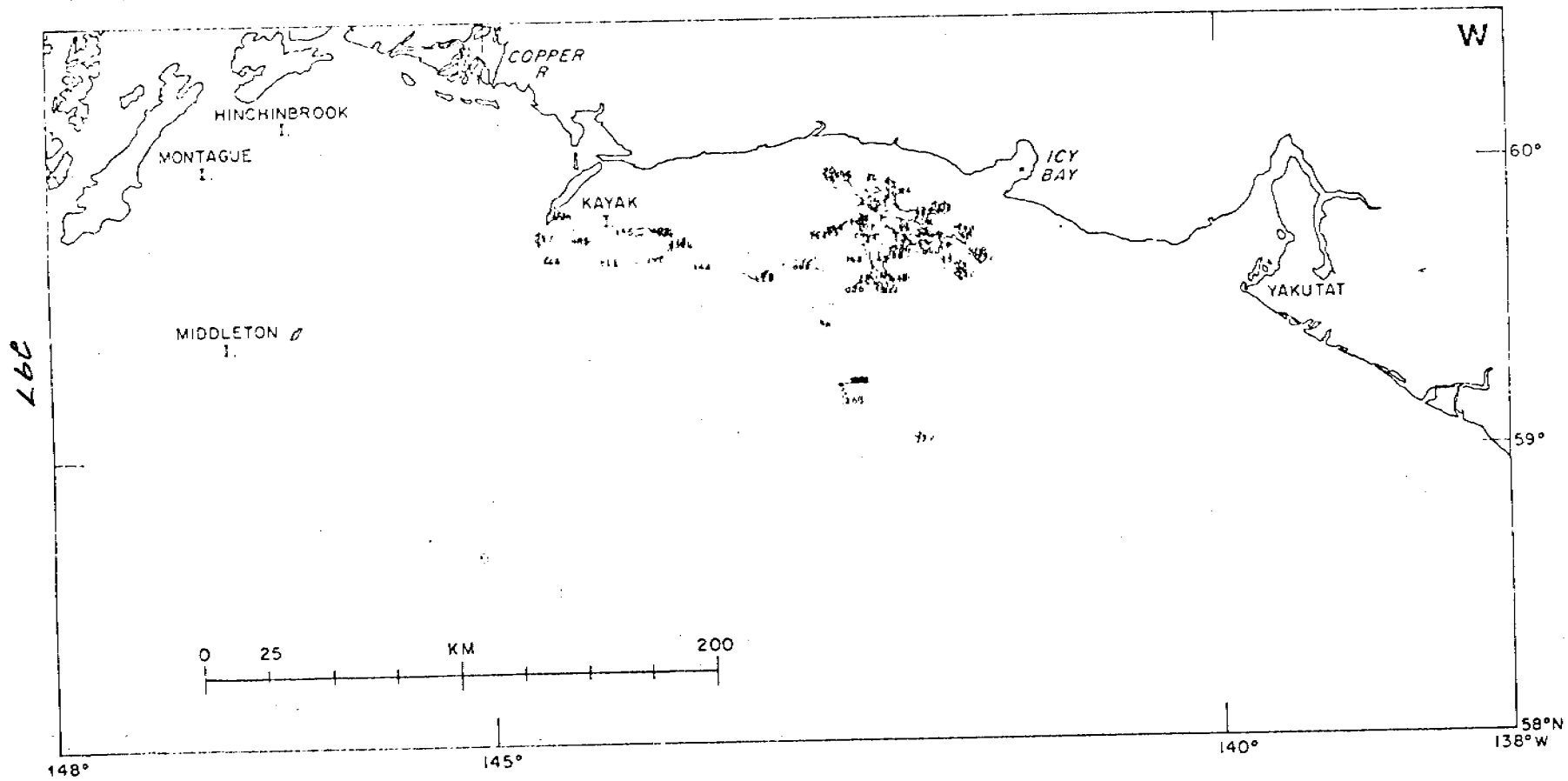


Figure 12j. Calculated trajectories at surface in NEGOA (Galt *et al.*, 1978).

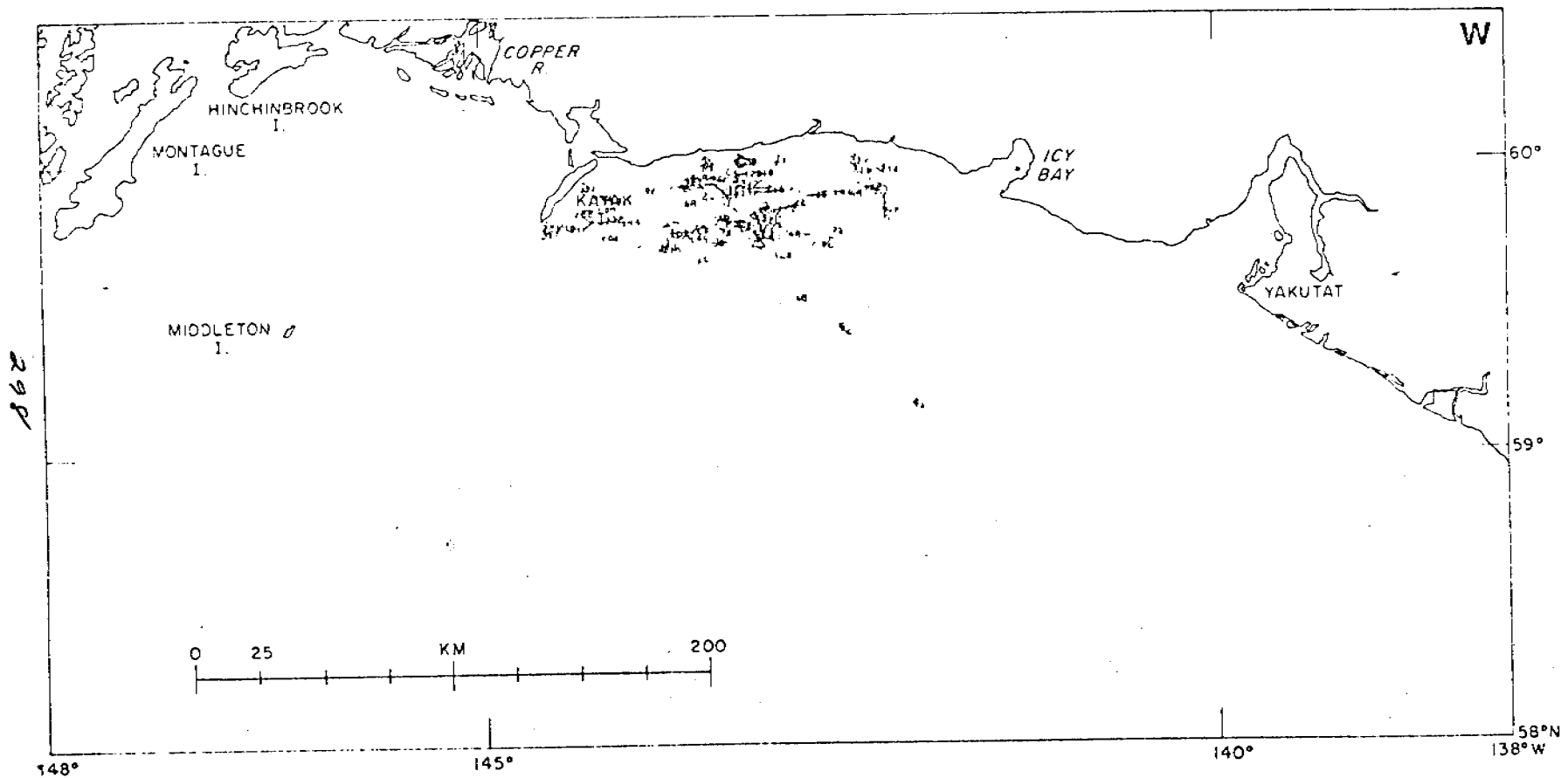


Figure 12k. Calculated trajectories at surface in NEGOA (Galt *et al.*, 1978).

and baroclinic flow will change over the course of a trajectory, but this is not incorporated in the numerical model. On some occasions, the density field used in the model is questionable due to local perturbations, such as eddies. This is not a fault of the model but rather one of the sampling scheme. The model should be run for other density fields, winds and currents where data are available.

Up to now, the major focus of the model has been to provide trajectories for potential oil spills. Now that this has been accomplished to some degree of success, the model should be used to better understand the processes which affect the circulation in the Gulf of Alaska. For example, what is the ocean's response to variations in the local wind field, both on and off the shelf? What is the response to an impulse of freshwater at the coast? Little communication has taken place between the descriptive investigators and modellers since the model has been developed and run. Numerous, numerical experiments should be attempted, like those outlined above.

#### IX. DEVELOPMENT OF A PROCEDURE TO PREDICT THE TRAJECTORY OF AN ACTUAL OIL SPILL

In case of an actual oil spill in the northern Gulf of Alaska, after the location of the spill has been established its path can be predicted from Galt's model. A density field must be selected that is appropriate to the season and the type of weather pattern established from current atmospheric pressure maps. Given those two input fields a reasonable guess of the spill trajectory can be made from previous model runs (see Galt *et al.*, 1978). The combined model can then be run using the appropriate wind and density fields along with the transition wind field to improve the

estimate. "Real time" modifications to this wind field should be incorporated as they become available. The trajectory model can thus be "stepped" through time for a better approximation.

#### X. RECOMMENDATIONS FOR FUTURE STUDIES

In addition to the modeling-descriptive interaction described previously, several other important problems have been ignored or overlooked up to now. First, the nearshore work is necessary to determine the circulation between the last hydrographic station and the beach. Apparently, much of the coastal jet has not been investigated and the wind stress effects (upwelling and downwelling) are a maximum there. In conjunction with these nearshore studies, the local winds must be better determined. For example, the argument of whether the actual winds are greater or less than those predicted from a large scale pressure network must be resolved. The small scale spatial variability of the wind field nearshore should also be investigated.

A serious fault of the previous physical oceanographic studies is a lack of knowledge of near surface circulation, particularly within the upper twenty meters. This has become especially important because of the vast amount of freshwater entering the system at the coast. We presently only have a hypothesis that this freshwater moves offshore creating an entrainment process. The technology is now available to attempt a solution to this problem.

Actual current measurements should be made in the coastal current to determine the current's response to freshwater discharge and wind forcing. These measurements should be made as close to the surface as possible

using a surface buoy and vector averaging current meters. Such a mooring could also provide necessary local wind field data.

The discovery of shelf break eddies in the Gulf of Alaska is very important to the understanding of lateral mixing on the shelf. The dynamics of these eddies is unknown. For example, how and where are they generated? Do they propagate or are they stationary? By what mechanism(s) do they dissipate? A study should be carried out to track one or more of these eddies and a numerical model should be utilized to investigate the nature of their formation.

The knowledge of the physical oceanography of the Gulf of Alaska resides with a number of individual scientists. This knowledge has not been integrated or synthesized with the exception of a brief attempt in late summer 1978. While the initiative to further investigate the data must come from the principal investigator, OCSEAP should provide an incentive for this reinvestigation. Such an investigation should include those data for the Kodiak region as part of the system. Such questions to be addressed are. Can general trends in flow energy be seen throughout the region? What are large scale responses, does the shelf and estuary circulation act together? Can eddies be seen as they propagate from one region to another? What are the interannual variations on this shelf? Principal investigators should be given the opportunities to alter parameters in the numerical model to determine their effect on the circulation and to provide more insight and guidance to the models application. This parameterization study must be based on a thorough understanding of the important physical process affecting the dynamics (Haney, 1979). We must know the manner in which a process controls the circulation;

altering parameters (or turning knobs) does not tell you how the machine operates.

Additional analysis of the circulation within Prince William Sound is in order. Sufficient data have been acquired by OCSEAP and NOS to determine the seasonal cycle in circulation there. The data include weather and current observations and the seasonal temperature and salinity fields. A descriptive paper incorporating currents, temperature, salinity and sea level should be completed prior to the later running of a numerical model.

## XI. CONCLUSIONS

The knowledge of the physical oceanography of the northern Gulf of Alaska continental shelf has progressed from nearly complete ignorance to the stage where important mechanisms affecting the circulation are beginning to be understood. The studies have passed from planning stages through the observations to descriptive reports. Work has not progressed much beyond this descriptive stage. While we can describe past observed circulation patterns, we cannot predict future ones with any large degree of certainty. In order to predict, a better knowledge of the forcing mechanisms affecting the circulation is required. An operational numerical model which includes temporal changes and planetary forcing is the next step in arriving at the predictive model.

In a statistical sense, we can predict the path of spilled oil, that is, chances are good that it will move shoreward from most release points. We do not know what will occur in the nearshore zone. Will the freshwater lens keep it offshore or will the wind drive it ashore? Chances are good that an oil spill will occur during severe weather conditions. For the

Gulf of Alaska, this means high winds and seas. Such conditions must be taken into account for planning purposes.

In order to evaluate the impact of oil and gas development on the environment in the Northeast Gulf of Alaska, a complete interdisciplinary synthesis of data is necessary. That synthesis will give a more comprehensive overview of the environment there than will be given by the individual syntheses. The individual syntheses should be carried out first. Interdisciplinary meetings should be held and ideas exchanged with additional analysis of the data undertaken prior to the final general synthesis.

## XII. REFERENCES

- Bakun, A. 1973. Coastal upwelling indices: West coast of North America. NOAA Tech. Rept. NMFS SSRF-671, 103 pp.
- Bennett, E. B. 1959. Some oceanographic features of the northeast Pacific Ocean during August 1955. *J. Fish. Res. Bd. Can.* 16(5):565-633.
- Dodimead, A. J., F. Favorite and T. Hirano. 1963. Review of oceanography of the subarctic Pacific Region. Salmon of the North Pacific Ocean. *Bull. Int. N. Pac. Fish. Comm.* 13, 195 pp.
- Doe, L. A. E. 1955. Offshore waters of the Canadian Pacific coast. *J. Fish. Res. Bd. Can.* 12(1):1-34.
- Favorite, F. 1974. Flow into the Bering Sea through the Aleutian Island passes. *Oceanography of the Bering Sea*, Occas. Publ. No. 2, Inst. Mar. Sci., Univ. Alaska, 623 pp.
- Favorite, F., A. J. Dodimead and K. Nasu. 1976. Oceanography of the subarctic Pacific Region 1960-72. *Bull. Int. N. Pac. Fish. Comm.*, 33 (In press).
- Favorite, F. and W. J. Ingraham. 1977. On flow in the northwestern Gulf of Alaska, May 1972. *J. Oceanogr. Soc. Japan* 33:67-81.
- Galt, J. A. 1976. Circulation studies on the Alaskan continental shelf off the Copper River, NOAA, U.S. Department of Commerce, Wash. D.C., 46 pp.
- Galt, J. A. 1979. An analysis of northeast Gulf of Alaska current patterns, 31 pp. (Unpublished manuscript).
- Galt, J. A., J. E. Overland, C. H. Pease and R. J. Stewart. 1978. Numerical Studies, PMEL Rept. to OCSEAP, RU 140, 177 pp. (Unpublished manuscript).
- Haney, R. L. 1979. Discussion of process parameterization and the structure of ocean general circulation models. *Dynam. Atmos. Oceans.* 3:283-287.
- Hayes, S. P. 1979. Variability of current and bottom pressure across the continental shelf in the northeast Gulf of Alaska. *J. Phys. Oceanogr.* 9:88-103.
- Hayes, S. P. and J. D. Schumacher. 1976. Description of wind, current, and bottom pressure variations on the continental shelf in the northeast Gulf of Alaska from February to May 1975. *J. Geophys. Res.* 81:6411-6419.
- Heggie, D. T., D. W. Boisseau and D. C. Burrell. 1977. Hydrography, nutrient chemistry and primary productivity of Resurrection Bay, Alaska, 1972-75. Rept. R77-2, Inst. Mar. Sci., Univ. Alaska. 111 pp.
- Livingstone, D. and T. C. Royer. 1979. An analysis of observed surface winds at Middleton Island, Gulf of Alaska. *J. Phys. Oceanogr.* 10 (In press).



- Muench, R. D. and G. M. Schmidt. 1975. Variations in the hydrographic structure of Prince William Sound. Univ. Alaska Sea Grant Rept. R75-1, 135 pp.
- Muench, R. D. and D. T. Heggie. 1978. Deep water exchange in Alaskan sub-arctic fjords. Estuarine Transport Processes. Univ. S. Carolina Press, Columbia, S.C., pp. 239-268.
- Muench, R. D., R. K. Reed and J. D. Schumacher. 1978. Volume transport variations in the Pacific Subarctic Gyre. *EOS* 60(18):295 (Abstract only).
- Muench, R. D., J. D. Schumacher, S. P. Hayes and R. L. Charnell. 1978. Northeast Gulf of Alaska Program, Draft Final Report, R.U. 139, 114 pp. (Unpublished manuscript).
- Niebauer, H. J., J. Roberts and T. C. Royer. 1979. Current fluctuations near the shelf break in the northern Gulf of Alaska, 1976-77. (Unpublished manuscript).
- Reeburgh, W. S., R. D. Muench and R. T. Cooney. 1976. Oceanographic conditions during 1973 in Russell Fjord, Alaska. *Estuarine and Coastal Mar. Science* 4:129-145.
- Reed, R. K. 1979. Lagrangian measurement of recirculation in the Alaskan Stream. *EOS* 60(18):290 (Abstract only).
- Reed, R. K., R. D. Muench and J. D. Schumacher. 1980. On baroclinic transport of the Alaskan Stream near Kodiak Island. *Deep-Sea Res.* (In press).
- Reid, J. L. and A. W. Mantyla. 1976. The effect of the geostrophic flow upon coastal sea elevations in the northern North Pacific Ocean. *J. Geophys. Res.* 81:3100-3110.
- Reynolds, R. M., T. R. Hiester and S. A. Macklin. 1978. Coastal meteorology of the Gulf of Alaska, Icy Bay to Yakutat Bay. PMEL/ERL/NOAA Tech. Rept.
- Roden, G. I. 1969. Winter circulation in the Gulf of Alaska. *J. Geophys. Res.* 74:4523-4534.
- Royer, T. C. 1975. Seasonal variations of waters in the northern Gulf of Alaska. *Deep-Sea Res.* 22:403-416.
- Royer, T. C. 1979a. On the seasonal variations of the baroclinic transport of the Alaska Current. *EOS* 60(18):292 (Abstract only).
- Royer, T. C. 1979b. On the effect of precipitation and runoff on coastal circulation in the Gulf of Alaska. *J. Phys. Oceanogr.* 9(3):555-563.

- Royer, T. C., D. V. Hansen and D. J. Pashinski. 1979. Coastal flow in the northern Gulf of Alaska as observed by dynamic topography and satellite-tracked drogued drift buoys. *J. Phys. Oceanogr.* 9(4):785-801.
- Stommel, H. 1964. *The Gulf Stream*. University of California Press, 248 pp.
- Sverdrup, H. U., M. S. Johnson and R. H. Fleming. 1942. *The Oceans: Their Physics, Chemistry and General Biology*. Prentice-Hall, Inc., New York, 1087 pp.
- Tabata, S. 1965. Variability of oceanographic conditions of Ocean Station P in the Northeast Pacific Ocean. *Trans. Roy. Soc. Can.* 3:367-418.
- Thompson, T. G., G. F. McEwen and R. Van Cleve. 1936. Hydrographic sections and calculated current in the Gulf of Alaska, 1929. *Rept. Int. Fish. Comm.* 10, 32 pp.
- Tully, J. P. and F. G. Barber. 1960. An estuarine analogy in the subarctic Pacific Ocean. *J. Fish. Res. Bd. Can.* 17:91-112.
- Veronis, G. 1973. Model of world ocean circulation: I. Wind driven, two-layer. *J. Mar. Res.* 31(3):228-288.

Annual Report

Coastal Meteorology

(Synoptic Climatology Component)

James E. Overland

Carol H. Pease

Pacific Marine Environmental Laboratory  
Environmental Research Laboratories, NOAA

3711 15th Ave. N.E.  
Seattle, Washington 98105

Contract No. R7120898

Research Unit: 367

Period: 1 April 1979 -

31 March 1980

RU 367 Annual Report FY80

This document summarizes the work on marine winds and assessment climatology studies for the northern Bering Sea. It supplements "Marine Climatology of the Bering Sea," Chapter 2, The Bering Sea Shelf: Oceanography and Resources which also was completed as part of this R.U. The report is divided into five studies:

1. Calculation of marine wind fields in the Bering Sea
2. Cyclone climatology of the Bering Sea
3. Evaluation of two synoptic climatologies for northern Bering Sea
4. METLIB - a program library for calculating and plotting marine boundary layer wind fields - NOAA Technical Memorandum ERL/PMEL -20, by J.E. Overland, R. A. Brown, and C.D. Mobley (abstract only)
5. Case studies of four severe Gulf of Alaska storms - NOAA Technical Memorandum ERL/PMEL -19, by J.E. Overland and V.J. Cardone (abstract only)

Principal conclusions are:

1. Computing surface wind fields from quality sea level pressure analyses such as those of the Anchorage National Weather Service office should provide an excellent way of specifying spatially varying winds for the Bering. They are to be preferred to extrapolating shore station reports.
2. These wind fields can be improved by direct comparison to quality over water and over ice surface wind measurements.
3. In winter the northern Bering can be represented by a synoptic climatology such as Putnins or Barry. In summer there are no dominant persistent weather types.
4. Using a synoptic climatology based upon Nome is an adequate approach for providing a wind climatology for Norton Sound. The southern Bering, however, should be represented by representative storms and tracks rather than a synoptic climatology.

## Calculation of Marine Wind Fields in the Bering Sea

PMEL has produced a computer analysis library called METLIB (Overland, et al., 1980) which is capable of producing time series of geostrophic, gradient or surface winds from sea level pressure (SLP) and ancillary fields such as those produced by the National Weather Service. The library was developed to make best use of a "man-machine mix" which allows control over critical decisions which affect the accuracy of the results such as digitizing the SLP fields while highly automating spherical geometric calculations involving polar grids, plotting, and running atmospheric boundary layer models. This note documents the comparison of winds generated from METLIB with observed winds.

Surface analyses of SLP for the Bering Sea region at 00 GMT and 12 GMT of March 1 - March 31, 1979 were obtained from the National Weather Service Forecast Office in Anchorage and digitized for input to METLIB. The pressure fields and surface winds calculated from reducing the gradient wind speed by 0.8 and rotating the vector  $20^\circ$  toward low pressure are shown in Appendix A. Figure 1 shows a sample NWS analysis. These fields correspond to the time of the 1979 SURVEYOR cruise and are taken from Salo et al. (1980).

Figure 2 shows the comparison of winds derived from METLIB with those from Nome, Tin City, St. Paul and from the ship. The METLIB winds represent over the water winds, so there should be some quantitative differences between the fields. However, what is remarkable about the Bering compared to similar studies at lower latitude is how well the pressure field gradient winds track individual events in the observed wind records. Pressure field derived winds made from quality analyses are clearly capable of providing first order wind speed and wind stress estimates over the Bering. This is probably due to the large importance of the Coriolis term in the momentum balance at high latitudes.

The reduction and turning angles used in Salo et al. (1980) to obtain surface winds from gradient wind were chosen arbitrarily. As a first attempt to tune METLIB for the Bering we have calculated reduction factors and turning angles from the station records. Table I indicates that turning angles of  $10^{\circ}$  -  $40^{\circ}$  and reduction factors of .7 - .9 are reasonable for the Bering. Nome has a low speed ratio and higher standard deviations than other stations for both turning angle and speed reduction. If we assume that gradient winds are a good source for predicting over water winds then Nome is a less ideal location to use for extrapolation.

Variation in inflow angle and speed reduction depends upon surface roughness, for instance that of ice versus water, and atmospheric stability. Twenty percent error in speed reduction can lead to forty percent error in wind stress that moves oil, water or ice. Therefore even though the gradient wind can track meteorological events very well, quality onsite measurements should be taken to determine the most appropriate turning angles and reduction factors.

### References

Overland, J.E., R.A. Brown and C.D. Mobley, (1980): METLIB - A program library for calculating and plotting marine boundary layer wind fields. NOAA Tech. Mem. ERL PMEL-20, 82 pp.

Salo, S.A., C.H. Pease and R.W. Lindsay, (1980): Physical environment of the Eastern Bering Sea. NOAA Tech. Mem. ERL PMEL-21, 119 pp.

Table I

	Nome	Tin City	St. Paul	Cruise winds
Directional differences:				
Mean	-45.9°	-40.1°	-17.8°	-34.0°
Standard Deviation	38.1°	32.4°	29.2°	22.3°
Median	-44.4°	-44.0°	-17.0°	-37.1°
Magnitude differences:				
Mean	- 9.1m/s	- 4.2m/s	- 3.6m/s	- 0.9m/s
Standard Deviation	4.4m/s	4.8m/s	4.4m/s	2.7m/s
Median	- 9.7m/s	- 3.6m/s	- 2.9m/s	- 0.8m/s
Reduction ratio using all available winds:				
Mean	.37	.76	.78	.92
Standard Deviation	.23	.34	.30	.38
Median	.33	.68	.75	.89
Reduction ratio using predicted winds greater than 5m/s:				
Mean	.34	.77	.75	.87
Standard Deviation	.18	.26	.28	.26
Median	.31	.72	.70	.89

Negative directional error: model direction is clockwise from observed direction.

Magnitude difference = observed magnitude - model magnitude.

Reduction ratio = observed speed/model speed.





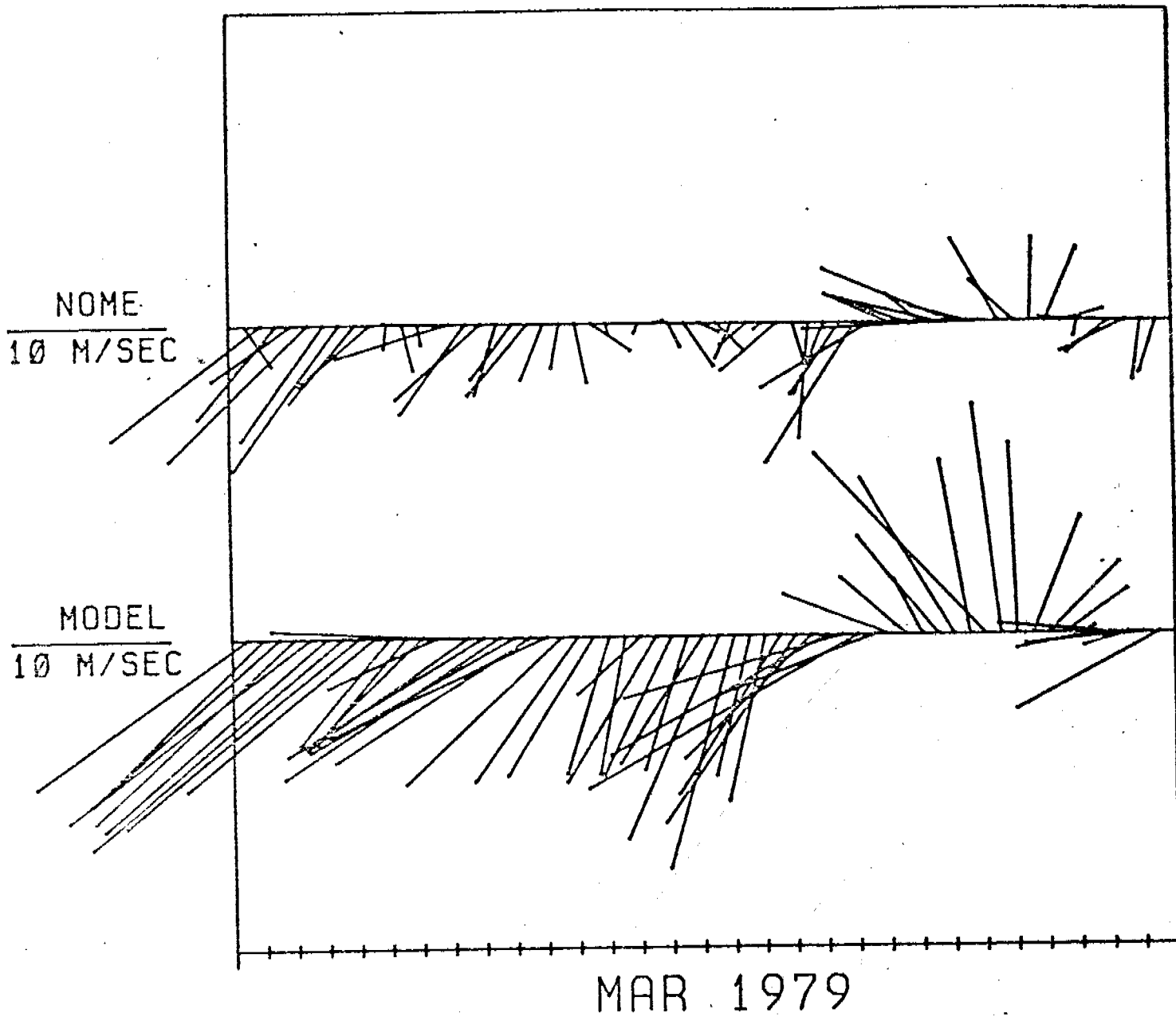


Figure 2A. Calculated surface wind compared to winds measured at the ship and three surface stations.

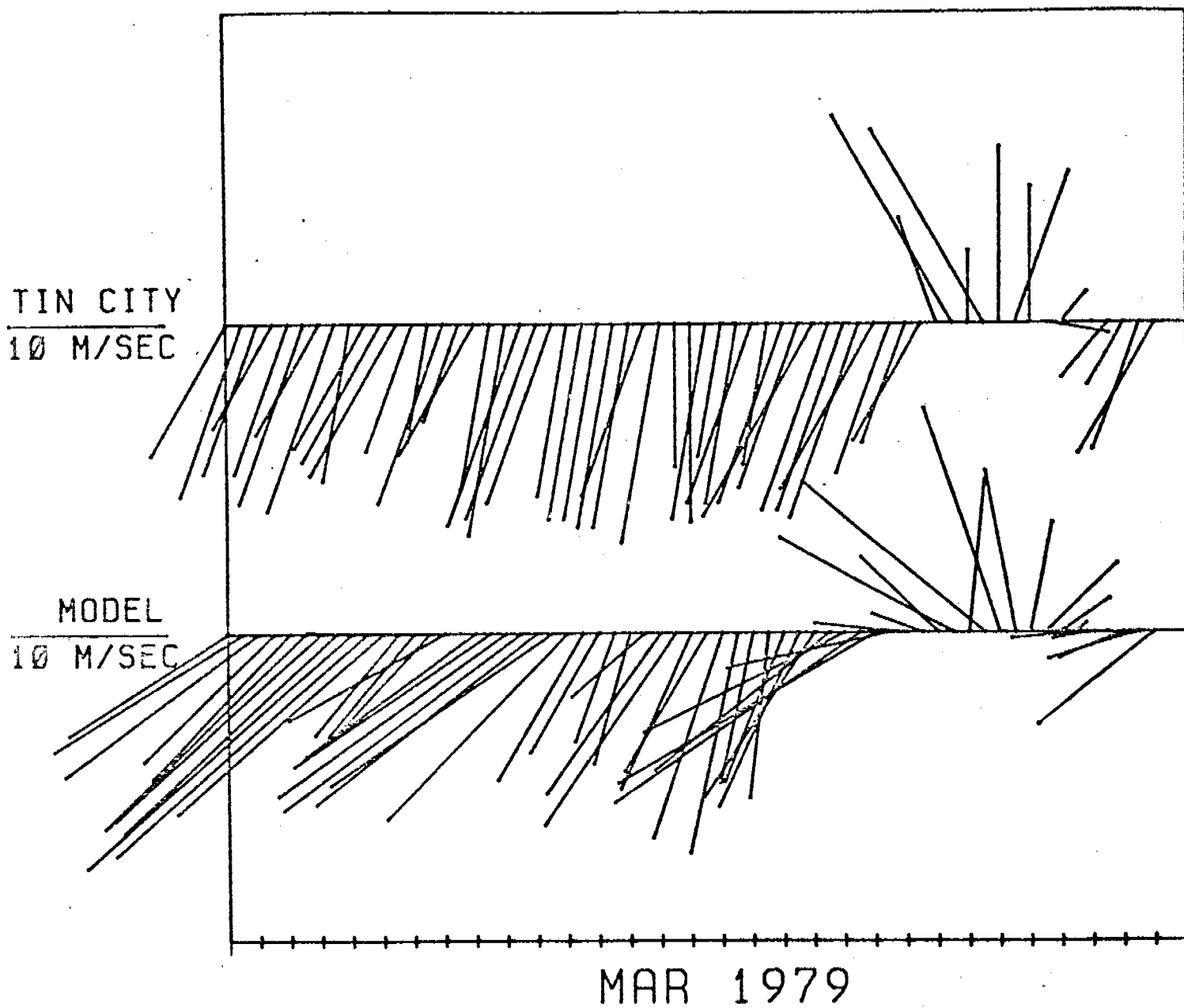


Figure 2B. Calculated surface wind compared to winds measured at the ship and three surface stations.

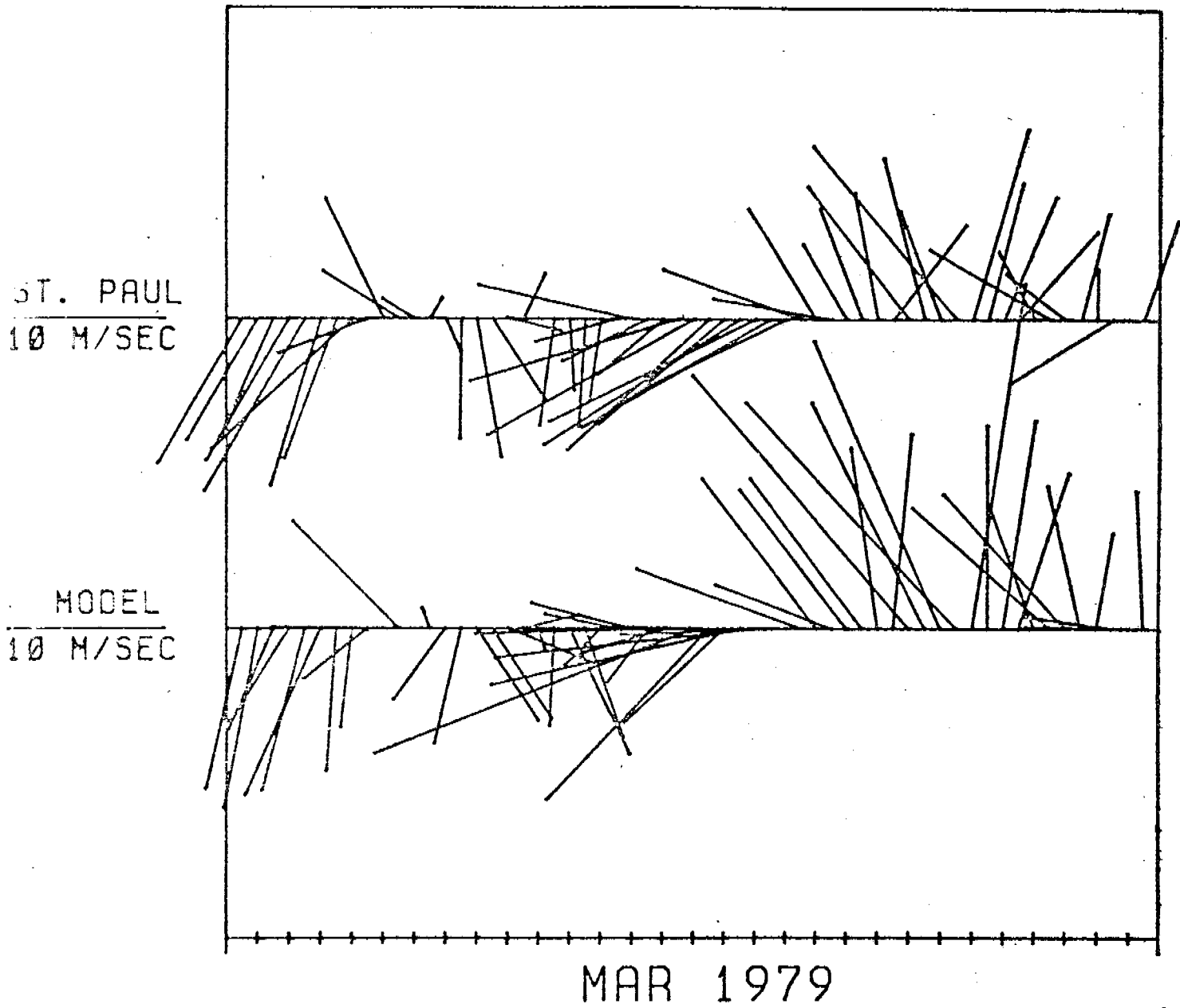


Figure 20. Calculated surface wind compared to winds measured at the ship and three surface stations.

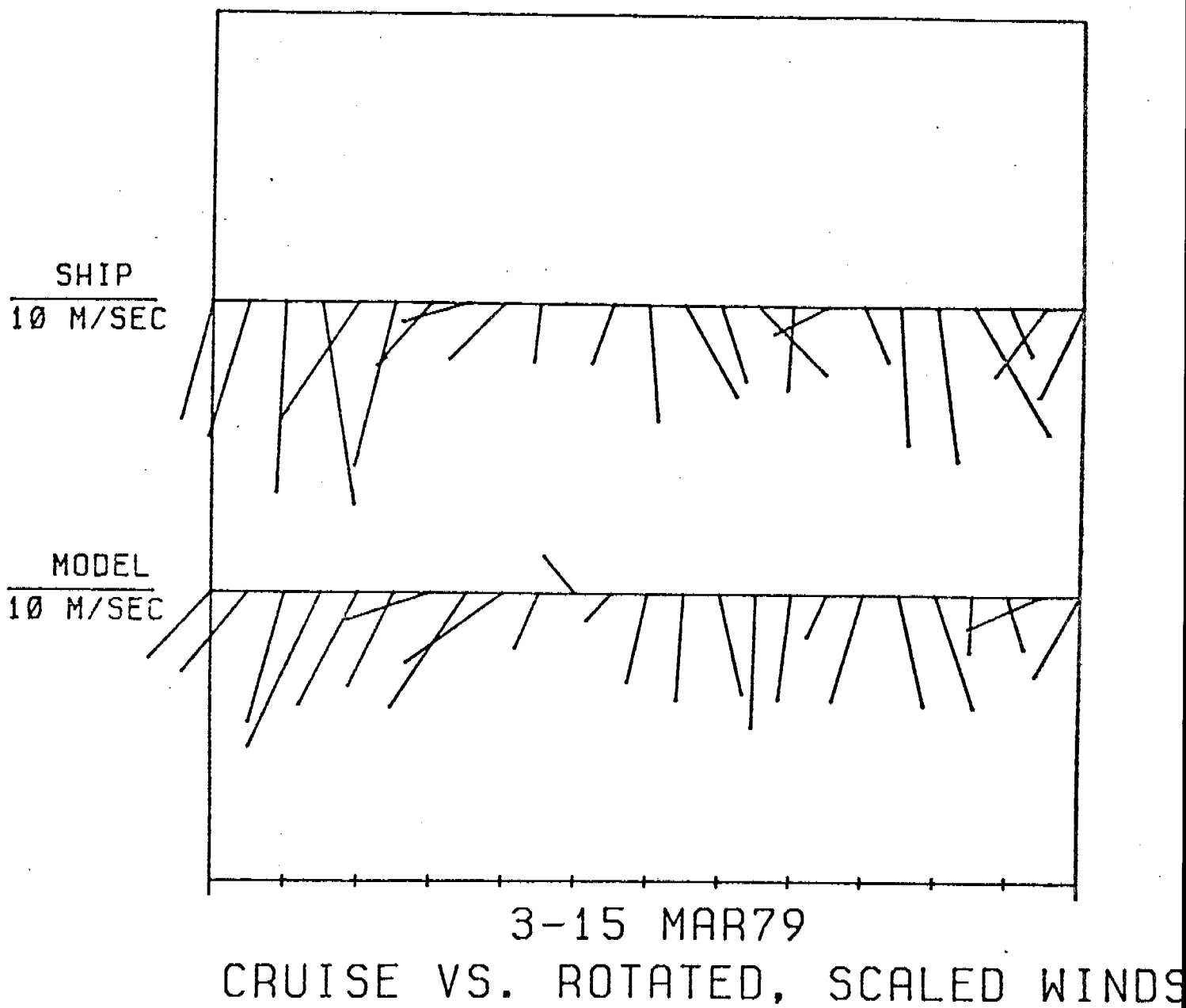
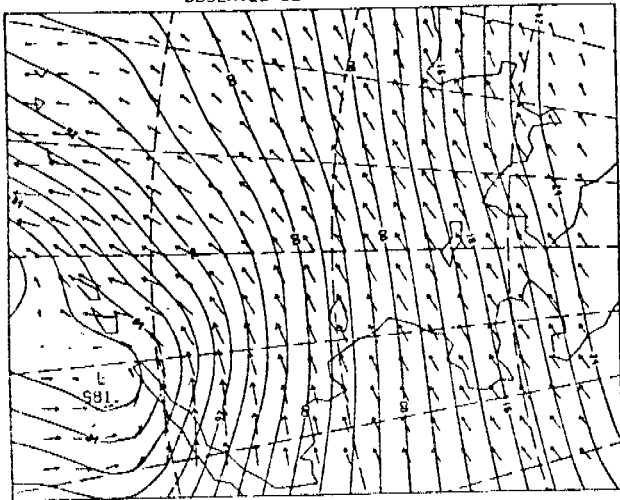


Figure 2D. Calculated surface wind compared to winds measured at the ship and three surface stations.

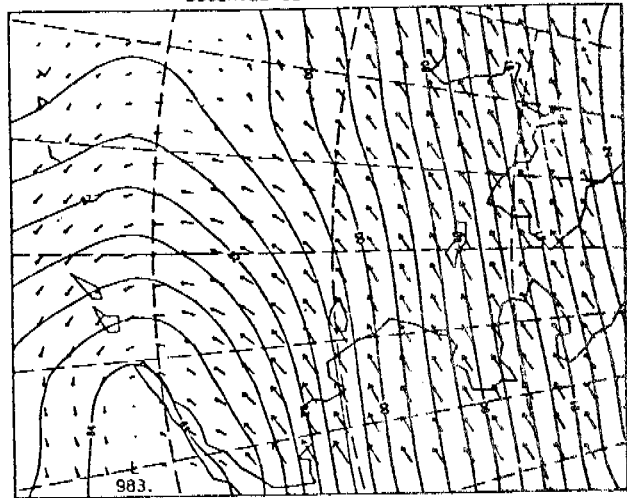
APPENDIX : SURFACE WINDS DERIVED FROM THE WSFO SURFACE ANALYSES.

OBSERVED SLP AND WINDS 4



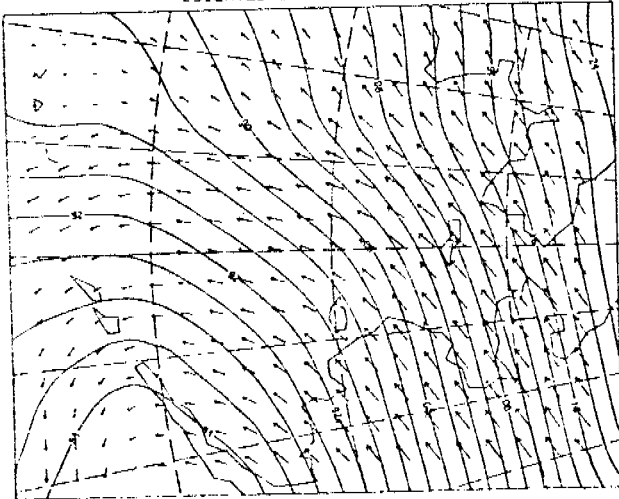
00Z 1 MAR 1979

OBSERVED SLP AND WINDS 4



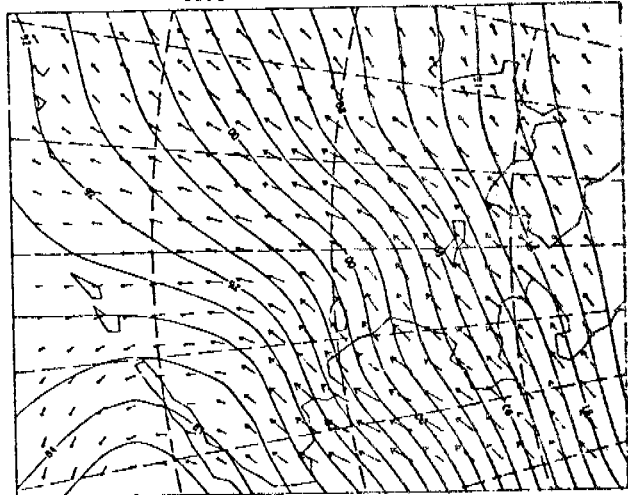
12Z 1 MAR 1979

OBSERVED SLP AND WINDS 4



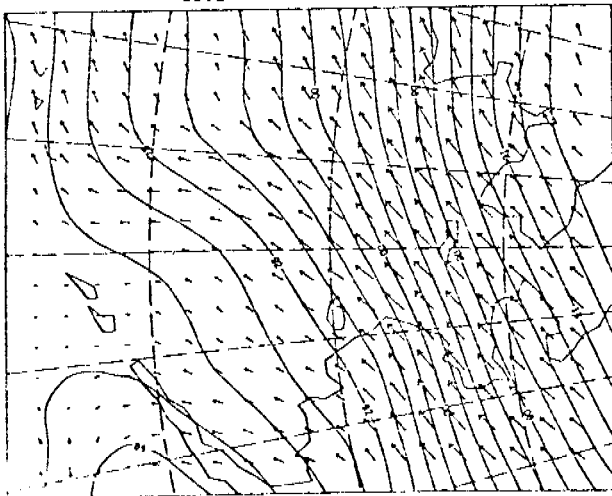
00Z 2 MAR 1979

OBSERVED SLP AND WINDS 4



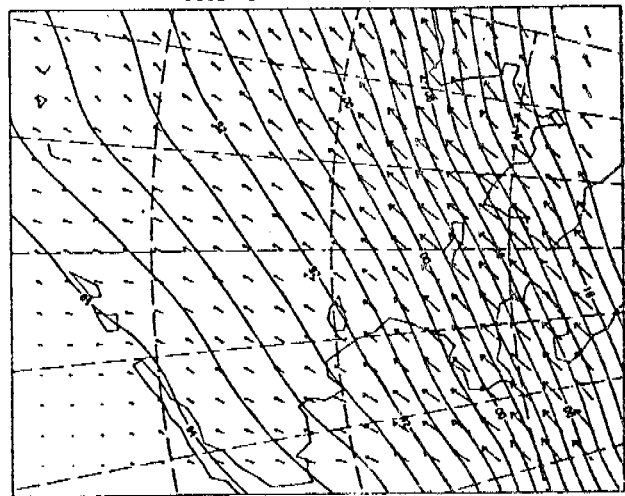
12Z 2 MAR 1979

OBSERVED SLP AND WINDS 4



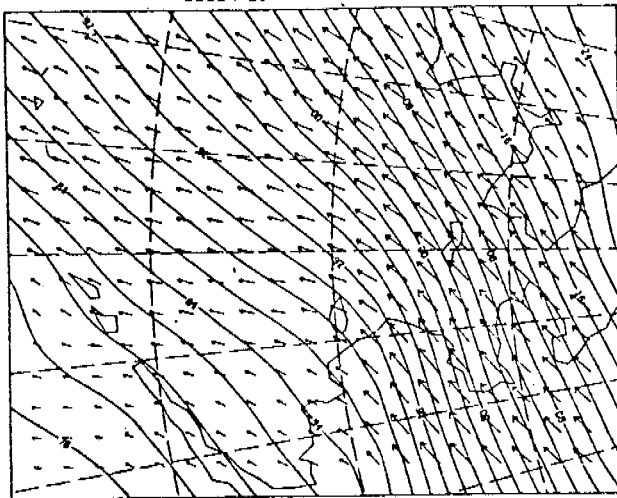
00Z 3 MAR 1979

OBSERVED SLP AND WINDS 4



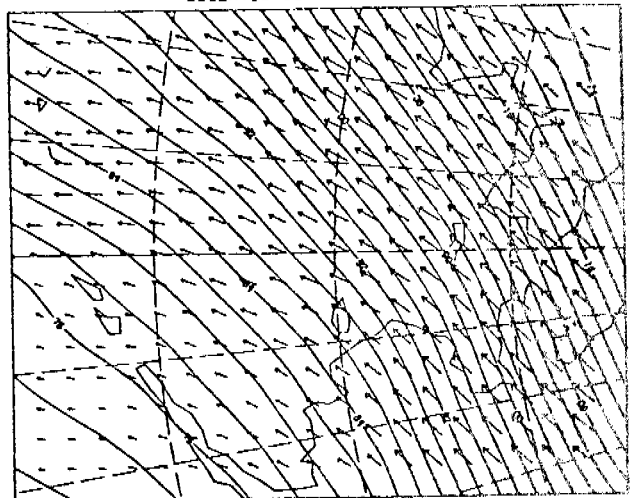
12Z 3 MAR 1979

OBSERVED SLP AND WINDS 4



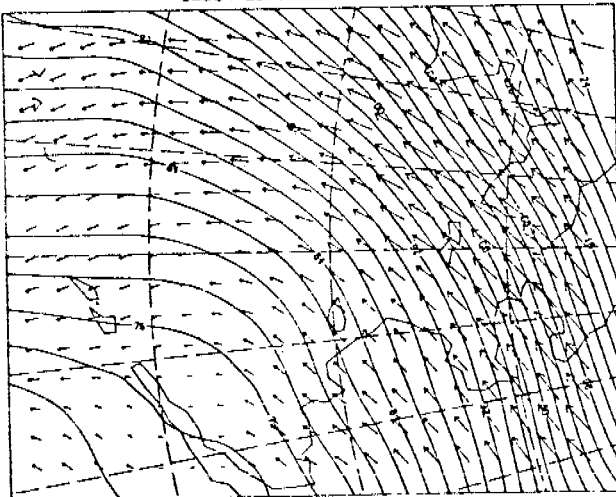
00Z 4 MAR 1979

OBSERVED SLP AND WINDS 4



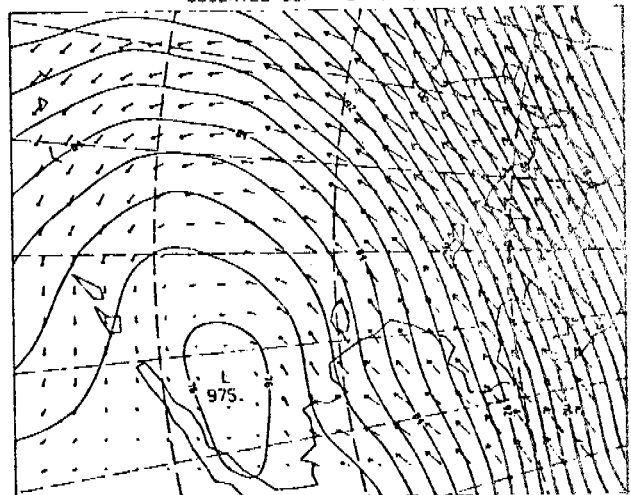
12Z 4 MAR 1979

OBSERVED SLP AND WINDS 4



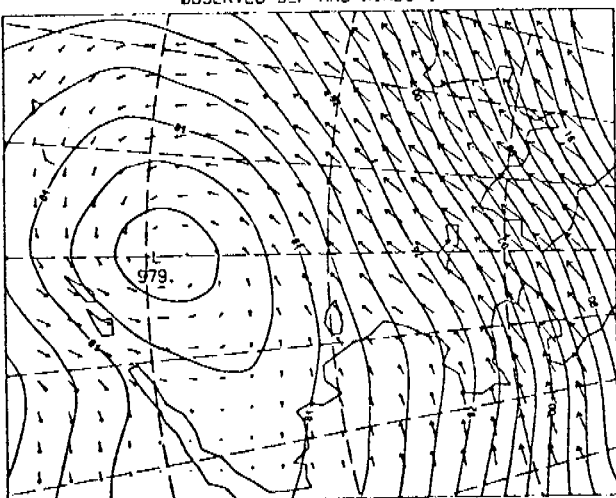
00Z 5 MAR 1979

OBSERVED SLP AND WINDS 4



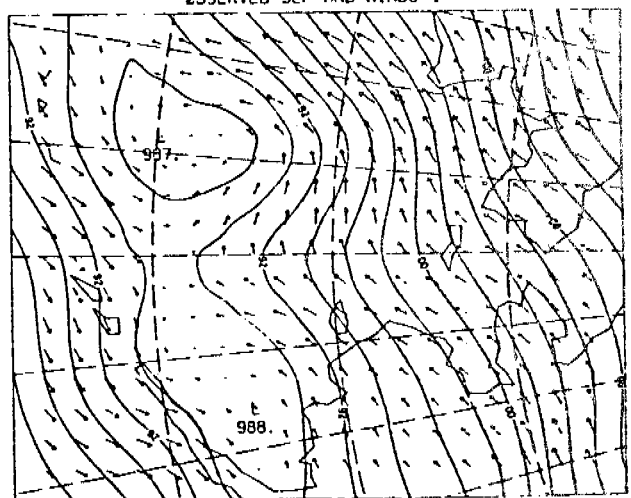
12Z 5 MAR 1979

OBSERVED SLP AND WINDS 4



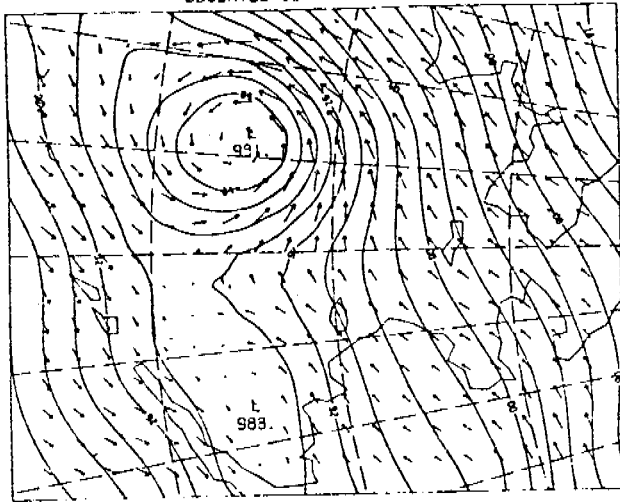
00Z 6 MAR 1979

OBSERVED SLP AND WINDS 4



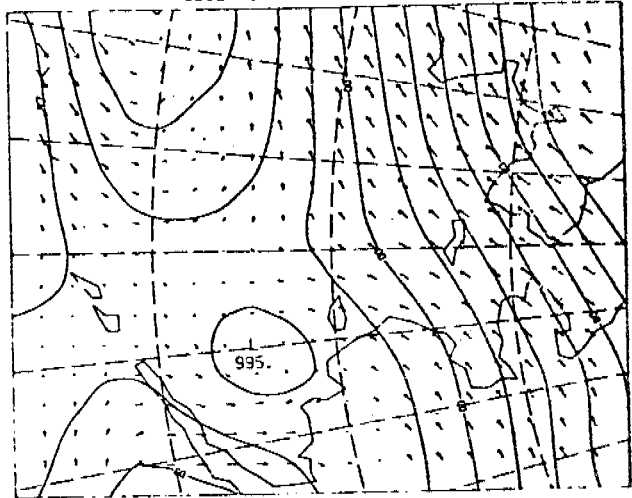
12Z 6 MAR 1979

OBSERVED SLP AND WINDS 4



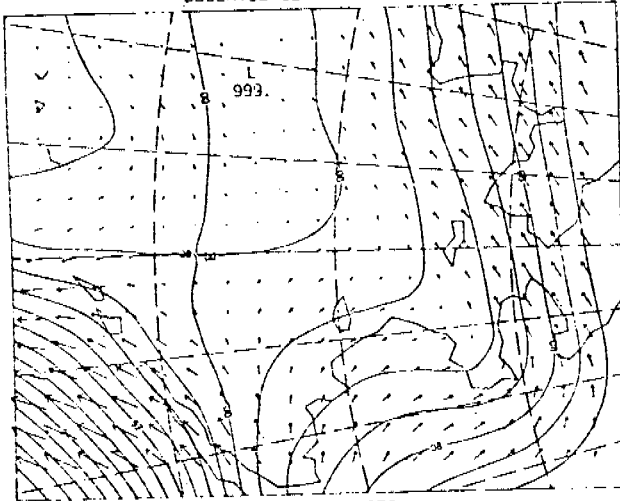
00Z 7 MAR 1979

OBSERVED SLP AND WINDS 4



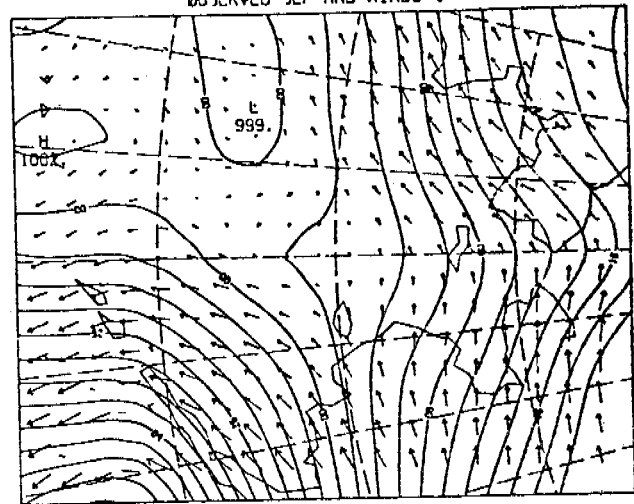
12Z 7 MAR 1979

OBSERVED SLP AND WINDS 4



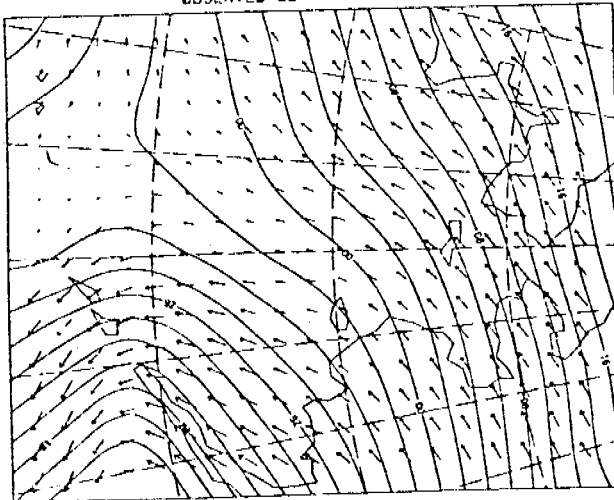
00Z 8 MAR 1979

OBSERVED SLP AND WINDS 4



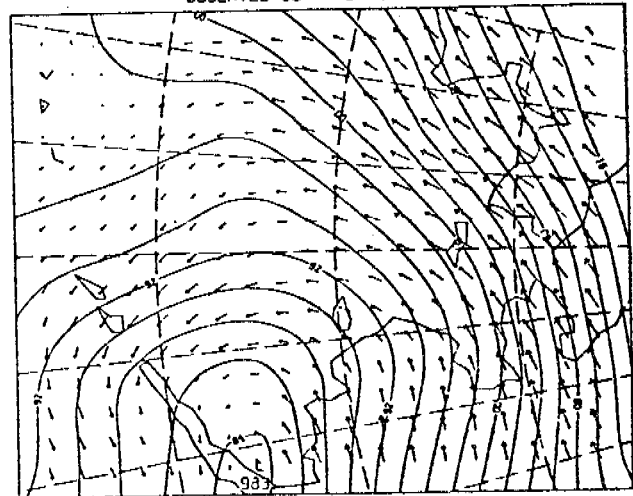
12Z 8 MAR 1979

OBSERVED SLP AND WINDS 4



00Z 9 MAR 1979

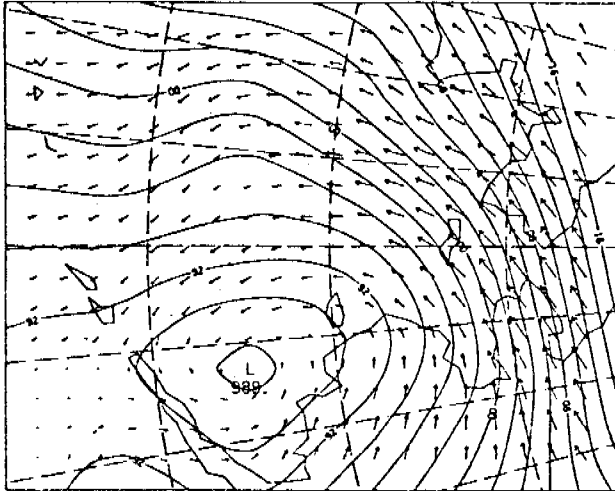
OBSERVED SLP AND WINDS 4



12Z 9 MAR 1979

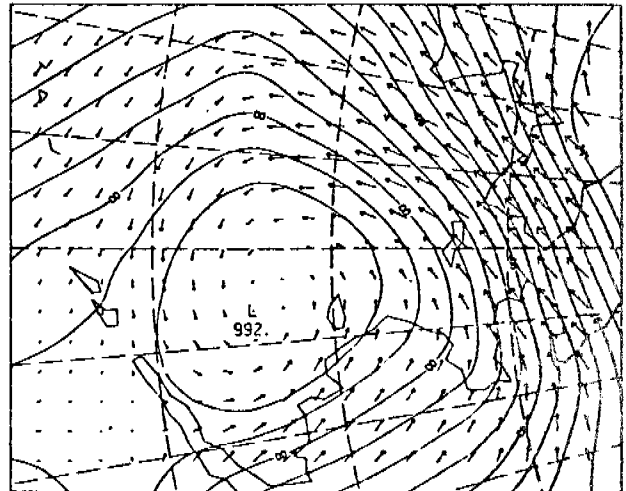


OBSERVED SLP AND WINDS 4



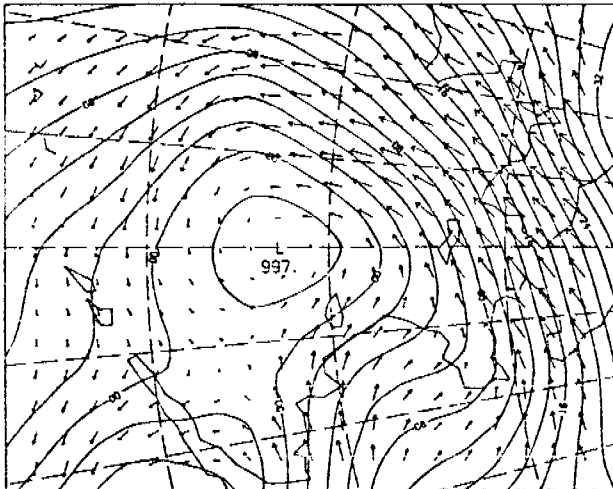
00Z 10 MAR 1979

OBSERVED SLP AND WINDS 4



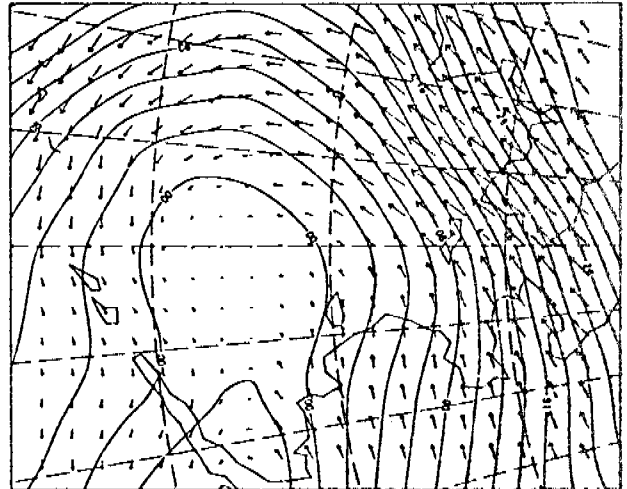
12Z 10 MAR 1979

OBSERVED SLP AND WINDS 4



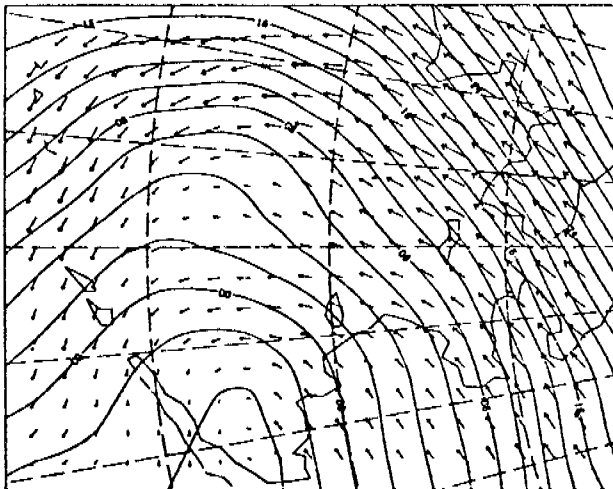
00Z 11 MAR 1979

OBSERVED SLP AND WINDS 4



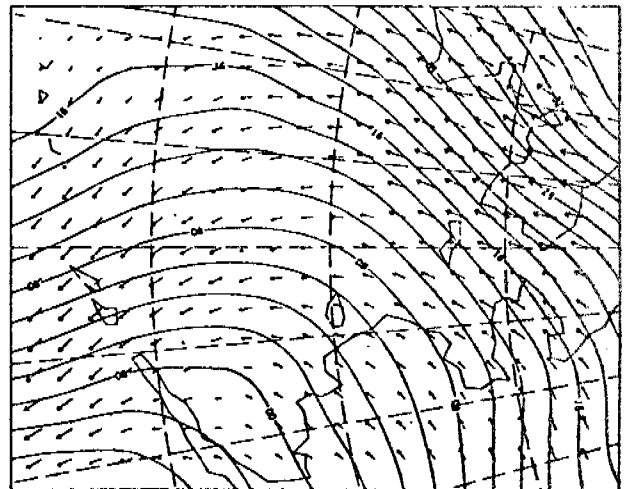
12Z 11 MAR 1979

OBSERVED SLP AND WINDS 4



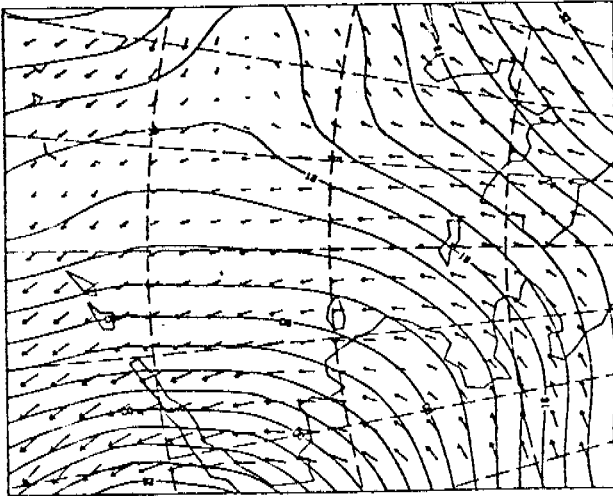
00Z 12 MAR 1979

OBSERVED SLP AND WINDS 4



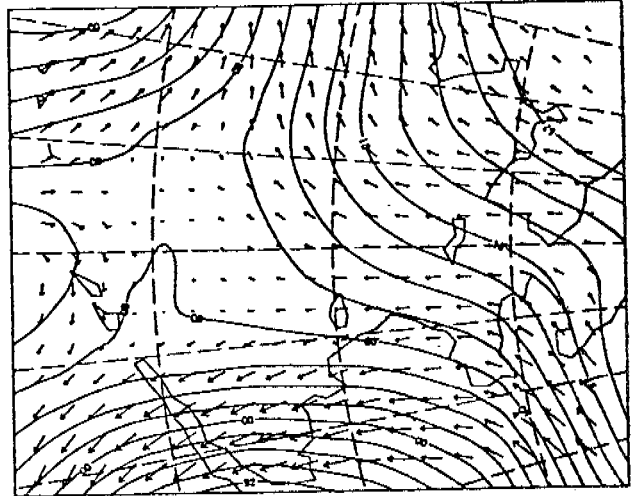
12Z 12 MAR 1979

OBSERVED SLP AND WINDS 4



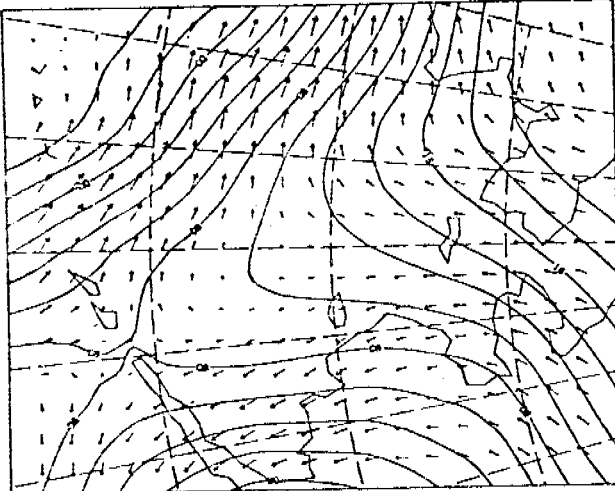
00Z 13 MAR 1979

OBSERVED SLP AND WINDS 4



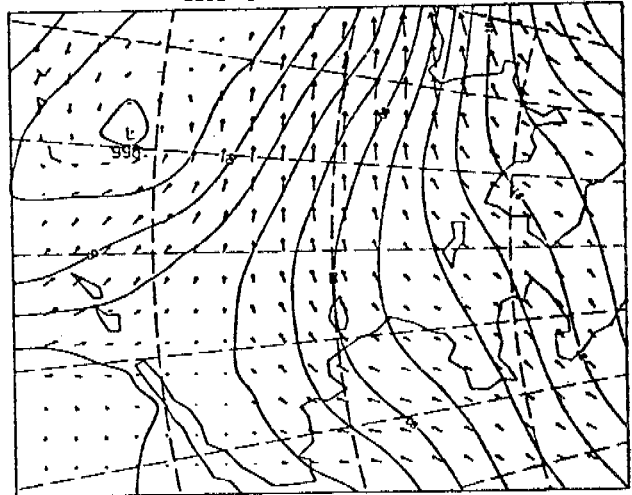
12Z 13 MAR 1979

OBSERVED SLP AND WINDS 4



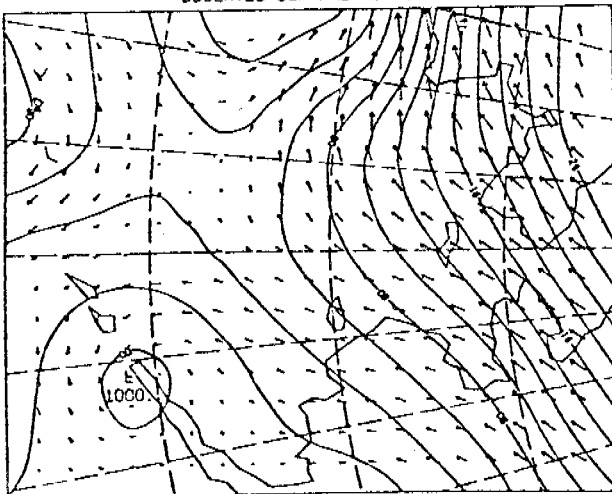
00Z 14 MAR 1979

OBSERVED SLP AND WINDS 4



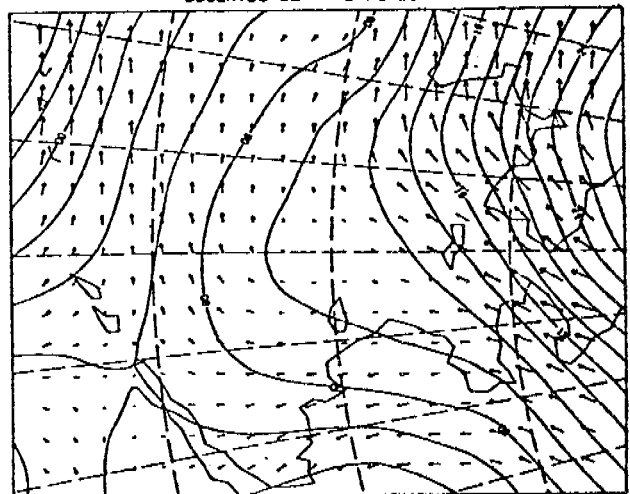
12Z 14 MAR 1979

OBSERVED SLP AND WINDS 4



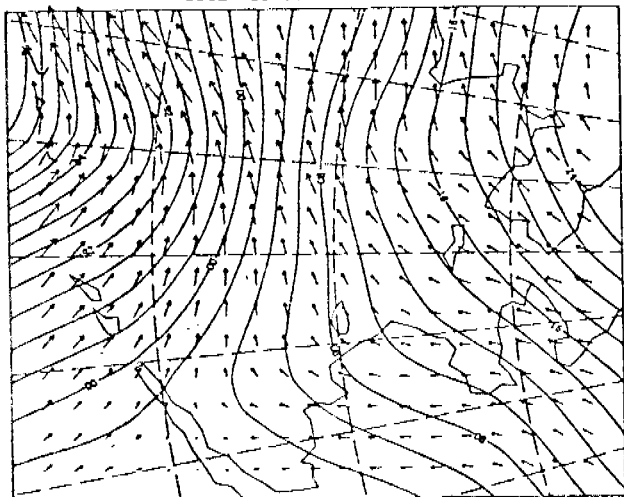
00Z 15 MAR 1979

OBSERVED SLP AND WINDS 4



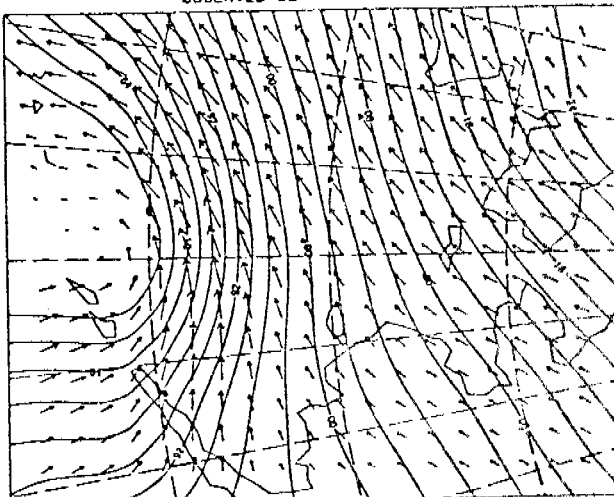
12Z 15 MAR 1979

OBSERVED SLP AND WINDS 4



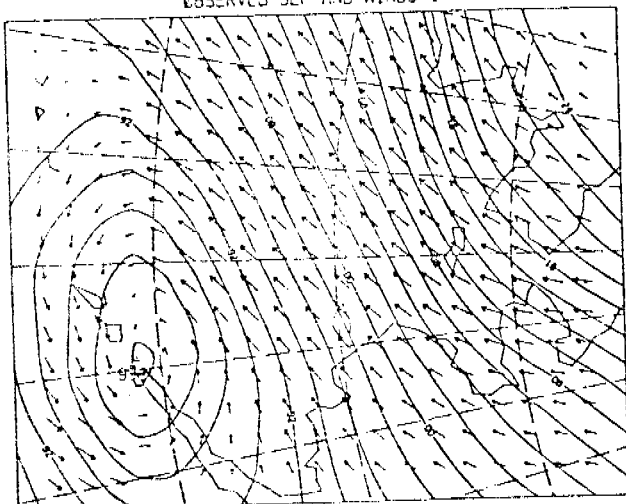
00Z 16 MAR 1979

OBSERVED SLP AND WINDS 4



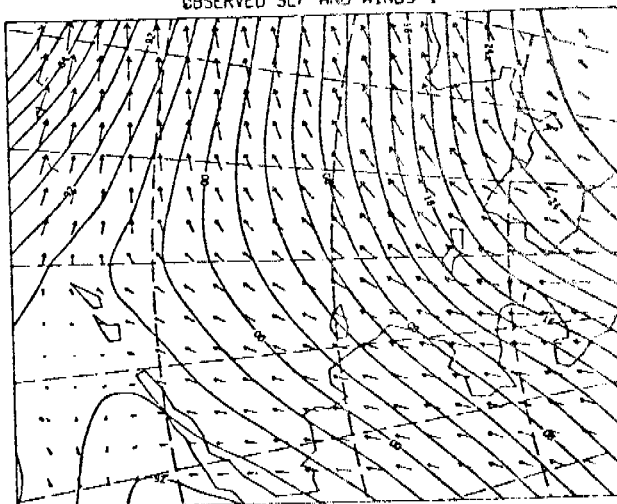
12Z 16 MAR 1979

OBSERVED SLP AND WINDS 4



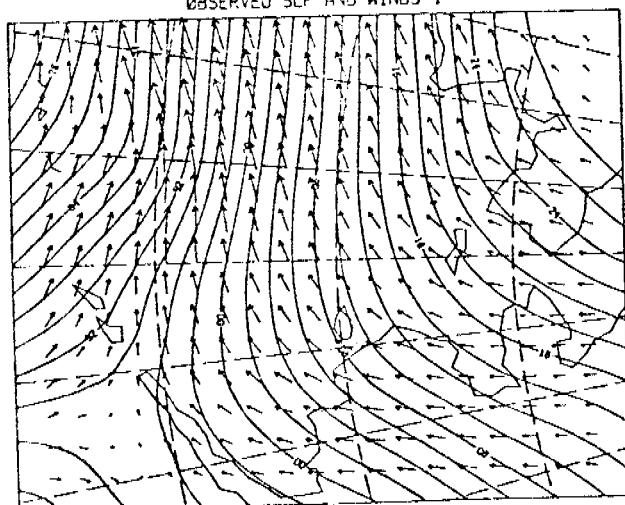
00Z 17 MAR 1979

OBSERVED SLP AND WINDS 4



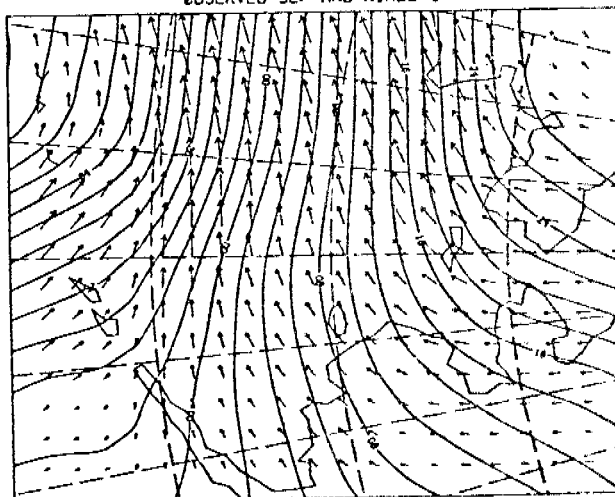
12Z 17 MAR 1979

OBSERVED SLP AND WINDS 4



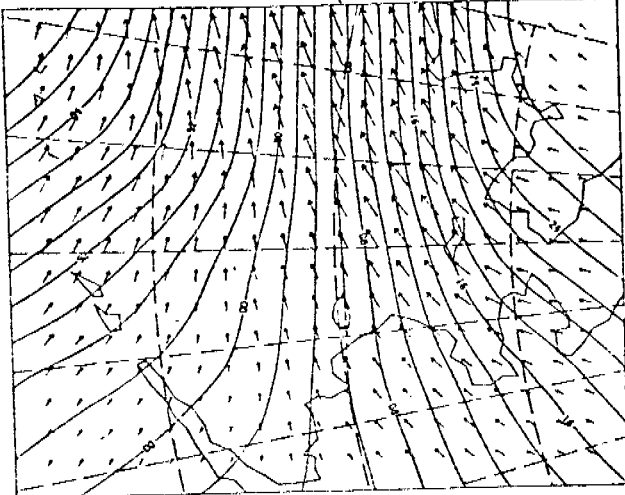
00Z 18 MAR 1979

OBSERVED SLP AND WINDS 4



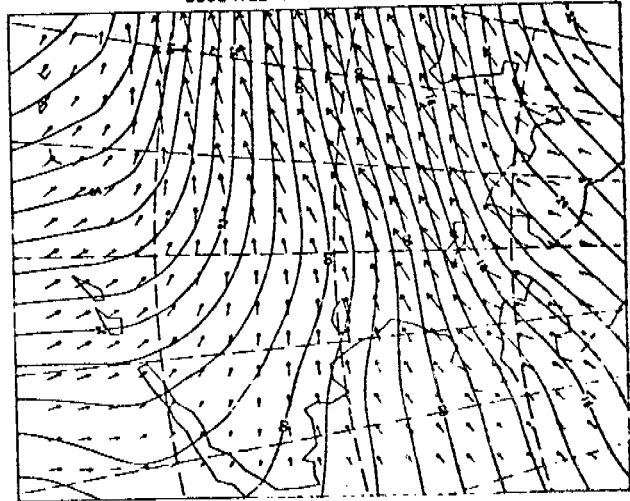
12Z 18 MAR 1979

OBSERVED SLP AND WINDS 4



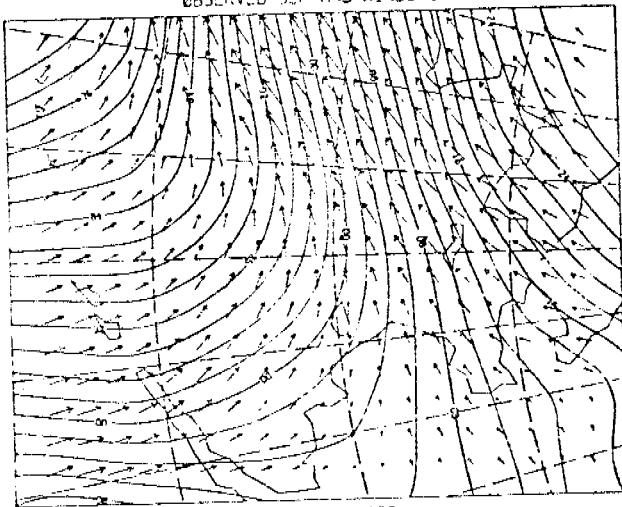
00Z 19 MAR 1979

OBSERVED SLP AND WINDS 4



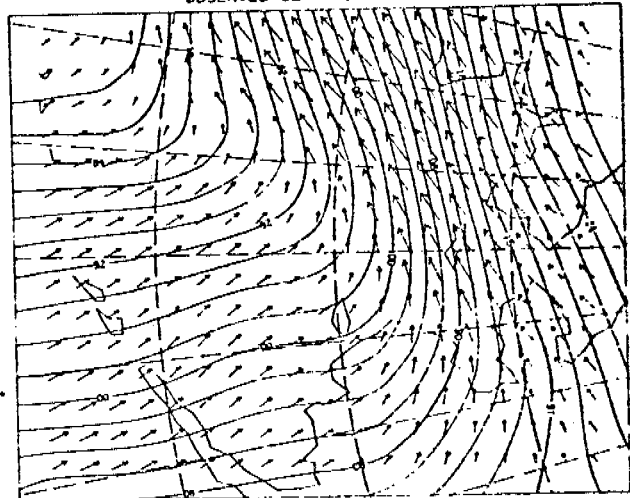
12Z 19 MAR 1979

OBSERVED SLP AND WINDS 4



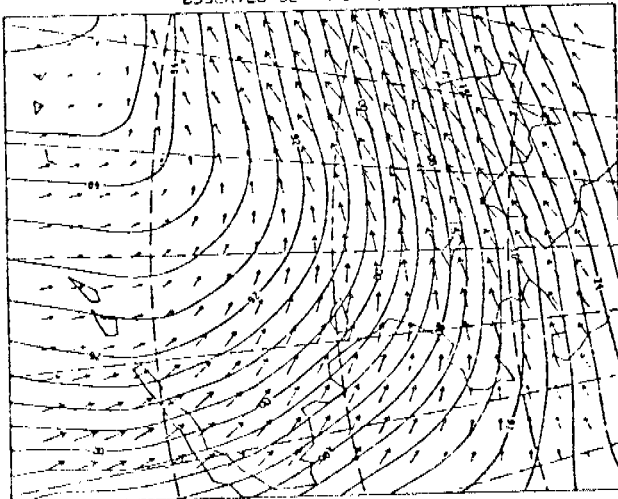
00Z 20 MAR 1979

OBSERVED SLP AND WINDS 4



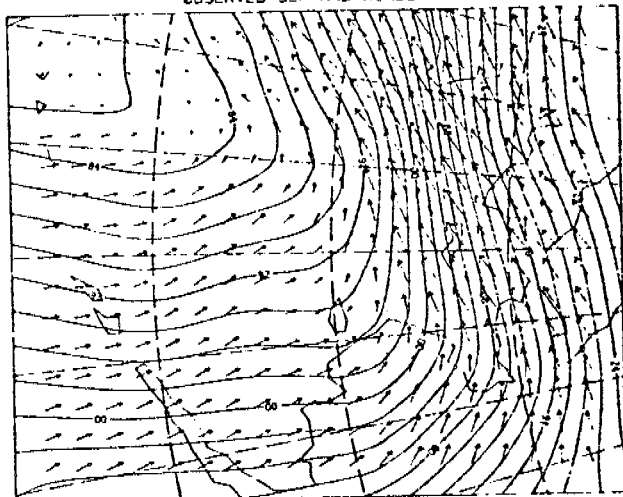
12Z 20 MAR 1979

OBSERVED SLP AND WINDS 4



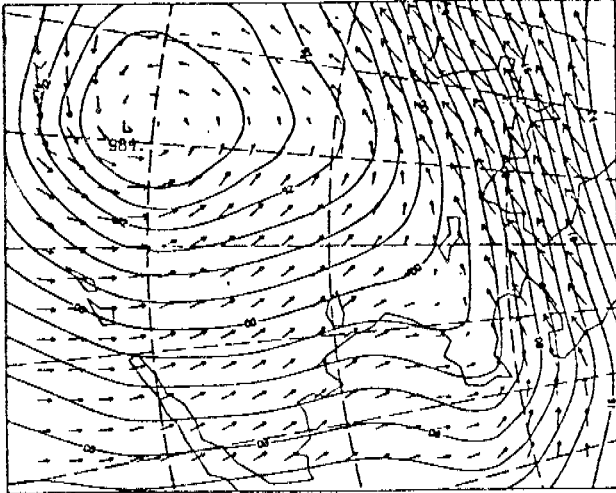
00Z 21 MAR 1979

OBSERVED SLP AND WINDS 4



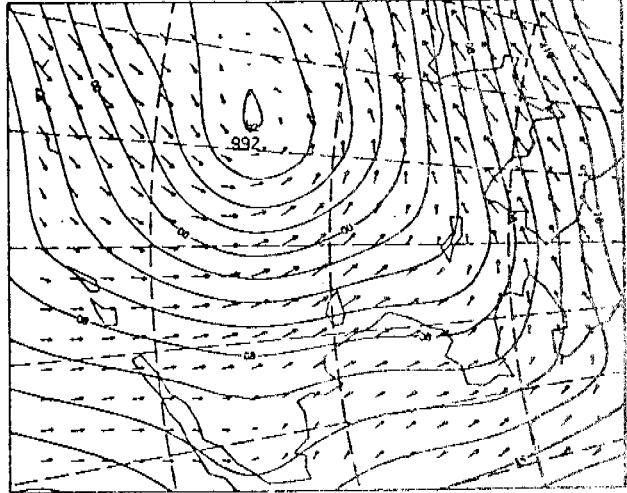
12Z 21 MAR 1979

OBSERVED SLP AND WINDS 4



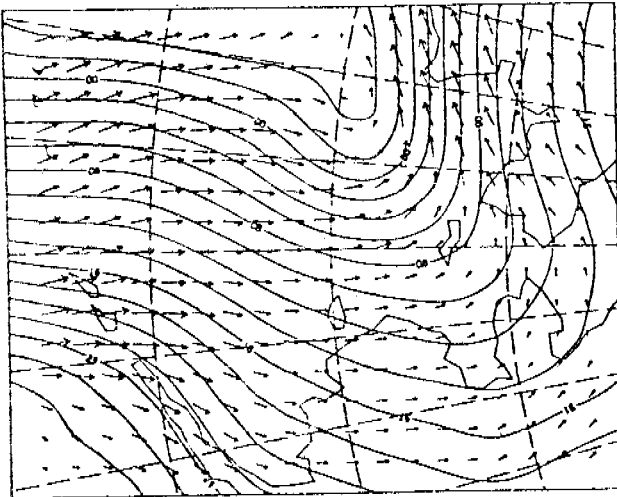
00Z 22 MAR 1979

OBSERVED SLP AND WINDS 4



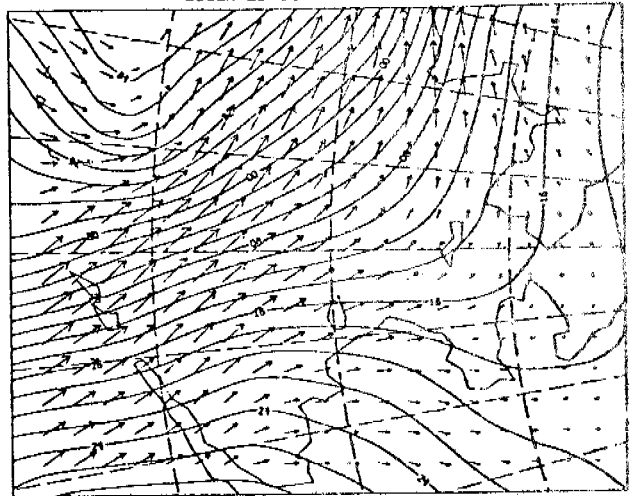
12Z 22 MAR 1979

OBSERVED SLP AND WINDS 4



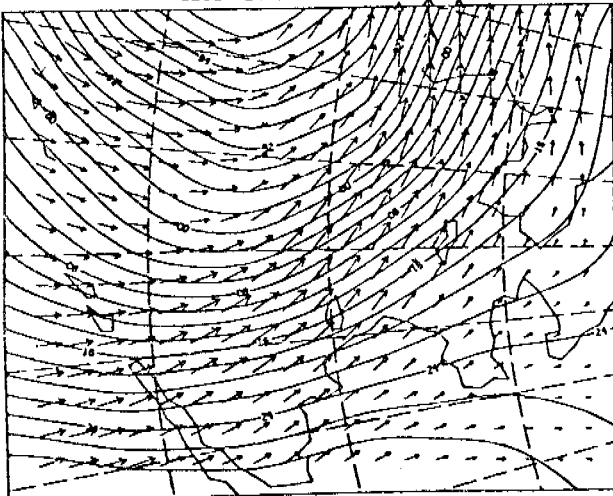
00Z 23 MAR 1979

OBSERVED SLP AND WINDS 4



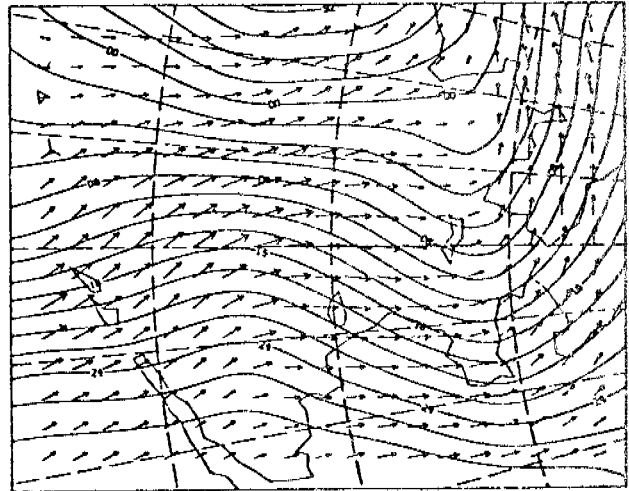
12Z 23 MAR 1979

OBSERVED SLP AND WINDS 4



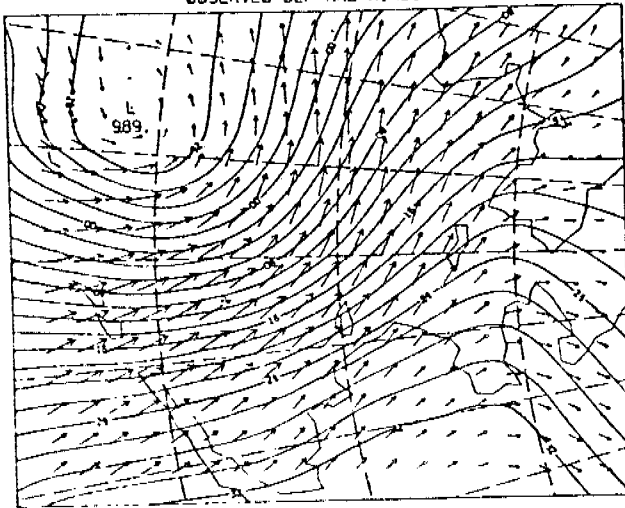
00Z 24 MAR 1979

OBSERVED SLP AND WINDS 4



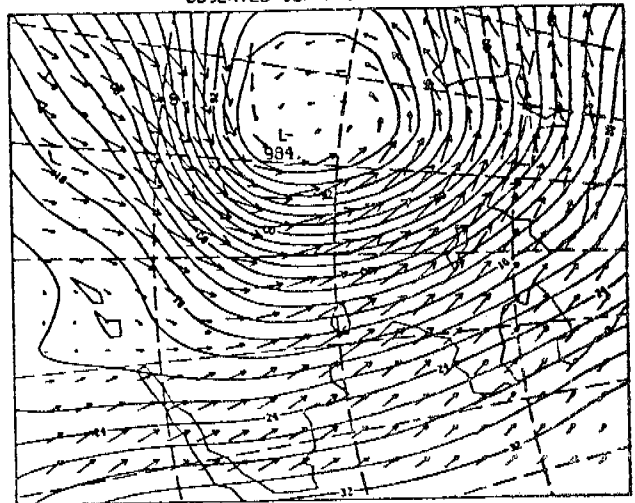
12Z 24 MAR 1979

OBSERVED SLP AND WINDS 4



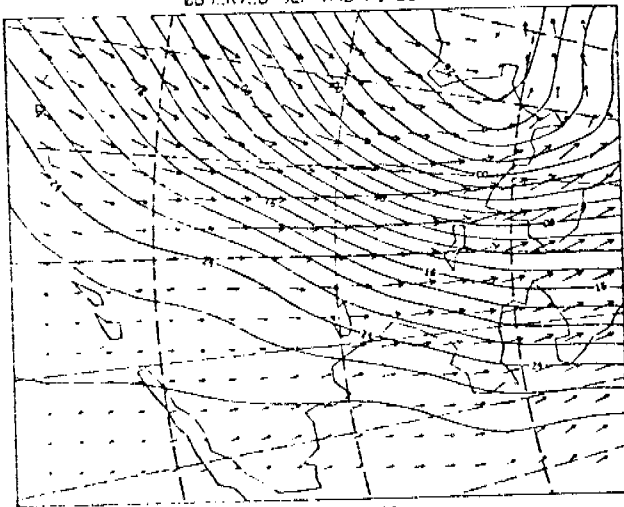
00Z 25 MAR 1979

OBSERVED SLP AND WINDS 4



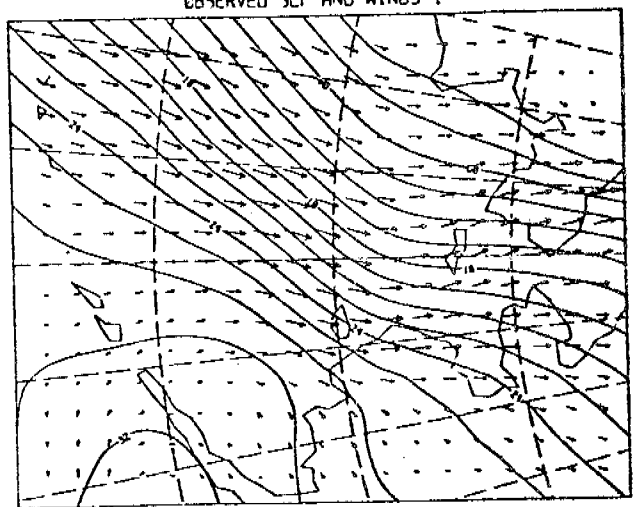
12Z 25 MAR 1979

OBSERVED SLP AND WINDS 4



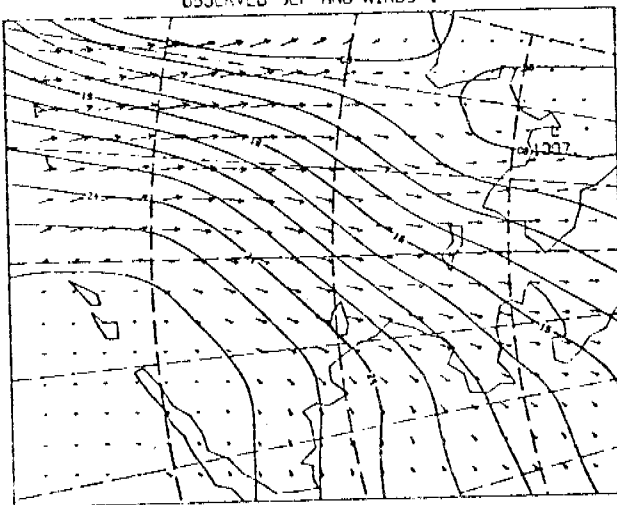
00Z 26 MAR 1979

OBSERVED SLP AND WINDS 4



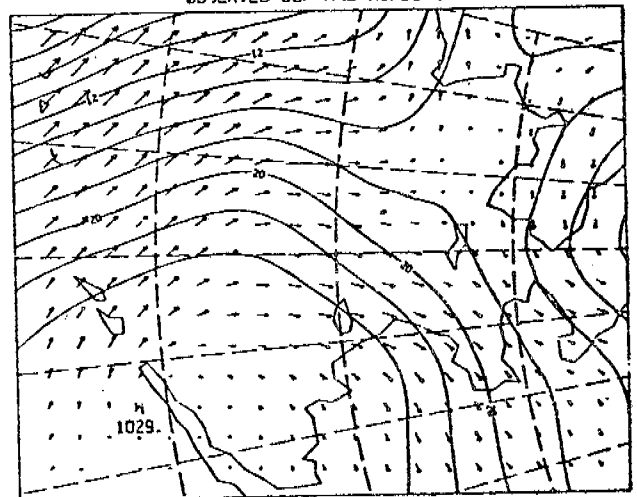
12Z 26 MAR 1979

OBSERVED SLP AND WINDS 4



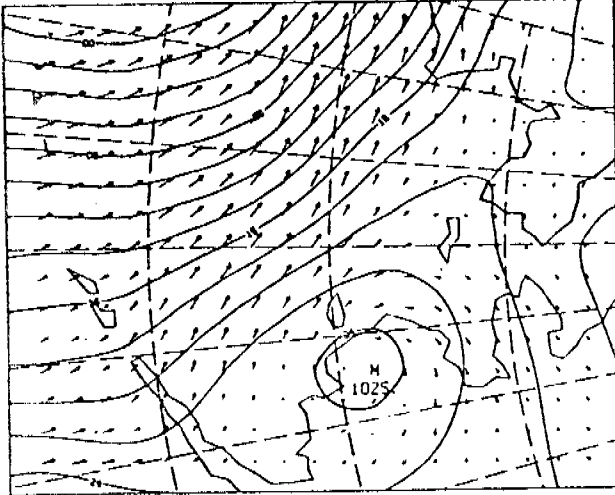
00Z 27 MAR 1979

OBSERVED SLP AND WINDS 4



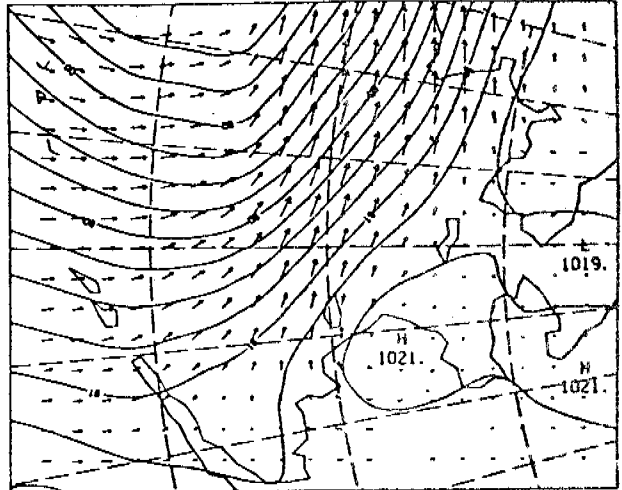
12Z 27 MAR 1979

OBSERVED SLP AND WINDS 4



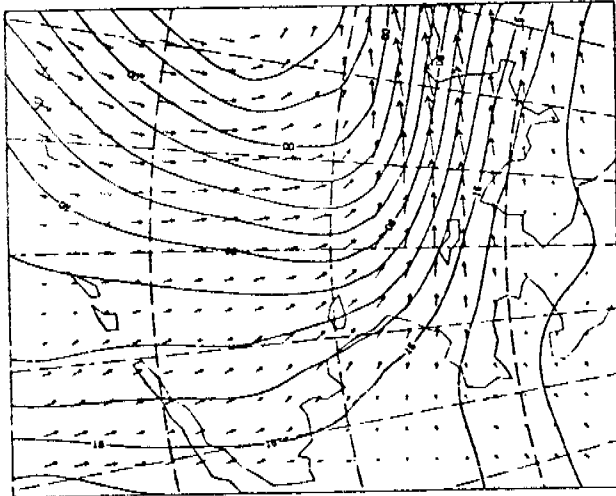
00Z 28 MAR 1979

OBSERVED SLP AND WINDS 4



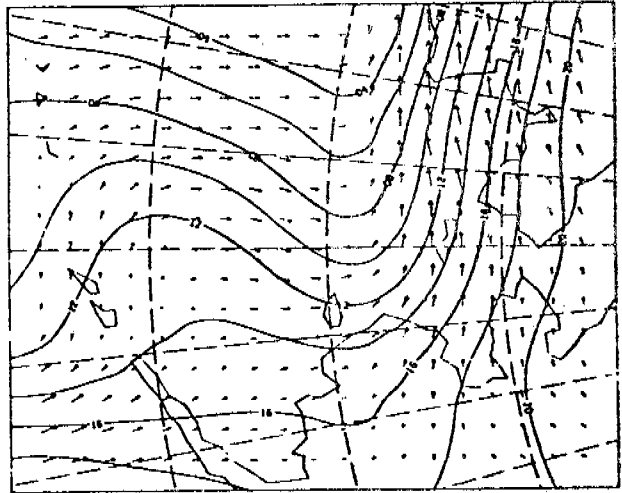
12Z 28 MAR 1979

OBSERVED SLP AND WINDS 4



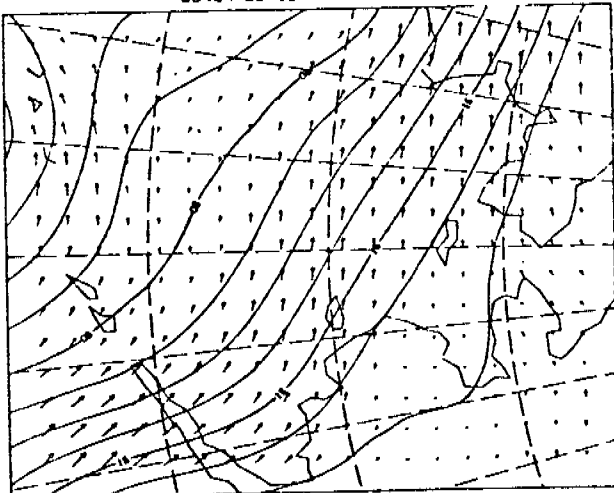
00Z 29 MAR 1979

OBSERVED SLP AND WINDS 4



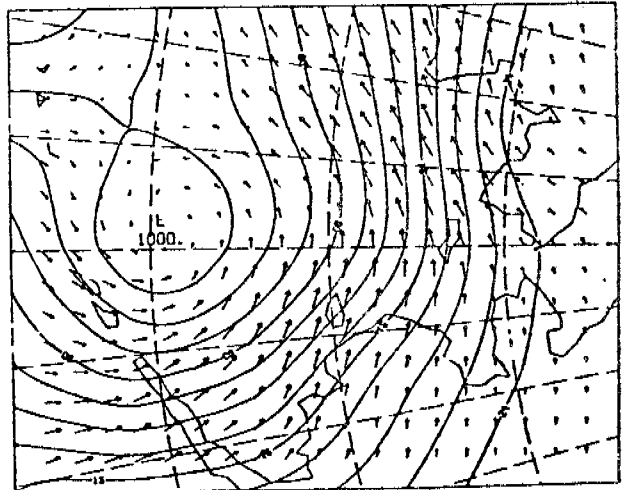
12Z 29 MAR 1979

OBSERVED SLP AND WINDS 4



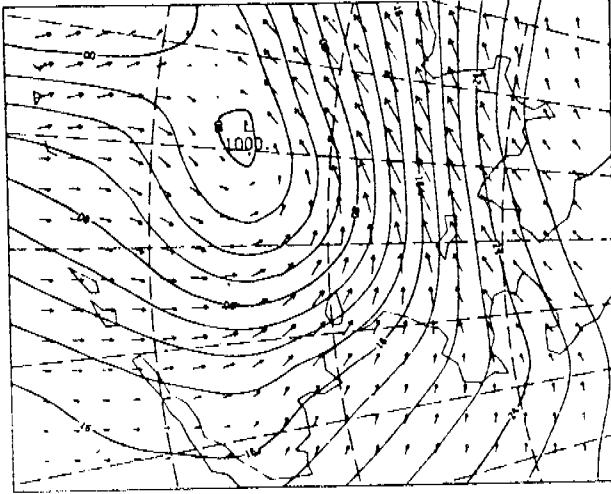
00Z 30 MAR 1979

OBSERVED SLP AND WINDS 4



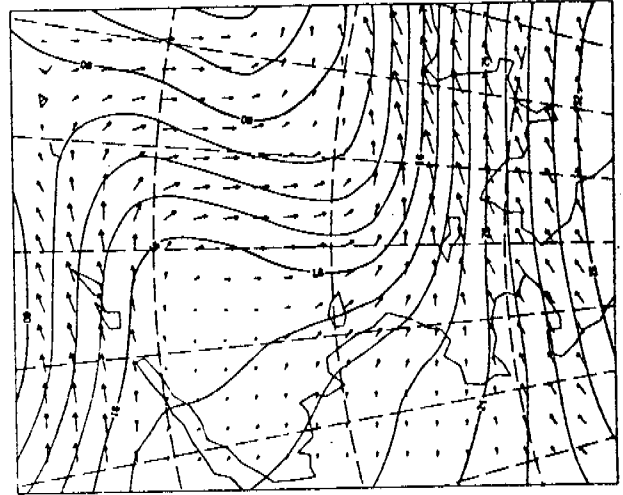
12Z 30 MAR 1979

OBSERVED SLP AND WINDS 4



00Z 31 MAR 1979

OBSERVED SLP AND WINDS 4



12Z 31 MAR 1979



## Cyclone Climatology of the Bering Sea

There are two basic approaches to generalize the synoptic variability in a given region, the use of a synoptic climatology (Barry and Perry, 1973), which regards patterns of weather as an implicit function of the static sea level pressure distribution, and the kinematic approach in which synoptic weather maps are classified in terms of principal storm tracks. A synoptic climatology is most appropriate in regions where a portion of the features form or decay in situ or are persistent such as the Gulf of Alaska (Suckling and Hay, 1978; Overland and Hiestler, 1980). The two synoptic climatologies for the northern Bering (Putnins, 1966; Barry 1979, unpublished) indicate a major first weather type associated with Arctic high pressure. The remaining types, however, all have nearly the same frequency of occurrence and appear arbitrary in location indicating that there are no fixed locations for synoptic features. The later difficulty combined with the previous study of Klein (1957) suggest that storm track climatology is the most appropriate technique for the Bering.

Past analyses of cyclone/anticyclone frequency patterns have included the Bering Sea only when the studies have been over large areas such as the hemispheric studies of Peterson (1956) and Klein (1957). Klein used a 5° latitude/5° longitude grid to determine the spatial distribution of cyclone and anticyclone frequencies for individual months based upon the daily synoptic series for 1899-1939. He constructed principal tracks drawn through axes of maximum frequency. Methodologies have developed as applied to North America (Reitan, 1974; Zishka and Smith, 1980) and to limited regions (Hurley, 1954; Colucci, 1976; Hayden, 1980). Three papers of note are Keegan (1958) and Reed and Kunkel (1960), which discuss Arctic circulation north of 60°N for winter and summer respectively, and Walsh (1978),

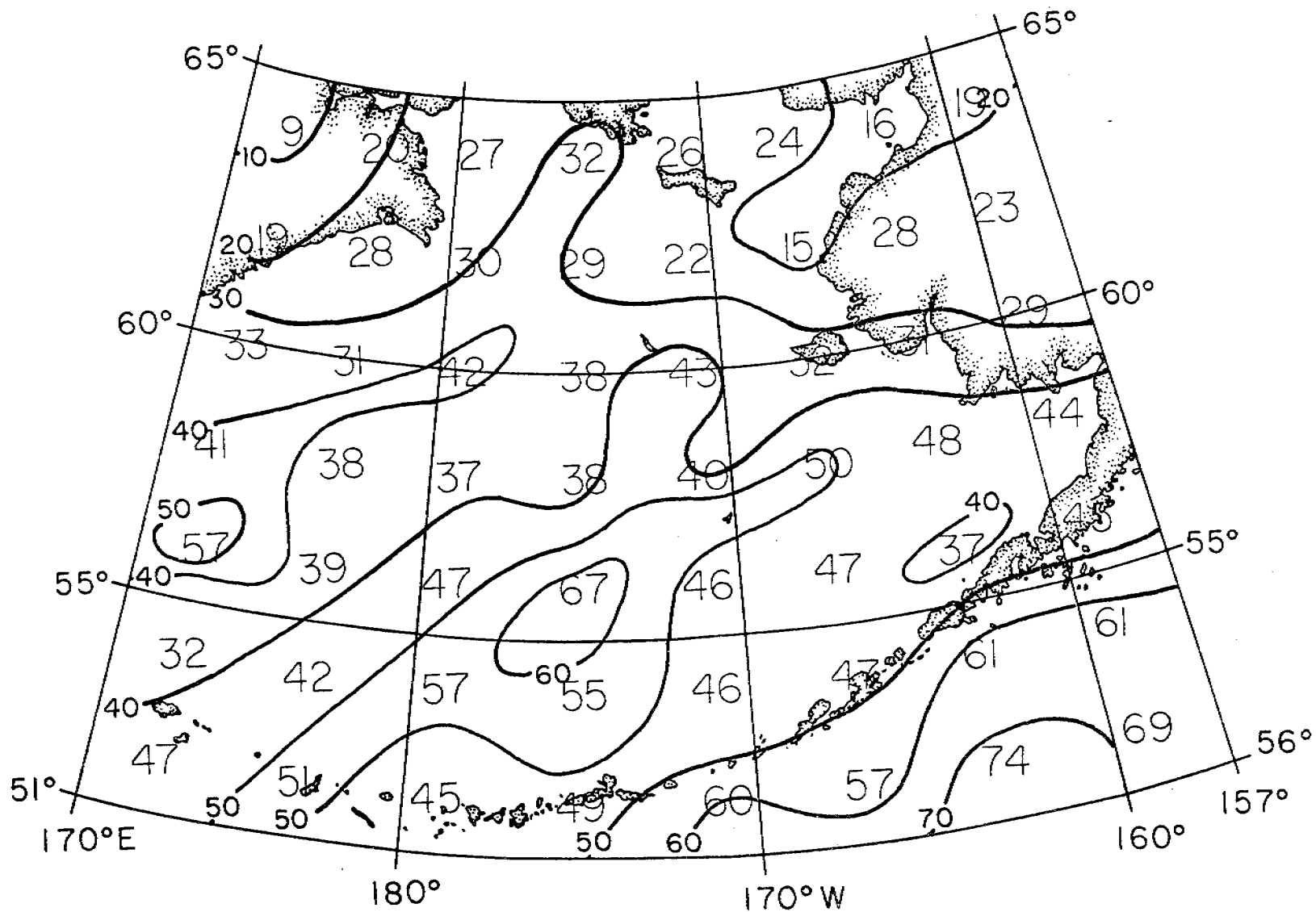
The data used in this study were derived from monthly cyclone maps published by NOAA in the Mariners Weather Log for November 1957 through April 1980. Twelve hourly pressure center locations are given on these charts for 00 and 12 GMT. Storm tracks for October 1957 were computed directly from daily sea level pressure charts to complete the ice year for winter 1957-1958. To study horizontal distributions  $2^\circ$  latitude/ $4^\circ$  longitude grids were prepared and cyclone frequencies were determined by counting the number of cyclone tracks that passed through each quadrangle in a particular month and year. Although the area enclosed by the quadrangles decreases with increasing latitude, no areal corrections are made (Zishka and Smith, 1980). The size of the quadrangles was considered minimum as a smaller area did not provide statistically stable estimates for frequency of cyclonic weather.

Figures 1-8 show the number of storms passing through each quadrangle for the twenty-three year period 1957-1979 for the months of October through December and 1958-1980 for January through April. The remaining months are free of ice in the Bering. October shows a tendency for two tracks, one starting in the lower left corner at  $180^\circ\text{W}$ ,  $50^\circ\text{N}$  heading east-northeast parallel to the Aleutian Islands. The other track enters at  $170^\circ\text{E}$ ,  $56^\circ\text{N}$  and curves northward toward Bering Strait and the Chukotka Peninsula. This northerly track is not evident in following months as the dominate Siberian high pressure is established in the northwest corner of the region. November has a maximum at  $170^\circ\text{W}$ ,  $55^\circ\text{N}$  with an indication of two tracks passing through this region, one parallel to the Aleutians as in October and one curving north into the Bering along  $170^\circ\text{W}$ . This northerly track persists through February; however, the absolute frequency drops substantially with latitude in all months. The relative importance of the northern track peaks in January when the frequency along the track is of similar magnitude as south

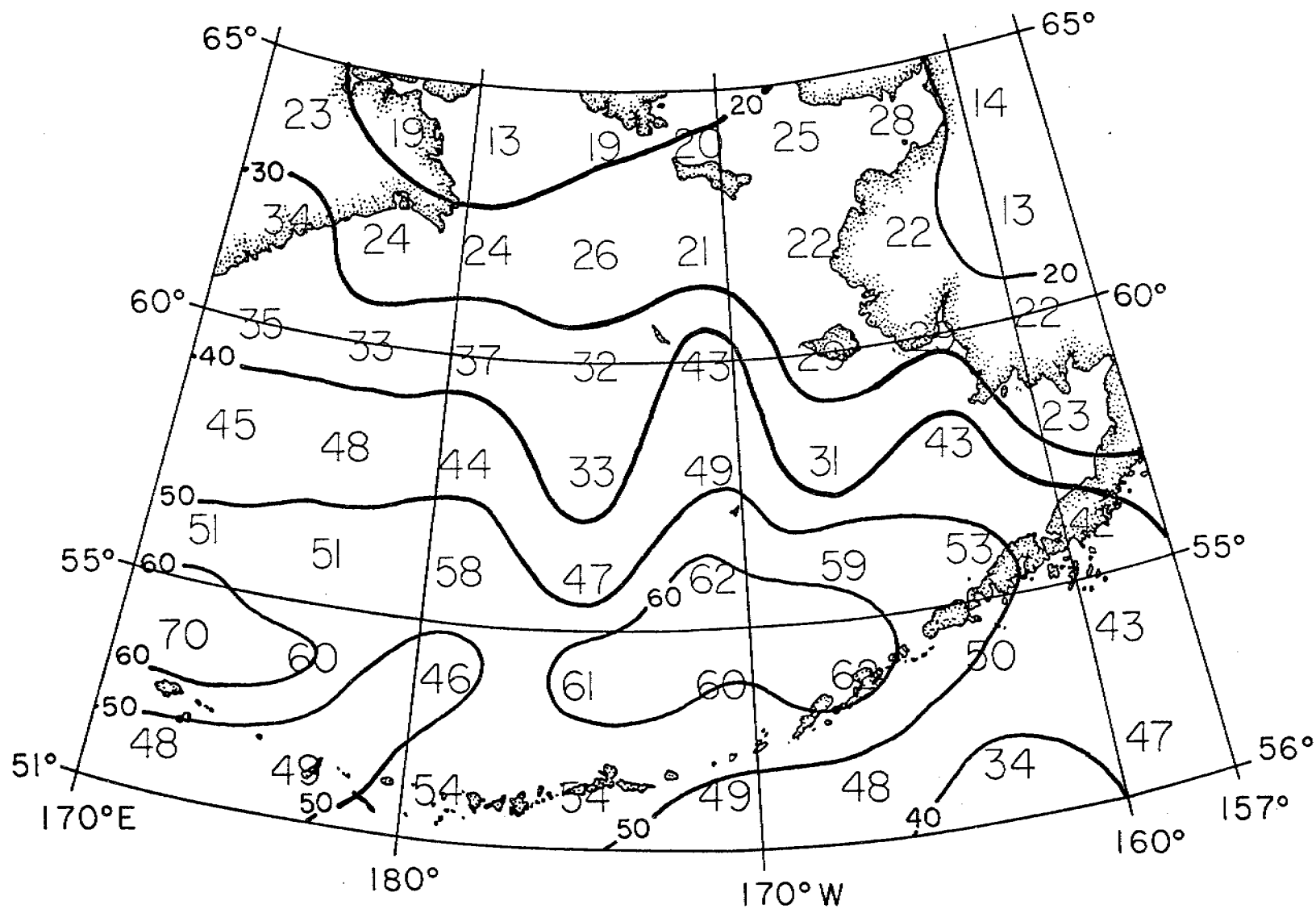
of the western part of the Aleutians. This month corresponds to maximum blocking ridge activity as given by White and Clark (1975). They show 29% of the 31 Januarys from 1950 to 1970 had blocking ridge activity as compared to 10% for the months November, December and February. In March and April the overall storms activity increases and the frequencies have a more zonal character than mid-winter. Figures 9 and 10 show the number of storms per  $2^{\circ}$  latitude by  $4^{\circ}$  longitude box for October - February for the years with the maximum ice cover and with the minimum ice cover. Note the lack of storms penetrating the Northern Bering in years with maximum ice cover.

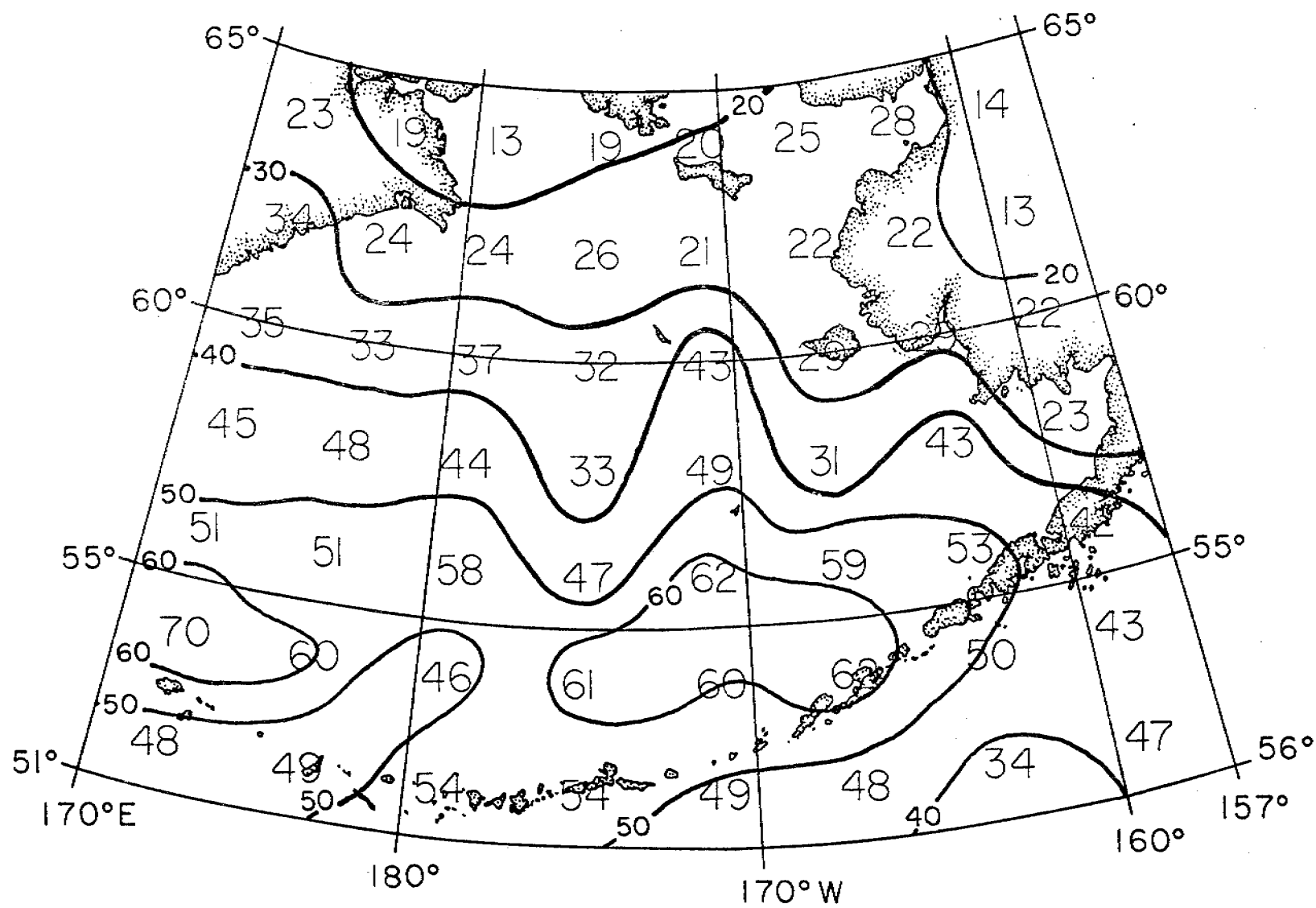
## References

- Berry, R.G., 1979: Shorefast sea ice. Surface morphological characteristics. Beaufor sea coast: Prudhoe sector.
- Colucci, S.J., 1976: Winter cyclone frequencies over the eastern United States and adjacent western Atlantic. Bull. Amer. Meteor. Soc., 57, 548-553.
- Hayden, B.P., 1980: Atlantic coast extra tropical cyclones: characteristic frequency patterns and their secular variation. Conference on application of statistics to meteorology, AMS, 192-197.
- Hurley, J.C., 1954: Statistics on the movement of and deepening of cyclones in the middle West. Mon. Wea. Rev., 82, 116-122.
- Keegan, T.J., 1958: Arctic synoptic activity in winter. J. Meteor., 15, 513-521.
- Klein, W.H., 1957: Principal tracks and mean frequencies of cyclones and anti-cyclones in the Northern Hemisphere. Re. Pap. No. 40, US Weather Bureau, Washington, D.C., 60 pp.
- Mariners Weather Log, 1957 to 1980. NOAA/EDIS, U.S. Dept. of Commerce.
- Petterson, S., 1956: Weather Analysis and Forecasting. Vol. 1, McGraw-Hill, 422 pp.
- Putnins, P., 1966: The sequence of baric pressure patterns over Alaska. Studies on the meteorology of Alaska. First Interim Report, Environmental Data Service, ESSA, Washington, D.C., 57 pp.
- Reed, R.J. and Bruce A. Kunkel, 1960: The Arctic circulation in summer. J. Meteor. 17, 489-506.
- Reitan, C.H., 1974: Frequencies of cyclones and cyclogenesis for North America, 1951-1970. Mon. Wea. Rev., 102, 861-868.
- U.S. Weather Bureau: Daily series synoptic weather maps. Washington, D.C.
- Walsh, J.E., 1958: Temporal and spatial scales of the Arctic circulation. Mon. Wea. Rev., 106, 1532-1535.
- Zishka, K.M. and P.J. Smith, 1980: The climatology of cyclones and anticyclones over North America and surrounding ocean environs for January and July, 1950-77. Mon. Wea. Rev., 108, 387-401.

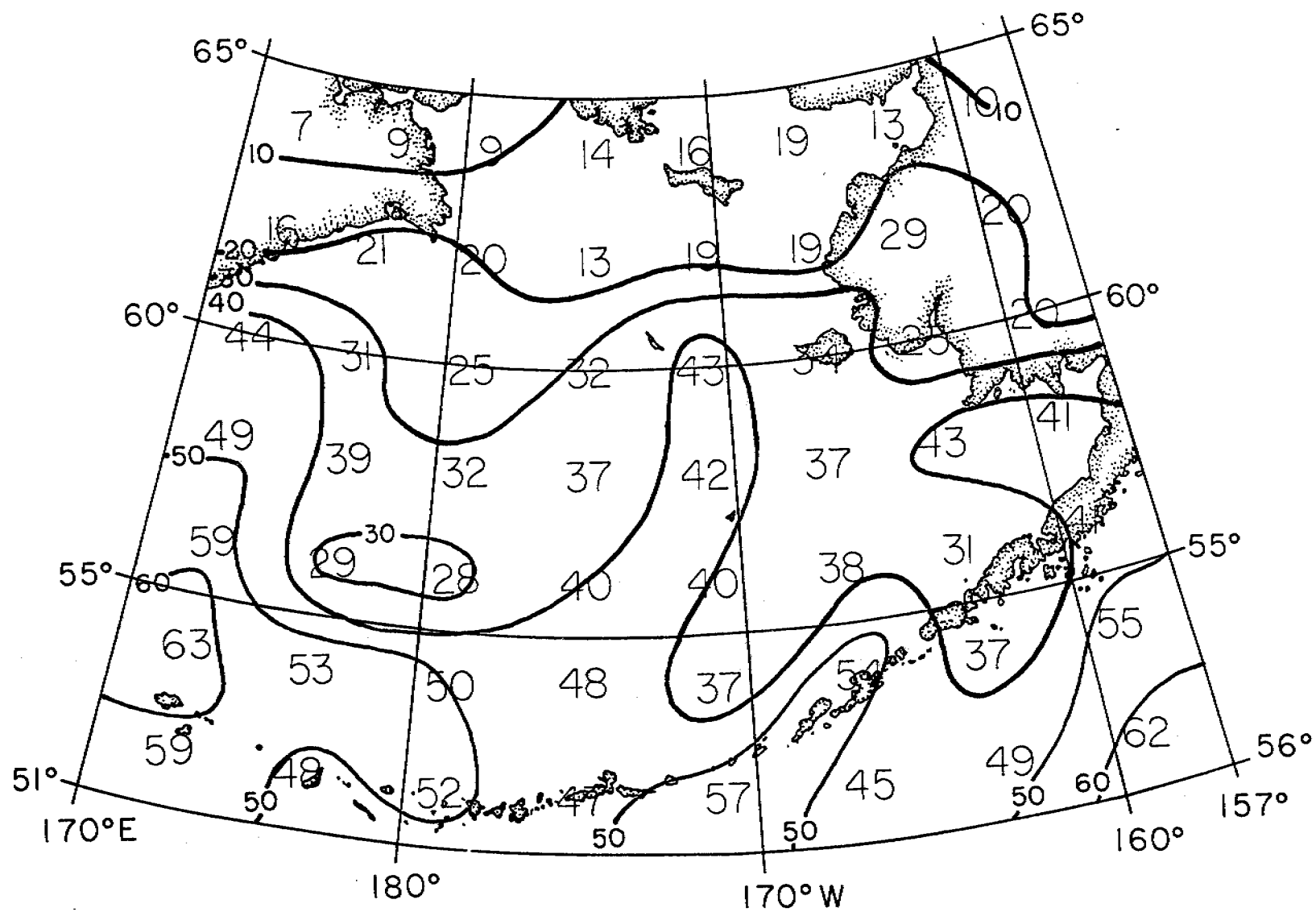


OCT-SUMS

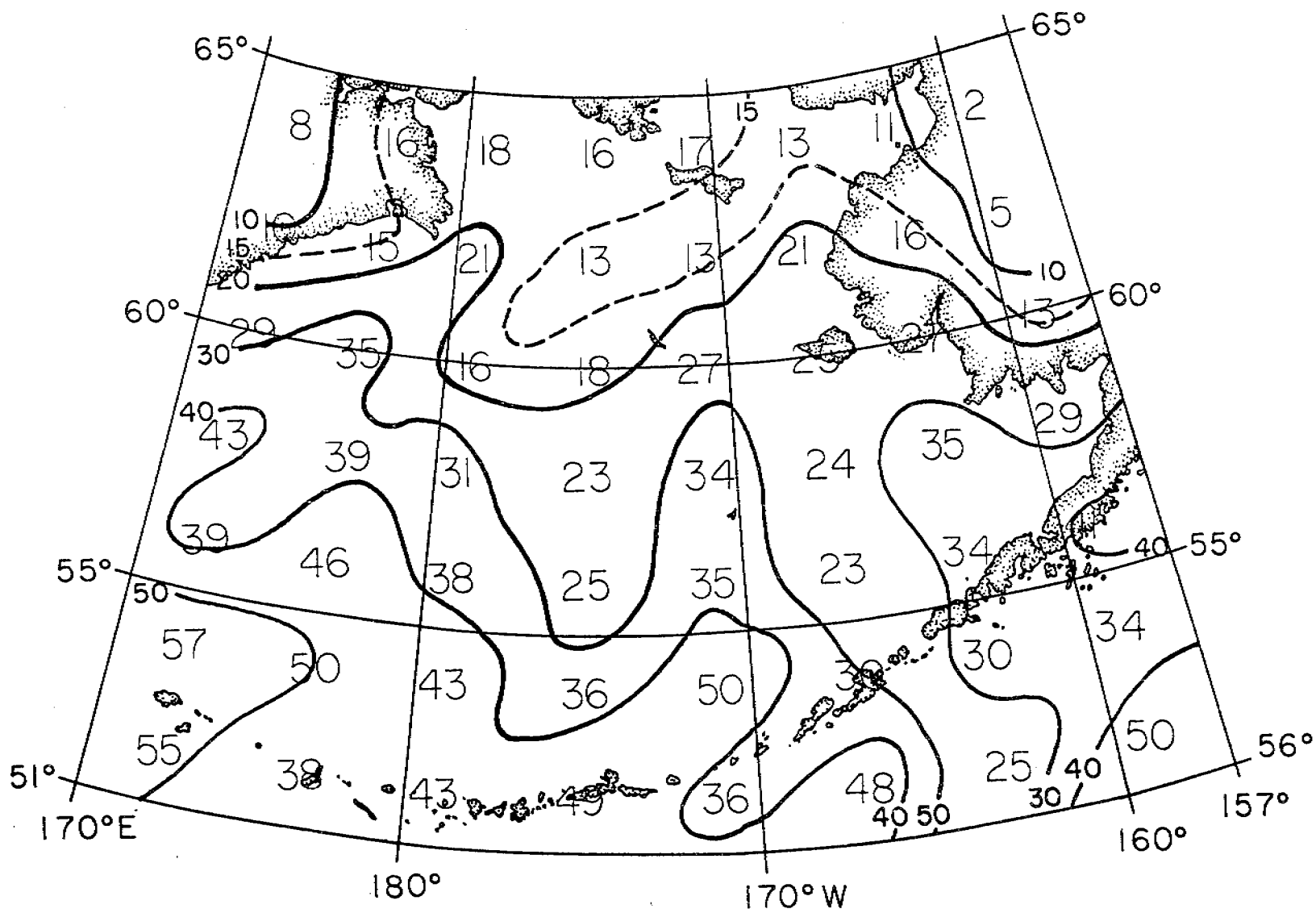
NOV-SUMS



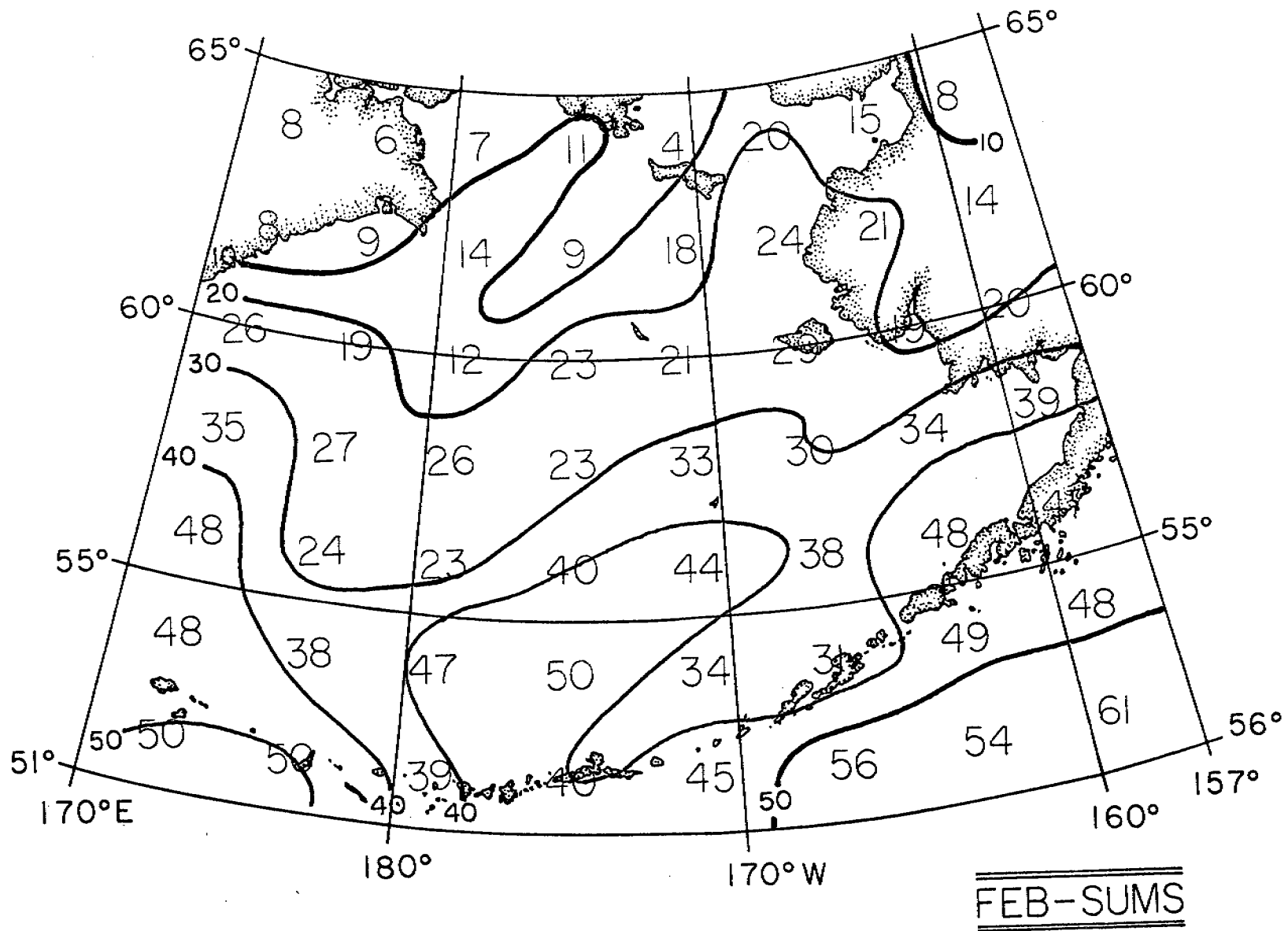
NOV-SUMS

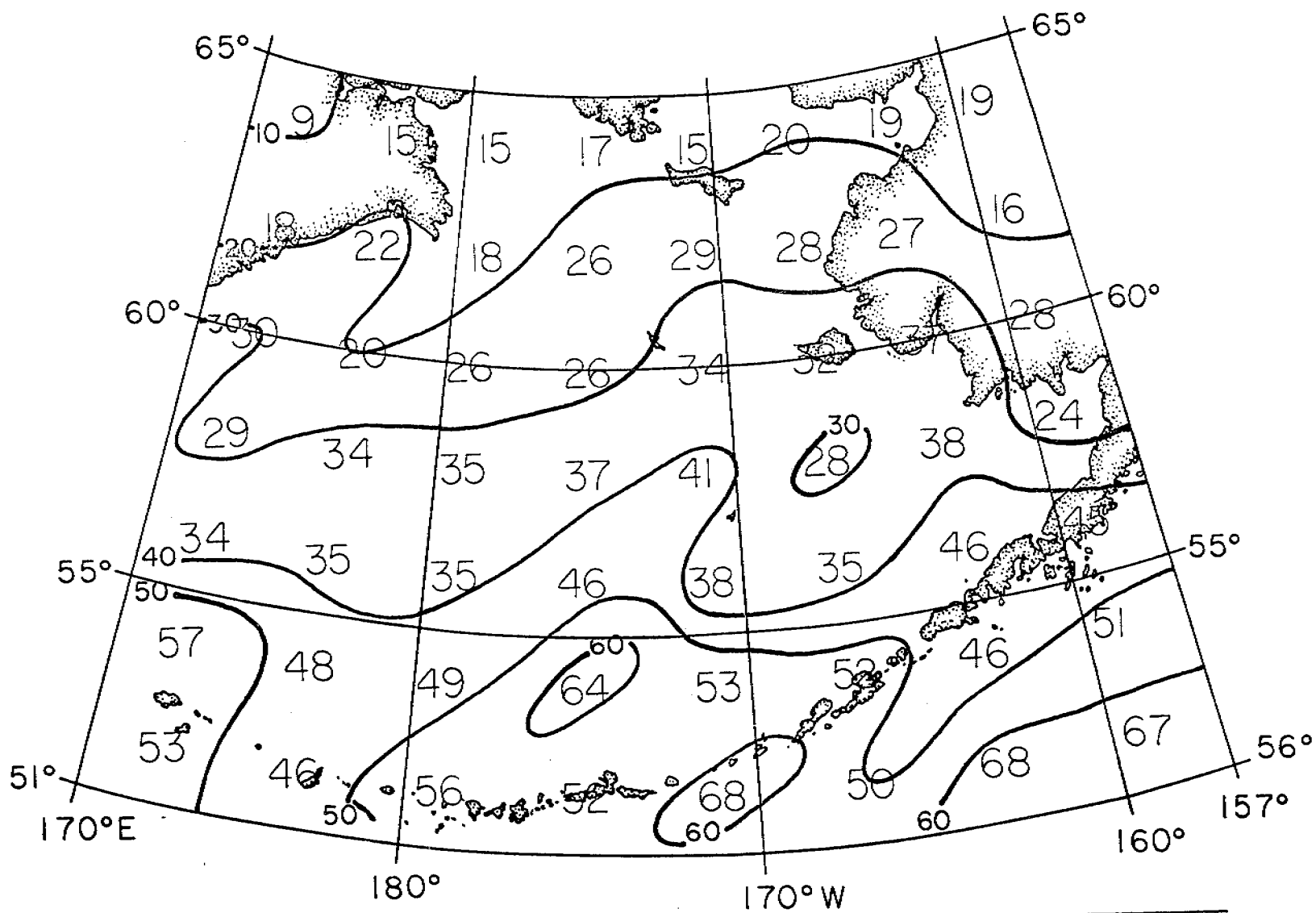
DEC-SUMS



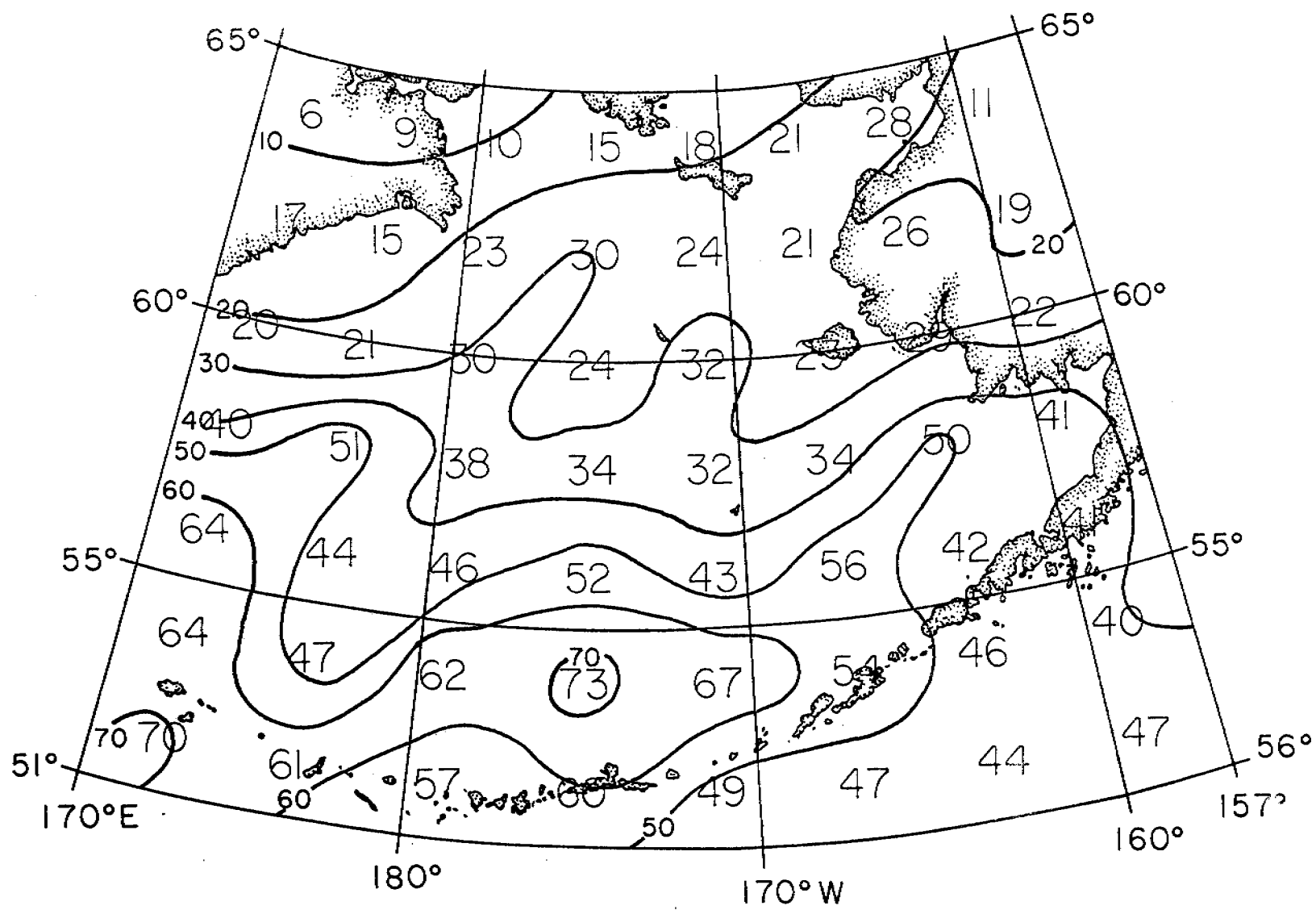


JAN-SUMS





MAR-SUMS



APR-SUMS

YEARS

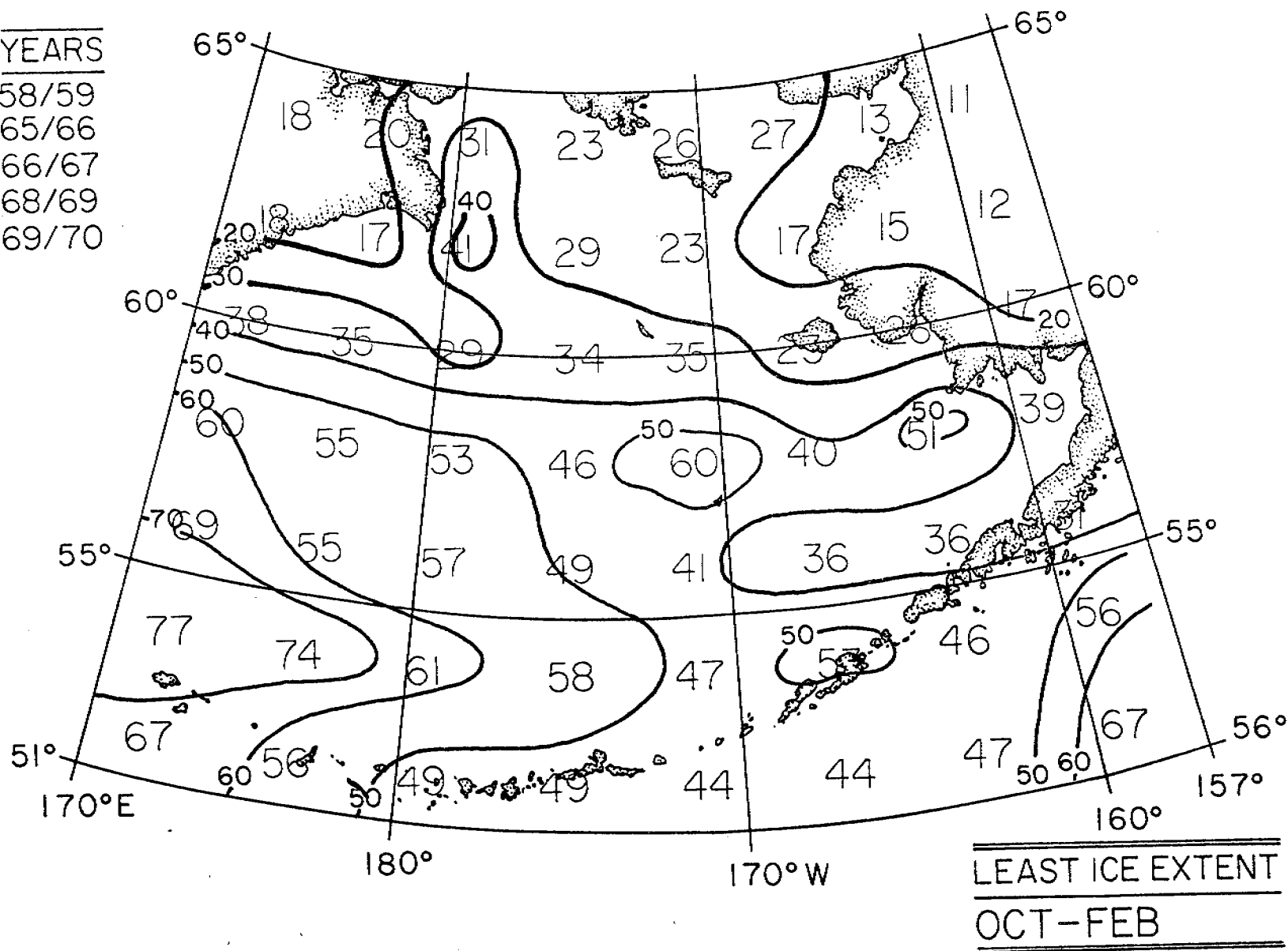
58/59

65/66

66/67

68/69

69/70



YEARS

57/58

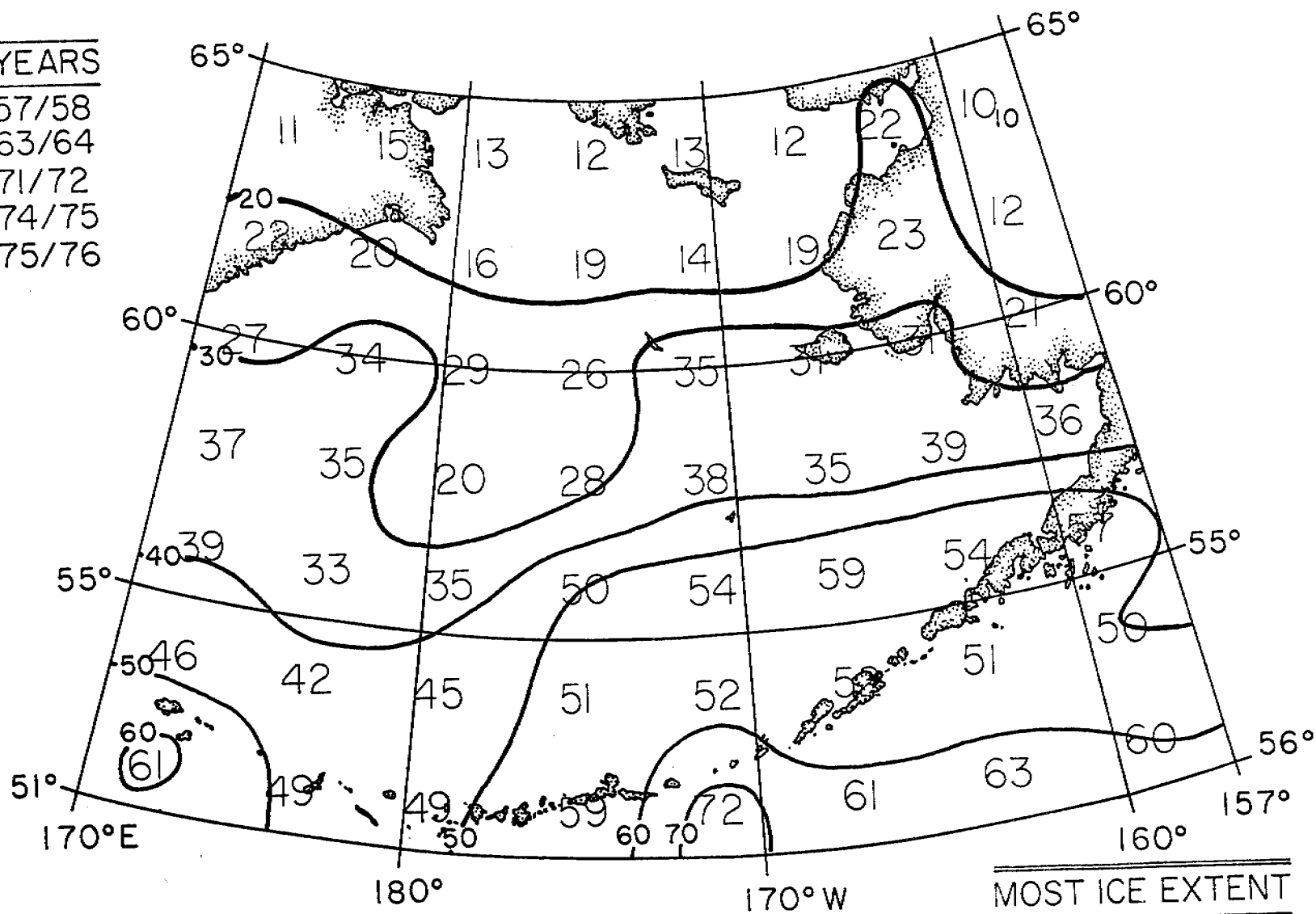
63/64

71/72

74/75

75/76

342



MOST ICE EXTENT  
OCT-FEB

## Evaluation of Two Synoptic Climatologies for Northern Bering Sea

### I. Introduction

In simulating space and time variable wind fields for climatological studies there are in general two approaches. One can pick a set of representative storms and representative storm tracks and run a trajectory model with various combinations of storms and tracks or one can use the synoptic climatology approach. In the later one picks a finite set of static weather situations, assigns frequencies to each weather type, and determines the transition probabilities between each type. Model runs are then made by starting with a type and then performing a first order Markov process using the transition probabilities. Overland and Hiester (1980) provided this later approach running the Galt spill model in NEGOA, where storms tend to be stationary. This note looks at two synoptic climatologies for the northern Bering Sea and analyzes whether using a synoptic climatology to represent regional weather is appropriate in this area.

### II. Norton Sound Weather Types

Putnins produced a synoptic climatology which covers all of Alaska. This creates some problem in applying the climatology to a small area as some differences in the patterns may be due to geographic regions not in the area of interest. Another problem with Putnins' types is that they were derived to emphasize land regions. A second synoptic climatology was derived by Barry for the Chuckchi Sea. Again this climatology covers northern Bering Sea but was not optimized for this region. Appendix A shows 22 types for Barry and the 21 weather types for Putnins plotted for the Bering Sea using METLIB (Overland et al., 1980). Note that north is to the right in these figures.

We wish to compare these climatologies with 13 years of twice daily weather charts. That is take digitized weather charts and by automated techniques

assign each chart to its most similar climatology chart. This can be done by simply calculating the correlation coefficient of the grid points that make up each map and weather type as was done in Overland and Hiester (1980). This time a slightly more sophisticated approach is taken which does not change the basic idea of matching. First the Empirical Orthogonal Functions (EOF's) for sea level pressure in the northern Bering were computed from twice daily weather charts for 1972. These functions are formed based upon the shape of the region and the variation of the meteorological signal. These functions form a basis set, the same way cosines form a basis set in Fourier series, for expanding any given daily chart or synoptic climate weather type. We have determined any weather chart can be represented as the sum of four EOF's with different weights or coefficients for each one. The number four was determined by a method proposed by R. Preisendorfer and these four EOF's can explain 95% of the variance of the yearly meteorological record. This procedure has two advantages. First charts can be compared by comparing the four coefficients of the EOF's rather than all data points. Second the EOF's probably give more generalized patterns than the original analysis. For example what is not resolved in a daily map by the four EOF's is likely to be a specific local event that should be excluded from a climatology. Also since both the 13 years of charts and the synoptic climatologies were expanded using the same set of EOF's it is likely that there will be a better match of the underlying meteorological structure in comparing both fields than by using other methods. Appendix B shows the EOF's for the northern Bering Sea and the entire Bering Sea. Since each weather chart is represented by a weighted sum of these functions individual EOF's will not represent a given weather map or weather type.



### III. Statistics

A large number of statistics can be computed from the data set. One has twenty-two Barry types, twenty-one Putnins types, and eleven Rand types which are the eleven Putnins types chosen as a subset for representing Norton Sound climatology. We have computed transition probabilities for each set at lags of 12 - 72 hours for four seasons and for a year. Rather than list all these numbers, we summarize our evaluation of using the synoptic climatology procedure by the following example.

Table I and II give the diagonal elements of the transition matrix for lags of 12 to 72 hours for Barry's climatology for winter and summer, that is the probability for a weather type to remain in each type as a function of duration. They also show the percent frequency of each type. Probabilities are given in tenths of percent so 812 is a 0.812 probability that type 1 will remain in type 1 for the next twelve hours. Barry's type 1 and type 4 represent domination of Arctic high pressure over the northern Bering. In winter these types show persistence to 72 hours, a sign that these patterns represent good examples of synoptic weather types. They represent 35% of the winter weather maps. The summer statistics are in marked contrast. Not only are fewer types persistent but almost all types are present, indicating little preference for any given weather types.

In summary in winter the northern Bering can be assigned clear weather types corresponding to Barry's types 1 and 4 for 35% of the time. The remainder is made up of other weather situations which have some characteristics of persistence. In summer all types tend to be represented with quick transition to other types indicating that storm tracks rather than a synoptic climatology would be a better generalization.

### References

- Overland, J.E., and T.R. Hiester (1979): Development of a synoptic climatology for the northeast Gulf of Alaska. J. of Appl. Meteor., 19(1), Jan. 1980.
- Overland, J.E., R.A. Brown and C.D. Mobley (1980): METLIB - A program library for calculating and plotting marine boundary layer wind fields. NOAA Tech. Mem. ERL PMEL-20, 82 pp.

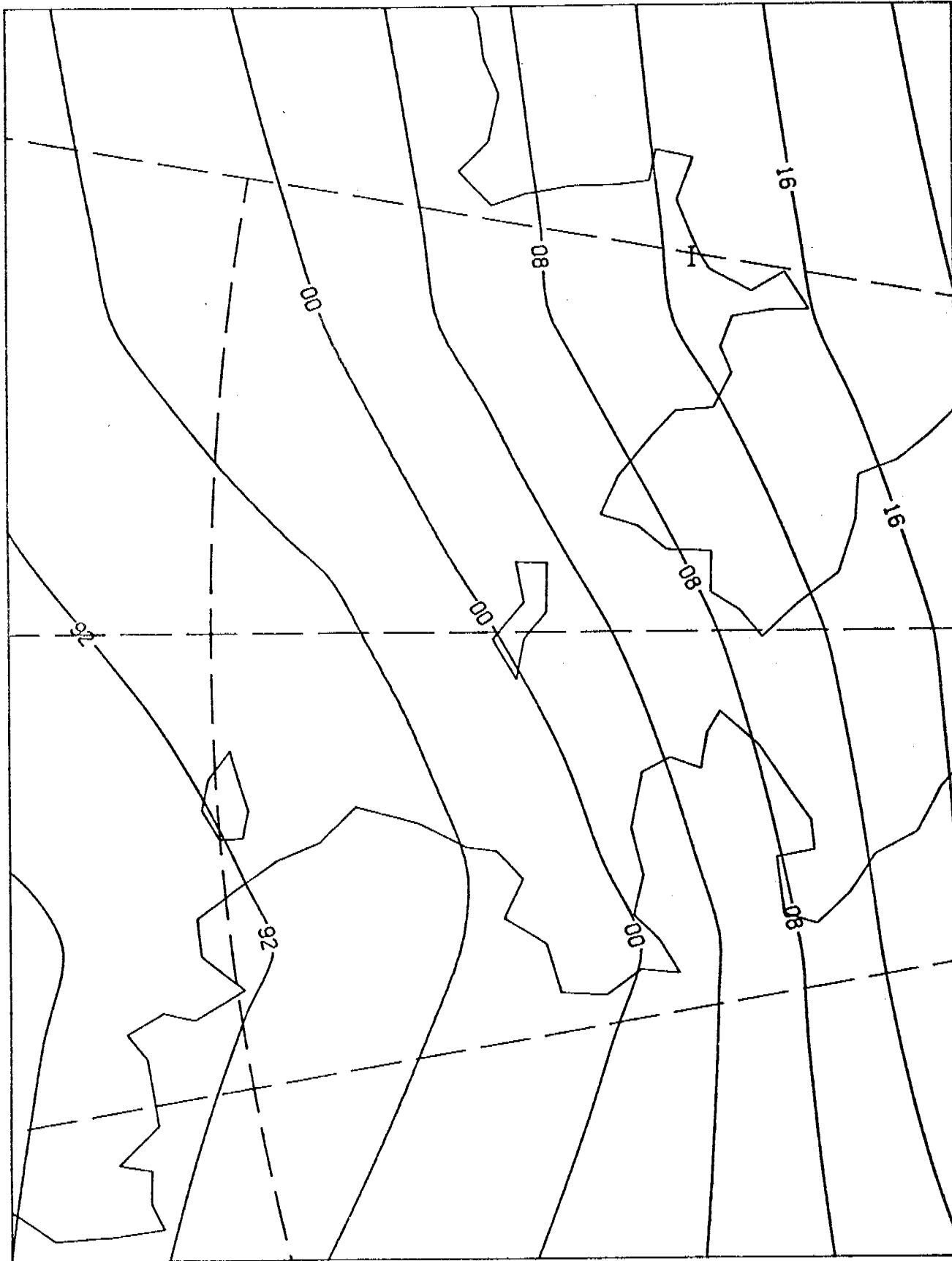
Table I Barry Types - Winter

Types	12 hrs	24 hrs	36 hrs	48 hrs	60 hrs	72 hrs	Frequency
1	812	669	585	517	469	437	228
2	629	434	330	278	224	198	52
3	597	333	215	172	172	172	35
4	666	453	340	295	250	235	121
5	241	71	0	0	0	0	13
6	528	292	177	130	114	114	48
7	166	55	0	0	0	0	8
8	492	259	184	159	147	124	57
9	465	210	140	160	120	50	26
10	90	0	0	0	0	0	5
11	387	114	64	90	104	89	28
12	593	376	273	261	216	146	39
13	460	220	150	90	90	81	45
14	508	304	242	226	137	125	78
15	76	0	0	0	0	0	5
16	666	464	300	230	187	157	52
17	514	317	242	203	118	130	47
18	200	32	64	66	34	37	13
19	285	0	0	0	0	0	3
20	90	0	0	0	0	0	5
21	298	122	87	36	35	17	26
22	640	435	333	283	235	222	57

Table II Barry Types - Summer

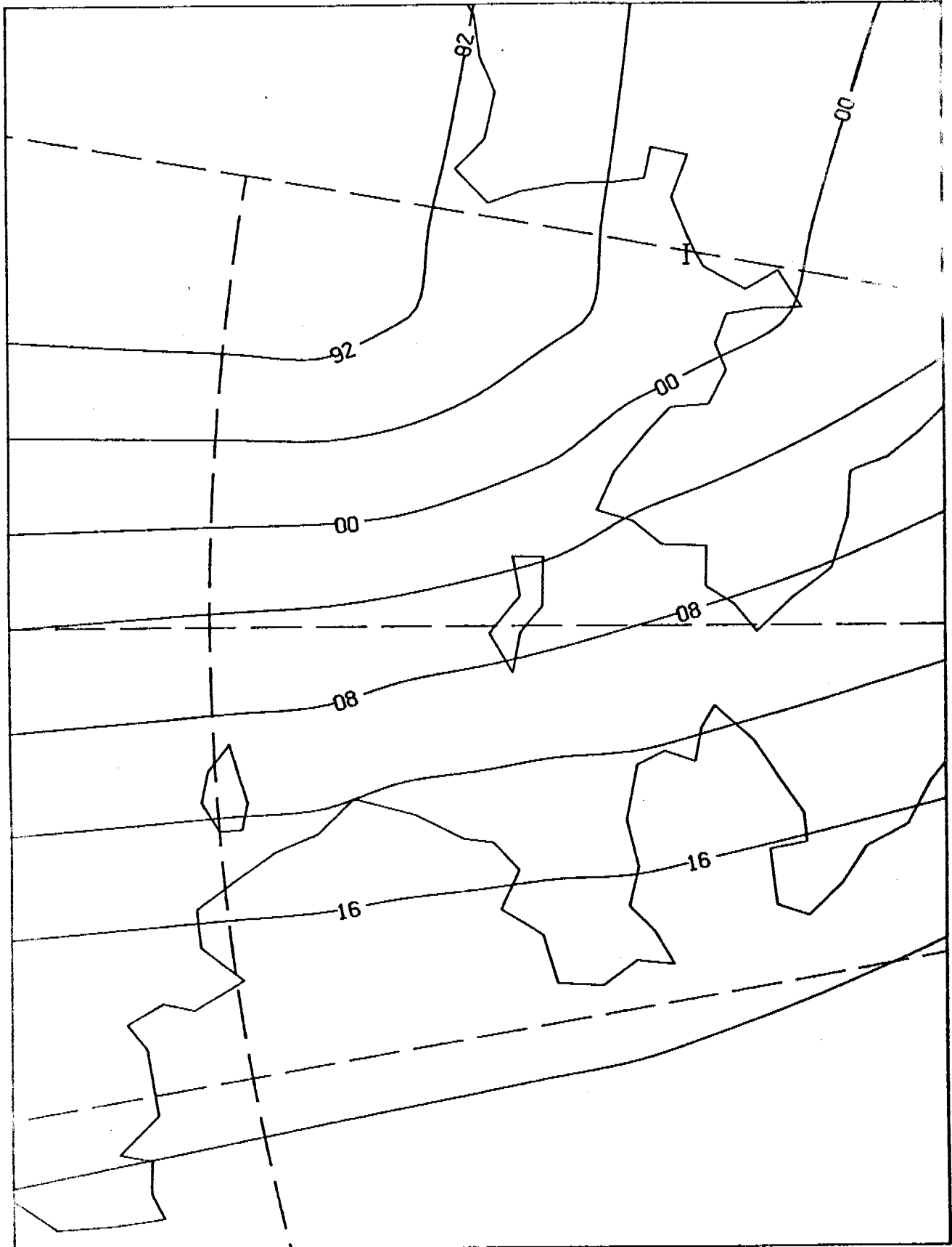
Types	12 hrs	24 hrs	36 hrs	48 hrs	60 hrs	72 hrs	Frequency
1	562	250	121	31	0	0	1
2	487	219	100	48	0	0	18
3	769	538	416	250	83	0	6
4	142	0	0	0	0	0	3
5	665	482	358	292	234	196	169
6	333	0	0	0	0	0	1
7	574	311	204	183	161	139	100
8	363	166	90	0	0	0	5
9	484	242	114	88	28	28	15
10	261	93	23	0	0	0	19
11	531	239	108	63	0	20	21
12	633	402	273	198	125	126	65
13	522	313	196	179	141	128	62
14	519	264	128	79	40	50	47
15	449	183	100	82	73	92	50
16	0	0	0	0	0	0	0
17	541	322	206	141	108	116	44
18	620	395	297	220	196	192	147
19	611	375	253	171	115	88	33
20	488	275	188	166	177	169	99
21	575	345	233	173	103	58	74
22	0	0	0	0	0	0	0

ØBSERVED SLP



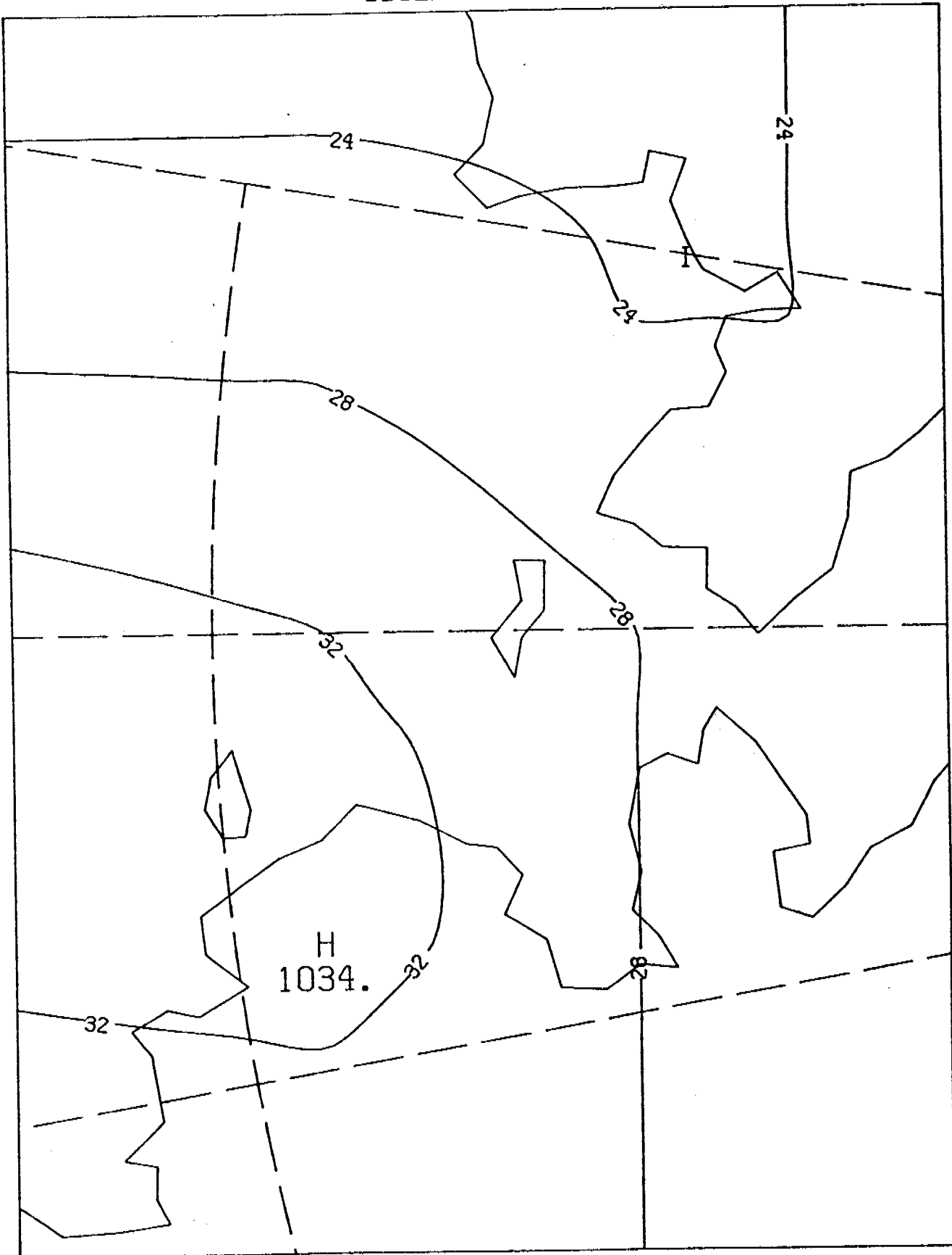
00Z 14 MAR 1970  
BERRY

OBSERVED SLP



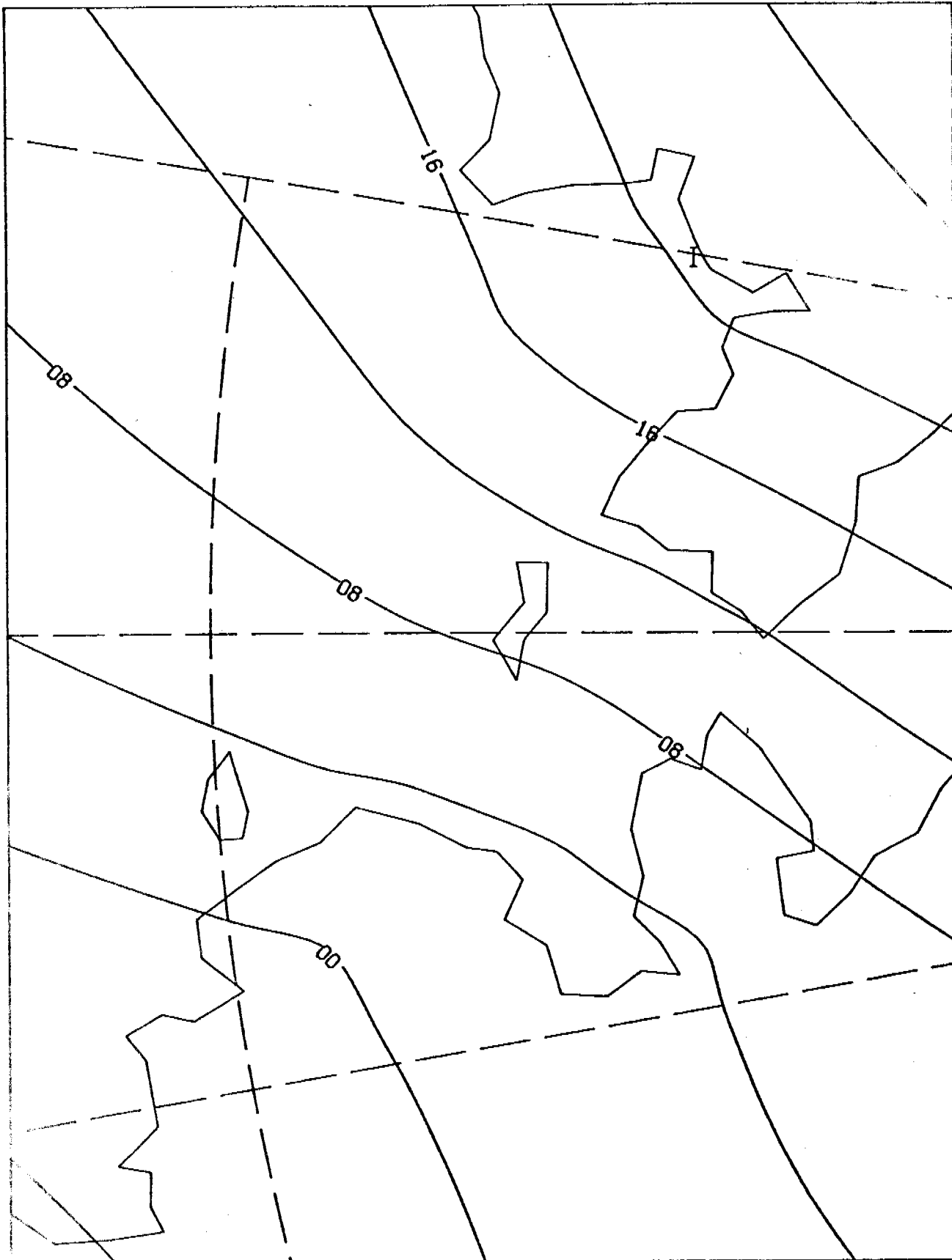
00Z 7 AUG 1968  
BERRY

ØBSERVED SLP



00Z 20 MAR 1967  
BERRY

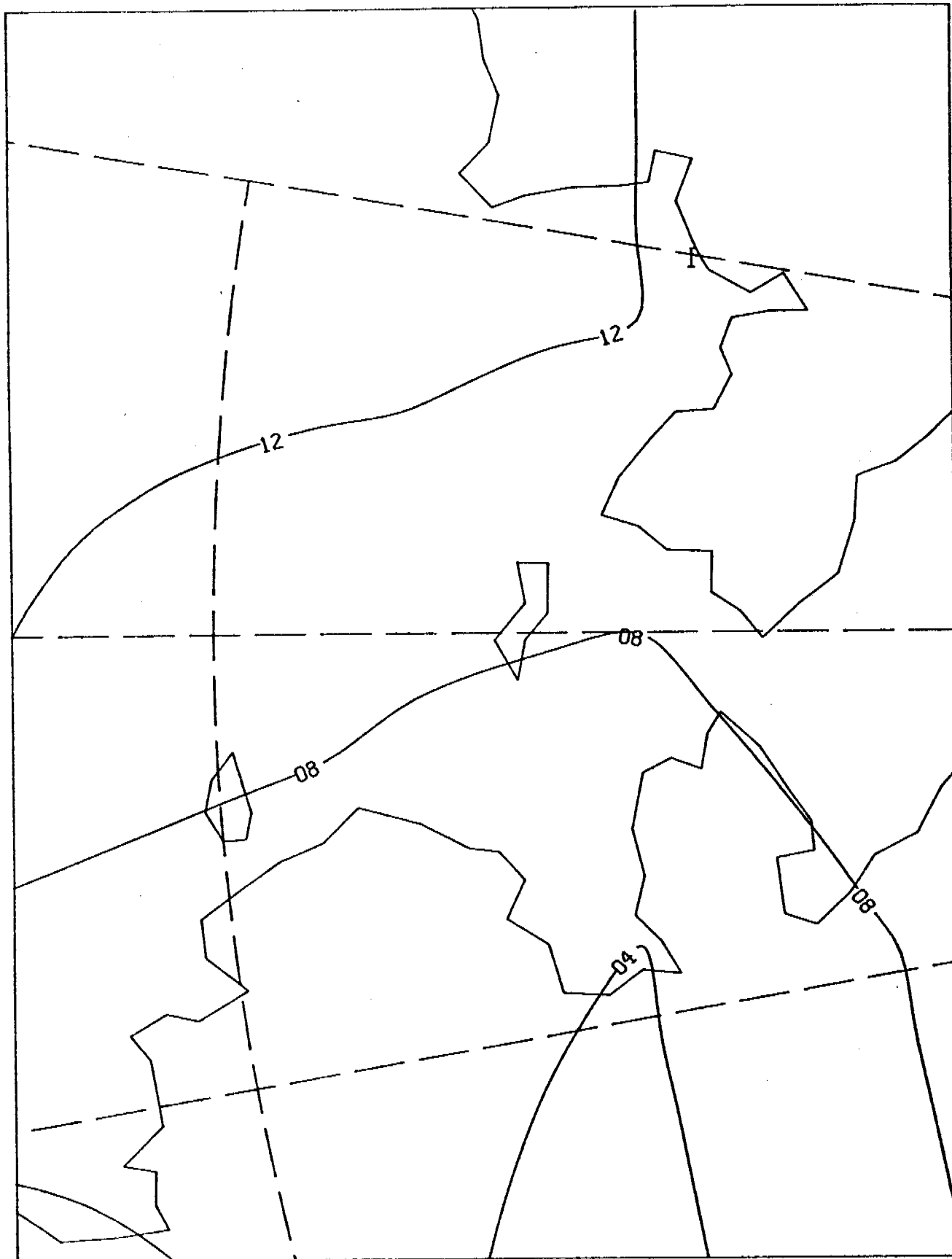
ØBSERVED SLP



00Z 2 FEB 1961  
BERRY

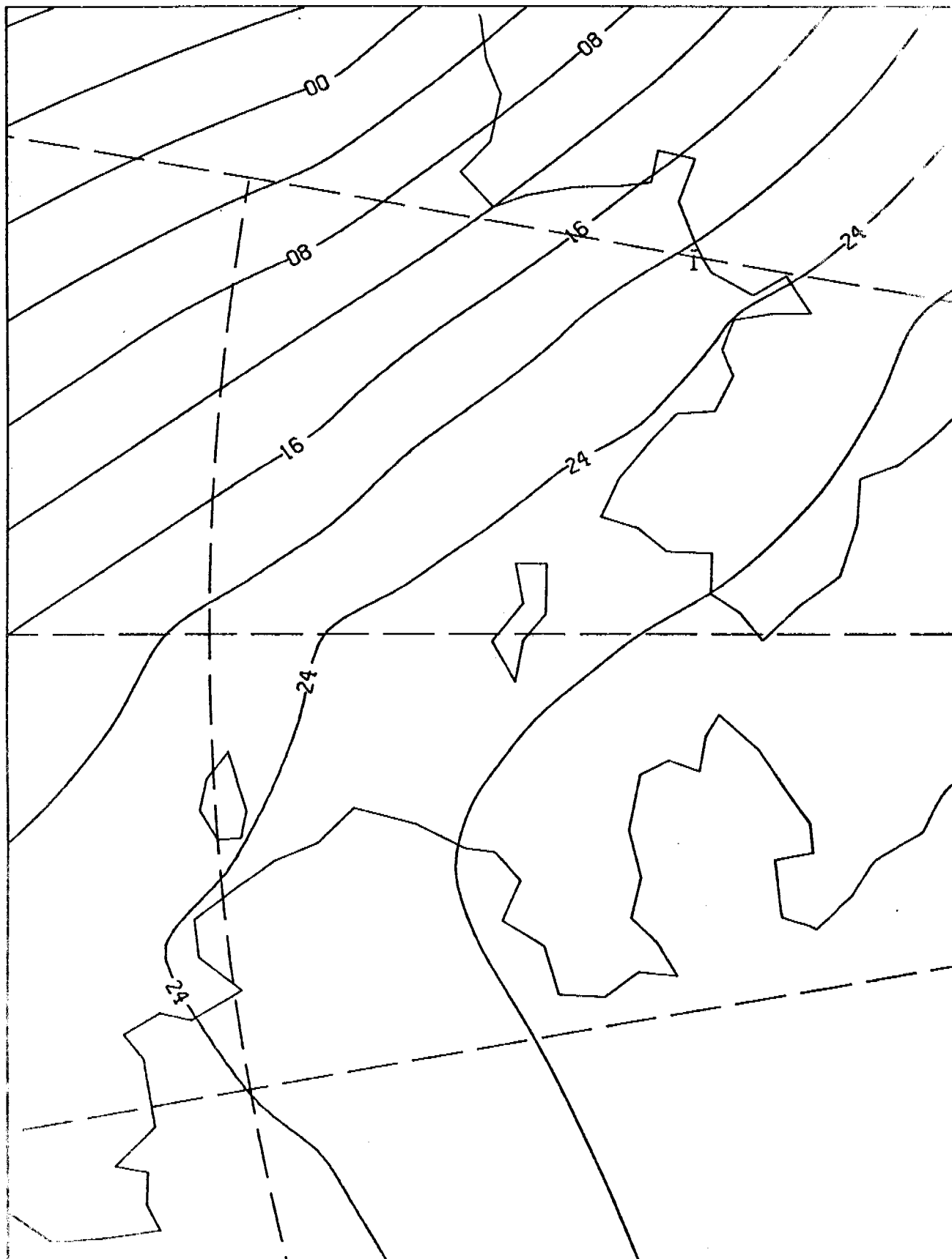


ØBSERVED SLP



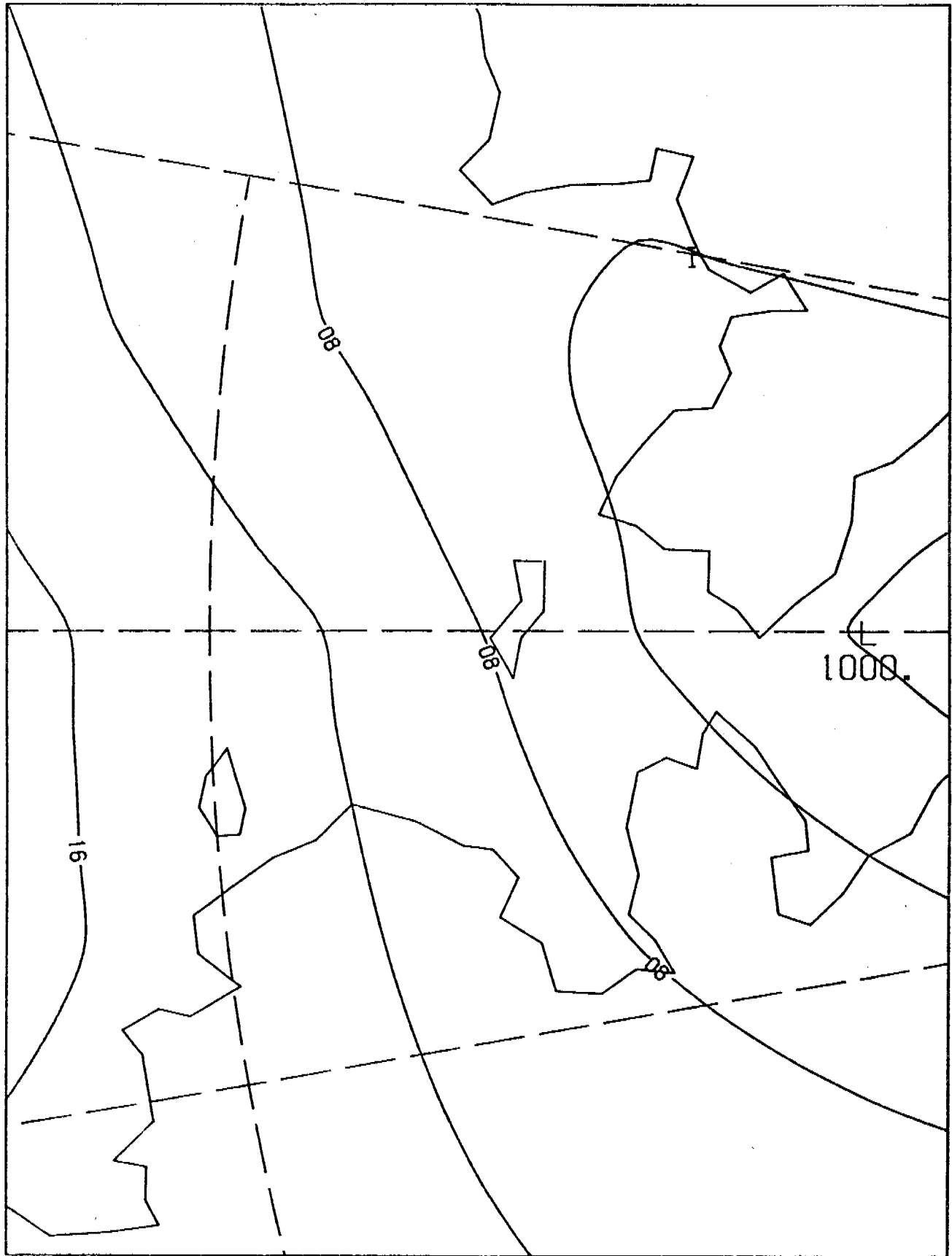
00Z 23 JUN 1969  
BERRY

OBSERVED SLP



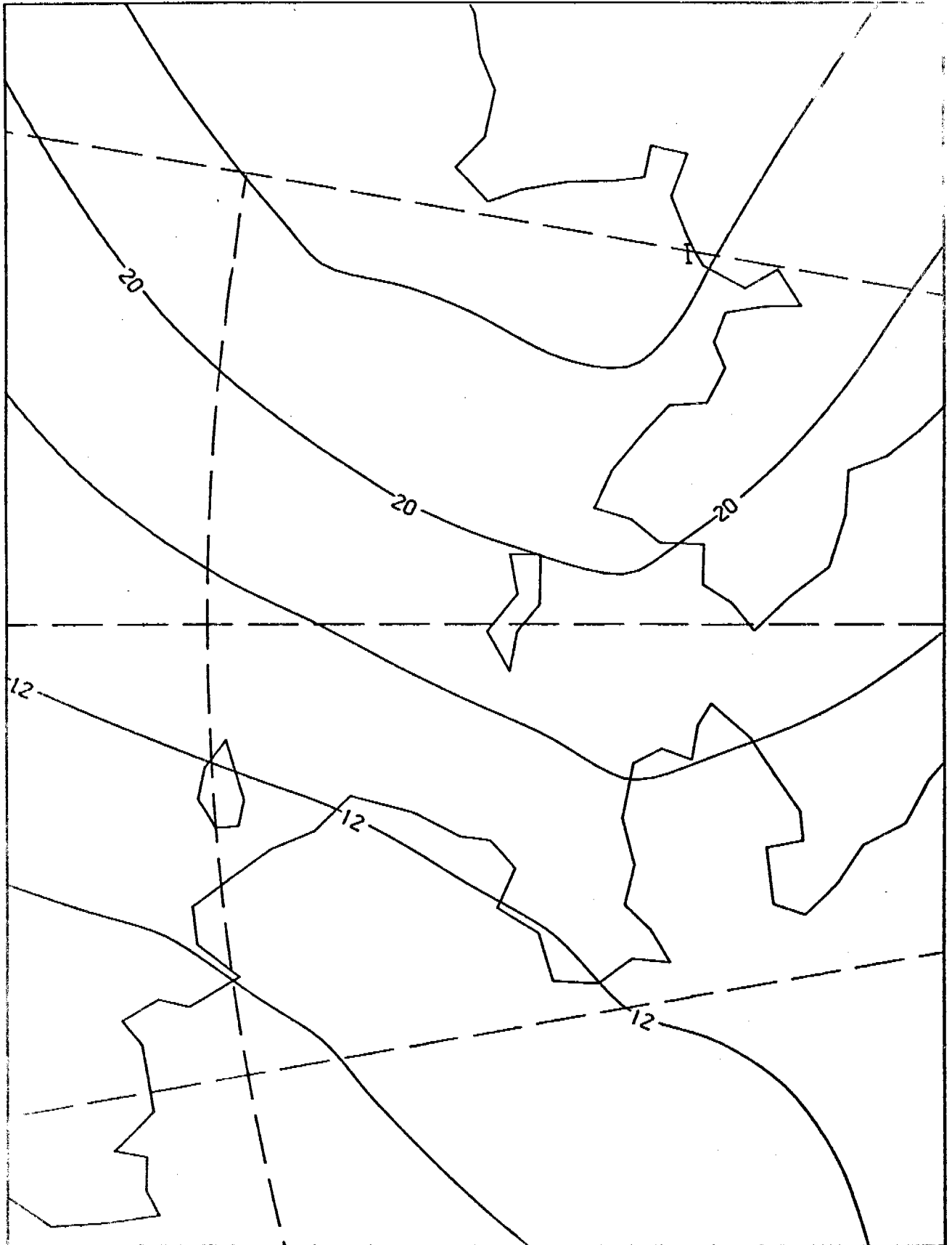
00Z 12 MAR 1955  
BERRY (354)

OBSERVED SLP



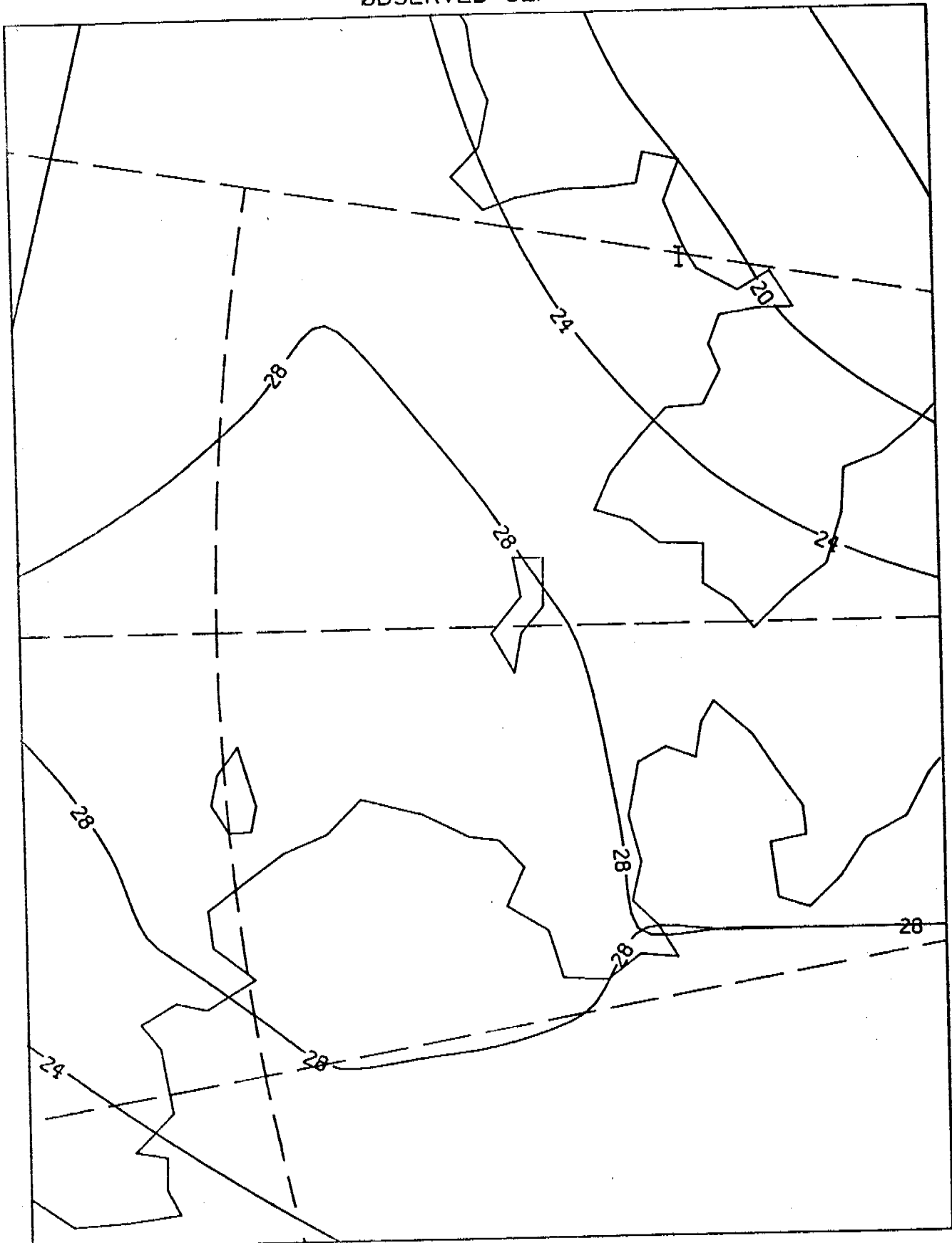
00Z 16 JUL 1966  
BERRY (355)

OBSERVED SLP



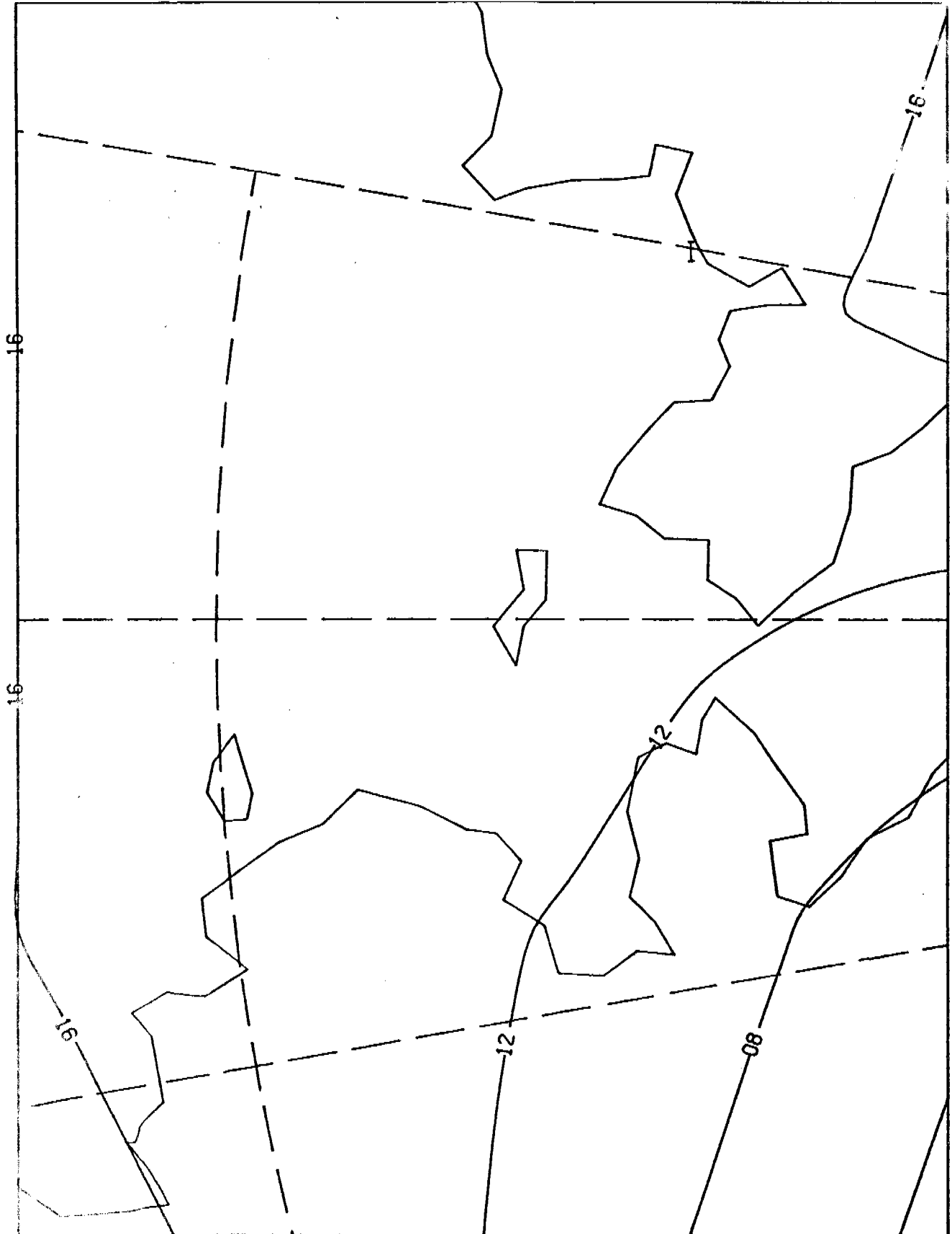
00Z 26 SEP 1957  
BERRY (356)

ØBSERVED SLP



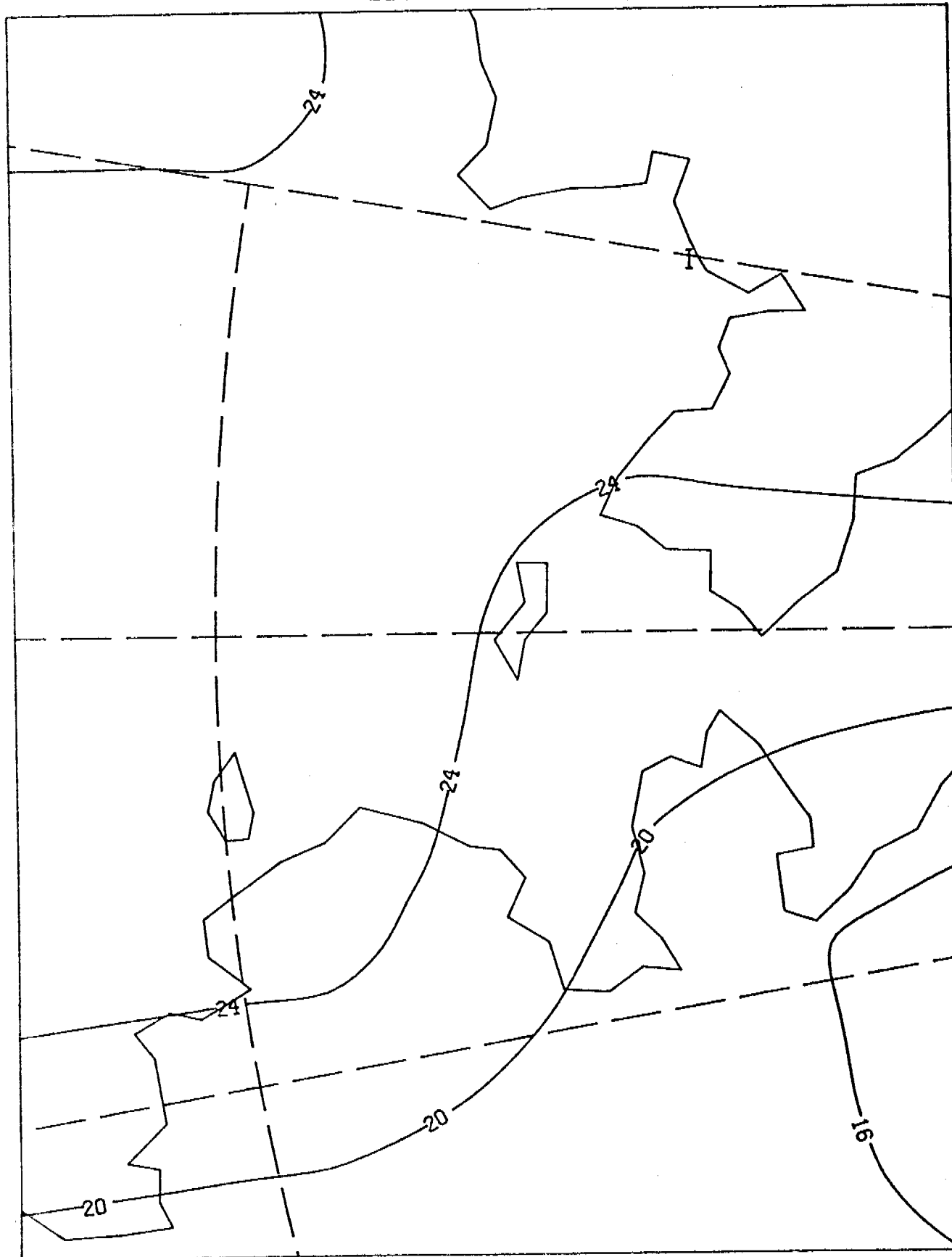
00Z 17 APR 1948  
BERRY (357)

ØBSERVED SLP



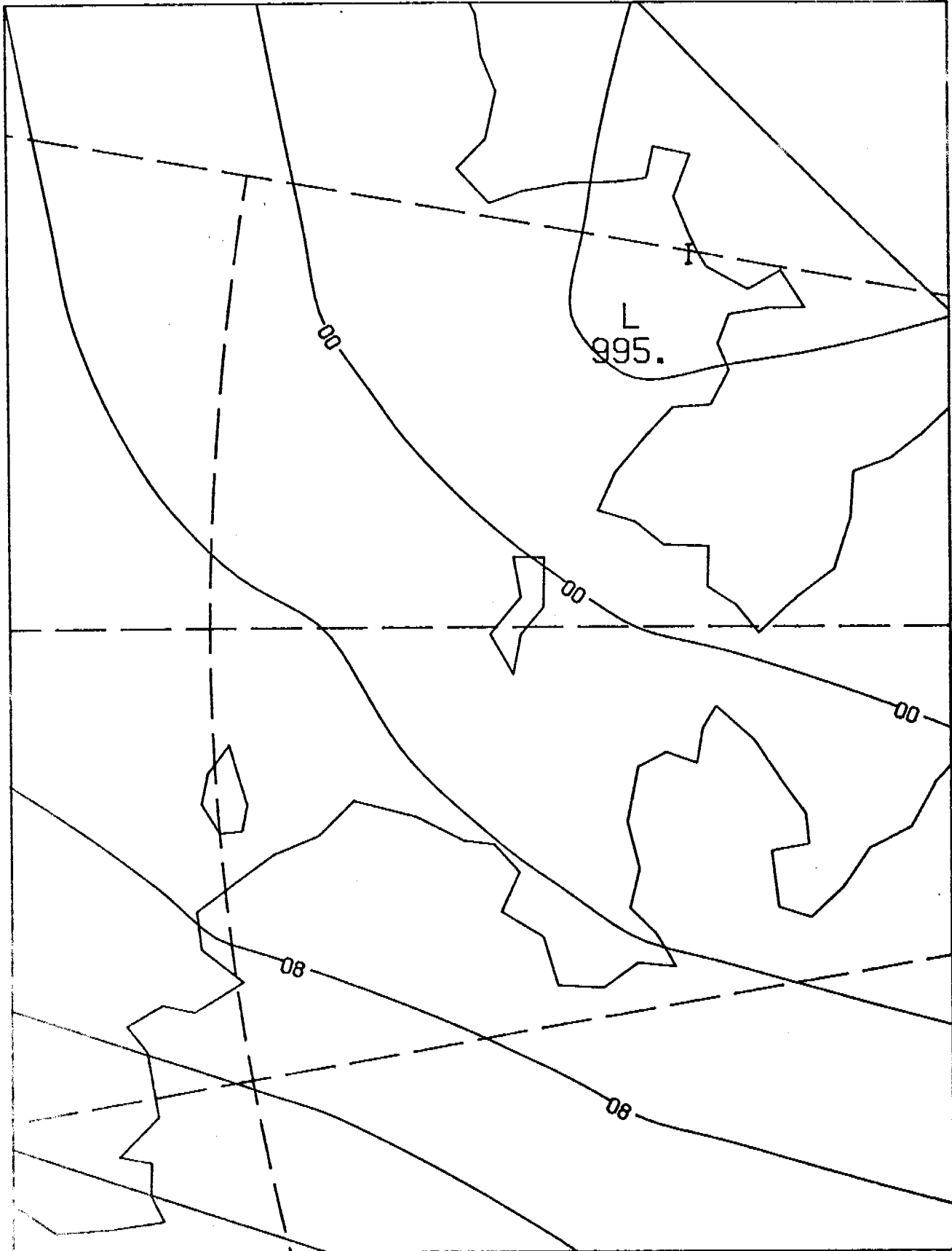
00Z 28 AUG 1948  
BERRY (358)

OBSERVED SLP



00Z 4 FEB 1955  
BERRY (35-9)

OBSERVED SLP

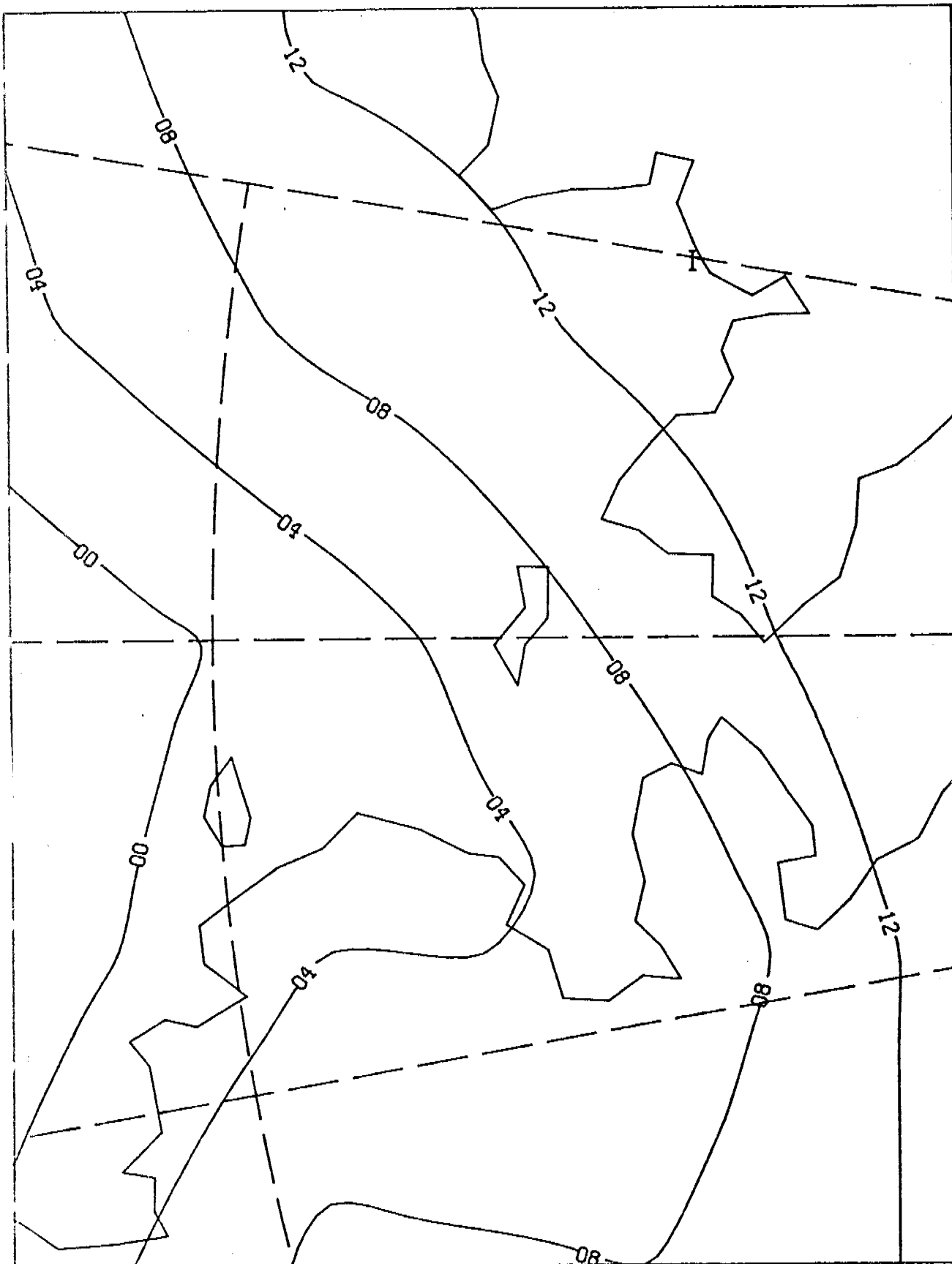


00Z 8 SEP 1946

BERRY (360)

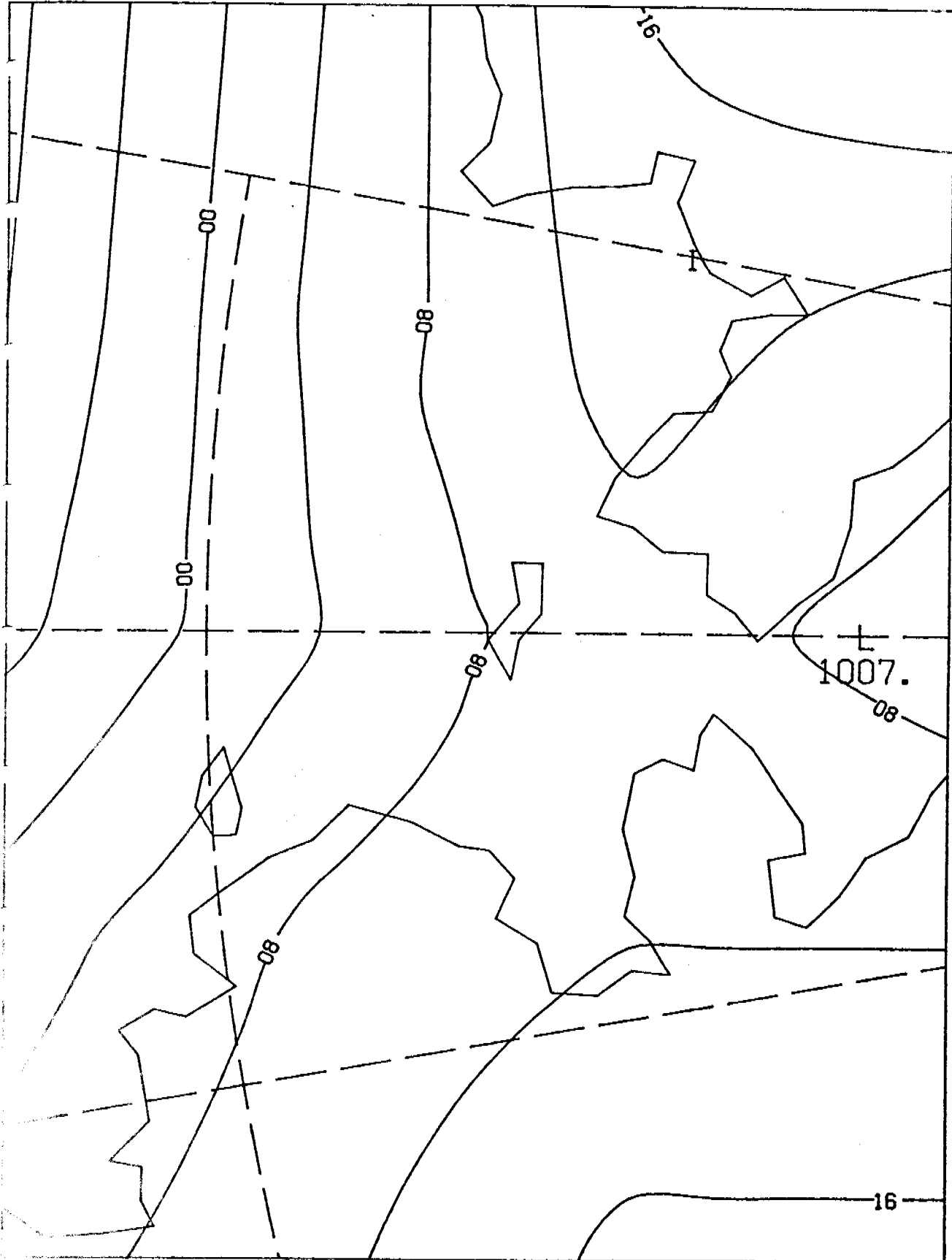


OBSERVED SLP



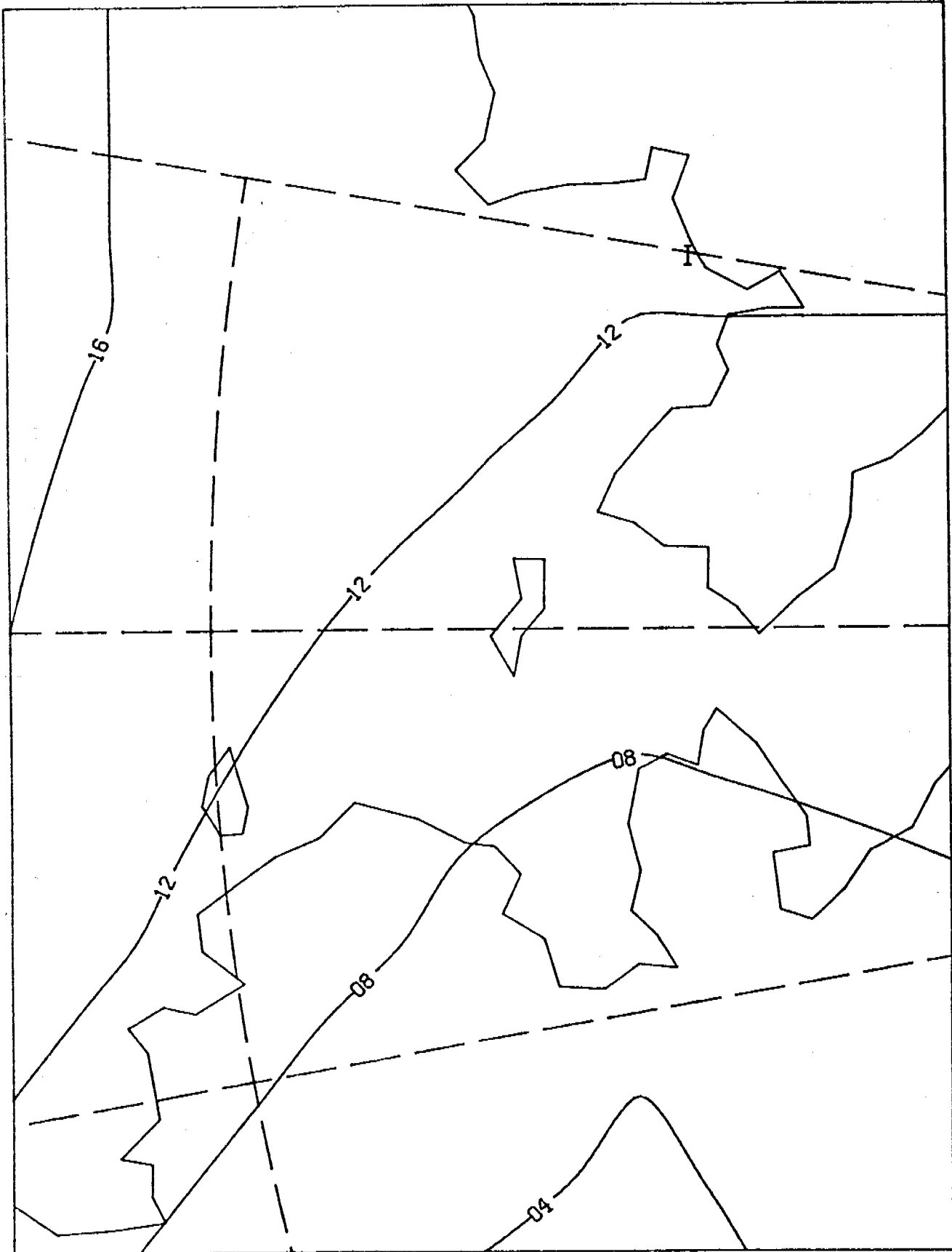
00Z 16 JUN 1969  
BERRY (361)

OBSERVED SLP



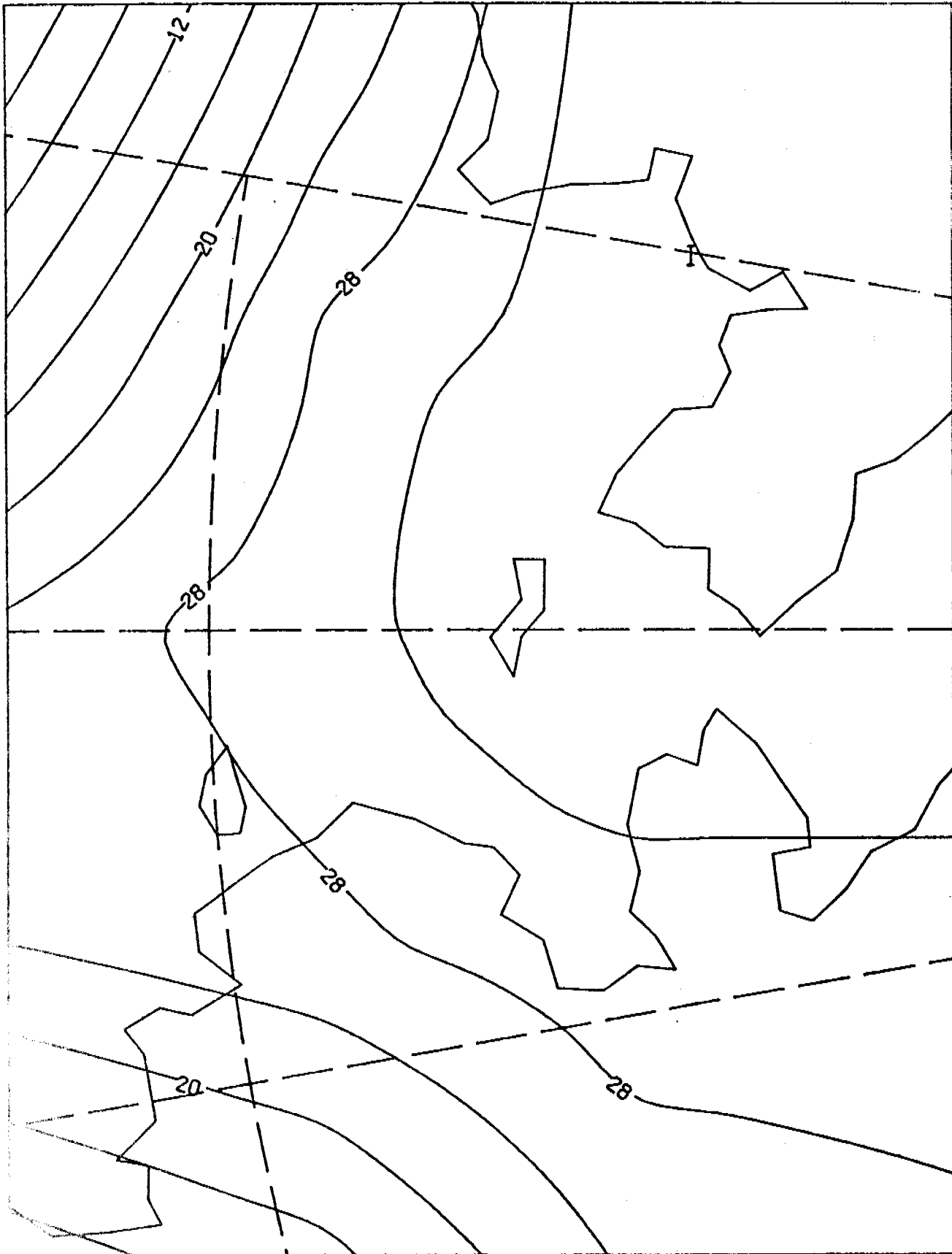
00Z 19 DEC 1966  
BERRY (3 2)

OBSERVED SLP



00Z 16 JUN 1960  
BERRY (363)

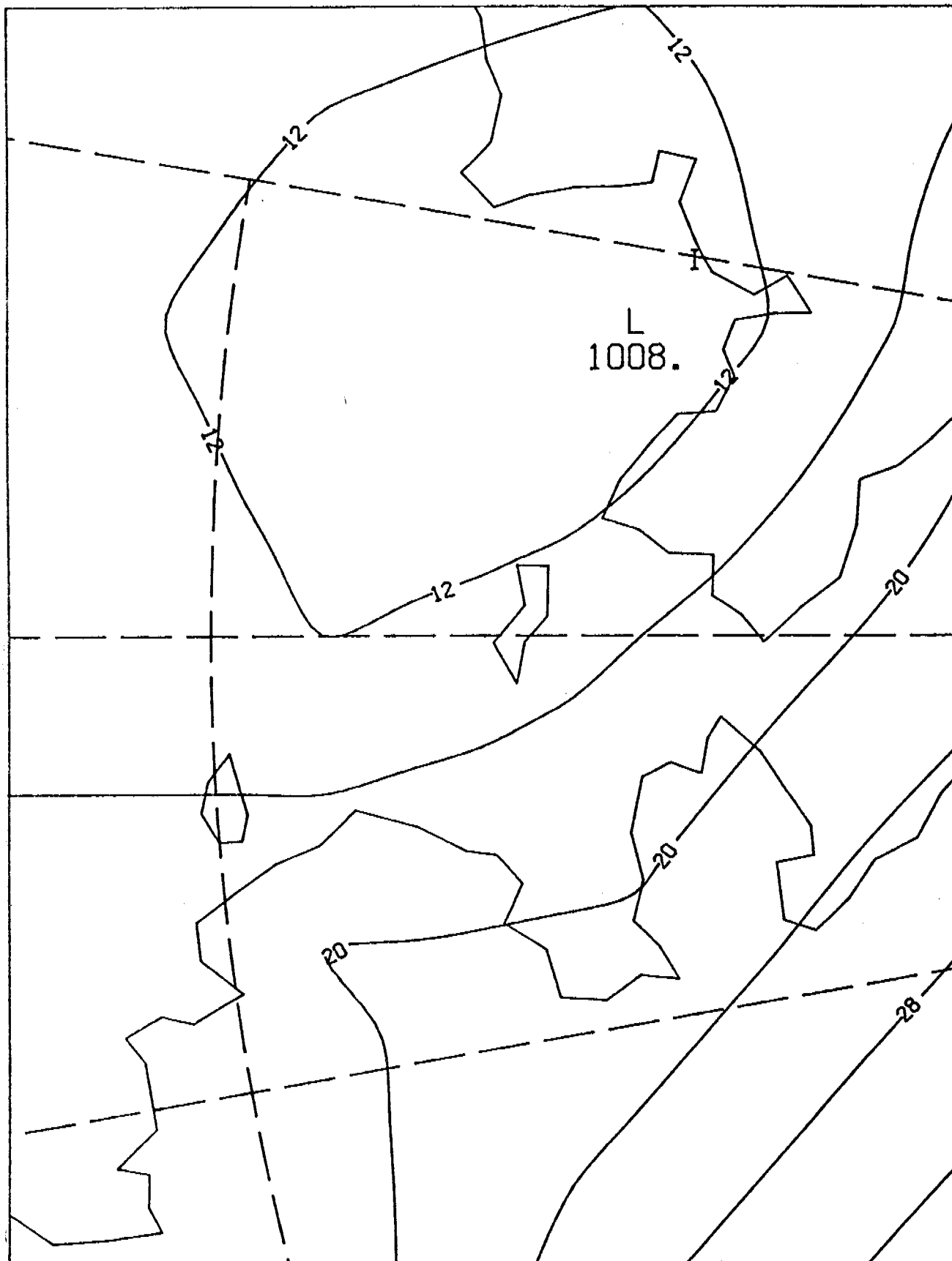
OBSERVED SLP



00Z 4 MAR 1956

BERRY 364

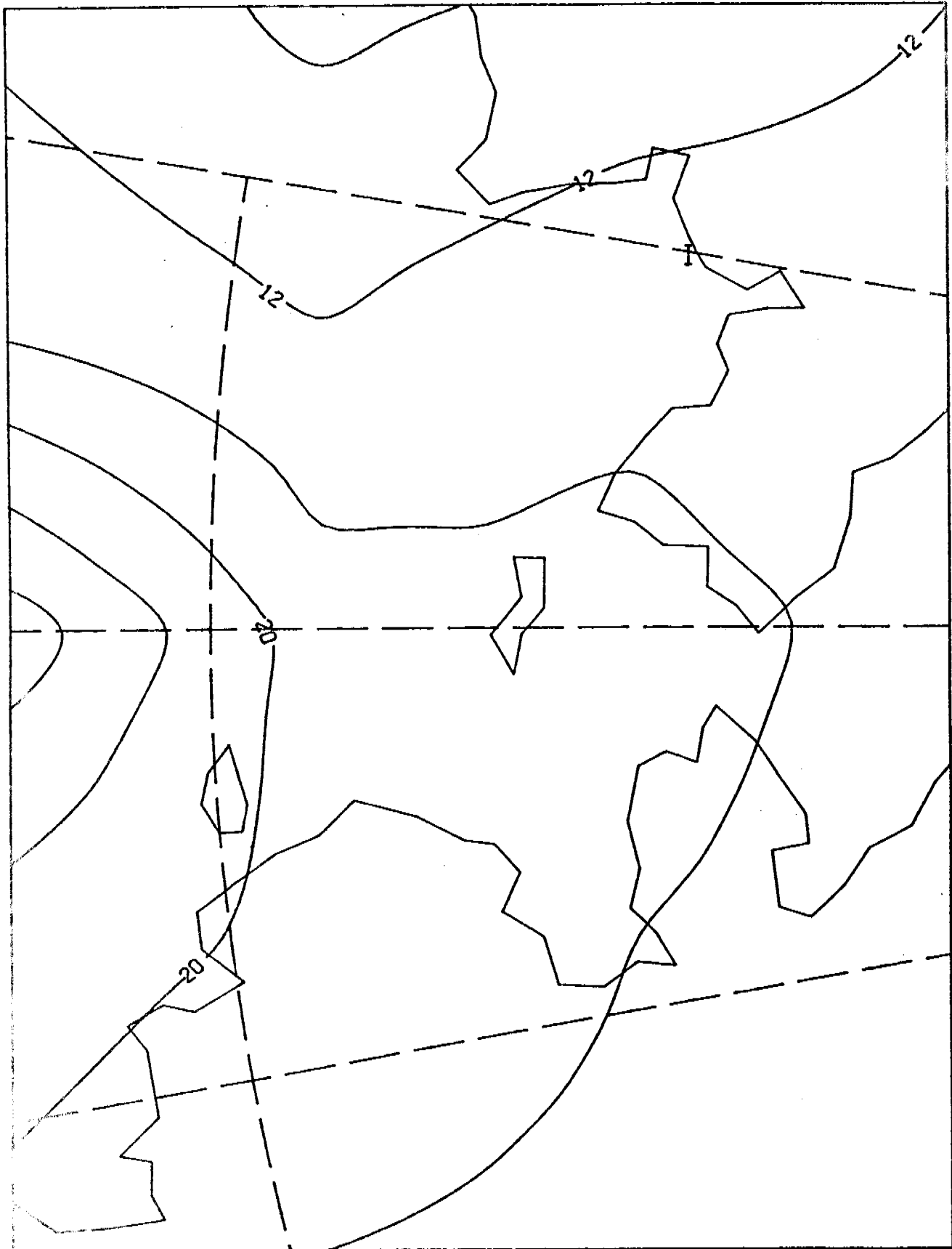
ØBSERVED SLP



00Z 26 DEC 1968

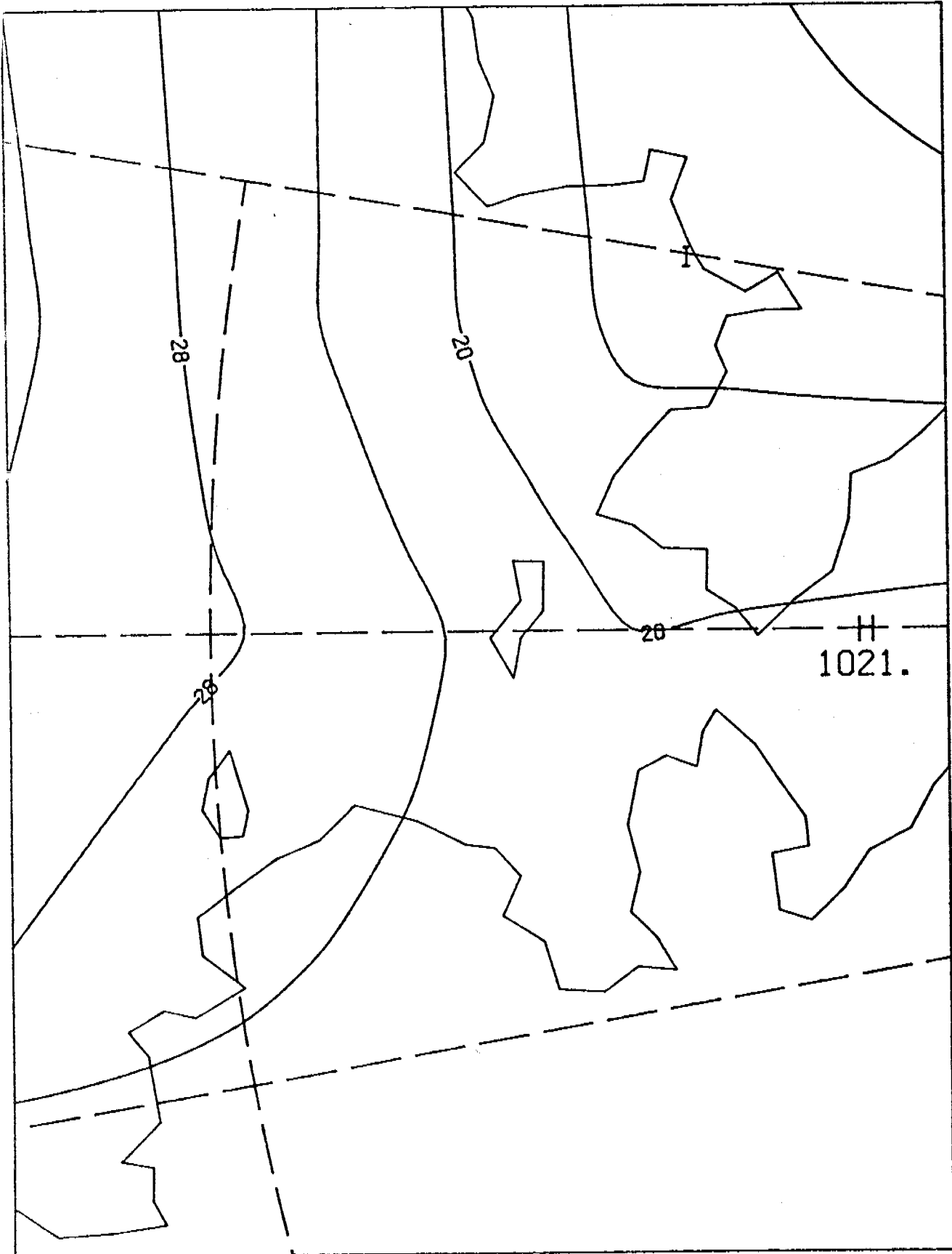
BERRY 365

OBSERVED SLP



00Z 19 JUL 1963  
BERRY 346

ØBSERVED SLP

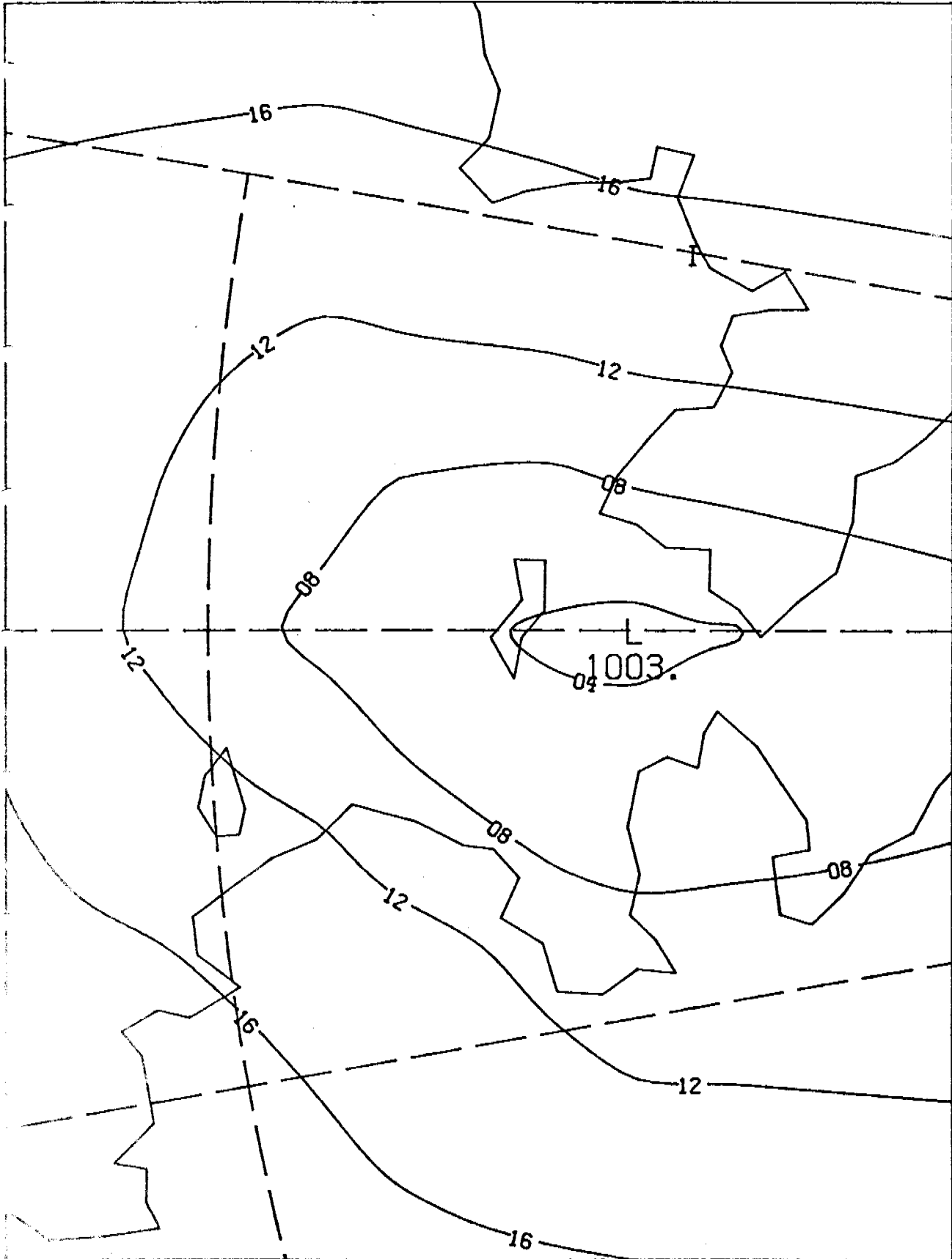


00Z 17 ØCT 1964

BERRY

367

OBSERVED SLP

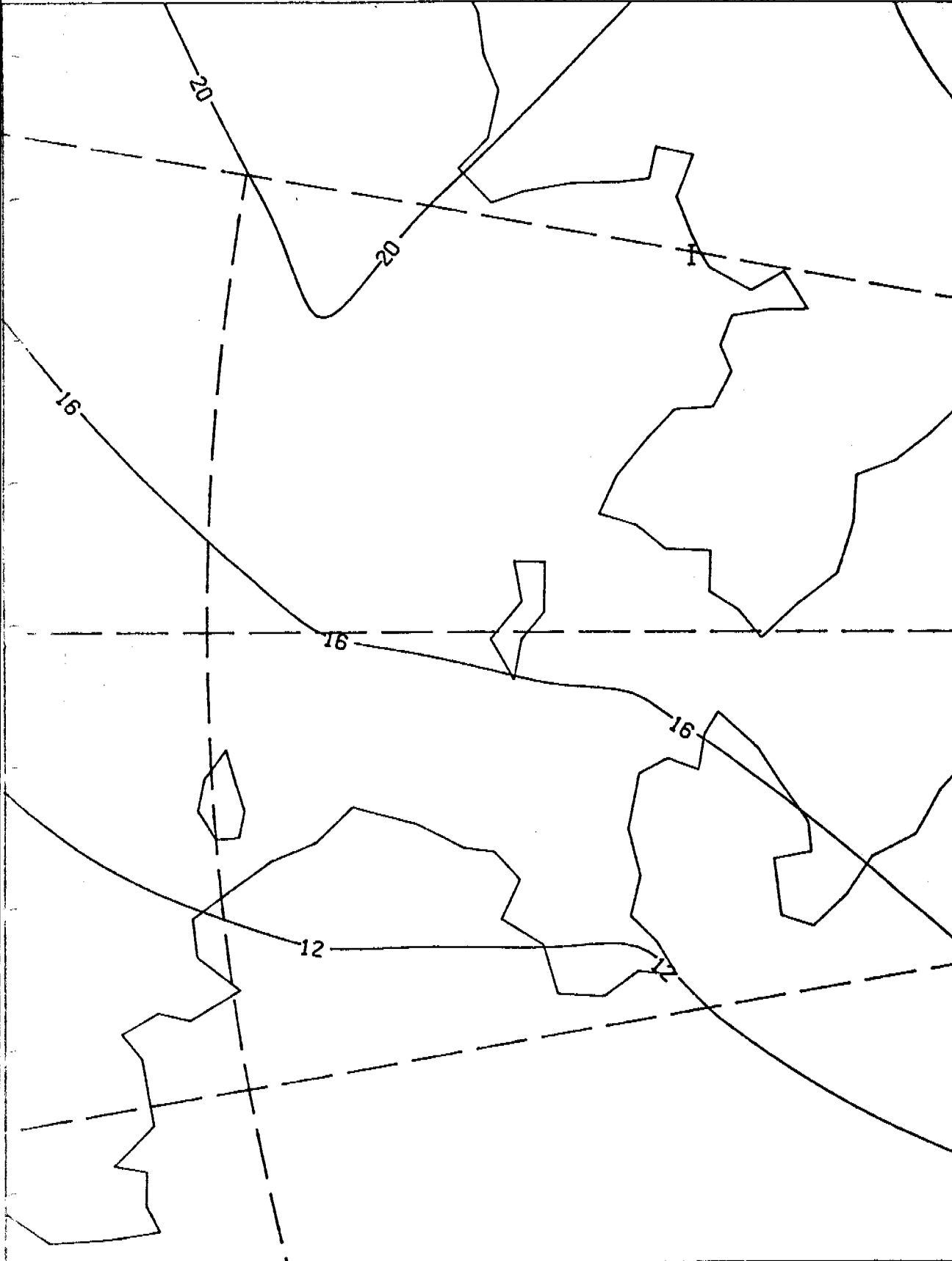


00Z 24 APR 1959

BERRY 368

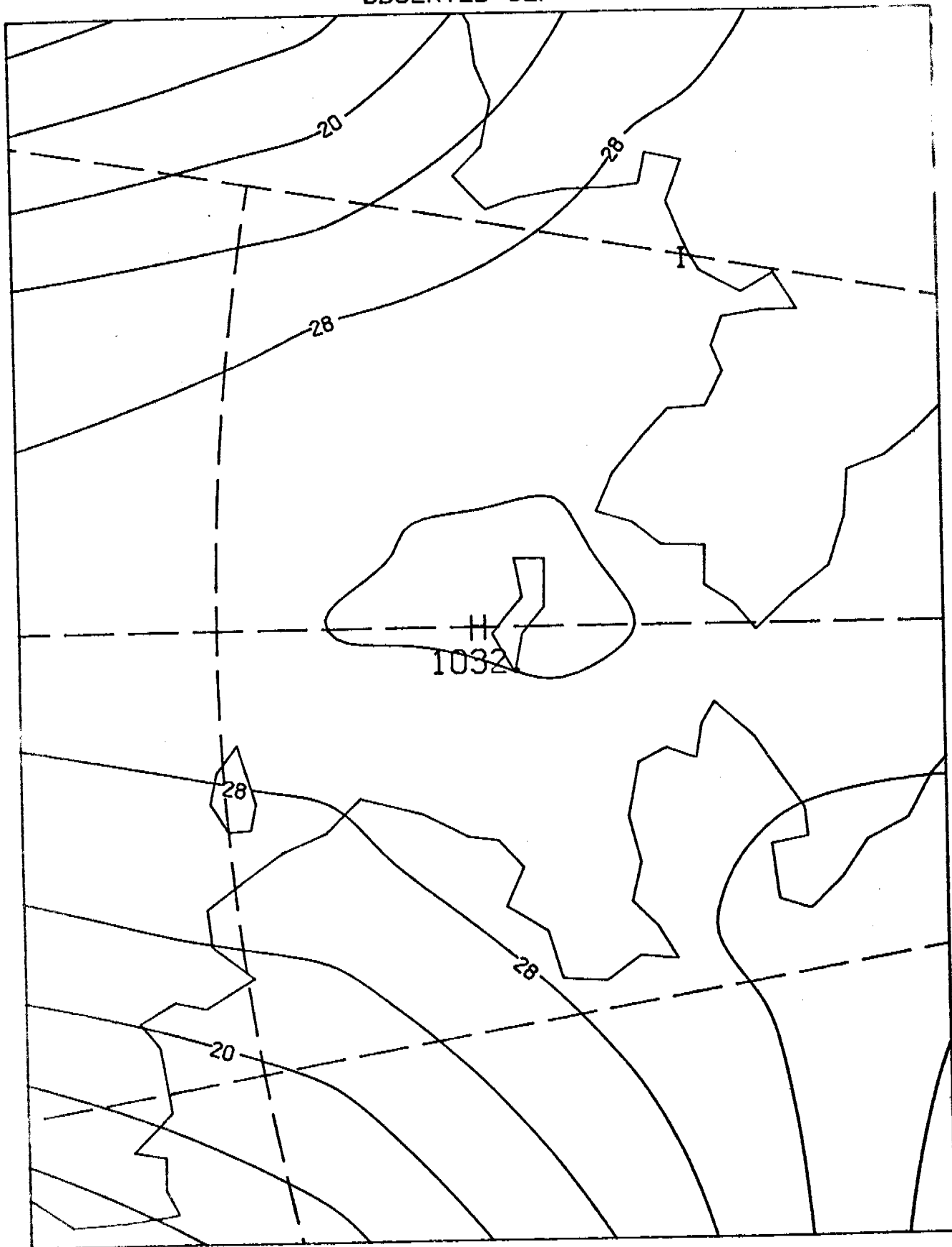


ØBSERVED SLP



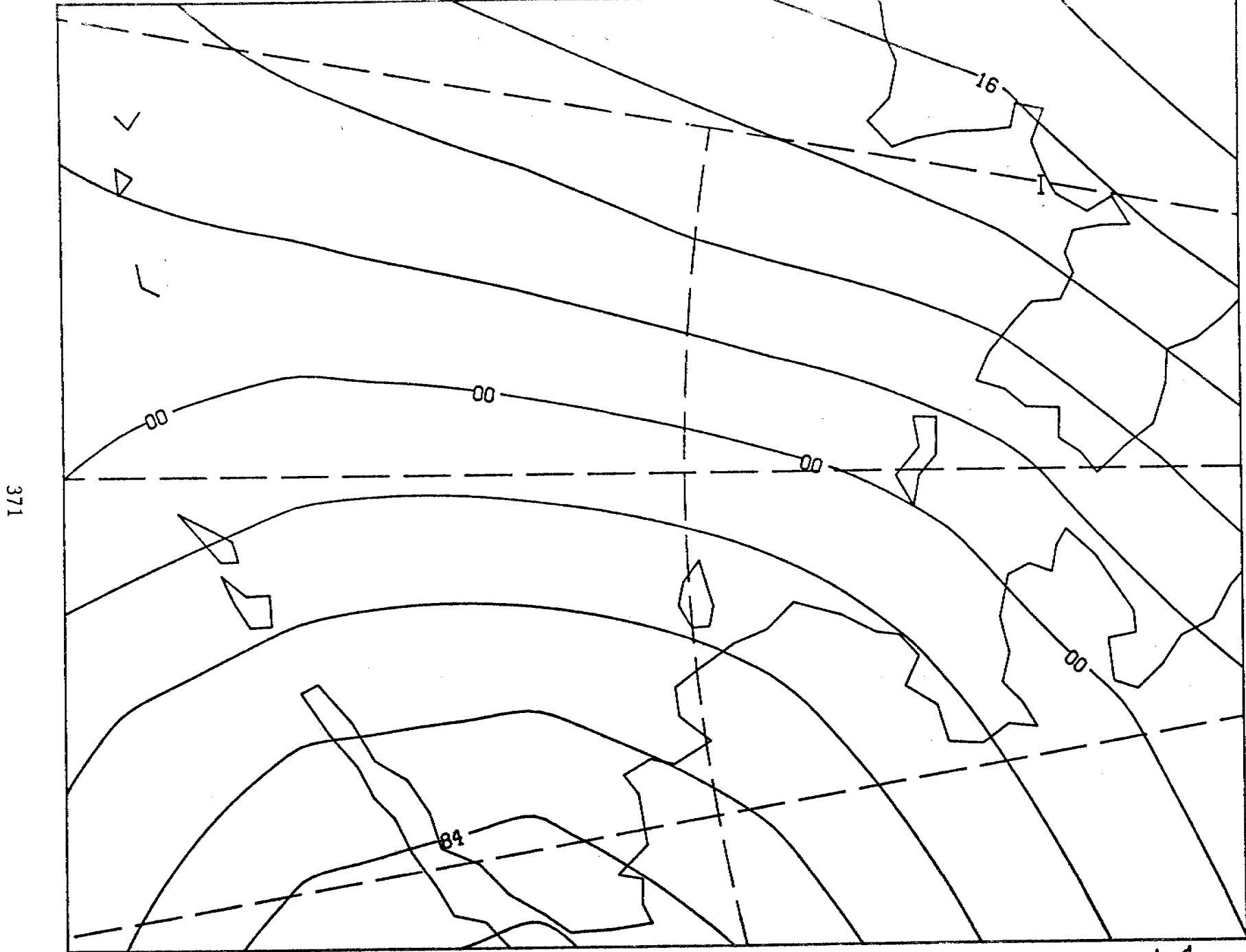
00Z 7 JUN 1970  
BERRY 309

OBSERVED SLP



00Z 1 JAN 1956

BERRY 320

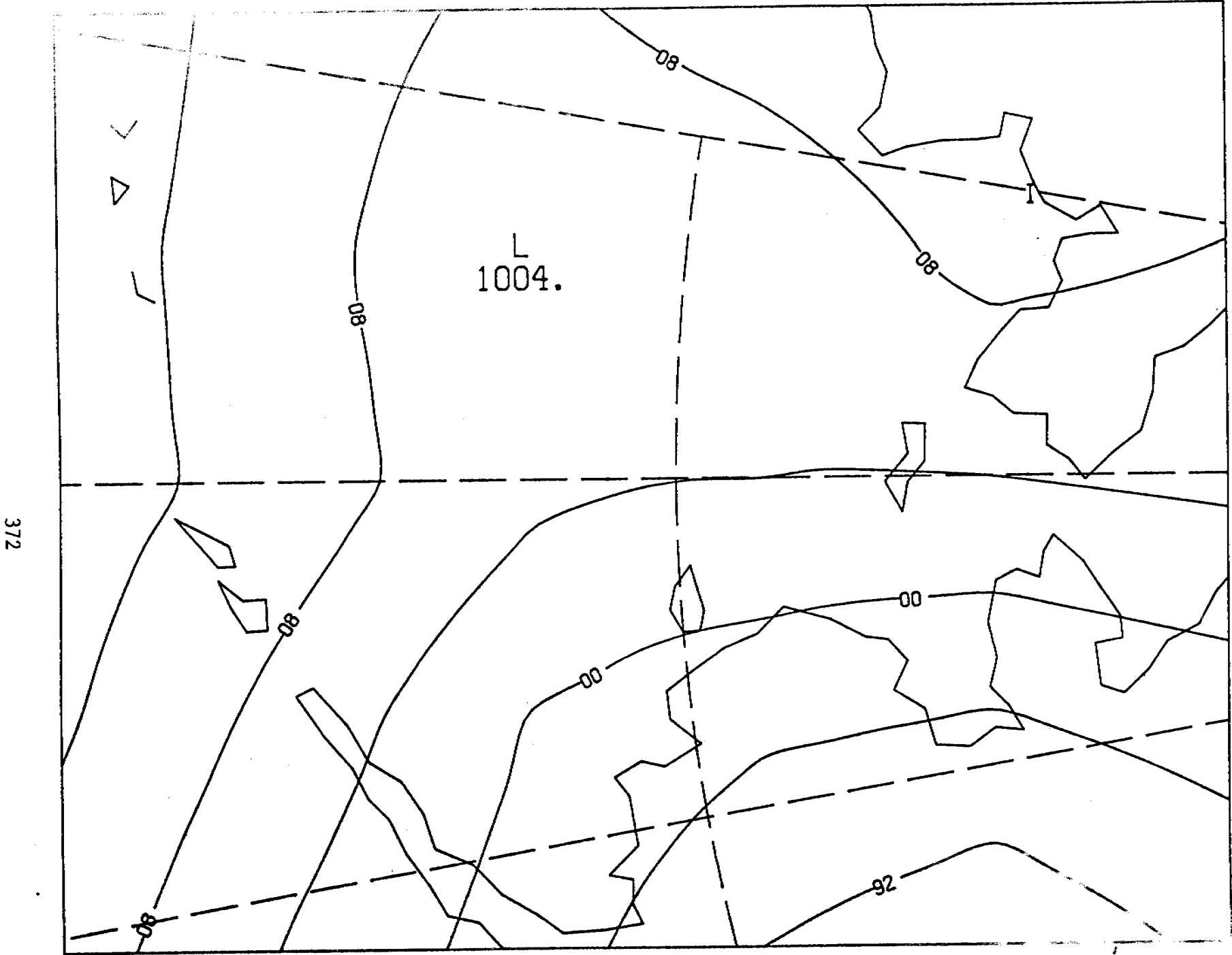


371

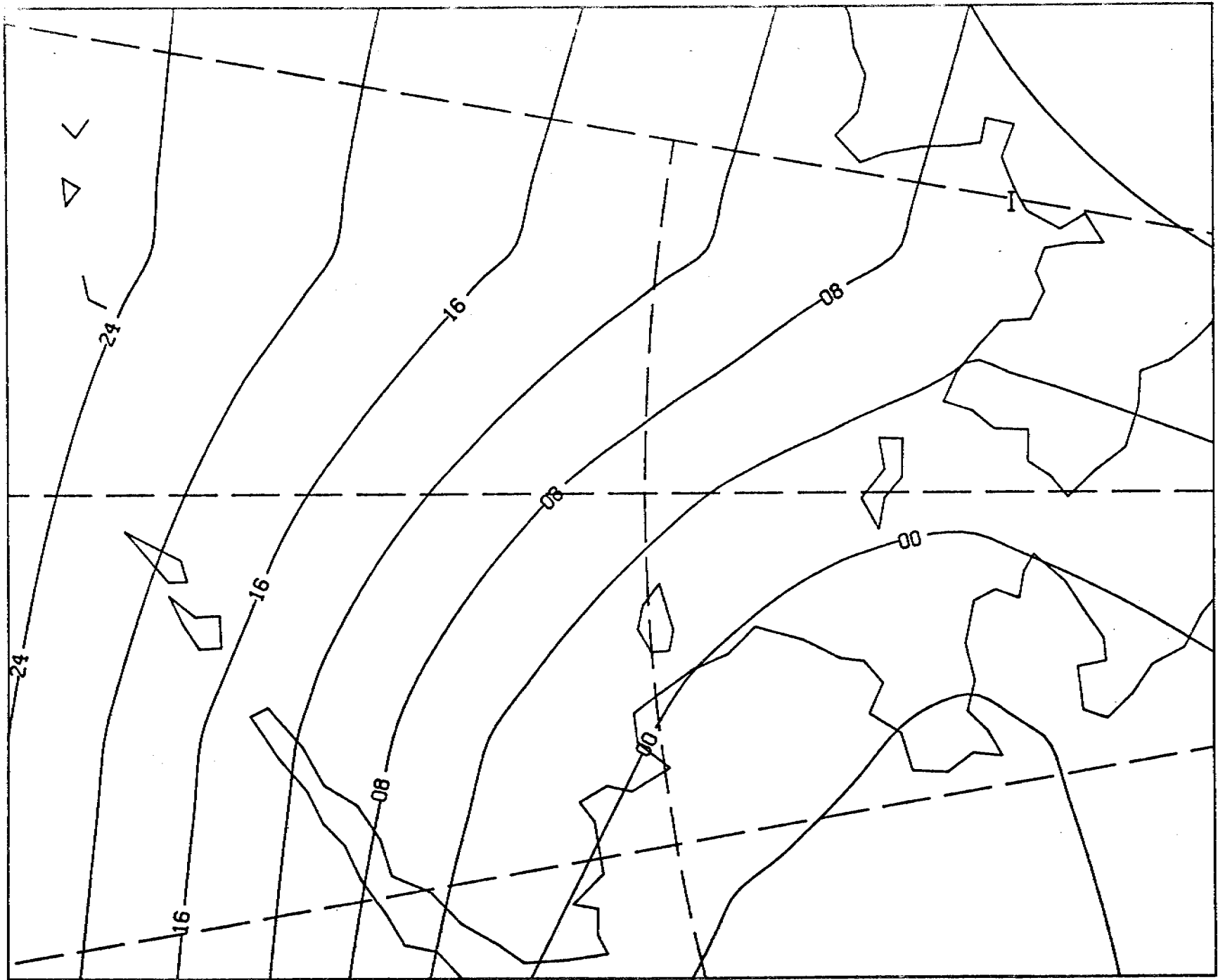
12Z 20 DEC 1958  
PUTNIN

A, Ac

OBSERVED SET



12Z 11 SEP 1947  
PUTNIN



373

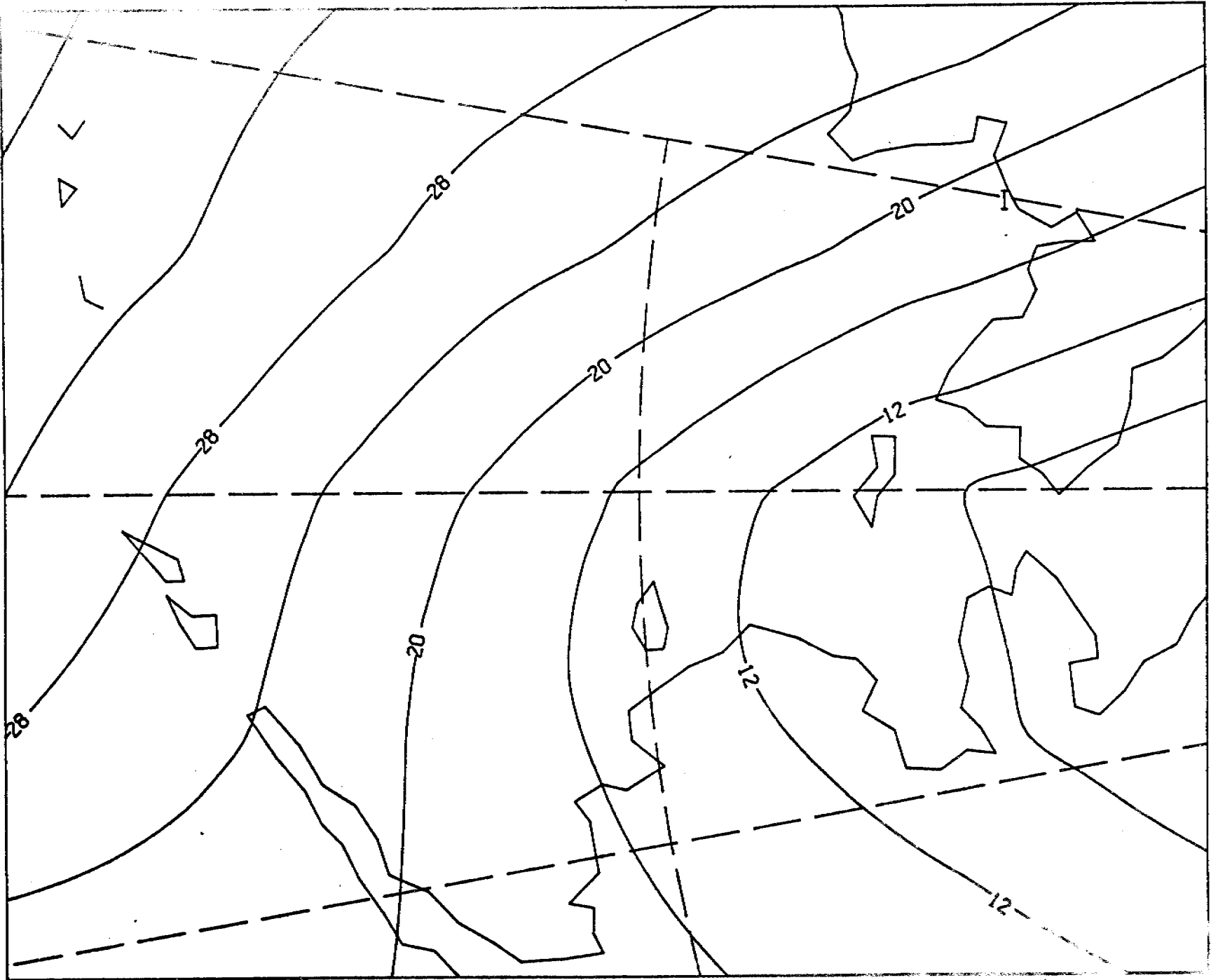
12Z 8 OCT 1946

PUTNIN

A''

OBSERVED SLP

374

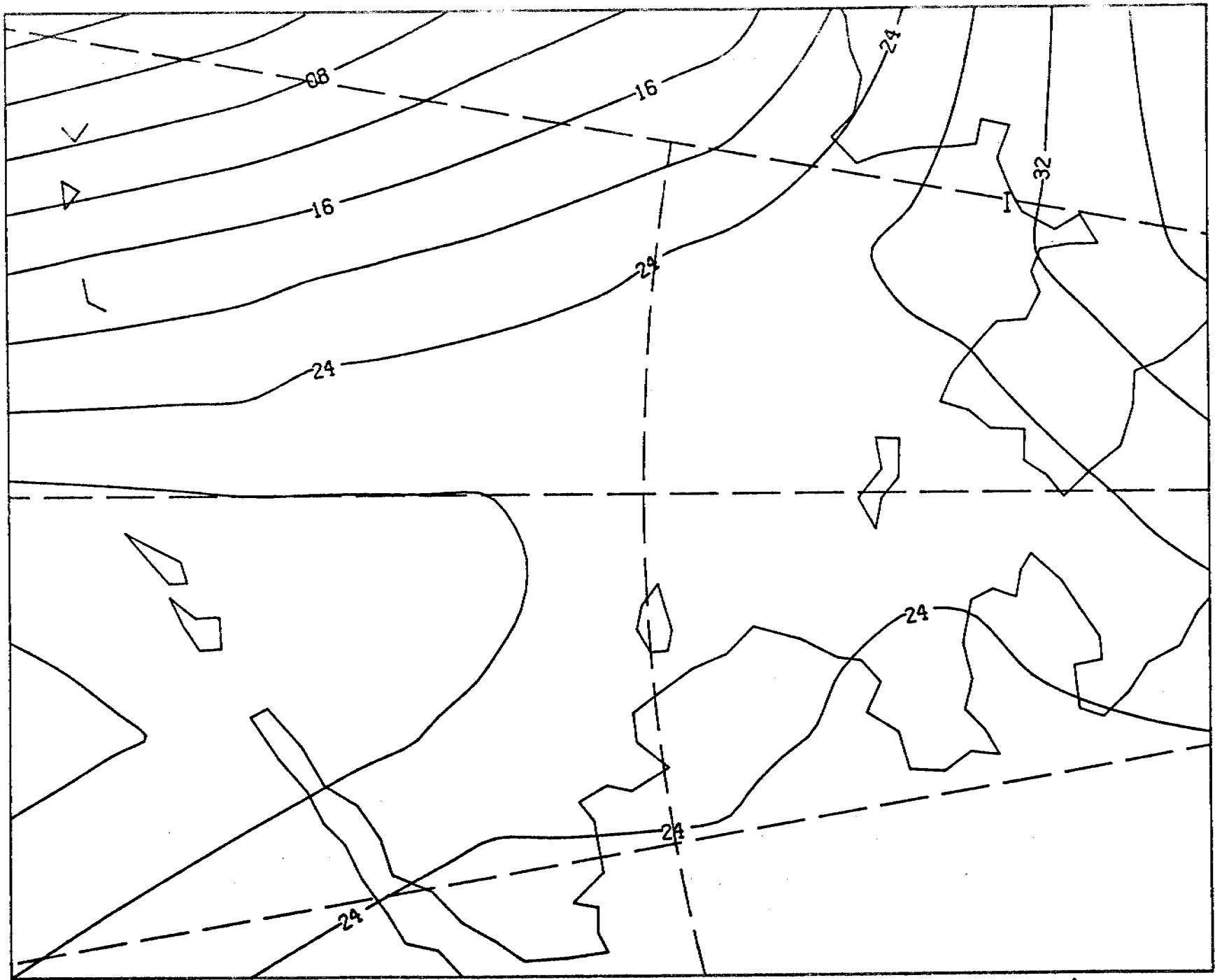


12Z 11 NOV 1950

PLTNN

A'''

375

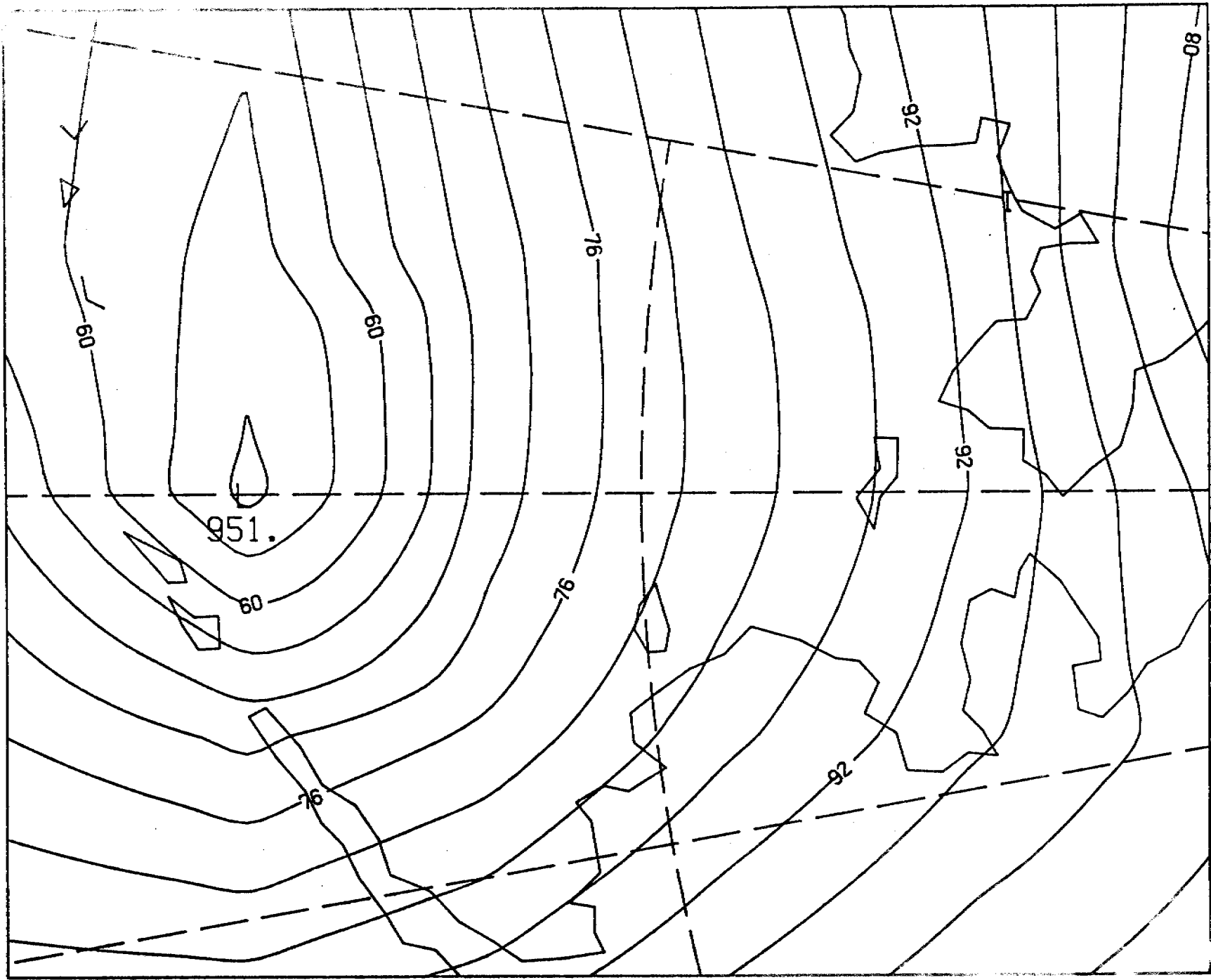


12Z 30 DEC 1958  
PUTNIN

A<sub>1</sub>

OBSERVED SLP

376



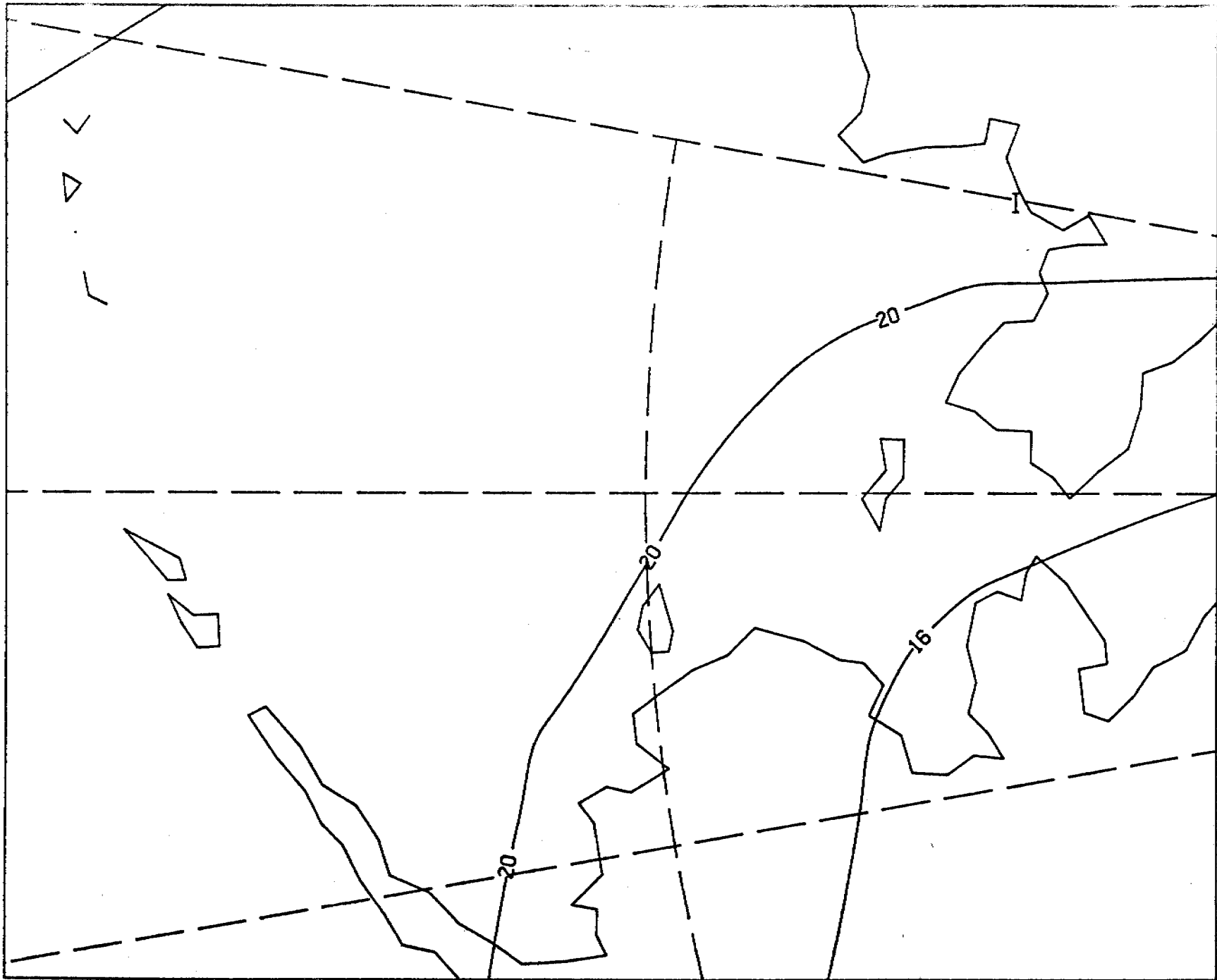
12Z 4 JAN 1958

PUNIN

A<sub>2</sub>



377

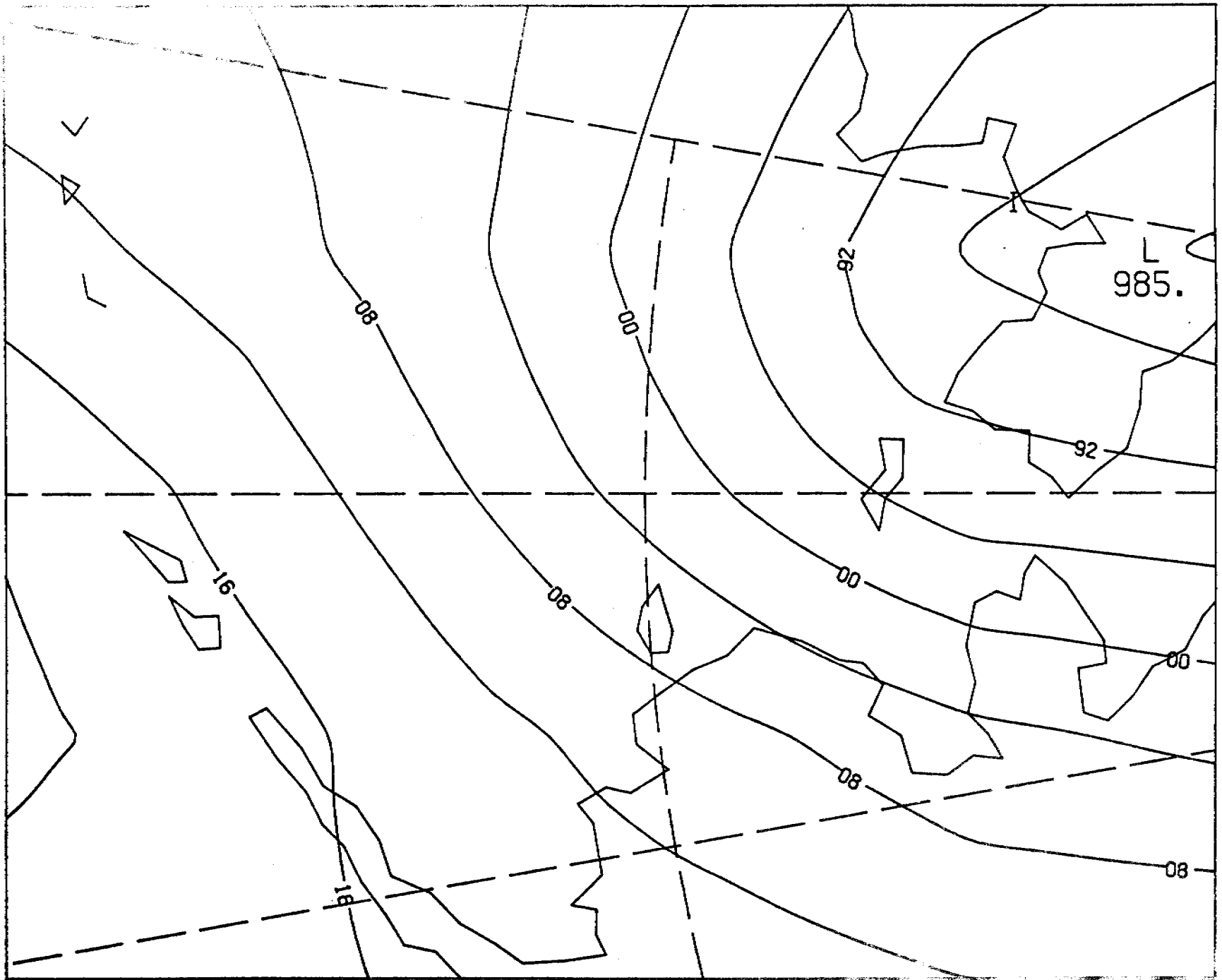


12Z 27 SEP 1958  
PUTNIN

A3

OBSERVED SLP

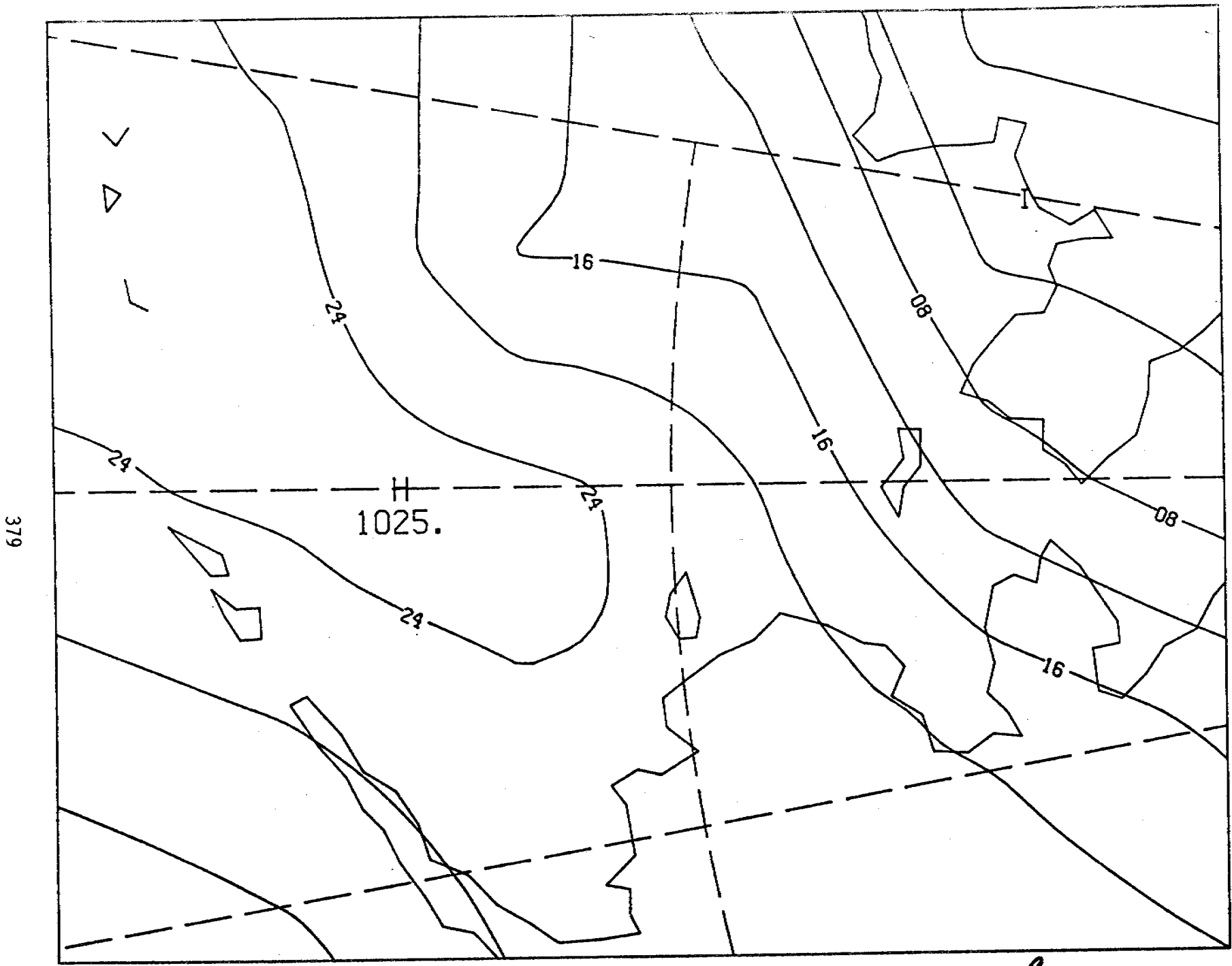
378



12Z 26 OCT 1952

PLITNIN

OBSERVED SLP

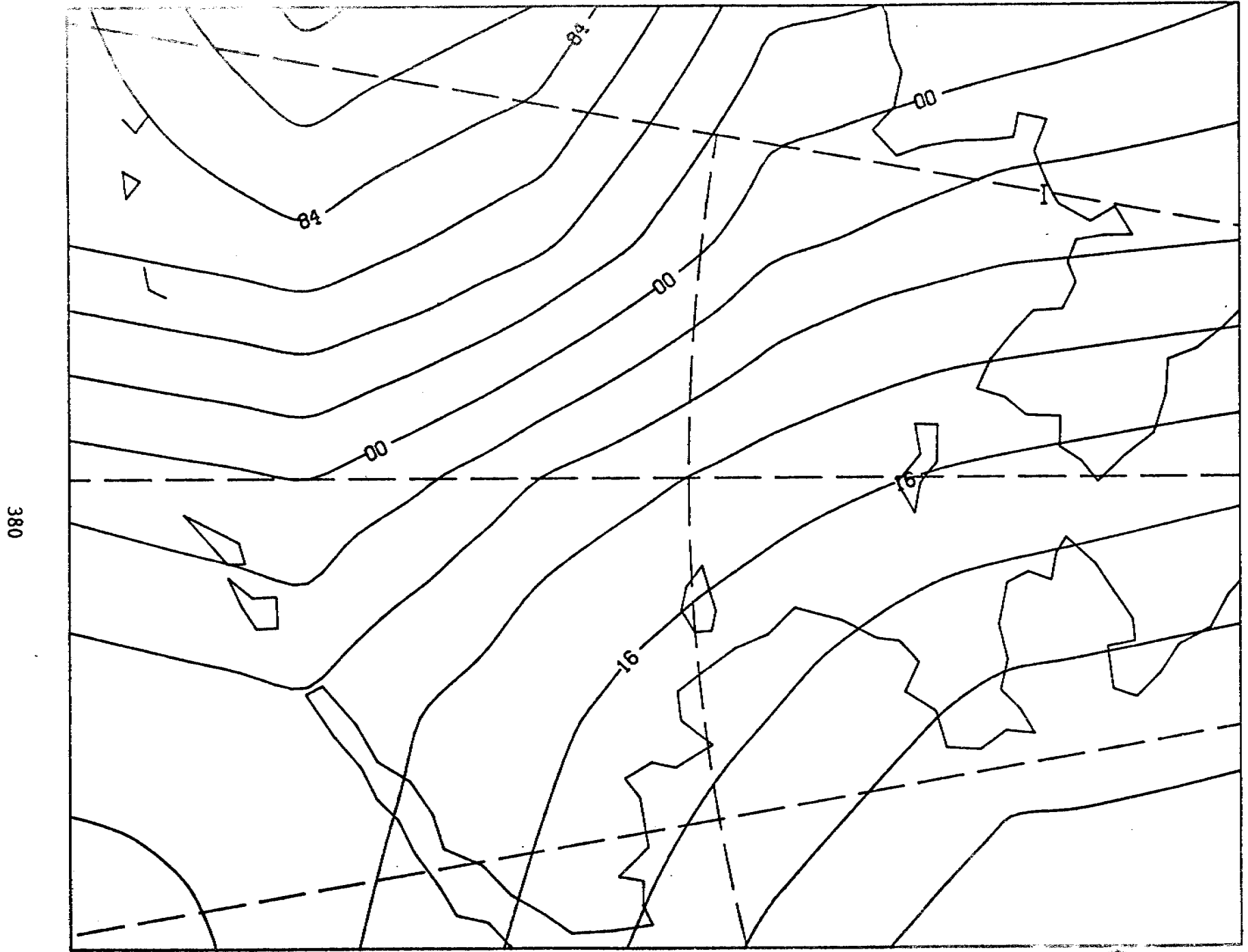


12Z 22 APR 1945

PUTNIN

e

OBSERVED SLP

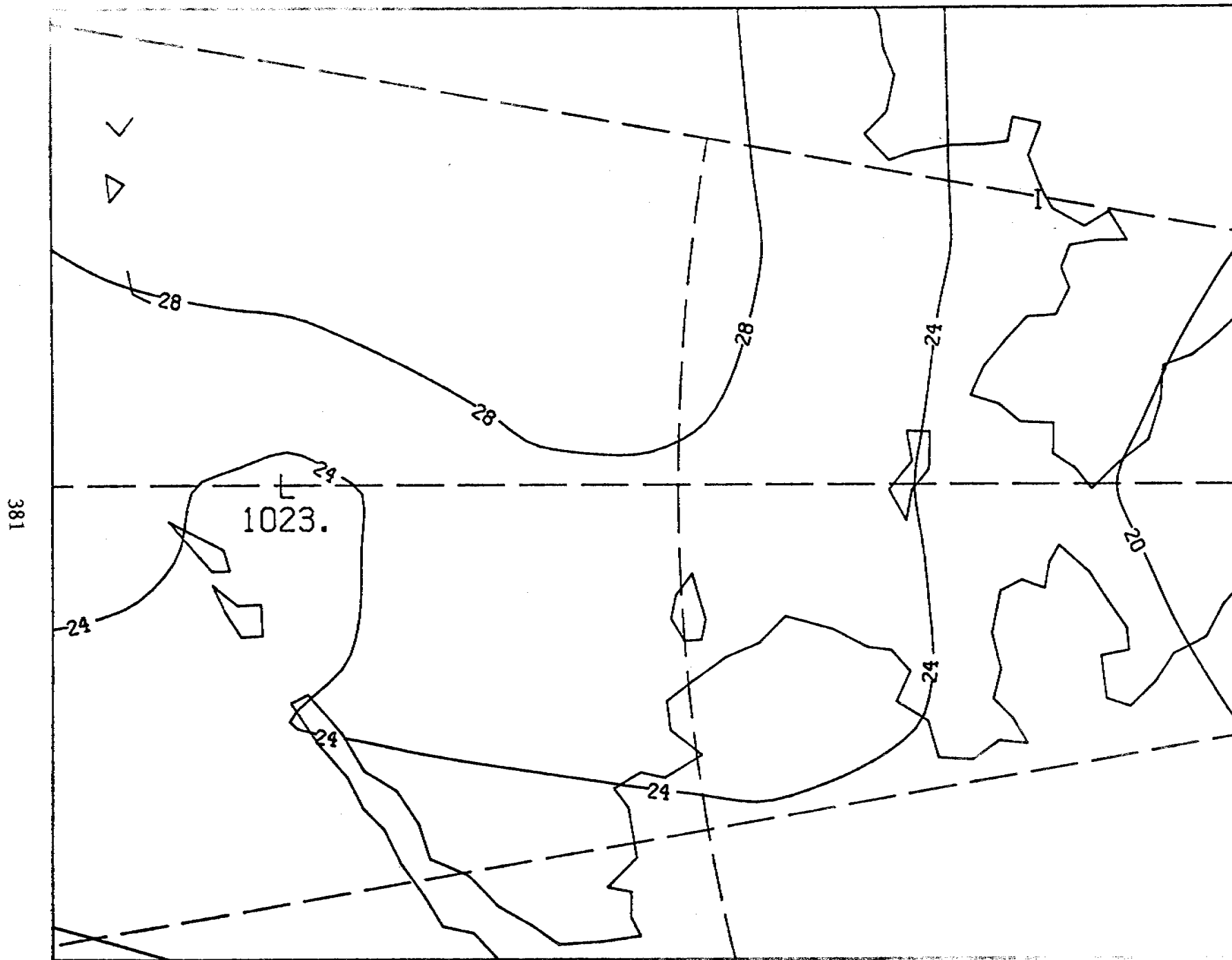


12Z 5 DEC 1958

PUTNIN

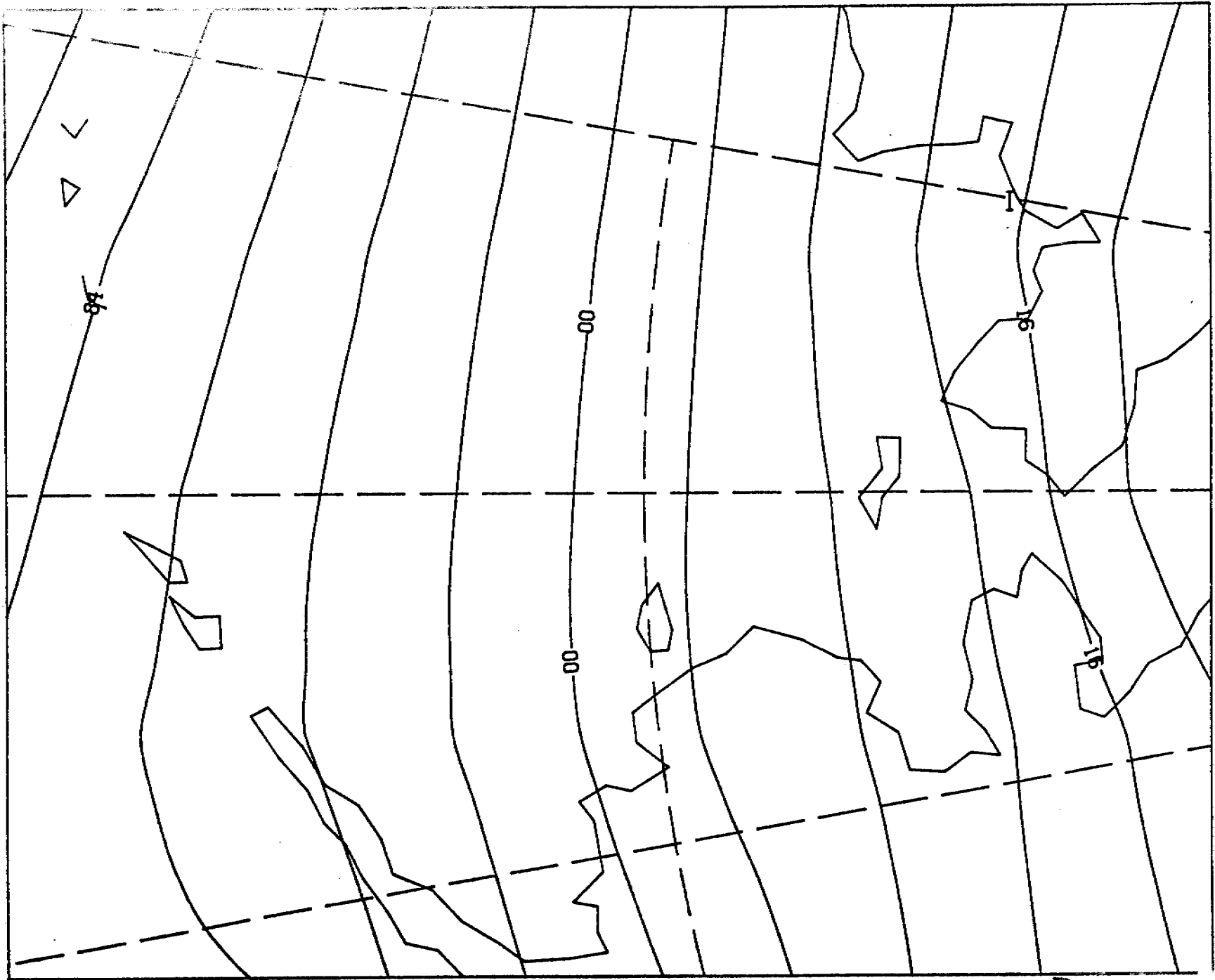
*D*

OBSERVED SET



20Z 21 DEC 1955  
PUTNIN

ØBSERVED SLP

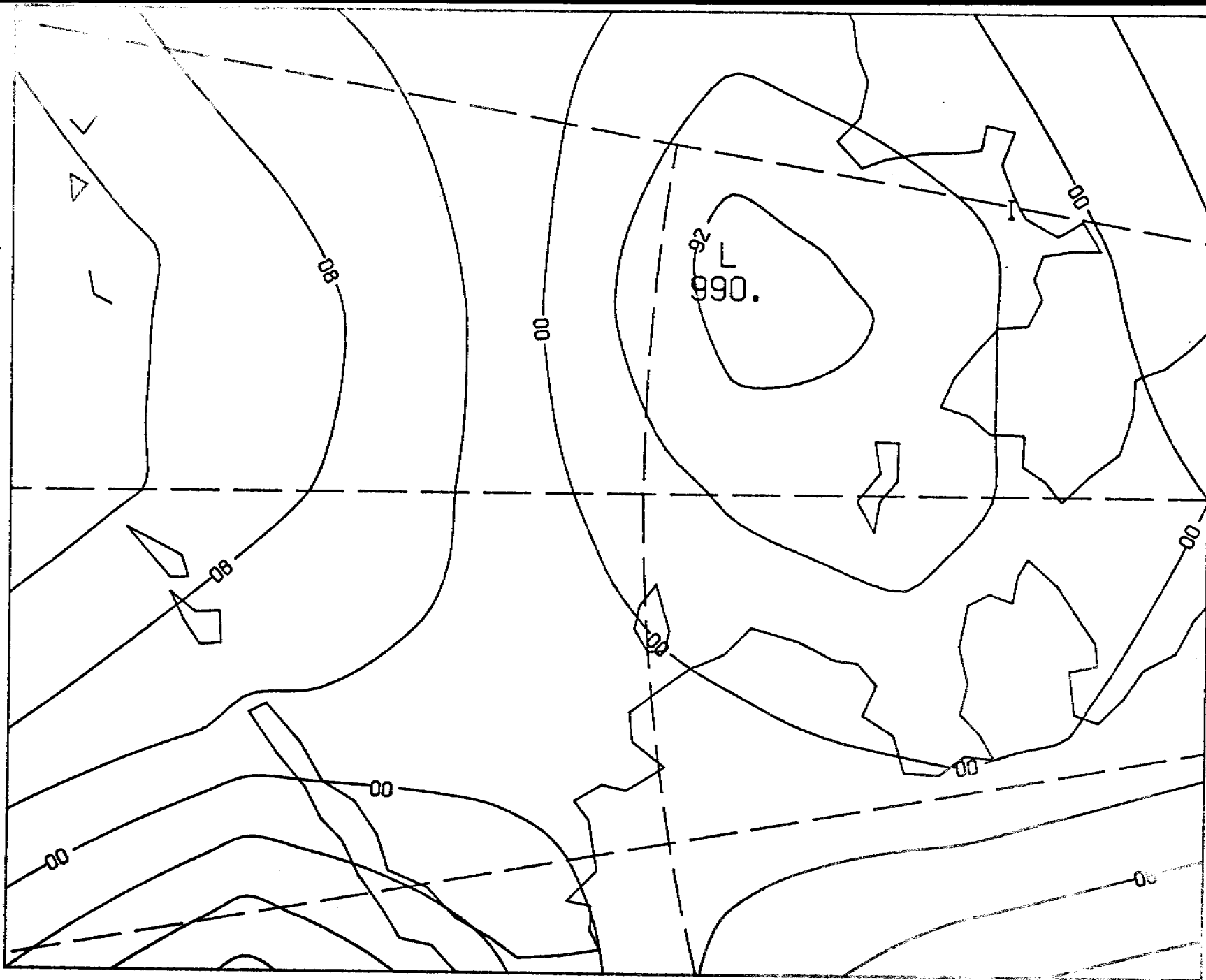


12Z 15 FEB 1958

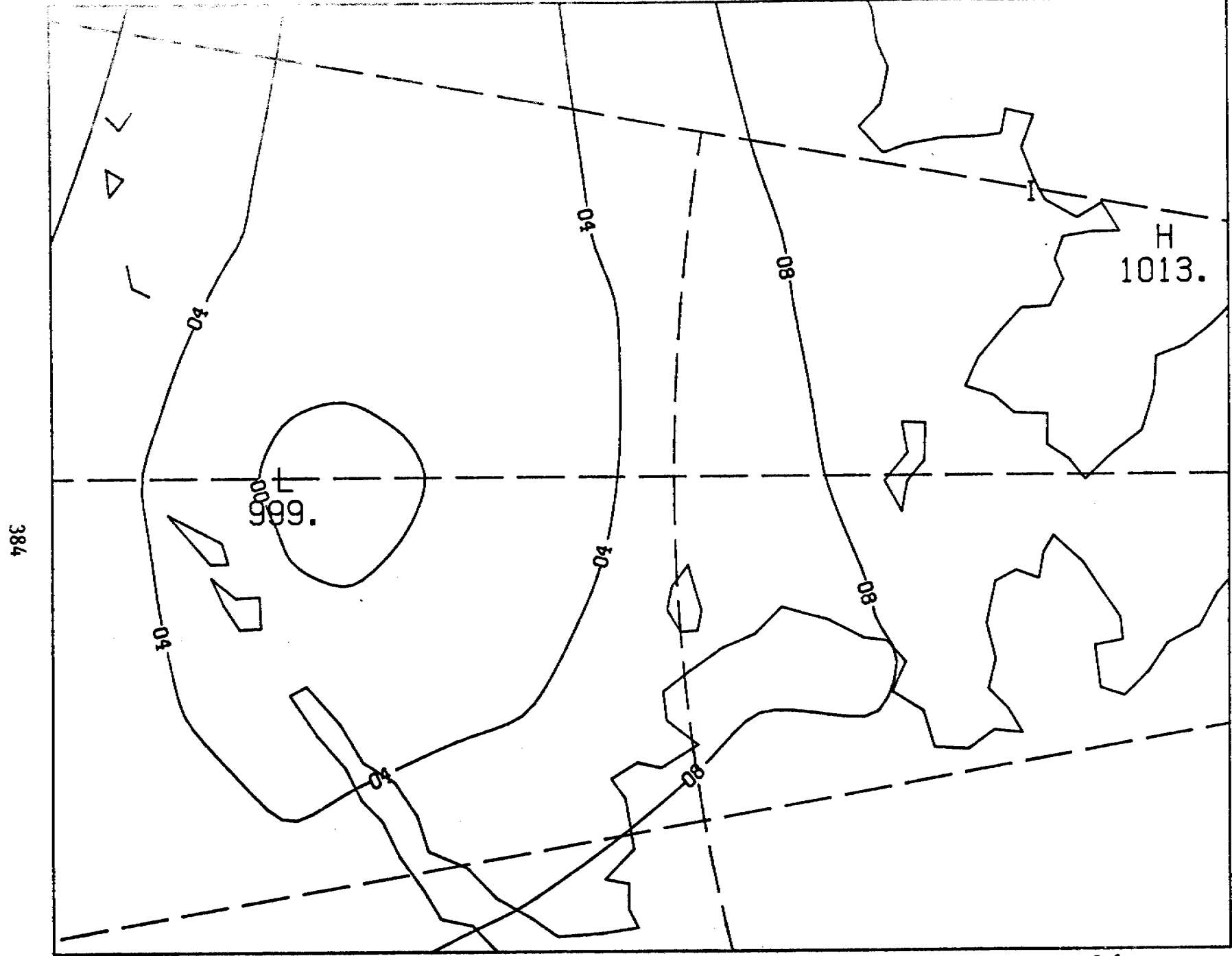
D<sub>i</sub>

382

383



12Z 15 NOV 1958  
PUTNIN



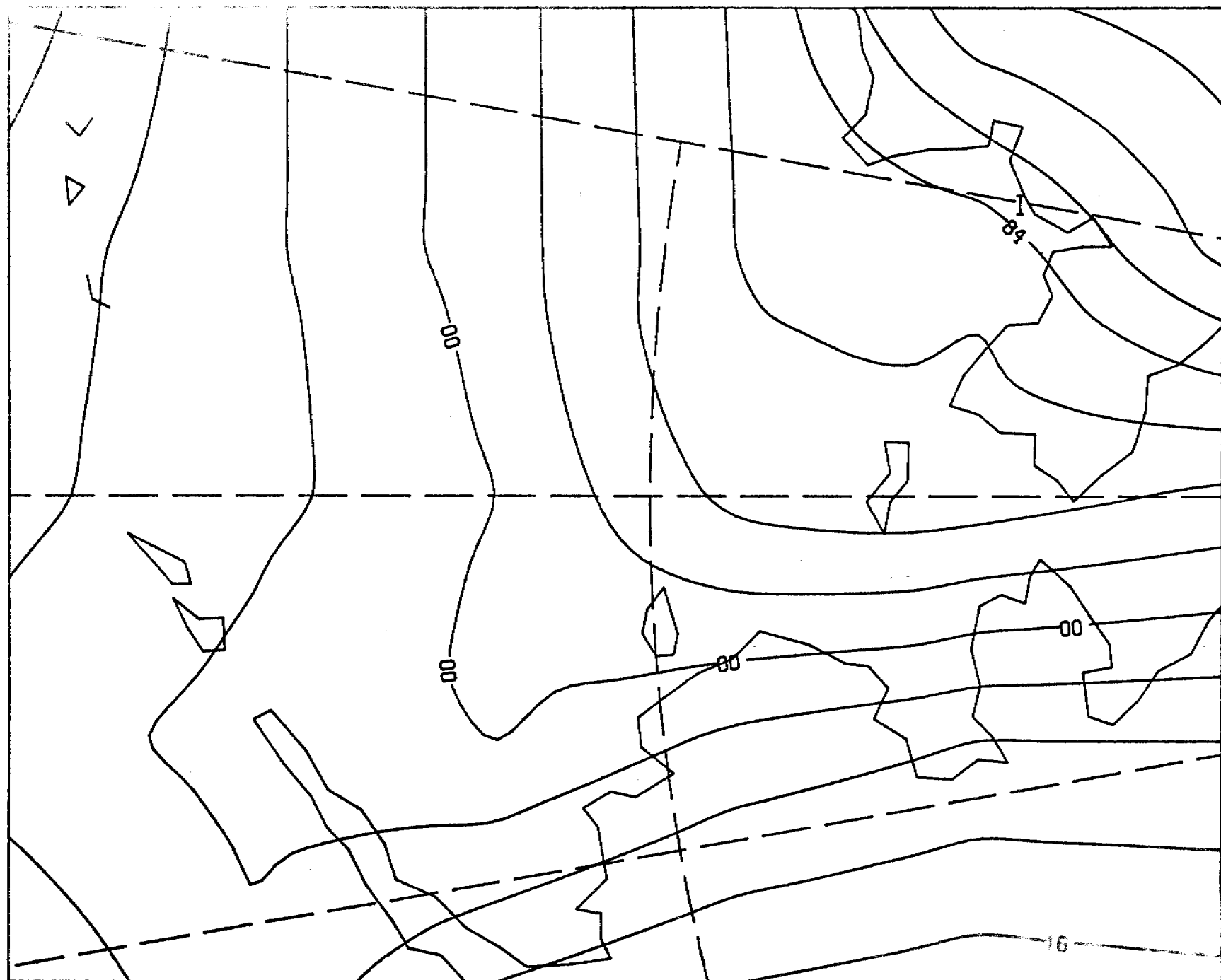
384

12Z 2 JUN 1958  
PUTNIN

E'



385



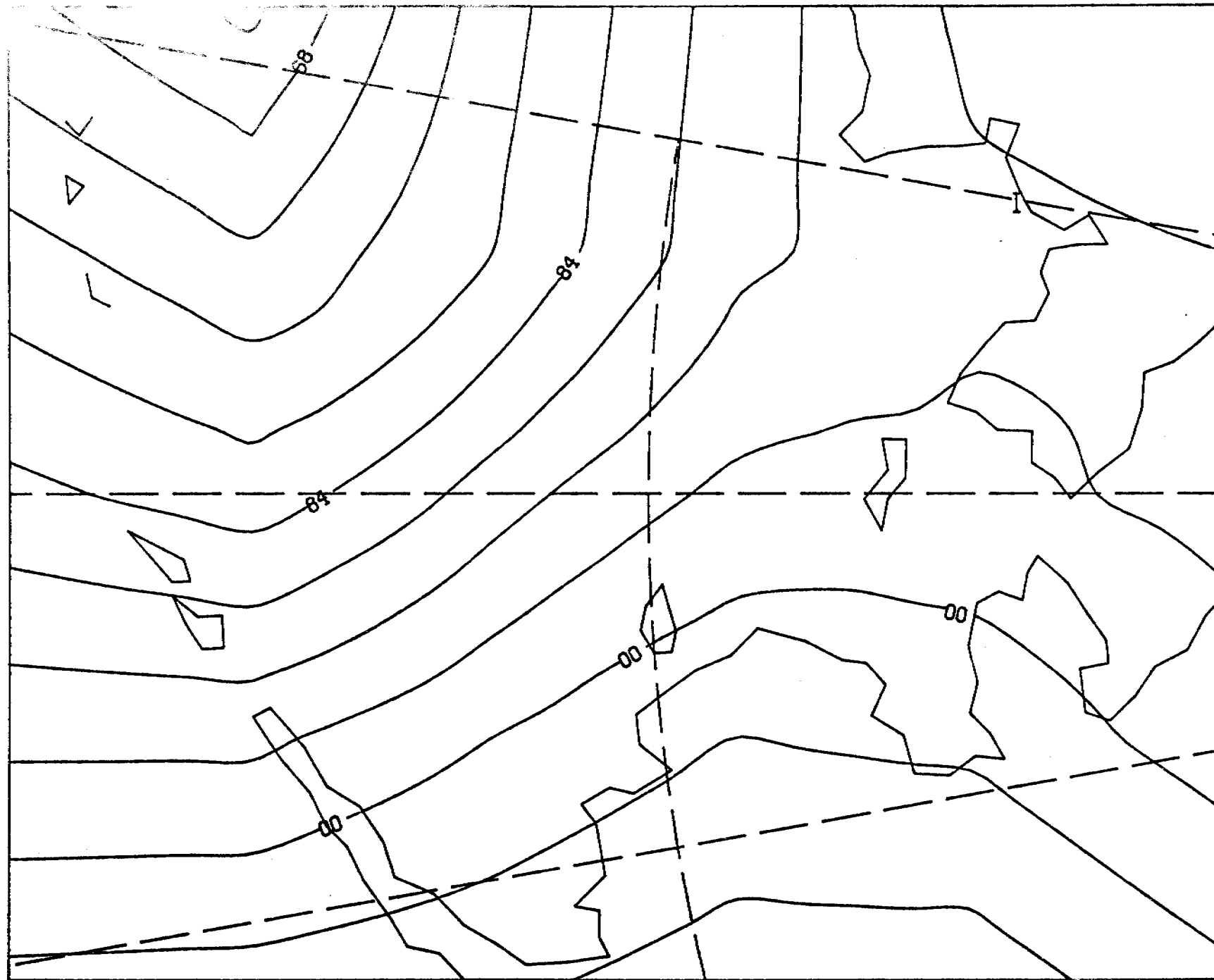
12Z 17 NOV 1950  
PUTNIN

16

1.9

OBSERVED SLIP

386



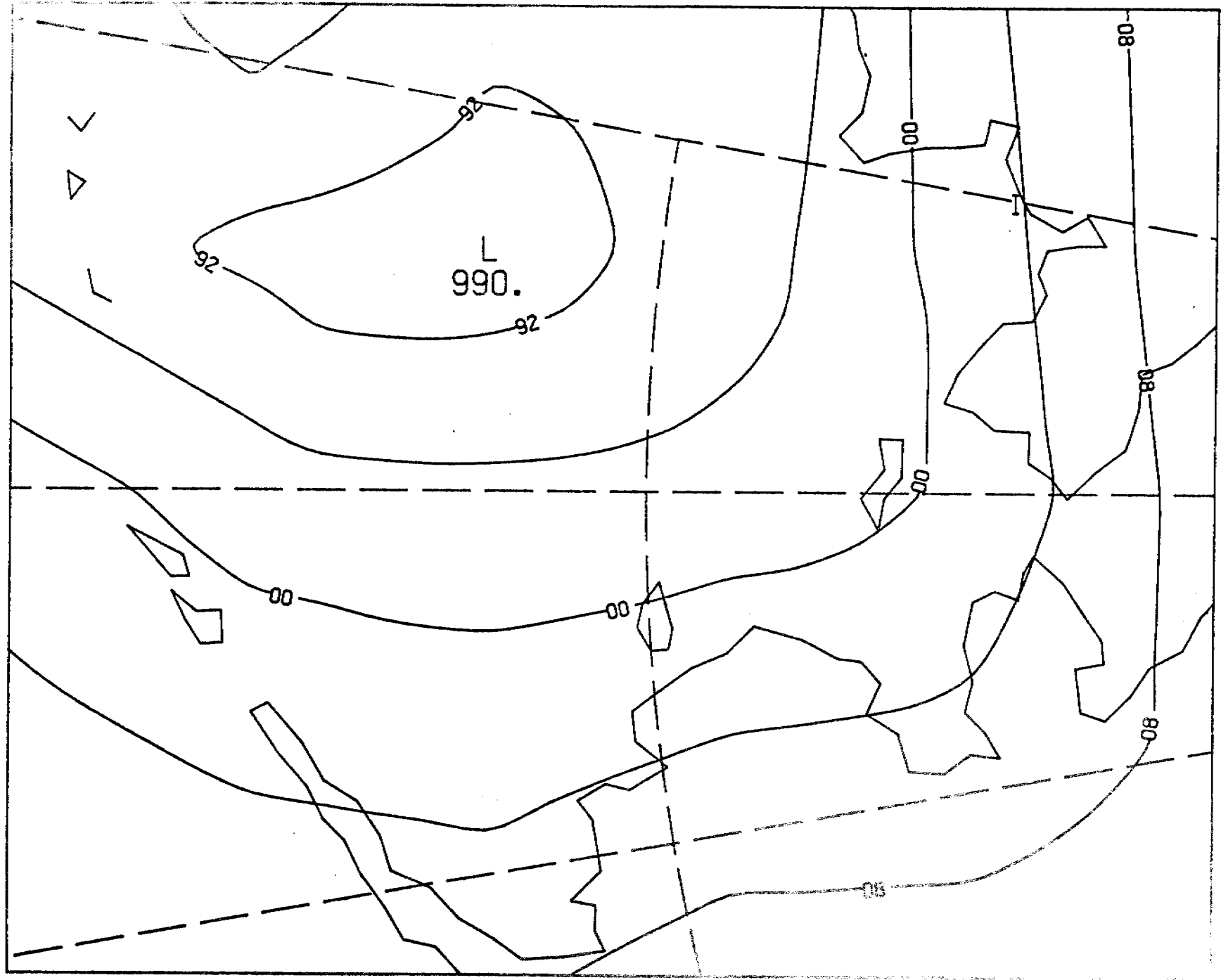
12Z 27 OCT 1952

PUTNIN

E<sub>1</sub>

OBSERVED SLP

387

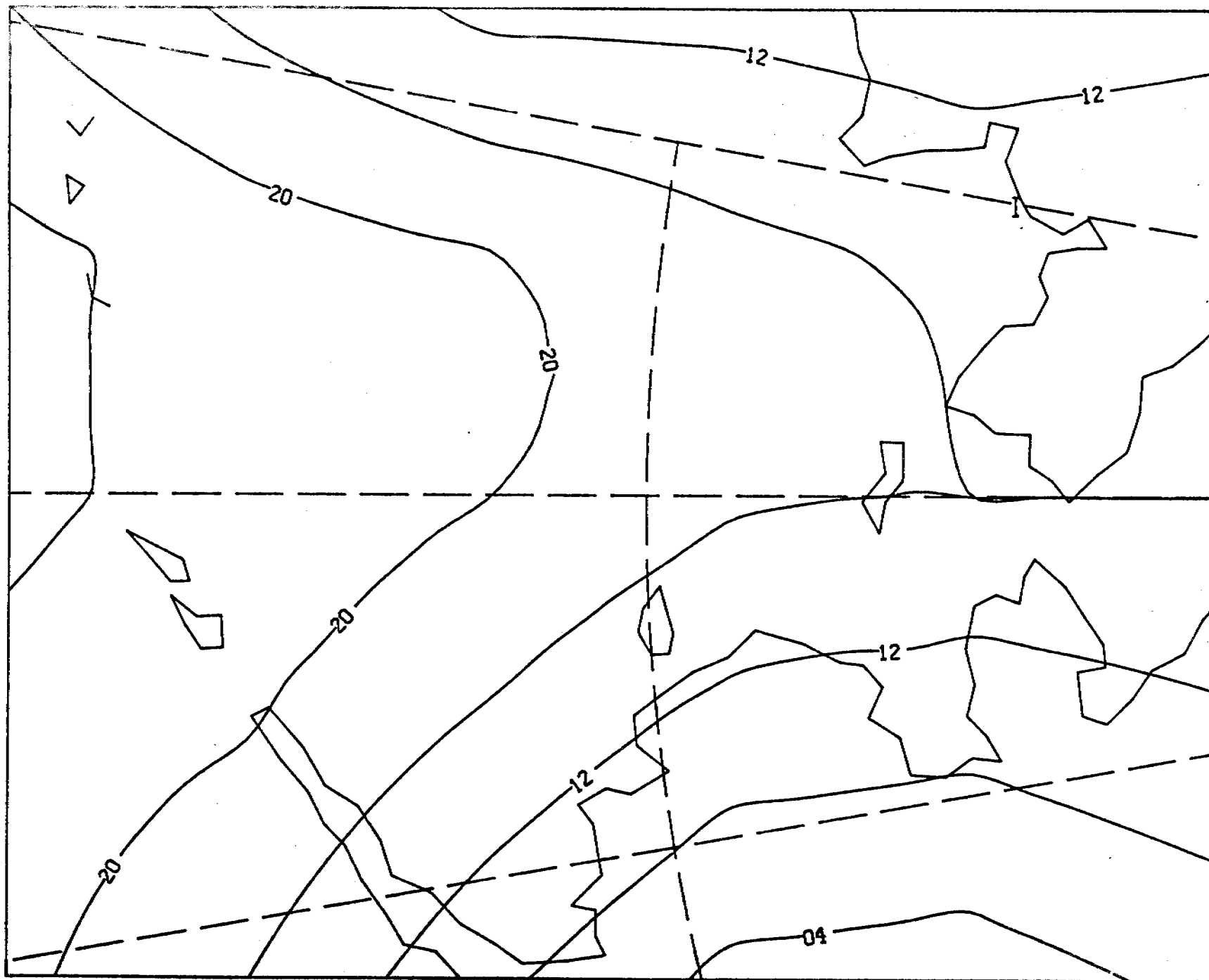


12Z 10 SEP 1958

PUTNIN

ØBSERVED SLP

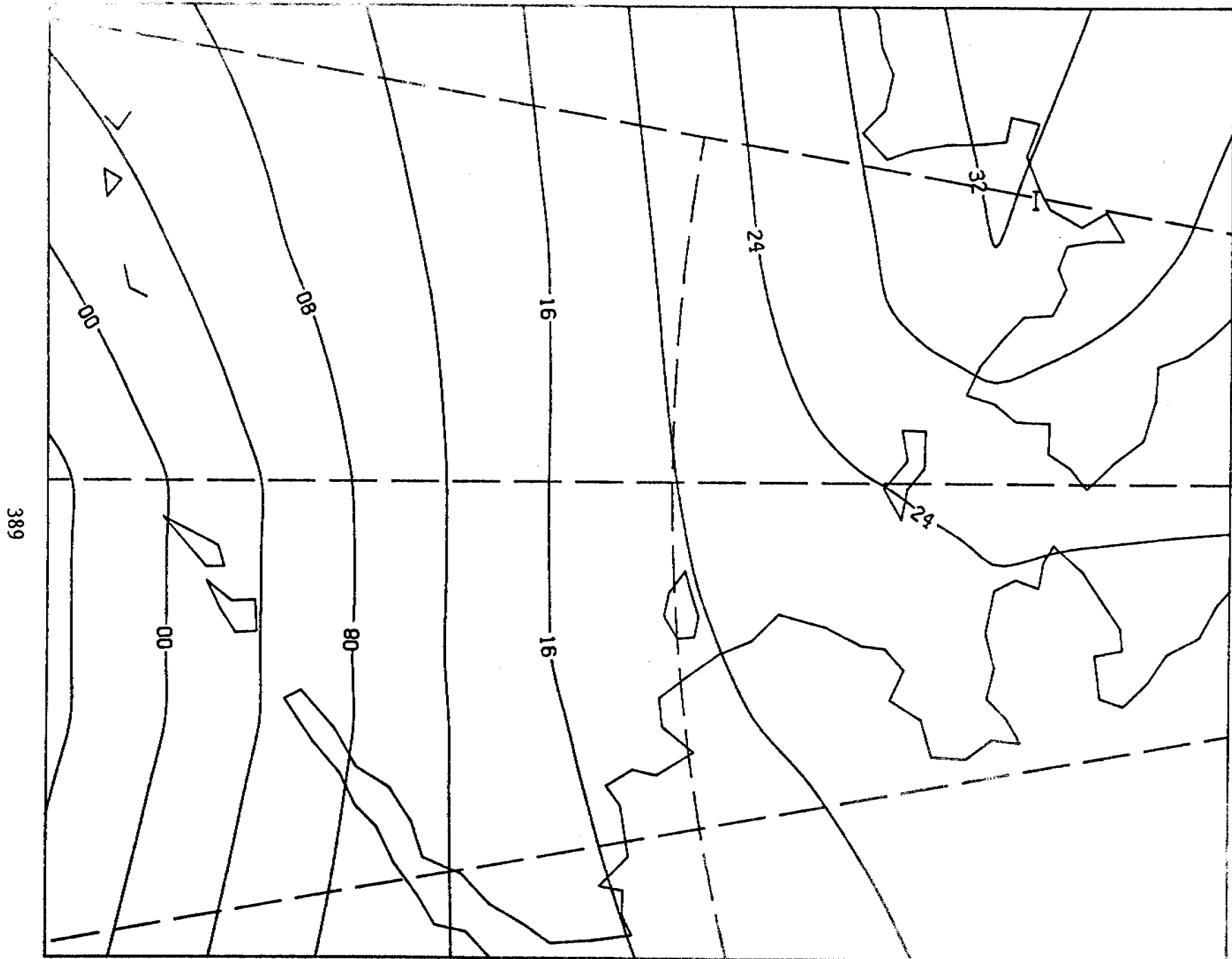
388



12Z 24 SEP 1955

F

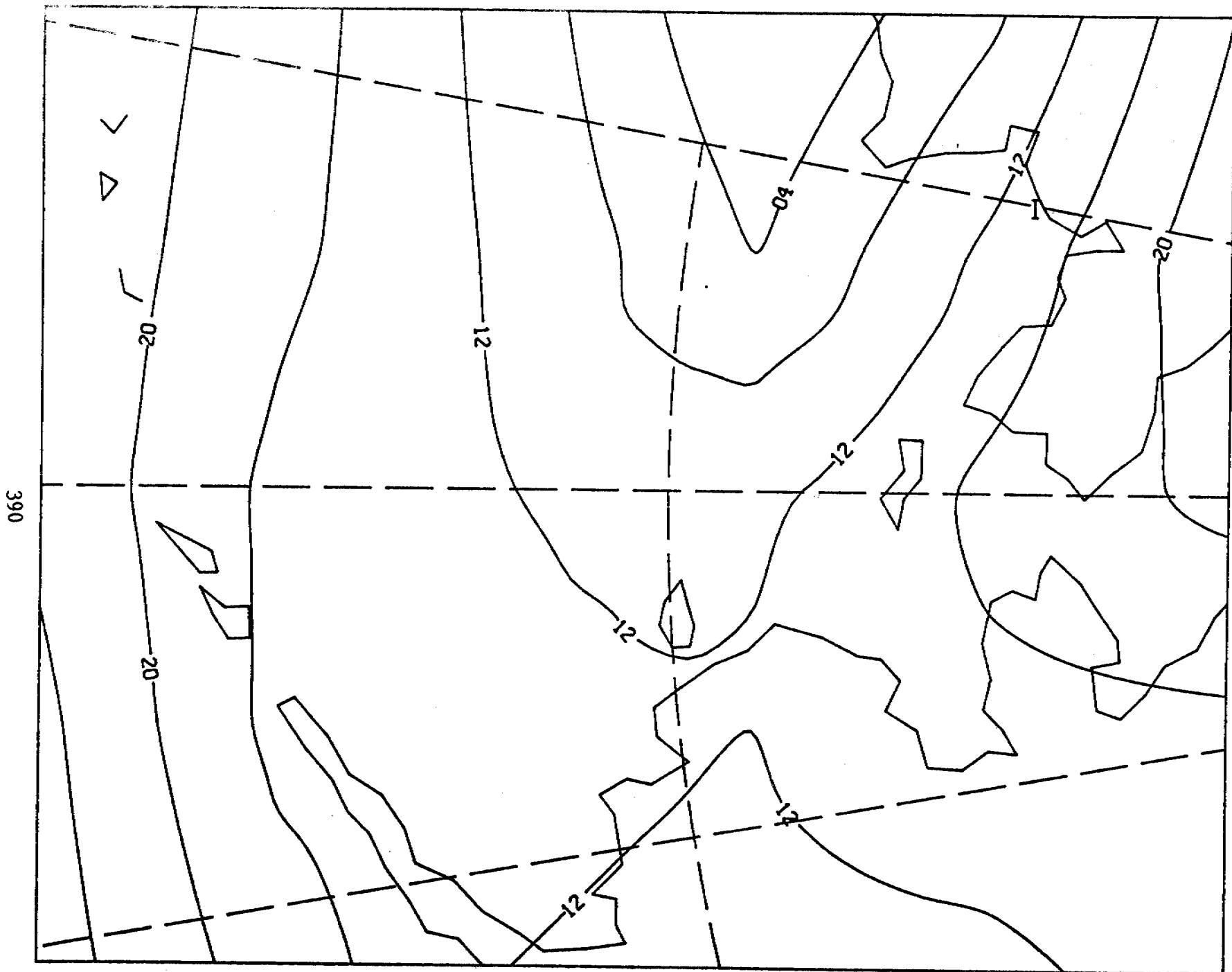
OBSERVED SLP



12Z 3 NOV 1955

PUTNIN

ØBSERVED SLP

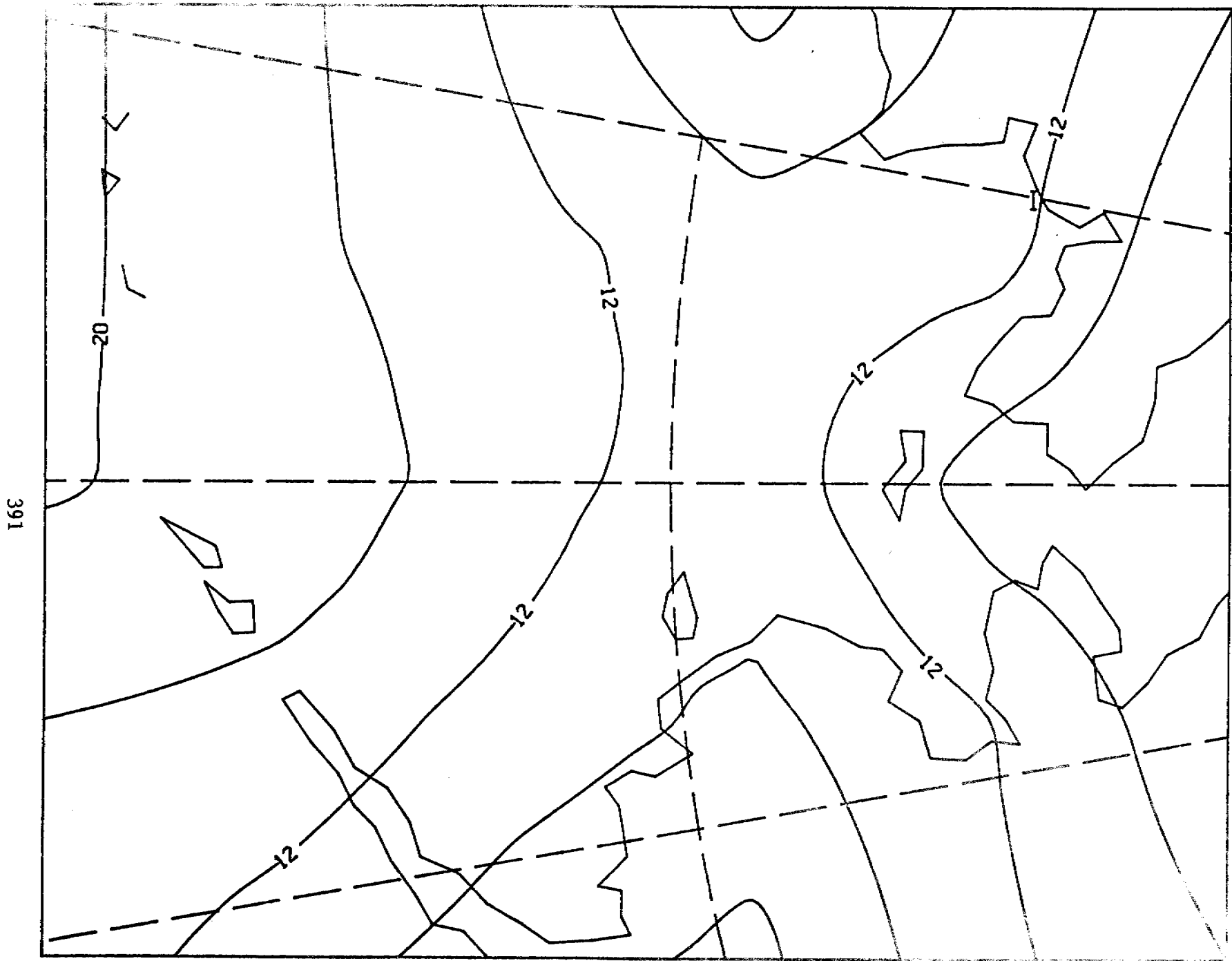


390

127 15 DEC 1957

G

OBSERVED SLP

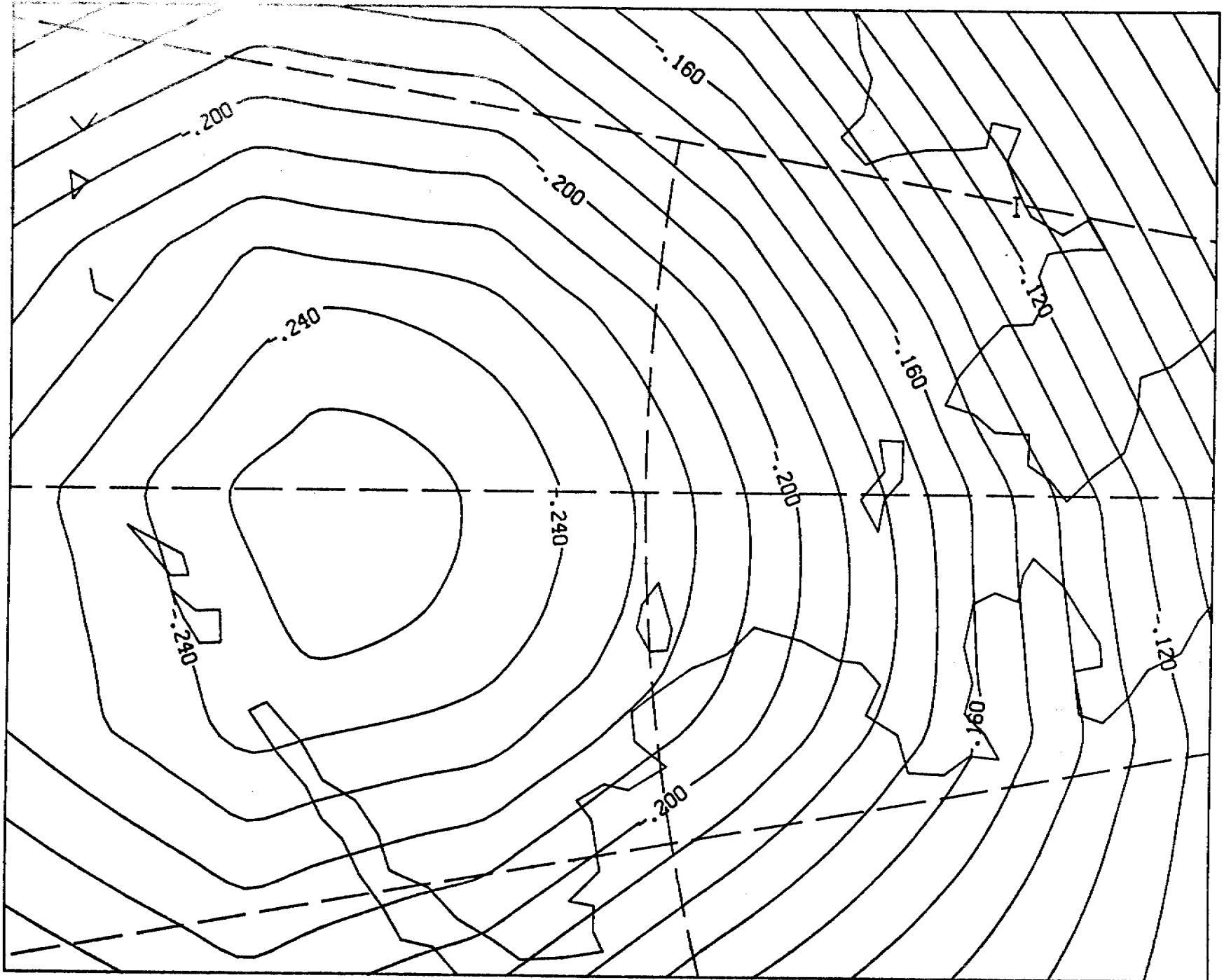


391

12Z 16 DEC 1957

PUTNIN

H

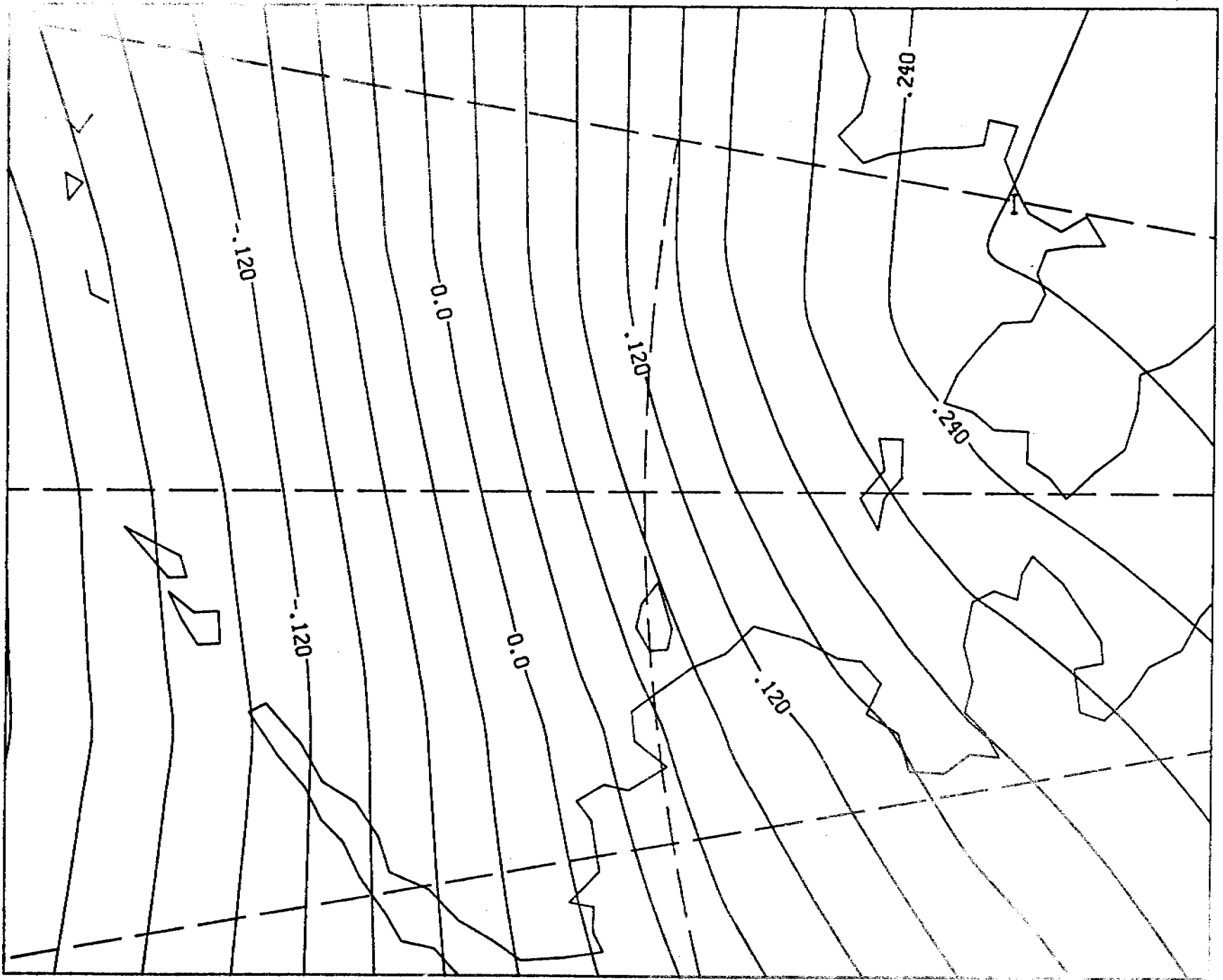


392

12Z 1 DEC 1972  
EIGENFUNCTION

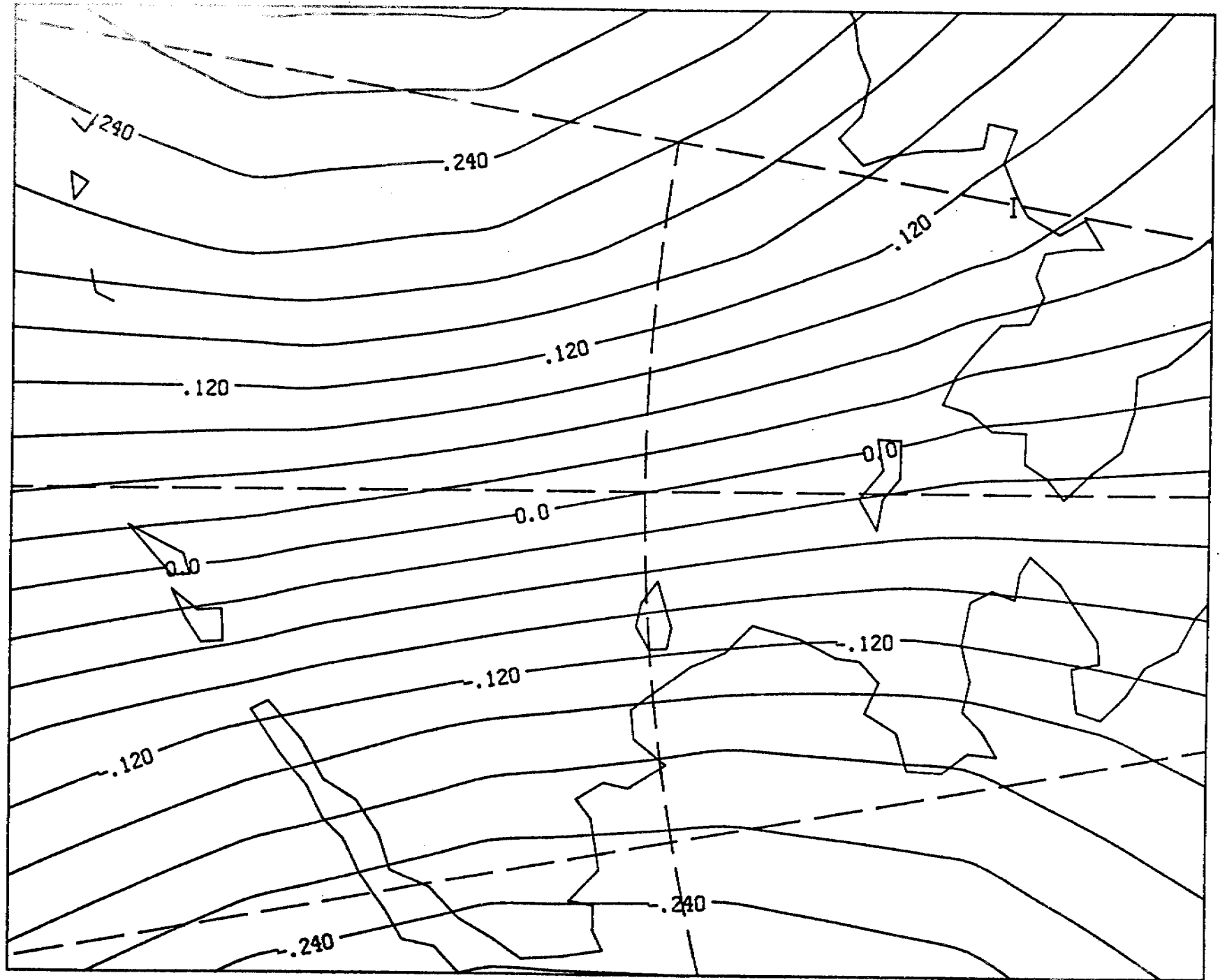


393



12Z 2 DEC 1972  
EIGENFUNCTION

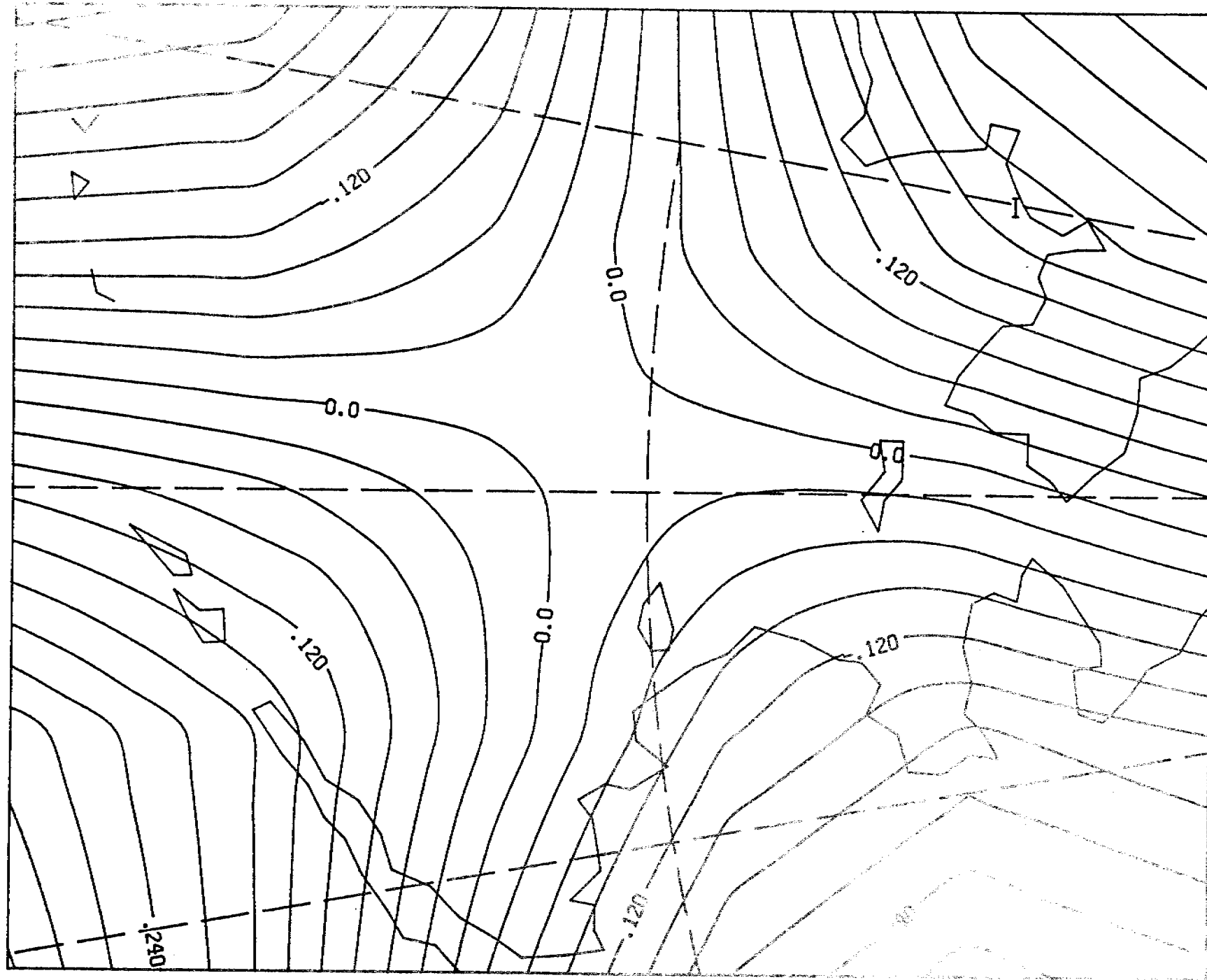
394



12Z 3 DEC 1972

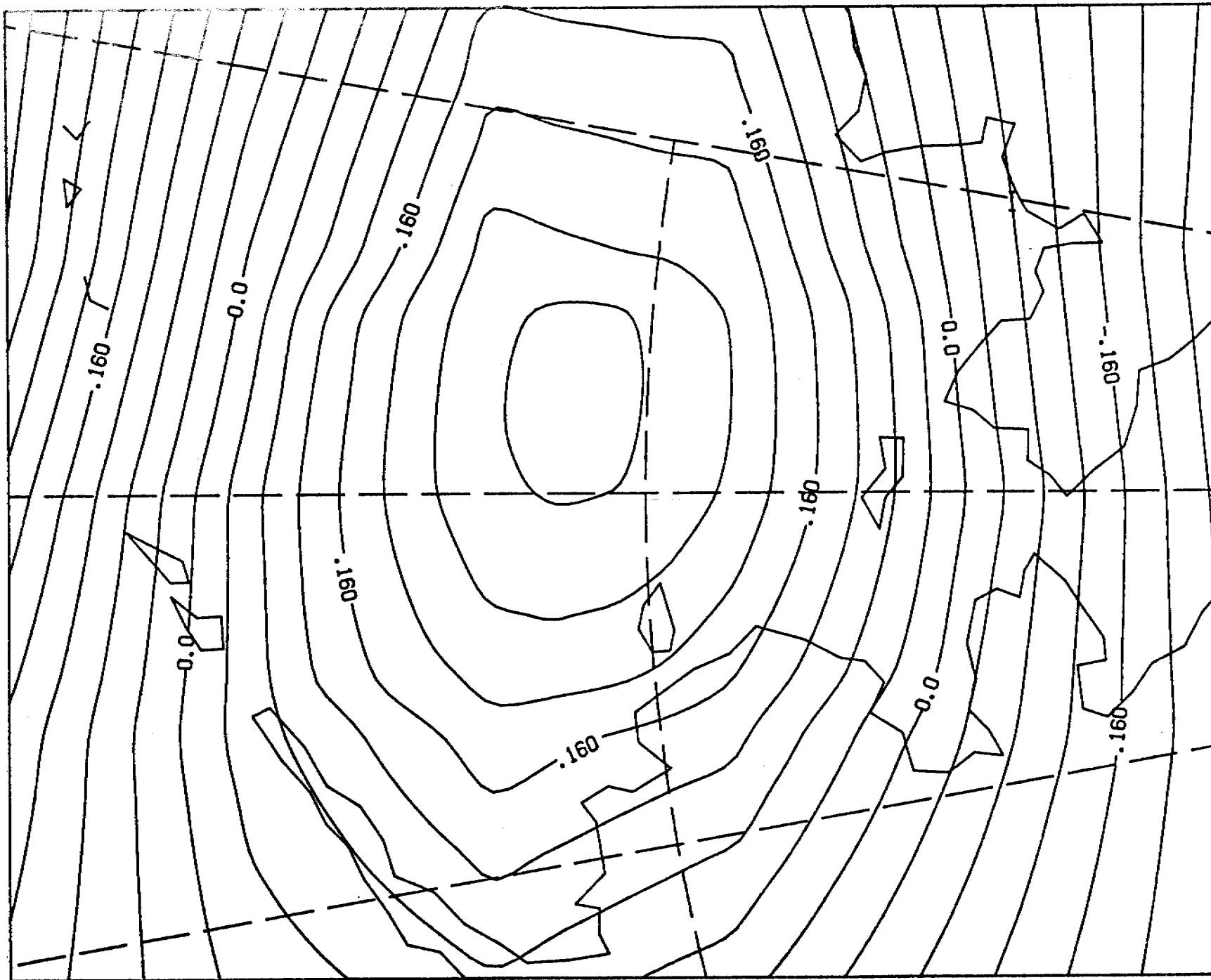
EIGENFUNCTION

395



12Z 4 DEC 1972  
EIGENFUNCTION

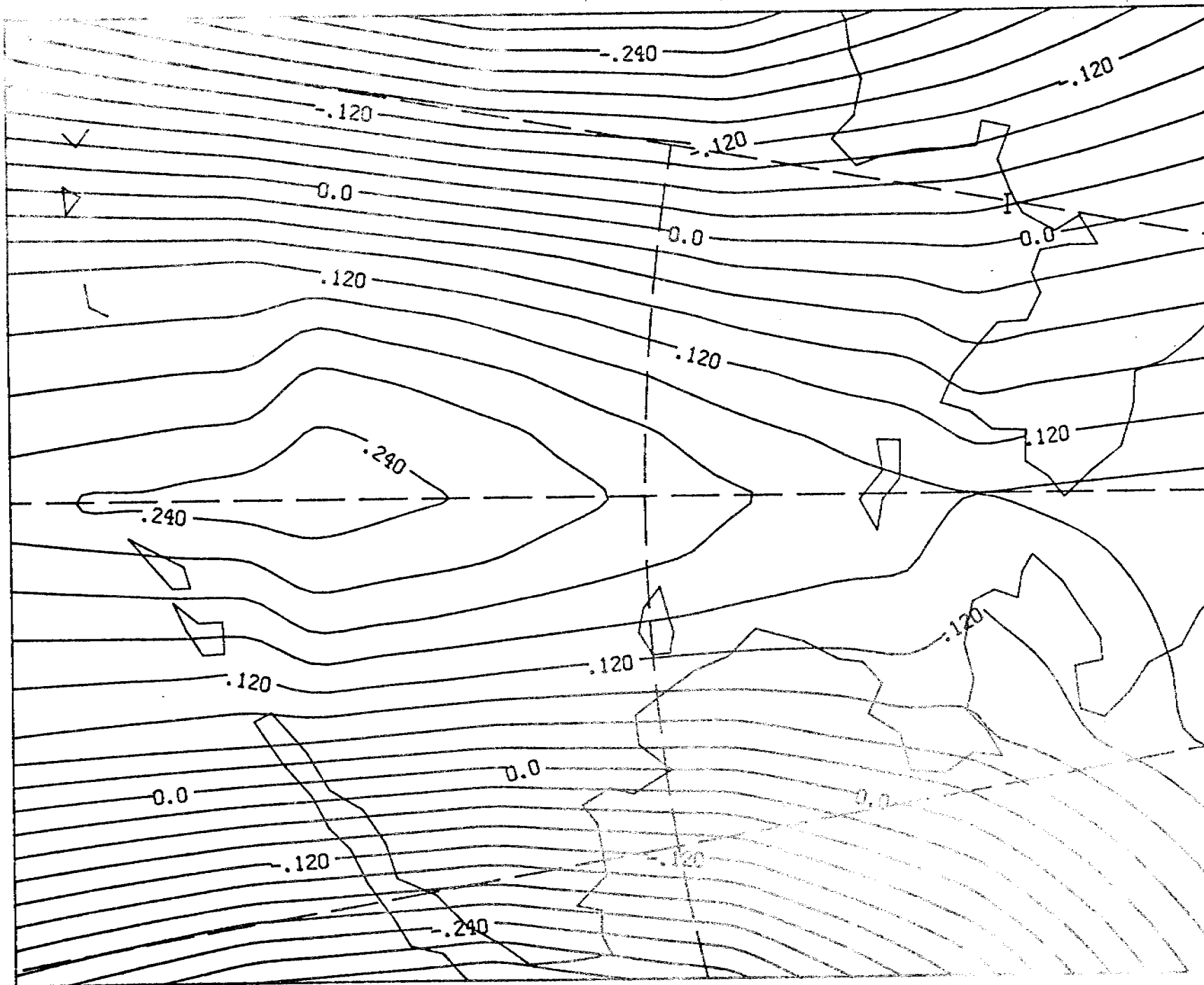
396



12Z 5 DEC 1972

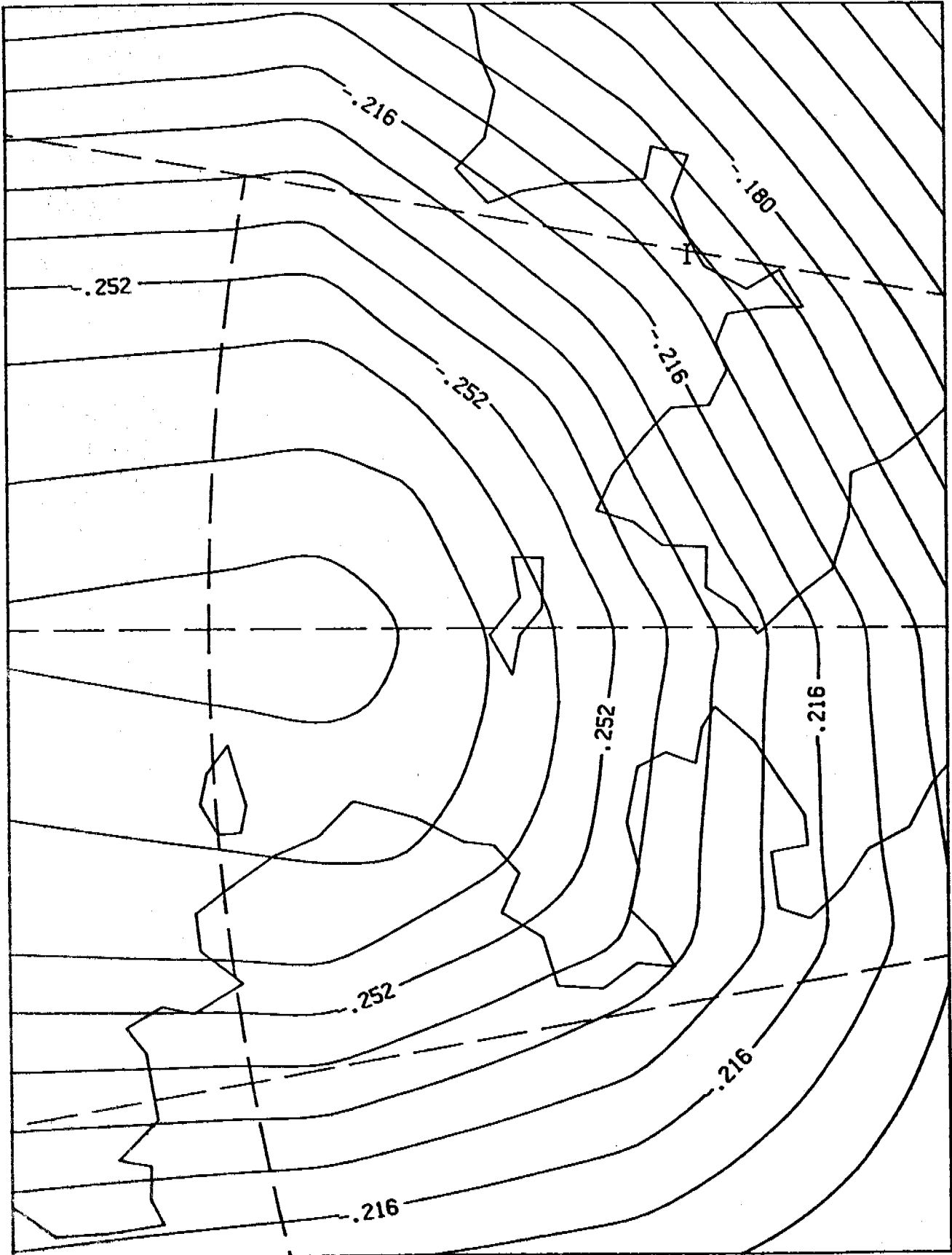
EIGENFUNCTION

397



12Z 6 DEC 1972  
EIGENFUNCTION

CLIMATE 901

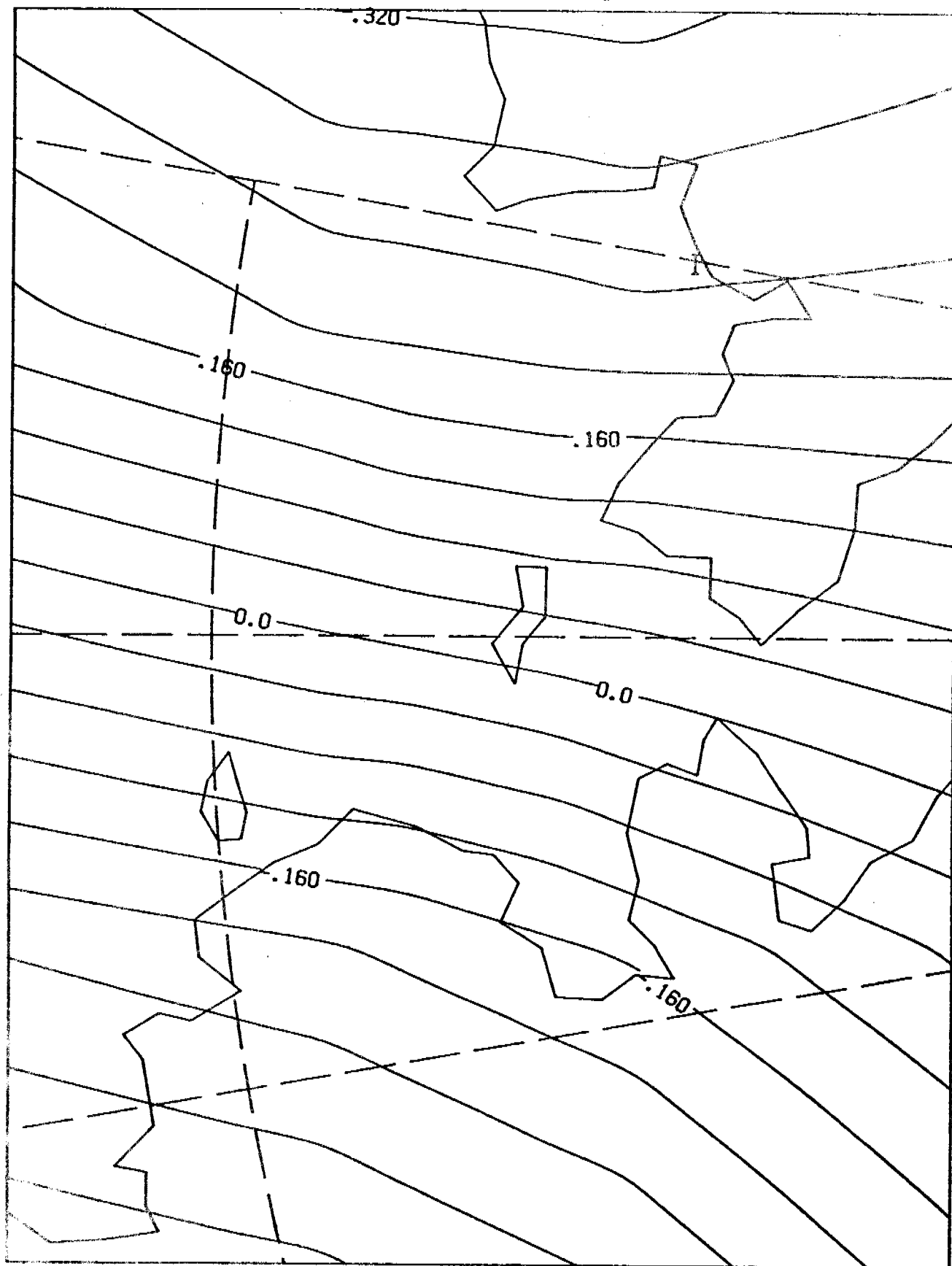


12Z 1 DEC 1972

FTCNEFUNCTION

398

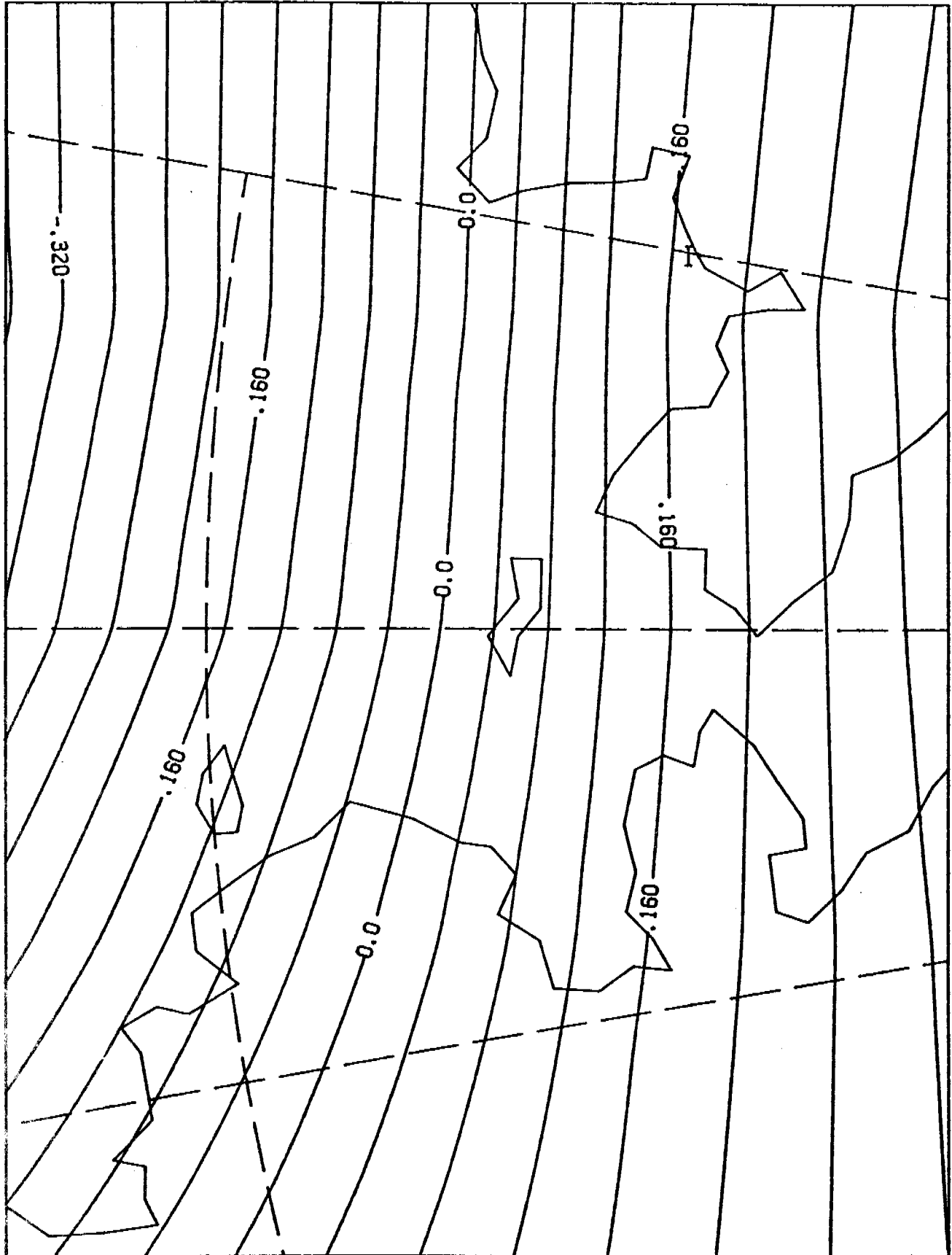
CLIMATE 901



12Z 2 DEC 1972  
EIGENFUNCTION

399

CLIMATE 901

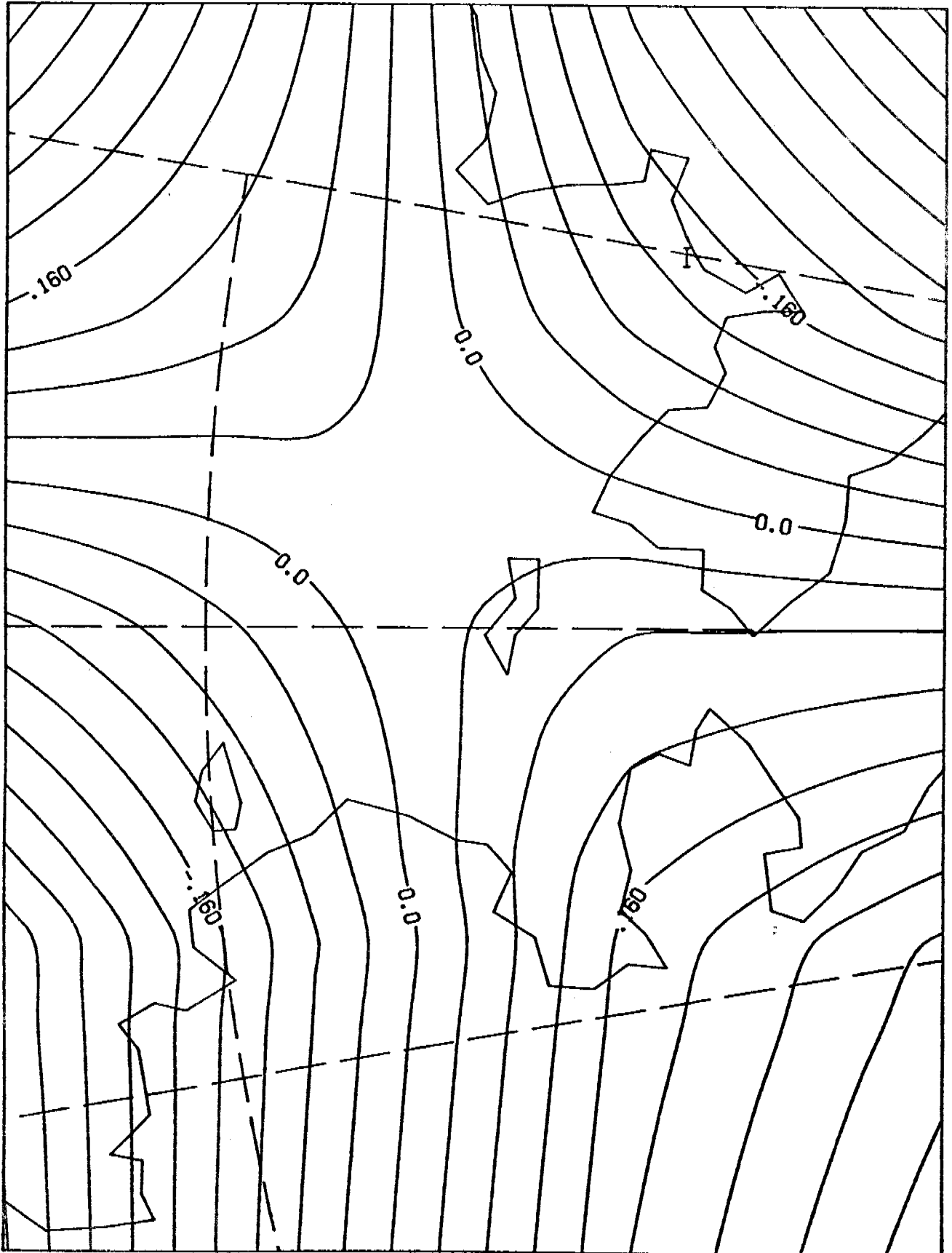


12Z 3 DEC 1972  
EIGENFUNCTION

400

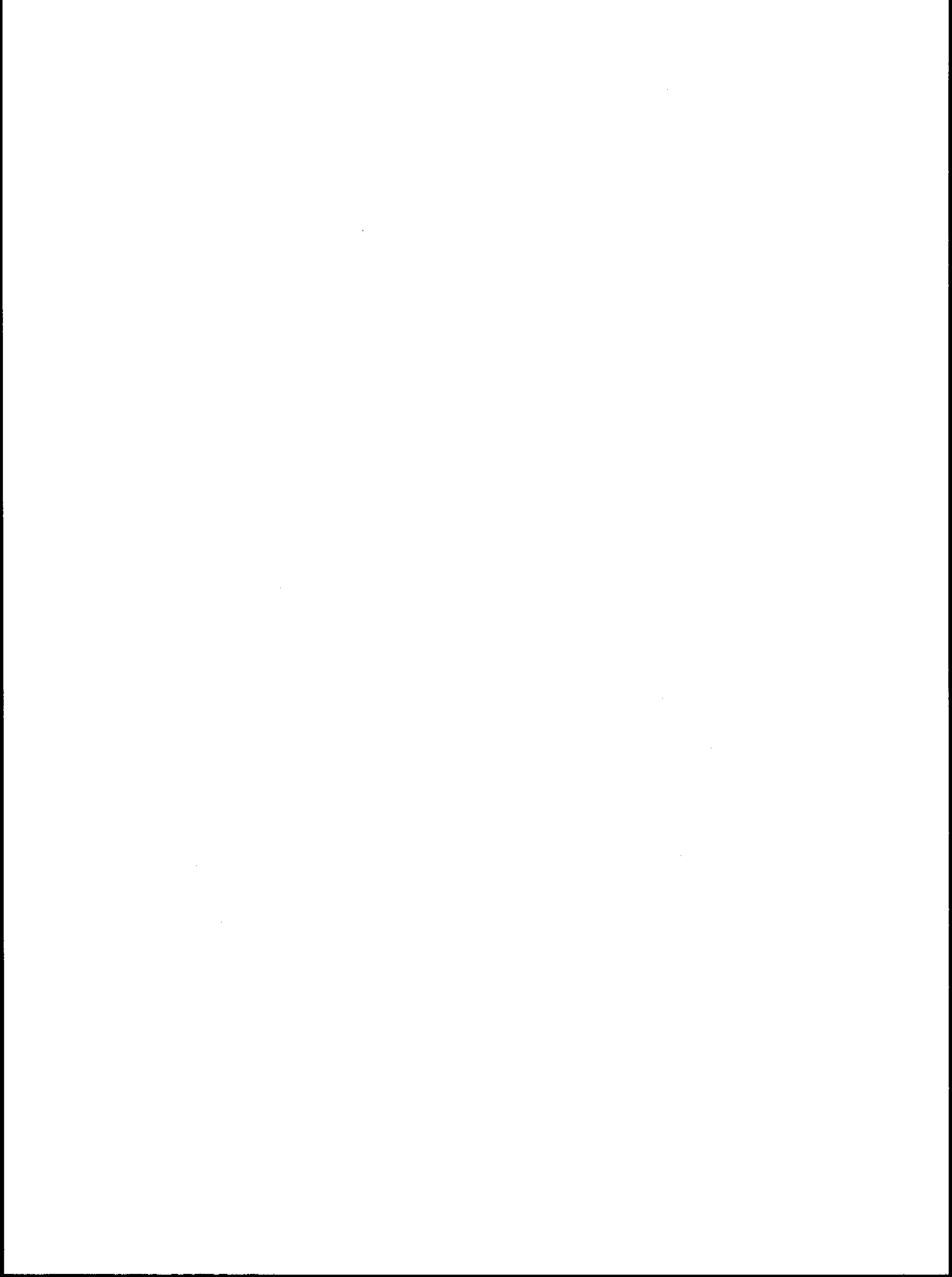


CLIMATE 901



12Z 4 DEC 1972

EIGENFUNCTION 401



APPENDIX

NOAA Technical Memorandum ERL PMEL-20

METLIB - A PROGRAM LIBRARY FOR CALCULATING  
AND PLOTTING MARINE BOUNDARY LAYER WIND FIELDS

J. E. Overland  
R. A. Brown  
C. D. Mobley

Pacific Marine Environmental Laboratory  
Seattle, Washington  
June 1980



**UNITED STATES  
DEPARTMENT OF COMMERCE**  
Philip M. Klutznick, Secretary

NATIONAL OCEANIC AND  
ATMOSPHERIC ADMINISTRATION  
Richard A. Frank, Administrator

Environmental Research  
Laboratories  
Wilmot N. Hess, Director

#### NOTICE

The Environmental Research Laboratories do not approve, recommend, or endorse any proprietary product or proprietary material mentioned in this publication. No reference shall be made to the Environmental Research Laboratories or to this publication furnished by the Environmental Research Laboratories in any advertising or sales promotion which would indicate or imply that the Environmental Research Laboratories approve, recommend, or endorse any proprietary product or proprietary material mentioned herein, or which has as its purpose an intent to cause directly or indirectly the advertised product to be used or purchased because of this Environmental Research Laboratories publication.

## CONTENTS

	Page
Abstract .....	406
1. INTRODUCTION .....	406
2. DATA SOURCES .....	407
3. DATA MANAGEMENT .....	408
4. MAIN PROGRAMS .....	413
4.1 Use of METLIB .....	413
4.2 UNPACK (Used to Extract Subsets from Large Temporal or Geographic Data Sets Such as NCAR) .....	413
4.3 DECKS (Creates a Standard Format File from Digitized Fields) ...	414
4.4 WINDS (Calculations of Winds) .....	415
4.5 PTWIND (Time Series of Winds) .....	417
4.6 PLOTGRD (Plotting) .....	418
4.7 MAP (Plotting Map Backgrounds) .....	426
4.8 PLOTW,PLOT2W,PLOT2W2 (Combined Submit Files) .....	427
5. SUBROUTINE DOCUMENTATION .....	431
5.1 Introduction .....	431
5.2 Interpolation (NTERP) .....	431
5.3 Location on Subgrid (W3FB00,W3FB01) .....	431
5.4 Speed and Direction (W3FC02,W3FC00) .....	433
5.5 Thermal Wind (TMWIND) .....	433
5.6 GRIDSET (GRIDSET) .....	433
5.7 Geostrophic Wind (GEOWIN,EDGE) .....	434
5.8 Gradient Wind (GRDWD) .....	434
5.9 Empirical Constants (MODEL4) .....	434
5.10 Model 2 (MODEL2) .....	434
5.11 Models 6-8 (MODEL6,MODEL8,BROWN,CARDON, etc) .....	435
6. ACKNOWLEDGEMENTS .....	436
7. REFERENCES .....	437
APPENDIX A: DERIVATION OF THE UNIVERSITY OF WASHINGTON (BROWN) PLANETARY BOUNDARY LAYER MODEL .....	438
APPENDIX B: DERIVATION OF CARDONE MODEL .....	472

METLIB - A PROGRAM LIBRARY FOR CALCULATING AND PLOTTING  
MARINE BOUNDARY LAYER WIND FIELDS\*

J. E. Overland  
Pacific Marine Environmental Laboratory  
Seattle, Washington

R. A. Brown  
C. D. Mobley  
University of Washington  
Seattle, Washington

METLIB is a FORTRAN program library for deriving earth-located time series of geostrophic, gradient, or surface winds from sea level pressure (SLP) and ancillary fields gridded on a polar stereographic projection. Such fields are generated at the National Meteorological Center (NMC) and at Fleet Numerical Oceanographic Central (FNOCC). They can also be generated by digitizing SLP charts analyzed manually. The library also contains programs for contouring scalars, such as SLP or wind speed, and for plotting vector arrows with a map background. Plotting is based upon the NCAR graphics routines. A major advantage to the library is that spherical geometric calculations involving polar stereographic grids are internal to the programs. The relationship between gradient wind and surface wind can be assigned from speed reduction and turning angle constants or by a baroclinic, stability-dependent, single point boundary layer model.

## 1. INTRODUCTION

This document provides an introduction to the program library, discusses the data structure used by the library, and provides documentation of the geophysical algorithms used to derive various parameters and perform geometric calculations. It provides a description of the SUBMIT files for accessing the library as of date of publication. The library is divided into four program divisions, UNPACK or DECKS, WINDS, PTWIND, and PLOTGRD and two subroutine libraries, WSUBLIB and those called by PLTPROC.

---

\*Contribution No. 451 from NOAA/ERL Pacific Marine Environmental Laboratory.

UNPACK extracts data from a larger data set, normally tapes such as those supplied by NCAR or NMC, and creates a master file in a standard format for all subsequent programs. DECKS performs the same function as UNPACK for card or terminal input of fields that have been digitized from manual analyses. Program WINDS inputs a series of sea-level pressure (SLP) fields in standard format and, depending upon the option, can also input air temperature, air-sea temperature difference and dew point depression fields. It outputs u and v components at each grid point. Output winds can be geostrophic, gradient, empirical reduction and turning of the gradient wind, or calculated from a planetary boundary layer (PBL) model. Two of the three PBL models have the option of outputting stress or heat flux in place of surface wind. PTWIND can take u and v fields generated by WINDS, interpolate them to any specified latitude and longitude, and convert the grid components to speed and direction relative to north. PLOTGRD can input and contour up to two scalar fields and can plot their difference. It can draw arrow plots of a vector field or the difference of two vector fields, and can plot a vector field with contours of a scalar, including contours of the magnitude (isotachs) of the vector field itself or the difference in magnitude of two vector fields. All routines are intended to be machine-independent FORTRAN programs.

For use at PMEL or other locations with access to the Environmental Research Laboratories' CDC 6600 computer in Boulder, Colorado, SUBMIT files are shown for WINDS, PLOTGRD and their combination. These SUBMIT files are specific to the NOS 1.3 operating system in use at the time of publication. RWINDS submits WINDS and RPLLOT submits PLOTGRD. PLOTW inputs scalar fields, calculates wind fields and plots the results (i.e., runs WINDS and PLOTGRD together). PLOT2W inputs scalars, runs WINDS twice, and plots vector differences. PLOT2W2 inputs two separate sets of SLP scalars, calculates winds for each and plots their difference.

## 2. DATA SOURCES

NMC currently produces SLP and surface air temperature (SAT) analyses at 0000 and 1200 GMT on one of two polar stereographic meshes: the PE 65 x 65 point grid, with a spacing of 381 km at 60°N covering the northern

hemisphere; and the LFM 53 x 57 point grid, a fine-mesh grid with a spacing of 190.5 km at 60°N, covering North America and the adjacent waters (Fig. 1 and 2). PE and LFM are historical names standing for "Primitive Equation" and "Limited Area Fine-Mesh Model". The PE data are archived at the National Center for Atmospheric Research (NCAR) (Jenne, 1975) and the National Climate Center (NCC). At present the LFM data are not routinely archived for general distribution. Pressure fields are also produced by Fleet Numerical Oceanographic Central (FNOC) on a 63 x 63 point grid with the same scale and orientation as the PE grid. All grids are uniformly spaced upon a polar stereographic map projection, which preserves angles.

Over the ocean, SLP and SAT values for operational forecast models are obtained from ocean-station vessel, buoy and ship observations analysed by a variety of objective analysis techniques (Cressman, 1959; Flattery, 1970; Holl and Mendenhall, 1971). For many research purposes it is necessary to reanalyze the SLP charts making use of reports that were not included in the NMC analysis. To this end, the reanalysis is done on a standard polar stereographic projection (either the PE or LFM) and digitized at a uniform spacing compatible with the program library.

Internal north-pole coordinates are (33,33) for the present PE grid and (27,49) for the LFM. The FNOC pressure fields use pole coordinates of (32,32). For PE data prior to 1976 the NMC "octagon" was used. The number of grid points was 47 x 51, the pole location was (24,26), and the data were stored in a one-dimensional array. This is the format used by NCAR to store much of their NMC PE data.

### 3. DATA MANAGEMENT

All master data files created by UNPACK or DECKS are in a standard format for subsequent analysis routines. Master data sets are arranged chronologically and separated by type (e.g., SLP or wind speed) and geographical region (e.g., the Gulf of Alaska). Thus, one file might have a 1-yr time series of observed SLP's in a 10 x 10 grid for the Gulf of Mexico; another file might consist of model-generated, u-component winds for the same period, etc.



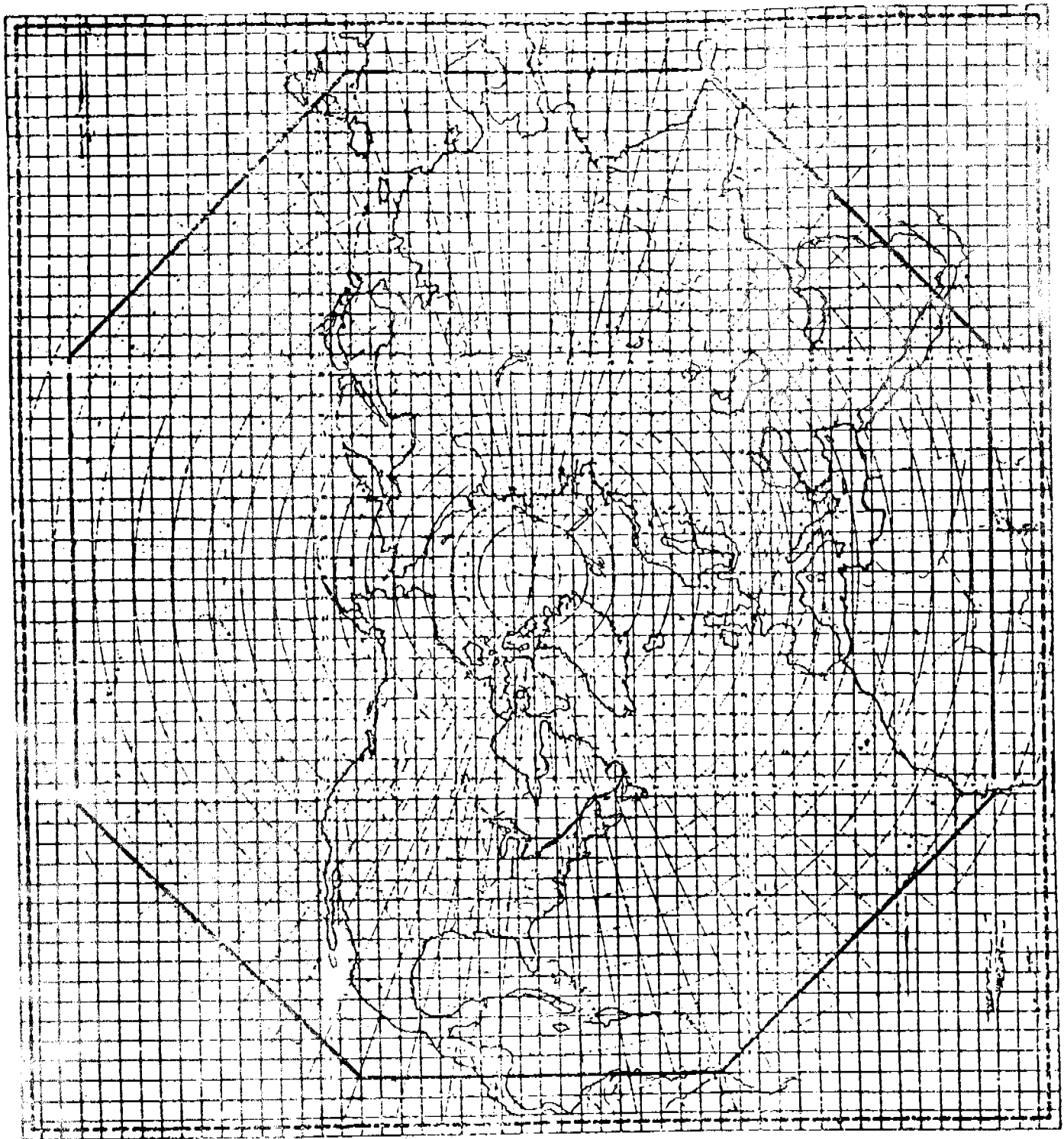


Figure-1. The NMC octagon 47 x 51 point grid. The 65 x 65 grid in present use has the same mesh point locations but covers a larger area.

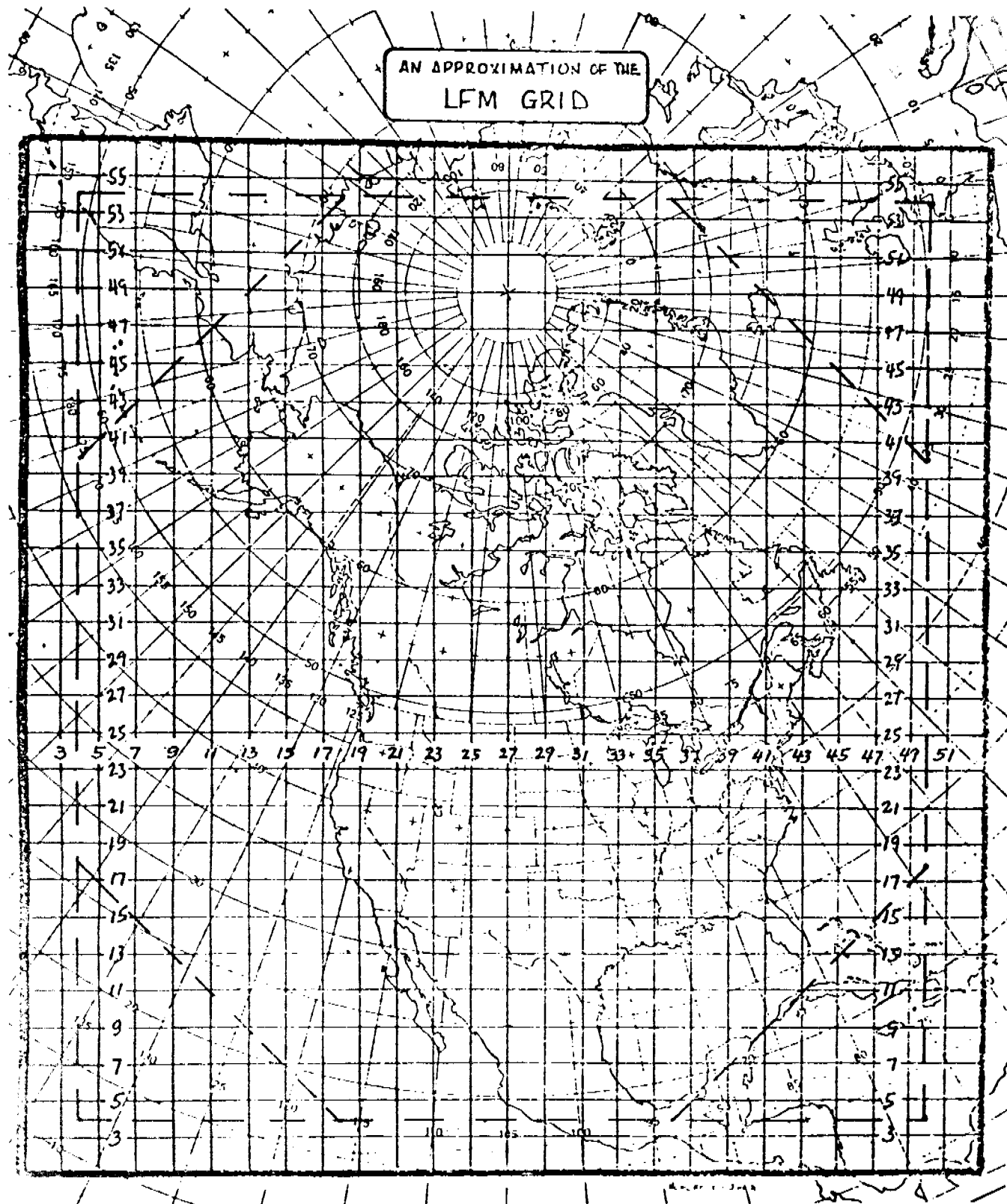


Figure 2. LFM 53 x 57 point grid (NMC).

All records are generated by FORTRAN unformatted write statements and are stored in an unpacked form. Every file is identified by a file header. This header consists of six words and identifies the particular grid on which the data are stored:

<u>Word</u>	<u>Quantity</u>
1	IGRID. Identifies the grid used: 1 means PE IGRID = 2 means LFM 3 means NMC octagonal (PE) 4 means FNOC
2,3	XIS,XJS. The (I,J) coordinates (relative to the above grid) of the lower left corner of the data subregion.
4,5	IMC,JMC. The (I,J) dimensions of the coarse (uninterpolated) grid subregion covered by the data.
6	IFACT Specifies the degree to which the data have been interpolated relative to the standard mesh. 1 means no interpolation, i.e., same as PE or LFM IFACT = 2 means interpolation to 1/2 mesh 4 means interpolation to 1/4 mesh.

For example, if SLP were hand digitized on a grid twice as fine as the PE, IMC and JMC would equal the size of the equivalent coarse PE array, but IFACT would equal 2.

The header is followed by as many data groups as necessary. Each group consists of seven identification words followed by the data. The identification words specify the date and data characteristics as follows:

<u>Word</u>	<u>Quantity</u>
1	IYEAR. "68" means 1968
2	MONTH. "11" means November
3	IDAY.
4	Ihour. "12" means 12 GMT
5	ITYPE. Data type coded as in NMC office note 84 (1973): 8 pressure in mb 16 air temperature in °K 18 dew point depression in °K

- 30 air-sea temperature difference in °K
  - 48 u wind component w/r to grid in  $\text{cm s}^{-1}$ \*
  - 49 v wind component w/r to grid in  $\text{cm s}^{-1}$ \*
  - 50 wind speed in  $\text{cm s}^{-1}$ \*
  - 55 direction from which wind is blowing with respect to north in degrees
  - 148 u wind stress component relative to grid in  $\text{dynes cm}^{-2}$
  - 149, 150, 155 same as 49, 50, 55 for stress
  - 180 Total heat flux in  $\text{watts m}^{-2}$
  - 182 Latent heat flux in  $\text{watts m}^{-2}$
  - 183 Sensible heat flux in  $\text{watts m}^{-2}$
  - 384 Sea surface temperature in °K
- 6 IOBS. Gives the type of forecast
- 0 means observed data
  - 12 means 12-hr forecast data
  - IOBS = 24 means 24-hr forecast data, etc.
  - 910 means climate type 1.0
  - 920 means climate type 2.0, etc.
- 7 IFLAG. Flags missing data
- 0 means data are complete
  - IFLAG = 1 means data are missing

Following these identification words, the data array is written in words 8, 9, 10, etc. Missing data are given the value 9999. Two-dimensional arrays, A(I,J), are structured so that I and J increase in the same direction as I and J of the weather forecasting grids, with A(1,1) at the lower left corner of the subregion and the arrays reading ((A(I,J), I=1, IMC), J=1, JMC).

\*Note that standard NMC and SI. format is  $\text{m s}^{-1}$ .

## 4. MAIN PROGRAMS

### 4.1 Use of METLIB

METLIB consists of a collection of programs and subroutines along with a set of SUBMIT files to run them. These libraries and example files are stored under USER, METLIB on the ERL 6600 computer. This USER is meant for read-only storage of programs. All data files and personal copies of SUBMIT and main program files should be stored in separate USER areas. Normal procedure is to copy the desired files from METLIB into a new area and then modify the files as necessary for a particular application. This entails changing the SUBMIT files and the dimension statements of the main programs to match the data array size.

### 4.2 UNPACK (Used to Extract Subsets from Large Temporal or Geographic Data Sets such as NCAR)

UNPACK performs three tasks. It unpacks the data, if necessary; extracts the appropriate time series, subregion, data type, and forecast type as specified; and organizes the data set into the standard format for use by the subsequent analysis routines. Since the raw data tapes come in different formats, a separate UNPACK must be written for each grid used (NMC octagonal, FNOC, etc.). For the version of UNPACK that is compatible with the NMC octagonal grid obtained from NCAR, the user specifies the starting and stopping time of the file to be generated, the lower left-corner coordinates and dimensions of the region to be analyzed, the data type and the forecast types on an input data card (13I2) as follows:

IYSTRT. . . . The year of the first desired datum (e.g. 71 for 1971)  
IMSTRT. . . . The month (e.g. 3 for March)  
IDSTRT. . . . The day  
IYSTOP. . . . The year of the last desired datum  
IMSTOP. . . . The month  
IDSTOP. . . . The day  
ILL . . . . The lower left (I,J) coordinates measured on the NMC  
JLL . . . . octagonal grid of the desired geographical region.  
IMC . . . . The number of (NMC octagonal) grid points to be taken in

JMC            the I and J directions to cover the desired geographical region. The point (ILL,JLL) is counted as the first point. The dimension of array is IMC by JMC.

IFUNC . . . . The NCAR function code specifying the data type:  
                  =10 for air temperatures  
                  =28 for sea-level pressures  
                  =47 for sea-surface temperatures.

IFCST . . . . The forecast type  
                  =0 for observed data  
                  =12 for 12-hr forecast data, etc.

ISMO . . . . =1,2,4 to interpolate the original data to a finer mesh.

The file generated by UNPACK is in standard format with a file header and a time series of data records.

#### 4.3 DECKS (Creates a Standard Format File from Digitized Fields)

DECKS performs for manually digitized fields the same function that UNPACK performs for the NCAR data sets. A uniform mesh compatible with the locations of the grid points of either the LFM or PE is laid over a hand-analysed polar stereographic National Weather Service sea level pressure chart or hand analyses performed on charts produced by program MAP (section 4.6), and values are extracted. The grid can be either at the standard, half or quarter mesh spacing.

The first card read by DECKS gives IGRID, XIS, XJS, IMC, JMC, IFACT, ITYPE, N, OFACT on a (I3,2F3.0,6I3) format. The first six words are the standard header from section 3.0. The number of fields to be read is N. OFACT is the resolution of the digitized input fields relative to the standard PE or LFM resolution; OFACT can be 1, 2, or 4 with the same meaning as IFACT. If IFACT is greater than OFACT, the digitized fields will be interpolated to a finer mesh by biquadratic interpolation. This card is followed by the data sets, each beginning with a header card (6I2) specifying IYEAR, IMONTH, IDAY, IHOOR, IOBS, IFLAG, and the data read in (user specifies format):

```
DO 10 J=1,JM
10 (ARRAY(I,J),I=1,IM)
```

In DECKS the dimension of ARRAY(IM,JM) is set at the size of the input array and the dimension of OUTPUT (IMM,JMM) and W(IMM,JMM) are set at the size of the array written on file in standard format. Values on the DATA statement following the DIMENSION statement must also be set.

#### 4.4 WINDS (Calculations of Winds)

Program WINDS uses any of several models to compute surface wind fields. Input always consists of a time series of sea-level pressures defined at each point of a spatial grid. Models 6-9 require the time sequence of surface air temperatures and air minus sea-temperature differences. The Brown model has the option of dew-point depression fields as well. The information in the file header record on each data set (i.e., IGRID, XIS, XJS) completely defines the parameters necessary for geometric manipulations on the polar stereographic grid. Output consists of time series for u and v components of winds.

Figure 3 shows a sample SUBMIT file for running WINDS on the CDC 6600. TAPE10 has the grid-point pressure fields in standard format, while TAPE11, TAPE12 and TAPE13 have the surface air temperature, air-sea temperature difference, and dew point depression grid fields. TAPE14 and TAPE15 are the output u and v fields. WSUBLIB contains the library of all subsequently called subroutines. The input data card is in (4I2,I4,I2,2F5.1,I2) format. The parameters are:

IYSTRT. . . The year (e.g., 68) of the starting time  
IMSTRT. . . The month (e.g., 11)  
IDSTRT. . . The date  
IHSTRT. . . The hour  
KSETS . . . The number sets to be analyzed  
MODEL . . . The model to be used to compute the surface winds.  
Values 1-5 are reserved for temperature-independent models. At present MODEL =  
1 for geostrophic winds  
2 for surface winds by the balance equation  
(Mahrt, 1975)

3 for gradient winds  
 4 empirical constants  
 6 use of Brown's model  
 8 use of Cardone's model.

**CNST1** If MODEL = 4 is specified, CNST1 is the fraction of the gradient wind speed used as the surface wind speed and

**CNST2** CNST2 specifies the inflow turning angle in degrees to the left of the geostrophic wind direction:  
 For MODEL = 6 or greater, CNST1 specifies the anemometer height (cm) assumed for the calculations. CNST2 specifies the default relative humidity (decimal fraction).  
 If MODEL = 6 and CNST2 < 0, dew-point depression will read from TAPE13.

**ICNST =** 0 wind components as output on TAPE14 and 15  
 = 1 wind stress components as output  
 = 2 total heat flux and latent heat flux  
 = 3 total heat flux and sensible heat flux.

The value for ITYPE written on the output files is

**ITYPE =** 480 + MODEL for the u velocity component  
 490 + MODEL for the v velocity component  
 500 + MODEL for the u stress component  
 510 + MODEL for the v stress component  
 520 + MODEL for total heat flux  
 530 + MODEL for latent heat flux  
 540 + MODEL for sensible heat flux

so that ITYPE = 482 designates a surface u field generated by MODEL = 2. The only program changes that need to be considered are array dimensions in WINDS.



```

00100 /JOB
00110 EXAMPLE,T270,
00120 ACCOUNT(METLIB)
00130 CHARGE(RP)
00140 GET,WINDS/UN=METLIB.
00150 GET(TAPE10=SLP)
00160 GET(TAPE11=SAT)
00170 GET(TAPE12=ASTD)
00180 GET,TAPE13=DPTD.
00190 GET(WSUBLIB/UN=METLIB)
00200 FTH,I=WINDS,R=3.
00210 LDSET(LIB=WSUBLIB)
00220 LGO.
00230 REPLACE(TAPE14=UFIELD)
00240 REPLACE(TAPE15=VFIELD)
00250 /EOR
00260 68110118 104 0.8 30. 00
      END OF INFORMATION ENCOUNTERED.
/

```

Figure 3. SUBMIT file RWINDS for running WINDS.

#### 4.5 PTWND (Time Series of Winds)

PTWND inputs the u (TAPE14) and v (TAPE15) components of winds and creates time series of winds at up to five specific geographic locations by interpolation. The first data card is formatted (4I2,I4,2I2) and specifies the starting time, number of data sets in the time series, and the parameters NPT and IOU:

NPT . . . Number of points at which the time series is to be created.

IOU. . . Specifies whether u and v components of winds or speed and direction of winds are to be used.

IOU = 0 for u and v components

1 for speed and direction.

Cards 2 through NPT+1 specify the latitude and west longitude (degrees) of each point in (2F5.1) format. Modifications to PTWND can be used to access the u and v fields for almost any purposes.

#### 4.6 PLOTGRD (Plotting)

PLOTGRD is the main program for performing graphical analysis on the data sets generated by the METLIB wind analysis routines. Both scalar and vector fields can be processed in a number of ways, and contour plots and vector fields can be drawn on a continental outline background.

The primary purpose of PLOTGRD is for the user to set up arrays with the proper dimensions. All subroutines use variable-dimensioned arrays and need not be changed when data sets are changed.

The secondary purpose of PLOTGRD is to set default values for a number of parameters which control the plotting. These values can be changed as desired by the user.

Figure 4 shows a listing of RPLLOT, the SUBMIT file for running PLOTGRD. The program uses up to six arrays corresponding to a first and second scalar field and u and v components for two vector fields. The

```
00100 /JOB
00110 EXAMPLE,T270.
00120 USER,METLIB.
00130 CHARGE,RP.
00140 GET,MAIN=PLOTGRD.
00190 GET,TAPE11=BSLP.
00191 GET,TAPE12=BSAT.
00192 GET,TAPE13=U6.
00193 GET,TAPE14=V6.
00194 GET,TAPE15=U1.
00195 GET,TAPE16=V1.
00230 GET,PLTPROC/UN=METLIB.
00231 CALL,PLTPROC(PLOTTER=1TK4010)
00232 REPLACE,TAPE2=EXAMPLT.
00290 /EOR
00300 0,0,0,3,2,3
00310 0,0,0,0,1,0
00320 10FINAL TEST
```

Figure 4. SUBMIT file RPLLOT for running PLOTGRD.

logical unit numbers are assigned as TAPE11 through TAPE16. These files only need be attached if they are to be used. For example for plotting vectors only, TAPE11 and TAPE12 may be omitted.

The "PLOTTER=" parameter specifies the device which will perform the plotting:

PLOTTER = 1TK4010 specifies a Textronics 4010 terminal  
 PLOTTER = 1CCWIDE specifies a CALCOMP plotter with wide paper  
 PLOTTER = 1CCNARO specifies a CALCOMP plotter with narrow paper.

The first data card specifies what plots are to be made. The second card specifies the starting time and the number of plots to be made. Cards 1 and 2 are read as list-directed (free format) input, so data values need only be separated by commas or blanks. Card 3 is optional and is used to specify an additional title for the bottom of the plot.

Data Card 1:

<u>Variable</u>	<u>Value</u>	<u>Comment</u>
IS1	0	no scalar fields are to be processed. If IS1=0, set IS2=IS12=0 also.
	1	scalar field 1 (array S1) is to be contoured.
	2	scalar field 1 is to be read in but is not to be contoured (i.e., is to be used only for differencing, see IS12).
IS2	0	no second scalar field is to be processed.
	1	scalar field 2 is to be contoured.
	2	scalar field 2 is to be read in but not contoured.
IS12	0	the difference of the scalar fields S1-S2 is not to be contoured.
	1	the difference S1-S2 is to be contoured.
IV1	0	no vector fields are to be processed, if IV1=0, set IV2=IV12=0 also.
	1	wind vectors (arrows) only are to be drawn for vector field 1 (arrays U1 and V1).

	2	vector field 1 is to be read in but not processed (i.e., is to be used only for differencing, see IV12).
	3	isotachs only of vector field 1 are to be drawn.
	4	both 1 and 3, i. e., both arrows and isotachs of vector field 1 are to be drawn.
IV2	0	controls processing of vector field 2 the same as IV1 controls processing of vector field 1.
	1	
	3	
	4	
IV12	0	no differencing of vector fields is to be done.
	1	arrows only of vector field 1 minus vector field 2 are to be drawn.
	2	isotachs only of magnitude of vector field 1 minus magnitude of vector field 2 are to be contoured.
	3	both 1 and 2, i.e., arrows and isotachs of the differences.

Data Card 2:

<u>Variable</u>	<u>Value</u>	<u>Comment</u>
IYSTRT	0	If plotting is to begin with the first data set found on the input data files. Otherwise IYSTRT gives the year of the beginning time for data processing, e.g. 71 for 1971.
IMSTRT	0	As for IYSTRT, if plotting is to begin with the first data set. Otherwise, IMSTRT gives the month of the beginning time, e.g. 6 for June.
IDSTRT	0	As for IYSTRT. Otherwise, IDSTRT gives the starting day of the month, e.g. 15.
IHSTRT	0	As for IYSTRT. Otherwise IHSTRT gives the hour of the beginning time, e.g. 12 for 1200Z.

KSETS	0	If all data from the starting time until the end of the input data files are to be processed. If KSETS is greater than zero, then KSETS of data will be processed, beginning with the data set at time IYSTRT, IMSTRT, IDSTRT, IHSTRT. Note that setting IYSTRT=IMSTRT=IDSTRT=IHSTRT=KSETS=0 means that all data found on the input files will be processed.
IBACK	0	no background of continental outlines is to be drawn.
	N	Where N = 1,2, etc. a continental outline is to be drawn every Nth map.

Data Card 3: This card provides any desired title at the bottom of the plot, given the specification of 2 variables:

<u>Variable</u>	<u>Format</u>	<u>Comment</u>
NAUXTL	I2	The number of characters in the auxiliary title.
AUXTIT	7A10,A8	The character string which comprises the title. Up to 78 characters are allowed.

If no auxiliary title is desired, either omit this data card entirely or give NAUXTL the value 0. An example of data card 3 is: 13EXAMPLE TITLE.

After running the example RPLOT of Figure 4 (via SUBMIT, RPLOT, E=PMEL), one can view the generated plots on a Textronix terminal by typing

```
GET,EXAMPLT.  
LNH, F=EXAMPLT.
```

If PLOTTER=1CCNARO is specified in RPLOT, then type

```
GET,EXAMPLT
```

ROUTE, EXAMPLT, DC=PR, UN=PMELTRM to send the plot to the CALCOMP plotter PMEL.

Figures 5 and 6 are sample plots.

The next set of variables is assigned within PLOTGRD (Fig. 7) and can be changed by editing a copied version of the program.

JGRID . . . . The interval for drawing latitude and longitude lines.  
Default is 10°.

IUSOUT. . . . Determines whether or not US state outlines are to be  
drawn if continental outlines are drawn. Default of 1  
gives state outlines. Set to 0 for no outlines.

IDOT. . . . . 0 for continental outlines drawn by solid lines (default)  
1 for continental outlines drawn by dotted lines

NHI . . . . . 0 if highs and lows are labelled by H and L respectively  
on all contour maps (pressure maps are always labelled  
H and L). -1 if highs and lows are not to be labelled  
(default).

Contour intervals for various types of data are as follows:

PRESIN. . . . The contour interval for pressure fields. Default is 4.0 mb.

TEMPIN. . . . The contour interval for temperature fields. The default  
is 1.0°C.

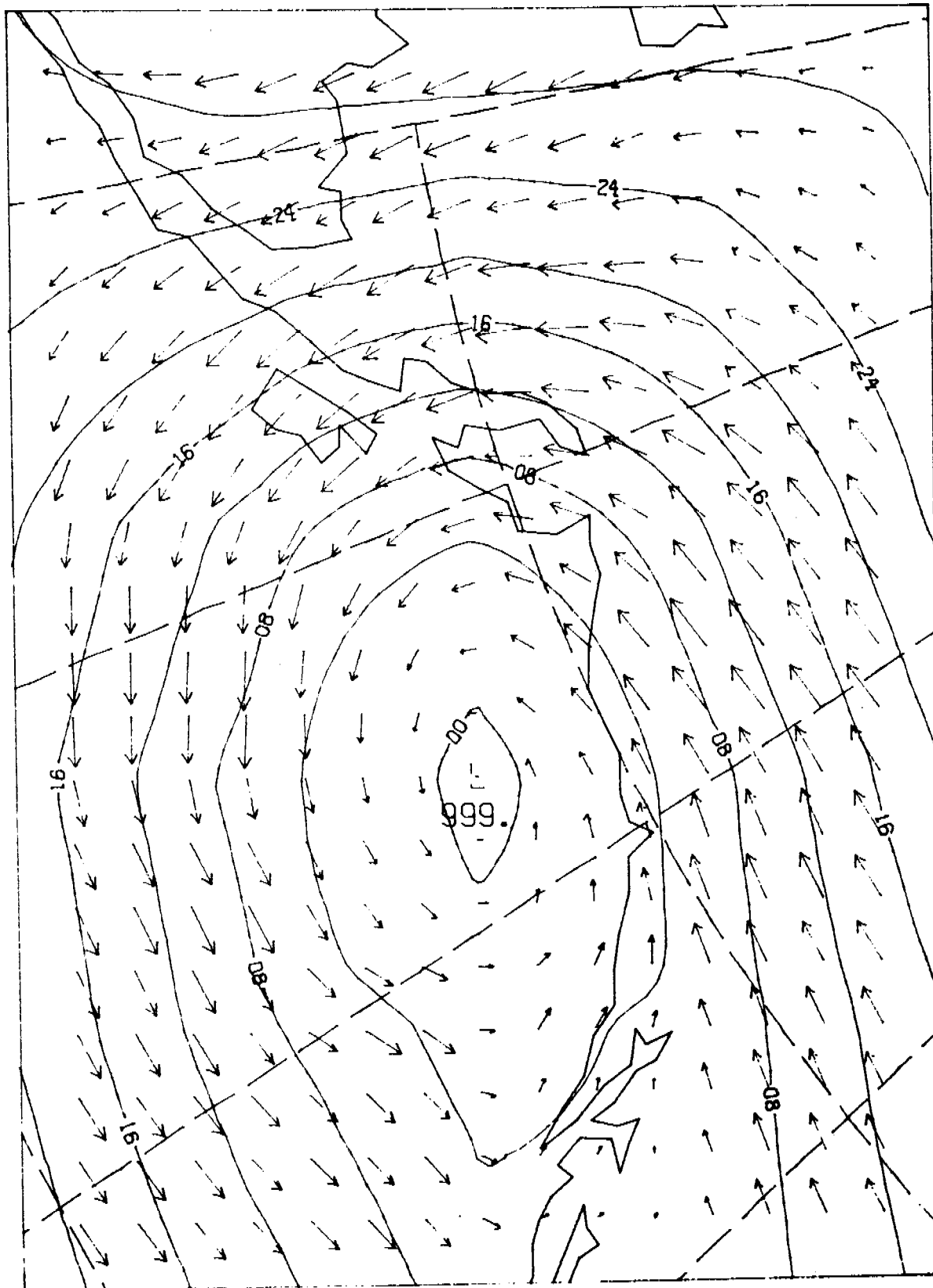
WINDIN. . . . The contour interval for isotachs of the wind fields.  
Default is 400.0 cm sec<sup>-1</sup>.

OTHRIN . . . . The contour interval for any other data type. The  
default of 0.0 allows the NCAR routine to examine  
the data and choose an appropriate interval.

Contour intervals for differences of data fields are as follows:

PDIFIN. . . . The contour interval for contouring the differences of  
two pressure fields. Default is 2.0 mb.

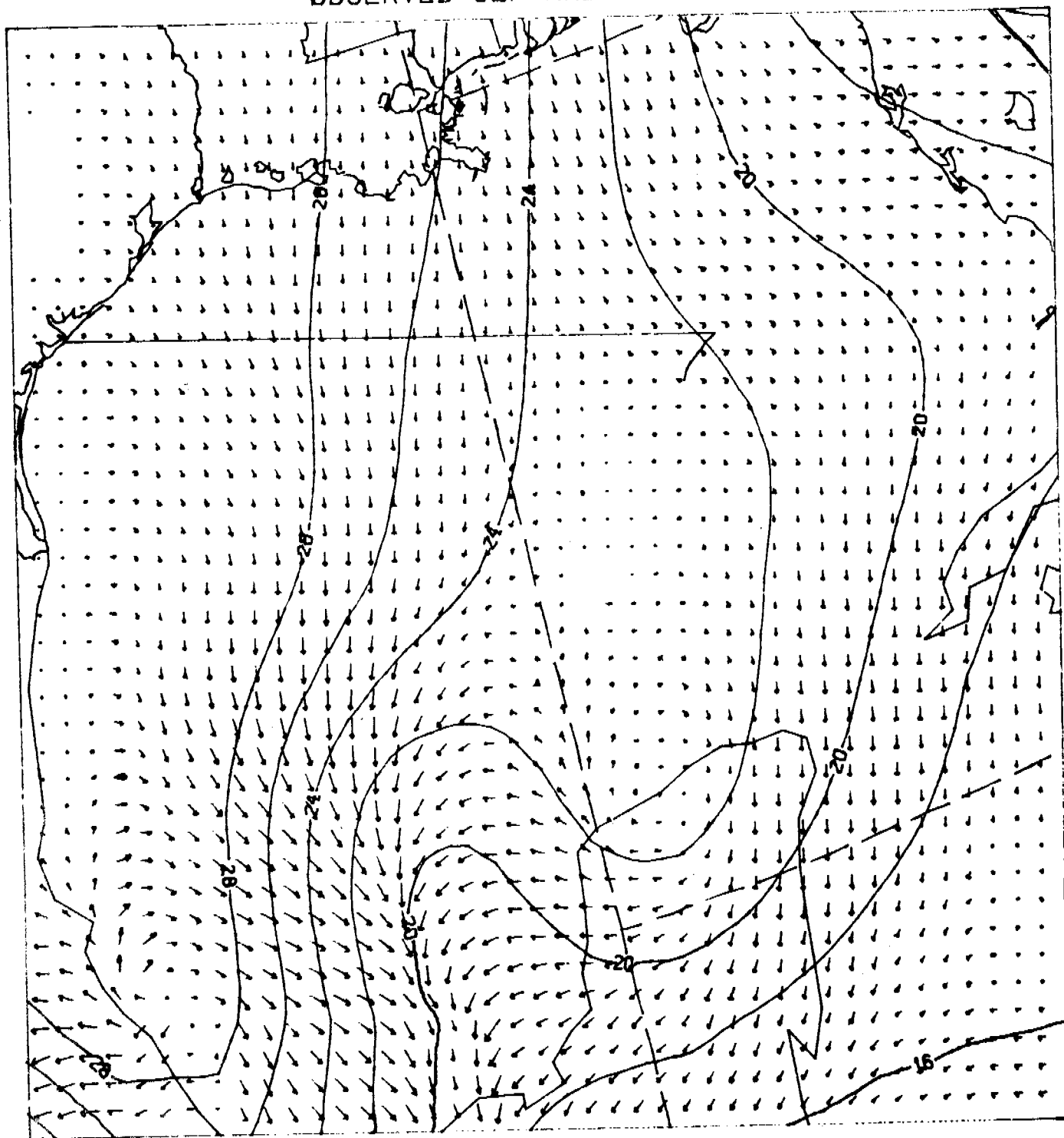
OBSERVED SLP AND WINDS 4



00Z 28 JAN 1974

Figure 5. Winds generated by model 4 and pressures plotted for in the Gulf of Alaska.

OBSERVED SLP AND WINDS 2



00Z 22 FEB 1978

Figure 6. Winds generated by model 2 and pressures plotted for in the Gulf of Mexico.





- VECMIN. . . . .The smallest vector magnitude to be drawn. Default is 0.0.
- VECMAX. . . . .The largest vector magnitude to be drawn. The plot is scaled so that an arrow of this length will just reach from one data point to the next. Default is 2000.0 cm sec.<sup>-1</sup>.
- VDIFMN. . . . .The smallest vector magnitude to be drawn when the difference of two vector fields is being plotted. Any vector smaller than this will not be plotted. Default is 1.0 cm sec.<sup>-1</sup>.
- VDIFM . . . . .The largest vector magnitude to be drawn when the difference of two vector fields is being plotted. Default is 500.0 cm sec.<sup>-1</sup>.

#### 4.7 MAP (Plotting Map Backgrounds)

This program and its SUBMIT file (Fig. 8) create plots of the polar stereographic background used with PLOTGRD. The primary purpose of MAP is to generate working base maps for hand plotting and analyzing meteorological data for later digitization. The one input card is in the same format as the primary card for DECKS. The "PLOTTER=" options are the same as in RPLOT.

```

00100 /JOB
00110 DRAWMAP,T270.
00120 USER,METLIB.
00130 CHARGE,RP)
00140 GET,MAIN=DRAWMAP/UN=METLIB.
00230 GET,MAPPROC/UN=METLIB.
00231 CALL,MAPPROC(PLOTTER=1CCHIDE)
00240 REPLACE,TAPE2=MAP.
00290 /EOR
00300 1,23.,25.,8,11,1
      -END OF FILE-
?
```

Figure 8. SUBMIT file for RMAP for running MAP.

#### 4.8 PLOTW,PLOT2W,PLOT2W2 (Combined Submit Files)

These routines combine RWINDS and RPLLOT so that plots of wind fields or differences between wind fields can be made from scalar input (Fig. 9,10,11). Figure 9 shows PLOTW which calculates and plots a given series of wind fields. The data cards correspond to those of RWIND followed by RPLLOT. PLOT2W (Fig. 10) reads one set of scalars and creates two wind fields corresponding to two different models. PLOT2W2 (Fig. 11) allows the two wind fields to be calculated from different analyses of data for the same observation time. Figure 12 is a sample session running PLOT2W.

```
00100 /JOB
00110 EXAMPLE,T270,
00120 ACCOUNT(METLIB)
00130 CHARGE(RP )
00140 GET,WINDS/UN=METLIB.
00150 GET(TAPE10=SLP)
00160 GET(TAPE11=SAT)
00170 GET(TAPE12=ASTD)
00180 GET,TAPE13=DPTD.
00190 GET(WSUBLIB/UN=METLIB)
00200 FTN,I=WINDS,R=0,L=0.
00210 LDSET(LIB=WSUBLIB)
00220 LGO.
00230 REPLACE(TAPE14=UFIELD)
00240 REPLACE(TAPE15=VFIELD)
00250 RETURN(TAPE10,TAPE11,TAPE12,TAPE13,TAPE14,TAPE15)
00260 GET,MAIN=PLOTGRD.
00270 GET,TAPE11=SLP.
00280 GET,TAPE12=SAT.
00290 GET,TAPE13=UFIELD.
00300 GET,TAPE14=VFIELD.
00310 REWIND(LGO)
00320 GET(PLTPROC/UN=METLIB)
00330 CALL,PLTPROC(PLOTTER=1TK4010)
00340 REPLACE,TAPE2=EXAMPLT.
00350 /EOR
00360 68110118000104 0.8 30.000
00370 0 0 0 4 0 0
00380 0 0 0 0 1 1
00390 09WIND TEST
  END OF INFORMATION ENCOUNTERED.
/
```

Figure 9. SUBMIT file PLOTW for producing wind-field plots from scalar data.

```

00100 /JOB
00110 EXAMPLE,T270,
00120 ACCOUNT(METLIB)
00130 CHARGE(RP)
00140 GET,WINDS/UN=METLIB.
00150 GET(TAPE10=BSLP/UN=SSDATA)
00160 GET(TAPE11=SAT)
00170 GET(TAPE12=ASTD)
00180 GET,TAPE13=DPTD.
00190 GET(WSUBLIB/UN=METLIB)
00200 FTH,I=WINDS,R=0,L=0.
00210 LDSET(LIB=WSUBLIB)
00220 LGO.
00230 REPLACE(TAPE14=UFIELD)
00240 REPLACE(TAPE15=UFIELD)
00250 REWIND(TAPE10,TAPE11,TAPE12,TAPE13)
00260 RETURN(TAPE14,TAPE15)
00270 LDSET(LIB=WSUBLIB)
00280 LGO.
00290 REPLACE(TAPE14=UFIELD2)
00300 REPLACE(TAPE15=UFIELD2)
00310 REWIND,LGO.
00320 RETURN(TAPE10,TAPE11,TAPE12,TAPE13,TAPE14,TAPE15)
00330 GET(PLTPROC/UN=METLIB)
00340 GET(TAPE11=SLP)
00350 GET(TAPE12=SAT)
00360 GET(TAPE13=UFIELD)
00370 GET(TAPE14=UFIELD)
00380 GET(TAPE15=UFIELD2)
00390 GET(TAPE16=UFIELD2)
00400 GET,MAIN=PLOTGRD.
00410 CALL,PLTPROC(PLOTTER=1TK4010)
00420 REPLACE(TAPE2=EXM2PLT)
00430 /EOR
00440 68110118000102
00450 68110118000103
00460 0 0 0 2 2 3
00470 0 0 0 0 1 1
  END OF INFORMATION ENCOUNTERED.
/

```

Figure 10. SUBMIT file PLOT2W for plotting differences between two model runs initialized by the same input data.

```

00100 /JOB
00110 EXAMPLE, T270,
00120 ACCOUNT(METLIB)
00130 CHARGE(RP)
00140 GET, WINDS/UN=METLIB.
00150 GET(TAPE10=SLP)
00160 GET(TAPE11=SAT)
00170 GET(TAPE12=ASTD)
00180 GET, TAPE13=DPTD.
00190 GET(WSUBLIB/UN=METLIB)
00200 FTH, I=WINDS, R=0, L=0.
00210 LDSET(LIB=WSUBLIB)
00220 LGO.
00230 REPLACE(TAPE14=UFIELD)
00240 REPLACE(TAPE15=VFIELD)
00250 REWIND(TAPE10, TAPE11, TAPE12, TAPE13)
00260 RETURN(TAPE10, TAPE14, TAPE15)
00265 GET(TAPE10=SLP2)
00270 LDSET(LIB=WSUBLIB)
00280 LGO.
00290 REPLACE(TAPE14=UFIELD2)
00300 REPLACE(TAPE15=VFIELD2)
00310 REWIND, LGO.
00320 RETURN(TAPE10, TAPE11, TAPE12, TAPE13, TAPE14, TAPE15)
00330 GET(PLTPROC/UN=METLIB)
00340 GET(TAPE11=SLP)
00350 GET(TAPE12=SAT)
00360 GET(TAPE13=UFIELD)
00370 GET(TAPE14=VFIELD)
00380 GET(TAPE15=UFIELD2)
00390 GET(TAPE16=VFIELD2)
00400 GET, MAIN=PLOTGRD.
00410 CALL, PLTPROC(PLOTTER=1CCNARO)
00420 REPLACE(TAPE2=EXM2PLT)
00430 /EOR
00440 68110118000102
00450 68110118000103
00460 0 0 0 2 2 3
00470 0 0 0 0 1 1
  END OF INFORMATION ENCOUNTERED.

```

Figure 21. SUBMIT file PLOT2W2 for plotting differences between wind fields created from different SLP fields.

CALL "RATE", 1200, 0, 2  
CALL "TERMIN"

80/07/14. 12.09.23. NOS 1.4 509/508.04  
N O A A / E R L 6600A 80/07/13.  
FAMILY:  
USER NUMBER: METLIB  
PASSWORD  
■■■■■■■■  
TERMINAL: 101, TTY  
RECOVER/ CHARGE: CHARGE, RP, 00000000  
\$CHARGE, RP, 8C697160.  
/GET, PLOT2W  
/USER, PMELTRM  
USER, PMELTRM.  
/CHARGE, RP, 00000000  
ACSR, 2.007UNTS.  
/SUBMIT, PLOT2W  
12.10.52. AETACCU  
/USER, METLIB  
USER, METLIB.  
/CHARGE, RP, 00000000  
ACSR, 2.050UNTS.  
/ENQUIRE, JN=CCU  
AGZYCCU NOT FOUND.  
/GET, EXAMPLT  
/LNH, F=EXAMPLT

Figure 12. Sample session with PLOT2W.

## 5. SUBROUTINE DOCUMENTATION

### 5.1 Introduction

A catalog of subroutines on WSUBLIB is in Figure 13. Consult source listings on WSUBS for calling sequences.

### 5.2 Interpolation (NTERP)

NTERP is a general subroutine for interpolating values to an arbitrary fractional I-J location from a regular grid-point array. To call NTERP, first determine whether the point is closer than one grid from a boundary, in which case the value is assigned via linear interpolation (i.e. KQUAD=5). For an interior point, biquadratic interpolation is used, which utilizes the values at the 16 surrounding points and is consistent with procedures in use at NMC.

### 5.3 Location on Subgrid (W3FB00,W3FB01)

W3FB01 calculates the latitude,  $\phi$ , and longitude,  $\lambda$ , from polar stereographic grid locations. The transformation equations are:

$$\lambda = 360^\circ - \tan^{-1} \left( \frac{XJ}{XI} \right) - 90^\circ + \text{ORIENT}$$

$$\phi = 90^\circ - 2 \tan^{-1} \left[ \frac{\text{XMESHL} \sqrt{(XI)^2 + (XJ)^2}}{a (1 + \sin 60^\circ)} \right]$$

Where XI and XJ are grid coordinates with the origin translated to the north pole and  $a = 6371.2$  km, the mean radius of the earth. XMESHL is the mesh length for the particular model. The orientation angle, ORIENT, is  $80^\circ$  for the PE and  $105^\circ$  for the LFM. This is the west longitude which is parallel to the j axis.

W3FB00 calculates the coordinates on the I-J grid given latitude and longitude by solving the transformation equations:

$$XI = \frac{11888.85}{(\text{XMESHL})} \frac{(\cos\phi)(\cos\alpha)}{(1 + \sin\phi)}$$

REC	CATALOG OF WSUBS NAME	TYPE	FILE LENGTH	1 CKSUM	DATE
1	GEOWIN	TEXT	736	0006	
2	GRDWD	TEXT	1567	6123	
3	TMWHD	TEXT	650	5741	
4	W3FB00	TEXT	426	0124	
5	W3FB01	TEXT	725	3543	
6	EDGE	TEXT	703	4573	
7	W3FC00	TEXT	171	6007	
8	W3FC02	TEXT	224	0004	
9	MODEL2	TEXT	410	1366	
10	SMOGRD	TEXT	216	7317	
11	GRID	TEXT	405	7525	
12	MODEL4	TEXT	110	7002	
13	FIRST	TEXT	61	5654	
14	BROWN	TEXT	3025	1625	
15	CARDON	TEXT	2413	7363	
16	HTERP	TEXT	1420	0073	
17	* EOF *		SUM =	16774	
CATALOG COMPLETE.					
/+					

Figure 13. Catalog of subroutines in WSUBS.  
WSUBLIB is the library version of WSUBS.



$$XJ = \left( \frac{(11888.85)}{XMESHL} \right) \left( \frac{(\cos\phi) (\sin\alpha)}{1 + \sin\phi} \right),$$

where  $\alpha = 360^\circ - (\lambda + 90^\circ - \text{ORIENT})$ . The pole location is then subtracted to locate the point on the standard grids.

#### 5.4 Speed and Direction (W3FC02,W3FC00)

W3FC02 computes the speed and direction in the meteorological convention of the wind from grid-oriented vector components. The speed is simply  $\text{SQRT}(u^2 + v^2)$ . The wind direction is found from

$$D = \text{TAN}^{-1} \frac{XJ}{XI} - \text{TAN}^{-1} \frac{V}{U}$$

where XI and XJ are defined as in W3FB00. W3FC00 performs the reverse operation.

#### 5.5 Thermal Wind (TMWND)

This subroutine calculates the non-dimensional thermal u and v wind component fields. These calculations are made only if one of models 6-10 is to be used. The vertical gradient of the geostrophic wind in the boundary layer is assumed to depend only on the surface horizontal temperature gradient computed by central differences and the Coriolis parameter:

$$u_T \equiv - \frac{g}{f^2 \bar{T}} \frac{\partial \bar{T}}{\partial y} \qquad v_T \equiv \frac{g}{f^2 \bar{T}} \frac{\partial \bar{T}}{\partial x}$$

where g is the gravitational acceleration; f, the Coriolis parameter; and air temperature (SAT) is taken for the boundary layer average temperature,  $\bar{T}$ , at each grid point.

#### 5.6 GRIDSET (GRIDSET)

GRIDSET reads in IGRID, IFACT, and other parameters and adjusts them according to the degree of interpolation and the grid system used.

### 5.7 Geostrophic Wind (GEOWIN,EDGE)

The components of the pressure gradient at each point of a grid field are found by central differences, dividing by twice the earth distance between adjacent grid points at that latitude. Both the earth-grid distance and the Coriolis parameter depend on the latitude of the grid point. The density of air is specified as constant.

Subroutine EDGE assigns values to the boundary points from the closest interior points.

### 5.8 Gradient Wind (GRDWD)

A method of successive approximations is used for computing the gradient wind at each interior point (Endlich, 1961). In GRDWD the geostrophic wind speed and the radius of curvature are calculated at each point. The equation  $C = C_g - \frac{C^2}{fr}$  is iterated, where  $C$  is the gradient wind speed,  $C_g$  is the geostrophic wind speed, and  $r$  is the radius of the curvature (negative for a clockwise trajectory). EDGE is called at the end to assign gradient wind values to perimeter points.

### 5.9 Empirical Constants (MODEL4)

Model 4 currently reduces the gradient wind by a set amount and rotates the direction as specified in the calling program.

### 5.10 Model 2 (MODEL2)

Model 2 utilizes the vertically integrated equations of motion, as suggested by Mahrt (1975) and by Augstein and Heinricy (1976), to yield a first-order approximation of surface winds from geostrophic winds. The equations are:

$$U = U_o + R_o U_1$$

$$V = V_o + R_o V_1$$

where  $R_o$  is the Rossby number ( $R_o = V_g (fl)^{-1}$ ;  $l$  is horizontal length scale;  $R_o = 0.2$  is assumed by subroutine). The solution without inertia is

$$U_o = (1 + C_D^*)^{-1} (U_g - C_D^* V_g)$$

$$V_o = (1 + C_D^*)^{-1} (V_g + C_D^* U_g)$$

where  $C_D^*$  is the nondimensional drag coefficient given by  $C_D^* = C_D V_g / fH$  where  $H$  is the vertical length scale chosen (1 km) and  $U_g$  and  $V_g$  are the components of the geostrophic wind.  $U_1$  and  $V_1$  are given by

$$U_1 = L(1+C_D^{*2})^{-3} \left[ 2C_D^* \frac{\partial U_g}{\partial x} + (C_D^{*2} - 1) \frac{\partial V_g}{\partial x} - 2C_D^* \frac{\partial U_g}{\partial y} + C_D^*(C_D^{*2} - 1) \frac{\partial V_g}{\partial y} \right]$$

$$V_1 = L(1+C_D^{*2})^{-3} \left[ (1-C_D^{*2}) \frac{\partial U_g}{\partial x} - 2C_D^* \frac{\partial V_g}{\partial x} + C_D^*(1-C_D^{*2}) \frac{\partial U_g}{\partial y} - 2C_D^* \frac{\partial V_g}{\partial y} \right]$$

where  $L$  is twice the mesh length and the partials are in the finite difference form. Another version of MODEL2 specifies  $H$  as proportional to  $u_* / f$ , where  $u_*$  is the friction velocity.

#### 5.11 Models 6-8 (MODEL6, MODEL8, BROWN, CARDON, etc)

Models 6-8 use the magnitude and direction of the thermal wind, the air-sea temperature difference, and the latitude to correct for stability and baroclinicity of the boundary layer in deriving surface-wind speed and inflow angle from the gradient wind. MODEL6 uses the model of R. Brown, summarized in Appendix A. MODEL8 uses the model provided by V. Cardone, summarized in Appendix B.

## 6. ACKNOWLEDGEMENTS

This report is a contribution to the Marine Services Project at Pacific Marine Environmental Laboratory. Subroutines W3FB00 and W3FB01 and subroutine NTERP are adaptations of subroutines in use at the National Meteorological Center. Our thanks to Clifford M. Fridlind, Matthew H. Hitchman, Steven Ghan and Jon O. Nestor who have contributed to the development of METLIB. T. Liu contributed substantially to Appendix A. V. Cardone provided a copy of the computer program of his boundary layer model. R. Brown was supported in part by the Jet Propulsion Laboratory during preparation of this memorandum.

## 7. REFERENCES

- Augstein, E. and D. Heinricy (1976): Actual and geostrophic wind relationships in an accelerated marine atmospheric boundary layer. Beitrage zur Physik der Atmosphere 49, 55-68.
- Cressman, G. (1959): An Operational Objective Analysis System. Mon. Wea. Rev., 87, 367-374.
- Endlich, R.M. (1961): Computation and Uses of Gradient Winds. Mon. Wea. Rev., 89, 187-191.
- Flattery, T.W. (1970): Spectral models for global analysis and forecasting. Proceedings, Sixth AWS Technical Exchange Conference, AWS Tech. Rept., 242, Scott AFB, Ill., 42-54.
- Holl, M., and B. Mendenhall (1971): FIB-fields by information blending. Final report to Commanding Officer, Fleet Numerical Weather Central, Project M-167, 66 pp.
- Jenne, R. L. (1975): Data sets for meteorological research. NCAR Tech. Note NCAR-TN/1A-111, 194 pp.
- Mahrt, L. (1975): The influence of momentum advections on a well mixed layer, Quart. J. R. Met. Soc., 101, 1-11.
- Wright, T. (1977): NCAR graphics software. NCAR Technical Note, Preliminary Edition.

Appendix A: DERIVATION OF THE UNIVERSITY OF WASHINGTON (BROWN)  
PLANETARY BOUNDARY LAYER MODEL

1. SOLUTION FOR THE PBL WITH NEUTRAL STABILITY

An appropriate set of non-dimensionalized equations for a non-accelerating lower atmosphere is

$$V + E^2 (KV_z)_z - P_x/\rho = 0 \quad (1)$$

$$U - E^2 (KV_z)_z + P_y/\rho = 0 \quad (2)$$

where E is an Ekman number defined by  $E = \delta/H$ , with  $\delta^2 = 2\bar{K}/f$ ; H is an arbitrary scale height; f is the Coriolis parameter; K is an eddy coefficient,  $\bar{K}$  is its mean;  $V_0$  is the characteristic velocity scale;  $z = \hat{z}/H$ ;  $V = \hat{V}/V_0$ . Hats denote dimensional variables while characteristic values are always dimensional:  $u_x, G, \delta, z_0, \rho_0, T_0$ , and L. All other terms use standard notation. A continuous solution for the domain  $0 \leq z \leq \infty$  can be obtained by considering three scale heights H and the appropriate solution for each regime is given in Table 1.

Table 1: Flow Solutions for Scale Heights H above the Surface

H	E	Equations	Solutions
$\rightarrow \infty$	$\rightarrow 0$	$\nabla \sim + \nabla P/\rho = 0$	Geostrophic (w/corrections)
$0[\delta]$	$0[1]$	(1&2) with $E=1$	Ekman/Taylor layer (3)
		$K = \text{constant}$	$\frac{\hat{U}}{G} = \cos \alpha - e^{-\zeta} [\cos(\alpha-\zeta) - \frac{\hat{U}_0}{G} \cos \zeta]$
		$V_0 \equiv G$	$\frac{\hat{V}}{G} = \sin \alpha + e^{-\zeta} [\sin(\alpha-\zeta) - \frac{\hat{U}_0}{G} \sin \zeta]$
			$\hat{U} \rightarrow G \text{ at } \zeta \rightarrow \infty$
			$\hat{U} \rightarrow \hat{U}_0 \text{ at } \zeta \rightarrow 0$

Cont.

Table 1: Flow Solutions for Scale Heights H above the Surface (continued)

H	E	Equations	Solutions
			$\zeta \equiv \hat{z}/\delta$
			$\alpha$ is angle between $\vec{V}_g$ and $\vec{U}_o$
			Surface Layer
$0[z_o]$	$\infty$	$(KU_z)_z = 0$	$\hat{U} = \frac{u_*}{k} \ln \frac{\hat{z}}{z_o}$ (4)
			$K = ku_* \hat{z}, K_o = ku_* z_o$
			$u_* = (\tau_o/\rho_o)^{1/2} = V_o$

where  $\tau_o, \rho_o, K_o$  and  $z_o$  are stress, density, eddy viscosity and height (roughness scale) at  $U = 0$ .

The velocity  $V_o$  can be related to the turning angle,  $\alpha$ , using Taylor's lower boundary condition that near the surface, the velocity and stress are in the same direction.

$$\hat{U}_o = G(\cos \alpha - \sin \alpha) \quad (5)$$

With equations 3, 4, and 5, velocity profiles can be calculated through the PBL provided that:  $u_*$  and  $z_o$  are known for the surface layer; either  $h_p$ , the height of the surface layer, or  $\alpha$ , the turning angle between  $G$  and  $u_*$ , is known; and  $G$  and  $\delta$  are known for the outer layer. By examining the matching requirements for the two-layer solution, the need for  $h_p$  and  $\delta$  will be reduced to only the need for the ratio  $h_p/\delta = \lambda$ .

When the velocity, shear and eddy viscosity in the surface layer and the Ekman/Taylor layer are matched, one obtains

$$\begin{aligned} kG/u_* \sin \alpha &= -B \\ kG/u_* \cos \alpha &= -A', \end{aligned} \quad (6)$$

where  $A'$  and  $B$  are similarity parameters which depend on the single similarity parameter,  $\lambda$ . So,

$$u_* / G = k(B^2 + A'^{-2})^{-1/2} \quad (7)$$

$$B = e^\lambda / (2\lambda \cos \lambda)$$

$$A' = -\ln \lambda E_s - (\cos \lambda - \sin \lambda) / (2\lambda \cos \lambda) \quad (8)$$

with  $E_s = \delta / z_o$ ,  $\delta = 2k\lambda u_* / f$ .

The solution is completed by adding an empirical relation for  $z_o$  as a function of  $u_*$  and assigning values to the similarity parameter,  $\lambda$ .

There exist several choices for  $z_o(u_*)$ . We have examined several possibilities and have chosen the empirical relation from Kondo (1975) (see Section IX) for use in the model. An iterative solution for  $u_*$  is needed.

## 2. THE NEUTRAL PBL WITH SECONDARY FLOW IN THE EKMAN/TAYLOR LAYER

It has been shown that the first-order closure (K-theory) solution for the Ekman/Taylor layer is unstable to infinitesimal perturbations and therefore doesn't exist (see, e.g., Brown, 1974). There is a non-linear equilibrium finite perturbation solution (Brown, 1970) and this correction has been incorporated in the model. The basic mean flow is altered such that  $(U, V, W) = (U_E, V_E) + (U_2, V_2) + (u_2, v_2, w_2)$  where  $(U_E, V_E)$  is the solution of the homogeneous equation (3),  $(U_2, V_2)$  are the mean flow modifications, and  $(u_2, v_2, w_2)$  are the zero mean secondary flow. The finite perturbation modifies the basic Ekman/Taylor equation (3) with a forcing function depending on  $\overline{w_2 v_2}$  on the right-hand side of the second equation.

The amended equations for  $u_*$  is

$$\frac{u_*}{kG} = \frac{-\gamma A' - \beta B + [A'^2 + B^2 - (\gamma B - \beta A')^2]^{1/2}}{A'^{-2} + B^2} \quad (9)$$

$$\frac{kG}{u_*} (\sin \alpha + \beta) = -B \quad (10)$$



$$\frac{kG}{u_*} (\cos\alpha + \gamma) = -A' \quad (11)$$

where

$$\beta = \frac{-e^\lambda}{2 \cos \lambda} U_{2\zeta}(\lambda)$$

$$\gamma = \frac{\cos \lambda - \sin \lambda}{2 \cos \lambda} U_{2\zeta} + U_2$$

evaluated at  $\zeta = \lambda$ .

The neutral value of  $U_2$  is given in Brown (1970).

### 3. THE MODIFIED EKMAN/TAYLOR LAYER WITH THERMAL WIND

When thermal wind is added to the model, the pressure gradient term in (1) and (2) becomes a function of  $(T_x, T_y)$ , and, under the approximation that the temperature gradient is constant with height,

$$P_x/\rho = (P_x/\rho)_{z=0} + (g/T_0) \hat{T}_x \hat{z}.$$

The equation for the geostrophic balance throughout the layer may be written

$$(U_g, V_g) = (U_{go}, V_{go}) + (u_T, v_T) \zeta$$

$$(u_T, v_T) = \frac{g}{fT_0} (-T_y, T_x), \quad (U_{go}, V_{go}) = (\cos \alpha, \sin \alpha).$$

The thermal wind must be added to (3) and the equations for  $\beta$  and  $\gamma$  become:

$$\beta = \frac{-e^\lambda}{2 \cos \lambda} \left[ u_T - \frac{\cos \lambda + \sin \lambda}{e^\lambda} v_T + U_{2\zeta} \right]_{\zeta=\lambda}$$

$$\gamma = \left\{ \left[ \frac{\cos \lambda - \sin \lambda}{2 \cos \lambda} + \lambda \right] u_T + \left\{ \frac{1}{2e^\lambda \cos \lambda} \right\} v_T \right. \\ \left. + U_2 + \frac{\cos \lambda - \sin \lambda}{2 \cos \lambda} U_{2\zeta} \right\}_{\zeta=\lambda}$$

while (9) remains the fundamental equation for  $u_*(G)$ .

#### 4. THE STRATIFIED PBL

Variation in the bulk stratification of the PBL has an effect on the surface-layer solution and upon the modified Ekman/Taylor-layer solution. The former effect has been empirically parameterized (Section 10) and (4) becomes

$$U = u_* [\ln(z/z_0) - \psi]/k, \quad (12)$$

where  $\psi$  is an empirical correction which depends on  $\hat{z}/L$ ;  $L$  is the Obukhov scale =  $-Tu_*^2/(gkT_*)$ ;  $T_* = -(\text{heat flux})/(\rho C_p u_*)$ . An iteration on the stratification correction is necessary since it depends upon  $u_*$ . The equations for  $A'$ ,  $B$  and  $\delta$  are

$$B = \frac{e^\lambda}{2 \lambda \cos \lambda} \left[ 1 - \lambda \psi_\zeta \right]_{\zeta=\lambda} \quad (13)$$

$$A' = - \left[ \ln \lambda E_s + \frac{\cos \lambda - \sin \lambda}{2 \lambda \cos \lambda} \right] - \left[ \psi + \frac{\cos \lambda - \sin \lambda}{2 \cos \lambda} \psi_\zeta \right]_{\zeta=\lambda}$$

$$\delta = 2k\lambda u_* / [f(1 - \lambda \psi_\zeta)].$$

The stratification effect on the outer layer appears in  $U_2/G$ . This is fairly strong and nearly constant in unstable stratification and decreases to zero when the Richardson number approaches 1/4. This stratification effect can be empirically related to a stratification parameter  $\mu = ku_*/(fL)$  from the magnitude calculations by Brown (1972):

$$\begin{aligned} U_2(\lambda) &= 0.05 & \mu &\leq 0 \\ U_{2\zeta}(\lambda) &= 0.1 & & \\ U_2(\lambda) &= 0.05 (\mu_{\max} - \mu)/\mu_{\max} & 0 \leq \mu \leq \mu_{\max} & (\text{Ri} = 0.25) \\ U_{2\zeta}(\lambda) &= 0.1 (\mu_{\max} - \mu)/\mu_{\max} & & \\ U_2 = U_{2\zeta} &= 0 & \mu &\geq \mu_{\max} \end{aligned} \quad (14)$$

## 5. HUMIDITY AND THE MOLECULAR SUBLAYER

In a marine atmosphere, the humidity can significantly change the buoyancy of the air since moist air is lighter than dry air. The model uses the relative humidity of the air to evaluate this term. To include this effect, the Obukhov length is defined as

$$L = -T_v u_*^2 / (gkT_{v*}),$$

where  $T_v = T(1 + 0.61Q)$ ,  $T_{v*} = T_*(1 - 0.61Q) + 0.61TQ_*$ ,  $T_* = -H_o / (c_p u_*)$ ,  $Q_* = -E_o / (\rho u_*)$ ,  $T$  is the potential temperature,  $Q$  is the specific humidity,  $H_o$  and  $E_o$  are the heat and moisture fluxes.

In order to determine  $L$ , the heat and moisture fluxes are determined with the diabatic profiles

$$\begin{aligned} (T - T_s) / T_* &= (\ln(z/z_T) - \alpha_T)(K_{H_o})^{-1} \\ (Q - Q_s) / Q_* &= (\ln(z/z_Q) - \alpha_Q)(K_{E_o})^{-1}, \end{aligned} \tag{15}$$

where  $\alpha_T = K_{H_o} / K_{M_o}$  and  $\alpha_Q = K_{E_o} / K_{M_o}$  are the ratios of turbulent diffusivities at neutral conditions. These profiles, however, are not valid close to the interface. While transport in air and water is facilitated by turbulent motion, the motion is suppressed near the interface and one expects molecular diffusion to dominate. Since diffusion is a much slower process in the regions on both sides of the interface, there is a reduction in exchanges between the ocean and the atmosphere. Most of the variation in velocity, temperature, and passive variable concentration in the lower part of the atmosphere and upper part of the ocean are found in these regions, which will be referred to as the interfacial sublayers. The lower boundary values  $z_T$  and  $z_Q$  in (15) depend on the temperature and moisture distributions in the sublayer in the air. Liu and Businger (1975) derived sublayer profiles based on the assumption of intermittent instability. The values of  $z_T$  and  $z_Q$  are determined by matching the sublayer profiles with (15) (Liu et al., 1979). Their values can be approximated by

$$\begin{aligned} z_T u_* / \nu &= a_1 Rr^b_1 \\ z_Q u_* / \nu &= a_2 Rr^b_2, \end{aligned} \tag{16}$$

where  $\nu$  is the kinematic viscosity. The values of  $a_1$ ,  $a_2$ ,  $b_1$ ,  $b_2$ , for ranges of the roughness Reynolds number  $Rr = zU/\nu$  are shown in Table 2.

Table 2: The Lower Boundary Values of the Logarithmic Profiles

$Rr$	$a_1$	$b_1$	$a_2$	$b_2$
0-0.11	0.177	0	0.292	0
0.11-0.826	1.376	0.929	1.808	0.826
0.925-3.0	1.026	-0.599	1.393	-0.528
3.0-10.0	1.625	-1.018	1.956	-0.870
10.0-30.0	4.661	-1.475	4.994	-1.297
30.0-100.0	34.904	-2.067	30.790	-1.845

## 6. MODEL SUMMARY

The University of Washington Planetary Boundary Layer (PBL) model is a composite which includes:

- 1) A surface layer with no turning of the wind and a velocity which increases logarithmically with height. The log profile is corrected for variable stratification using the Businger/Dyer model (Section 10). It is also corrected for variable humidity and diabatic effects in the interfacial layer.
- 2) An outer layer model in which velocity turning takes place from the top of the surface layer to the upper boundary flow condition--the free stream or geostrophic flow. This Ekman/Taylor layer flow is corrected for stratification effects directly through the variable secondary flows from Brown (1970) and for thermal wind.

- 3) A similarity relationship derived from matching the two layers. This involves the geostrophic flow  $G$ , the Ekman depth  $\delta = (2K/f)^{1/2}$ , the friction velocity,  $u_*$ , and the surface roughness scale,  $z_0$ , in an equation relating the geostrophic drag coefficient,  $u_*/G$ , to the similarity parameter,  $\lambda = h_p/\delta$ .
- 4) An assumed relation between  $z_0$  and  $u_*$  taken from Kondo (1975) (Section 9).

The basic equations are:

Surface layer:

$$\hat{u}/u_* = [\ln \hat{z}/z_0 - \psi(\hat{z}/L)]/k,$$

where  $\psi$  is determined empirically from the Businger and Dyer method (Section 10) and

$$L = \frac{-Tu_*^2}{kgT_*} \quad T_* = \frac{T_a - T_s}{\alpha k (\ln \frac{h_*}{z_0} - \psi)}$$

and  $h_*$  and  $z_0^*$  are obtained from Liu's (1978) correction for the interfacial layer, allowing for humidity effects.

Ekman/Taylor layer:

$$U = \cos \alpha + u_t \xi - e^{-\xi} [(\cos \xi - \sin \xi) \sin \alpha + v_t \cos \xi] + U_2$$

$$V = \sin \alpha + v_t \xi - e^{-\xi} [(\cos \xi + \sin \xi) \sin \alpha + v_t \sin \xi] + V_2$$

$$(U_g, V_g) = (\cos \alpha, \sin \alpha) + (u_t, v_t)$$

$$(u_t, v_t) = g\delta / (fGT_0) (-\hat{T}_y, \hat{T}_x) \text{ and } \alpha < u_*, v_g >$$

$$(\hat{U}_2, \hat{V}_2)/G \text{ are parameterized from the results of Brown (1972).}$$

Applying the Matching Condition gives the system:

$$\frac{kG}{u_*} (\sin \alpha + \beta) = -B$$

$$\frac{kG}{u_*} (\cos \alpha + \gamma) = -A'$$

$$u_* = kG \frac{-\gamma A' - \beta B + [A'^2 + B^2 - (\gamma B - \beta A')^2]^{\frac{1}{2}}}{A'^2 + B^2}$$

$$B = \frac{e^\lambda}{2 \lambda \cos \lambda} \left[ 1 - \lambda \psi_\zeta(\text{HL}) \right]$$

$$A' = -\ln \lambda E_s + \psi(\text{HL}) - \frac{\cos \lambda - \sin \lambda}{e^\lambda} B$$

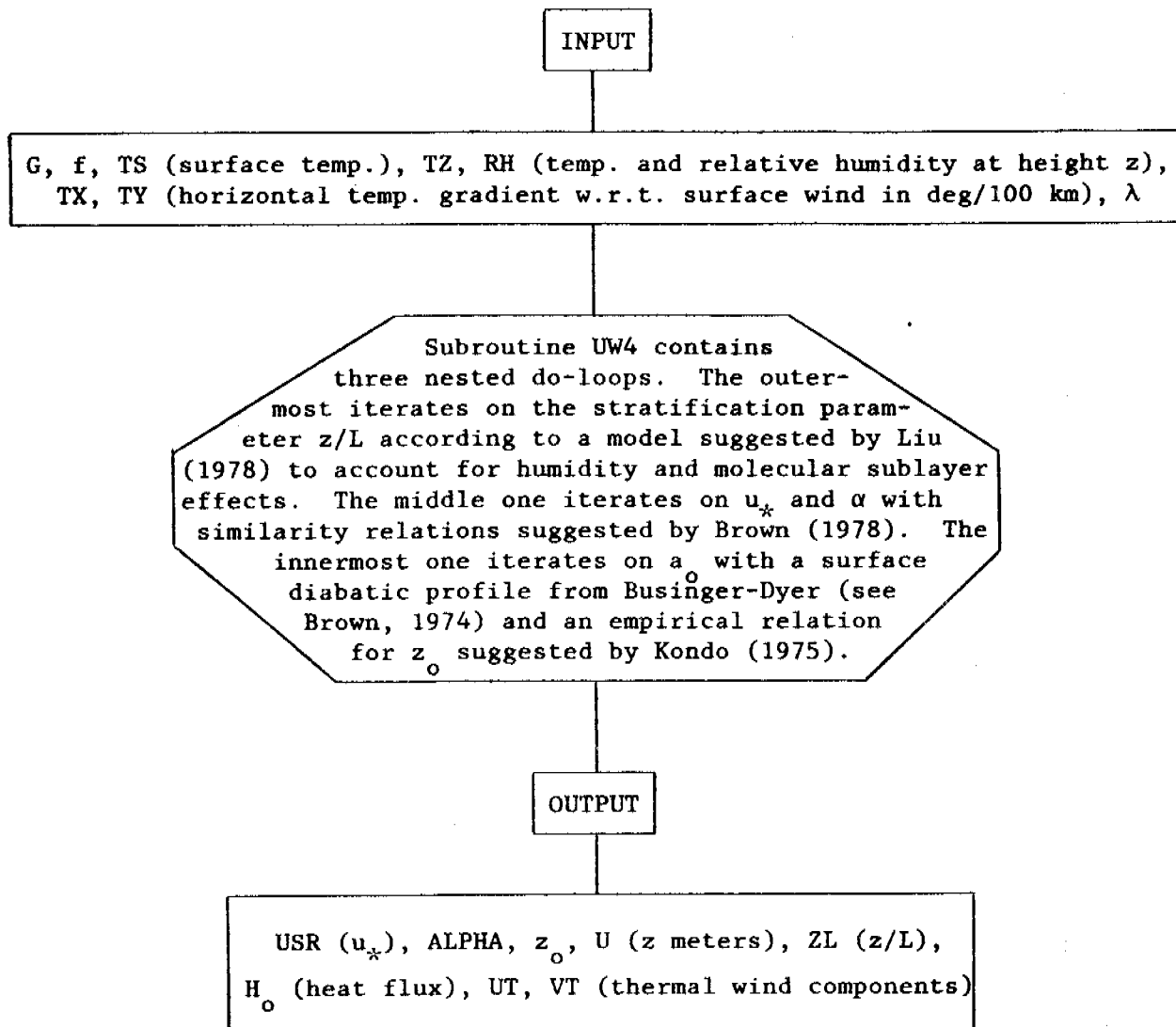
$$E_s = \delta / z_o = 2k\lambda u_* / [fz_o (1 - \psi_\zeta(\text{HL})]); \text{HL} = \frac{\lambda \delta}{L}$$

$$\beta = \frac{e^\lambda}{2 \cos \lambda} \left[ -u_T(\lambda) + \frac{\cos \lambda + \sin \lambda}{e^\lambda} v_T(\lambda) - U_{2\zeta}(\lambda) \right]$$

$$\gamma = \lambda u_T(\lambda) + \frac{\cos \lambda}{e^\lambda} v_T(\lambda) + U_2(\lambda) - \frac{\cos \lambda - \sin \lambda}{e^\lambda} \beta.$$

The roughness parameter,  $z_o(u_*)$ , is specified per Kondo (1975) and Liu (Section 9),  $\lambda = 0.15$  from Brown (1978), and  $U_2(\lambda)$  from Brown (1972). The value of  $L$  requires air-sea temperature differences and Businger/Dyer corrections (Section 10). The thermal wind ( $u_T$ ) requires horizontal temperature gradients.

## 7. PROGRAM FLOW DIAGRAM



## 8. MODEL SENSITIVITY

The model is based upon the  $\psi$  formulation of Businger-Dyer and the Kondo (1975)  $z_0(u_*)$  relation. Other aspects which differ from previous models are: the inclusion of equilibrium producing secondary flow in the outer layer; adding a molecular sublayer and relative humidity effect; and adding a thermal wind. The importance of each of these terms has been investigated by varying the basic parameters and checking output variations for representative cases.

Some changes due to secondary flow are shown in Table 3.

Table 3: Secondary Flow Effect (Neutral)

$G \text{ m sec}^{-1}$	$U_2$	$U_{2z}$	$z_0 \text{ cm}$	$U_{10} \text{ ms}^{-1}$	$u_* \text{ cm sec}^{-1}$	$\alpha \text{ deg.}$
10	0	0	.017	7.0	25	15
10	-0.05	0.1	.020	7.6	28	12

The variation of the surface roughness parameter  $z_0$  and the PBL height parameter,  $\delta$ , with  $G$  is shown in Figure 1. Both increase nearly linearly with freestream flow magnitude.

The default relative humidity is 0.7. The effect of humidity is shown in Figure 2. There is a change in stratification over the range of humidity, greatest in slightly stable regimes. The effect on  $\delta$  is shown, amounting to a 50 percent change near neutral stratification.

The effects of thermal wind on the model are shown in Figure 3. Variation of  $u_*$  and  $\alpha$  with  $T_x$  (temperature gradient in the  $U_{10}$  direction,  $T_y \equiv 0$ ) and with  $T_y$  ( $T_x \equiv 0$ ) are shown in Figure 3a. The effect of direction is shown in 3b, where a constant  $\nabla T \cong 4.0$  is rotated. This is a large thermal wind and the effect is significant. For  $\nabla T \leq 2^\circ/100 \text{ km}$ , the  $u_*$  error is  $\leq 10$  percent, and  $\alpha$  may change by  $\leq 5^\circ$ .

From the matching of  $K$  at the patching height;

$$\delta = 2k\lambda u_* / [f(1-\lambda\psi_z)].$$

Using Ekman's approximate boundary layer height,  $H = \pi\delta$ , this becomes:

$$\frac{Hf}{u_*} = 2\pi k\lambda / (1-\lambda\psi_z).$$



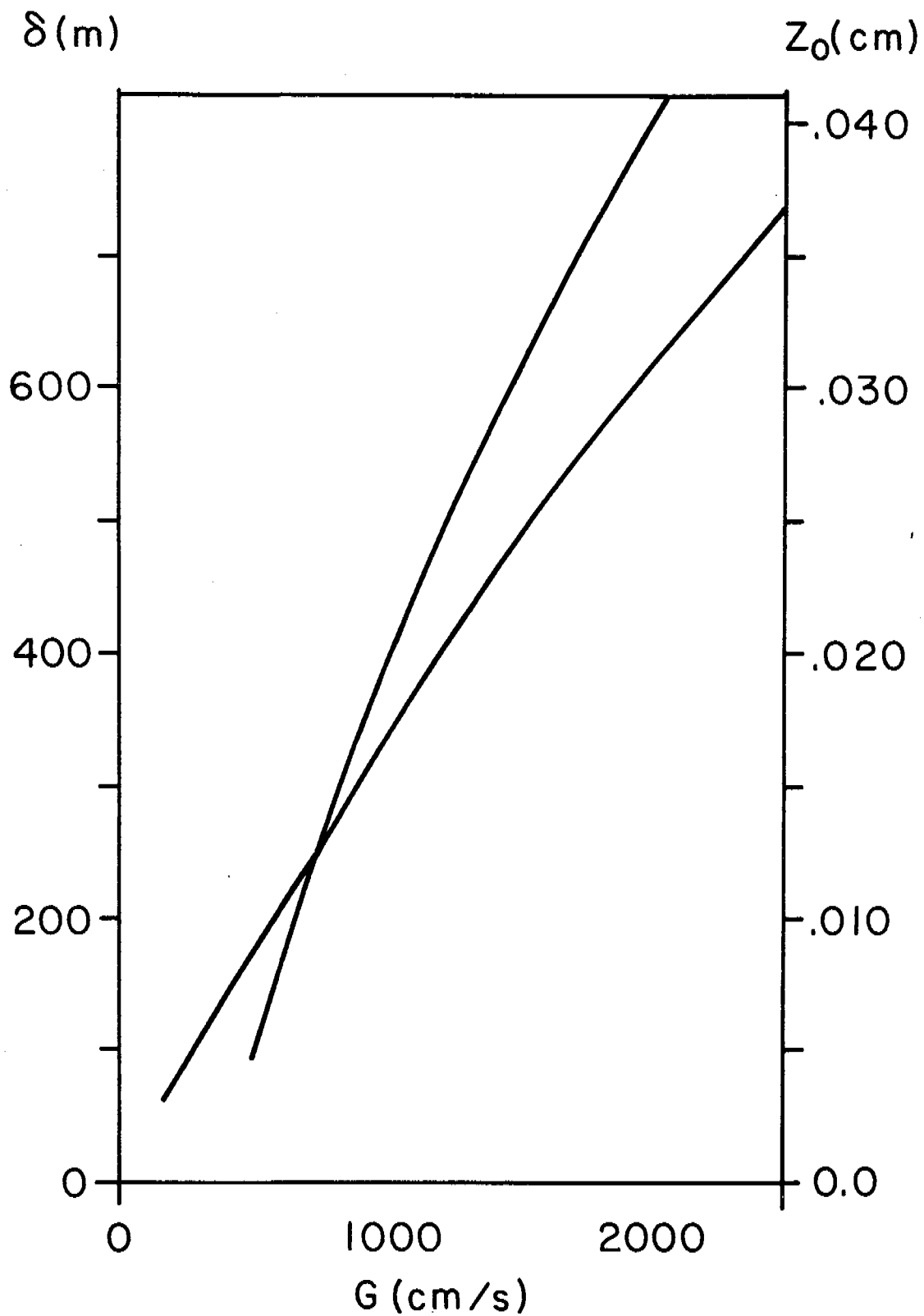


Figure 1 -- Roughness parameter  $z_0$  and depth of frictional resistance  $\delta$  versus geostrophic flow  $G$  (at  $45^\circ$  lat.,  $RH = 0.7$ , neutral stratification),  $u_x/G$  is approximately constant 0.028.

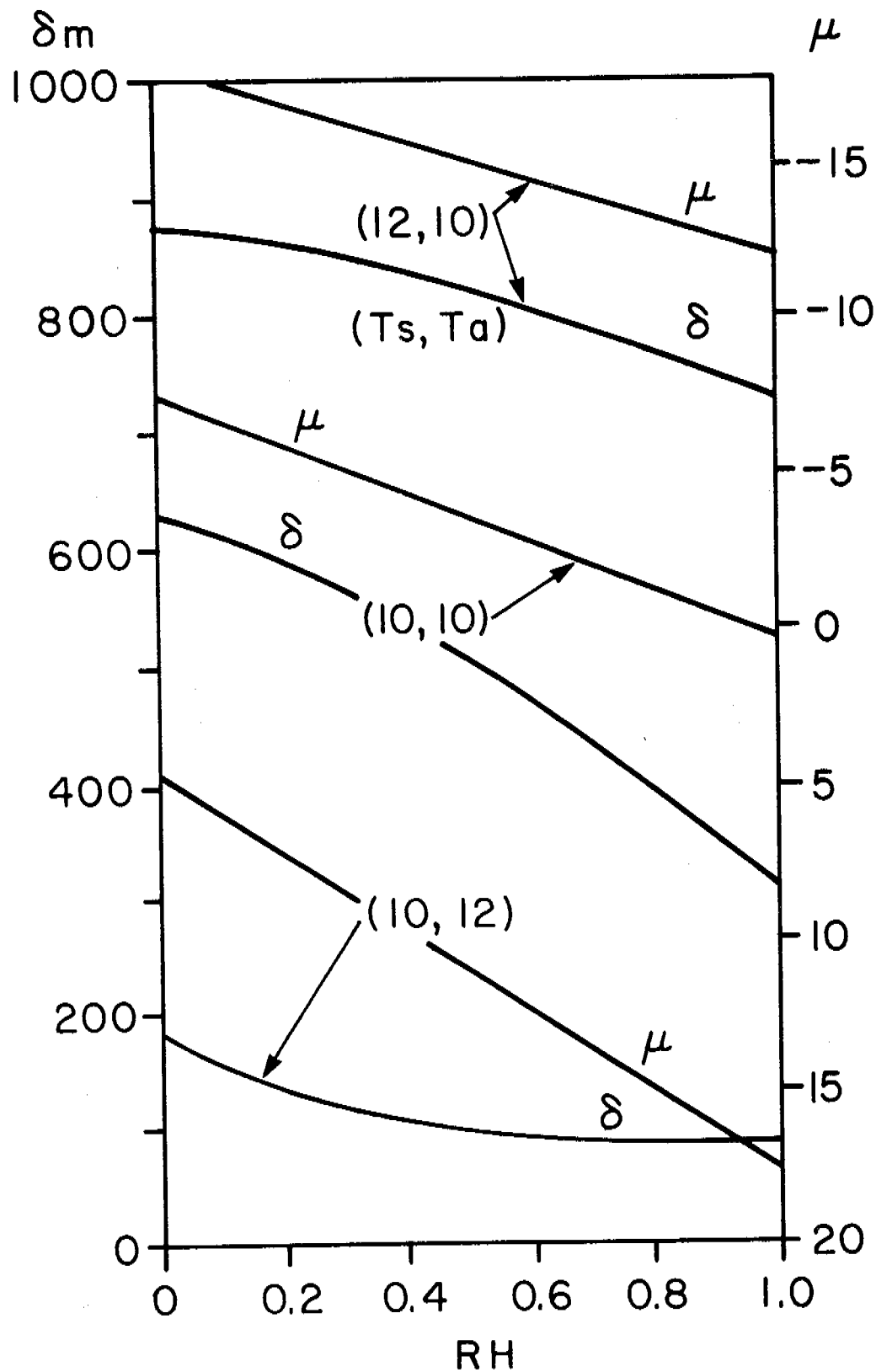


Figure 2 --  $u_*$ ,  $z_o$  and  $\delta$  versus relative humidity at stable ( $T_s = 10$ ,  $T_z = 12$ ), near neutral ( $T_s = T_z = 10$ ) and unstable ( $T_s = 12$ ,  $T_z = 10$ ) stratification (at  $45^\circ$  lat.,  $G = 10 \text{ m s}^{-1}$ ).

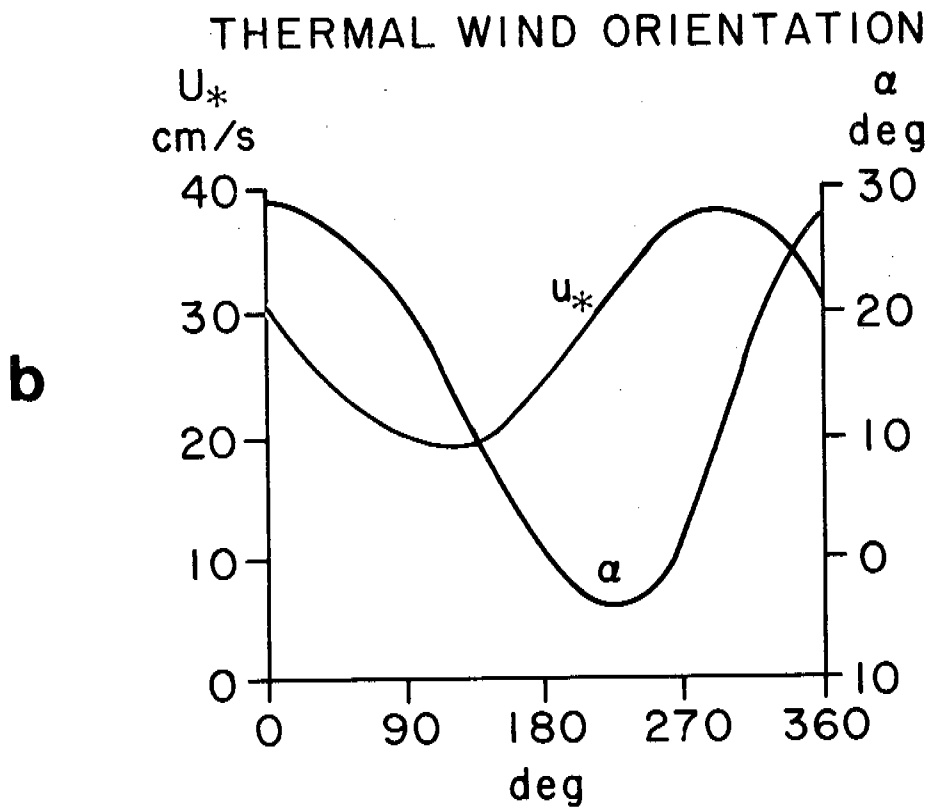
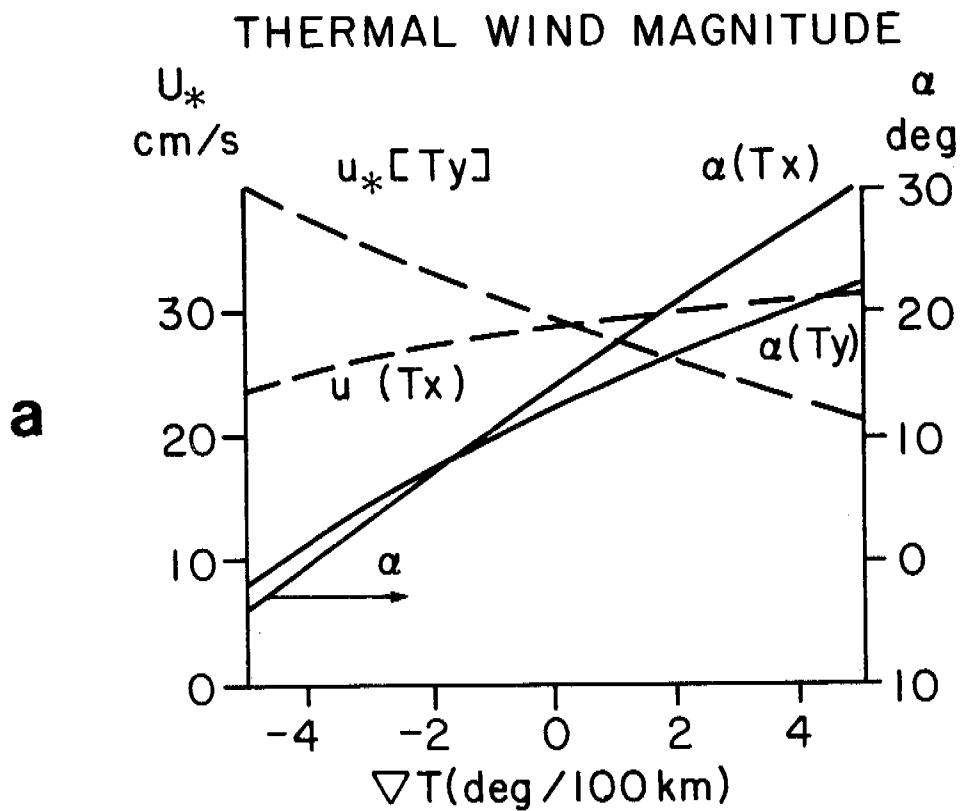


Figure 3 --  $u_*/G$  and  $\alpha$  (geostrophic departure) versus temperature gradient for variable gradient parallel to surface flow ( $T_y = 0$ ), normal to surface flow ( $T_x = 0$ ) and for constant gradient ( $\nabla T = 4$ ) at various angles to  $U_{10}$  (at  $45^\circ$  lat.,  $RH = 0.7$ ,  $G = 10 \text{ m s}^{-1}$ , neutral).

From Paulson's (1970) empirical expression for  $\Psi(\hat{z}/L)$ , model results for PBL height variation with stratification are shown in Figure 4.

The height of the PBL in stably stratified conditions has often been written:

$$\frac{Hf}{u_*} = a\mu^{-\frac{1}{2}}, \quad (17)$$

where  $\mu = u_*/fL$  and "a" has been found to be from 0.7 to 2, generally assumed to be near unity. With  $\Psi = -a_0 \hat{z}/L$  in stable stratification,

$$\frac{Hf}{u_*} = \frac{2\pi k\lambda}{1 - \frac{a_0\lambda\mu}{k\pi} \frac{Hf}{u_*}}$$

$$\frac{Hf}{u_*} = \frac{1 \pm (1 - 8a_0\lambda^2\mu)^{\frac{1}{2}}}{\frac{2a_0\lambda}{k\pi} \mu}$$

$$\frac{Hf}{u_*} = [(1 + 0.84\mu)^{\frac{1}{2}} - 1] / (1.1\mu) \quad (18)$$

when  $a_0 = -4.7$ ,  $k = 0.4$ , and  $\lambda = 0.15$

In case of large  $\mu$ , (18) is approximated by 17 with  $a = 0.8$ .

While the curve fit (17) breaks down at  $\mu = 0$ , (18) has no such problem, as shown in Figure 4.

Figure 5 shows the effects of stratification on  $u_*$ ,  $U_{10}$ ,  $U_{19.5}$  and  $\alpha$ . Stable stratification has a large effect, and small changes near neutral result in large change in  $\alpha$  and  $u_*$ . The decreased effect on  $U_{19.5}$  and  $U_{10}$  compared to  $u_*$  is evident, a result of the higher level flow being more influenced by the constant upper boundary condition,  $G = \text{constant}$  and less by the layer stratification.

#### 9. THE NEUTRAL DRAG COEFFICIENT AND ROUGHNESS PARAMETER

Under neutral conditions, the wind speed at height  $z$  in the atmospheric surface layer is given by

$$(\hat{U} - \hat{U}_s)/u_* = \ln(\hat{z}/z_0)/k, \quad (19)$$

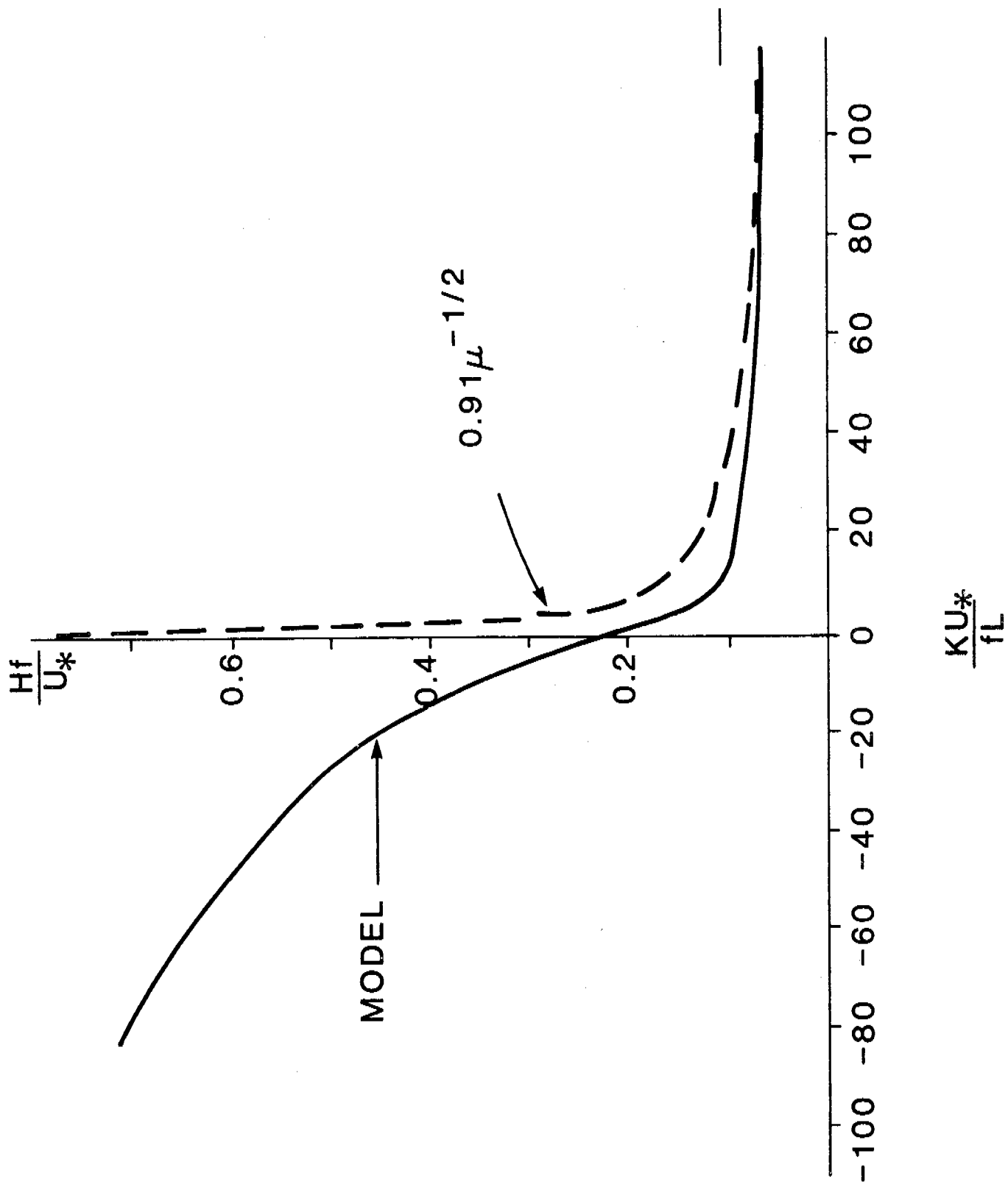


Figure 4 -- The PBL height from the model versus stratification (solid line). The dashed line is the approximate relation  $H = 0.9 \mu^{-1/2}$ ,  $RH = 0.7$ ,  $G = 10 \text{ m sec}^{-1}$ ,  $\text{lat.} = 45^\circ$  and  $H \sim \pi\delta$ .

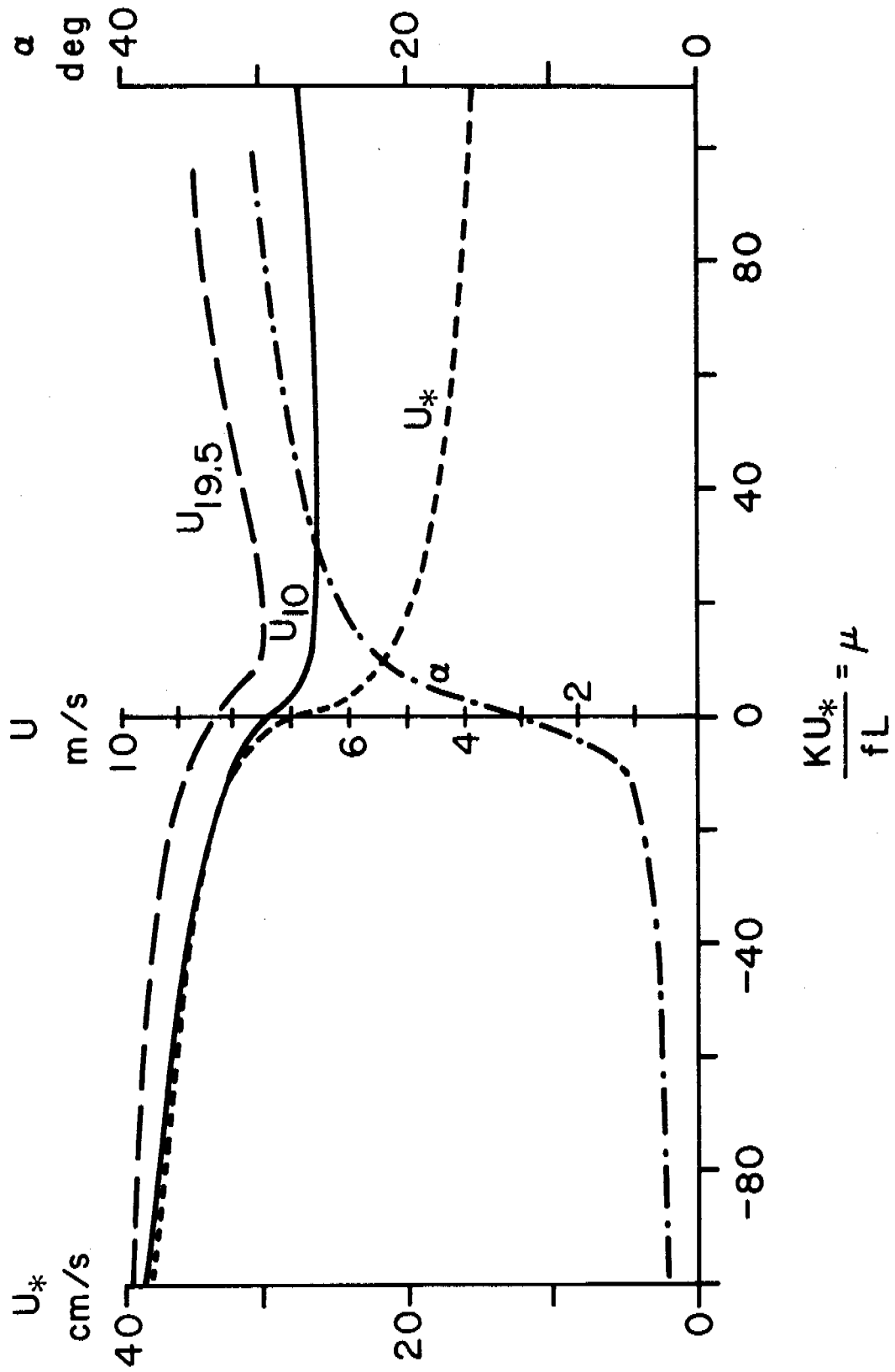


Figure 5 --  $U_{19.5}$ ,  $U_{10}$ ,  $u_*$  and  $\alpha$  versus stratification.  $RH = 0.7$ ,  $lat. = 45^\circ$ ,  $G = 10 \text{ m s}^{-1}$ .

where  $U_s$  is the surface drift. The drag coefficient,  $C_D$ , relates wind to stress:

$$\tau/\rho = C_D(\hat{U} - \hat{U}_s)^2. \quad (20)$$

By combining (19) and (20), a relation between  $z_o$  and  $C_D$  can be determined:

$$z_o = z \exp(-k/C_D^{1/2}). \quad (21)$$

The reference height for  $C_D$  is generally taken to 10 m.

Both the measurements of Nikuradse (1933) on pipe flow and those of Kondo (1973) at an air-sea interface indicate:

$$z_o = G_1 \nu / u_* \quad \text{for } \xi u_* / \nu \leq r_1 \quad (22a)$$

$$z_o = f(\xi u_* / \nu) \quad \text{for } r_1 \leq \xi u_* / \nu \leq r_2 \quad (22b)$$

$$z_o = G_2 \xi \quad \text{for } r_2 \leq \xi u_* / \nu. \quad (22c)$$

Nikuradse (1933) defined  $\xi$  as the actual mean diameter of the sand grains used as roughness elements and found  $r_1 = 5$ ,  $r_2 = 70$ ,  $G_1 = 0.11$  and  $G_2 = 0.03$ . Kondo (1973) defined  $\xi$  as the root-mean square waveheight for frequencies between 20 and 200 rad/sec<sup>-1</sup> and found  $r_1 = 5.7$ ,  $r_2 = 67$ ,  $G_1 = 0.11$  and  $G_2 = 0.07$ . These results separate the flow roughly into smooth, transition and rough regimes.

For a fully rough air-sea interface, Charnock (1955) obtained by dimensional reasoning

$$z_o = \frac{a u_*^2}{g}, \quad (23)$$

where  $g$  is the acceleration due to gravity and  $a$  is a universal constant. Wu (1969) found that for  $U_{10} < 3 \text{ m s}^{-1}$ , (22a) is valid; for  $3 \text{ m s}^{-1} < U_{10} < 15 \text{ m s}^{-1}$ , (23) is valid; and for  $U_{10} \geq 15 \text{ m s}^{-1}$ ,  $z_o$  is a constant.

Recently, a number of investigators have obtained empirical relations between  $C_D$  and  $U_{10}$ . Smith and Banke (1975) correlate  $C_D$  and  $U_{10}$  for 111 data runs and obtained

$$10 C_D = 0.63 + 0.066 U_{10} \quad (24a)$$

for  $U_{10}$  between 3 and 21  $m s^{-1}$ . Garrett (1977) obtained from 18 sets of data including those of Smith and Banke (1975)

$$10 C_D = 0.75 + 0.067 U_{10} \quad (24b)$$

for  $U_{10}$  between 4 and 21  $m s^{-1}$ . Both (24a) and (24b) agree with (23). Kondo (1975), by using wind-wave data from Kondo et al. (1973), obtained approximate relations in the form:

$$10^3 C_D = p + q U_{10}^r \quad (24c)$$

that agree with (22). The values of  $p$ ,  $q$ ,  $r$  for different ranges of wind speed are shown in Table 4. The difference between  $C_D$  given by (24a), (24b) and (24c) are small for moderate wind speeds. Garratt (1977) did not use the result of Kondo (1975) to evaluate (24b) but indicated that (24c) agrees well with the data he collected.

In a boundary layer model proposed by Cardone (1969), a relation is assumed

$$z_o = 0.684/u_* + 4.285 \times 10^{-5} u_*^2 - 4.43 \times 10^{-2} \quad (25)$$

Combining this relation with (21), a relation between  $C_D$  and  $U$  can be obtained.

In evaluating the above relations, the surface drift velocity is neglected by the investigators, i.e.,  $U_s$  is assumed to be zero. The drag coefficient and roughness parameter obtained with the  $U_s = 0$  assumption are related to the actual values,  $C'_D$  and  $z'_o$ ,

$$C_D^{-\frac{1}{2}} = C'_D^{-\frac{1}{2}} + U_s/u_* \quad (26)$$

$$z_o = z'_o \exp(-kU_s/u_*). \quad (27)$$



The ratio  $U_s/u_*$  is a parameter of wind-wave coupling and its effect on the drag has been discussed by Kitaigorodskii (1973) and Davidson (1974). Wu (1975) found by laboratory experiments that this ratio decreases gradually as the fetch increases and approaches approximately the relation  $U_s = 0.55 u_*$ .

Figure 6 shows the wind-speed dependence of the drag coefficient for the four models (24a), (24b), (24c), and (26).

Table 4: Parameters in Expressions for Neutral Bulk Transfer Coefficients

$U_{10}$ (m s <sup>-1</sup> )	p	q	r
0.3 to 2.2	0	1.08	-0.15
2.2 to 5	0.771	0.0858	1
5 to 8	0.867	0.0667	1
8 to 25	1.2	0.025	1
25 to 50	0	0.073	1

## 10. THE STABILITY FUNCTIONS

The surface stress and the surface heat flux can be determined from  $U$  and  $(T - T_o)$  by integrating the mean profiles.

$$\hat{U}/u_* = [\ln(\hat{z}/z_o) - \psi_U]/k \quad (28)$$

$$(T - T_o)/T_* = [\ln(\hat{z}/z_o) - \psi_T]/\alpha_N k, \quad (29)$$

where  $T_* = -H_o/(c\rho u_*)$ ,  $\alpha_N = K_H/K_M$  at neutral stability,  $K_H$  and  $K_M$  are the turbulent diffusivities for heat and momentum,  $c$  is the isobaric specific heat,  $U$  and  $T$  are the mean wind speed and potential temperature at height  $z$ , and  $T_o$  is the temperature at  $z_o$  given by the extrapolation of (29). The evaluation of  $z_o$  has been discussed in section 9. In this section we investigate the stability functions  $\psi_U$  and  $\psi_T$ .

For a diabatic surface layer, similarity theory suggests that the non-dimensional gradients are functions of the stability parameter,  $\zeta$ .

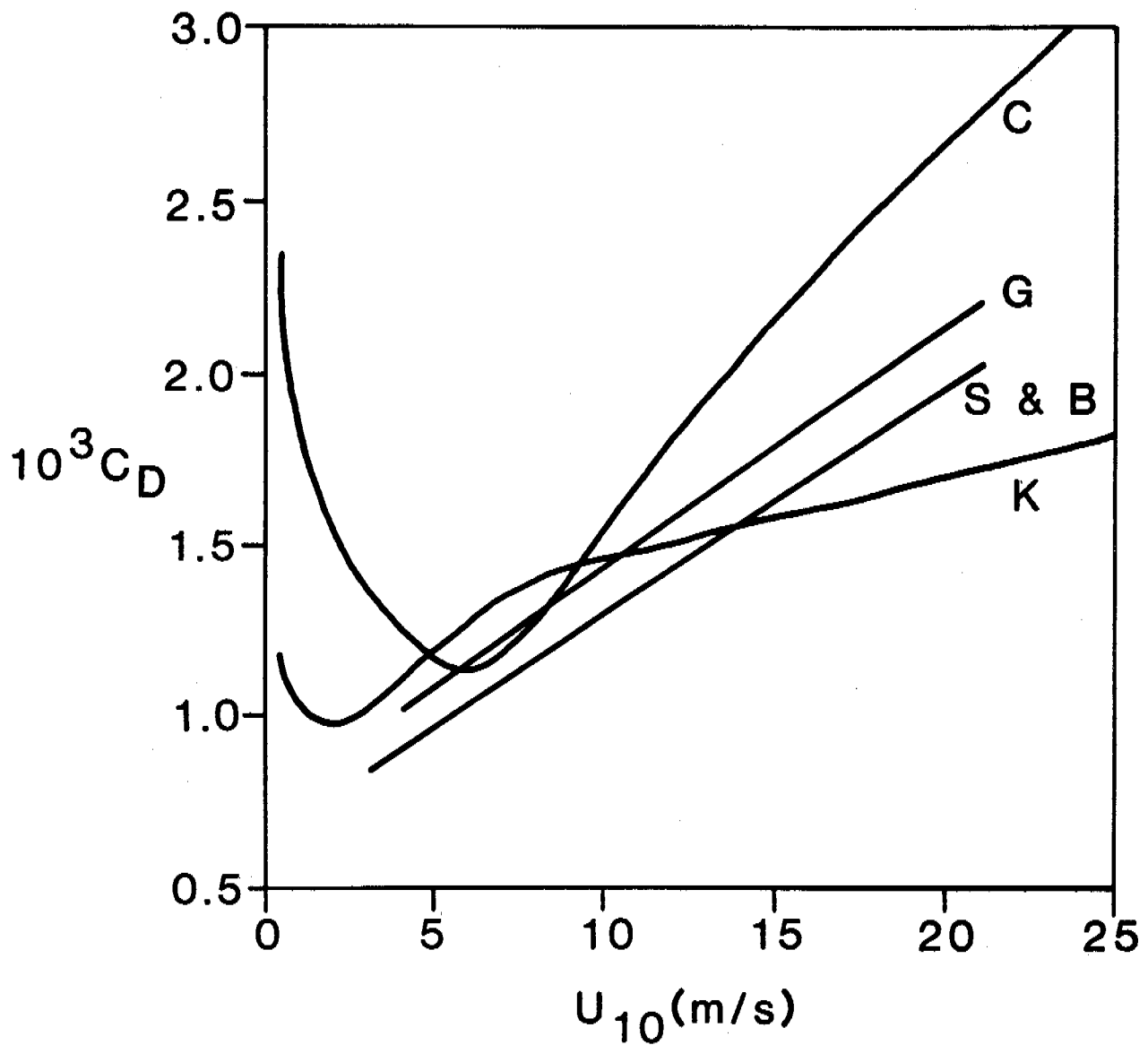


Figure 6 -- A plot of the neutral drag coefficient as a function of wind speed for four different assumptions (K = Kondo, S + B = Smith and Banke, G = Garratt, C = Cardon).

$$kz(\partial U/\partial z)/u_* = \phi_U(\xi) \quad (30)$$

$$\alpha_N kz(\partial T/\partial z)/T_* = \phi_T(\xi), \quad (31)$$

where  $\xi = z/L^1$  and  $L$  is the Obukhov's length. Combination of (28), (29), (30) and (31) gives

$$\psi_U = \int_{\xi_0}^{\xi} [(1 - \phi_U)/\xi^2] d\xi'$$

$$\psi_T = \int_{\xi_0}^{\xi} [(1 - \phi_T)/\xi^2] d\xi'.$$

Under unstable conditions, the KEYPS model (Panofsky et al., 1960) proposes

$$\phi_U^4 - a\xi\phi_U^3 = 1. \quad (32)$$

The adjustable constant  $a$  is taken to be 18 following Panofsky et al. (1960).

If the effect of moisture fluctuations on density is neglected, the Obukhov's length is defined as

$$L = -Tu_*^2/(kgT_*). \quad (33)$$

With the assumption that  $K_H/K_M$  is constant and equal to unity,  $\phi_T = \phi_U = \phi$ ,  $\psi_T = \psi_U = \psi$  and

$$L = -u_*^2 T [\ln(z/z_0) - \psi_0/k^2 g(T - T_0)]. \quad (34)$$

Recently, profile measurements in the surface layer have been successfully described by the Businger-Dyer model:

$$\psi_U = (1 - a_U \xi)^{-1/4} \quad (35)$$

$$\phi_T = (1 - a_T \xi)^{-1/2}. \quad (36)$$

<sup>1</sup>Note a new definition for  $\xi$ .

Results from the Kansas experiment (Businger et al., 1971) give  $a_U = 15$ ,  $a_T = 9$  while  $k = 0.35$  and  $\alpha_N = 1$ . However, Paulson (1970), with the assumption that  $k = 0.4$  and  $\alpha_N = 1$ , obtained  $a_U = a_T = 16$  in his analysis of Kerang data, in close agreement with Dyer (1967). The Businger-Dyer model differs from the KEYPS model in that the B-D model allows for the variation of  $K_H/K_M$  with stability. Paulson (1970) found that both models describe velocity distribution equally well but the B-D model gives better representation in temperature distribution. The two models also give different dependence of U and T on z when free convection is approached (see Businger et al., 1971 and Businger, 1973 for further discussion). Both the Kansas and Kerang data are measured over land. The B-D model has also been found to represent measurements over ocean in the Spanish Bank experiment (Miyake et al., 1970), the Indian Ocean experiment (Badgley et al., 1972), and the BOMEX experiment (Paulson et al., 1972).

Figure 7 shows the stress as a function of wind speed for unstable stratification of  $3^\circ\text{C}$  for the three models.  $z_o(u_*)$  relations from Cardone (1969) have been used in these calculations. Figure 8 shows the rate of heat flux evaluated for a range of air-sea temperature differences.  $T_{10}$  and  $U_{10}$  are potential temperature and wind speed at 10 m. Stresses evaluated with the B-D model with  $k = 0.4$  are about 1 percent lower than those evaluated with the KEYPS model at moderate wind speed but increase to 8 percent at  $1 \text{ m s}^{-1}$  wind. With  $k = 0.35$  the stress is about 30 percent lower. The heat fluxes evaluated by the B-D model with the two sets of constants are about 6 and 13 percent lower than those with the KEYPS model.

Under stable conditions, the log-linear model which was obtained by dropping the higher order terms in the power expansion of  $\phi_U$  and  $\phi_T$  are used:

$$\phi_U = 1 + b_U \zeta \quad (37)$$

$$\phi_T = 1 + b_T \zeta.$$

Cardone (1969) uses the values  $k = 0.4$ ,  $\alpha_N = 1$ ,  $b_T = b_U = 7$ . Similar values have been used by McVeil (1963) and others. Businger et al. (1971) suggested  $k = 0.35$ ,  $\alpha_N = 1.35$ ,  $b_U = 4.7$  and  $b_T = 6.35$ . However, the log-

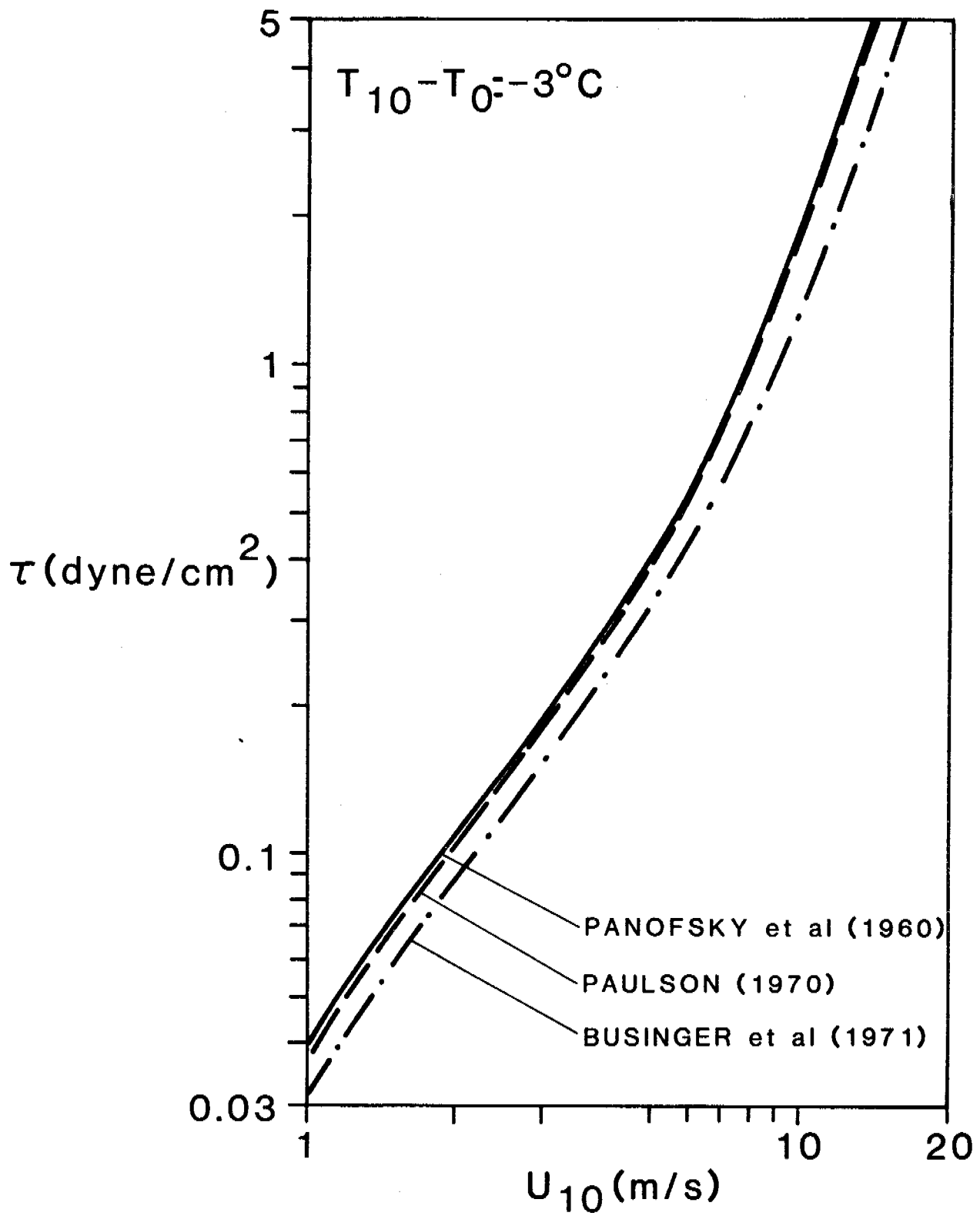


Figure 7 -- Stress versus wind speed for unstable stratification for three stability function models.

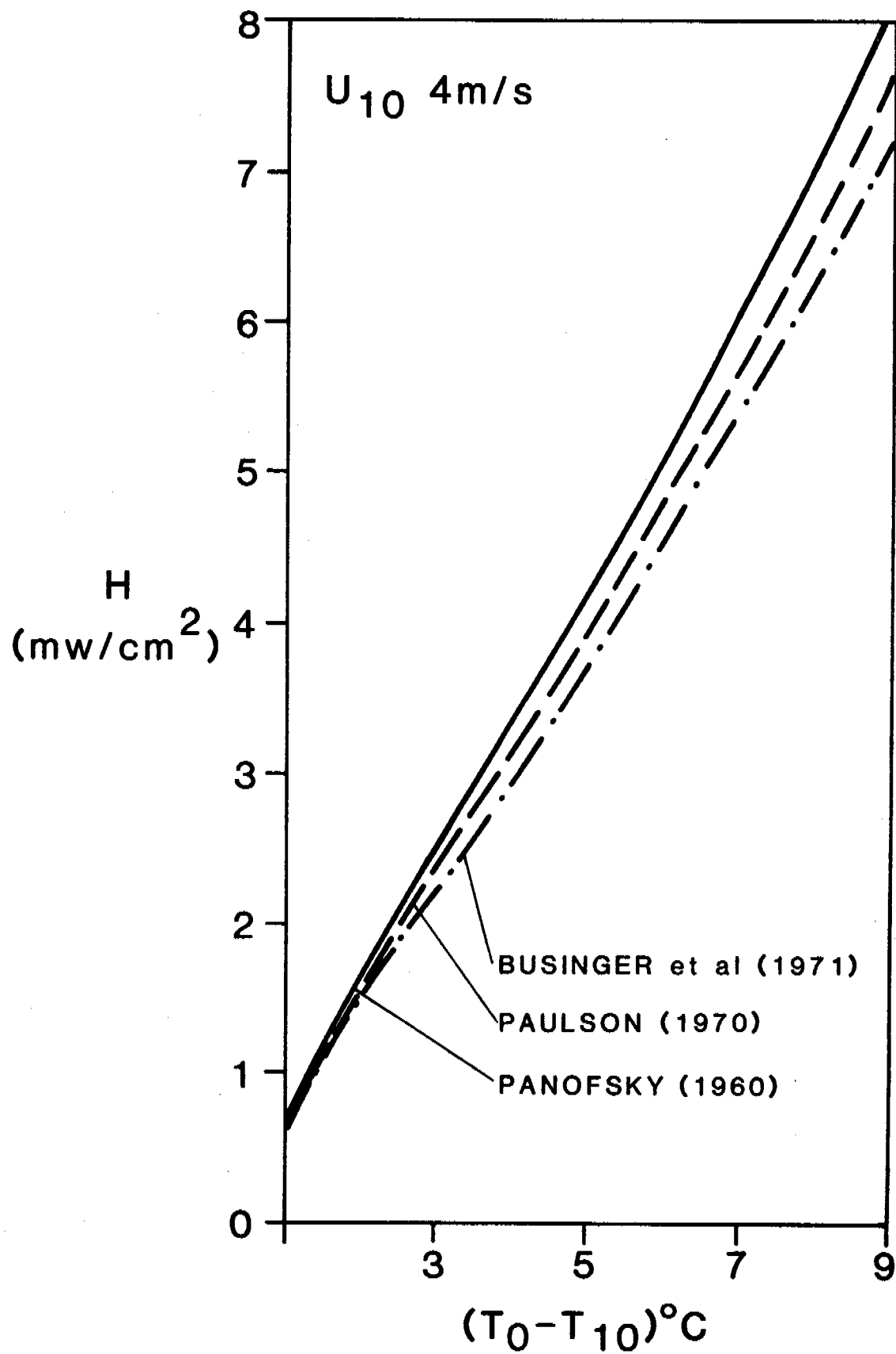


Figure 8 -- Heat flux as a function of unstable air sea temperature for three stability models.

linear model has its limitations. From the definition,

$$\zeta = \alpha_N \phi_U^2 Ri / \phi_T, \quad (38)$$

where  $Ri = g(\partial T / \partial z)^2$  is the Richardson number. For  $b_U = b_T = b$

$$\zeta = \frac{A}{1 + B},$$

where  $A = \alpha_N Ri$ ,  $B = \alpha_N Ri b$  and  $\zeta$  can be solved by fix-point iterations only if

$$B < 1$$

and

$$Ri < (\alpha_N b)^{-1}. \quad (39)$$

The quantity  $(\alpha_N b)^{-1}$  is also the asymptotic value of  $Ri$  as  $\zeta$  increases in value.

The criterion (39) is equivalent to

$$gz(T - T_0) / (TU^2) < (\alpha_N b)^{-1}.$$

For  $z = 10$  m,  $g = 981$  cm s<sup>-1</sup>,  $\alpha_N = 1$ ,  $b = 7$ ,  $T = 280^\circ\text{K}$ , in order to have a realistic solution,  $(T - T_0) / U^2 < 4.1 \times 10^{-5}$ . In other words, there is no solution when  $U_{10} < 157$  cm s<sup>-1</sup> for  $(T_{10} - T_0) = 1^\circ\text{C}$  and when  $U_{10} < 221$  cm s<sup>-1</sup> for  $(T_{10} - T_0) = 2^\circ\text{C}$ . Kondo (1975) suggested

$$\phi = 1 + 6\zeta / (1 + \zeta), \quad (40)$$

which is not subjected to the above condition for a solution.

The stresses evaluated with these models are compared in Figure 9. The stress evaluated with Cardone (1969) is lower than that evaluated with Kondo's model by 3 percent at a wind speed of 10 m s<sup>-1</sup> and by 59 percent at a wind speed of 2 m s<sup>-1</sup>. With the representation suggested by Businger et al. (1971), which means a different value of von Karman's constant, the stress is about 40 percent lower than the Kondo representation. Most of this is due to the smaller  $k$ .

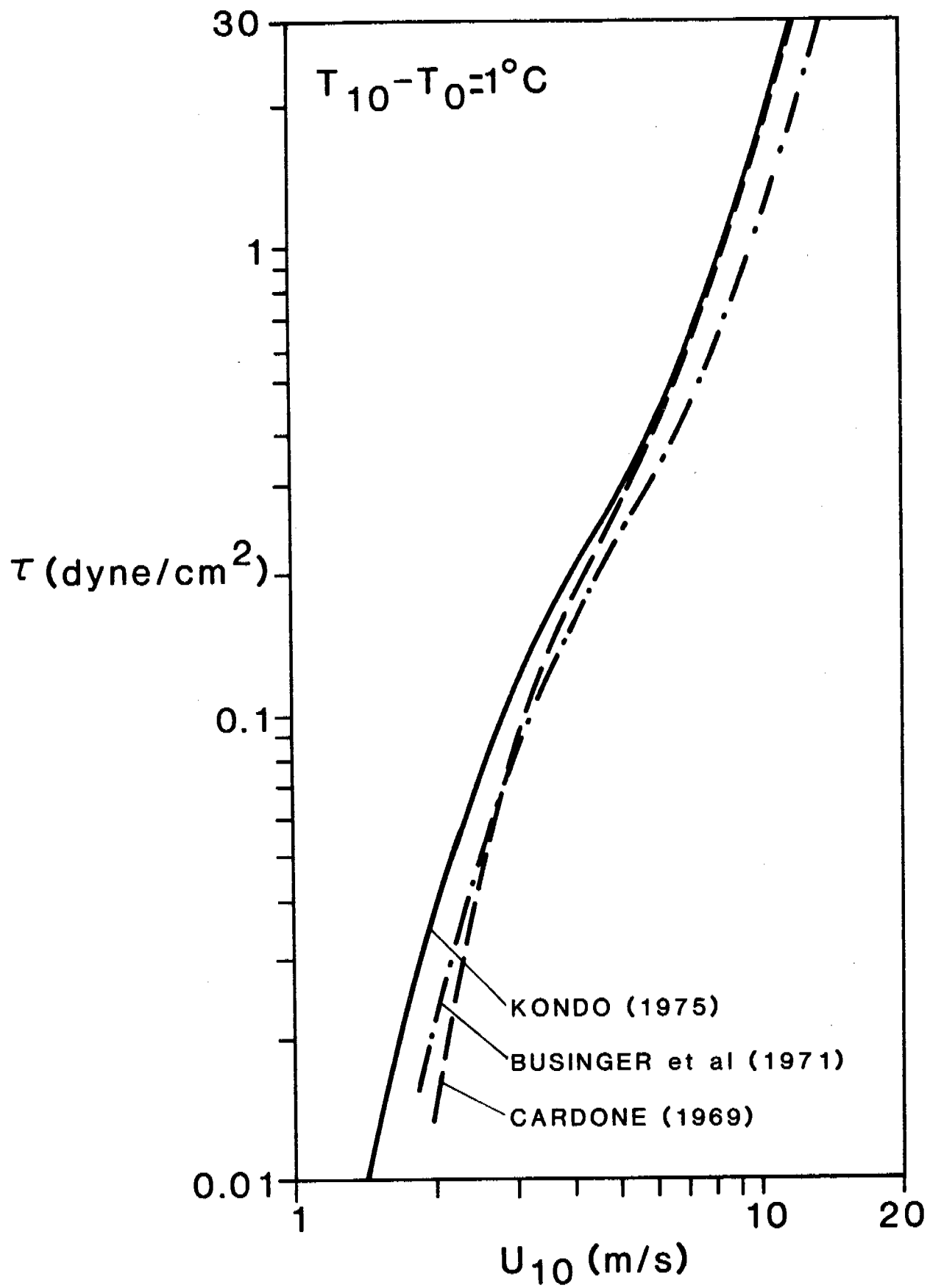


Figure 9 -- Stress versus wind speed for stable stratification for three stability function models.



Over water, the effect of moisture fluctuations on buoyancy may be important. The Obukhov length can be redefined to include this effect:

$$L = T_v u_*^2 / (gkT_{v*}),$$

where  $T_v = T(1 + 0.61Q)$  and  $T_{v*} = T_*(1 - 0.61Q) + 0.61TQ_*$ ,  $Q_* = -E/u_*$ ,  $E$  is the moisture flux,  $Q$  is the specific humidity at  $z$ . The moisture flux can be determined from the humidity profile

$$(Q - Q_0)/Q_* = [\ln(z/z_0) - \psi_Q] (\alpha_N' k)^{-1},$$

where  $\alpha_N' = K_E/K_M$  at neutral stability and  $K_E$  is the turbulent diffusivity of moisture. Assuming  $\alpha_N' = \alpha_N$ ,  $\psi_Q = \psi_T$ , the stress and heat flux can be evaluated for different values of relative humidity. The percentage difference between the values evaluated with the effects of moisture included and those with the effects excluded are shown in Tables 5 and 6. The difference in stress decreases with increasing wind speed because at low wind speed the buoyancy production becomes increasingly important relative to the shear production. The difference is larger the drier the air.

The sea-surface temperature  $T_s$ , rather than  $T_o$ , is generally available. Figure 10 shows that under slightly unstable conditions, the heat flux estimated by assuming  $T_o = T_s$  ( $z_T = z_o$ ) differs from those estimated by including a sublayer model (Liu, 1978) by 3 percent in low wind speed up to 27 percent for  $20 \text{ m s}^{-1}$  winds.

Table 5: Percentage Difference Between the Stress Evaluated with the Effects of Moisture on Buoyancy Included and those with the Effects Excluded.

$T_0 = 10^\circ\text{C}$						
$U_{10} (\text{m s}^{-1})$	$T_{10} - T_0 = 1^\circ\text{C}$			$T_{10} - T_0 = -3^\circ\text{C}$		
	R.H.			R.H.		
	100%	60%	0%	100%	60%	0%
1	20	64	159	1	4	6
5	1	6	18	1	2	3
10	0.3	2	7	1	1	4

---

$T_0 = 25^\circ\text{C}$						
$U_{10} (\text{m s}^{-1})$	$T_{10} - T_0 = 1^\circ\text{C}$			$T_{10} - T_0 = -3^\circ\text{C}$		
	R.H.			R.H.		
	100%	60%	0%	100%	60%	0%
1	13	5	169	3	8	14
5	-0.3	17	4	2	4	8
10	-8	7	10	1	5	12

Table 6: Percentage Difference Between the Heat Flux Evaluated with the Effects of Moisture on Buoyancy Included and those with the Effects Excluded ( $U_{10} = 5 \text{ m s}^{-1}$ )

	$T_0 = 10^\circ\text{C}$			$T_0 = 25^\circ\text{C}$		
	R.H.			R.H.		
$T_{10} - T_0$	100%	60%	0%	100%	60%	0%
$-3^\circ\text{C}$	1	2	3	2	4	7
$1^\circ\text{C}$	1	7	8	-0.3	18	28

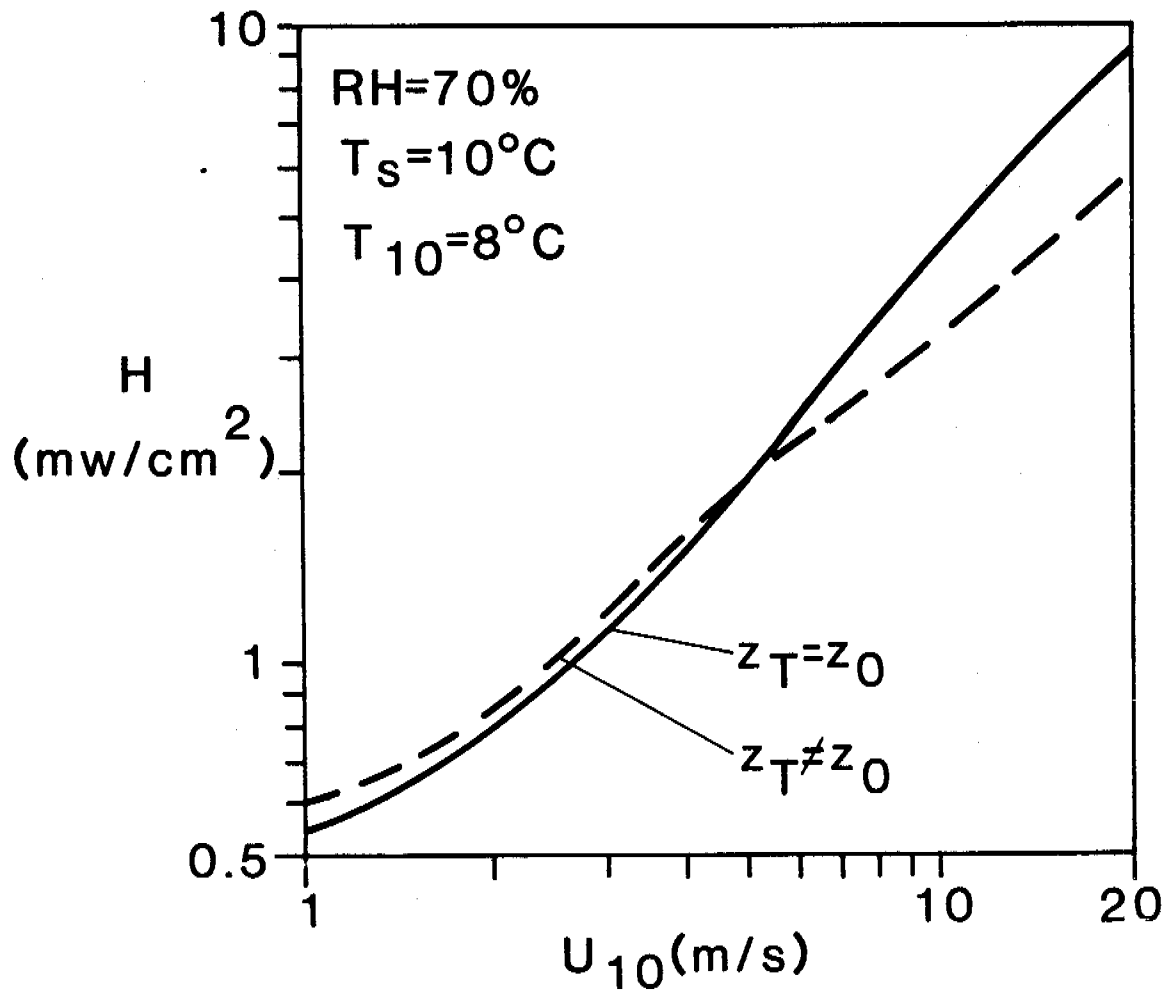


Figure 10-- Heat flux as a function of wind speed with the assumption of a sublayer adjacent to the surface,  $z_T \neq z_0$ .

REFERENCES (APPENDIX A)

- Badgley, F. I., C. A. Paulson and M. Miyake (1972): Profile of wind temperature and humidity over the Arabian Sea, International Indian Ocean Expedition. Meteor. Monograph, 6, 66.
- Brown, R. A. (1970): A secondary flow model for the planetary boundary layer. J. Atmos. Sci., 27, 742-757.
- Brown, R. A. (1972): The inflection point instability problem for stratified rotating boundary layers. J. Atmos. Sci., 29, 850-859.
- Brown, R. A. (1974): Analytical Methods in Planetary-Layer Modelling, Adam Hilger Ltd., London, and Halsted press, John Wiley & sons, N. Y. 148 pp.
- Brown, R. A. (1978): Similarity parameters from first-order closure and data. Boundary-Layer Meteorol., 14, 381-396.
- Businger, J. A. (1973): A note of free convection. Boundary-layer Meteorol., 4, 323-326.
- Businger, J. A., J. C. Wyngaard, Y. Izumi and E. F. Bradley (1971): Flux profile relationships in the atmospheric surface layer. J. Atmos. Sci., 28, 181-189.
- Cardone, V. J. (1969): Specification of the wind distribution in the marine boundary layer for wave forecasting. Report GSL-TR69-1, New York Univ., School of Engineering and Science, 131 pp.
- Charnock, H. (1955): Wind stress on a water surface. Quart. J. Royal Meteor. Soc., 81, 639-640.
- Davidson, K. L. (1974): Observational results on the influence of stability and wind-wave coupling on momentum transfer and turbulent fluctuations over ocean waves. Boundary-Layer Meteorol., 6, 305-331.

- Dyer, A. J. (1967): The turbulent transport of heat and water vapour in an unstable atmosphere. Quart. J. Roy. Meteor. Soc., 93, 501-508.
- Garrett, J. R. (1977). Review of drag coefficients over oceans and continents. Mon. Weather Rev., 105, 915-929.
- Hasse, L. (1970): On the determination of vertical transports of momentum and heat in the atmospheric boundary layer at sea. Technical Report 188, School of Oceanography, Oregon State University.
- Kitaigorodskiy, S. A. (1973). The Physics of Air-sea Interaction, Israel Program for Scientific Translation, Jerusalem.
- Kondo, J. (1975): Air-sea bulk transfer coefficients in diabatic condition, Boundary-Layer Meteorol., 9, 91-112.
- Kondo, J., Y. Fujinawa and G. Naito (1973): High frequency component of ocean waves and their relation to aerodynamic roughness. J. Phys. Oceanogr., 3, 197-222.
- Liu, W. T. (1978): The molecular effects of air-sea exchanges. Ph.D. dissertation, University of Washington, Seattle.
- Liu, W. T. and J. Businger (1975): Temperature profile in the molecular sublayer near the interface of a fluid in turbulent motion. Geophys. Res. Lett., 2, 403-404.
- Liu, W. T., K. B. Katsaros and J. A. Businger (1979): Bulk parameterization of air-sea exchanges of heat and water vapor including the molecular constraints at the interface, submitted to J. Atmos. Sci. for publication.
- McVeil, G. E. (1964): Wind and temperature profiles near the ground in stable stratification. Quart. J. Roy. Meteor. Soc., 90, 136-146.

- Miyake, M., M. Donelan, G. McBean, C. Paulson, F. Badgley and E. Leavitt (1970): Comparison of turbulent fluxes determined by profile and eddy correlation techniques. Quart. J. Roy. Meteor. Soc., 96, 132-137.
- Nikvradse, J. (1933): Laws of flow in rough pipes, N.A.C.A. Technical Memorandum 1292.
- Paulson, C. A. (1970): The mathematical representation of wind speed and temperature profiles in the unstable atmospheric surface layer. J. Appl. Meteorol., 9, 857-861.
- Paulson, C. A., E. Leavitt and R. G. Fleagle (1972): Air-sea transfer of momentum, heat, and water determined from profile measurements during BOMEX. J. Phys. Oceanogr., 2, 487-497.
- Panofsky, H. A., A. K. Blackadar and G. E. McVeil (1960): The diabatic wind profile. Quart. J. Roy. Meteor. Soc., 86, 390-398.
- Smith, S. D. (1973): Thrust-anemometer measurements over the sea reexamined, Report 73-1, Bedford Inst. Oceanography.
- Smith, S. D. (1974): Eddy flux measurements over Lake Ontario. Boundary-Layer Meteor., 6, 235-256.
- Smith, S. D. and E. G. Banke (1975): Variation of the sea surface drag coefficient with wind speed. Quart. J. Roy. Meteor. Soc., 101, 665-673.
- Wu, J. (1969): Wind stress and surface roughness at the air-interface. J. Geophys. Res., 74, 444-455.
- Wu, J. (1975): Wind-induced drift currents. J. Fluid Mech., 68, 49-70.
- Wu, J. (1979): Wind-wave interaction. Phys. Fluid, 13, 1926-1930.

## Appendix B: DERIVATION OF CARDONE MODEL

Cardone's model, an extension of Blackadar (1965), separates the boundary layer into two regions: a surface layer and an Ekman layer. The surface layer is assumed to be a constant-flux layer in which the eddy viscosity variation with height is specified as a function of the atmospheric stability according to the Monin-Obukhov similarity theory. The upper Ekman layer is assumed to have a constant eddy viscosity,  $K_m$  (Fig. B1) (Cardone 1969).

The surface layer assumes the standard Monin-Obukhov similarity hypothesis that the non-dimensional wind speed and potential temperature gradients defined by

$$\begin{aligned}\phi_u &= \frac{kz}{u_*} \frac{\partial u}{\partial z} \\ \phi_\theta &= \frac{z}{\theta_*} \frac{\partial \theta}{\partial z}\end{aligned}\tag{B1}$$

are universal functions of the stability parameter  $L$  or  $L'$ , where

- $L$   $= -\frac{u_*^3}{C_p \rho T} H$ , the Monin length
- $u$  mean wind speed
- $z$  vertical space coordinate
- $T$  mean temperature
- $k$  von Karman's constant ( $\approx 0.4$ )
- $u_*$   $(\tau/\rho)^{1/2}$ , friction velocity
- $H$   $C_p \rho \overline{w'T'}$ , turbulent heat flux
- $\theta_*$   $= -H/(ku_* \rho C_p)$ , a scaling temperature
- $\theta$   $T + \Gamma z$ , potential temperature
- $\Gamma$   $g/C_p$ , adiabatic lapse rate
- $g$  acceleration of gravity
- $C_p$  specific heat at constant pressure
- $\rho$  air density
- $\tau$  tangential stress



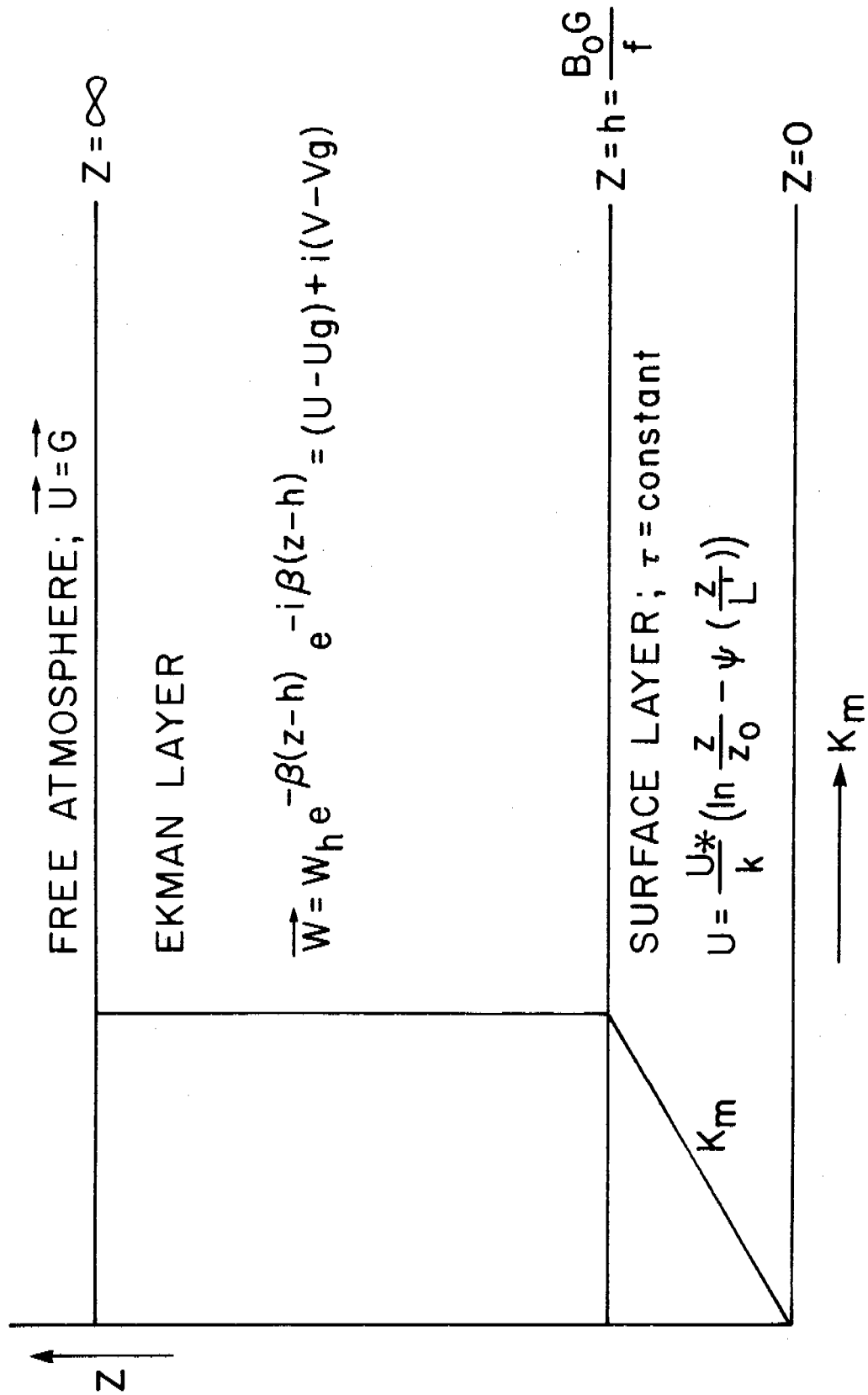


Figure B1. Model of the atmospheric surface boundary layer.

$K_m$   $u_*^2/(\partial u/\partial z)$ , turbulent transfer coefficient for momentum

$K_H$   $-H/(\rho C_p \partial \theta/\partial z)$ , turbulent transfer coefficient for heat

$a_h$   $K_H/K_m$ , reciprocal of the turbulent Prandtl number

$L'$   $a_h L$ .

Integrating the non-dimensional gradients gives:

$$u = \frac{u_*}{k} [\ln(z/z_0) - \psi_u(z/L')] \quad (B2)$$

$$\theta = \theta_s + \frac{\theta_*}{a_h} [\ln(z/z_0) - \psi_\theta(z/L')],$$

where  $z_0$  is the roughness length and

$$\psi_u(z/L') = \int_0^\xi \frac{1 - \phi_u(\xi)}{\xi} d\xi, \quad \xi = \frac{z}{L'} \quad (B3)$$

Under the assumption that the profile of wind and temperature are similar up to the anemometer height "a", i.e.,  $a_h \approx 1$ ,  $\phi_\theta \approx \phi_u$ , the stability length can be defined in terms of an anemometer height temperature

$$L' = a_h L = \frac{u_* T \partial u / \partial z}{kg \partial \theta / \partial z} \approx \frac{u_*^2 \bar{\theta} [\ln(a/z_0) - \psi_u(a/L')]}{k^2 g (\theta_a - \theta_s)} \quad (B4)$$

For  $a/L'$  small, with "a" a small fraction of the surface layer height, this is a good approximation. However, it would be an easy matter to carry both  $\psi_u$  and  $\psi_\theta$ . Our listing contrasts with Cardone's in that we have replaced  $a = 19.5$  m with  $a = 10.0$  m. Cardone uses the KEYPS representation for  $\phi$  which interpolates between neutral stability and free convection:

$$\phi_u^4 - \alpha'(z/L') \phi_u^3 - 1 = 0, \quad (B5)$$

with  $\alpha' = 18$ .

This is solved by defining an intermediate variable, the Richardson number:

$$R_i = \frac{g}{\theta} \frac{\frac{d\theta}{dz}}{\left(\frac{du}{dz}\right)^2} = \frac{z}{L'} \frac{1}{\phi_u(z/L')},$$

so that

$$\frac{z}{L'} = \frac{R_i}{(1 - \alpha' R_i)^{1/4}}$$

and

$$\phi_u = \frac{1}{(1 - \alpha' R_i)^{\frac{1}{4}}}$$

The KEYPS representation implies that both  $u$  and  $\theta$  vary asymptotically as  $z^{-1/3}$ . The B5 relation implies

$$\psi(z/L') = 1 - \phi - 3 \ln \phi + 2 \ln \left( \frac{1 + \phi}{2} \right) + 2 \tan^{-1} \phi - \frac{\pi}{2} + \ln \left( \frac{1 + \phi^2}{2} \right). \quad (B6)$$

An alternate form is the Businger-Dyer (B-D) profiles:

$$\begin{aligned} \phi_u &= [1 - \alpha'(z/L)]^{-\frac{1}{4}} \\ \phi_\theta &= [1 - \alpha'(z/L)]^{-\frac{1}{2}} \\ \psi_u &= 2 \ln [(1 + x)/2] + \ln [(1 + x^2)/2] - 2 \tan^{-1} x + \frac{\pi}{2} \\ \psi_\theta &= 2 \ln [(1 + x^2)/2], \end{aligned} \quad (B7)$$

where  $x = (1 - \alpha'z/L)^{\frac{1}{2}}$ .

The  $\psi_\theta$  profile is important only to level "a" (i.e., in defining  $L'$ ); however, the choice of the  $\psi_u$  profile is critical in matching velocities at the top of the surface layer. For stable boundary layers, Cardone has

$$\begin{aligned} \phi_u(z/L') &= 1 + \beta'z/L' \\ \psi_u(z/L') &= -\beta'z/L' \end{aligned} \quad (B8')$$

with  $\beta' = 7$ .

The linear profile in B8' is generally limited to  $z/L' < 0.3$  which in practice can be  $\theta_a - \theta_s < 2^\circ\text{C}$ . To extend the stable range we replace B8' by

$$\begin{aligned} \phi_u(z/L') &= 1 + \frac{\beta'(z/L')}{1 + z/L'} \\ \psi(z/L') &= -\beta' \ln(1 + z/L'). \end{aligned} \quad (B8)$$

Wave development is considered indirectly through the dependence of surface roughness upon  $u_*$  in the following relation:

$$z_0 = 0.684/u_* + 4.285 \times 10^{-5} u_*^2 - 4.43 \times 10^{-2}, \quad (B9)$$

where  $z_0$  is in cm and  $u_*$  in  $\text{cm s}^{-1}$ . The relation B9 implies a viscous sub-layer for small  $u_*$  and the Charnock (1955) relation ( $z_0 = a_c u_*^2/g$ ) for large  $u_*$ .

Equation B9 along with B2 implies a variation of the drag coefficient at neutral stability,  $[C_{10} = k^2/\lambda n(10m/z_0)]$ , as shown in Figure B2.

The structure of the planetary boundary layer is shown in Figure B1. A key assumption is specification of the height of the surface layer as

$$h = \frac{B_0 G}{f} \quad (B10)$$

where  $G$  is the wind speed at the top of the boundary layer,  $f$  is the Coriolis parameter, and  $B_0$  is an assignable constant,  $3.0 \times 10^{-4}$  (Blackadar, 1965).

Note that  $h$  is independent of stability. The outer layer is governed by an Ekman equation with constant eddy viscosity

$$if\vec{v} = if\vec{G} + K_m \frac{\partial^2 \vec{v}}{\partial z^2}, \quad (B11)$$

with boundary conditions

$$\vec{v} \rightarrow G \text{ at } z \rightarrow \infty$$

$$\vec{v} \frac{\partial \vec{v}}{\partial z}, \vec{\tau} \text{ continuous at } z = h. \quad (B12)$$

The solution to B11 in terms of a velocity deficit is

$$W = (u - u_g) + i(v - v_g)$$

$$W = W_h \exp[-\beta(1 + i)(z - h)], \quad (B13)$$

with  $W_h$  being the deficit between the wind speed at the top of the surface layer and the geostrophic velocity and with  $\beta = f/(2K_m)$ .

Figure B3 shows the barotropic boundary condition at the internal boundary height. Differentiating B12 with respect to  $z$  gives

$$\frac{\partial W}{\partial z} = -(1 + i)\beta W. \quad (B14)$$

Since  $\partial \vec{u}/\partial z$  is parallel to  $\vec{u}$  and  $\partial \vec{u}/\partial z|_h = \partial \vec{w}/\partial z|_h$ , the angular relationship between  $\vec{u}_h$  and  $\vec{w}_h$  is established as

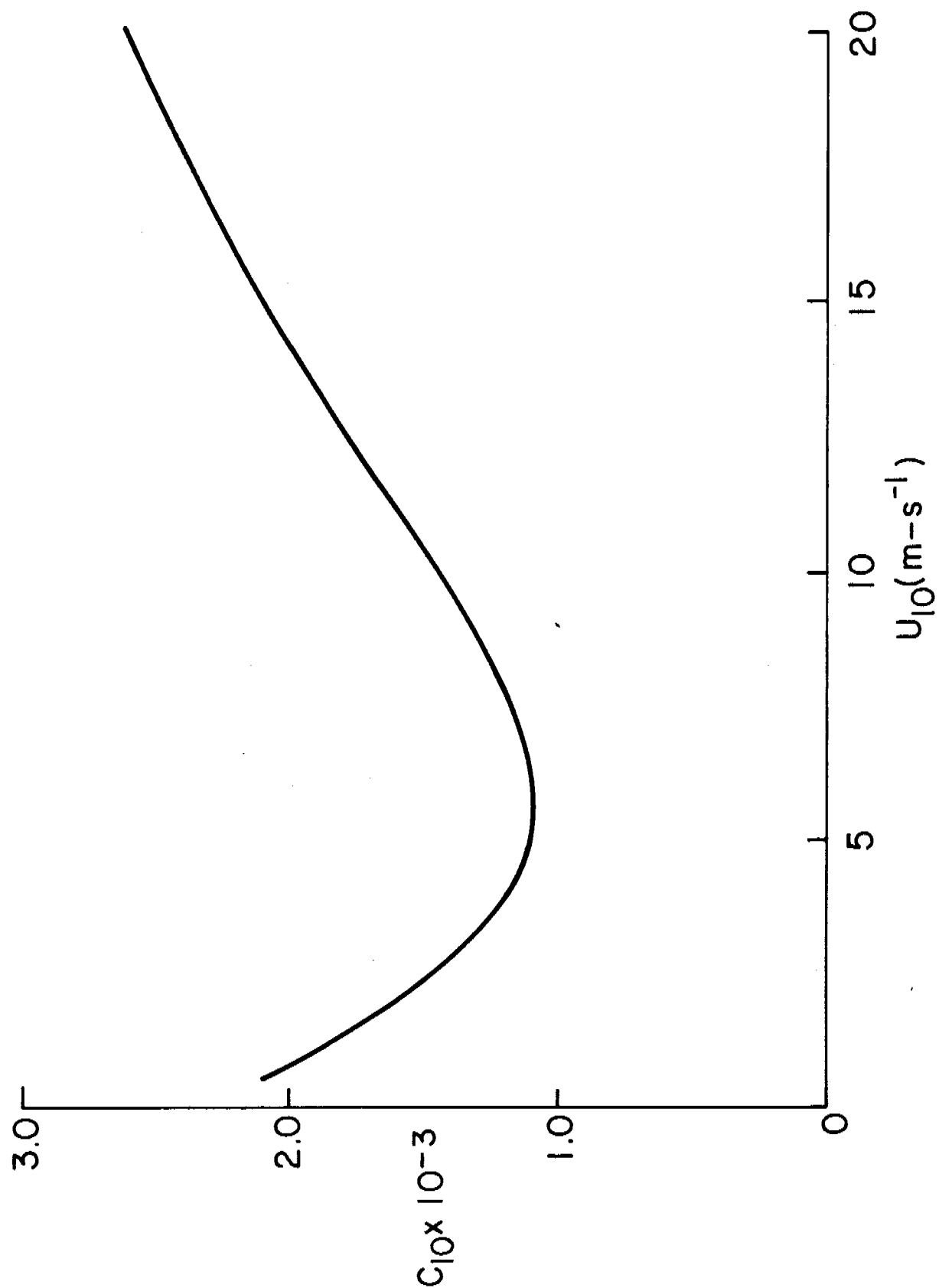


Figure B2. Drag coefficient with respect to 10 m as a function of 10-m wind speed for neutral conditions and roughness parameter specification Eq. B9.

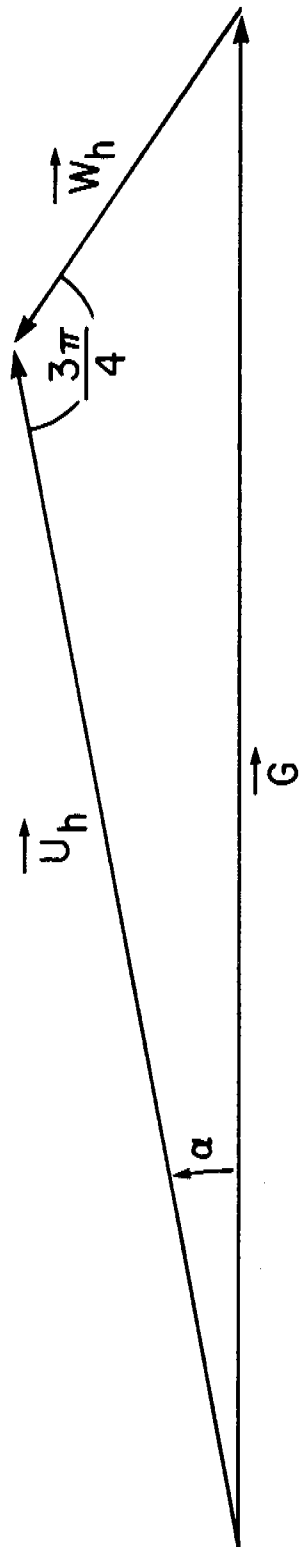


Figure B3. Barotropic boundary condition on the internal boundary surface.

$$\frac{\vec{u}_h}{u_h} = -(1 + i) \frac{\vec{w}_h}{w_h} . \quad (\text{B15})$$

By using the law of sines on Figure B3

$$\frac{u_h}{G} = \sqrt{2} \sin\left(\frac{\pi}{4} - \alpha\right), \quad (\text{B16})$$

and again

$$\frac{w_h}{G} = \sqrt{2} \sin \alpha. \quad (\text{B17})$$

The profile B1 in the surface layer implies

$$K_m = \frac{k u_* z}{\phi_u(z/L')} \quad z \leq h. \quad (\text{B18})$$

This relation combined with B10 and B12 implies

$$K_m = \frac{k u_* B_0 G}{f \phi_u(z/L')} \quad z \geq h \quad (\text{B19})$$

and

$$\beta = f \sqrt{\frac{\phi_u(z/L')}{2k u_* B_0 G}} . \quad (\text{B20})$$

The mixing coefficient in the upper layer is a function of stability in the sense that its magnitude is determined by the value where the profile B18 intersects height  $h$  and is larger for unstable stability and smaller for a stable regime. At  $z = h$

$$u_h = \frac{u_*}{k} \left[ \ln \frac{B_0 G}{f z_0} - \psi_u(h/L') \right] \quad (\text{B21})$$

$$\left. \frac{\partial u}{\partial z} \right|_{-h} = \frac{u_* f \phi_u(h/L')}{k B_0 G} \quad (\text{B22})$$

$$\left| \frac{\partial u}{\partial z} \right|_{+h} = \left| \frac{\partial w}{\partial z} \right|_{+h} = \sqrt{2} \beta |w_h|. \quad (\text{B23})$$

B22 and B23 imply

$$|w_h| = u_* f \phi_u(h/L') / (\sqrt{2} k B_0 G \beta). \quad (\text{B24})$$

Combining B17 and B24 gives

$$\frac{u_*}{G} = [2k B_0 \sin^2 \alpha / \phi_u (h/L')]^{1/3}, \quad (\text{B25})$$

and combining B16 and B21 gives

$$\frac{u_*}{G} = \sqrt{2} k \sin(\frac{\pi}{4} - \alpha) / [\ln \frac{B_0 G}{f z_0} - \psi(h/L')]. \quad (\text{B26})$$

B25 and B26 along with the definition of  $z_0$  and  $L'$  (B4 and B9) are solved by iteration.

The baroclinic derivation deviates from the barotropic in that the shear in the surface layer is matched to the sum of the geostrophic shear and the shear of the deficit velocity. Several secondary variables are defined, but the relations are straightforward in terms of the triangle geometry of the vector balance at height  $h$ . It is convenient to define a parameter

$$p = \frac{u_h}{\left. \frac{\partial u}{\partial z} \right|_h} = \frac{B_0 G}{f \phi_u} \left[ \ln \frac{B_0 G}{f z_0} - \psi \right]. \quad (\text{B27})$$

From this definition and boundary condition B12,

$$u_h = p \left[ \frac{\partial G}{\partial z} + \frac{\partial W}{\partial z} \right]_h. \quad (\text{B28})$$

In the same way as Figure B3 we can define Figure B4 to apply at level  $h$  with  $\eta$  as the angle between the thermal and geostrophic wind. By differentiation of  $W$  we again obtain a relation similar to B23:

$$p \left| \frac{\partial W}{\partial z} \right|_h = \sqrt{2} p' |W_h| \quad (\text{B29})$$

with

$$p' = \left( \frac{f^2 \phi_u}{2k u_* B_0 G} \right)^{\frac{1}{2}} p.$$

The magnitude of the thermal wind is defined by

$$r = \frac{1}{f} \left| \frac{\partial G}{\partial z} \right|. \quad (\text{B30})$$

One can construct a relation similar to B29 by setting

$$p \left| \frac{\partial G}{\partial z} \right| = r' G \quad (\text{B31})$$



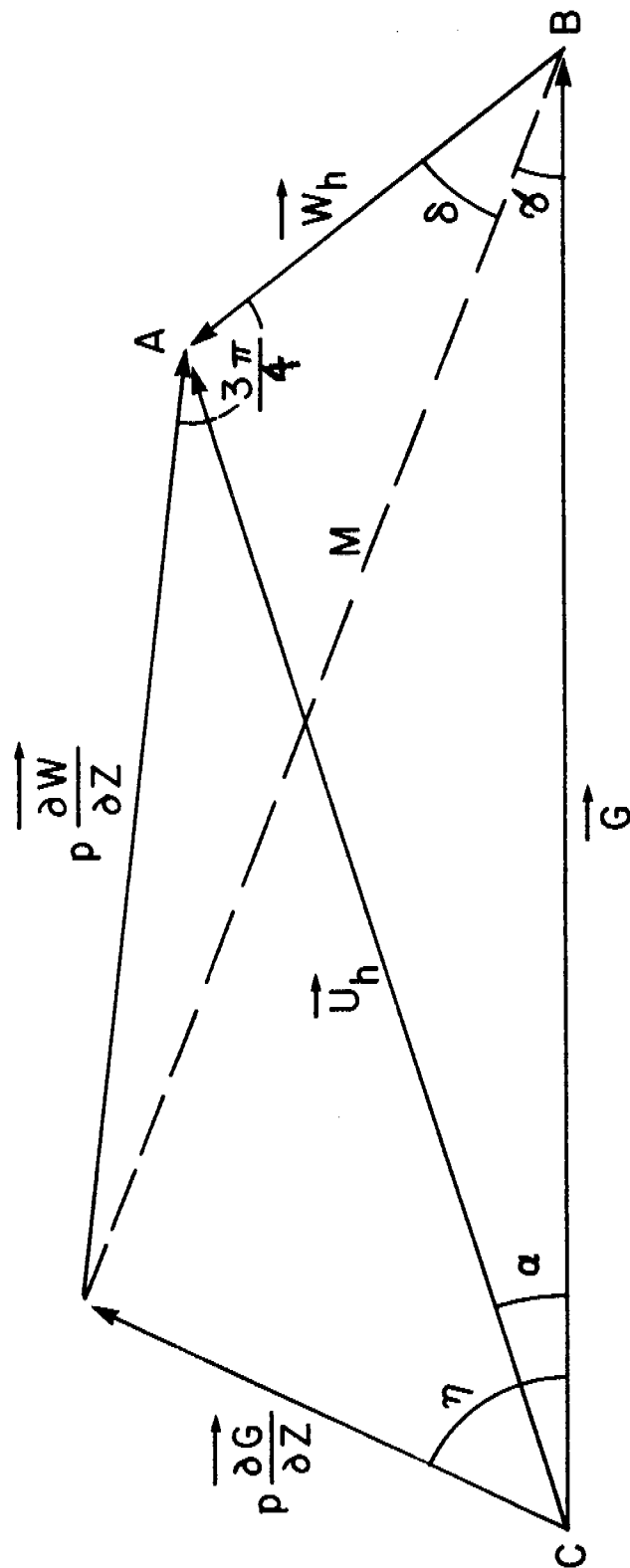


Figure B4. Baroclinic boundary condition on the internal boundary surface.

with

$$r' = \frac{r B_0}{\phi_u} \left[ \lambda n \frac{B_0 G}{f z_0} - \psi_u \right].$$

From the law of cosines of triangle ABD with interior angle  $3\pi/4$ ,

$$M^2 = p \left| \frac{\partial W}{\partial z} \right|^2 + W_h^2 - 2p \frac{\partial W}{\partial z} W_h \cos \frac{3\pi}{4} \quad (\text{B32})$$

or

$$M^2 = W_h^2 s^2$$

where

$$s^2 = 2p'^2 + 2p' + 1.$$

From the law of cosines of triangle BCD with interior angle  $\eta$ ,

$$M^2 = \left( p \frac{\partial G}{\partial z} \right)^2 + G^2 - 2p \left| \frac{\partial G}{\partial z} \right| G \cos \eta$$

or

$$M^2 = W_h^2 s^2 = G^2 q^2 \quad (\text{B33})$$

where

$$q^2 = 1 + r'^2 - 2r' \cos \eta.$$

From the law of sines for ABD and B32,

$$\sin \delta = \frac{p(\partial W / \partial z)}{\sqrt{2} M} = \frac{p'}{s}, \quad (\text{B34})$$

and from the law of sines for BCD and B33,

$$\sin \gamma = \frac{p \partial G / \partial z}{M} \sin \eta = \frac{R'}{q} \sin \eta. \quad (\text{B35})$$

The law of sines on ABC gives

$$u_h = W_h \frac{\sin(\delta + \gamma)}{\sin \alpha}. \quad (\text{B36})$$

The law of cosines on the same triangle taking  $(\delta + \gamma)$  as the interior angle gives

$$u_h^2 = G^2 W_h^2 - 2GW_h \cos(\delta + \gamma). \quad (\text{B37})$$

Taking  $\alpha$  as the interior angle,

$$W_h^2 = u_h^2 + G^2 - 2u_h G \cos\alpha. \quad (\text{B38})$$

Combining B36 and B38 gives

$$\tan\alpha = \frac{2 G W_h \sin(\delta + \gamma)}{G^2 + u_h^2 - W_h^2} \quad (\text{B39})$$

Substituting  $u_h$  from B37 and using B33,

$$\tan\alpha = \frac{\sin(\delta + \gamma)}{s/q - \cos(\delta + \gamma)} \quad (\text{B40})$$

Matching B36 to the surface layer velocity at  $h$ , i.e., B21, using  $W_h = q G/s$  from B33, gives

$$\frac{u_*}{G} = \frac{q \sin(\delta + \gamma) k}{s \sin\alpha \left[ \ln \frac{B_0 G}{f z_0} - \psi\left(\frac{z}{L'}\right) \right]}. \quad (\text{B41})$$

Secondary variables  $\delta$ ,  $\gamma$ ,  $s$ ,  $q$ ,  $p'$ , and  $p$  are defined in terms of known parameters. The inflow angle  $\alpha$  from B40 and geostrophic drag coefficient from B41 are again solved by iteration along with the equations for  $z_0$  and  $L'$ . A key point is that the influence of the thermal wind is included by matching the shear rather than an integrated effect through an assumed PBL depth.

Figures B5 through B7 present the plotted dependence of Cardone's model upon air-sea temperature difference, geostrophic wind and thermal wind. The strength of the thermal gradient is  $3^\circ/100 \text{ km}$ . Although not shown here, the overall dependencies are quite similar to observations and similarity theory relations.

Modern theory updates Cardone's model by Kondo's surface roughness relations (Appendix A, Garrett 1977) and by Businger-Dyer's stability relations (also Appendix A). Both these relations do not change Cardone's basic PBL theory (Halberstam, 1978), only quantitatively change the results. Both of these relations will be added to Model=8 in the near future.

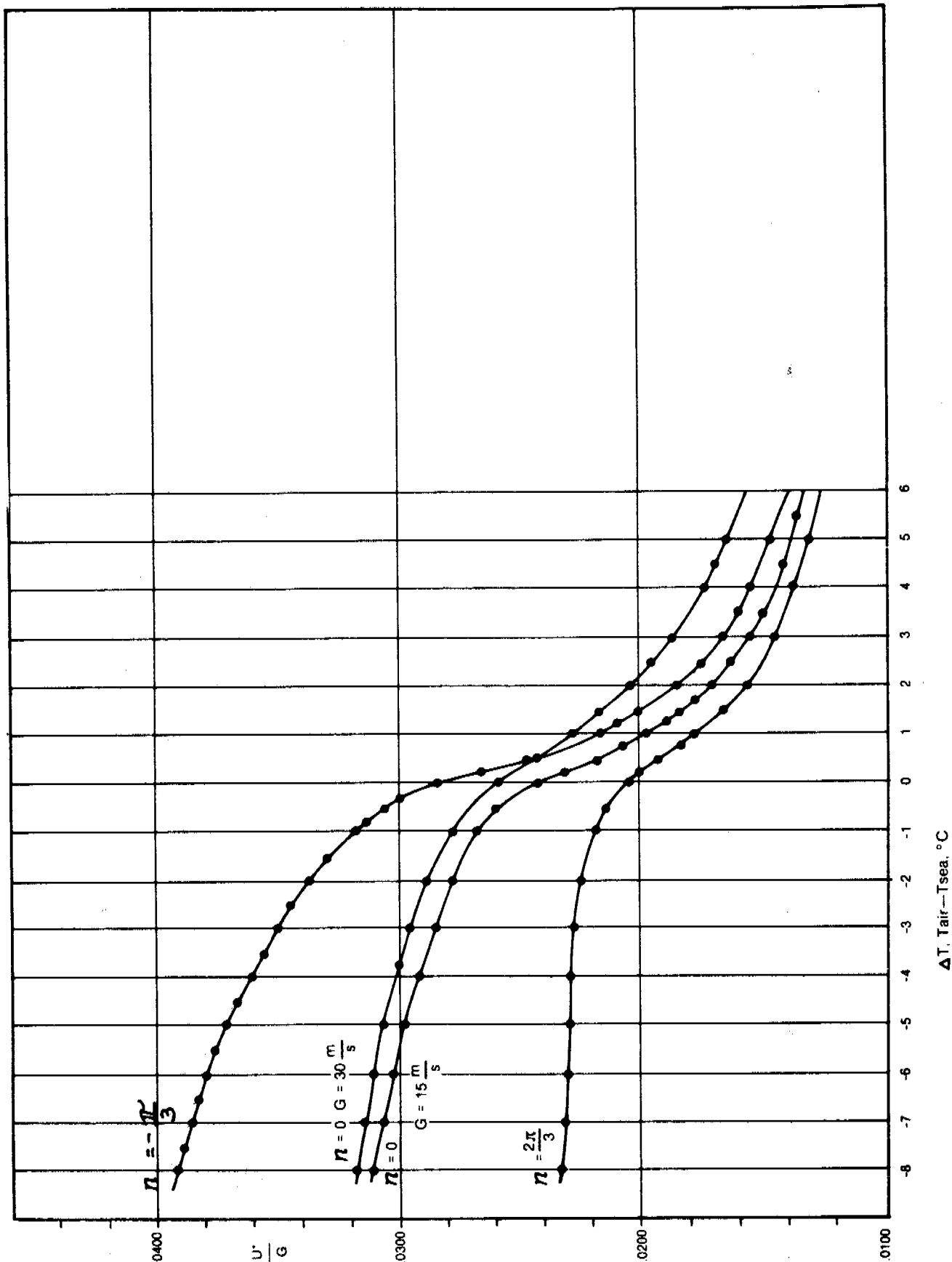


Figure B5. Dependence of the geostrophic drag coefficient on the air-sea temperature difference from Cardone's model. Two curves are given for  $15 \text{ m s}^{-1}$  and  $30 \text{ m s}^{-1}$  geostrophic wind and barotropic conditions. The high and low curves are for two orientations of the thermal wind for a surface air temperature gradient of  $3^\circ\text{C}/100 \text{ km}$ .

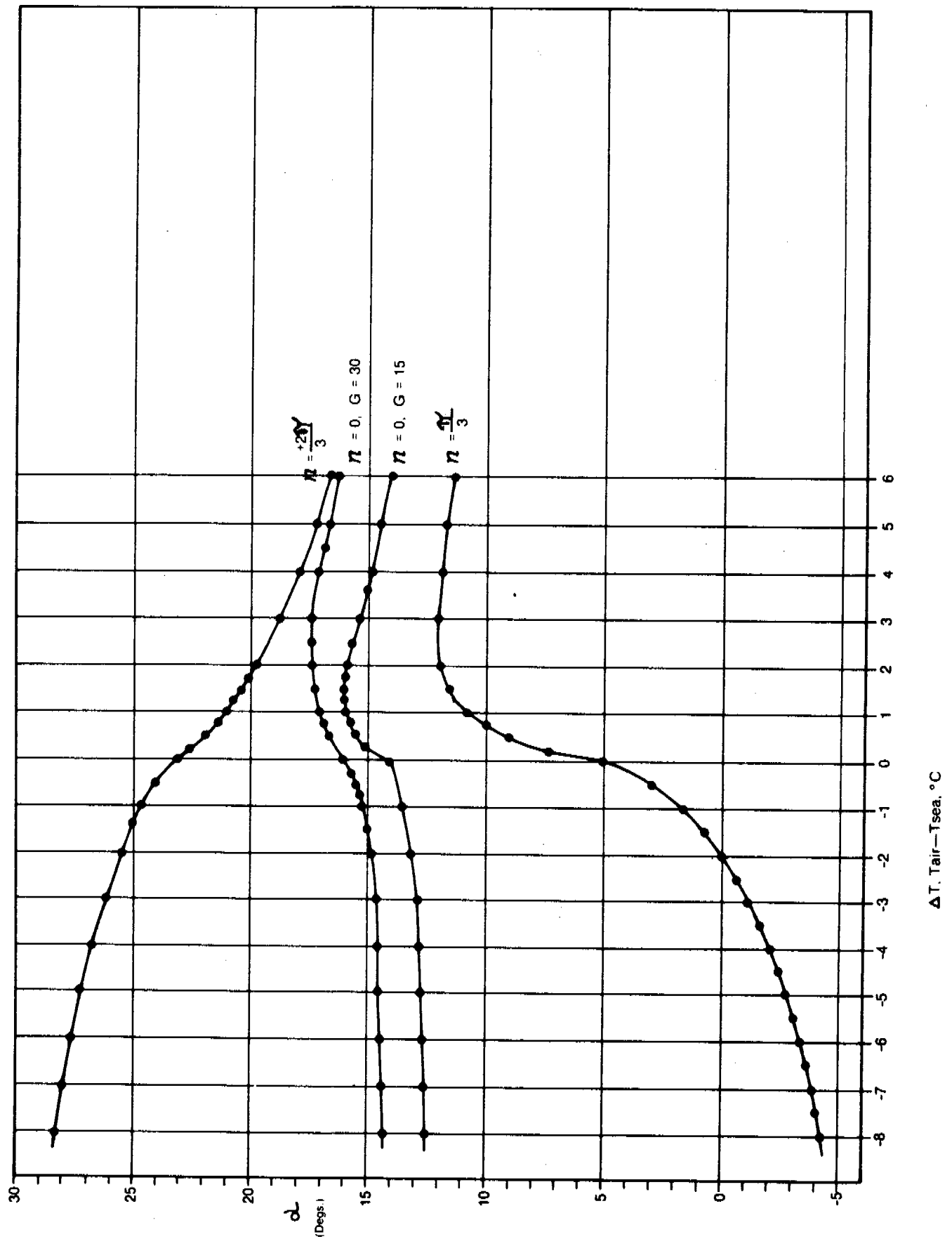


Figure B6. A similar set of curves as in A5 for inflow angle.

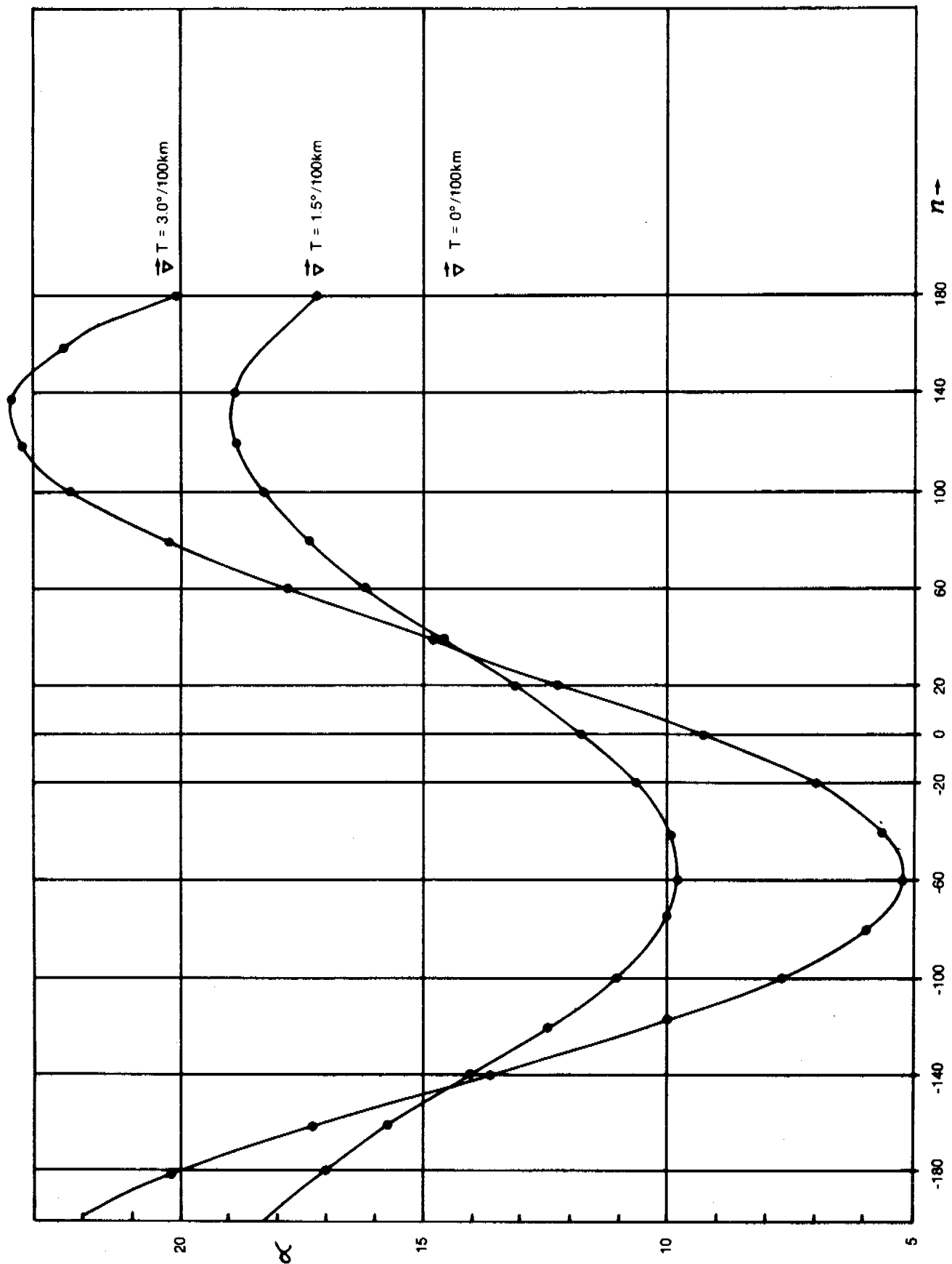


Figure B7. Influence of orientation of the thermal wind on inflow angle for three magnitudes of the thermal wind, 0, 1.5° and 3°C/100 km from Cardone's model. The geostrophic wind magnitude is 15 m s<sup>-1</sup>.

## REFERENCES (APPENDIX B)

- Blackadar, A.K.(1965): A simplified two-layer model of the baroclinic neutral atmospheric boundary layer. Air Force Cambridge Res. Lab. Report 65-531, pp 49-65.
- Cardone, V.J.(1969): Specification of the wind distribution in the marine boundary layer for wave forecasting. Report GSL-TR69-1, New York University, School of Engineering and Science, 131 pp.
- Charnock, H.(1955): Wind stress on a water surface. Quart. J. R. Met. Soc., 81, 639-640.
- Garrett, J.R. (1977): Review of drag coefficients over oceans and continents. Mon. Wea. Rev., 105, 915-929.
- Halberstam, I. (1978): The marine surface layer and its relationship to Seasat-A Scatterometer measurements. Jet Propulsion Laboratory (unpublished manuscript).

1

2

3

4

5

6



NOAA Technical Memorandum ERL PMEL-19

CASE STUDIES OF FOUR SEVERE GULF OF ALASKA STORMS

J. E. Overland, PMEL Coordinator  
V. J. Cardone

Pacific Marine Environmental Laboratory  
Seattle, Washington  
June 1980



**UNITED STATES**  
**DEPARTMENT OF COMMERCE**  
Philip M. Klutznick, Secretary

NATIONAL OCEANIC AND  
ATMOSPHERIC ADMINISTRATION  
Richard A. Frank, Administrator

Environmental Research  
Laboratories  
Wilmot N. Hess, Director

CONTENTS

	PAGE
ABSTRACT .....	491
1. INTRODUCTION .....	491
2. STORM 1: OCTOBER 27-31, 1974 .....	492
3. STORM 2: DECEMBER 29, 1974 TO JANUARY 1, 1975 .....	494
4. STORM 3: DECEMBER 16-21, 1975 .....	494
5. STORM 4: JANUARY 27-31, 1976 .....	496
6. ACKNOWLEDGEMENTS .....	497
7. REFERENCES .....	498

CASE STUDIES OF  
FOUR SEVERE GULF OF ALASKA STORMS\*

V. J. Cardone  
Ocean Weather Inc.  
White Plains, N.Y. 10601

ABSTRACT

This memorandum presents the meteorological development and life history of four severe storms from 1974-1976 which resulted in high winds in the inner Gulf of Alaska. Storm tracks and a narrative of each storm are provided along with sequences of sea-level pressure analyses, streamline-isotach analyses and wind variation at four offshore locations between Yakutat and Kodiak, Alaska. The four storms represent a variety of storm histories and a range of coastal wind response.

1. INTRODUCTION

The purpose of this study is to describe surface wind fields in severe storms for the northern Gulf of Alaska. Among other applications, such as STREX (Storm Transfer and Response Experiment), the wind fields will be used to assess the resolution errors inherent in the use of the synoptic climatology for this region developed by Overland and Hiester (1980).

The storms presented here were selected from cases treated in prior studies. Storms selected were all characterized by strong surface winds with an onshore component along the stretch of coast from Kodiak to Yakutat.

The method of wind field analysis employed is described in detail in Cardone et al. (1979). Briefly, a detailed postanalysis is performed using mainly hand analysis techniques to derive the surface wind distribution directly from the basic meteorological observations. Real-time data sources are augmented by archived observations from transient ships obtained from manuscript logs. Coastal and island station data are also used in the postanalysis. Surface winds are calculated from sea-level pressure gradients using a marine planetary boundary layer (PBL) model. PBL winds are retained only in uninteresting parts of the wind field, however, and are used only to guide the construction of streamlines and isotachs (kinematic analysis) in the areas of high winds near storms.

The accuracy of the wind fields produced by these techniques has been documented by Cardone et al. (1979). On the scales resolved (minimum length scale of 100-200 km), the wind speeds have an error of about 2.5

---

\*Contribution No. 458 from the NOAA/ERL Pacific Marine Environmental Laboratory

m sec<sup>-1</sup> rms about a negligible bias with wind direction errors of about 20°. The minimum resolvable length scale is determined by the basic data density in the northeast Pacific. Hence, the deforming influences of the shoreline topography along the Gulf of Alaska (GOA) on the near-shore field are not depicted in the wind fields presented here. In a storm environment such local influences are to be considered mesoscale and to influence the winds for a distance of perhaps 10-20 km offshore. However, the synoptic-scale wind field is also affected by the topography, since the orientation and intensity of isobaric gradients around intense extratropical cyclones are affected by the large-scale effects of the Alaskan Peninsula on storm speed and track. These synoptic-scale influences are included in the wind fields presented.

For each case study, the following material is presented:

1. Copies of microfilmed Northern Hemisphere 6-hourly surface maps at 12-hourly intervals throughout the storm (3-to 5-day period);
2. A storm track;
3. Several streamline/isotach charts covering the area between 130°W and 170°, and from 45°N to the Alaskan coast. The base maps show all winds reported from buoys, transient ships, and selected coastal and island stations;
4. Time histories of surface wind speed and direction at four offshore locations between Kodiak and Yakutat as follows:

Location 1	57°N	153°W
Location 2	59°N	149°W
Location 3	60°N	145°W
Location 4	59°N	141°W;

5. A narrative description of the storm.

## 2. STORM 1: OCTOBER 27-31, 1974

The storm track for this storm in the Gulf of Alaska is shown in Figure 1, while the complete history of the storm is shown in the series of surface analyses in Figures 2a-2i. Wind fields were constructed over the Gulf of Alaska beginning at 0600 GMT October 27, 1974, when, as seen in Figure 2a, the storm preceding the one of interest was producing winds of 30-35 kn along the Alaskan coast. Time histories of surface wind speed and direction at the offshore locations are shown in Figure 3. The preceding storm was of moderate intensity, reaching a central pressure of about 970 mb before stalling and filling in the GOA on October 27 and 28.

The intense storm of October 27-31 began as a wave (~1010 mb) on the polar front near 35°N, 180°W early on October 27. The low moved

northeastward at nearly 40 kn during October 27 and 28 and deepened to 986 mb, reaching 46°N, 160°W by 1800 GMT October 28. As seen in the detailed track obtained by postanalysis in Figure 1, the low slowed considerably after 0000 GMT October 29 and gradually curved northward. The minimum central pressure of about 950 mb was attained at 1800 GMT October 29, when the center was located 360 mi south of the Kenai Peninsula. The storm then drifted northward, filled slowly for about 12 hr, then filled more rapidly later on October 30 and 31. The storm ultimately drifted northwestward toward the Kenai Peninsula and filled.

The kinematic analyses are presented in Figures 4a-4d. The analyses are restricted to the region bounded by 130°W, 170°W, 45°N and the Alaskan coast. Ships' wind reports are plotted in standard fashion, except that two digits are shown next to the wind barb. The first digit resolves the tens' place of the wind direction reported while the second digit resolves the units' place of the wind reported in knots (e.g. <sup>04</sup> is a wind report of 300° at 14 kn). Isotachs are drawn at 5-kn intervals. Coastal and island reports, where plotted, are shown as open boxes; while ship and buoy reports are shown as open circles.

The analysis for 0000 GMT October 29, 1974, (Fig. 4a) shows the decaying wind pattern about the filling storm in the GOA and the increasing winds about the intensifying cyclone. At this time maximum winds of 40-45 kn occurred in a north-south band located about 300 mi east and south of the intensifying storm center with light winds to the north and northwest. Light winds (< 20 kn) were affecting the GOA nearshore area from Kodiak to Yakutat. By 1200 GMT October 29, 1974, winds were increasing rapidly offshore Kodiak and, soon thereafter, at the other locations (as shown in Fig. 3). The isotach maximum rotated to the northeast of the low center and, for the first time in the history of the wind field for this storm, strong winds developed in the northwestern quadrant. The winds there developed much closer to the center than in the northeastern quadrant.

By 0000 GMT October 30, 1974, the low center reached maximum intensity (central pressure near 950 mb) and winds in excess of 50 kn covered the eastern, northern and western quadrants with speeds between 55 and 60 kn northeast of the center as far as the GOA coast between Yakutat and Middleton Island. By 1200 GMT, winds began to decrease, but a ring of wind speeds in excess of 40 kn surrounded the center (Fig. 4d) with smaller areas of winds between 45 and 50 kn just northeast and southwest of the low center.

The most striking aspect of the time histories interpolated from the wind fields at the four coastal locations (Fig. 3) is the rapid increase in wind speed from less than 15 kn to greater than 50 kn in about 12 hr. All locations experience maximum winds at about the same time, with wind directions consistent with cyclonically curved flow about the approaching center. Only near Kodiak do the wind directions have an offshore component.

### 3. STORM 2: DECEMBER 29, 1974 TO JANUARY 1, 1975

This storm was not quite as intense as storm 1 but was unusual in that the strong winds were associated with wind directions between south and west between the Kenai Peninsula and Yakutat. Near Kodiak, winds of only moderate strength occurred and these were associated with offshore directions.

The time histories (Fig. 5) begin at 0000 GMT December 29, when a 979-mb low with a broad center containing relatively light winds was located in the GOA. The storm of interest here developed apparently in the broad westerly polar air stream. Figure 5a shows the trough near 50°N, 170°E in which the new low developed. This system moved eastward to near 50°N 165°W at 0000 GMT and began to acquire frontal wave characteristics. The detailed track (Fig. 1) shows the system turning east-northeastward and intensifying rapidly, passing near Middleton Island on October 31 with a central pressure of about 954 mb.

As seen most readily in Figure 5e, the storm had a fairly complicated isobaric pattern, with a deep trough extending southeastward from the center of lowest pressure. The strongest south and southeast winds, therefore, occurred well east of the center. Also, because of the near-shore track of the broad center, strong easterly winds did not occur along the GOA coastline. Rather, the strongest winds occurred after the center had crossed the GOA and moved into extreme southern Alaska. The indicated behavior is shown in the 12-hourly streamline/isotach analyses, Figures 7a-7d, covering the period 1200 GMT December 30, 1974, to 0000 GMT January 1, 1975.

The time histories of surface wind, Figure 6, indicate that 45- to 50-kn winds occurred offshore Prince William Sound-Yakutat. Those winds had an onshore component through much of the event, while weaker offshore winds affected the shelf near Kodiak.

The time scale of this storm was significantly longer, as winds increased over a 36-hr period, than that of storm 1.

### 4. STORM 3: DECEMBER 16-21, 1975

This event was selected to show the rapid succession of storms possible in the GOA. The period December 16, 1975, to December 21, 1975, included, at some sites, five separate events in which wind speeds exceeded 30 kn along at least some portion of the coast. East of Kodiak, the strong winds were mainly onshore.

The sequence of 12-hourly surface maps for the period is given in Figures 8a-8i. The broad scale sea-level pressure pattern shifted during this period. In the beginning of the period, a large extratropical cyclone centered in the Bering Sea dominated the north central North Pacific. During the period, a series of disturbances moved northeastward from the southern periphery of that low into the GOA, so that by the end of the period, the center of cyclonic action had shifted from the Bering Sea to the GOA.

Fig. 8a shows the first such disturbance just entering the GOA at 1200 GMT December 16, 1975. This system caused 40- to 45-kn onshore winds along the entire region between Kodiak and Yakutat. The second disturbance in the series reached the Alaskan coast shortly after 1200 GMT December 17 (Fig. 8c) but caused only a minor increase in wind speeds between Kenai Peninsula and Yakutat.

The strongest storm of the sequence apparently originated as an open wave on the polar front in the western Pacific. The wave (996 mb) is seen in Figure 8a near  $38^{\circ}\text{N}$ ,  $171^{\circ}\text{E}$ . The wave moved eastward without intensification for about another 24 hr, then turned northeastward and began to intensify sharply. By 1800 GMT December 18, 1980, the first position shown in Figure 1, central pressure had fallen below 960 mb. The system continued to curve northward, decelerate and deepen over the next 24 hr. The center passed just east of Kodiak around 1800 GMT December 19, with a central pressure near 950 mb, before drifting over the Kenai Peninsula and filling rapidly on the 20th.

Figures 10a through 10f show the wind field about the intense storm at several times. As the storm entered the GOA (Fig. 10a), the wind field was not unlike that depicted for storm 1, with strong winds mainly east and south of the center. Also, a band of strong surface winds developed well northeast of the center ahead of the occlusion (Figs. 10b, 10c), with lighter winds separating that area from the isotach maxima south of the center.

As observed in storm 1, the northwest quadrant of the circulation was the weakest, as stronger winds developed there only late in the history and covered a small area close to the center of circulation.

As the low center moved from east of Kodiak into Kenai (Figs. 10d and 10e), the isotach maximum located initially south of the center appears to have rotated to the southeast quadrant, producing the sharp east-west gradient in wind speed across the GOA evident on the 0000 GMT December 20 wind field.

The time histories shown in Figure 9 for this event are quite similar to those of storm 1, with a rapid increase in wind speed over a 12-hr period between 1800 GMT December 18 and 0600 GMT December 19. The secondary maximum in wind speed at the eastern locations 12- to 18-hr later is a response to the movement onshore of the strong southeastern quadrant of the circulation noted above in Figure 10e.

Southwesterly winds in the wake of the intense storm backed to easterly late on December 20 in advance of yet another strong impulse. This fourth impulse also formed as an open wave on the polar front around 0000 GMT December 19. At that time (Fig. 8f) a vigorous low, which had formed in the polar air stream, was located near  $45^{\circ}\text{N}$   $180^{\circ}\text{W}$ . Over the following 24-36 hr, the frontal wave moved northward and deepened, ultimately merging with and absorbing the circulation of the low in the polar air stream. By 1200 GMT 21 December, the combined system had deepened to 956 mb and was located about 200 miles northwest of weather ship "P". This low, however, did not move further northward into the GOA, but began to fill and drift eastward. Figure 10f shows

the wind field over the GOA at 0600 GMT December 21, when this storm was most intense. Easterly winds covered the entire GOA, with the strongest winds offshore Kodiak. Maximum winds probably did not exceed 50 kn throughout this storm.

The most striking feature of time histories for this last event of the sequence is the uniformity of wind direction across the shelf between Kodiak and Yakutat. This type of storm provides strong winds with an onshore component at Kodiak.

#### 5. STORM 4: JANUARY 27-31, 1976

A long period of moderate (20-30 kn) onshore flow along the entire upper GOA coast preceded this storm. The wind field history began at 0000 GMT January 27, 1976, as a relatively weak system moved northward through the GOA. The passage of the broad center of this low caused the shifting wind pattern evident in the time histories at all four offshore locations between 0000 GMT January 27 and 0000 GMT January 28 (see Figs. 11a-11i).

Between 0000 GMT January 28 and 0000 GMT January 30, the GOA was under the influence of a broad southerly flow. As an extratropical cyclone moved into the Bering Sea early on January 29, a minor increase in the flow is evident in the time histories at all sites between 0000 and 0600 GMT January 29.

The important storm in this sequence for the GOA is traceable to a flat wave on the polar front which had moved due eastward across the North Pacific along 35°N on January 28. By 0000 GMT January 29, this wave had begun to turn northeastward and deepen. The 6-hourly positions thereafter are indicated in Figure 1. This storm moved northeastward more rapidly than any of the other storms studied and decelerated only slightly as it approached the Alaskan coast. Indeed, the center moved quickly northward across western Alaska and reached Norton Sound by 0000 GMT January 31. The lowest central pressure attained in this storm was about 958 mb, when the center was 200 mi south of the Trinity Islands.

The streamline/isotach analyses presented in Figure 13a-13d show the wind field between 1200 GMT January 29 and 1800 GMT January 30. This storm is similar in many respects to storms 1 and 3 in that the southern and eastern quadrants of the wind field are much stronger than other quadrants as the low enters the GOA. It differs in that strong winds develop quickly in the northeast sector of the storm as the gradient is enhanced between the storm center and the Alaska coast. The enhancement apparently causes winds to increase between Kenai and Yakutat in advance of this type of low more rapidly than would be expected from simple advection of the wind field (Fig. 12).

It is interesting to note that in storm 4 the strong winds never develop to any discernible extent in the northwestern quadrant, despite the existence of strong surface pressure gradients there close to the center. This effect was also observed in storms 1 and 3, except that as those storms decelerated, stronger winds eventually developed northwest



of the center. This suggests that the acceleration of air entering the northwestern quadrant is retarded greatly by the highly cyclonic curvature which characterizes trajectories of air parcels there.

#### 6. ACKNOWLEDGEMENTS

This research is a contribution to the Marine Services Project at PMEL under purchase order 79-ABA-02699. It was supported in part by the Bureau of Land Management through interagency agreement with the National Oceanic and Atmospheric Administration, under a multiyear program responding to needs of petroleum development of the Alaskan continental shelf and is managed by the Outer Continental Shelf Environmental Assessment Program (OCSEAP) office.

## 7. REFERENCES

- Cardone, V. J., A. J. Broccoli, C. V. Greenwood, and J. A. Greenwood (1979): Error characteristics of extratropical storm windfields specified from historical data. Offshore Technology Conference, April 30-May 3, 1979, Houston, Texas. Paper OTC 3598. Also to appear in J. of Petroleum Technology, May, 1980.
- Overland, J. E., and T. R. Hiester (1980): Development of a synoptic climatology for the northeast Gulf of Alaska. J. Applied Met., 19, 1-14.

## FIGURES

	<u>Page</u>
Figure 1. Storm track map for the four storms.	500
Figure 2a-2i. Storm #1: sea level pressure analyses.	501
Figure 3. Storm #1: coastal winds.	510
Figure 4a-4d: Storm #1: streamline isotachs.	511
Figure 5a-5f: Storm #2: sea level pressure analyses.	515
Figure 6. Storm #2: coastal winds.	521
Figure 7a-7d: Storm #2: streamline isotachs.	522
Figure 8a-8l: Storm #3: sea level pressure analyses.	526
Figure 9. Storm #3: coastal winds.	538
Figure 10a-10f: Storm #3: streamline isotachs.	539
Figure 11a-11i: Storm #4: sea level pressure analyses.	545
Figure 12. Storm #4: coastal winds.	554
Figure 13a-13d: Storm #4: streamline isotachs.	555

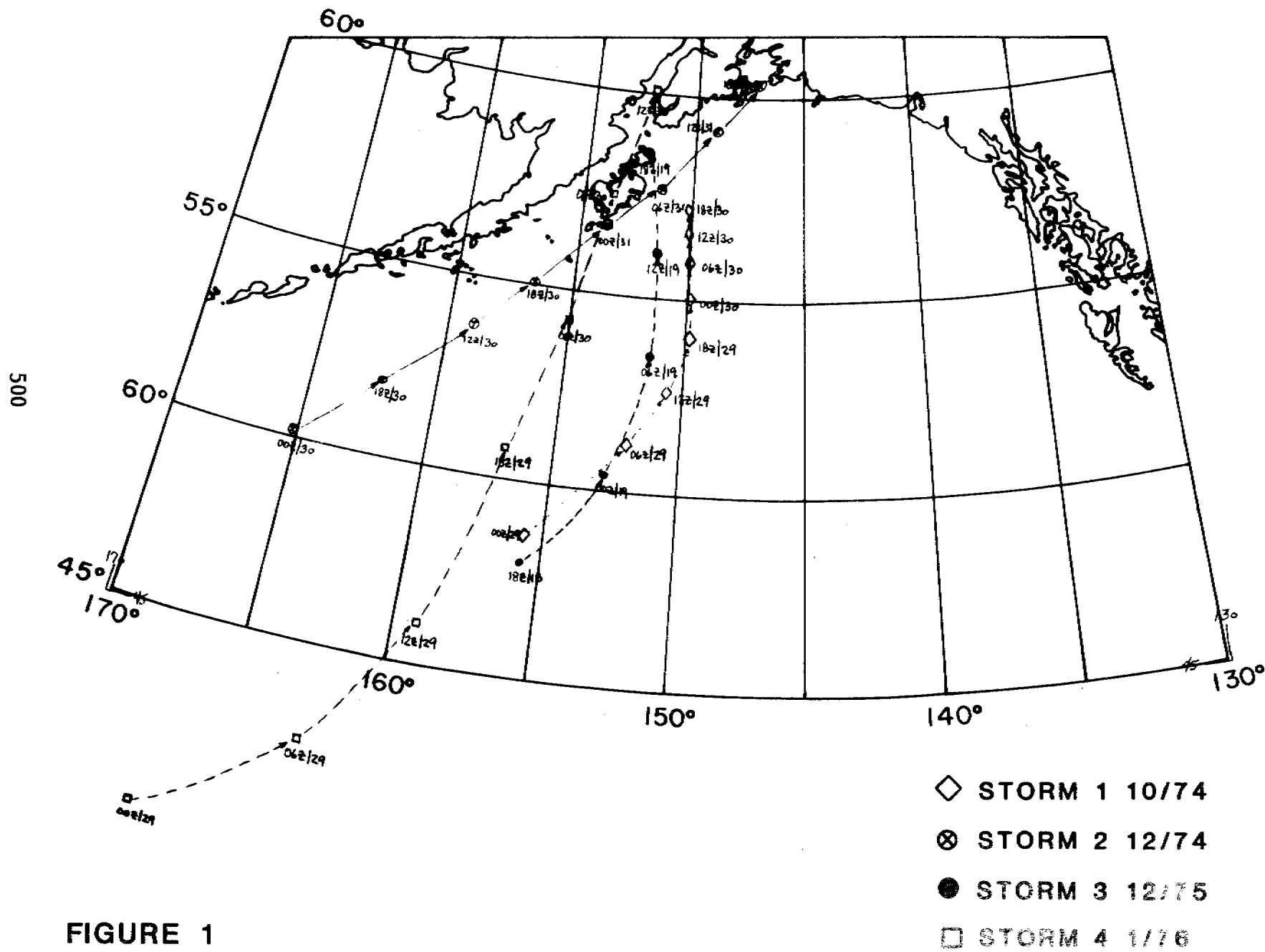


FIGURE 1

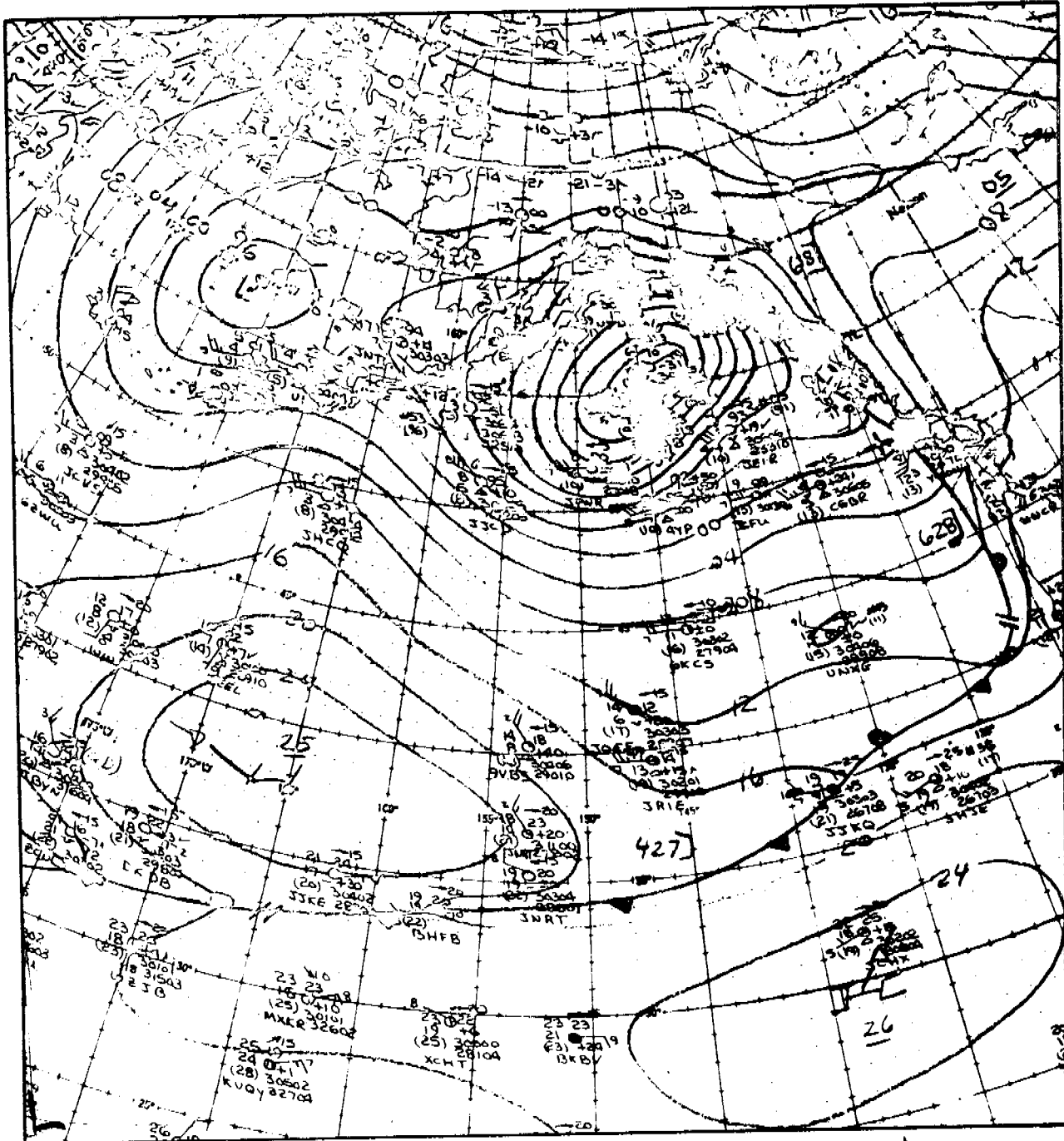


Fig.2a

06GMT 10/27/74





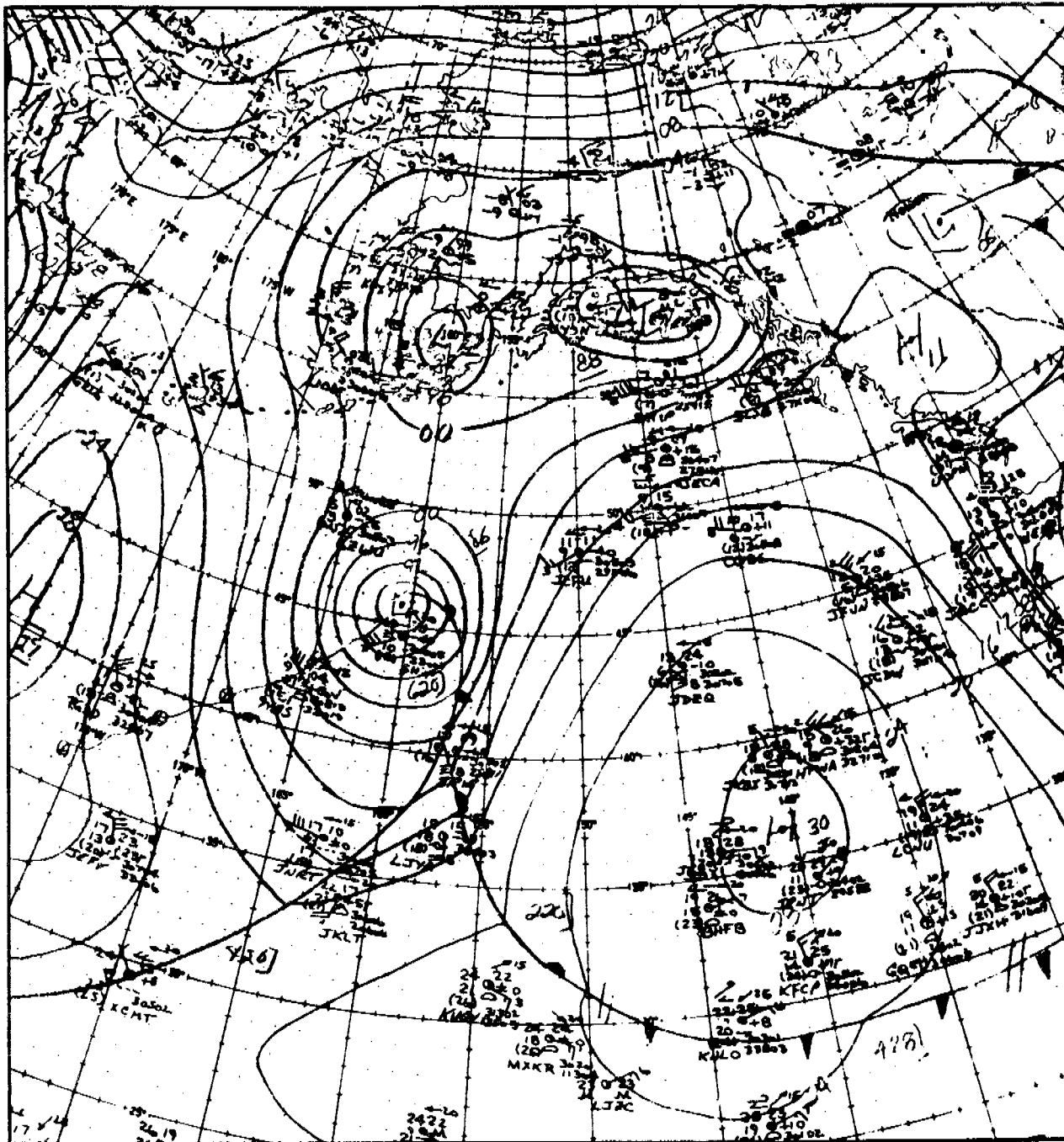


Fig.2d

18GMT 10/28/74



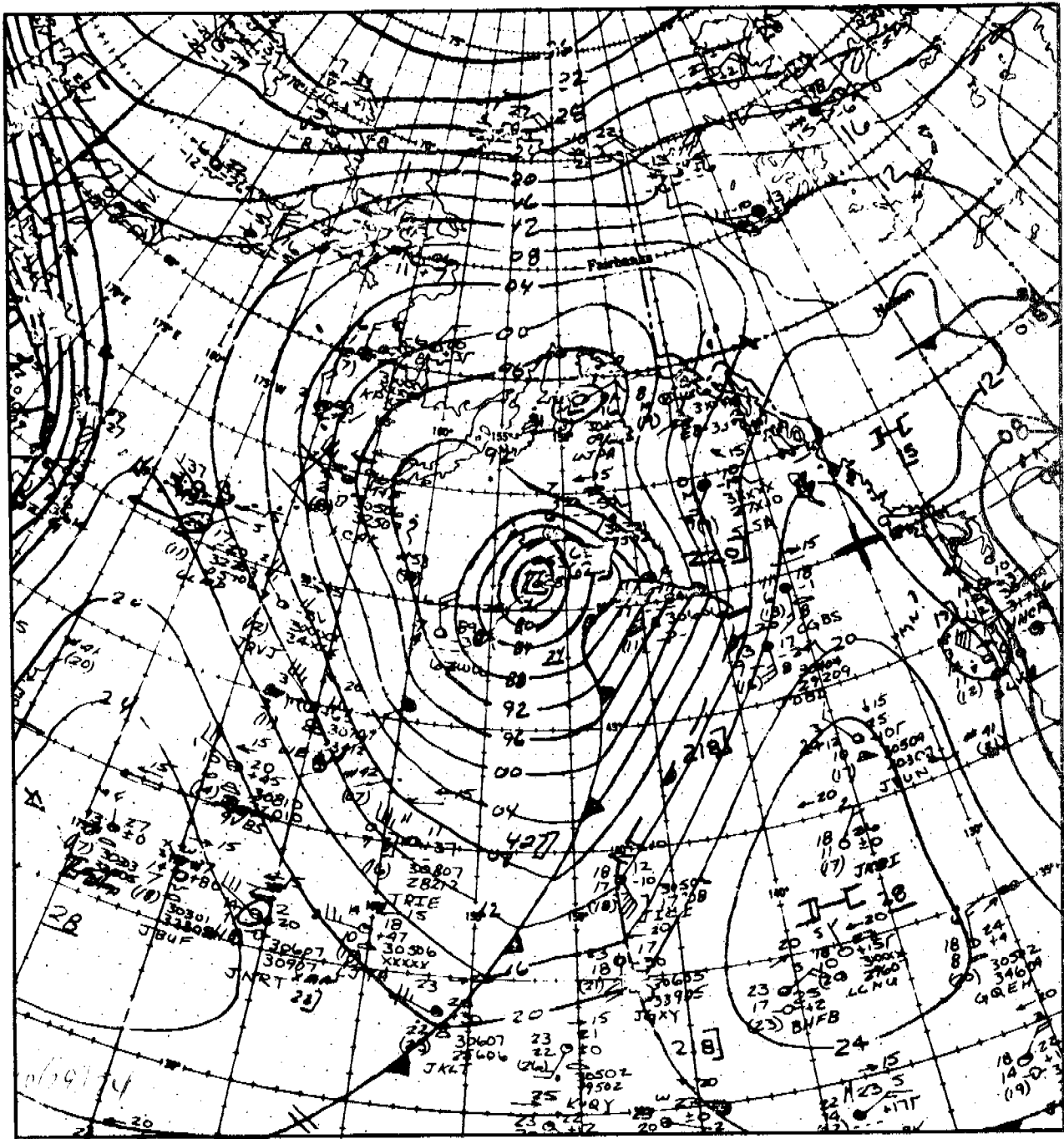


Fig.2e

06GMT 10/29/74

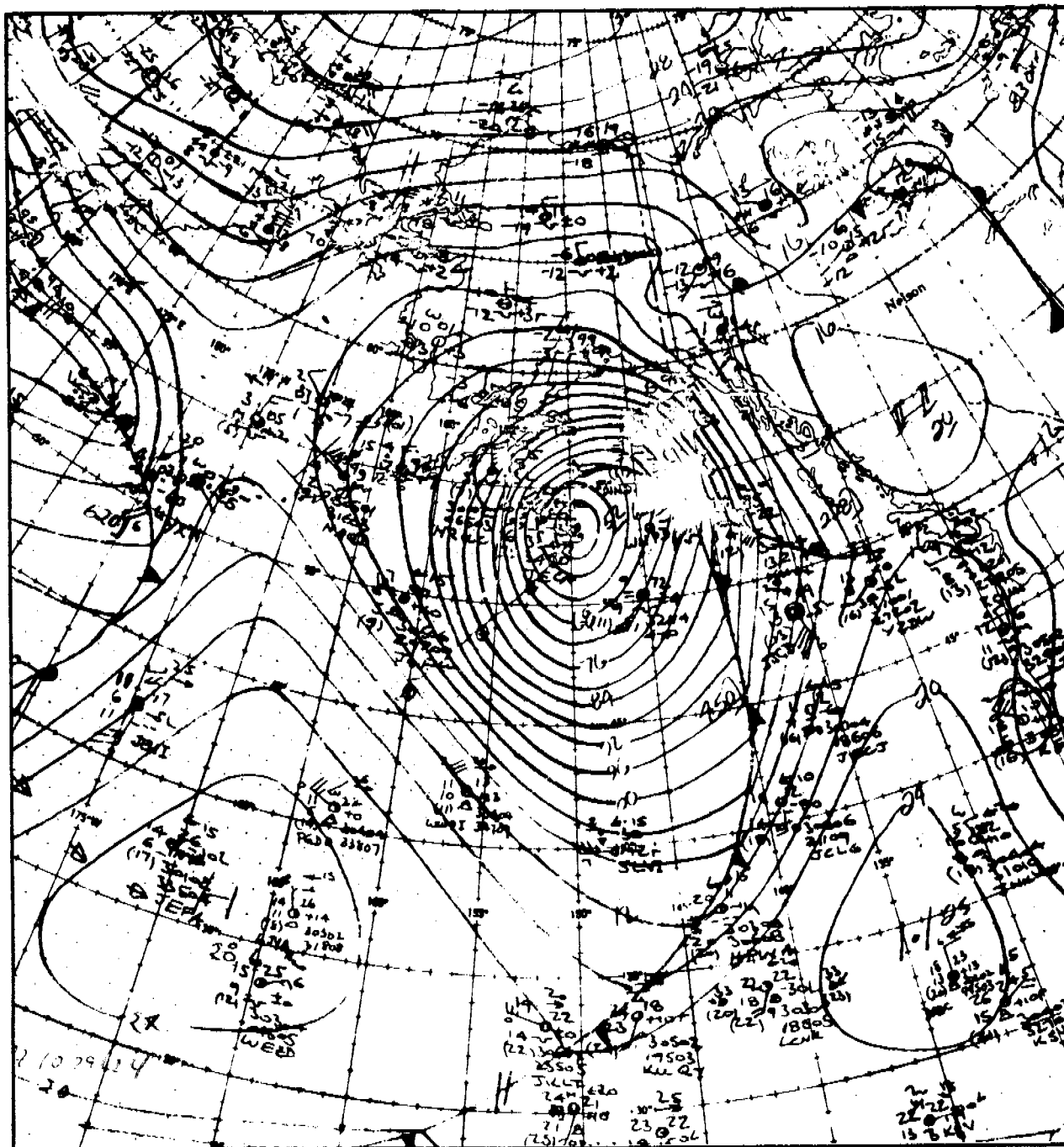


Fig.2f

18GMT 10/29/74

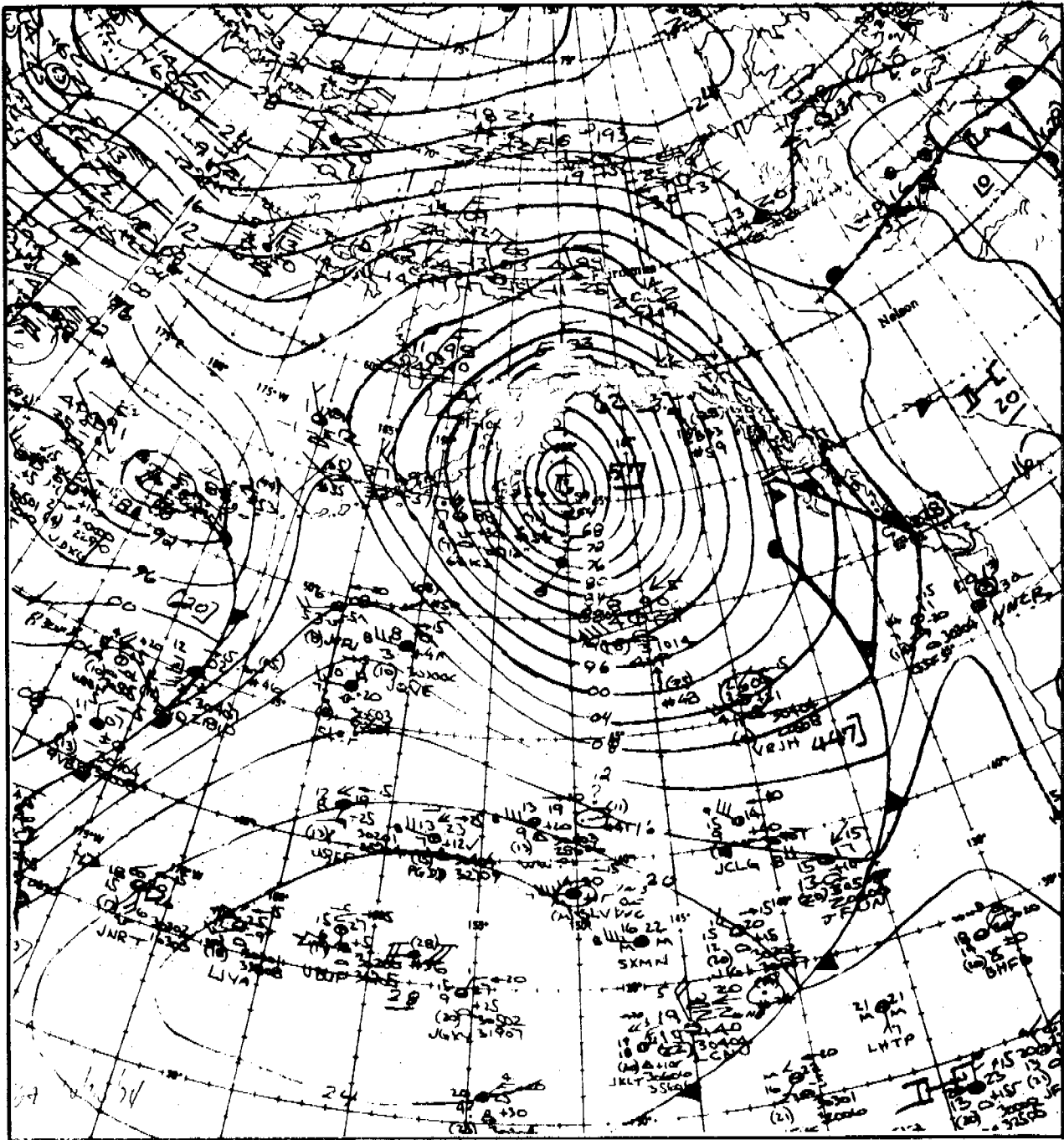


Fig.2g

06GMT 10/30/74

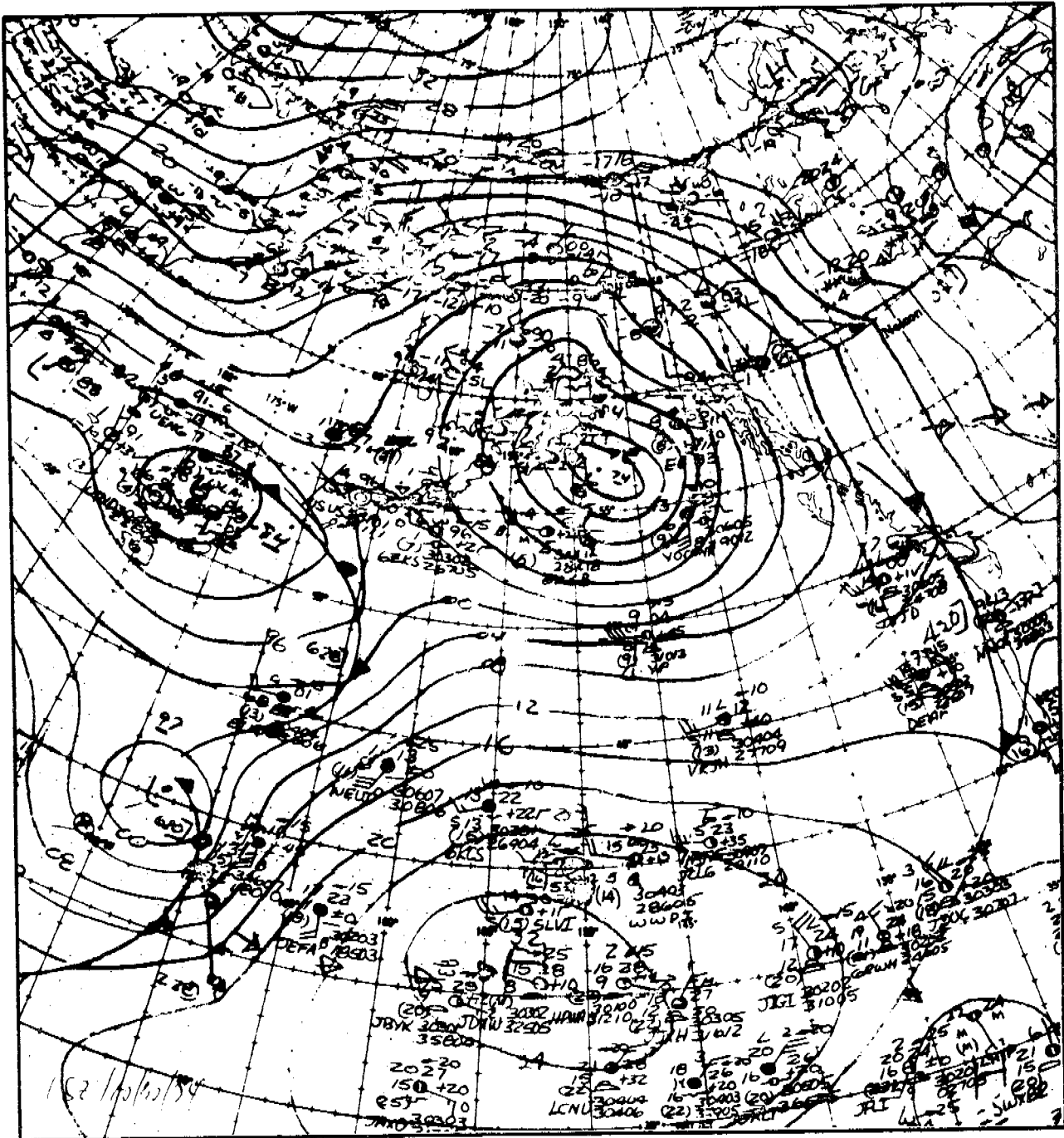


Fig.2h

18GMT 10/30/74



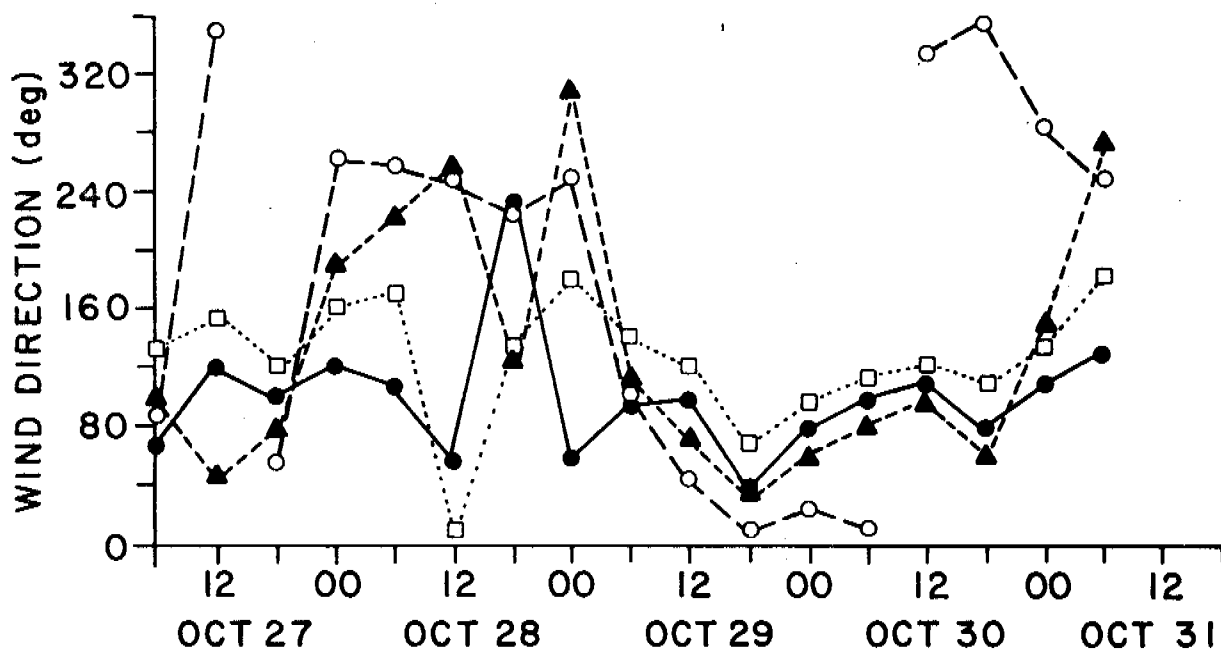
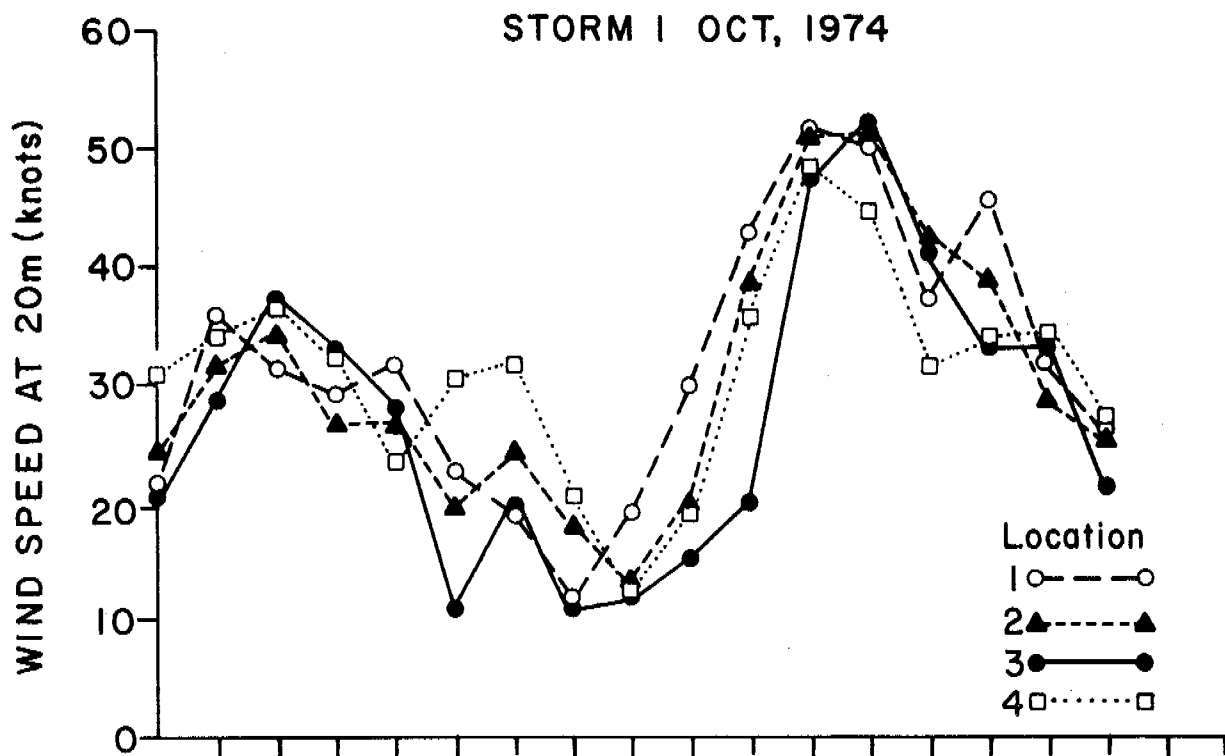


Figure 3

511

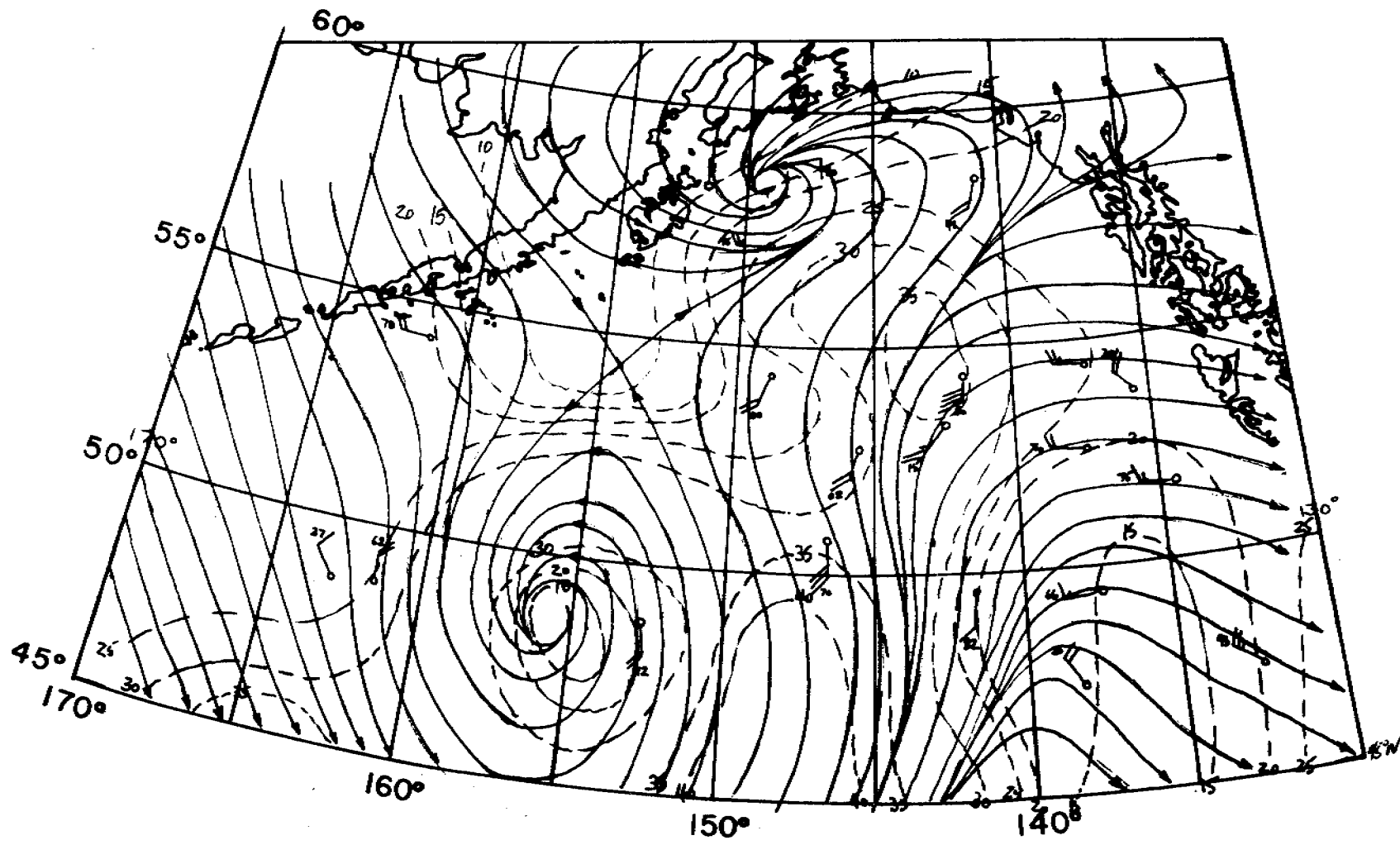


FIGURE 4a  
0000 GMT  
10/29/74

512

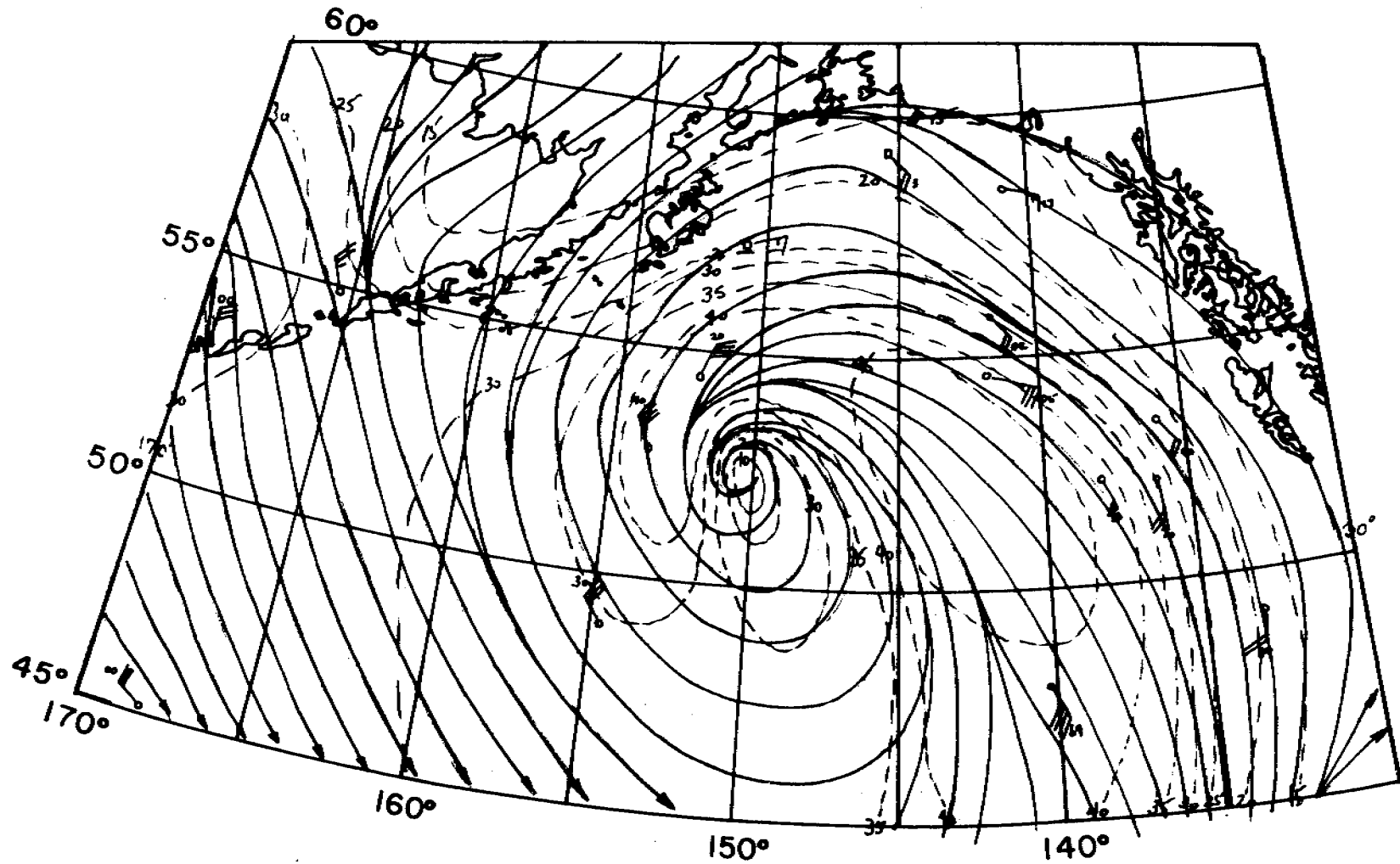


FIGURE 4b  
1200 GMT  
10/29/74



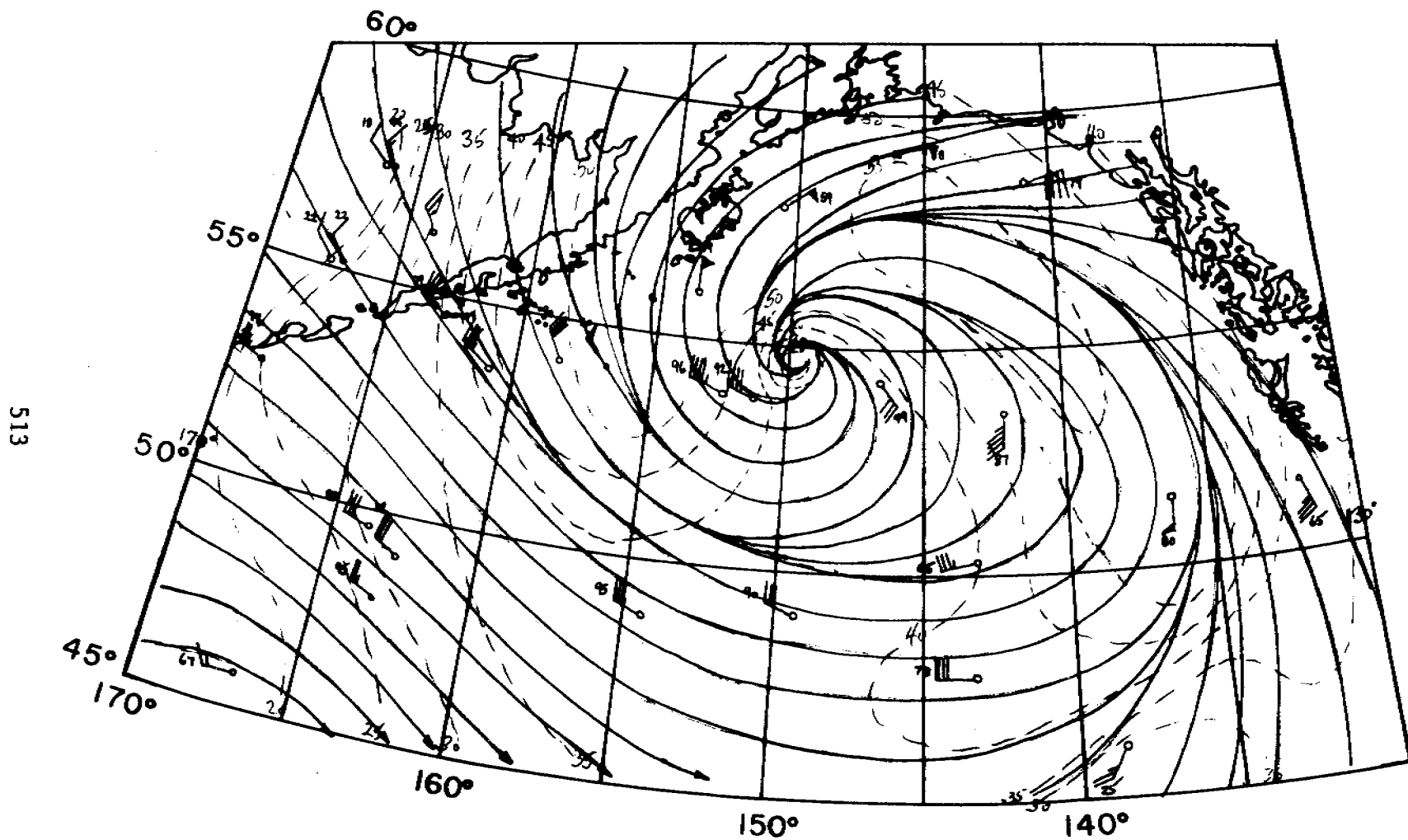


FIGURE 4c  
0000 GMT  
10/30/74

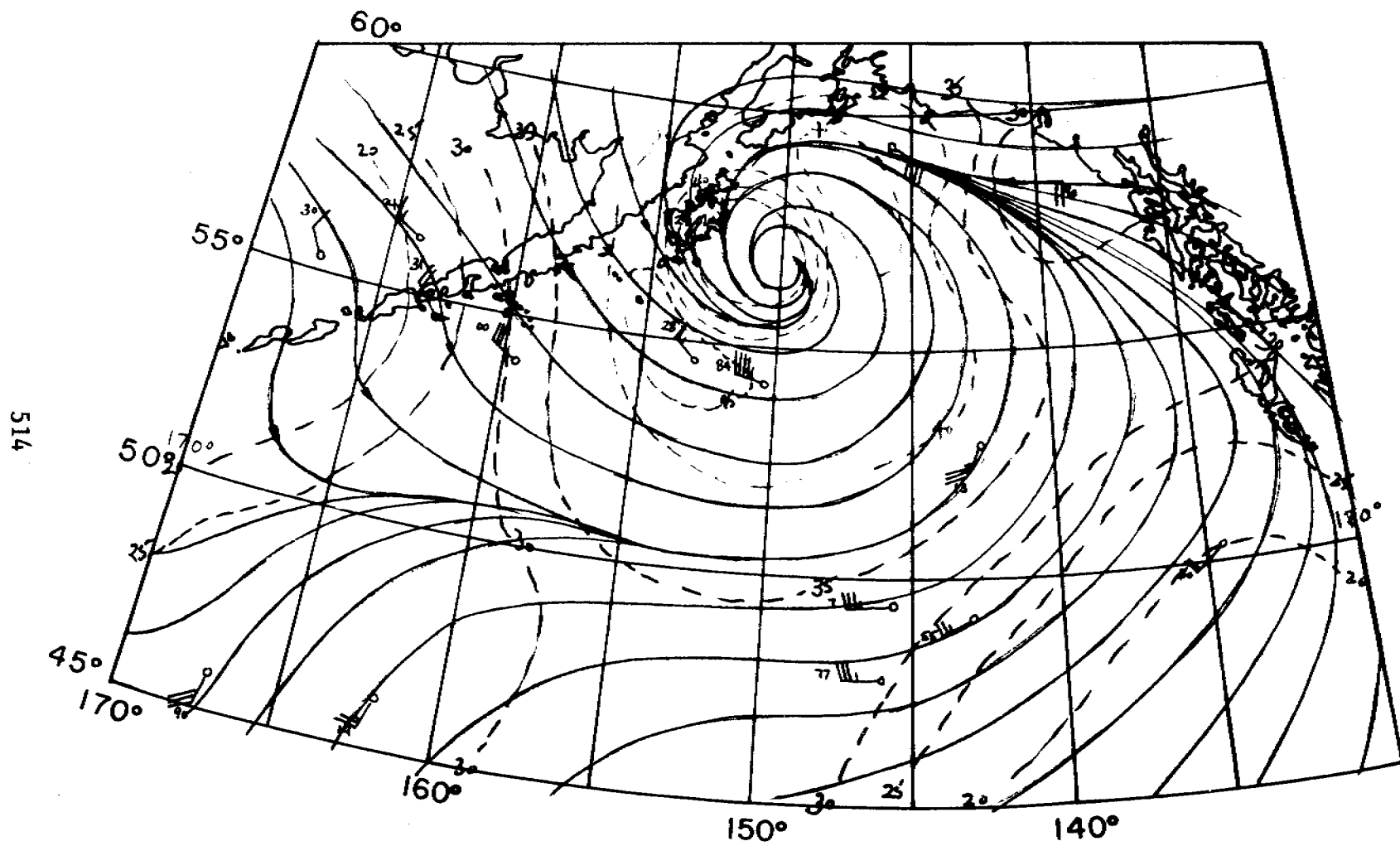


FIGURE 4d  
1200 GMT  
10/30/74



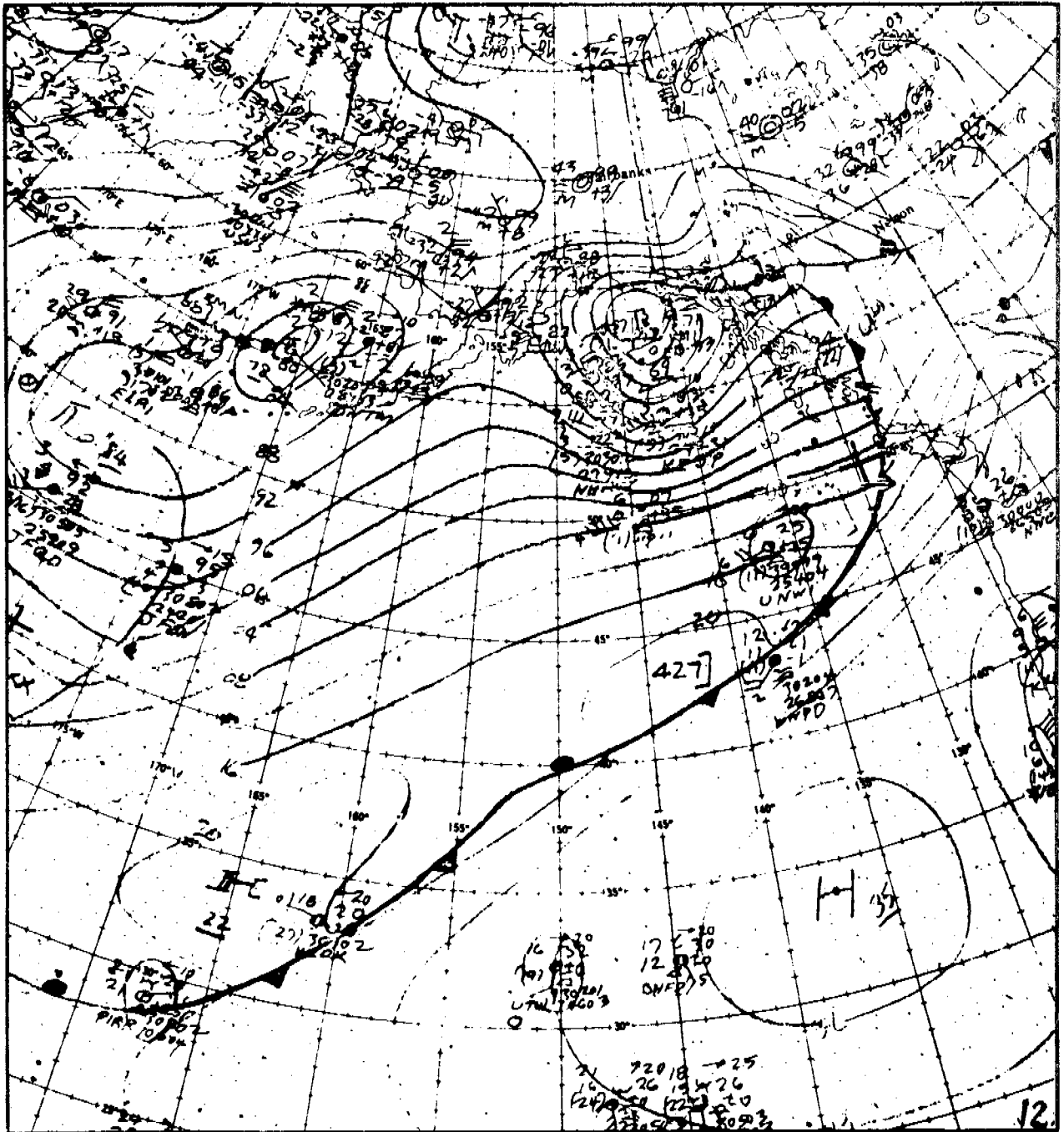


Fig.5b

12GMT 12/29/74

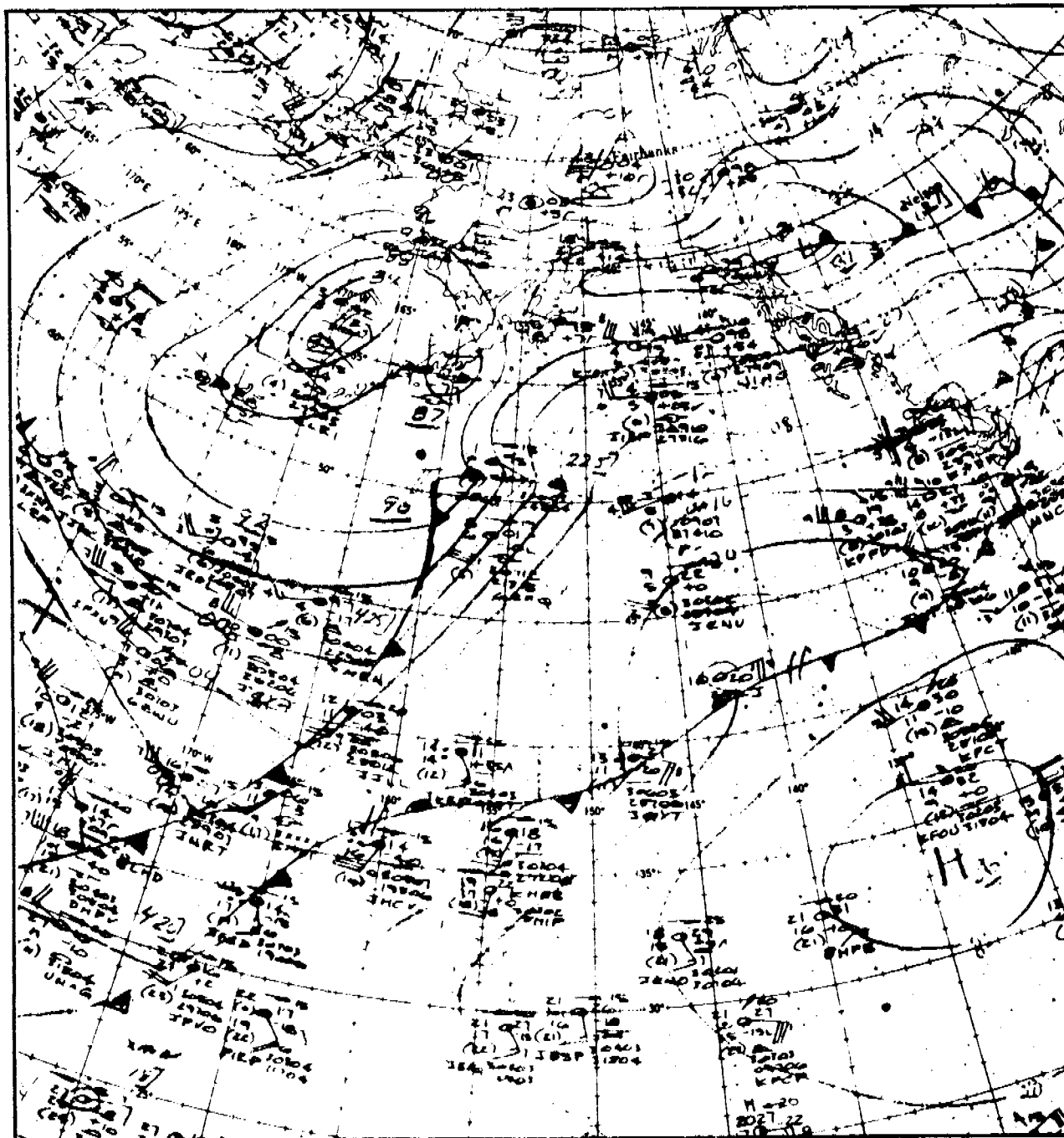


Fig.5c

00GMT 12/30/74

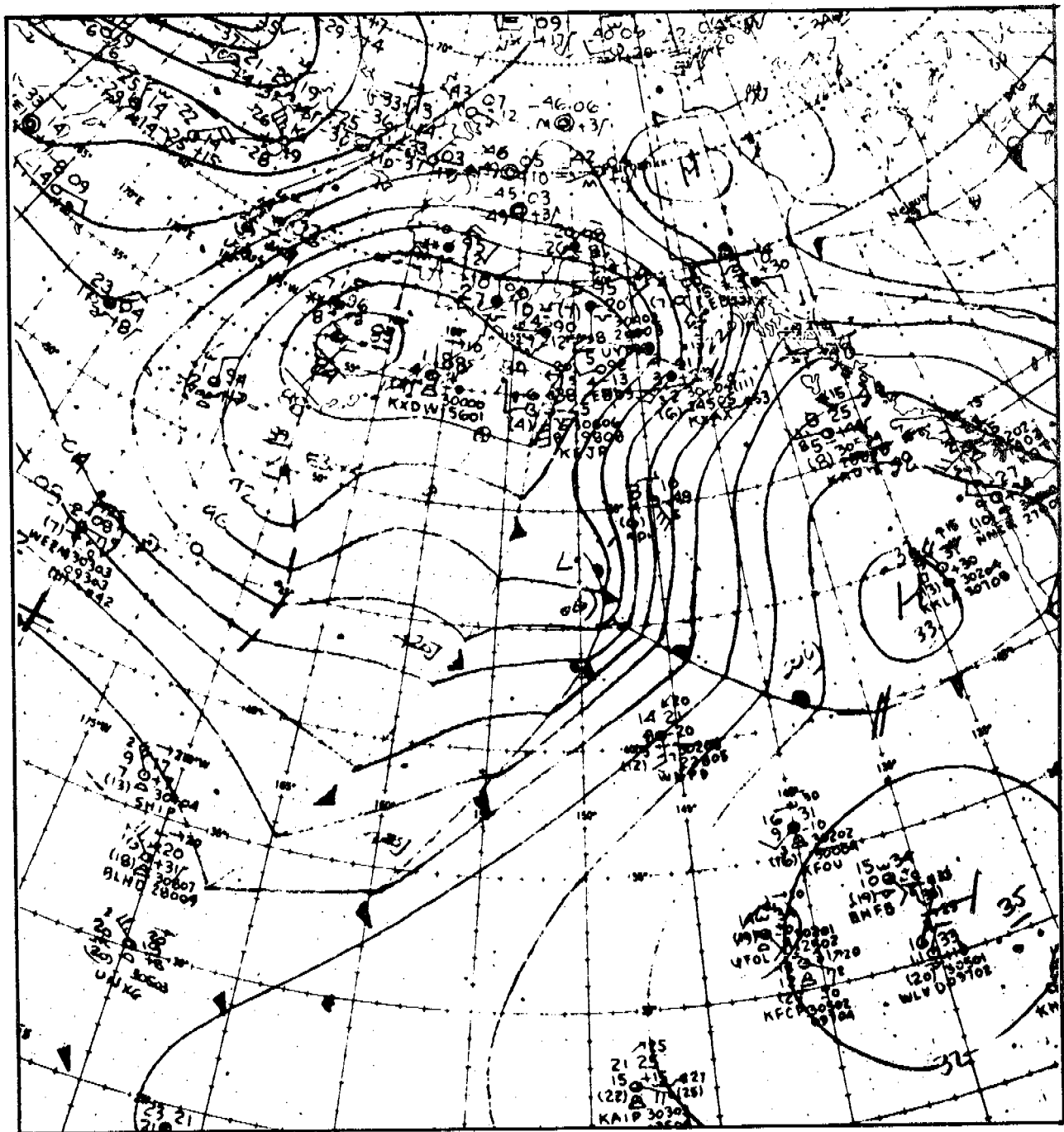


Fig.5d

12GMT 12/30/74

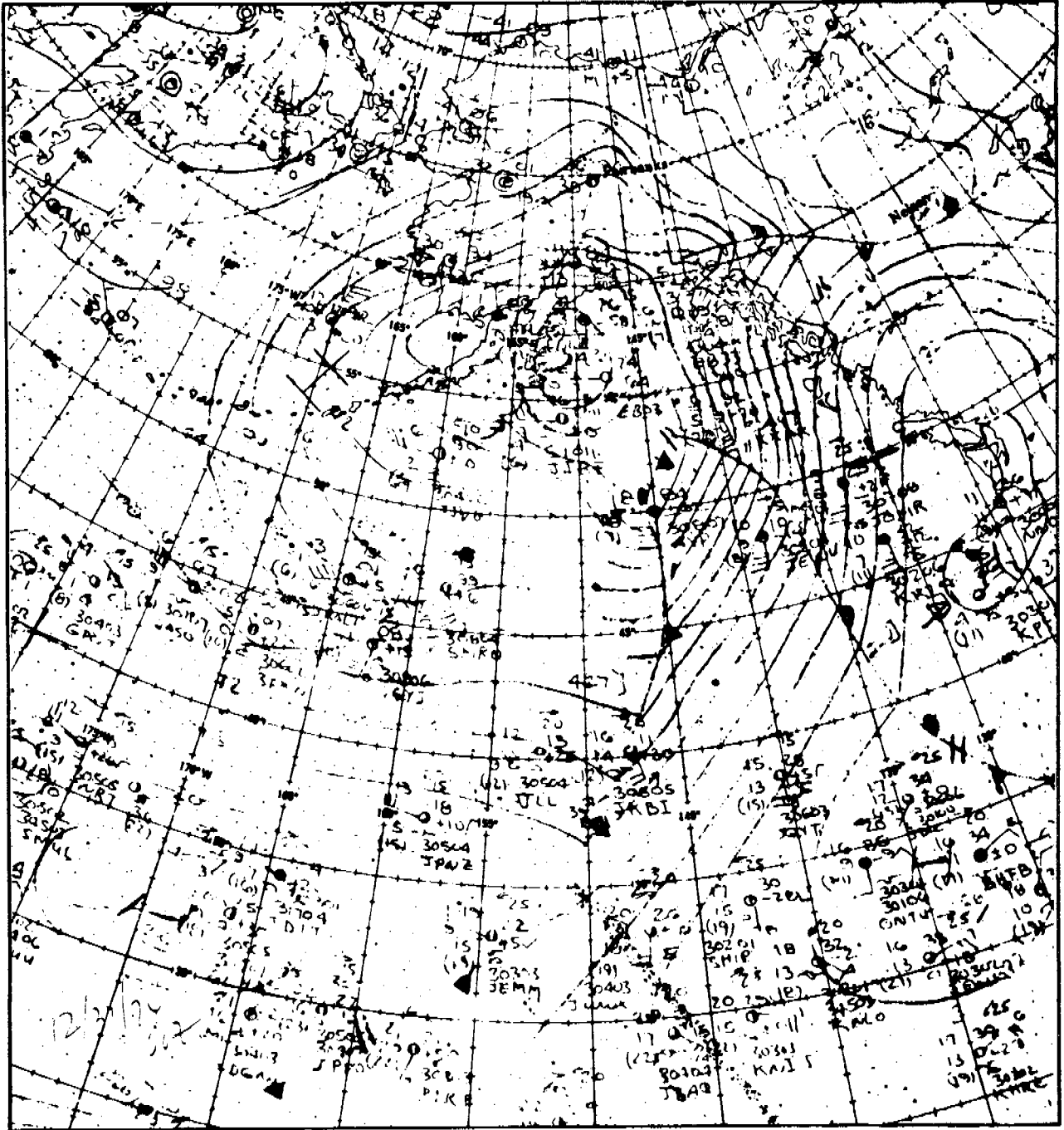


Fig.5e

00GMT 12/31/74

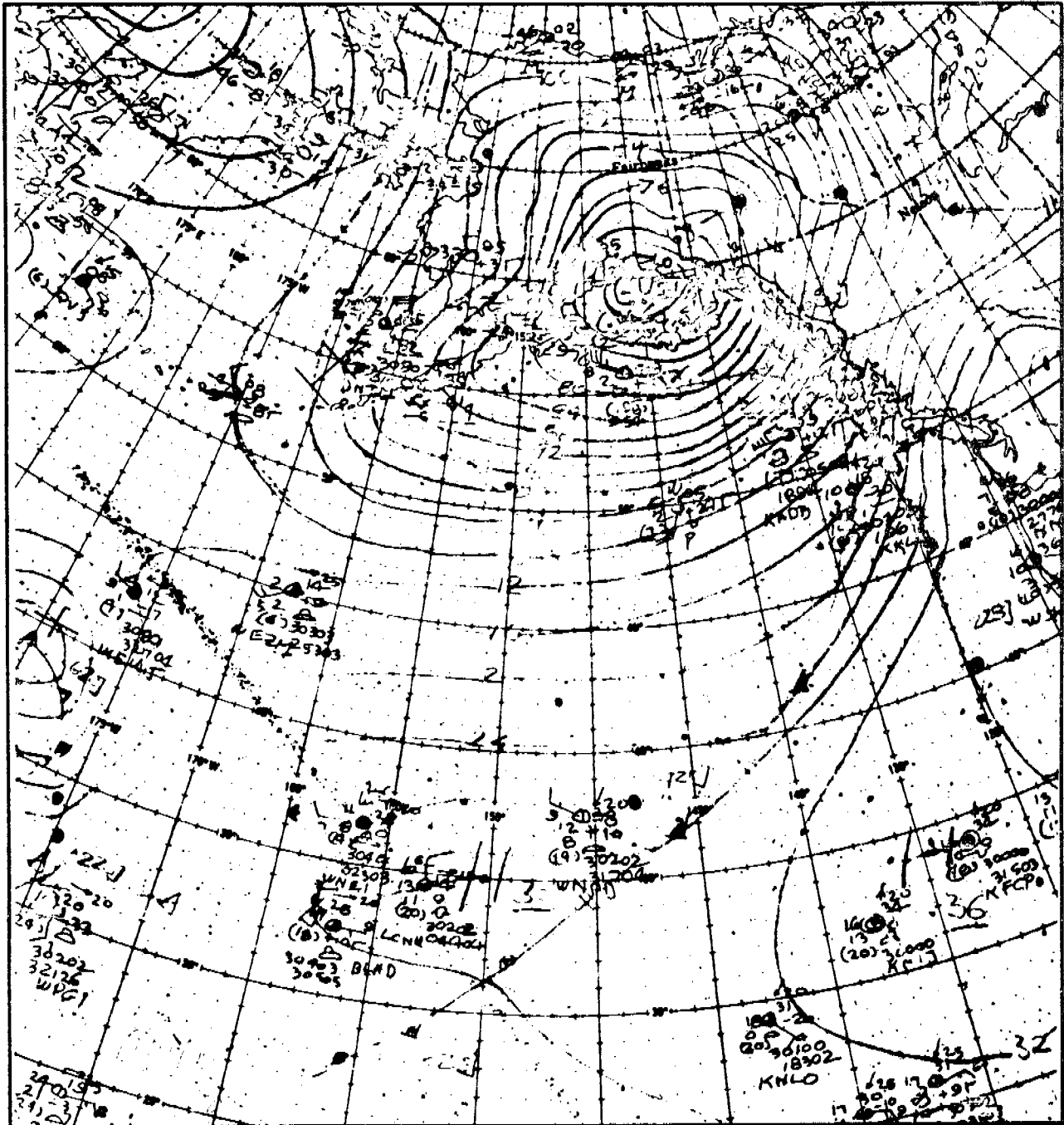


Fig.5f

12GMT 12/31/74



STORM 2 DEC, 1974 - JAN, 1975

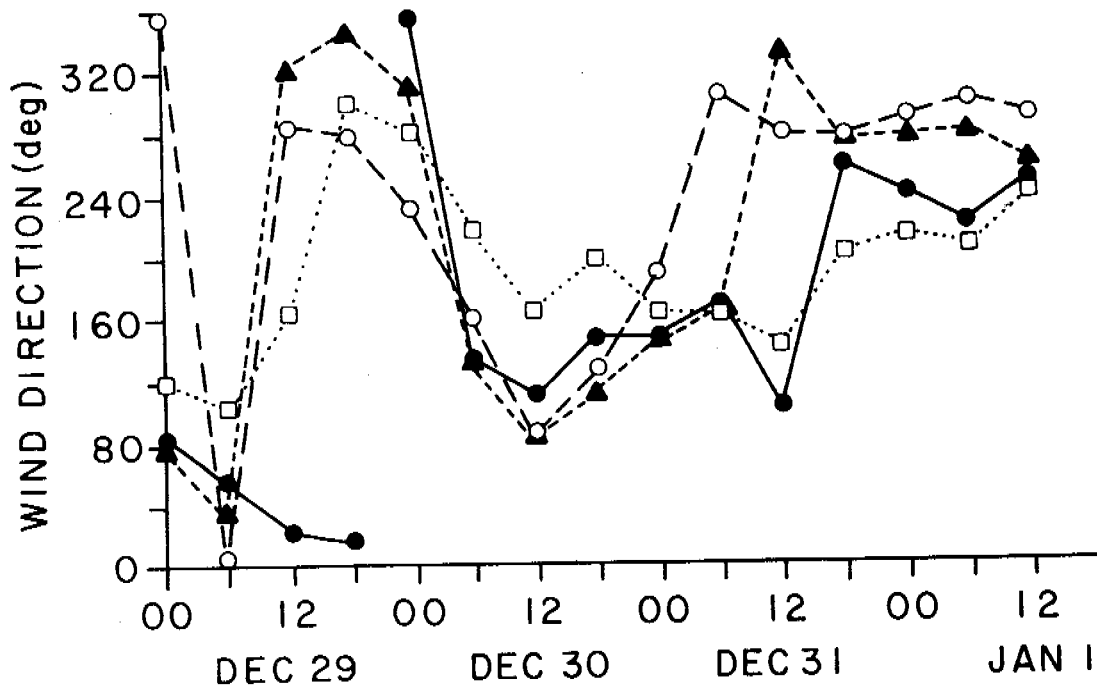
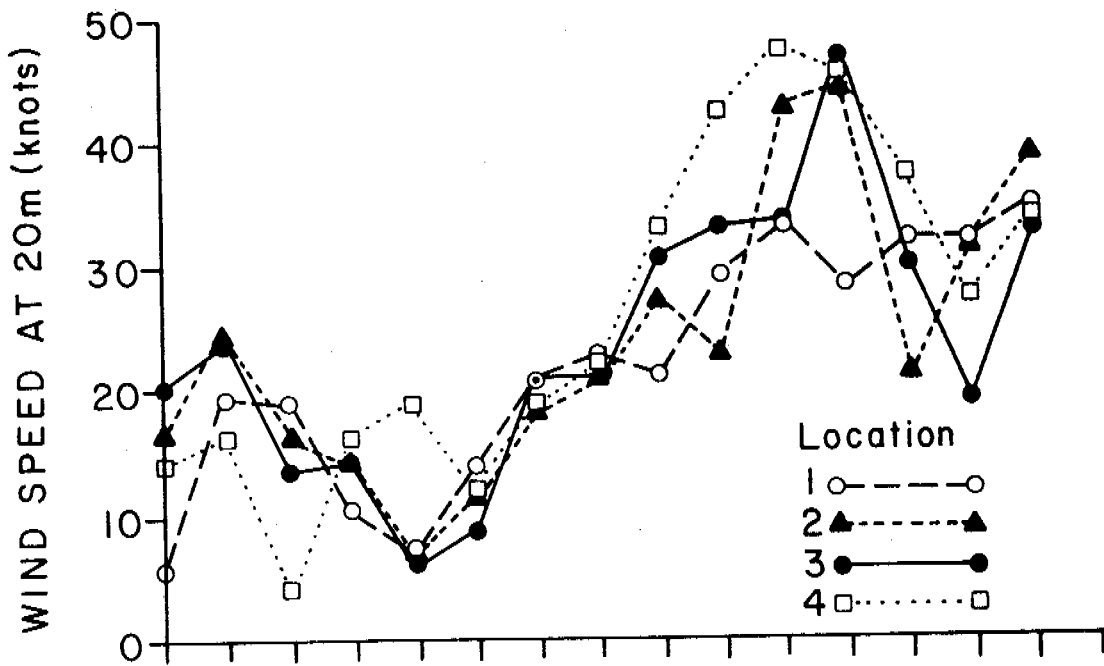


Figure 6

522

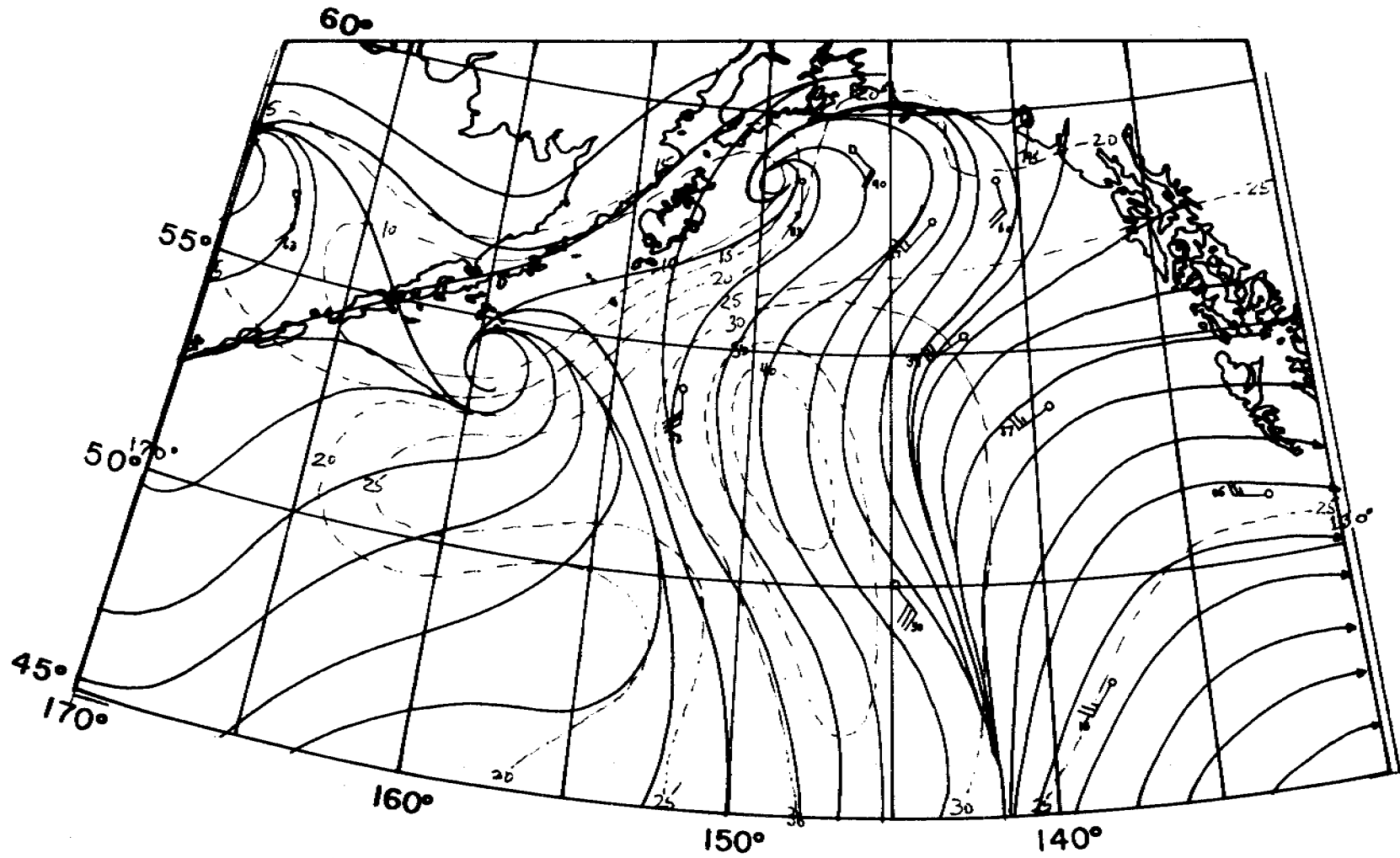
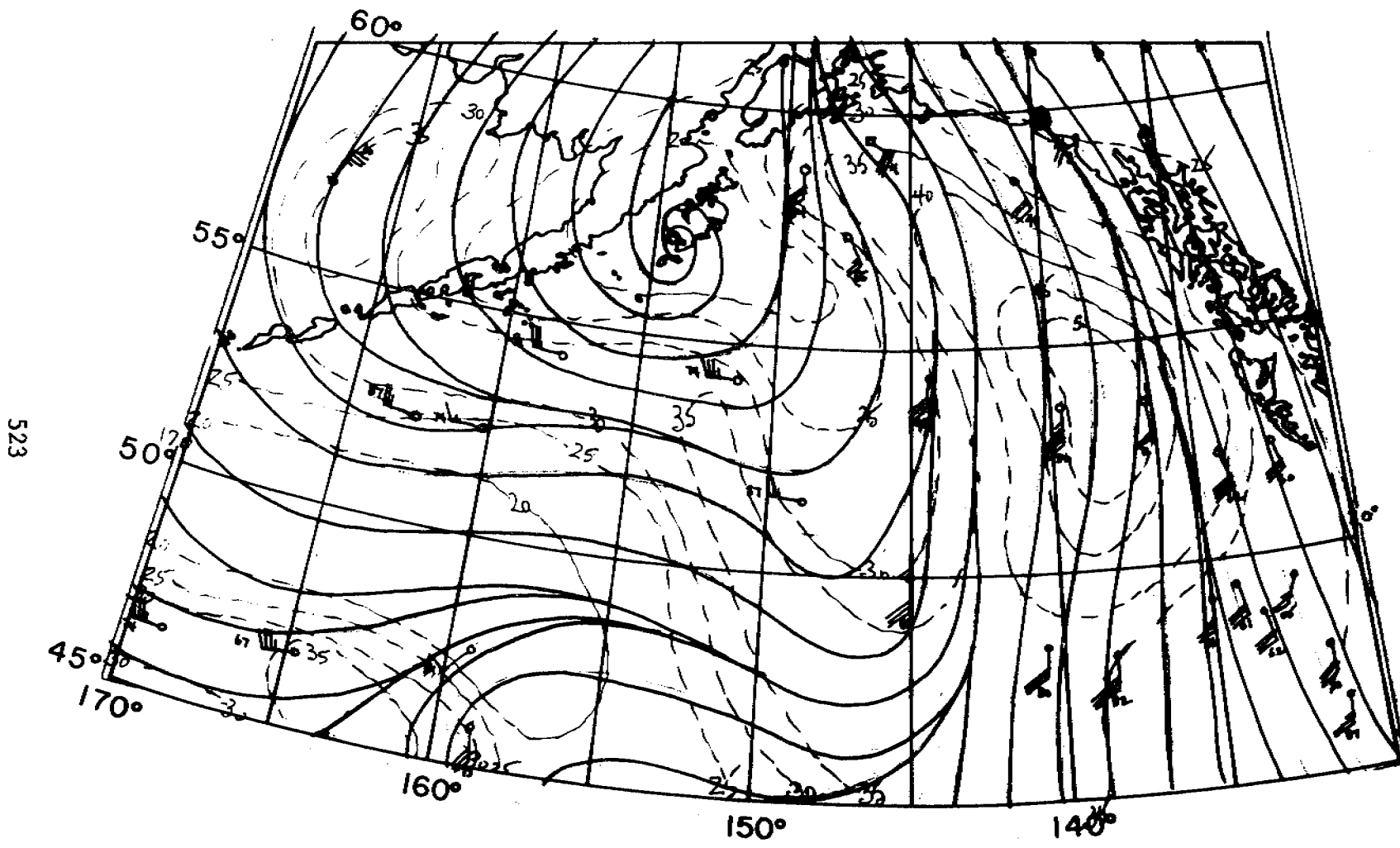


FIGURE 7a  
1200 GMT  
12/30/74



523

FIGURE 7b  
0000 GMT  
12/31/74

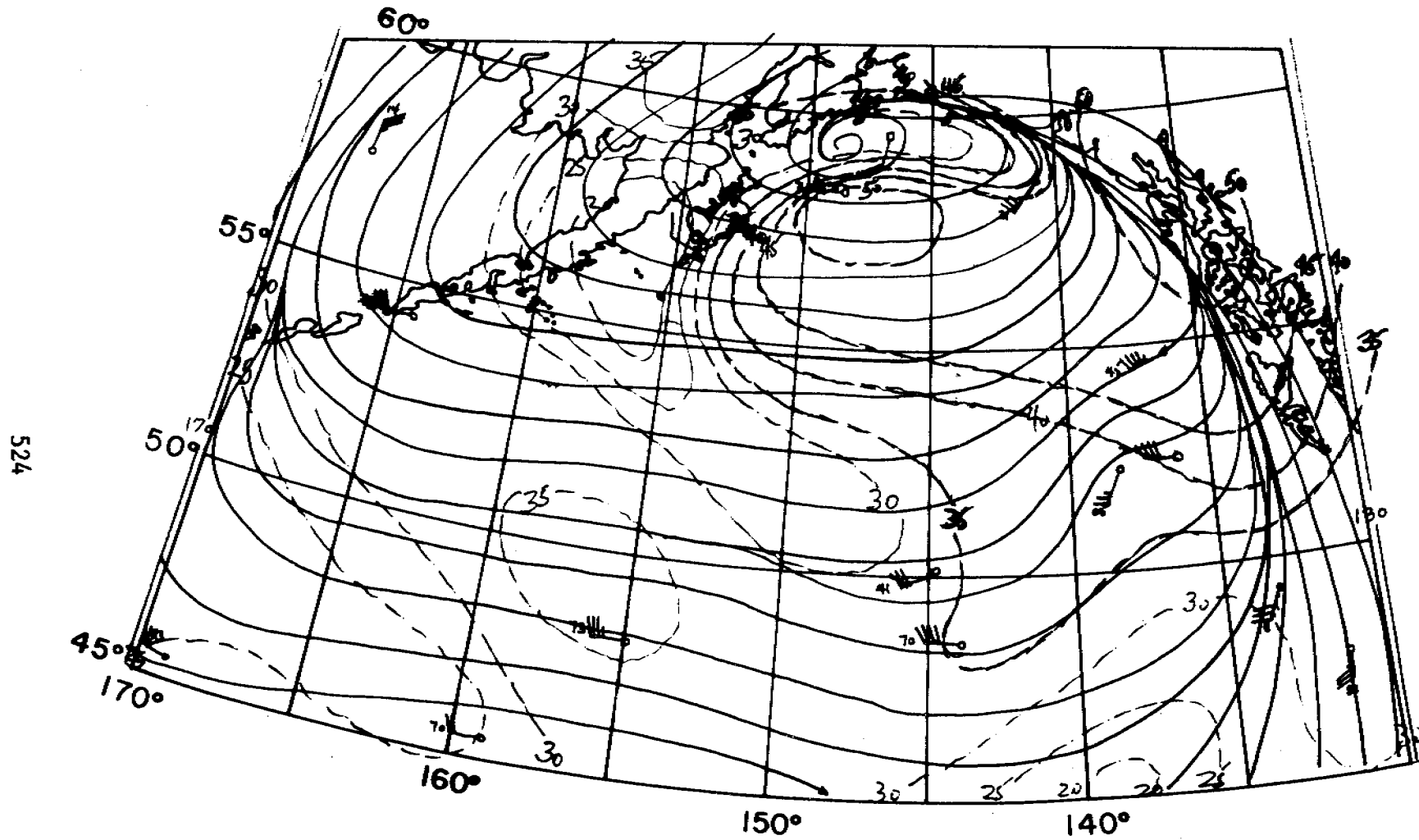


FIGURE 7c  
1200 GMT  
12/31/74

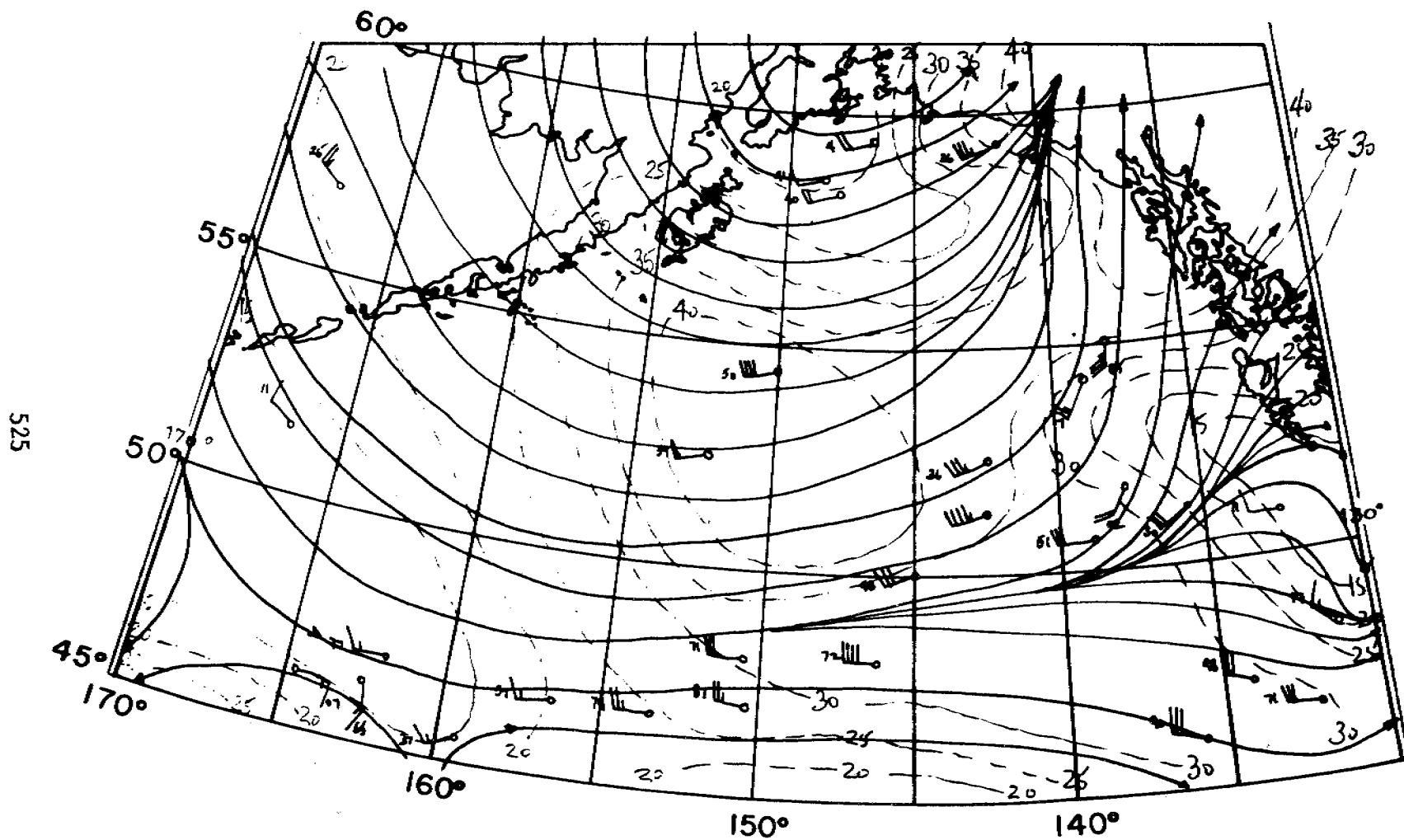


FIGURE 7d  
0000 GMT  
1/1/75

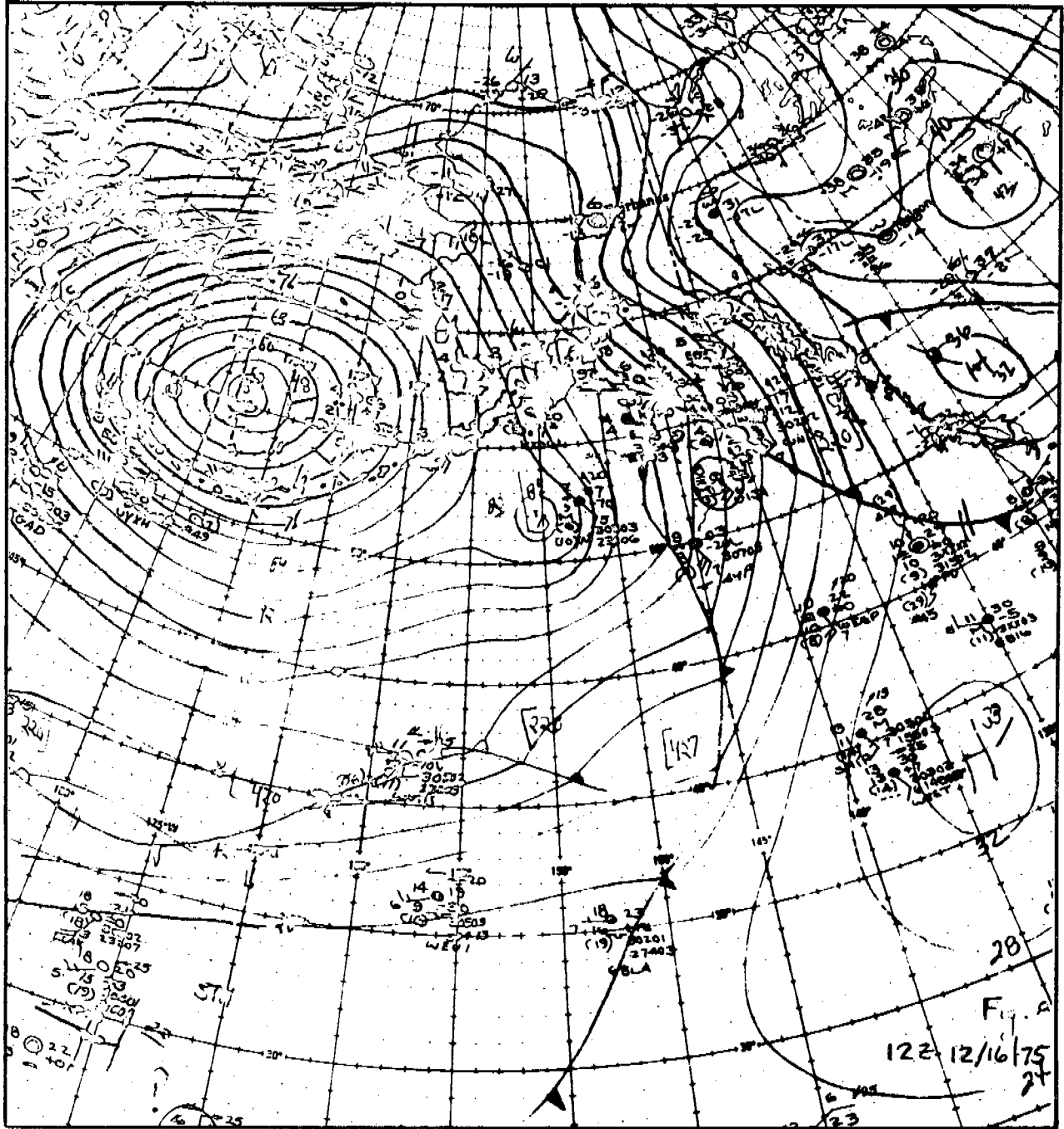


Fig. 8a

12GMT 12/16/75

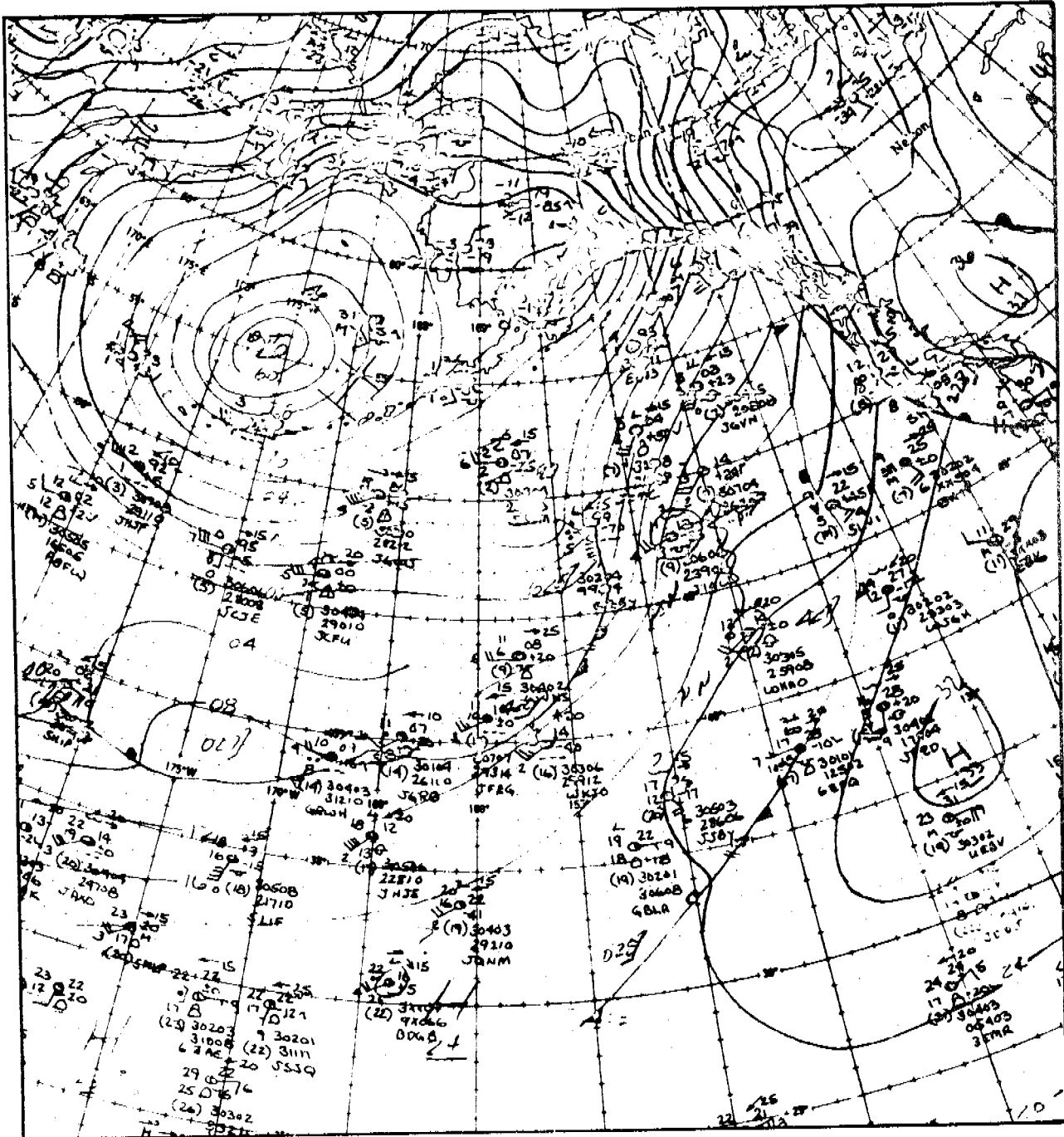


Fig.8b

00GMT 12/17/75

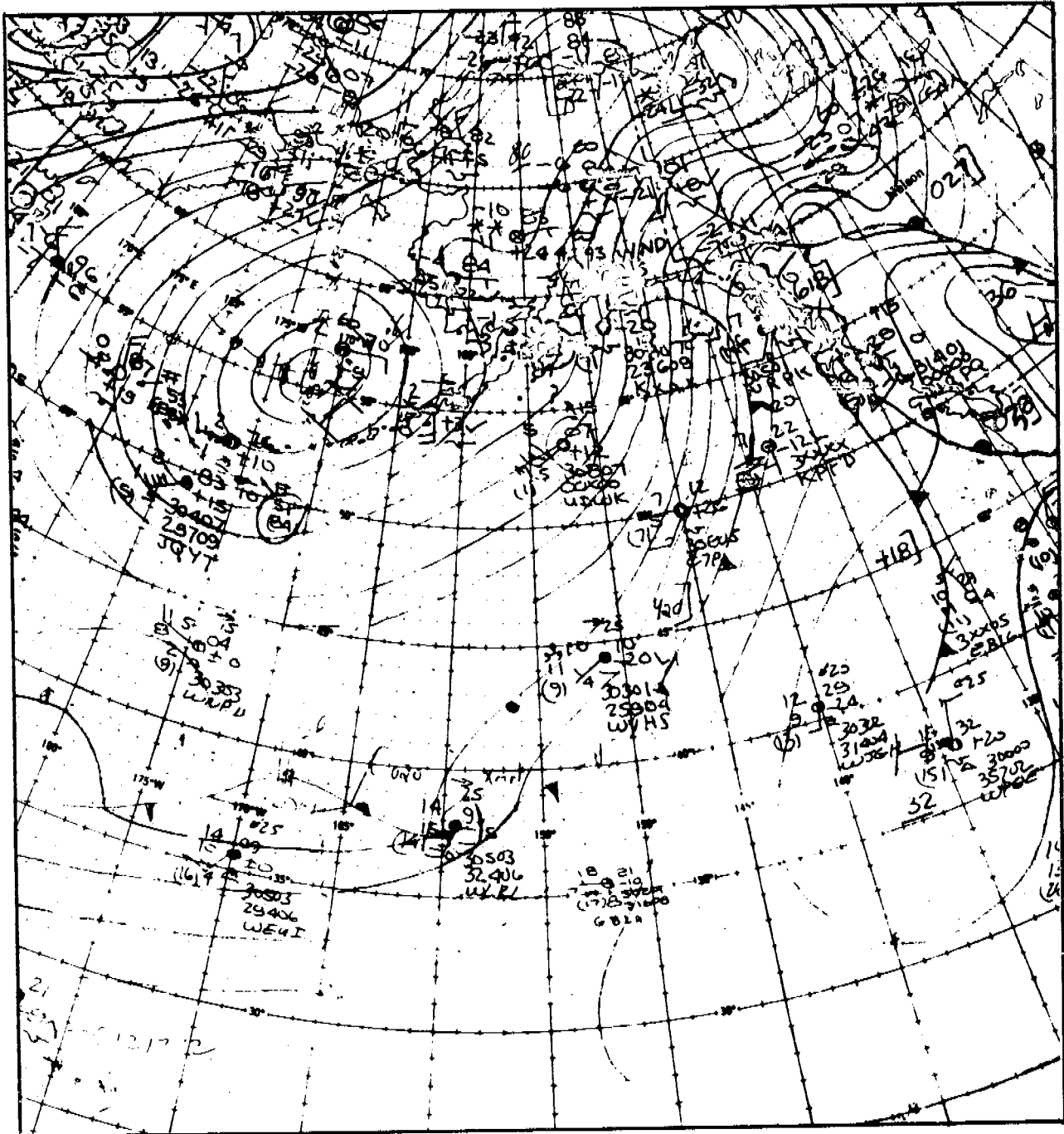


Fig.8c

12GMT 12/17/75



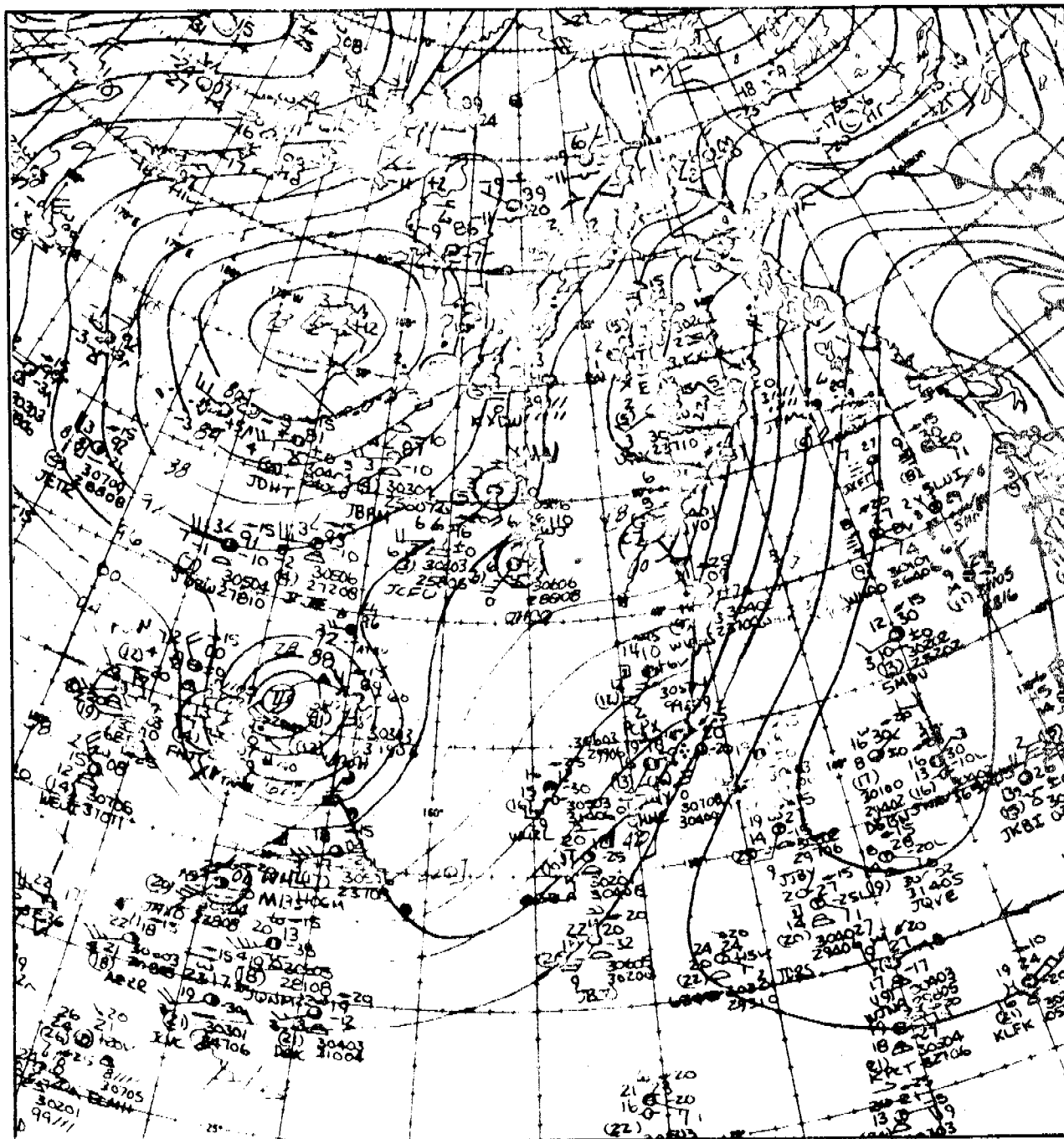


Fig.8d

00GMT 12/18/75

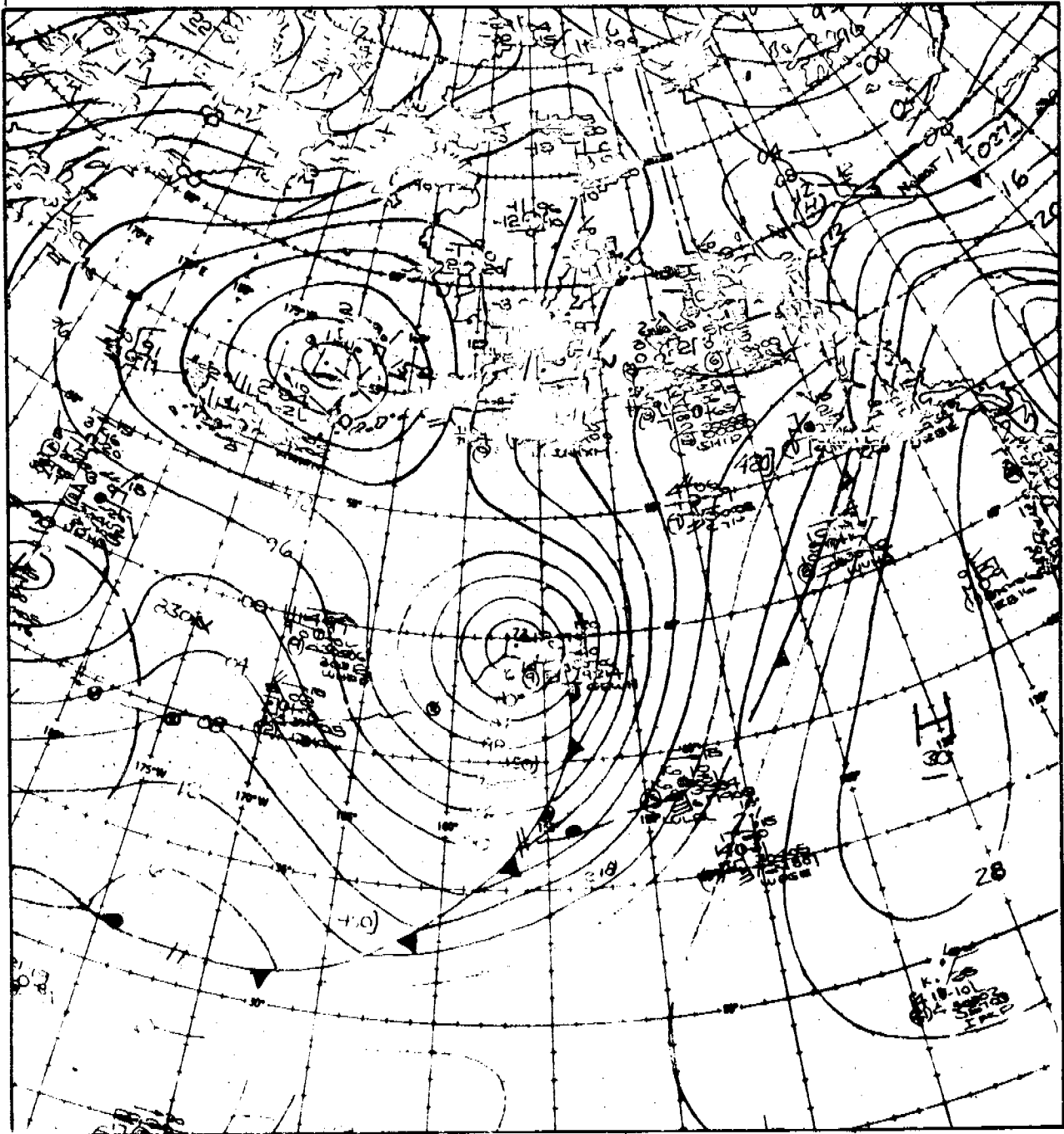


Fig.8e

12GMT 12/18/75

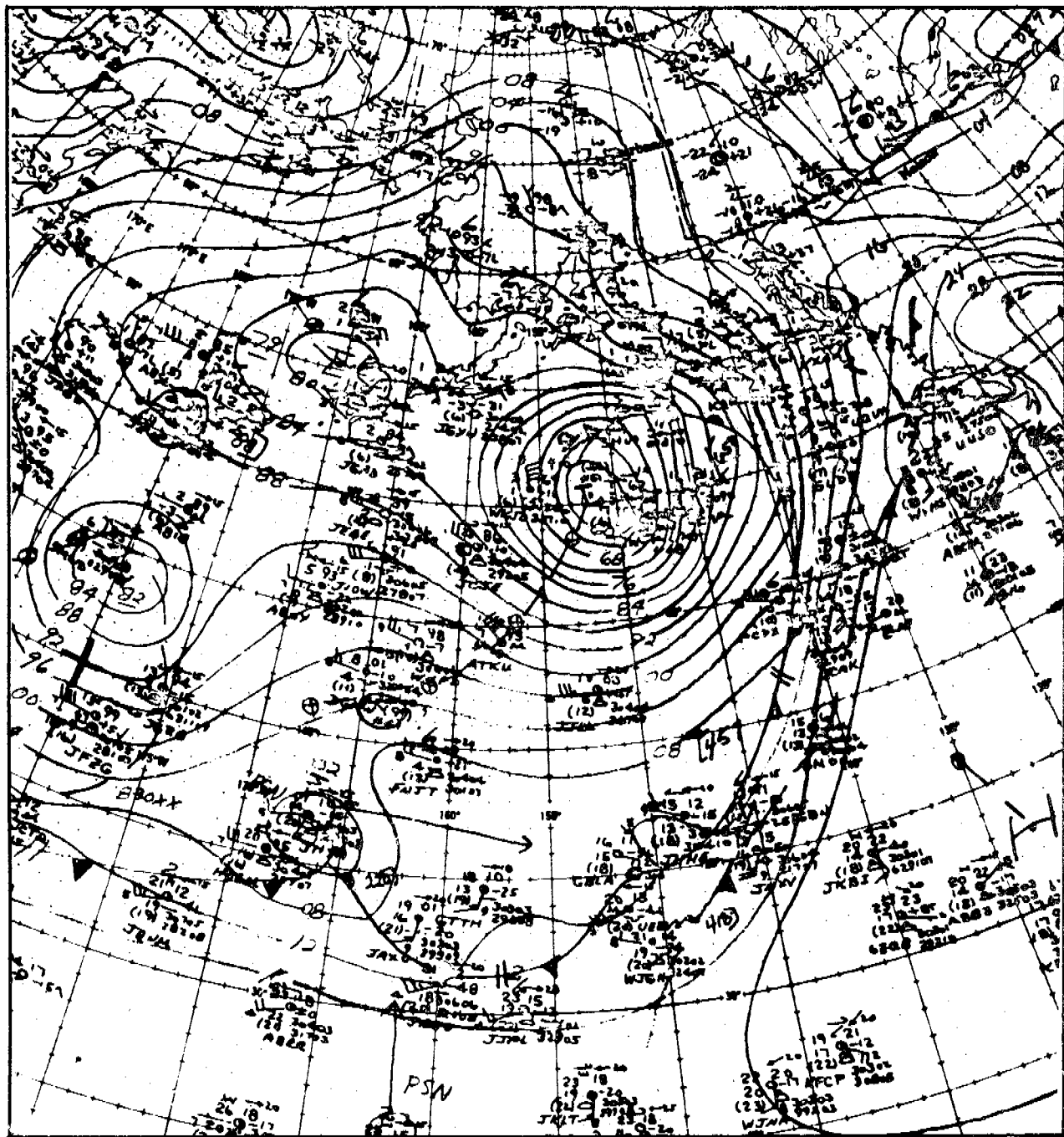


Fig.8f

00GMT 12/19/75

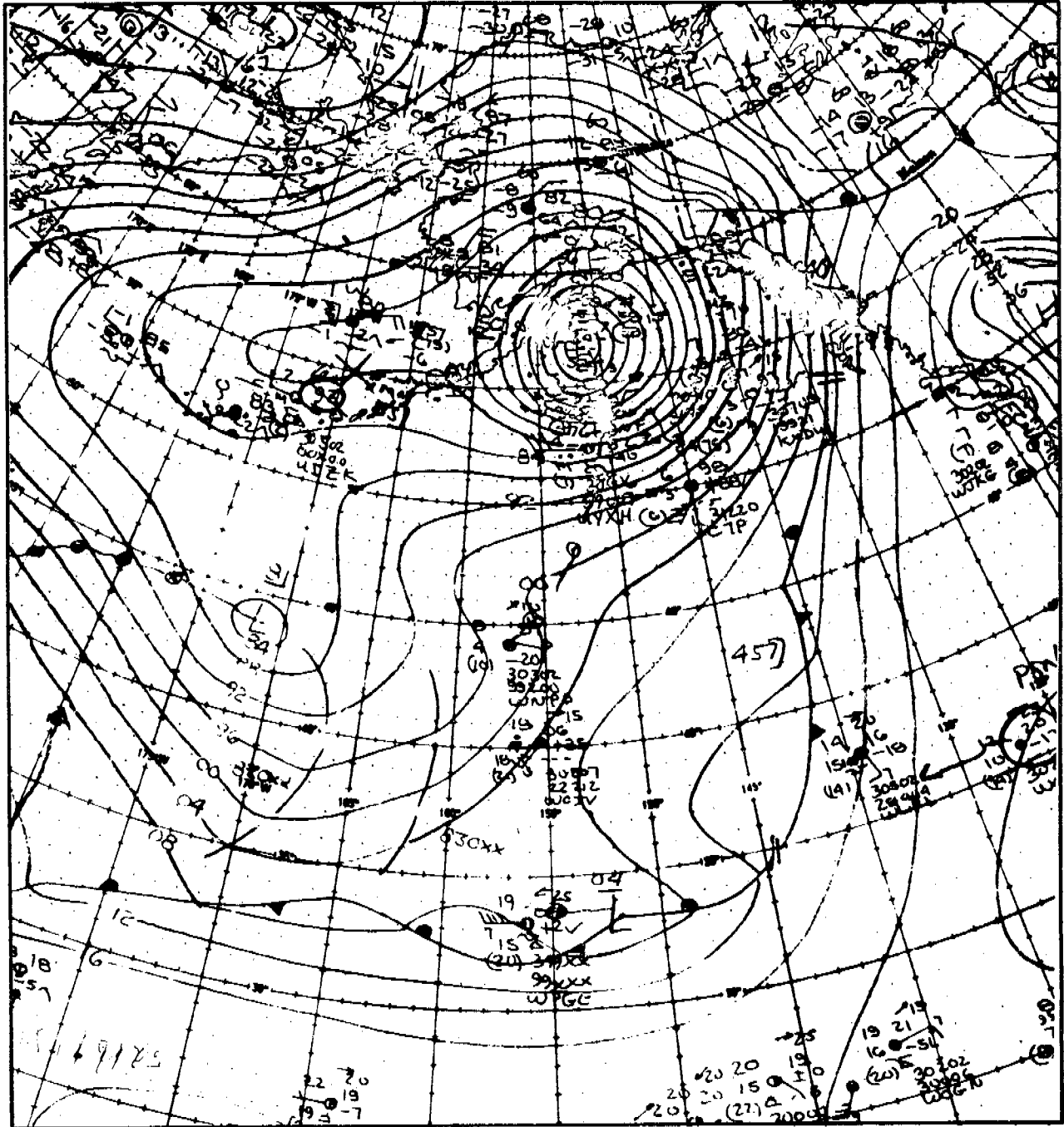


Fig.8g

12GMT 12/19/75

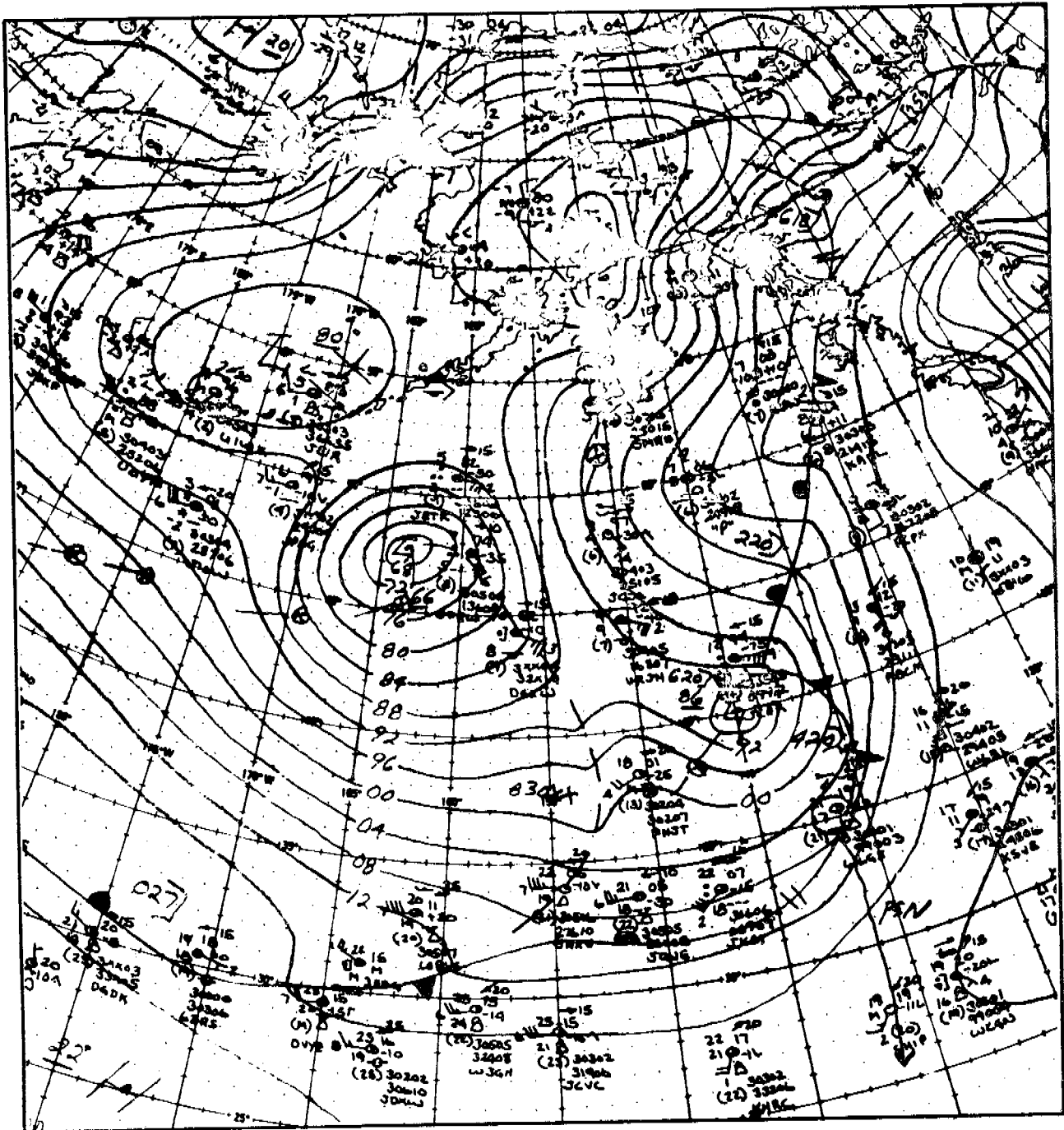


Fig.8h

00GMT 12/20/75

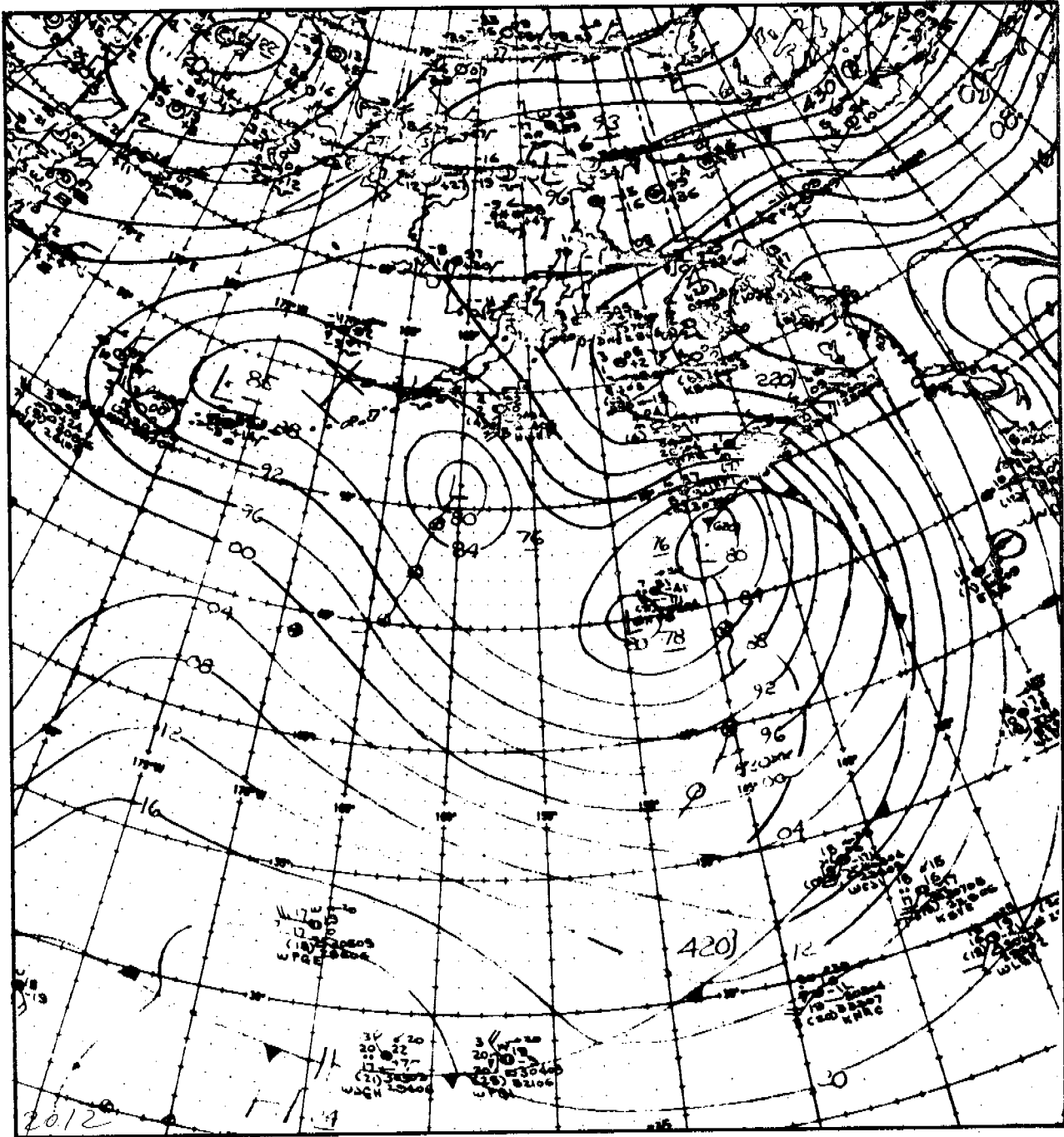


Fig.8i

12GMT 12/20/75

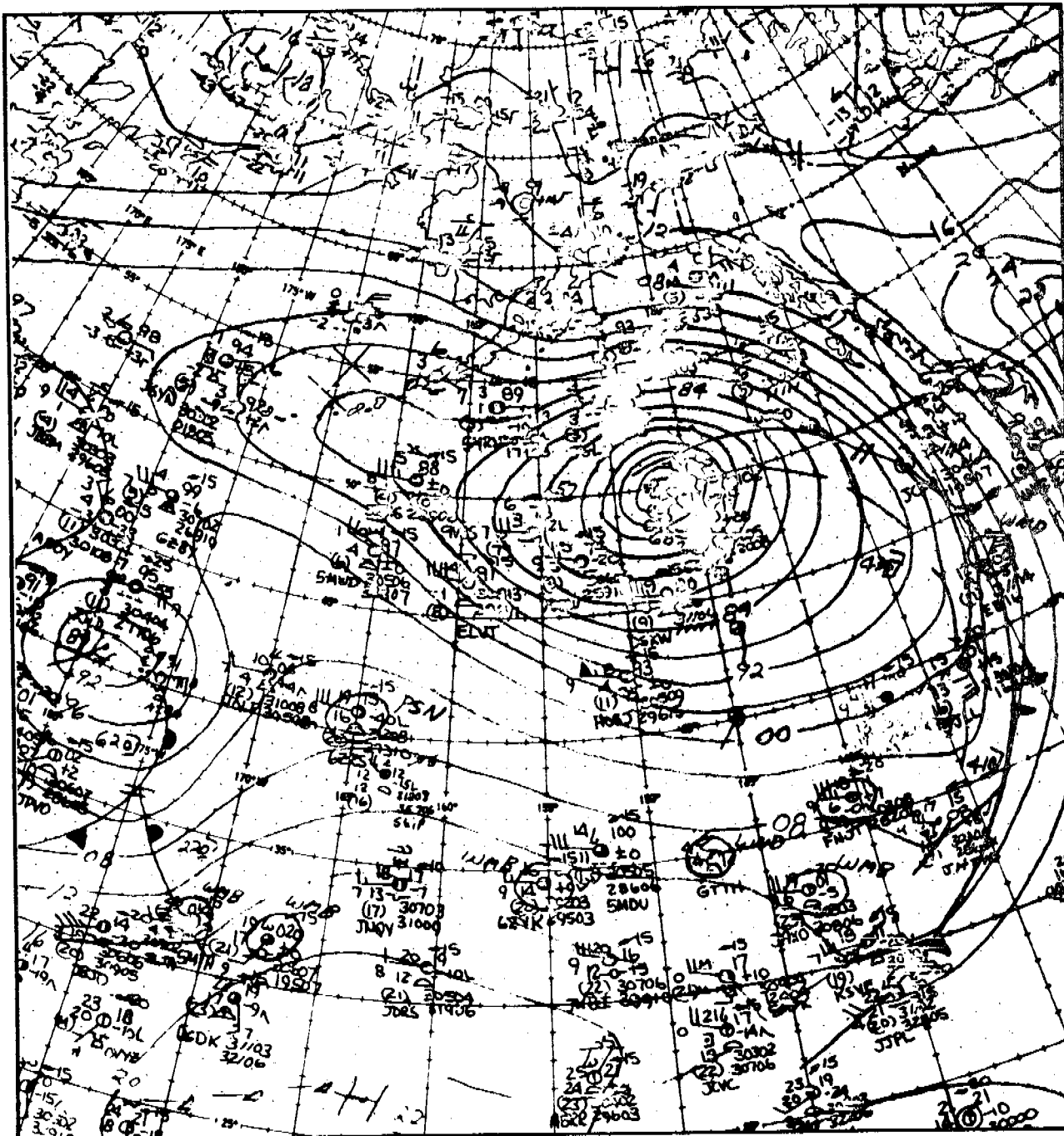


Fig.8j

00GMT 12/21/75

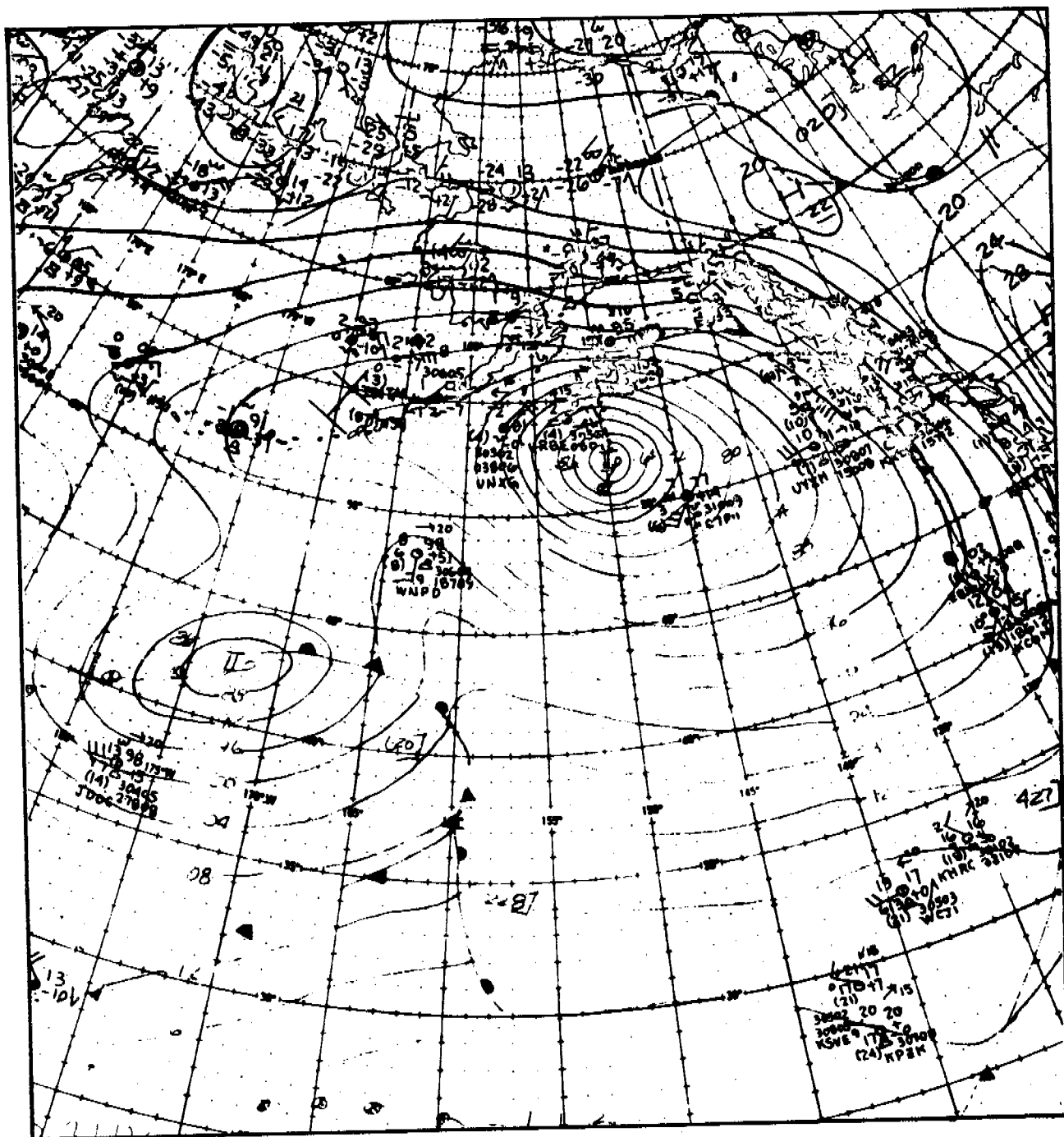


Fig. 8k

12GMT 12/21/75



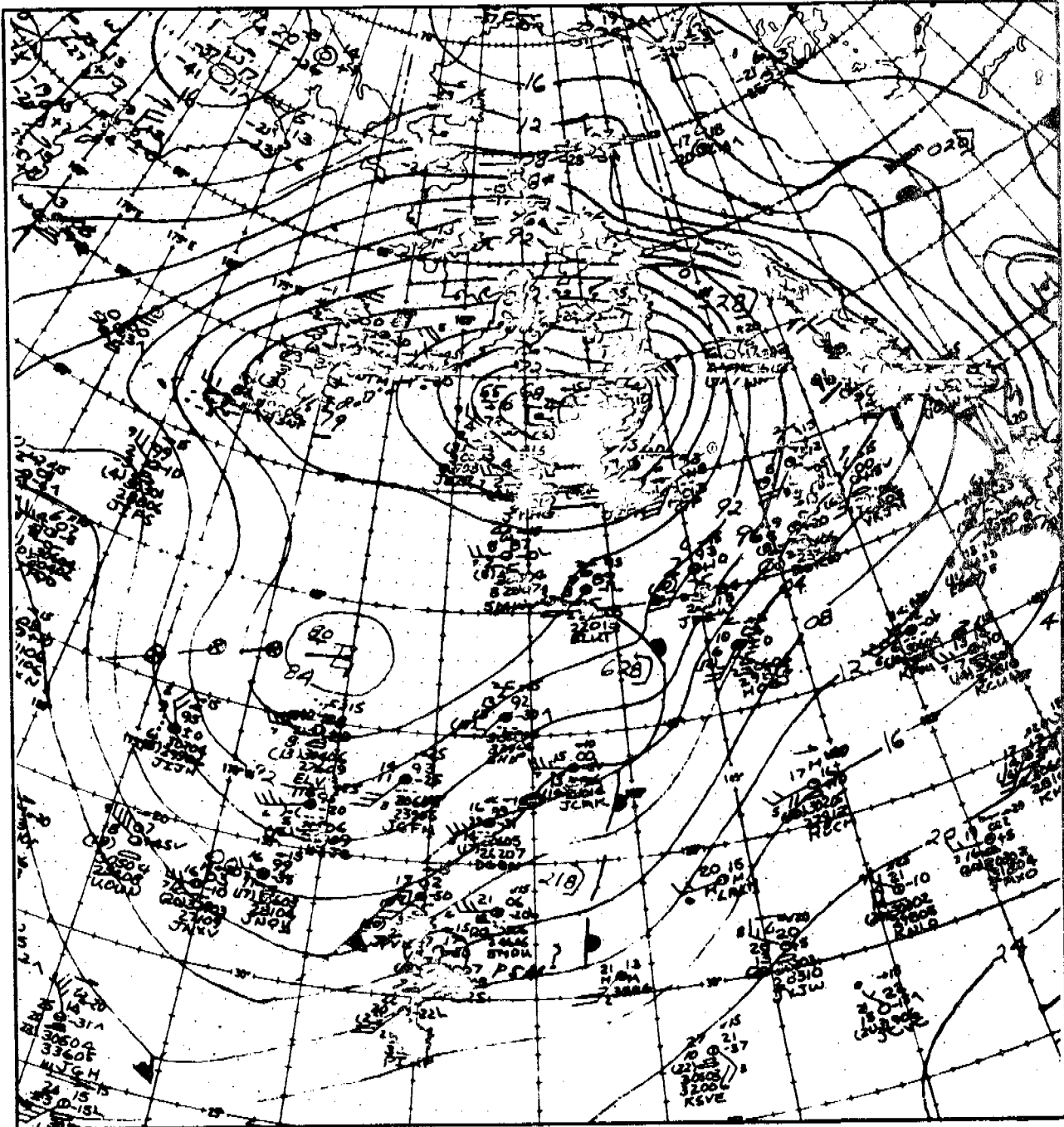


Fig. 81

00GMT 12/22/75

## STORM 3 DEC, 1975

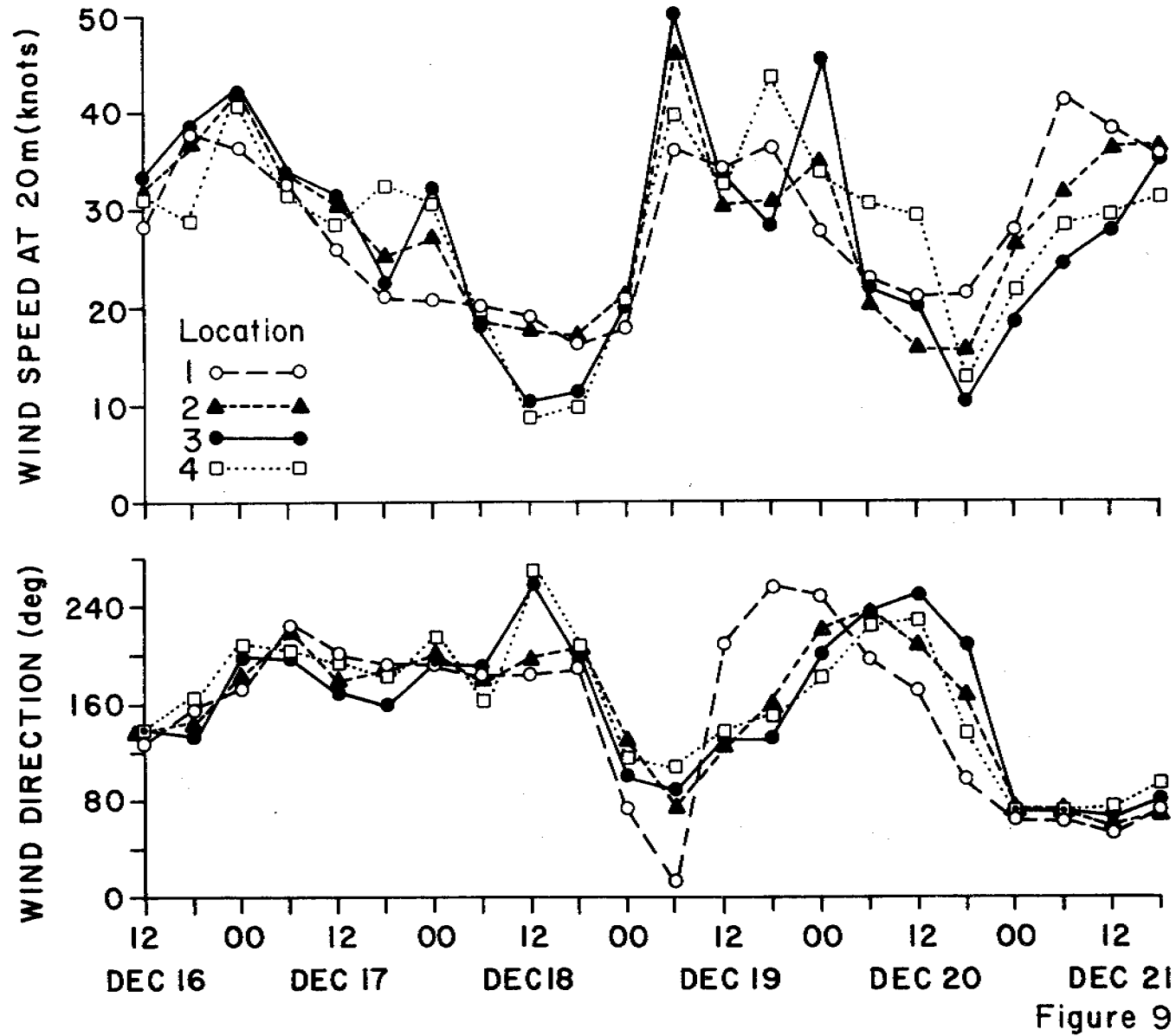


Figure 9

539

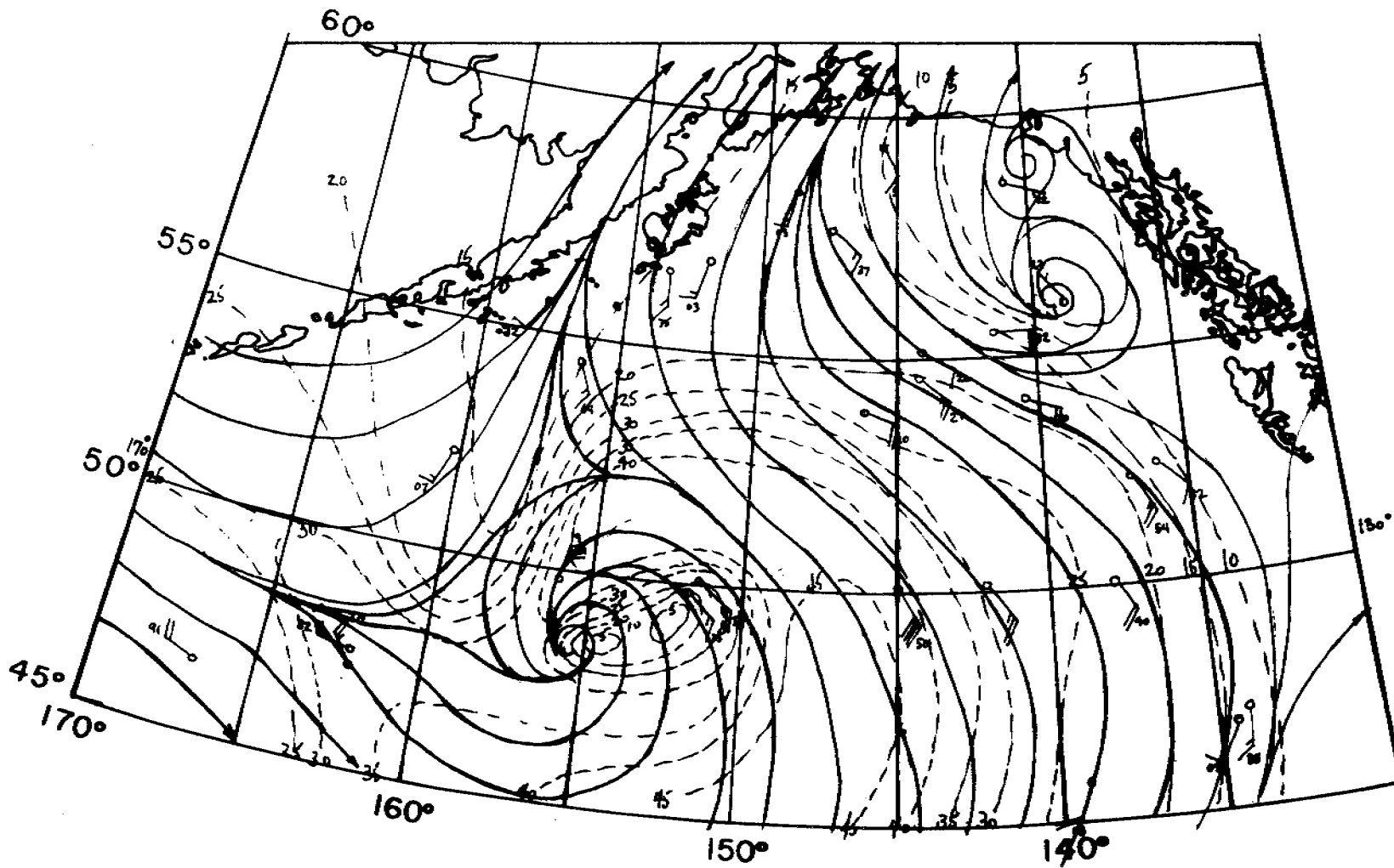


FIGURE 10a  
1800 GMT  
12/18/75

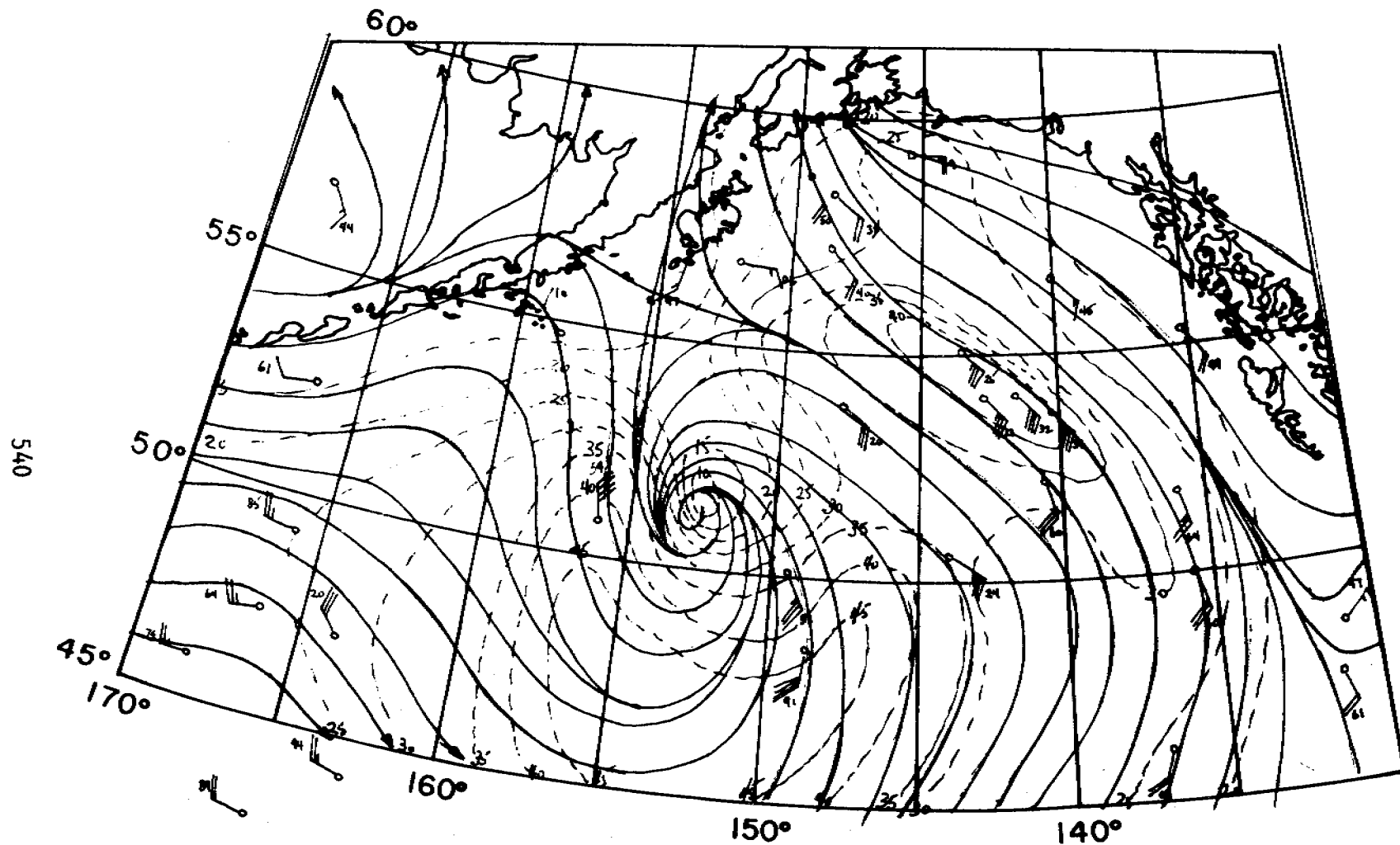
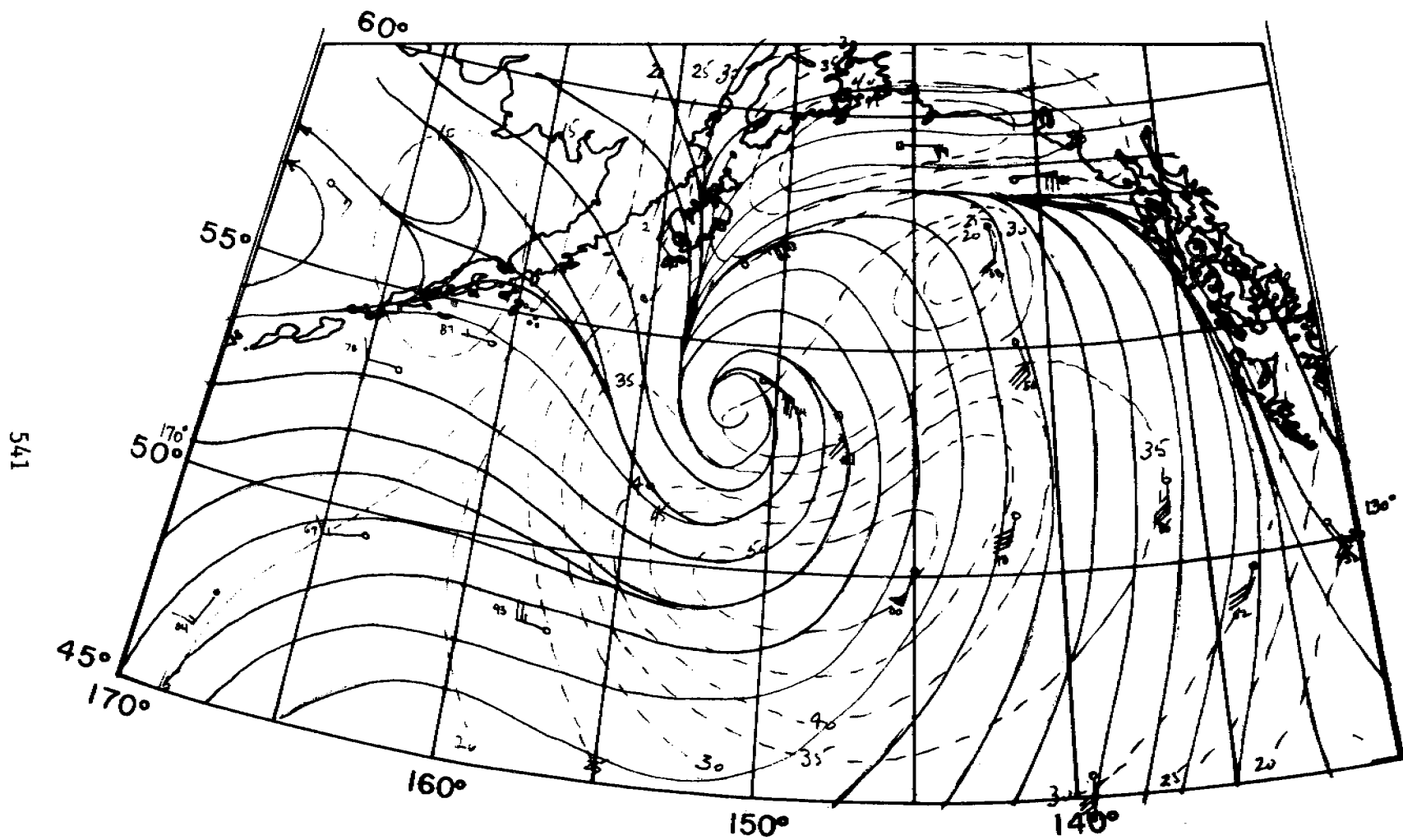
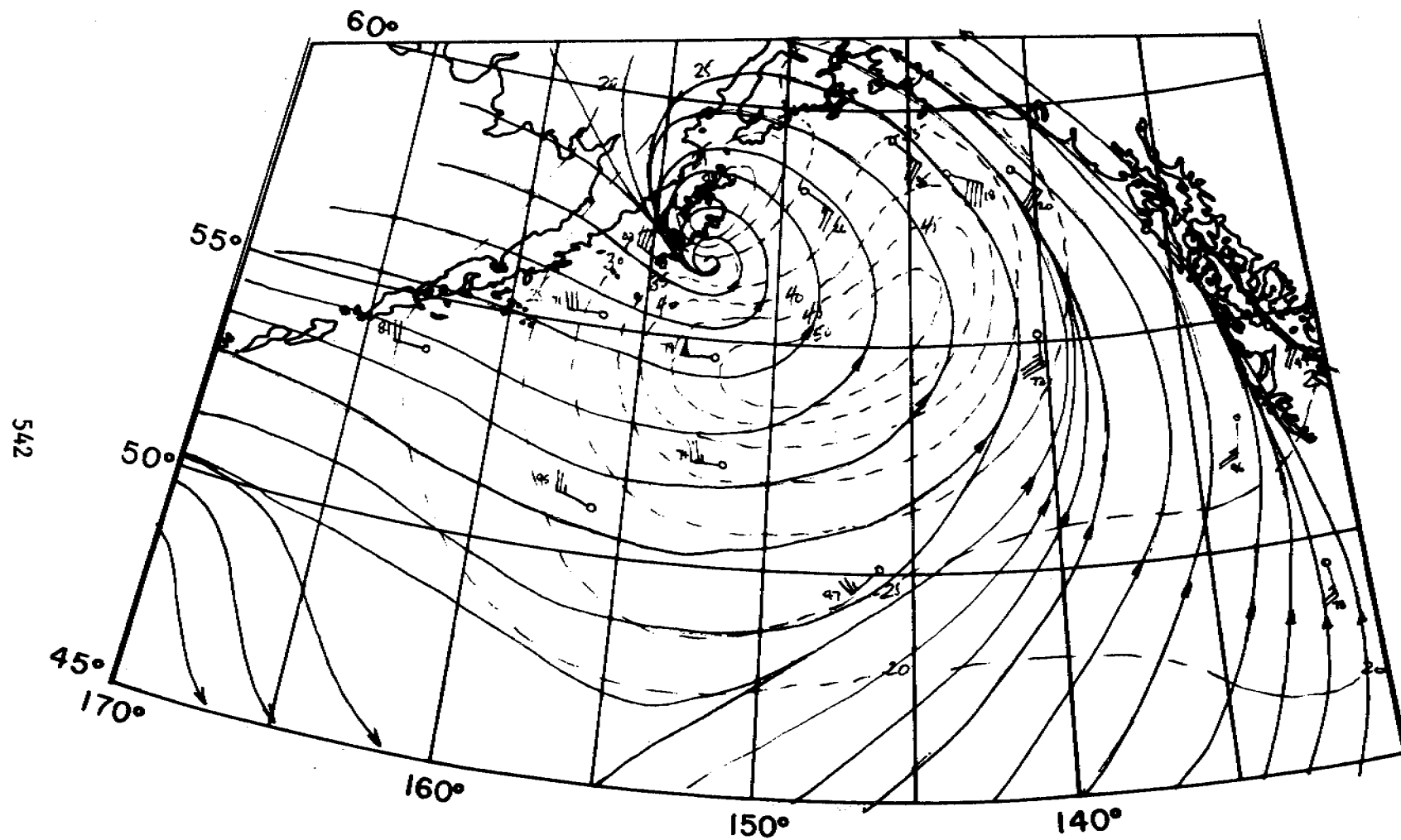


FIGURE 10b  
0000 GMT  
12/19/75



541

FIGURE 10c  
0600 GMT  
12/19/75



542

FIGURE 10d  
1200 GMT  
12/19/75

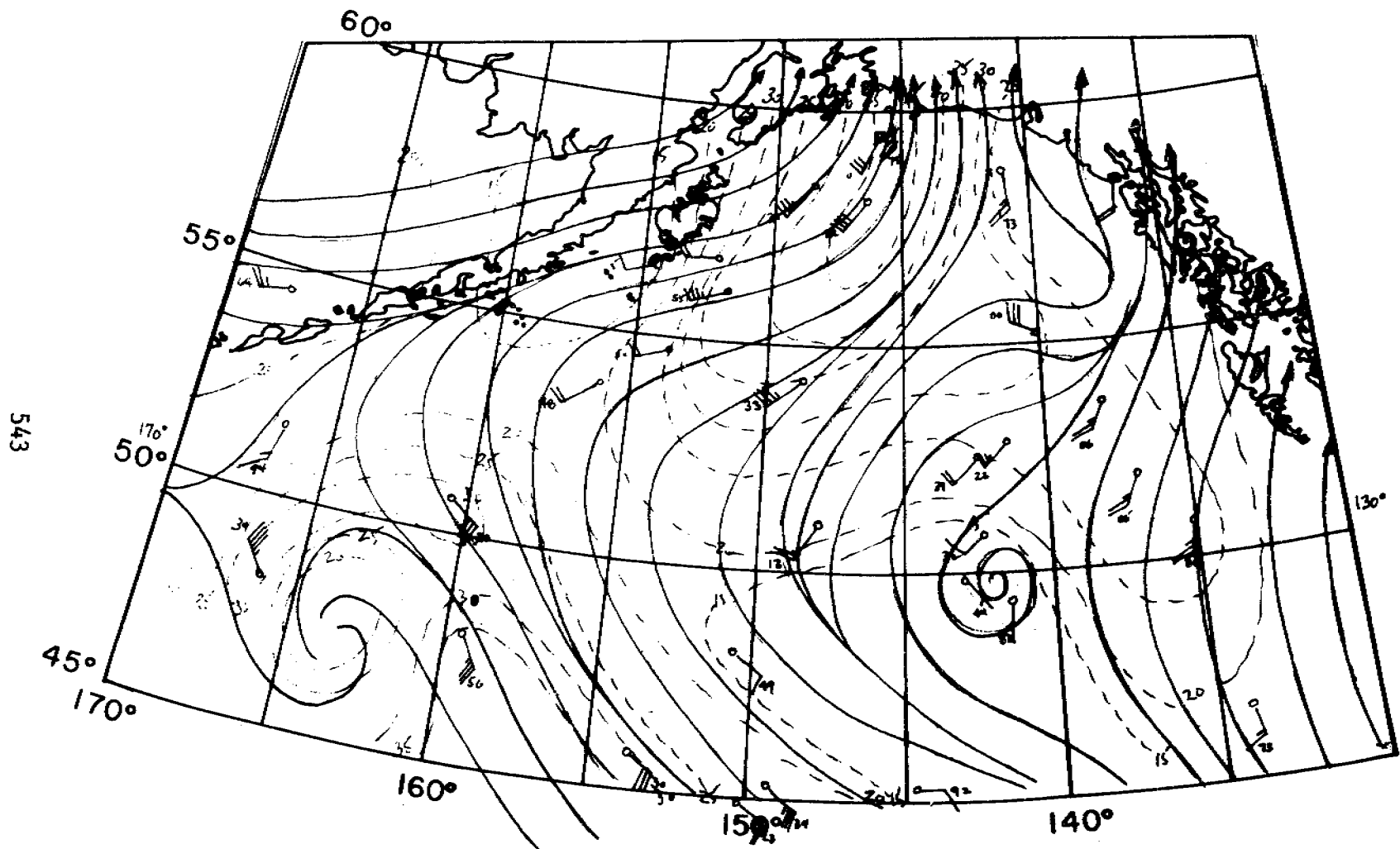


FIGURE 10e  
0000 GMT  
12/20/75

544

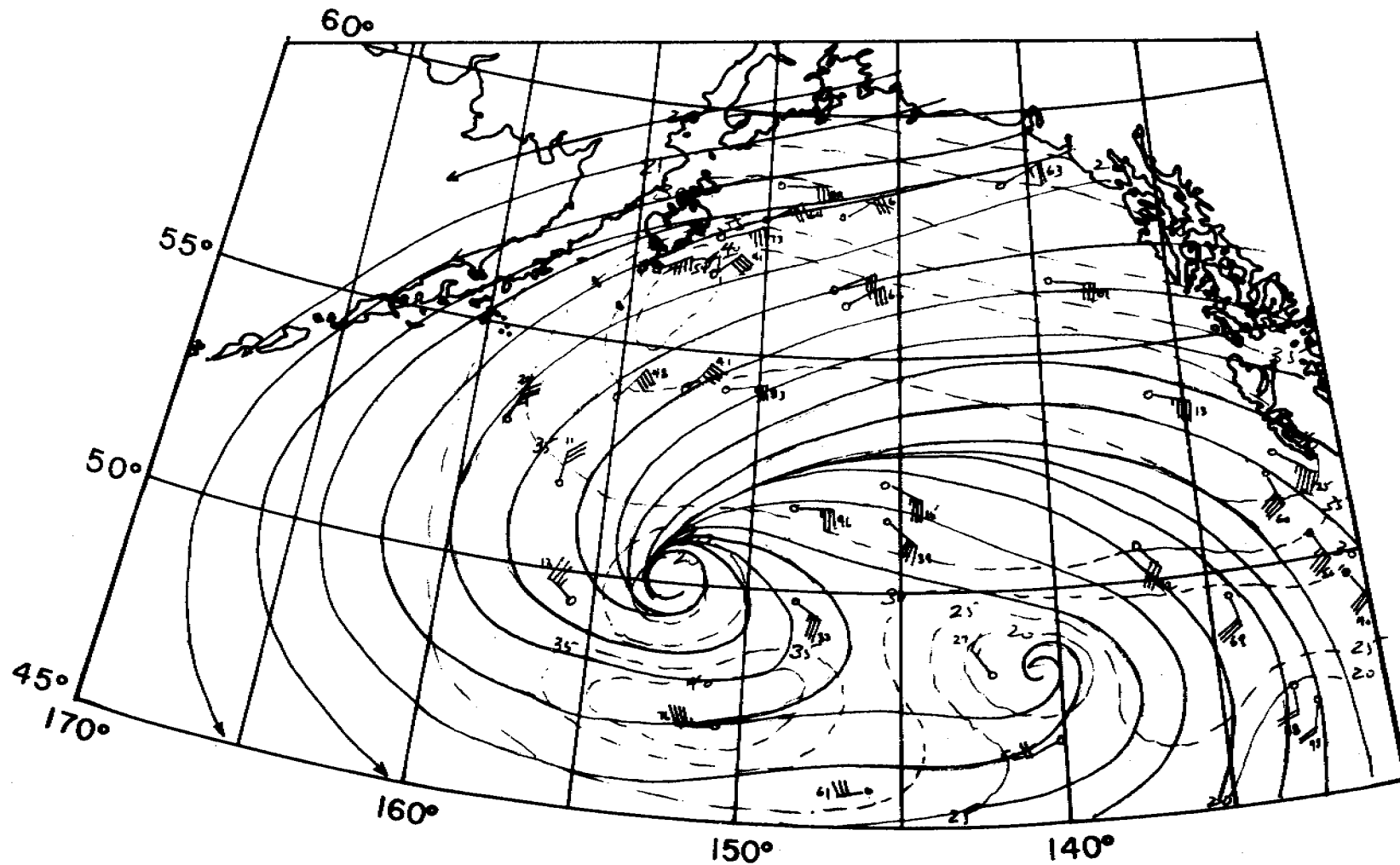


FIGURE 10f  
0600 GMT  
12/21/75



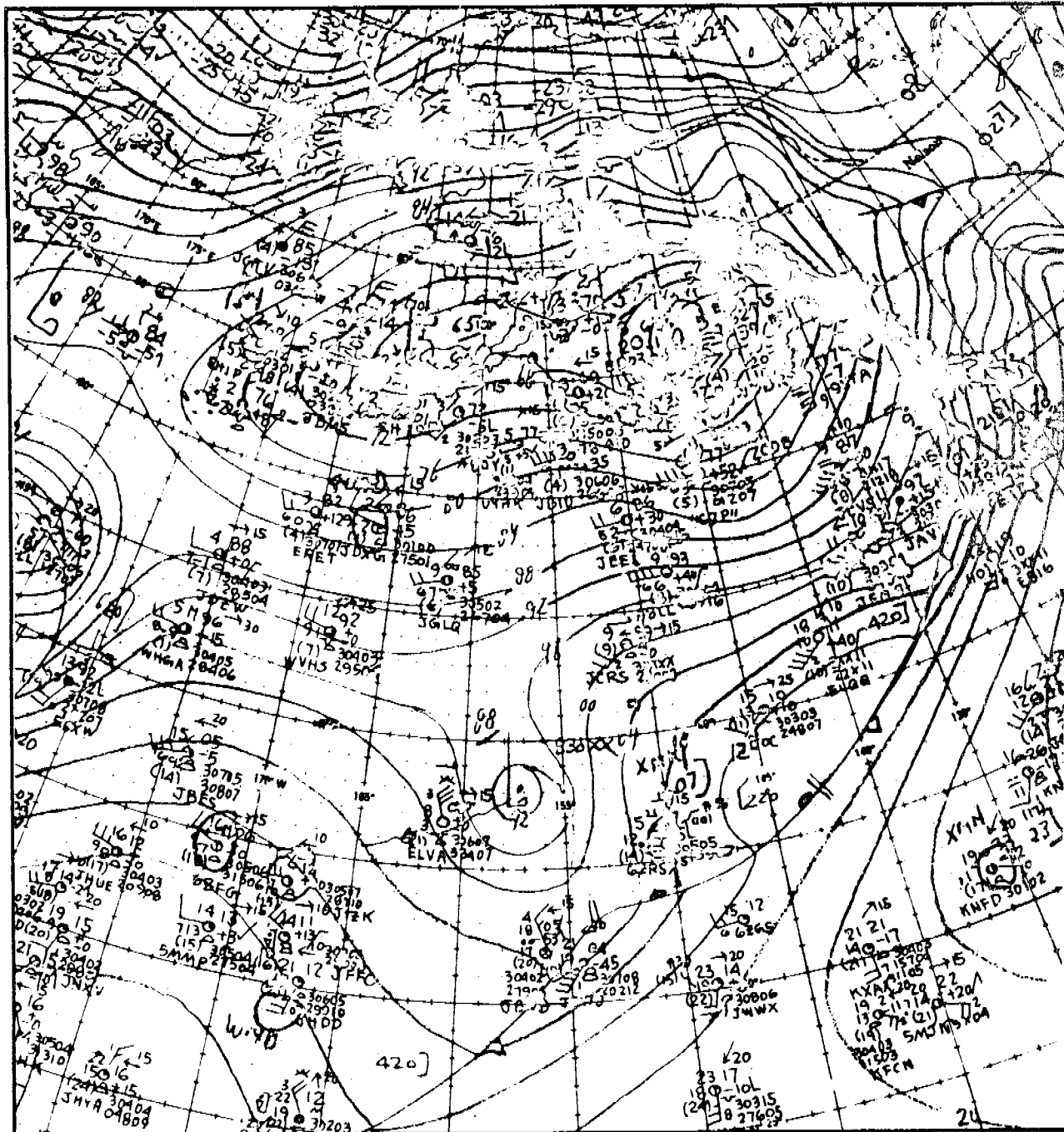


Fig. 11a

00GMT 1/27/76

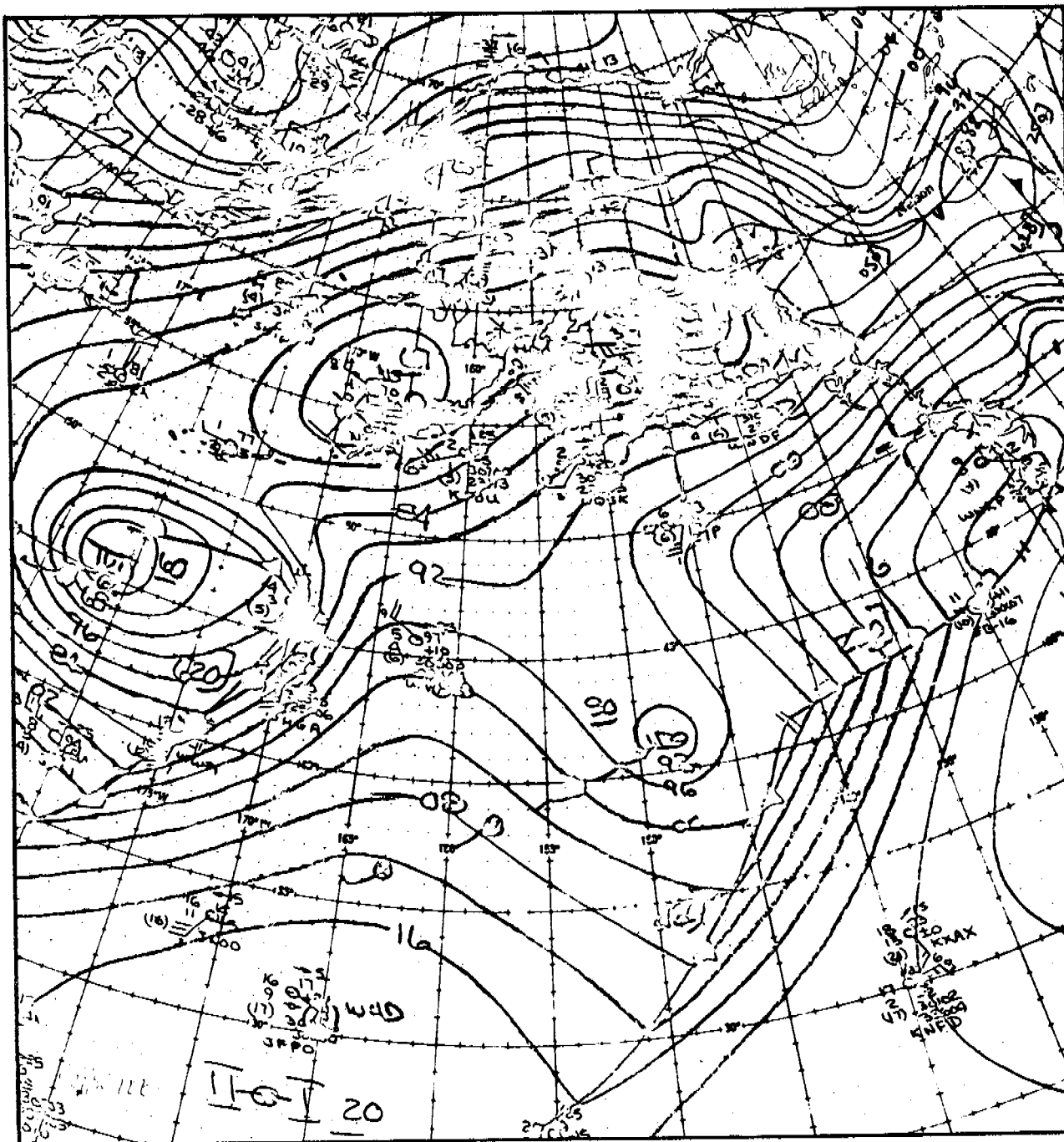


Fig.11b

12GMT 1/27/76

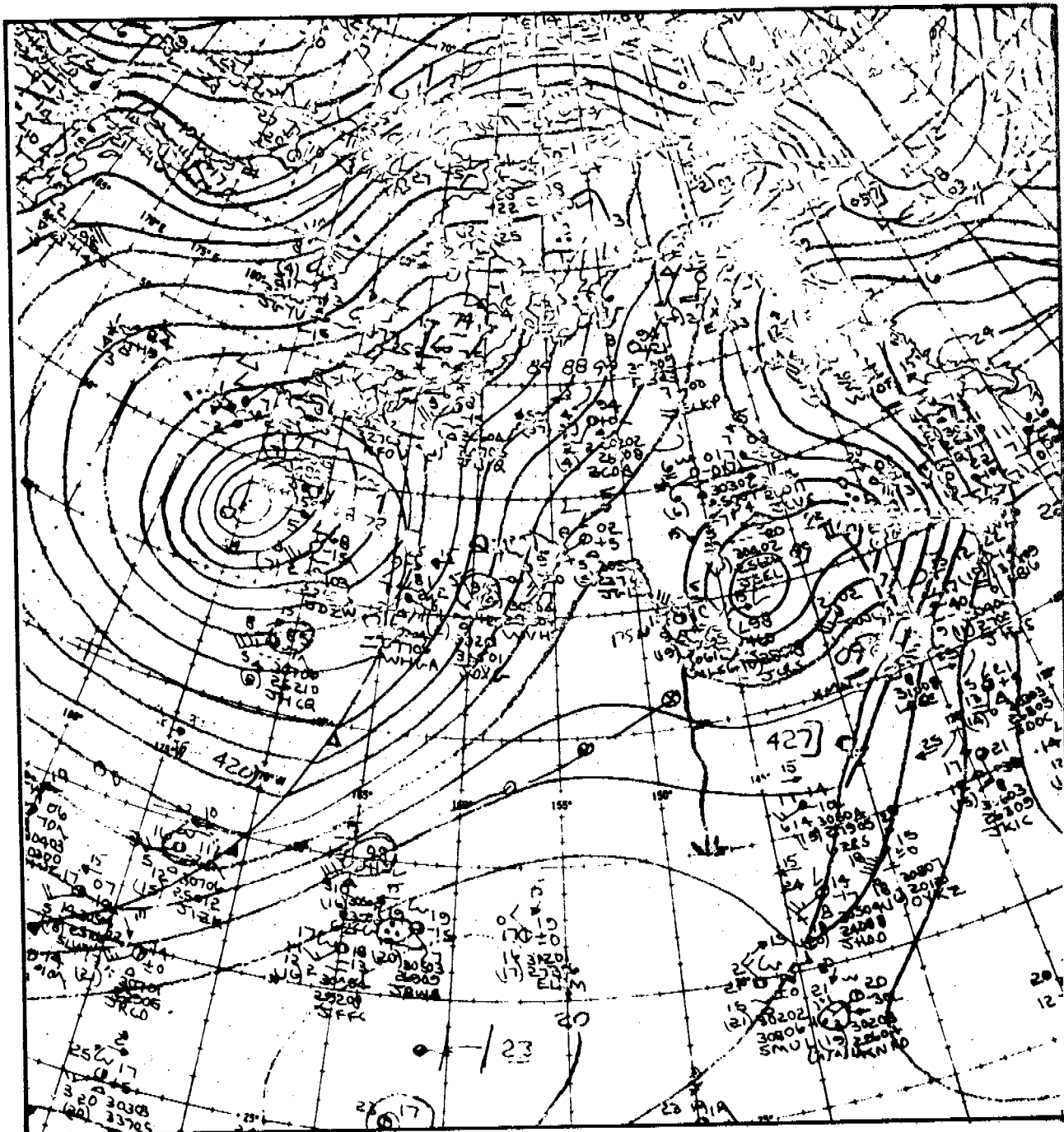


Fig. 11c

00GMT 1/28/76

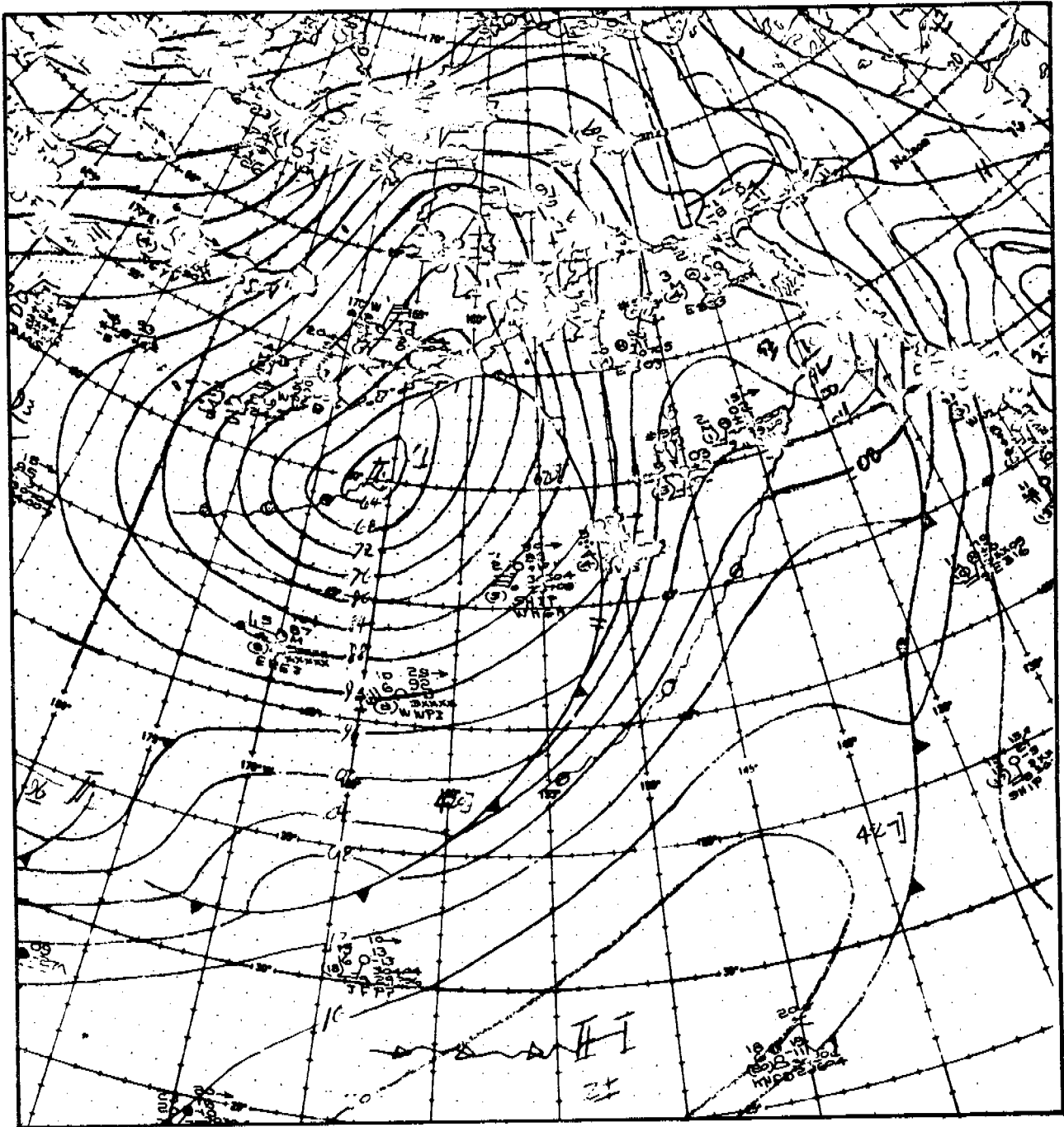


Fig. 11d

12GMT 1/28/76

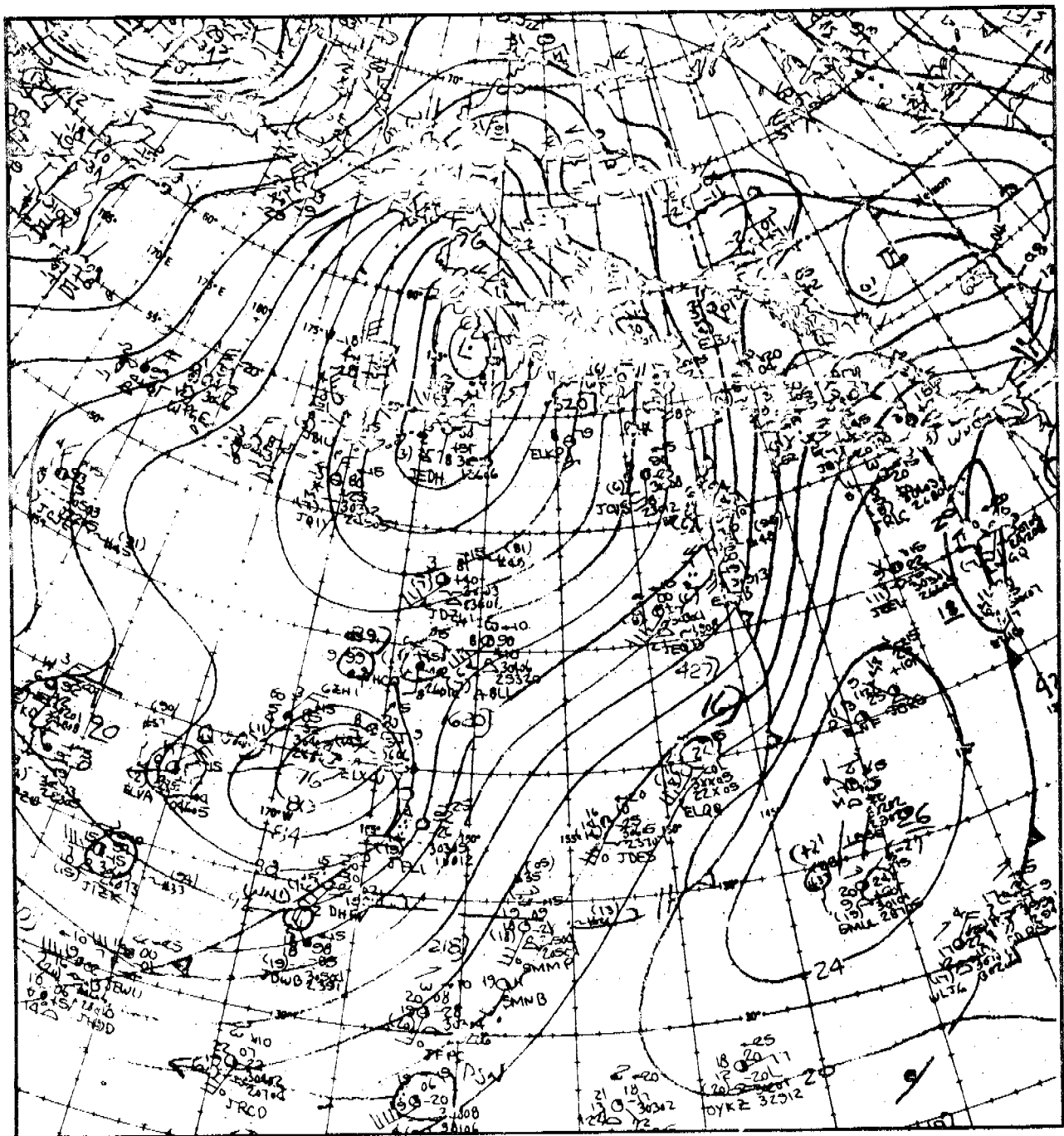


Fig.11e

00GMT 1/29/76

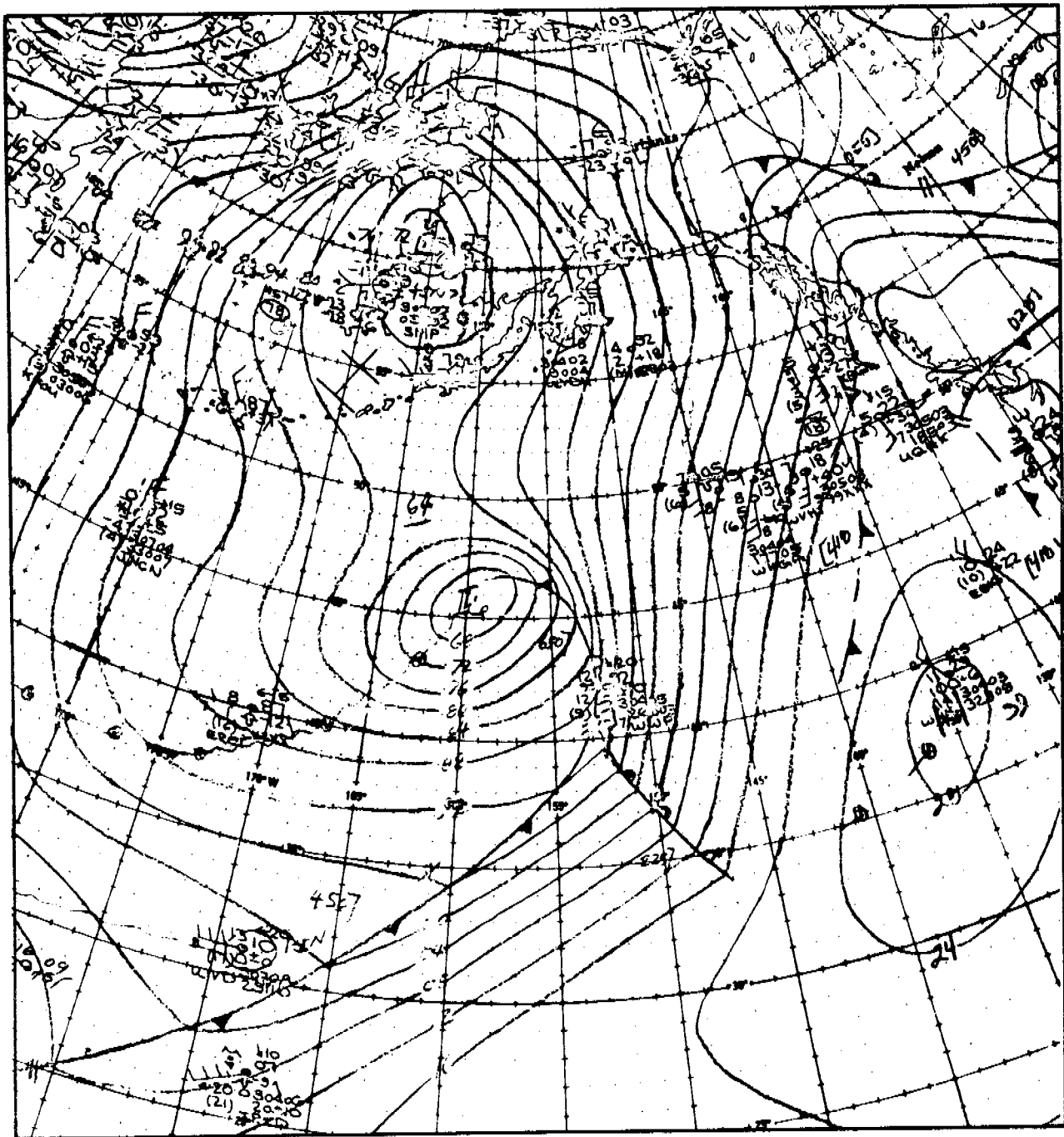


Fig.11f

12GMT 1/29/76



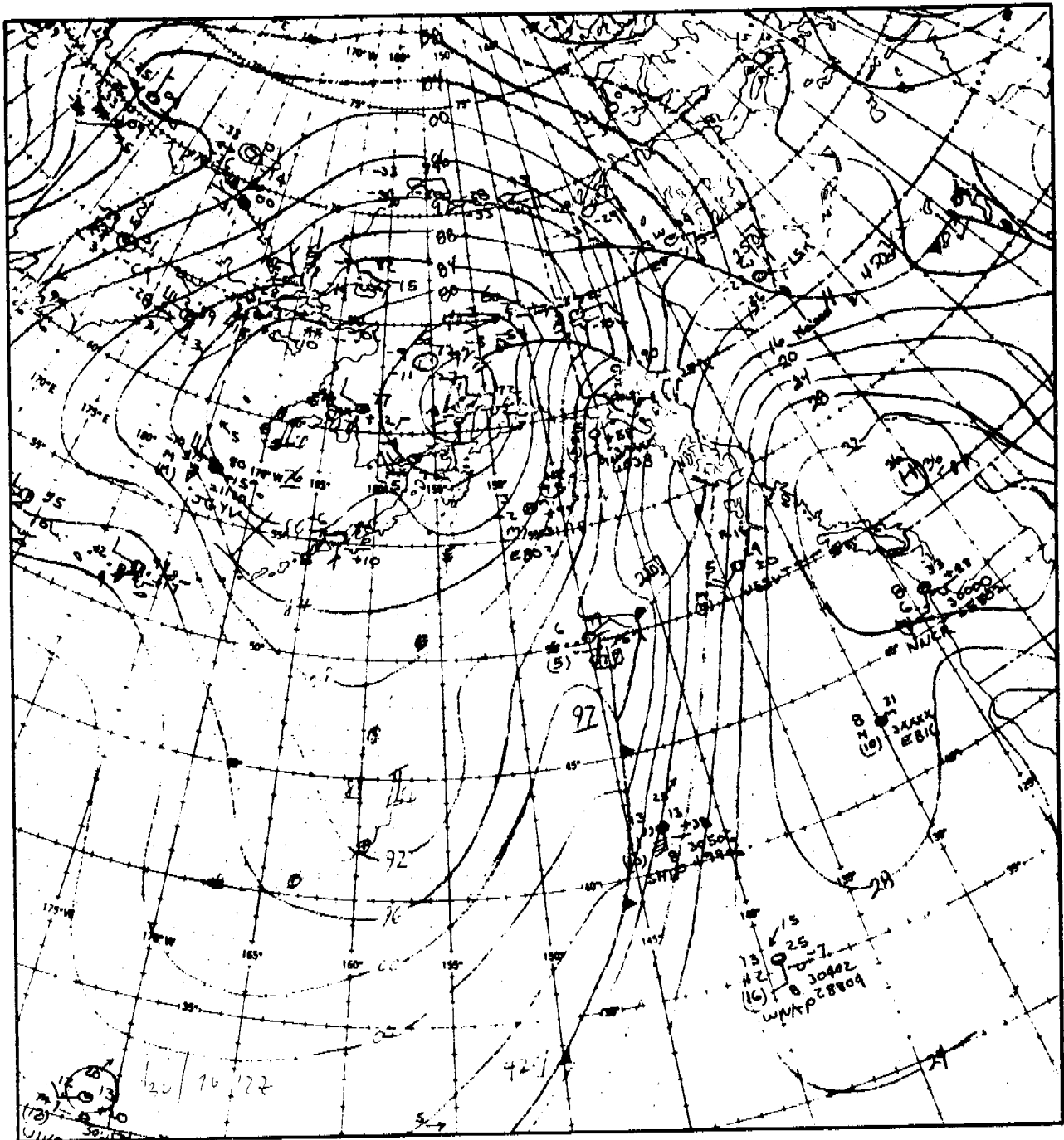


Fig. 11h

12GMT 1/30/76



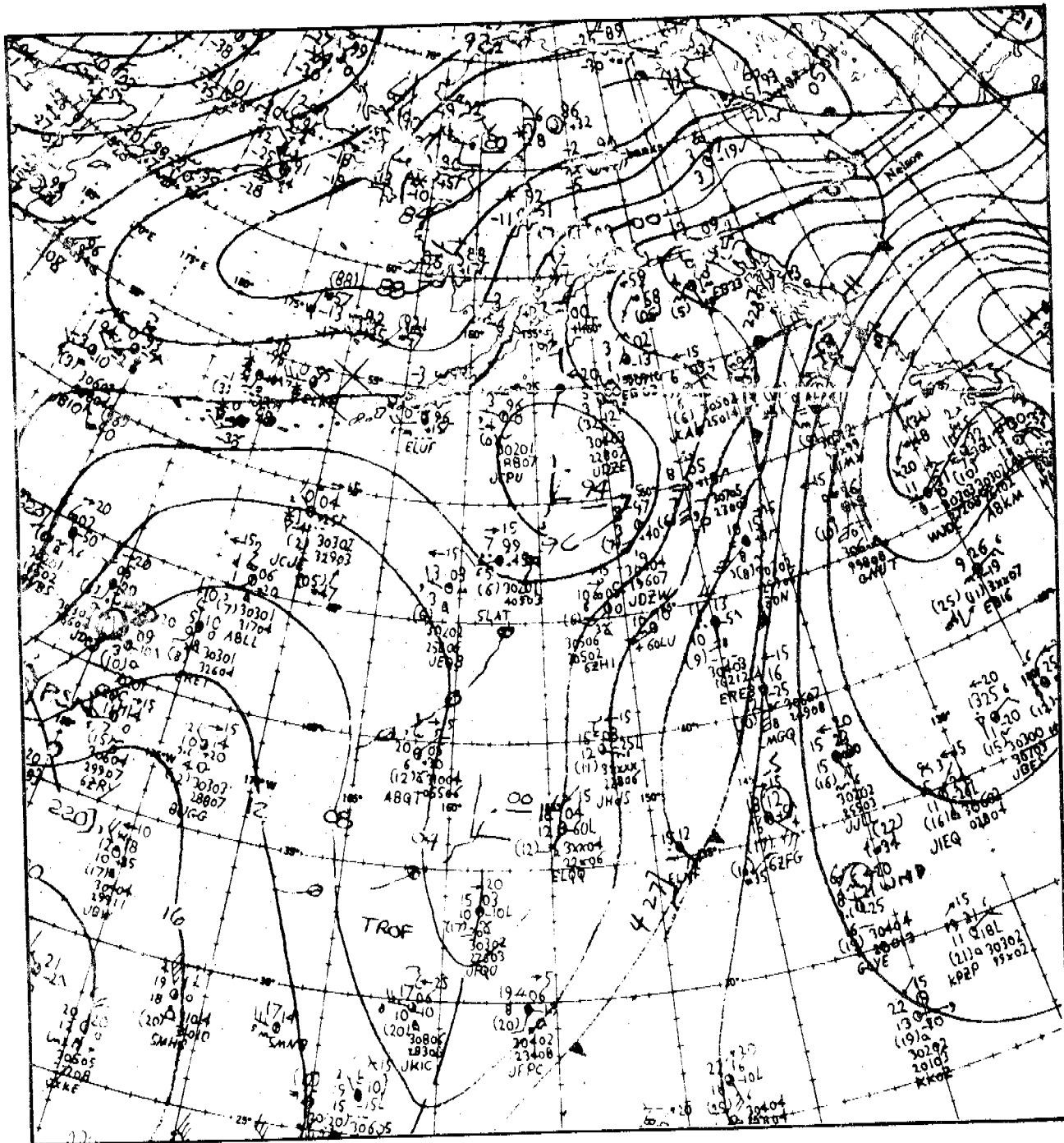


Fig. 11i

00GMT 1/31/76

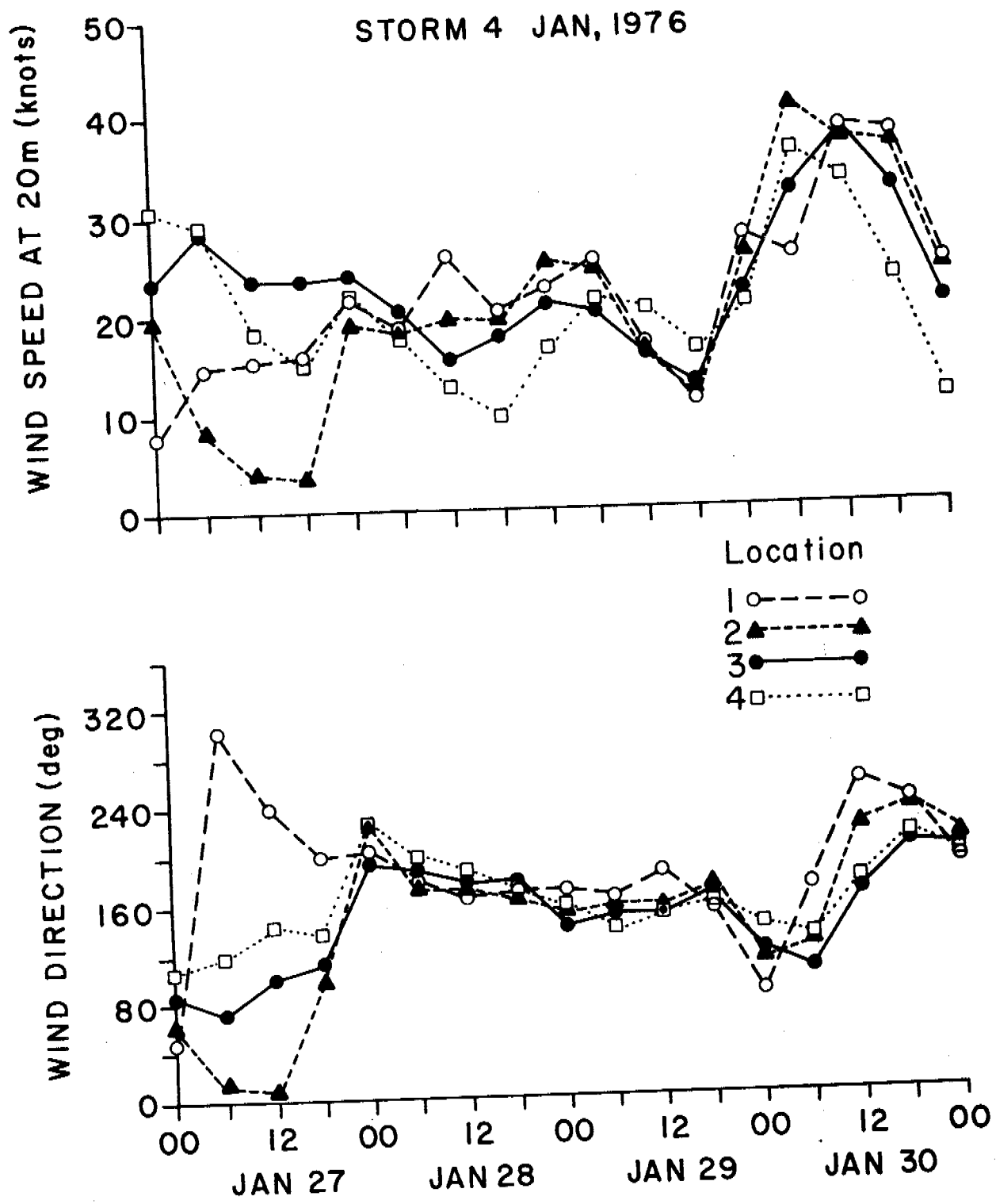


Figure 12

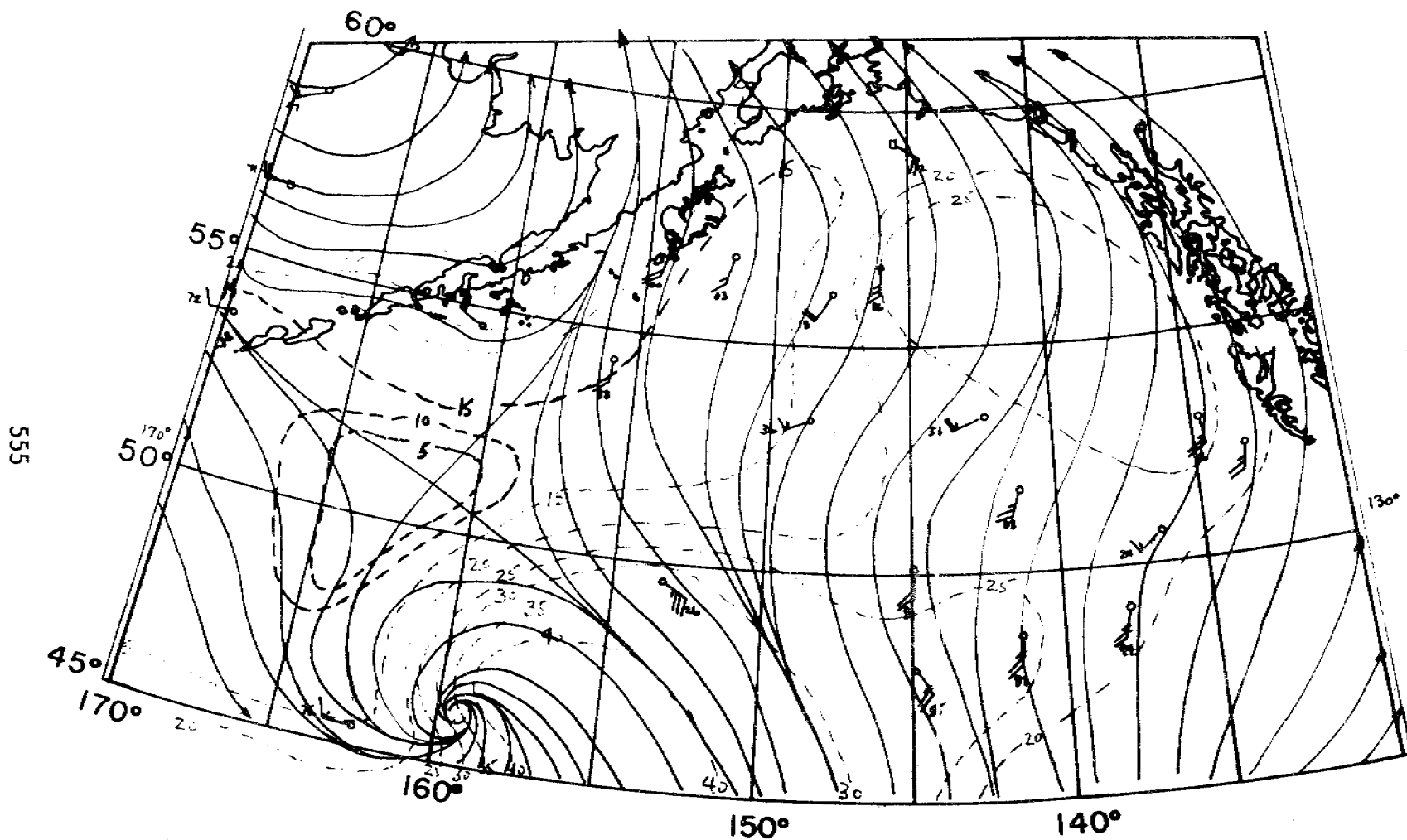


FIGURE 13a  
1200 GMT  
1/29/76

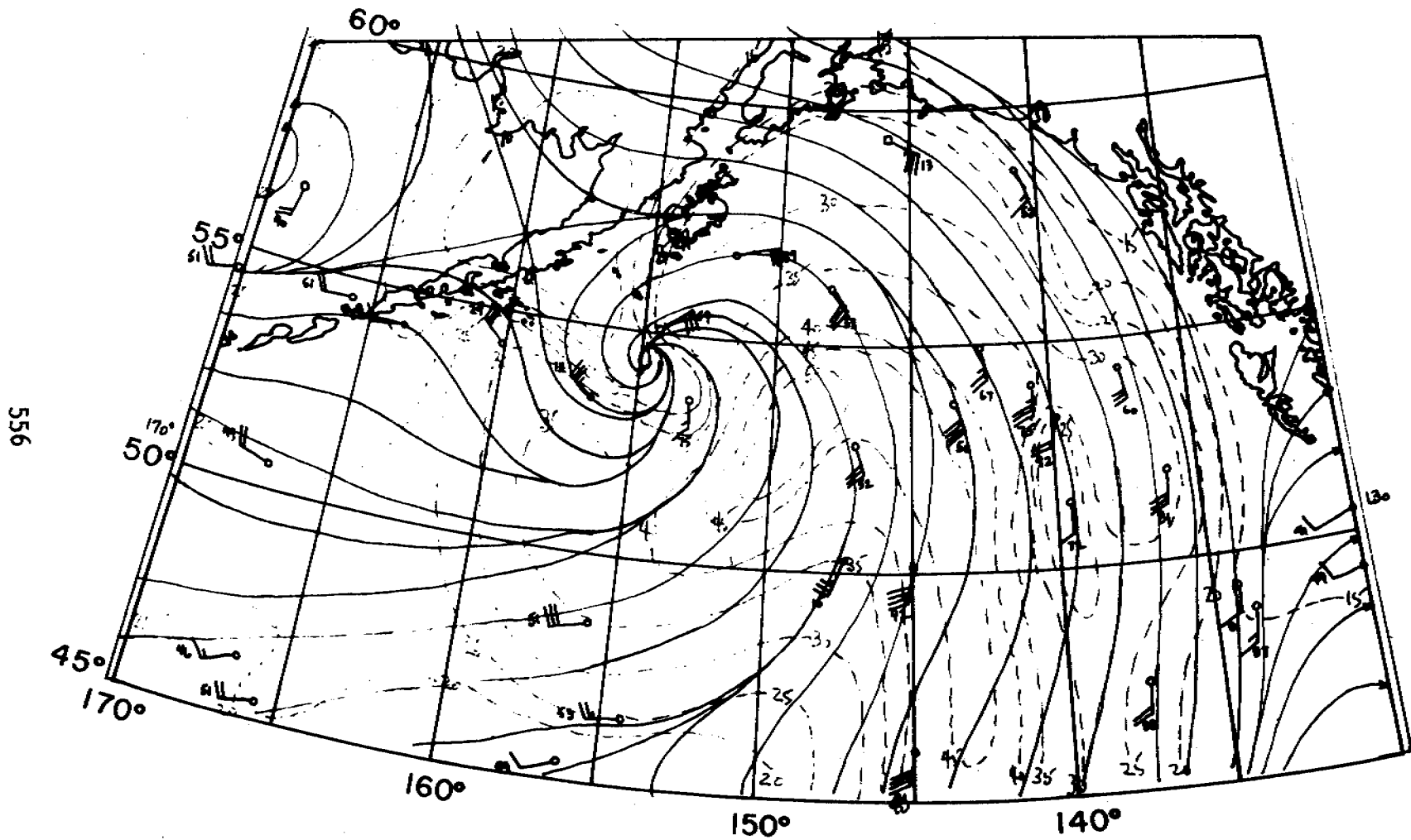


FIGURE 13b  
0000 GMT  
1/30/76

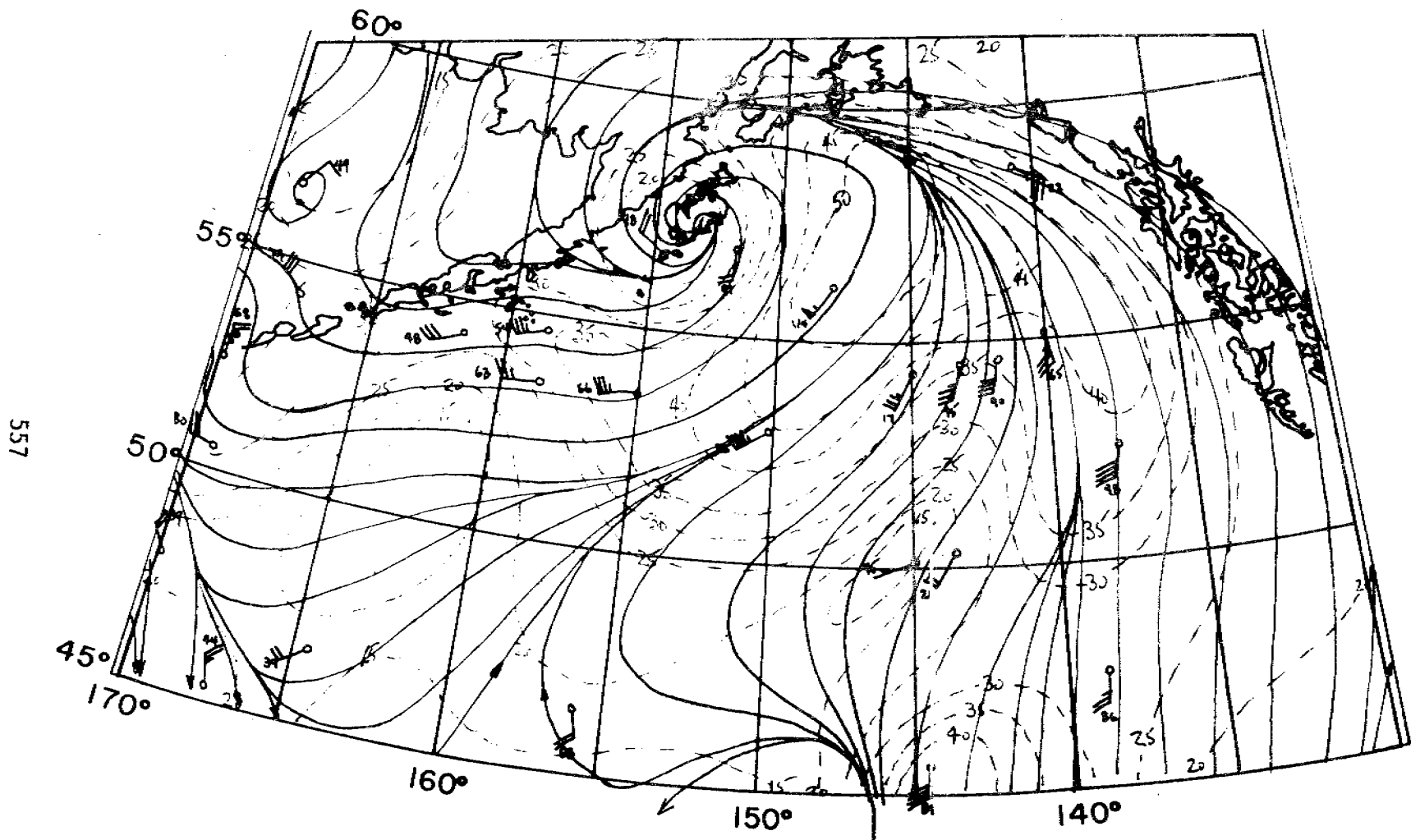


FIGURE 13c  
0600 GMT  
1/30/76

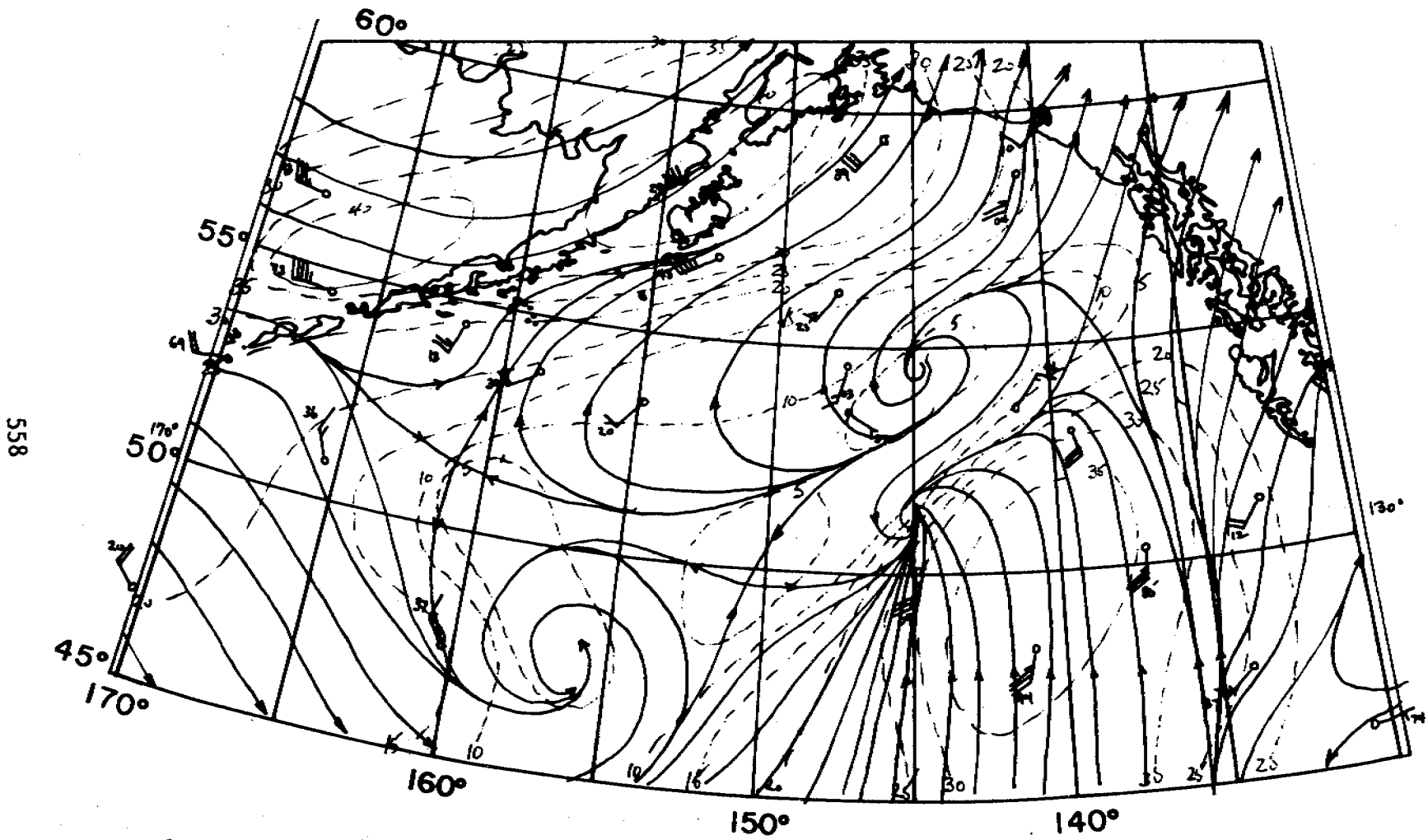


FIGURE 13d  
1800 GMT  
1/30/76

Annual Report  
April 1, 1979 - March 31, 1980  
Research Unit #435

MODELING OF TIDES AND CIRCULATIONS OF THE BERING SEA  
National Oceanic and Atmospheric Administration

J. J. Leendertse and S. K. Liu, Principal Investigators  
The Rand Corporation

April 1, 1980

Annual Report

MODELING OF TIDES AND CIRCULATIONS OF THE BERING SEA (RU 435)  
National Oceanic and Atmospheric Administration

April 1, 1979 - March 31, 1980

J. J. Leendertse and S. K. Liu

During the reporting period our efforts have been centered on carrying out modeling investigations of the St. George Basin-Bristol Bay area and of Norton Sound. For the first study area, we have:

- o Completed the final prediction and verification of the three-dimensional turbulent energy model and prepared a report describing the setup, adjustment and verification of this model (Ref. 1).
- o Made a series of simulation runs under the partial ice coverage conditions for the oil trajectory simulation.
- o Begun the adaptation of the response function model for calculation of oil spill trajectories near the St. George Basin beyond the area of the three-dimensional model so that 30-day spill trajectories can be accommodated.
- o Made a series of experimental 30-day oil spill trajectories to test the computational aspects of the oil trajectory model covering the extended area west of the St. George Basin.

For the Norton Sound study area, we have

- o Adjusted the Norton Sound three-dimensional model under ice-free conditions.
- o Compiled the existing ice cover data for the simulation of ice regions in Norton Sound.
- o Extended the oil trajectory model northwestward for the 30-day oil spill trajectory simulation.

BASIC MODEL DEVELOPMENT

For the basic three-dimensional model, during the reporting period we have revised the basic subgridscale (turbulent) energy computational scheme so that transient behavior of vertical density instability can be simulated more efficiently.

During periods of seasonal heating or cooling, vertical momentum-mass exchange and turbulence level are being suppressed or enhanced. The



quantitative level of suppression and enhancement have long been treated as functions of local Richardson number. Due to the scarcity of measurements, this functional relationship induces uncertainties in the vertical exchange computation. During the reporting period certain basic changes have been made in the computational method so that the exact gain in potential energy through the vertical mixing process is accounted for and taken out of the SGS turbulent energy balance. Therefore uncertainties in the turbulence and exchange computation are substantially reduced.

The ice model addition to the three-dimensional hydrodynamic model is completed. Since in the future the hydrodynamics should be simulated with not only a complete ice cover, but also with a partially covered area, we have now also included the capability of simulating partially-open ice covering conditions. It is now also possible to specify if ice floes, land-fast ice or rigid ice cover are included in the system. The inclusion of partial ice capability created difficulties at the open boundaries of the computational scheme; these problems have now been solved. With the final selected scheme a series of simulation tests have been conducted.

The formation, movements, and type of ice cover in Norton Sound and Bristol Bay are quite different from those observed in the areas of the Beaufort Sea and Bering Strait. To facilitate the initial ice condition for the oil trajectory computation in these areas, historic data, satellite photos and personal observations have been compiled and reviewed. Computed ice movements under different weather conditions are being compared with the observed movements by means of satellite tracking data.

#### NORTON SOUND AND ST. GEORGE BASIN-BRISTOL BAY MODELING AREA

As a result of a meeting held at the Sandy Point Project Office, Seattle, Washington, on August 23, 1979 current and water level data collected at station LD-5 during July-September 1978 have been used for the verification of the Norton Sound model under ice-free conditions. A magnetic tape containing digitized data for station LD-5 (Fig. 1) was transmitted from the University of Washington to Rand in mid-September of 1979. Using the weather data collected at Nome during the same period in 1978, the final phase of model adjustment and verification was carried out. Station LD-5, being the only current station in the middle of Norton Sound available for verification, is located approximately on the amphidromic point of the semidiurnal tidal component, making the model adjustment somewhat more difficult. In addition, due to the loss of one instrument in the latest NOAA survey, only three pressure records on the boundary of the model could be analyzed (Fig. 1). This analysis resulted in tidal amplitudes and phases of all major tidal constituents. These amplitudes and phases are used to describe the boundary conditions of the model. On the northwesterly boundary only one station was available; consequently the estimates of the amplitudes and phases probably induced errors in the computed horizontal and vertical tides.

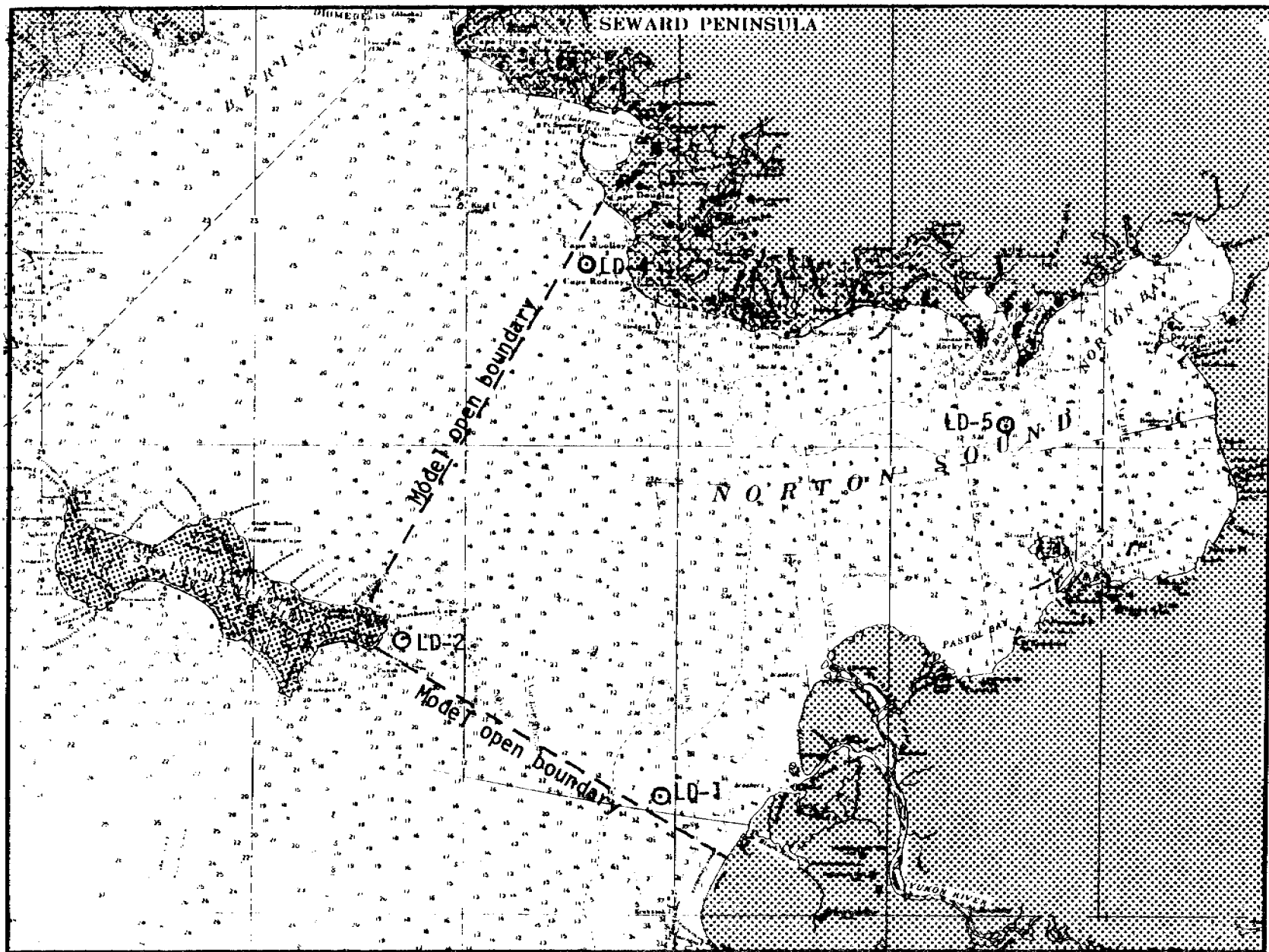


Fig. 1--Location map of Norton Sound model

Nevertheless, the appearance of the tidal chart of the semidiurnal tide in the model is similar to the chart for the  $M_2$  tidal component produced by NOAA from field data (Fig. 2). The amplitudes of the model results are larger due to the fact that in the model results the combined results of all semidiurnal tide components ( $M_2$ ,  $K_2$ , etc.) are shown, while in the NOAA chart only the  $M_2$  component is used.

The diurnal tidal charts obtained from the model results and from field data also have the same appearance, but in this case the computed amplitudes are lower than those estimated from the field data (Fig. 3).

We attribute this to the inclusion of storm-induced oscillations in the results of the observed tidal analysis. To investigate this behavior an analysis was made of the only available current record at station LD-5 in the interior (Figs. 4 and 5). Filtering the tidal oscillations out of these data, the resultant record suggests the existence of oscillations with periods of 50 hours and 26 hours (Figs. 6 and 7). From this we concluded that in future simulations the actual observed water levels at the boundary have to be used to obtain a good agreement between observed and computed water levels and currents.

At present the computed current (driven only with the predicted tides at the model boundaries) shows underestimates at alternating peaks (Figs. 8 and 9). A final verification run of the model will be made when the results of the present survey become available.

For the St. George Basin-Bristol Bay study area, the report describing the final adjustment and prediction of the model under ice-free conditions was published in September 1979 (Ref. 1). Present efforts for this area are directed toward simulating the conditions with partial ice coverage and extending the area for the oil trajectory response function model to cover an additional 220 km westward from the shelf break.

#### OIL TRAJECTORY MODELING

The computational program for oil trajectory simulation is nearly complete. Several tradeoffs between resolution and simulation cost have been studied. The computational system obtains its predictive impulse response function from the main simulation program. For the ice-free condition, five basic runs are made using the main program for calm, and under four (N.E.S.W.) wind directions of average wind speed, tide conditions and vertical density profiles. Wind stress is terminated after 12 hours, and the system is left to oscillate with only the inertial components. Differences in the velocity components between the condition with and without wind at each model's grid location are then used as the impulse response function for oil trajectory simulation.

During the oil trajectory simulation, every 12 hours a wind condition (speed and direction) is drawn from a certain weather 'type' which will last for 36 hours. The weather type is selected randomly from a transitional distribution derived from local weather statistics.

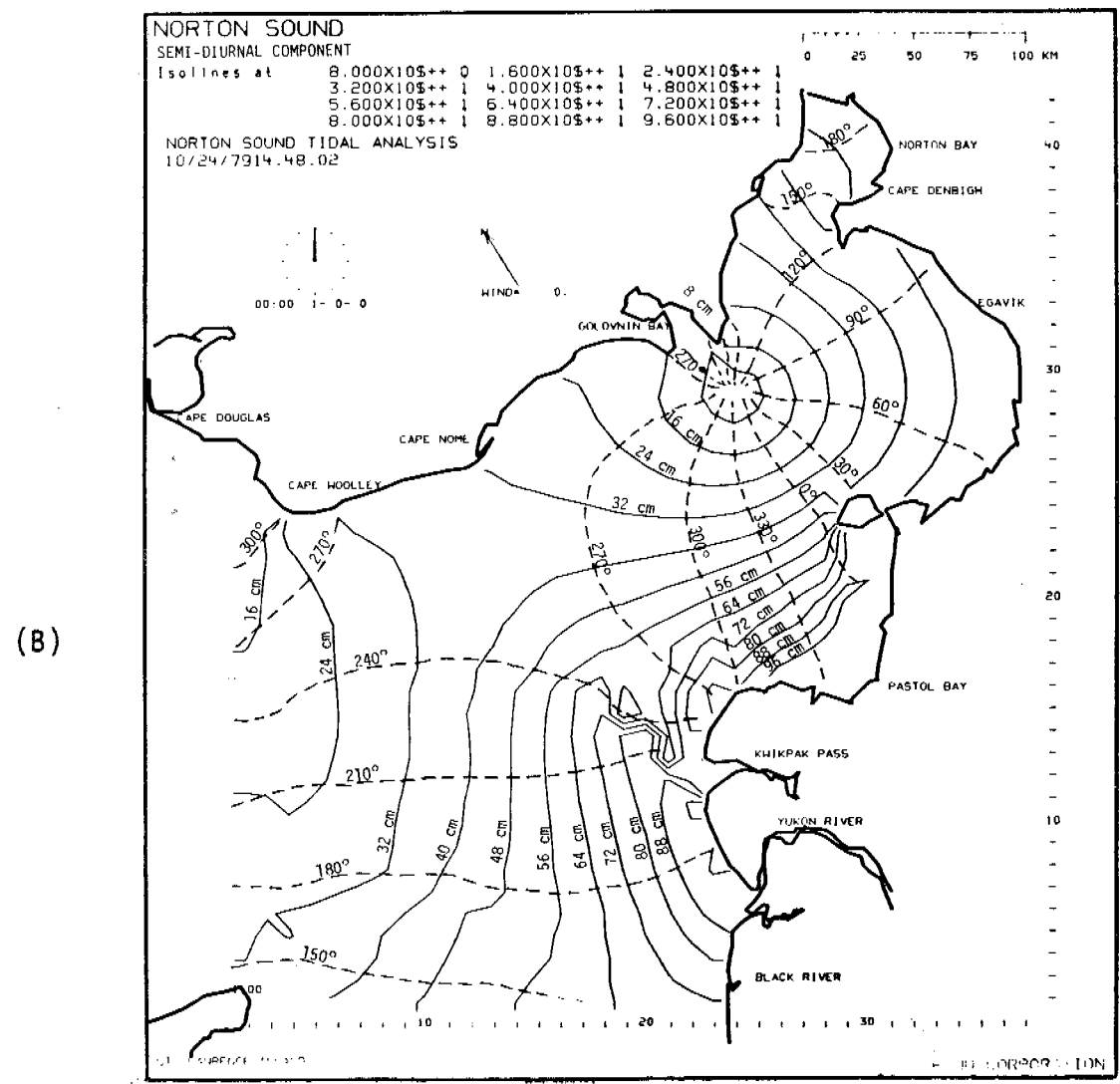
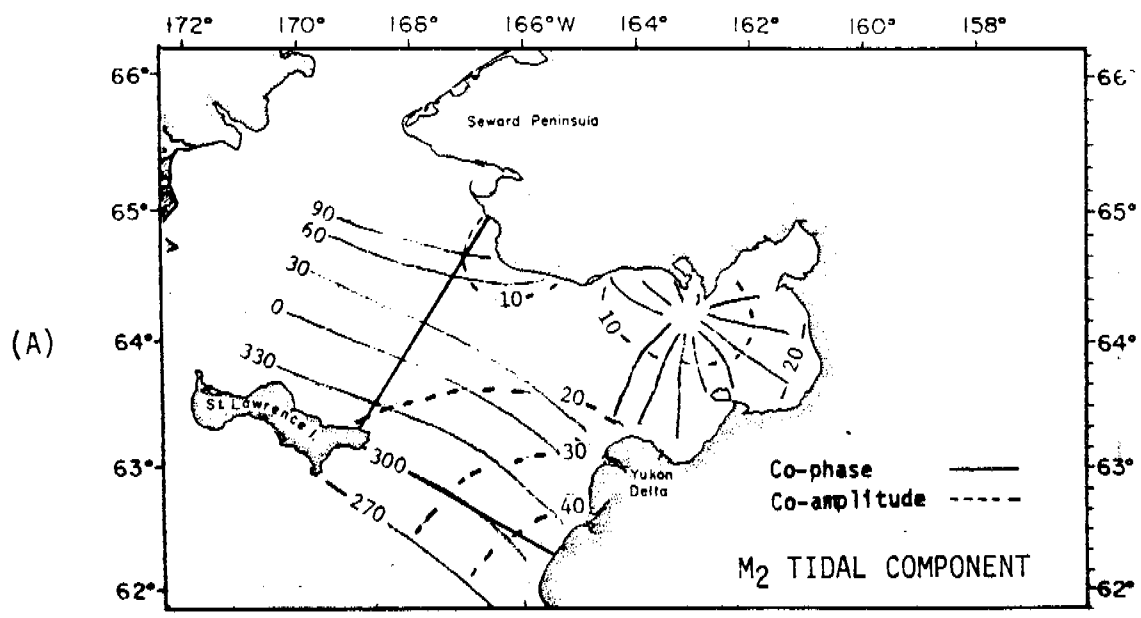


Fig. 2--Comparison between the computed (B) amplitude and phase of the semidiurnal tide in Norton Sound and a similar chart (A) derived from field data as compiled by the Pacific Marine Environmental Laboratory, National Oceanic and Atmospheric Administration.

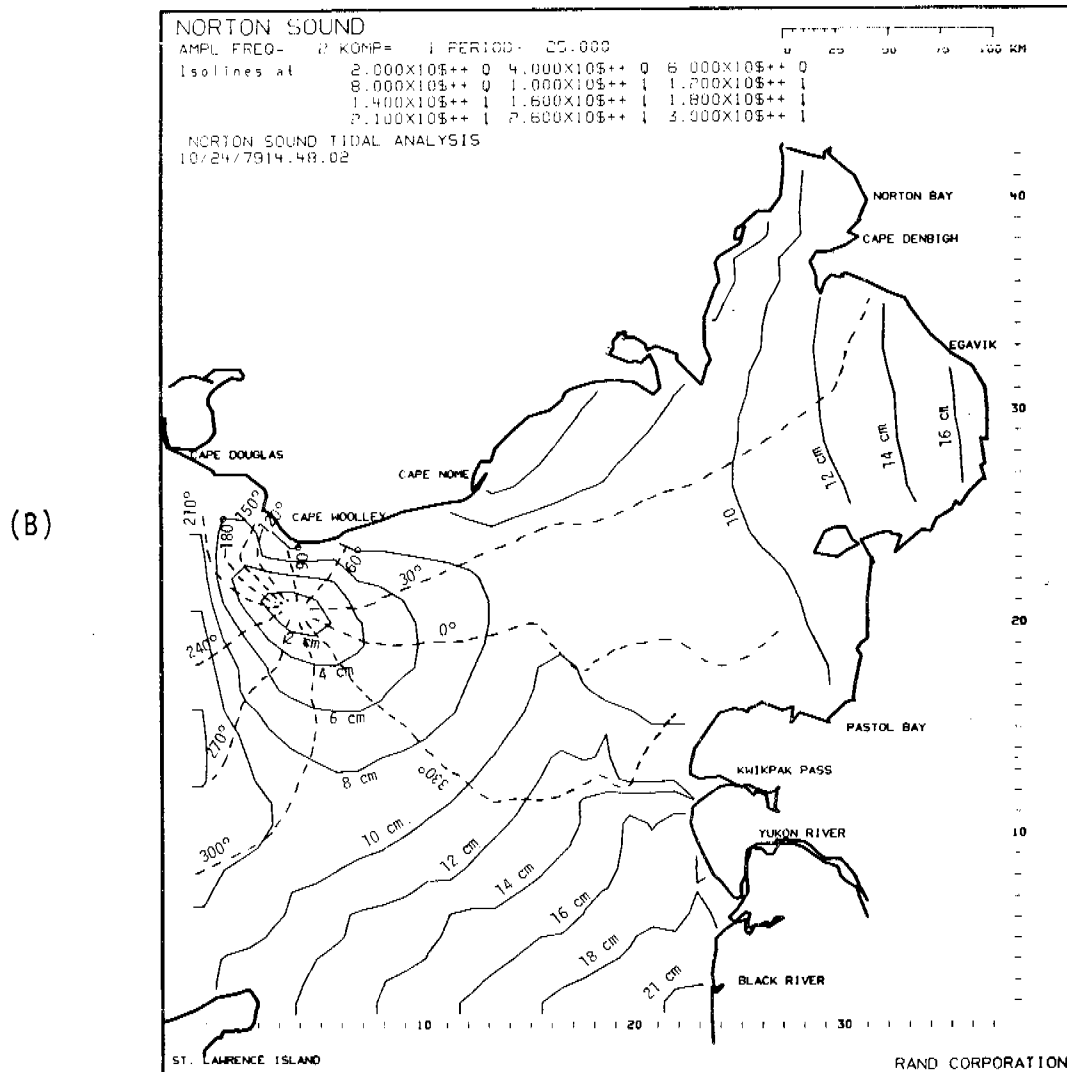
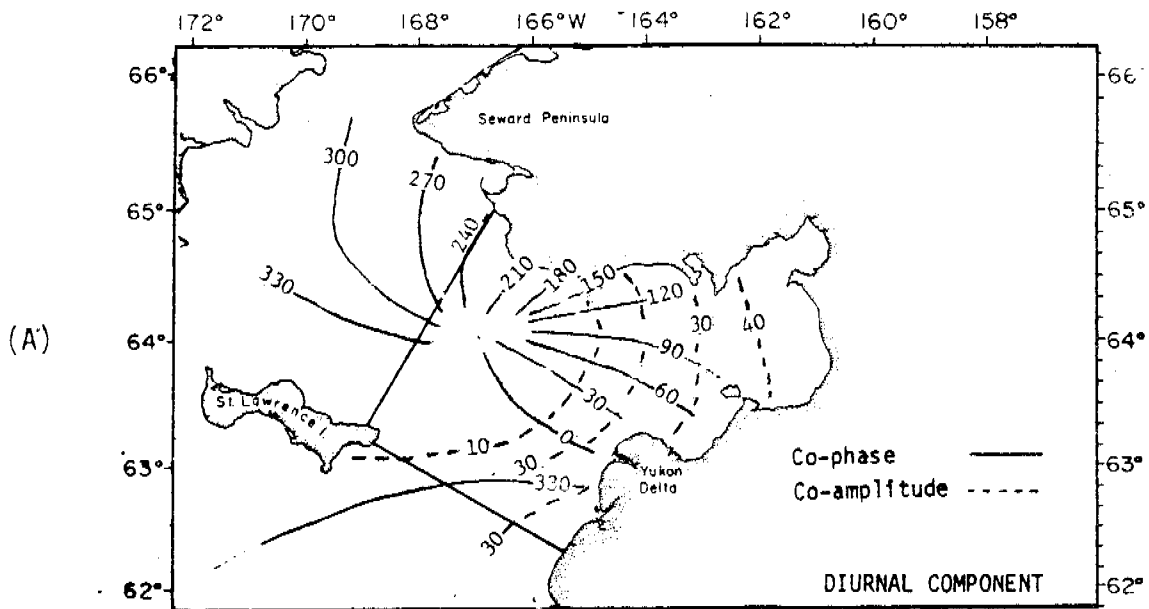


Fig. 3--Comparison between the computed (B) amplitude and phase of the diurnal tide in Norton Sound and a similar chart (A) derived from field data as compiled by the Pacific Marine Environmental Laboratory, National Oceanic and Atmospheric Administration.

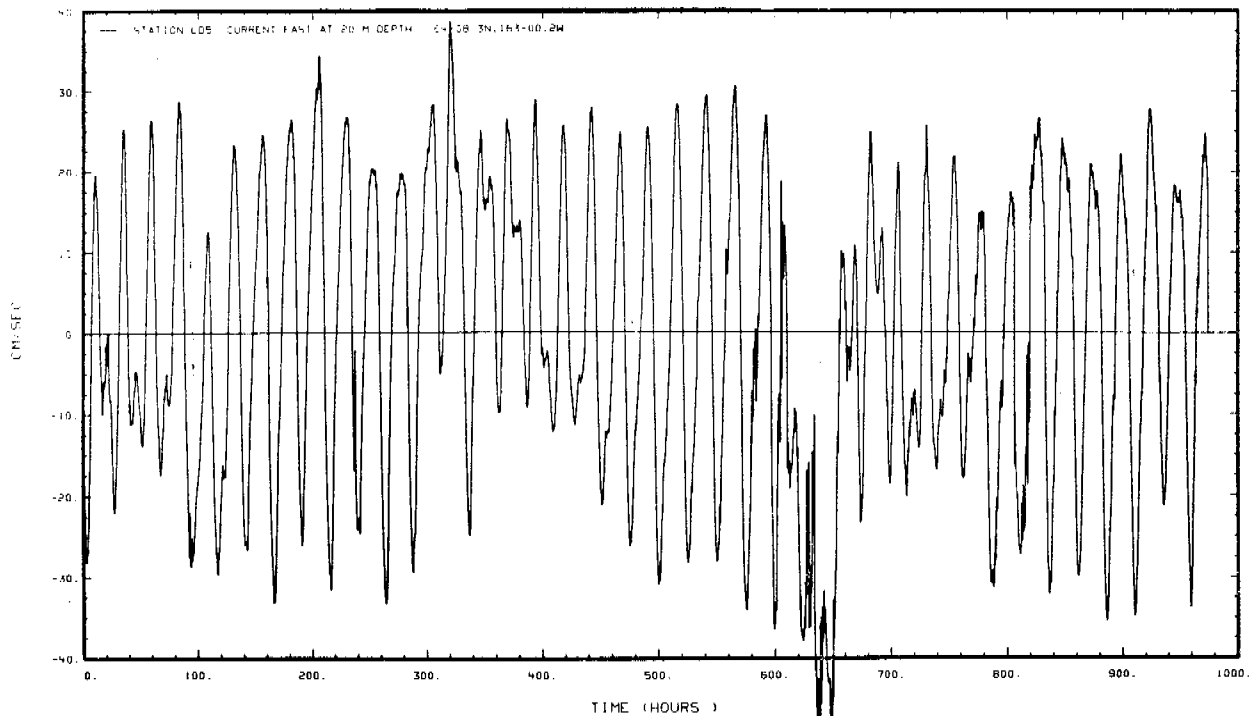


Fig. 4--Observed current component U near the bottom at station LD-5 in Norton Sound.

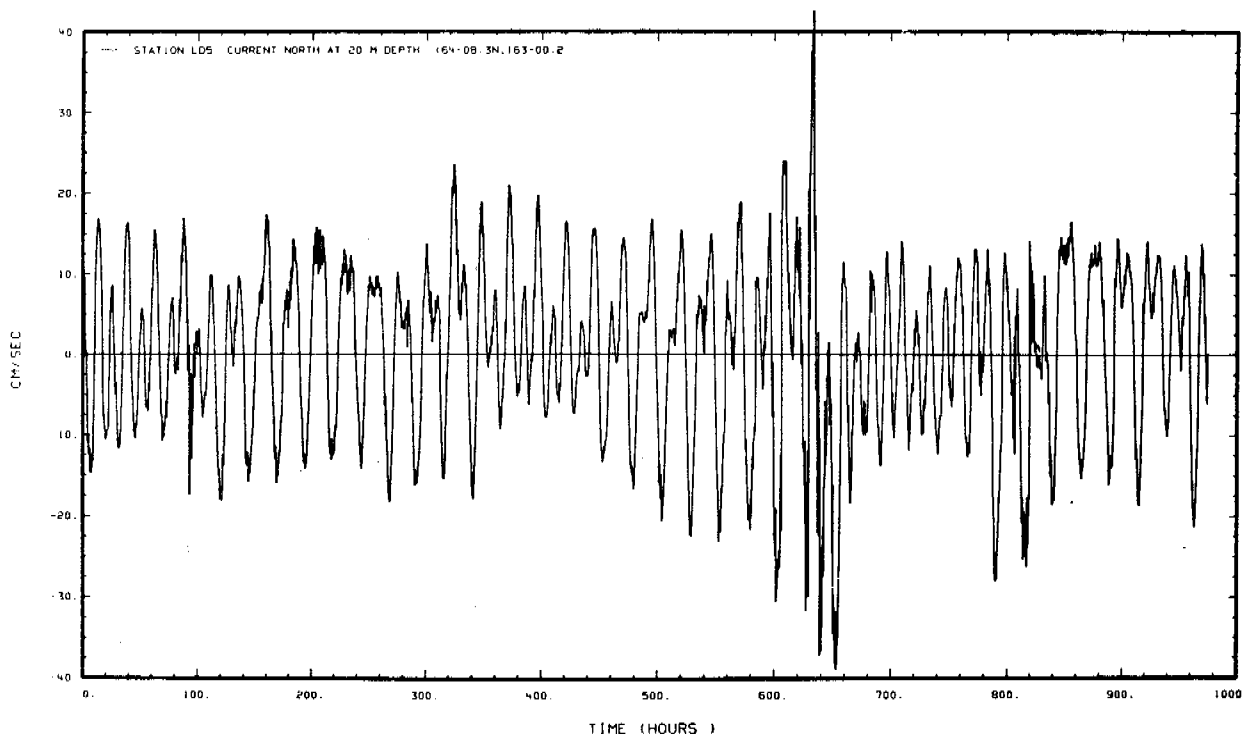


Fig. 5--Observed current component V near the bottom at station LD-5 in Norton Sound.

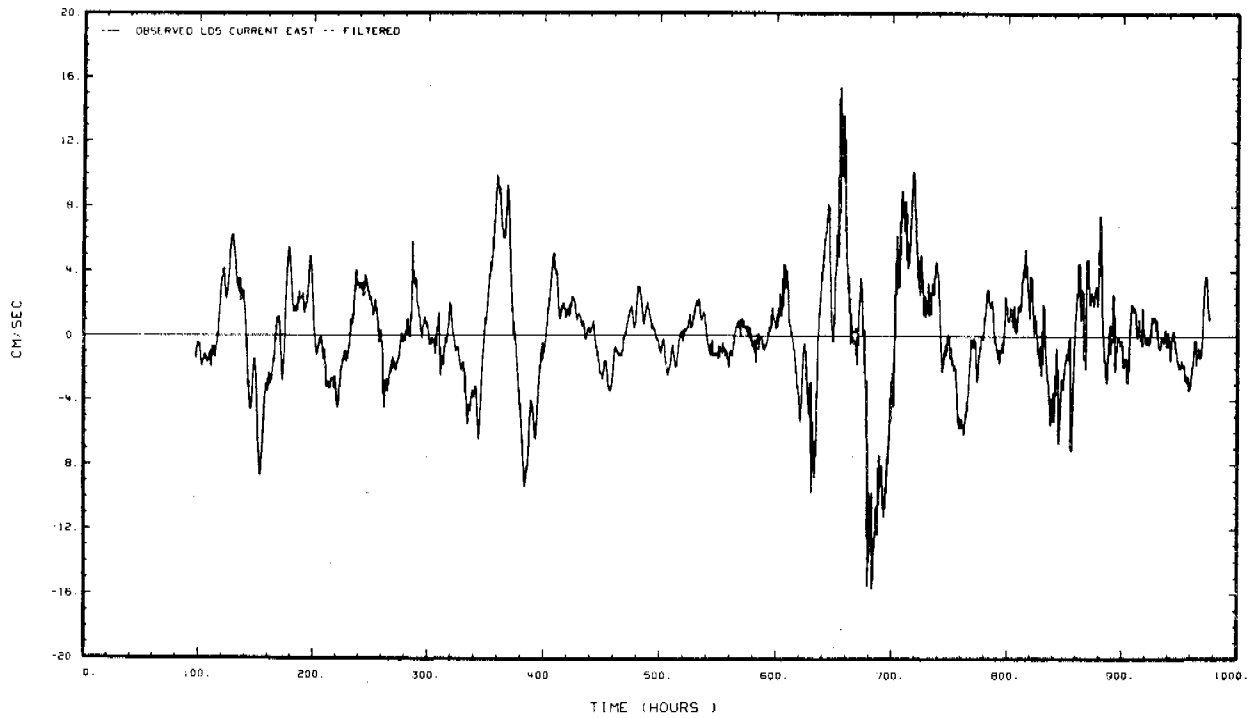


Fig. 6--Non-tidal oscillations in the east-west velocity component of the observed current at station LD-5, Norton Sound, after applying the numerical filter which filters out energies in the primary and higher tidal modes.

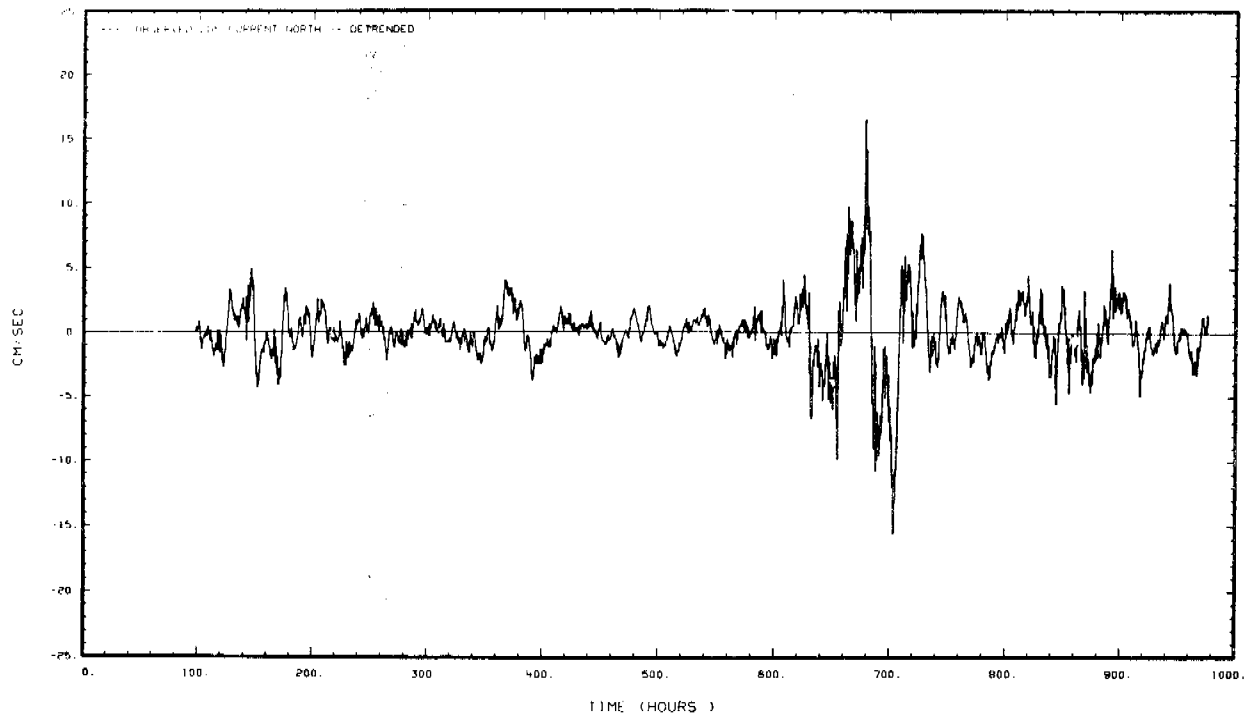


Fig. 7--Non-tidal oscillations in the north-south velocity component of the observed currents at station LD-5, Norton Sound, after applying the numerical filter which filters out energies in the primary and higher tidal modes.

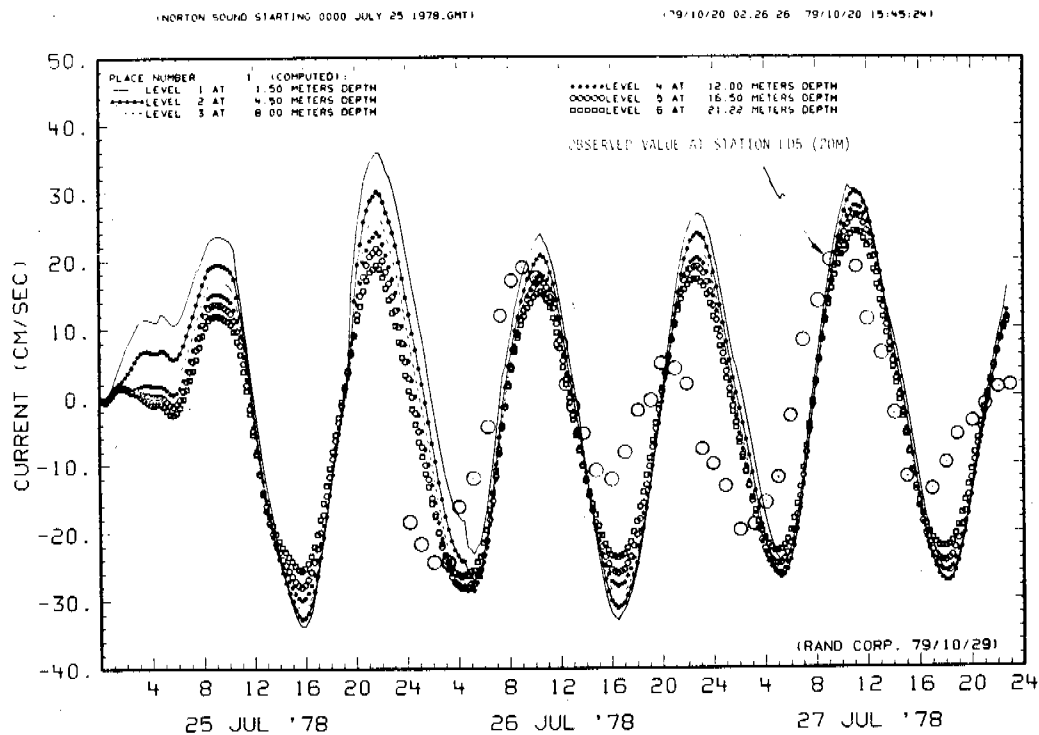


Fig. 8--Comparison between the computed and the observed current in Norton Sound in the x-direction at station LD-5 after the 24-hour run-in period.

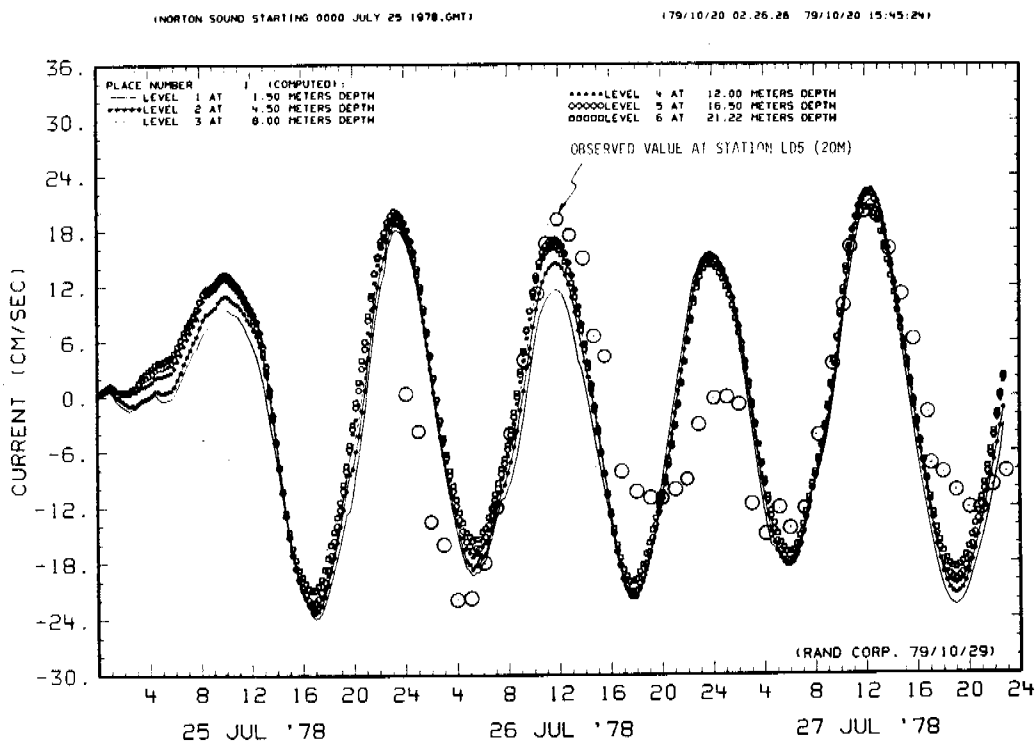


Fig. 9--Comparison between the computed and the observed current in Norton Sound in the y-direction at station LD-5 after the 24-hour run-in period.



Within each 12-hour period the current speed in the surface layer of each grid location is first computed by the convolution procedure and then extrapolated vertically upward to the water surface. The local surface drift velocity is added to the nonlinear water transport due to surface waves to obtain the final oil film transport. The wind speed and direction for the wave-induced surface transport is computed every 30 minutes from a Gaussian wind field having a mean value belonging to the 12-hour weather type plus certain assigned standard deviations. A typical oil trajectory simulation is expected to last for 30 days. A typical 30-day oil spill trajectory using the St. George Basin-Bristol Bay model will be used to illustrate the simulation procedure.

During the reporting period a series of simulations was made for the purpose of deriving the predictive response function for oil trajectory simulation. This procedure can best be described using graphs produced from the simulation series.

After the preliminary adjustment, a simulation of 60 hours (or longer) is made without the surface wind stress. Results obtained from this basic run, which contains tidal- and density-induced vertical shear structure for the entire field, are used to compare with four other runs under identical tidal and density conditions except that each one is under different wind stress from NESW directions for a period of 12 hours. After this period, the system is allowed to oscillate on its own inertia. Results from these four runs are then used to derive the response function by comparing them with the basic run. Figure 10 shows the response function for the surface drift current components  $u$  and  $v$  under an easterly wind of 10 knots at the model's grid location ( $M=12$ ,  $N=13$ ). Similar functions for the model's grid location ( $M=10$ ,  $N=16$ ) are plotted in Fig. 11. The first 12-hour period when wind stress is in effect is marked on each diagram.

From Figs. 10 and 11 it is clearly evident that under given wind components the behavior of surface drift current at each location is markedly different due to the local tide-induced energy level, vertical density-induced shear coupling, and the boundary's influence on the inertial components.

A similar set of response functions ( $M=16$ ,  $N=21$ ) due to a north wind for the St. George Basin and Bristol Bay is shown in Fig. 12.

During the reporting period, the response function model of St. George Basin-Bristol Bay has been extended offshore to compute off-shelf trajectories beyond the present three-dimensional model boundaries (Fig. 13), covering some additional 80,000 sq km offshore beyond the 1000-fathom contour. As shown in Fig. 14, the computational grid of the original model is represented by a (+), while the extended area is covered in dots.

In order to test the extended model, nine hypothetical oil spill locations were selected to compute the trajectories for a 30-day period

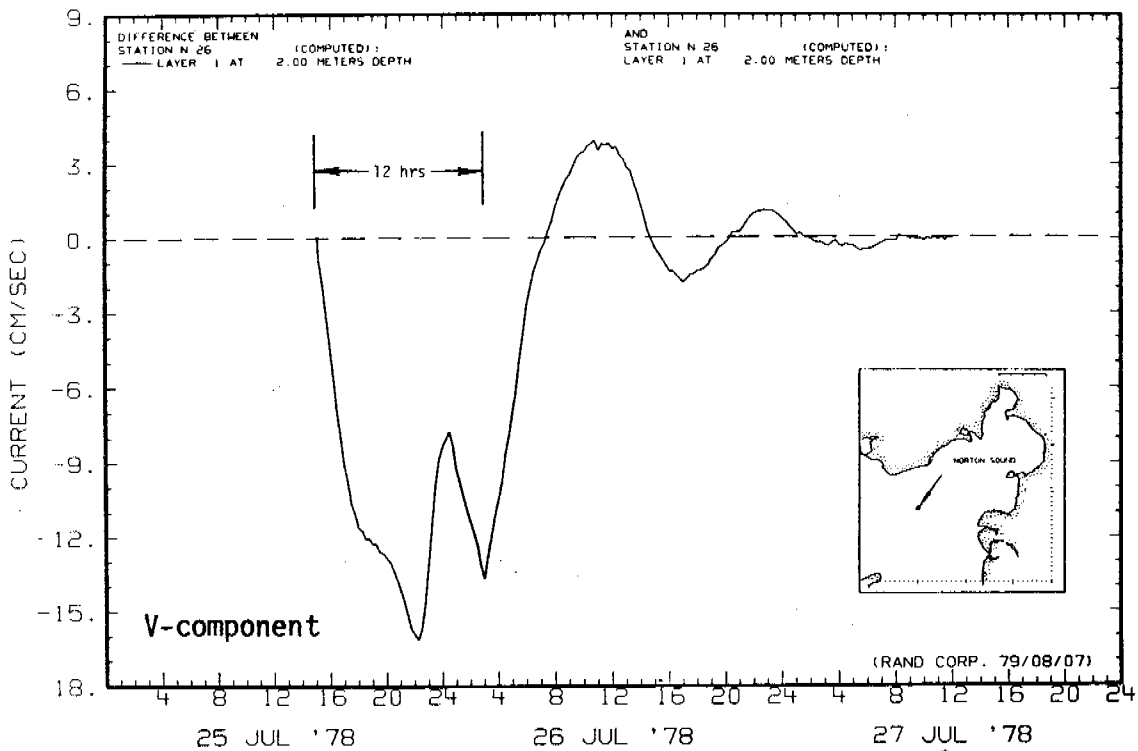
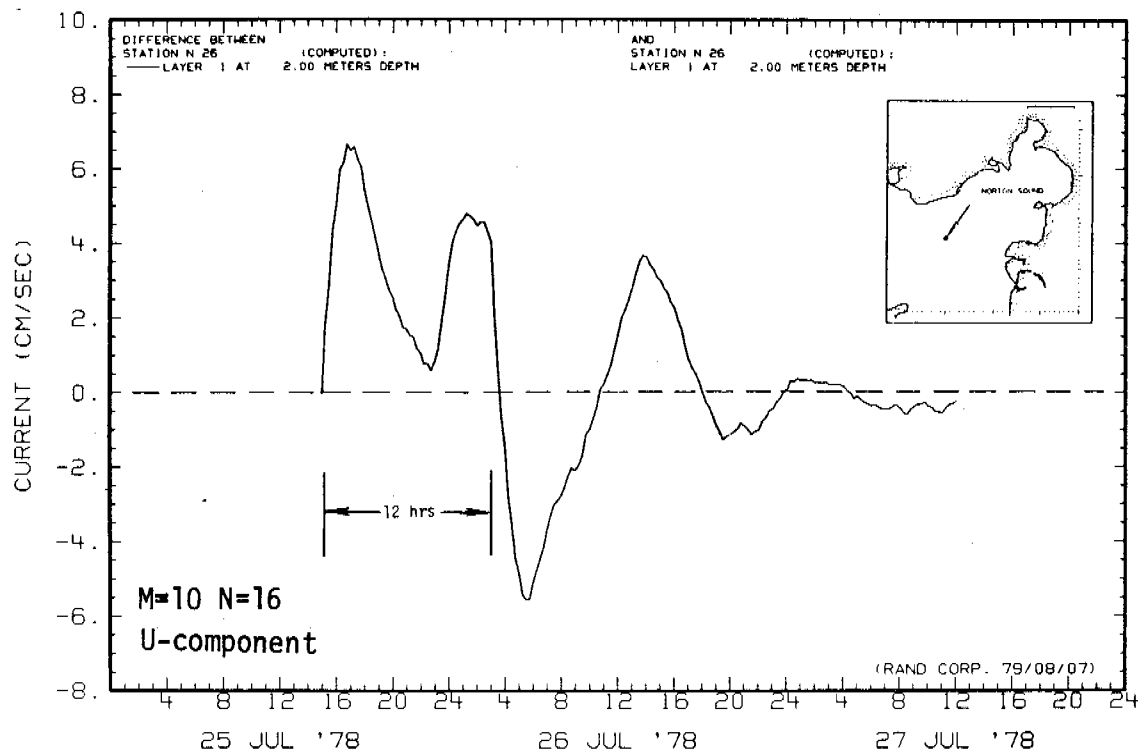


Fig. 10--U- and V-components of the response function for the surface drift under easterly wind of 10 knots at grid location M=10, N=16, Norton Sound model.

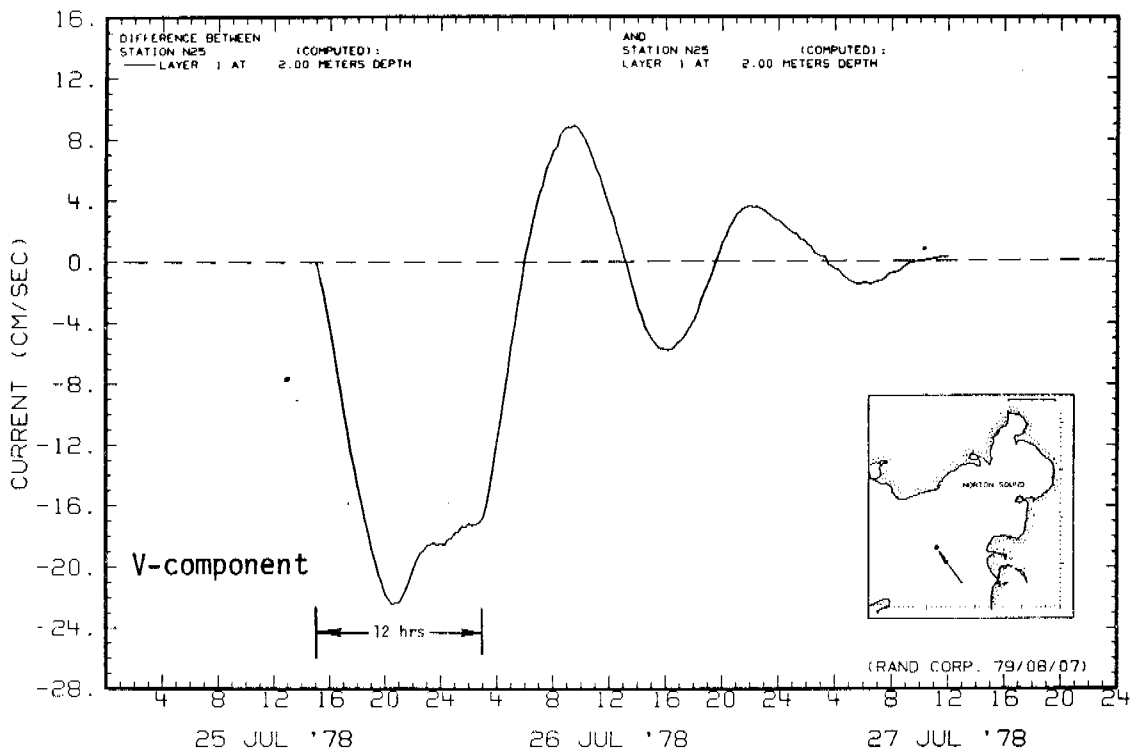
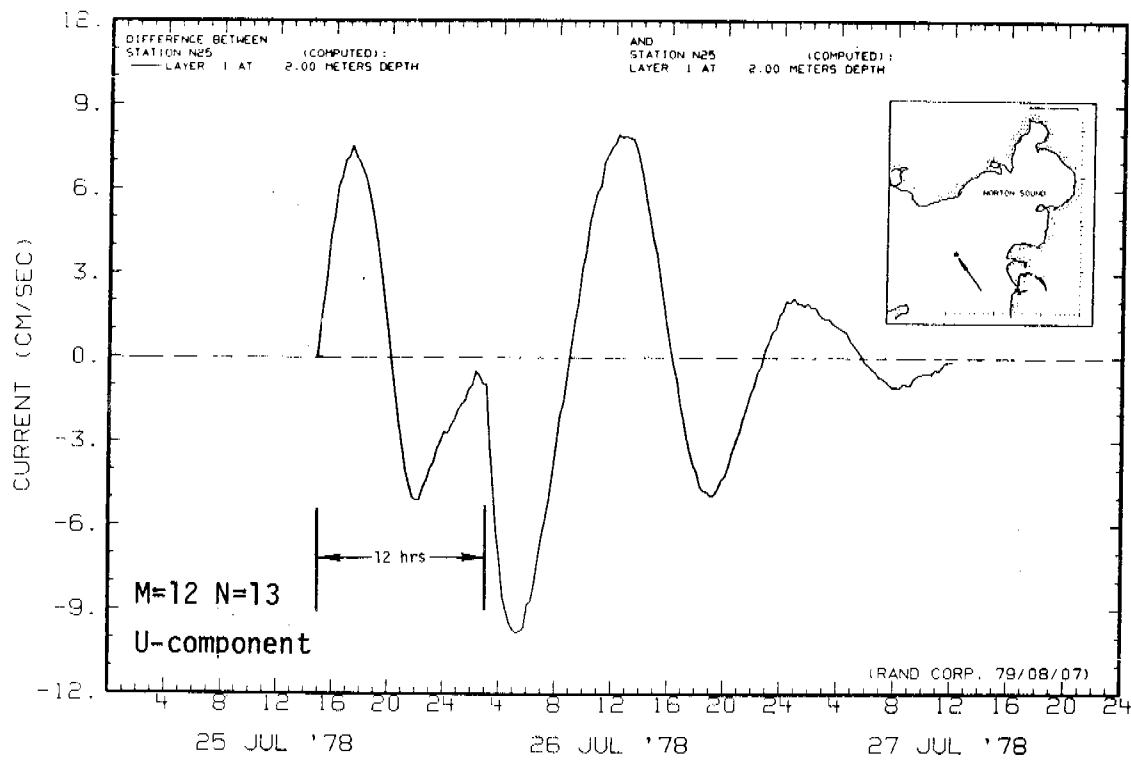


Fig. 11--U- and V-components of the response function for the surface drift under easterly wind of 10 knots at grid location M=12, N=13, Norton Sound model.

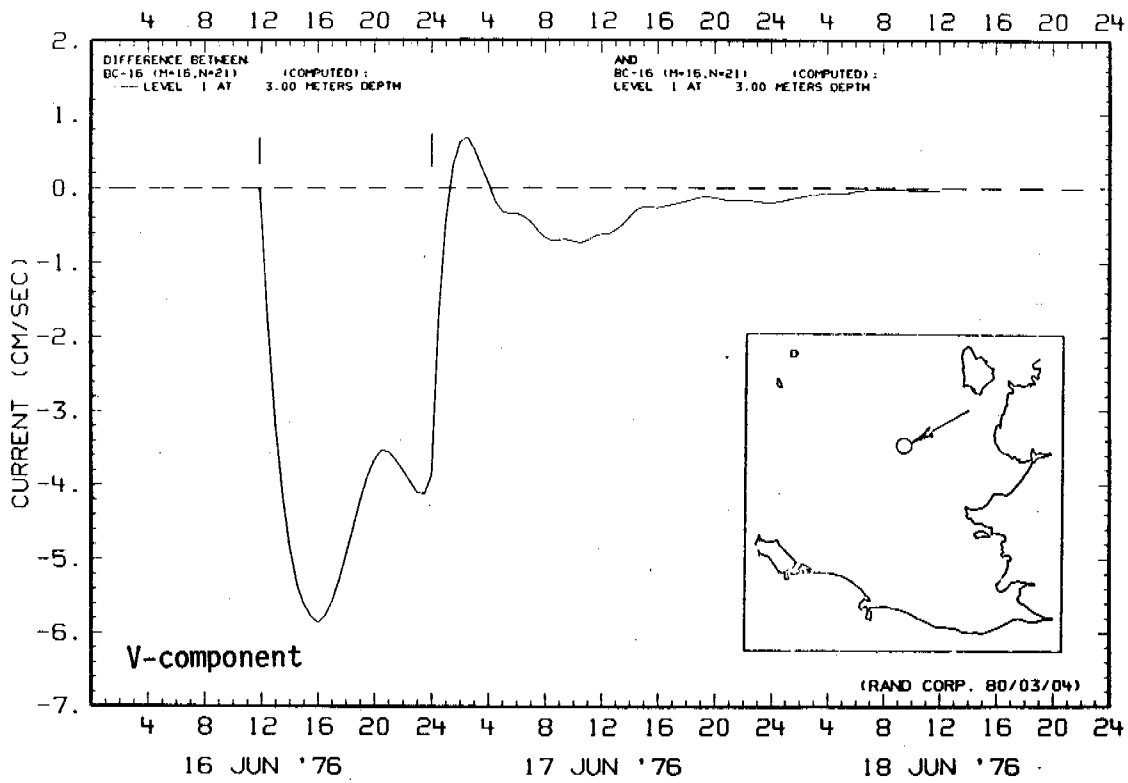
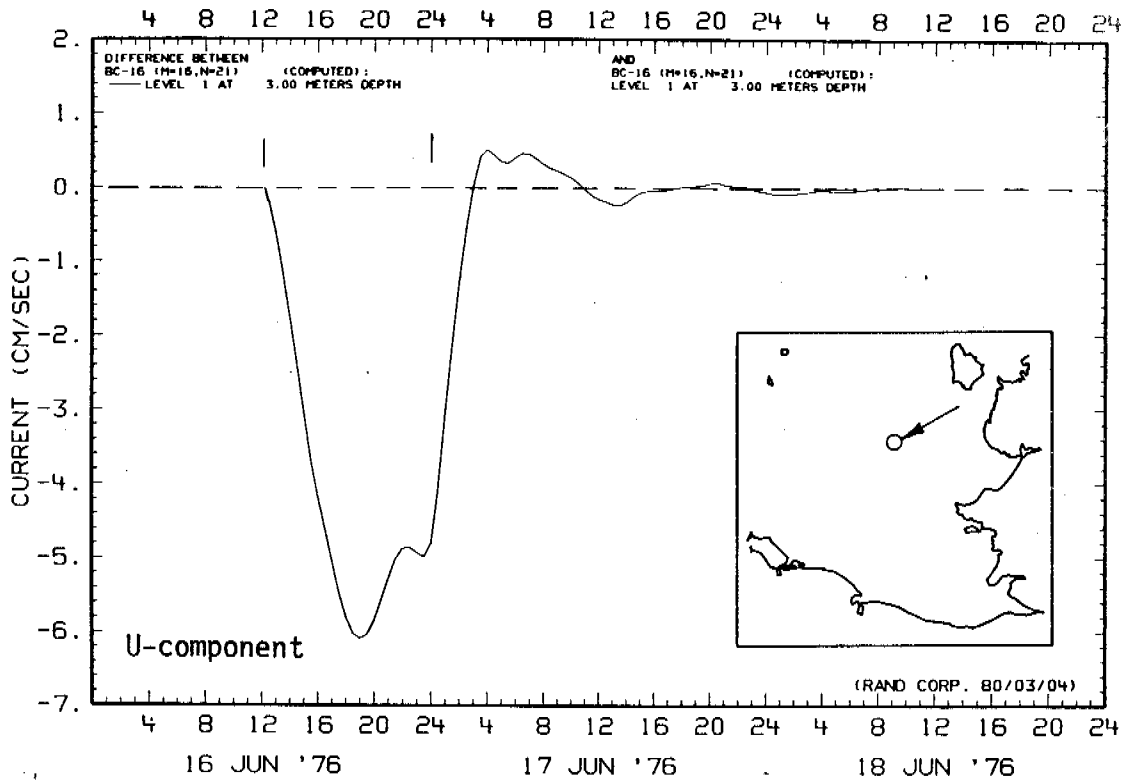


Fig. 12--U- and V-components of the response function for the surface drift under north wind of 10 knots at grid location M=16, N=21, Bristol Bay model.

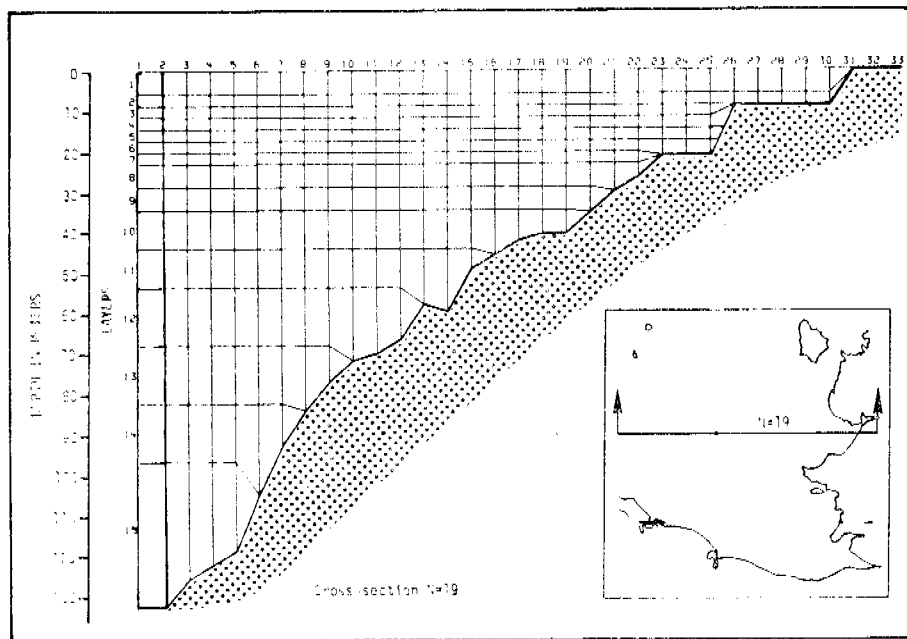
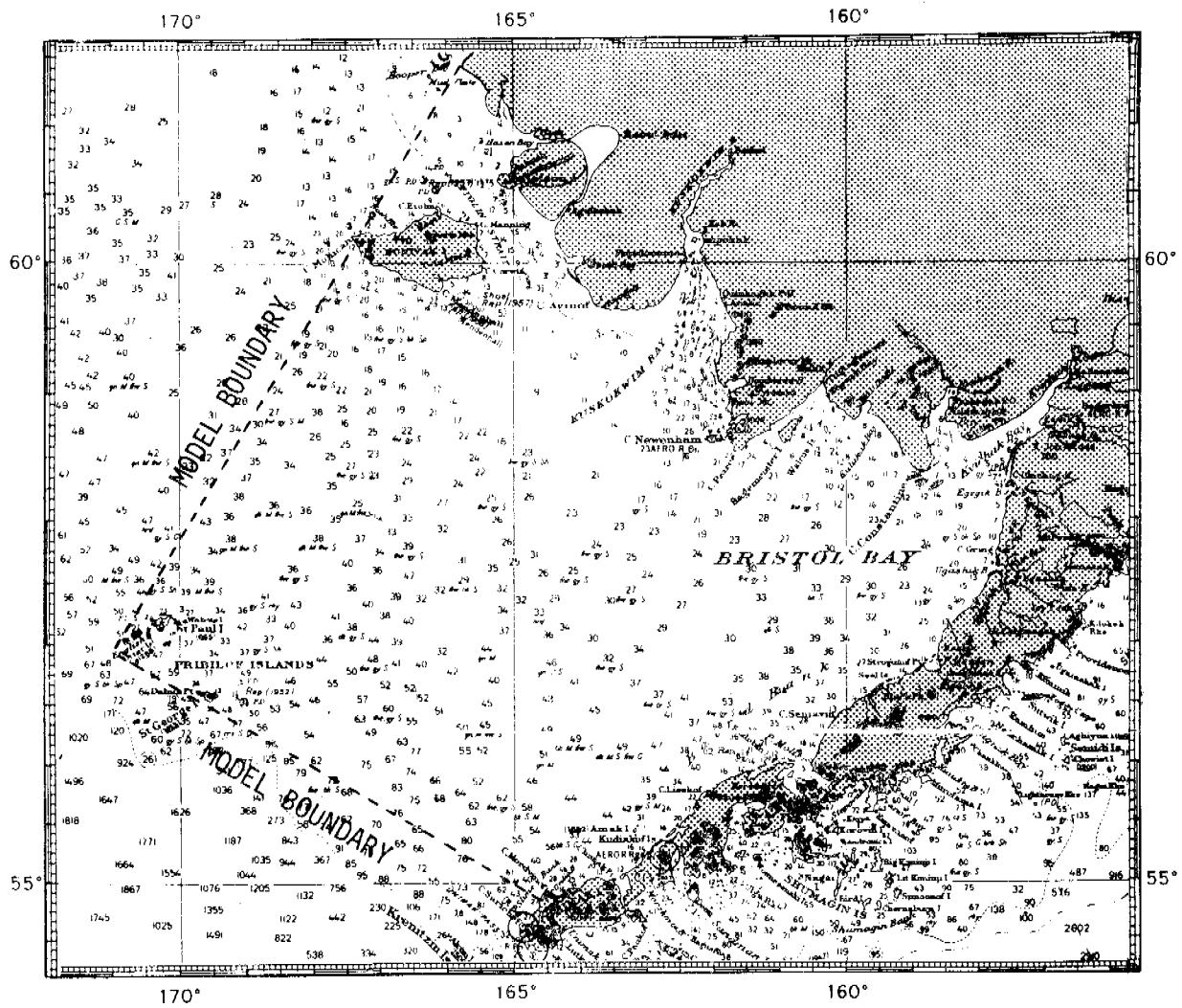


Fig. 13--Delineation of St. George-Bristol Bay model and a typical bathymetric profile of the modeled area.

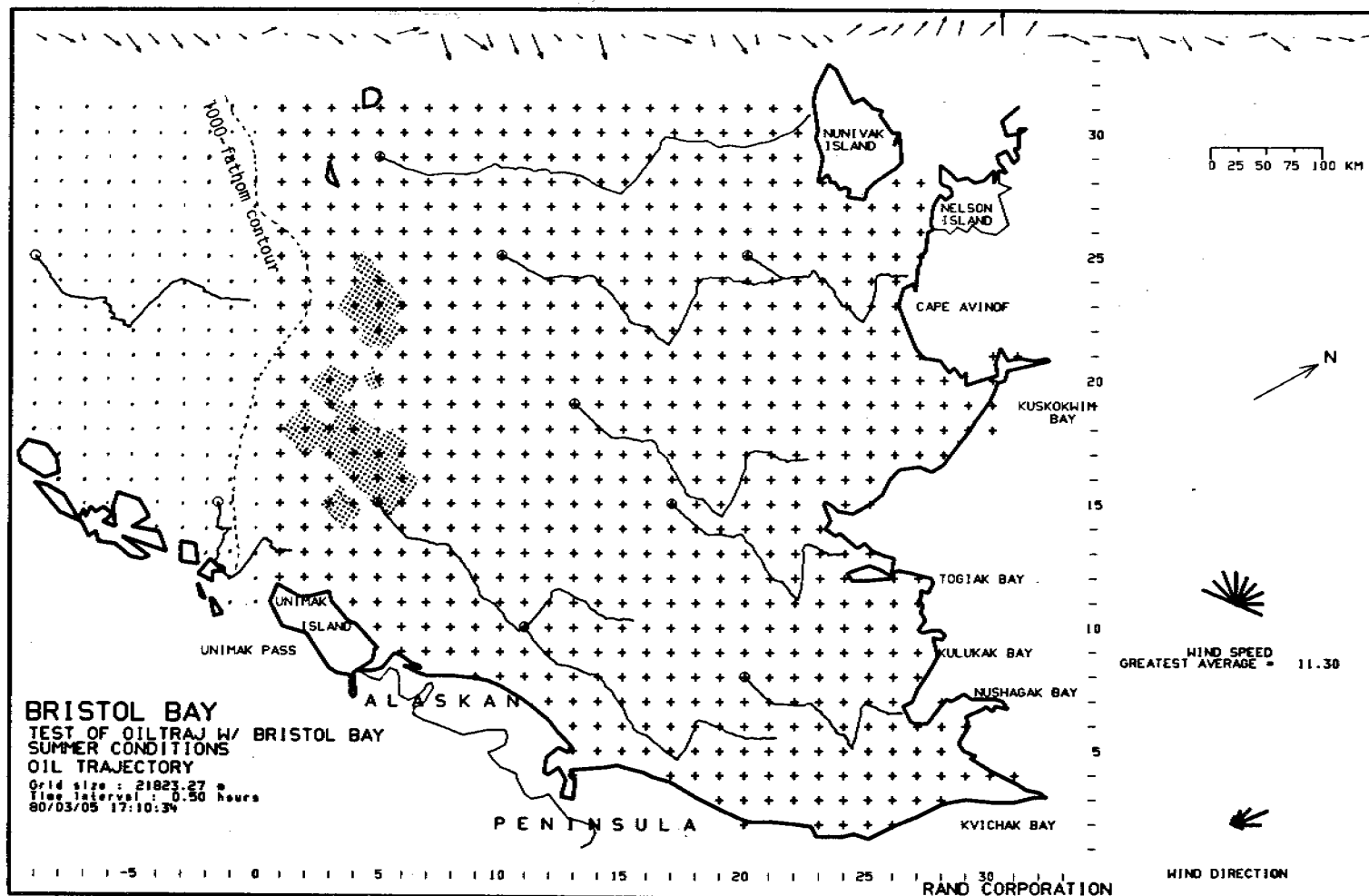


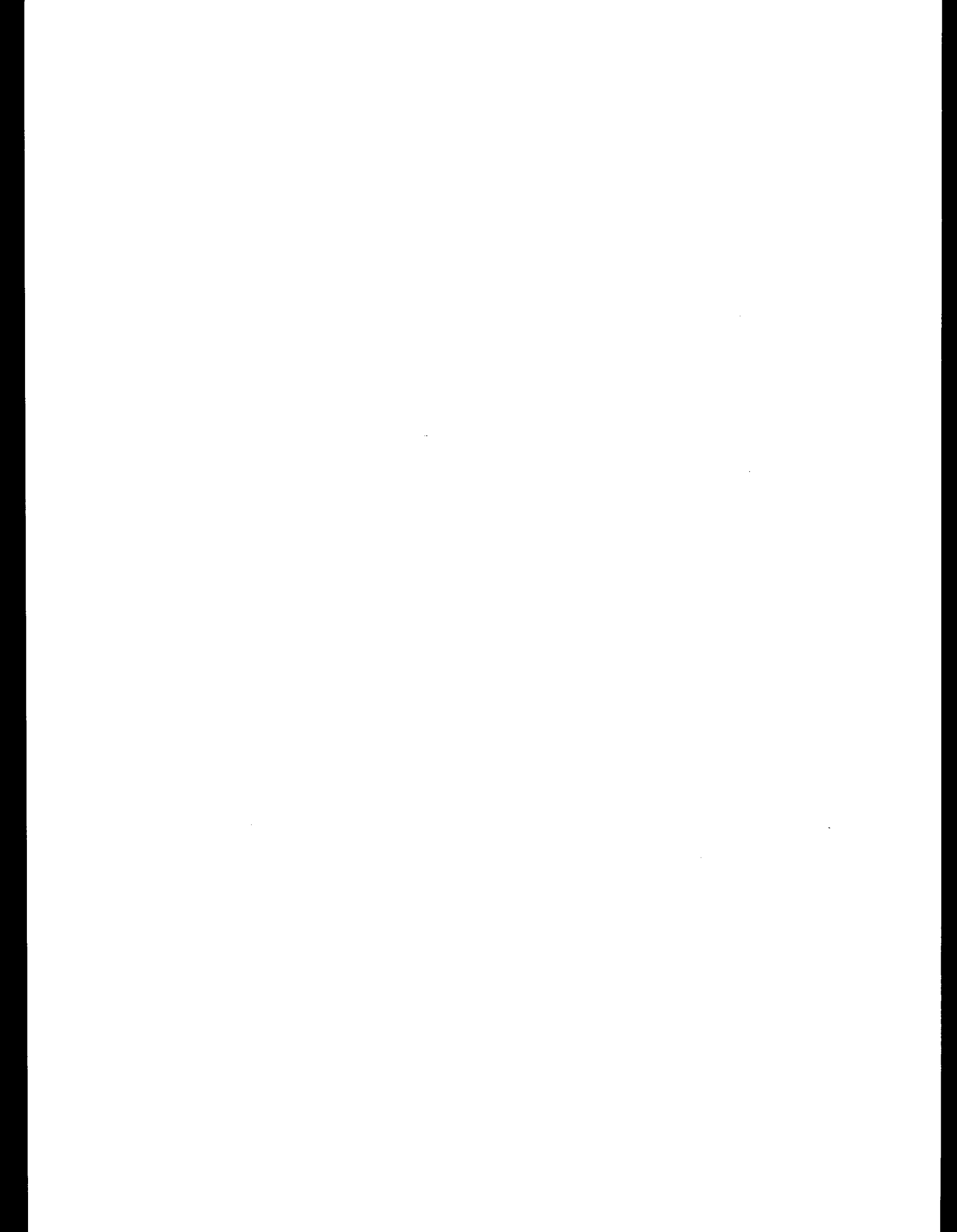
Fig. 14--A typical 30-day oil spill trajectory map of St. George Basin covering a 220 km extension beyond the 1000-fathom contour. Nine hypothetical spill sites are used in the simulation. Shaded areas represent potential lease areas under consideration. Spill sites are denoted by circles.

under ice-free conditions with a weather scenario typical of the summer-fall period. The wind conditions under this 30-day weather scenario are represented at 12-hour intervals by a series of wind vectors along the upper part of Fig. 13. Under an identical weather scenario, spilled oil originating from different sites would experience complex routes induced by the local tidal residual current, inertia component, vertical density effects, and the random components in the short-wave-induced nonlinear mass transport. Considering all nine sites, the total traveled distance of the spilled oil, when compared with the 30-day average wind speed, represents a ratio range from 1.1% to 3.3% of the wind speed. One of the nine hypothetical sites is located within the possible lease area (shaded) under consideration. During the 30-day simulation period, the average wind speed is approximately 9.6 knots, with the predominant wind coming from WSW.

We intend to complete the oil spill risk analyses for the Bering Sea-Norton Sound area by December 31, 1980 and the analyses for the St. George Basin by April 15, 1981.

#### Reference

1. Liu, S. K., and J. J. Leendertse, *A Three-Dimensional Model for Estuaries and Coastal Seas: Volume VI, Bristol Bay Simulations*, The Rand Corporation, R-2405-NOAA, September 1979.





ANNUAL REPORT

Contract #03-5-022-55  
Research Unit #526-77  
Task Order #13  
Reporting Period: 1 April 1976  
31 March 1980  
Number of Pages:

CHARACTERIZATION OF THE NEARSHORE HYDRODYNAMICS  
OF AN ARCTIC BARRIER ISLAND-LAGOON SYSTEM

J. B. Matthews  
Geophysical Institute  
University of Alaska  
Fairbanks, Alaska 99701

March 1980

## I. SUMMARY

Data are presented for under-ice water quality and current both for a site in a protected lagoon and for a location in the shear zone beyond the barrier islands in the Beaufort Sea. The data show two different regimes apply at the two sites.

For the site in Stefansson Sound a regime is shown in which brine is formed in early winter and travels consistently seaward. The seaward motion has peak velocities of 10 cm/sec. in November falling to peak values of 5.8 cm/sec in January. The seaward current in the bottom 2 meters of water showed strong semi-diurnal tidal influence. The water salinity increased steadily from a value of about 32.5‰ in early November to values of more than 34.5‰ by mid January. Temperatures are always close to the freezing point for that salinity, falling from about -1.8°C in November to about -2.0°C in February. The currents flow is always offshore in the lower layers and it is suggested that a return shoreward flow must exist in the upper water layers, just beneath the ice canopy. This shoreward flow was computed to have values of 22 cm/sec in early November. This water mass is the source for ice and brine formation.

For the site off Brownlow Point the same temperature and salinity characteristics were observed as at the lagoon site. However, the current regime was dominated by a longshore flow with superimposed tidal ellipses. The net flow was towards the east between November and March.

Sealevel changes of 1.2m were observed in early November. A negative surge in November resulted in a 40‰ volume change in Stefansson Sound. Surges in the winter, especially when ice growth decreases the water volume in lagoons can be major influences in reversing the restricted lagoon waters.

## II. INTRODUCTION

### A. General Nature and Scope of Study

The general scope of the study is to provide physical oceanographic data on the coastal and estuarine regimes of the Beaufort Sea Shelf. Originally planned as an integral part of the "Beaufort Sea Barrier Island - Lagoon Ecological Process Studies", Research Unit 467, the project was expanded in FY79 to include winter studies in the Beaufort Sea. At the same time the work was extended beyond the barrier island lagoon system into the shear zone in order to bridge the gap to Aagaard's study region along the outer shelf (RU 91 and RU 151). The scope comprises, with Aagaard, studies of the physical oceanographic processes on a seasonal basis in the region offshore of the Beaufort Sea Lease Area.

### B. Specific Objectives

Major objectives for this reporting period have been to complete the recovery of instruments previously deployed and begin detailed analysis of any data collected. Within these overall objectives the specific objective of analyzing data from the Stefansson Sound boulder patch has been given first priority in support of the work of Dunton (RU 536) Schell (RU 537), Naidu (RU 529) and others concerned with the winter studies program

### C. Relevance to Problems of Petroleum Development

The physical oceanographic processes determine the physical properties of the Beaufort Sea ecosystem. These processes, as well as determining the trajectories and movements of sediments, muds and spilled oil, control the flow of nutrients into and out of the ecosystem. The studies undertaken therefore have both direct and indirect relevance to the problems attendant to petroleum development.

## II. CURRENT STATE OF KNOWLEDGE

Much of what is known about the circulation on the nearshore regions of the Beaufort Sea is based on summer observations. Discussion of summer conditions has been made in earlier annual reports. The basic processes during the period from break-up to freeze-up will be briefly reviewed again then the state of knowledge of winter conditions developed.

There have been several measurements of currents in the lagoon and nearshore regions. Dymas (1975) reported observations of waves near Oliktok Point and has discussed some of the physical oceanographic characteristics of Simpson Lagoon. Wiseman et al, (1974) have discussed observations at several sites along the Beaufort Sea Coast including Simpson Lagoon. Barnes et al., (1977), Hufford et al, (1974) and Aagaard (1977) have all made observations of nearshore waters in the summer season. The conclusions have been that the coastal waters are

wind-driven throughout the open-water season and come under the influence of the prevailing winds from the east. The work of Matthews (this RU 526) and Mungall (RU 531) confirmed this observation and, for Simpson Lagoon, showed currents were 3 to 4% of the wind speed and travelling in the wind direction. During the periods of strong winds, which occur at approximately 10-day intervals during the summer, currents greater than 50 cm/sec are not infrequent. Observations of surface drifters by Barnes et al, (1977) and by Matthews (this RU) have shown that drifters released before a strong easterly blow can travel from Prudhoe Bay to Point Barrow (about 360 km) at an average speed of at least 40 cm/sec computed from time of recovery to time of release of the drifter.

The water masses, in summer, show very large ranges of temperature and salinity in both space and time. Hufford et al, (1974) and Barnes et al, (1977) point out that year-to-year variations can be almost as large as the variations in one year. We reported in the last annual report the observations at Egg Island Channel off the Kuparuk River. When the Kuparuk River overflowed the land-fast ice, water of 43‰ and temperature -1.8°C was flushed by fresh river water at 0°C in less than the 5-minute sampling interval. The salinity gradually increased over the period of a month at which time a salinity of 30‰ was reached. Fluctuations occur throughout the summer as parcels of warm (>6°C), brackish (< 28‰) water pass along the coast separated by oceanic water at temperatures close to 0°C and salinities near 30‰. By mid August temperature and salinity fluctuations decrease until, by early September, the coastal waters are in the range 30-32‰ and close to the freezing point for that salinity.

Until this winter studies program was initiated, there had been no reported winter observations of the under-ice circulation in the Beaufort Sea lagoons. Aagaard (1977) has made winter observations across the Beaufort Sea shelf in depths greater than 50 m but, inshore, inferences were based on a few scattered measurements and observations in the Canadian arctic. It was known that salinities can reach values over 40‰ in the winter inside protected lagoons and temperatures are near the freezing point for the salinity. Currents under the ice were unknown but it was believed that both tidal pumping and thermohaline convection was important. The thrust of the winter studies program under this research unit were directed toward understanding more of the details of the under-ice circulation, particularly in the region of the boulder patch in Stefansson Sound but also in the shear ice zone beyond the barrier islands.

#### IV. STUDY AREA

The study area extends from Brownlow Point to Oliktok Point and out to the mid shelf region in water depths of 40 m. This encompasses the entire area of the lease sale of December 1979.

## V. SOURCES METHODS AND RATIONALE OF DATA COLLECTION

The data collection methods have been developed specially for this project and have been discussed extensively in previous reports. Briefly, we rely on moored recording current meters and tide gauges which can be deployed, serviced and recovered by divers. A typical deployment schematic is shown in Figure 1. The instruments, floats, anchors and accessories are all arranged in modular units so they can be carried by helicopter and assembled on the ice. Aanderaa instruments were chosen because of their known performance characteristics in high latitude waters. Calibrations of all instruments is carried out both before and after each deployment.

## VI. RESULTS

Instruments were recovered from the sites shown in Figure 2 during April and May 1979 as reported in the June 1979 quarterly report. Instruments were recovered from sites numbered 1 through 10 but instruments were not recovered at sites 11, 12, 13 or 15. The Stefansson Sound (#7 on Figure 2) instruments were serviced and recovered on 16 August 1979. The instruments had disappeared from the mooring when attempts to recover them were made in November 1979. The Egg Island Channel (#5) instruments were partially buried under 1.2 m of sediments and special dredging techniques were employed to recover two current meters. The Milne Point instrument (#14) was recovered. Because of poor visibility and thin ice offshore of the barrier islands, instruments at sites Narwhal Island (#6), Oliktok, (11 and 15) and Flaxman Island (#8) were not recovered. Attempts to recover the remaining instruments will be made in April 1980.

Data have been analyzed for Stefansson Sound and Brownlow Point and the tide gauge at Narwhal Island. The Stefansson Sound site location is shown in detail in Figure 3. The Stefansson Sound current meter data are shown in Figures 4 and 5. The plots show the entire data set from two instruments at depths of 4 and 5 m in 6 m of water. The temperature and salinity data are shown to the same scales so that differences can be visualized. The results show that the salinity rises gradually from the beginning of the record in November until early January. There appear to be fluctuations in salinity after January although it continues to rise to mid February when the data-set ended. Deviations of the lower salinity record from those recorded on the upper meter are always towards higher salinity values. This suggests that brine is found near the bottom in January and February but does not extend beyond 1 to 1.5 m above the bottom.

The temperature record shows that the temperatures are within about 0.1°C of each other and the freezing temperature for that salinity throughout the record except in late January and February. The lower instrument shows a period in late January and early February when very cold water masses were observed. It is suspected that freezing may have occurred at this time for the lower instrument. These data may be erroneous as a result. This will be addressed later in the report.

Current vectors are shown in the lower plots in Figures 4 and 5. A semi-monthly tidal inequality can be clearly seen but the most striking

feature of the plots is that both sets show consistently north north easterly flow. The average is close to 50°T for both records. The location map for the instrument site (Figure 3) shows that 50°T is directly offshore. Maximum velocities are near 10 cm/sec. This suggests that a return flow must exist above the level of our instruments to maintain mass balance. It should be noted also that the currents in the lower meter, at 5 m depth, were generally greater than those observed at 4 m depth.

These data will be examined in more detail later in the narrative but first we will present the overall conditions. Figure 6 shows data from Brownlow Point (#10 in Figure 2) for the period from November 1978 to February 1979. Here again the salinity increases steadily through February. However there appear to be more fluctuations than were observed in the Stefansson Sound records. However, the steady increase from about 32.5‰ in salinity is common to both sites. Here again in mid January we find that the record changes to one showing more violent fluctuations. It is difficult to determine what is real and what is an artifact due to ice accretion and freezing of the instrument. The temperature record suggests that freezing took place in late January when the temperature fell below the freezing temperature for that salinity. Overall currents are quite different from the uni-directional currents observed in Stefansson Sound. The prevailing direction is NW-SE which is along the coastline rather than the offshore flow seen in Stefansson Sound. Brownlow Point is not protected by barrier islands.

Before examining the records in detail, sea level records for the period will be presented. Figure 7 shows the hourly sea level records for Narwhal Island. The striking feature of the records, is the marked low sea level on 26 November following the high value on 13 November. This shows a negative surge of 1.3 m over 13 days with 80 cm of that occurring over 3 tidal cycles. Other variations in sea level are seen throughout the record, but none are as large as the November surge. There is also a tendency for the mean sea level to decrease from November to May.

Figures 8 and 9 show detailed salinity, temperature and current records for Stefansson Sound Boulder Patch (Figure 3) for depths 4.02 m and 5.08 m respectively for the period 11 November through 11 December 1978. Salinity shows a generally increasing trend with steeper increases over a 1 to 2 day period. The upper salinity runs from 32.47‰ to 33.39‰ and the lower salinity from 32.31‰ to 33.23‰ for the month. Temperatures fall from -1.79°C to -1.85°C in both instruments. Maximum currents are 9.5 cm/s with mean currents 1.4 cm/s at 50°T. Currents at the lower instrument tend to be higher than at the lower instrument. A strong semi-diurnal tidal component can be seen in both records but with no current reversals. Note also that the mean current direction of 50°T derives from a 60°T current superimposed on a 36°T current.

The tidal record is identical to the fuller record shown for Narwhal Island in Figure 7. A peak sea level is shown for 13-14 November at 604 cm and a trough on 26 November of 447 cm arbitrary datum units. The semi-diurnal tidal range is 10 cm.

Figures 10 and 11 show salinity, temperature and current records for Stefansson Sound at 4 and 5 m depths. Both instruments register an overall increase in salinity and decrease in temperature for the month. Currents again both shown semi diurnal tidal pulses with no current reversals and a mean 50°T direction. Temperatures fell from -1.85°C to -1.90°C and salinities from 33.23‰ to 33.93‰ for the lower meter and from 33.39‰ to 34.08‰ for the upper meter. Maximum currents near 8.1 cm/s for the lower meter and 5.8 cm/s for the upper meter with means of 1.9 and 0.7 cm/s respectively at 98°T.

Figures 12 and 13 show salinity temperature and current records for Stefansson Sound at 4 and 5 m depths. The lower instrument shows pulses of what appears to be saline water which do not appear on the upper record. Also the temperature record for the lower meter shows a cooling effect which suggests freezing, since it is below the freezing temperature for the water salinity. If freezing occurs, ice crystals in the conductivity sensor would alias the signal. The upper current meter shows little change over the period of the record. Temperatures were in the range -1.9°C to -2.0°C and salinities 33.95‰ to 34.62‰. Currents on the upper meter reached a maximum of 5.8 cm/sec and fell to zero after 22 January although weak currents maintained the vane at 48°T. The lower instrument continued to show currents with an average of 1.6 cm/sec at 40°T and peak at 7 cm/sec. Sea level ranged from a low of 545 cm on 11 January to high of 613 cm on 20 January 1979 with a semi diurnal and semi monthly in equality of the tide. Data are shown from Narwhal Island because of instrument failure at Stefansson Sound.

## VII. DISCUSSION

The results show a buildup of brine as the season progresses from November when only about 0.6 m ice were present until March when there was 2 m of ice. The Stefansson Sound data show a pulsating current regime in the waters 1 m and 2 m above the bottom with the current flowing directly offshore at 50°T peak currents are about 10 cm/sec in early November and gradually decrease in magnitude into March. In late January the currents ceased to influence the instrument 2m above the bottom although the current vane still showed a consistent direction. The salinity and temperature data at the upper meter are unreliable in late February at the same time that no currents were registered. Since the ice is nearly 2 meters thick and the float extends above the instrument array, it is suggested that frazil ice accreted on the instrument. This idea is supported by the temperature measurements which fell below -2°C in late February 1979. The conductivity cell with ice in it gives meaningless results and of course a frozen rotor registers no current.

These results are consistent with the observations of Lake and Lewis (1970) and other under-ice observations showing salt rejection during sea ice formation. In our case the brine falls to the sea floor and moves consistently seaward. A tidal regime is superimposed on the density current. This led us to attempt to compute a return flow of oceanic water in the upper water layers, immediately beneath the ice. The resultant current vectors, assuming three layers of flow are shown in Figure 14. The upper layer of shoreward flowing sea water was allowed to vary with the observed sea level and a constant ice growth rate of 1 cm/day. Current were computed with a maximum velocity of 22 cm/sec early in the record and falling to

peaks of 18 cm/sec in mid-December. The observations suggest that tidal pumping is the major circulation mechanism in winter and that this dominates the density-induced currents. However, the tidal currents are strongly baroclinic; flowing shorewards near the surface and seawards near the bottom. The currents decrease towards the end of our observations. This could be because ice formed at a slower rate leading to lower density currents and because the lagoon volume is much restricted by shorefast ice leading to lower tidal currents. There is also the possibility that ice in the rotor bearing may serve to decrease the responsiveness of the equipment.

The data from Brownlow Point show the same trends of increasing salinity and decreasing temperature. The current regime from the one instrument analysed to date is altogether different. At this site with no protective barrier islands to seaward the current regime shows a marked longshore drift superimposed on rotating tidal currents. This suggests that ice formation yields brine. The brine after passing seaward through the lagoon then gets carried by the longshore current regime beyond the barrier islands. The mean drift in November was westward, contrary to the currents observed by Aagard at the outer edge of the shelf. Considerably more light will be thrown on this longshore current when the data from other instruments are analysed.

#### VIII. CONCLUSIONS

It is concluded that brine resulting from ice formation leads to a steadily seaward flow along the bottom in the early winter in the lagoons. A counter-current of seawater at lower salinity must exist just below the ice. Detailed analyses, yet to be done, should shed light on the details of the mechanism of ice formation and brine production. Currents are highest in the early winter when brine and ice formation are most rapid. Peaks of 10 cm/sec were observed in the lower layers and 22 cm/sec were computed for the upper layers. Tidal pumping plays an important role and dominates the observed current regime. Salinities build up from near 32‰ in November to 34‰ in February. Temperatures are very close to the freezing point for that salinity throughout the observations.

Seaward of the barrier islands a longshore current and tidal current dominate the observations. The same buildup in salinity and drop in temperature observed in the protected lagoons is also seen in this shear zone at the edge of the landfast ice.

Sea level variations are about 10 cm range due to tides and over 10 times larger due to surge motions. The sea level ranged between 445 cm and 605 cm in November when there was 60 cm of ice. This water depth (excluding the ice sheet) fell from 454 cm to 385 cm. This suggests that 40% of the volume of the lagoon can be flushed by surge activity under the ice.

Work, presently going on, should throw more light on the many processes occurring under the ice throughout the winter.

#### IX. NEEDS FOR FURTHER STUDY

There is a need to continue evaluating the data already taken. After this is accomplished a detailed study plan can be presented, based upon the process revealed in this preliminary analyses.



X. SUMMARY OF JANUARY-MARCH QUARTER

A. Ship or Laboratory Activities

1. Ship or field trip schedule
  - a. Dates
    - (i) Departed Fairbanks for Prudhoe Bay on 18 March 1980.
  - b. Name of Vessel
    - (i) None
  - c. Aircraft
    - (i) NOAA helicopter
2. Scientific Party
  - a. Steve Petersen - University of Alaska, Diver-Technician  
Cliff Moore - University of Alaska, Diver-Technician  
Jeanette Moore - University of Alaska, Diver-Technician
3. Methods
  - a. Field Sampling  
Search and recovery attempts will be made for all outstanding instrument arrays noted in the last quarterly report.
  - b. Laboratory Analysis  
Analysis by computer methods described in earlier reports.
4. Sample Localities/Ship or Aircraft Tracklines  
shown in figure 2 are the stations locations.
5. Data Collected or Analysed
  - a. Number and types of samples/observations  
Brownlow Point data for salinity temperature and current speed and direction and the same data for Stefansson Sound were analysed. Details have been given in the annual report.
  - b. Number and types of analyses  
Data from the tide gauge (#303) at Narwhal Island and the top current meter (#3419) from the station 0.5 km north of Brownlow Point were edited and plotted.  
  
Data from the lower current meter (#3420) from the station 0.5 km north of Brownlow Point is in the editing process.
  - c. Miles of trackline  
None.

#### REFERENCES

- Aagaard, K., 1977. STD measurements in possible dispersal regions of the Beaufort Sea. Annual Reports, R.U. 151 Arctic Project Office OCSEAP.
- Barnes, P., E. Reimnitz and D. McDowell, 1977. Current meter and water level observations in Stefansson Sound, summer 1976. U.S.G.S Open File Report 77-477, 7 pp.
- Dygas, J. A., 1975. A study of wind, waves and currents in Simpson Lagoon in Environmental studies of an arctic estuarine system. Final Report EPA-660/3-75-026. National Environmental Research Center, Office of Research and Dvelopment, U.S. Environmental Protection Agency, Corvallis, Oregon, 97330
- Hufford, G. L., S. H. Fortier, D. E. Wolfe, J. F. Foster and D. L. Noble, 1974. Physical oceanography of the Western Beaufort Sea in Marine ecological survey of the western Beaufort Sea. U. S. Coast Guard Oceanographic Report No CG-373-64.
- Lake, R. A. and E. L. Lewis, 1970. Salt rejection by sea ice during growth, J. Geophys. Res., 75(3):583-597.
- Wiseman, W. J., J. N. Suharda, S. A. Hsu and C. D. Walters, 1974. Characteristics of nearshore oceanographic environment of Arctic Alaska, in The coast and shelf of the Beaufort Sea Arctic Institute of North America, p. 49-64.

## FIGURE CAPTIONS

- Figure 1. Typical instrument array for under-ice oceanographic observations.
- Figure 2. Complete station location map of winter studies physical oceanography program.
- Figure 3. Stefansson Sound Boulder Patch station location.
- Figure 4. Salinity, temperature and current record from Stefansson Sound boulder patch at 4.02 m for November 1978 to November 1979.
- Figure 5. Salinity, temperature and current record from Stefansson Sound boulder patch at 5.06m depth from November 1978 to February 1979.
- Figure 6. Salinity, temperature and current records for a mooring 0.5km north of Brownlow Point.
- Figure 7. Narwhal Island sea level record for period 12 November 1978 to 7 May 1979.
- Figure 8. Salinity, temperature, current records and sea level for Stefansson Sound at 4 m depth for period 11 November to 11 December 1978.
- Figure 9. Salinity, temperature, current records and sea level for Stefansson Sound at 5.0 m depth for period 11 November to 11 December 1978.
- Figure 10. Salinity, temperature and current records for Stefansson Sound at 4 m depth and sea level record for Narwhal Island for period 11 December 1978 to 11 January 1979.
- Figure 11. Salinity, temperature and current records for Stefansson Sound at 5 m and sea level for Narwhal Island for period 11 December 1978 to 11 January 1979.
- Figure 12. Salinity, temperature and current record for Stefansson Sound at 4 m depth and Narwhal Island sea level record for period 11 January 1979 to 11 February 1979.
- Figure 13. Salinity, temperature and current record for Stefansson Sound at 5m depth and Narwhal Island sea level record for period 11 January 1979 to 11 February 1979.
- Figure 14. Current vectors from 4 and 5m depth and computed for a hypothetical upper layer on the basis of mass conservation.

6.1m ABOVE BOTTOM

ICE

5.6m ABOVE BOTTOM

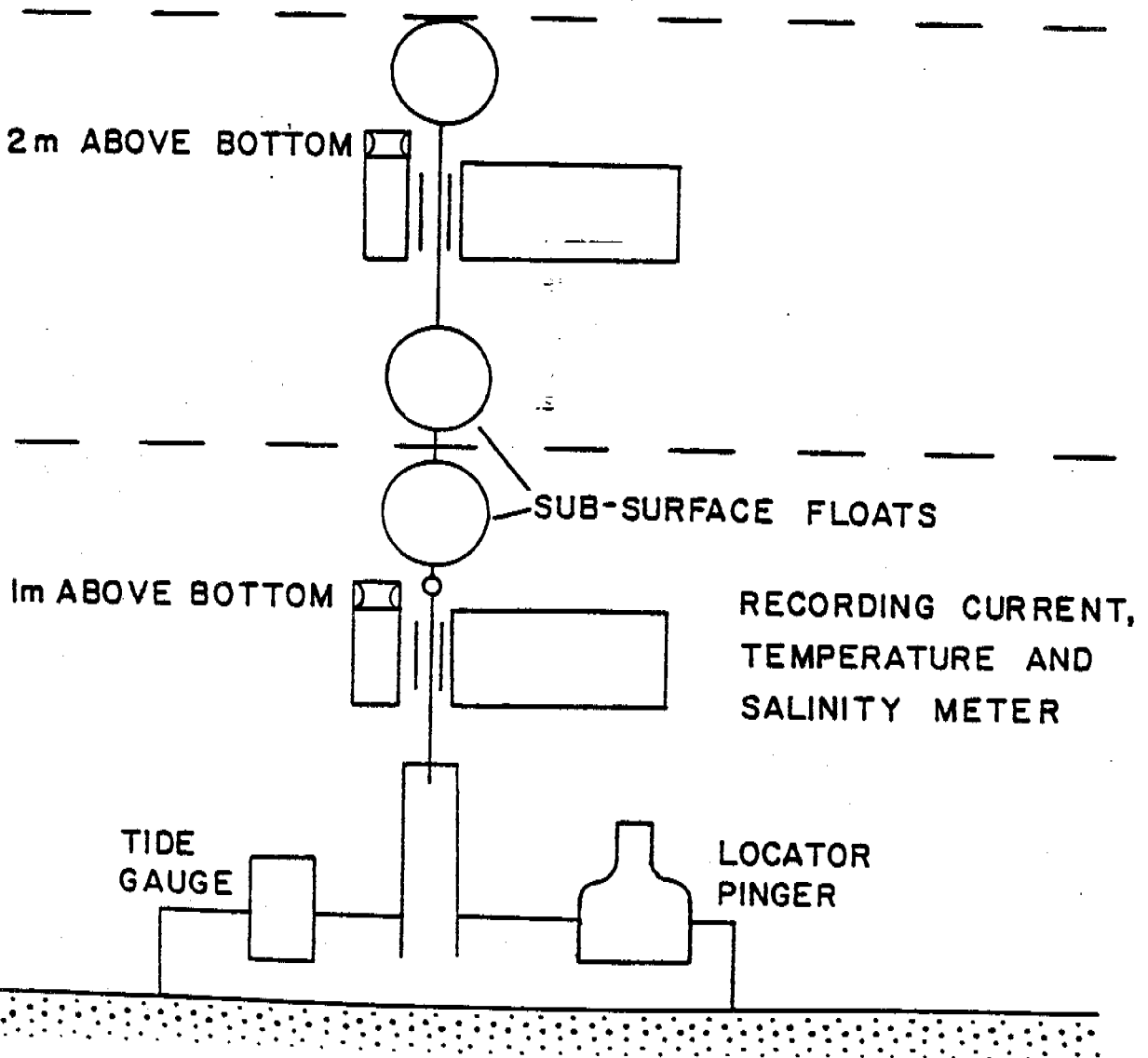
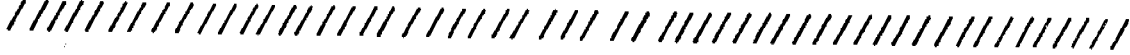


Figure 1. Typical instrument array for under-ice oceanographic observations.

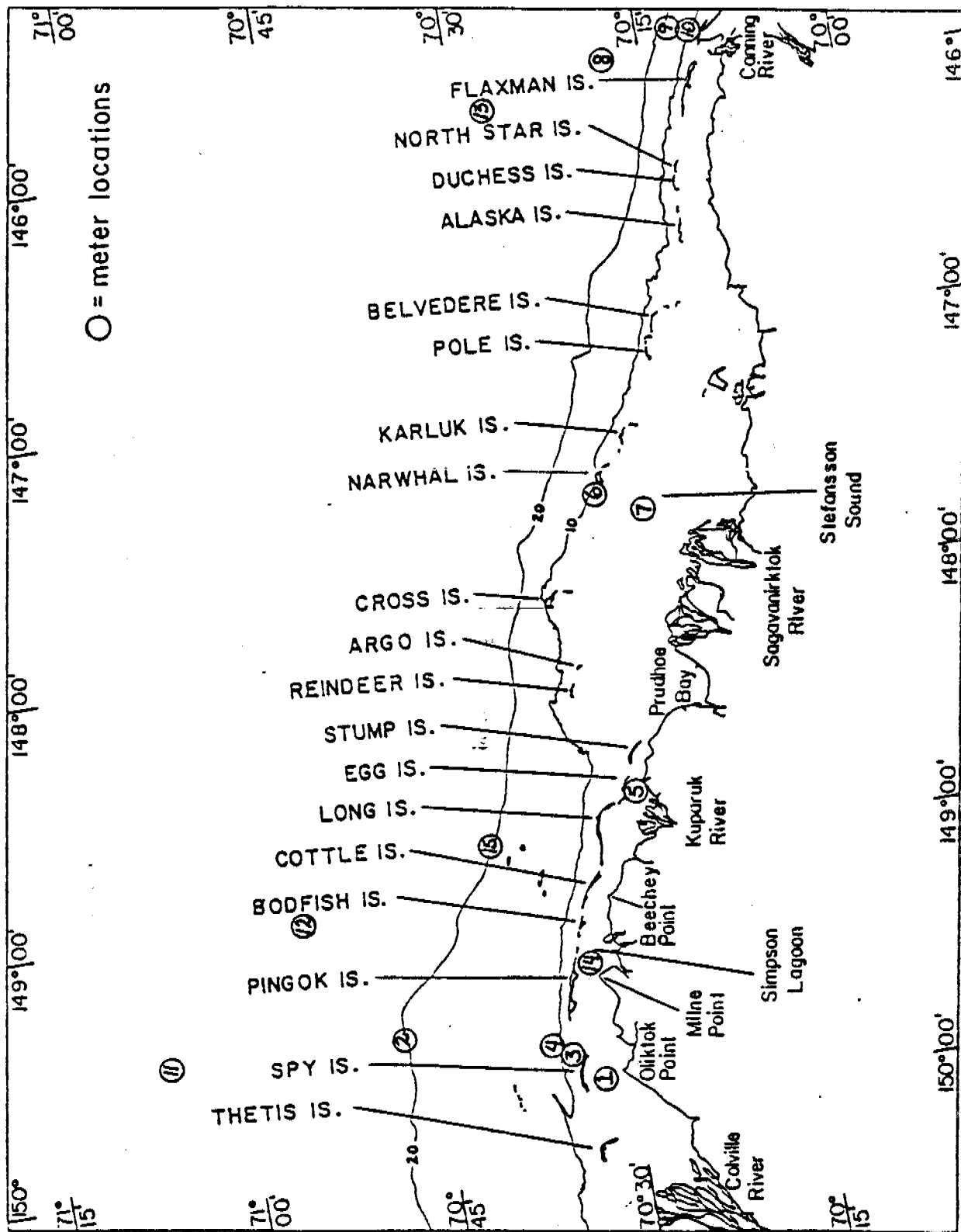


Figure 2. Complete station location map of winter studies physical oceanography program.

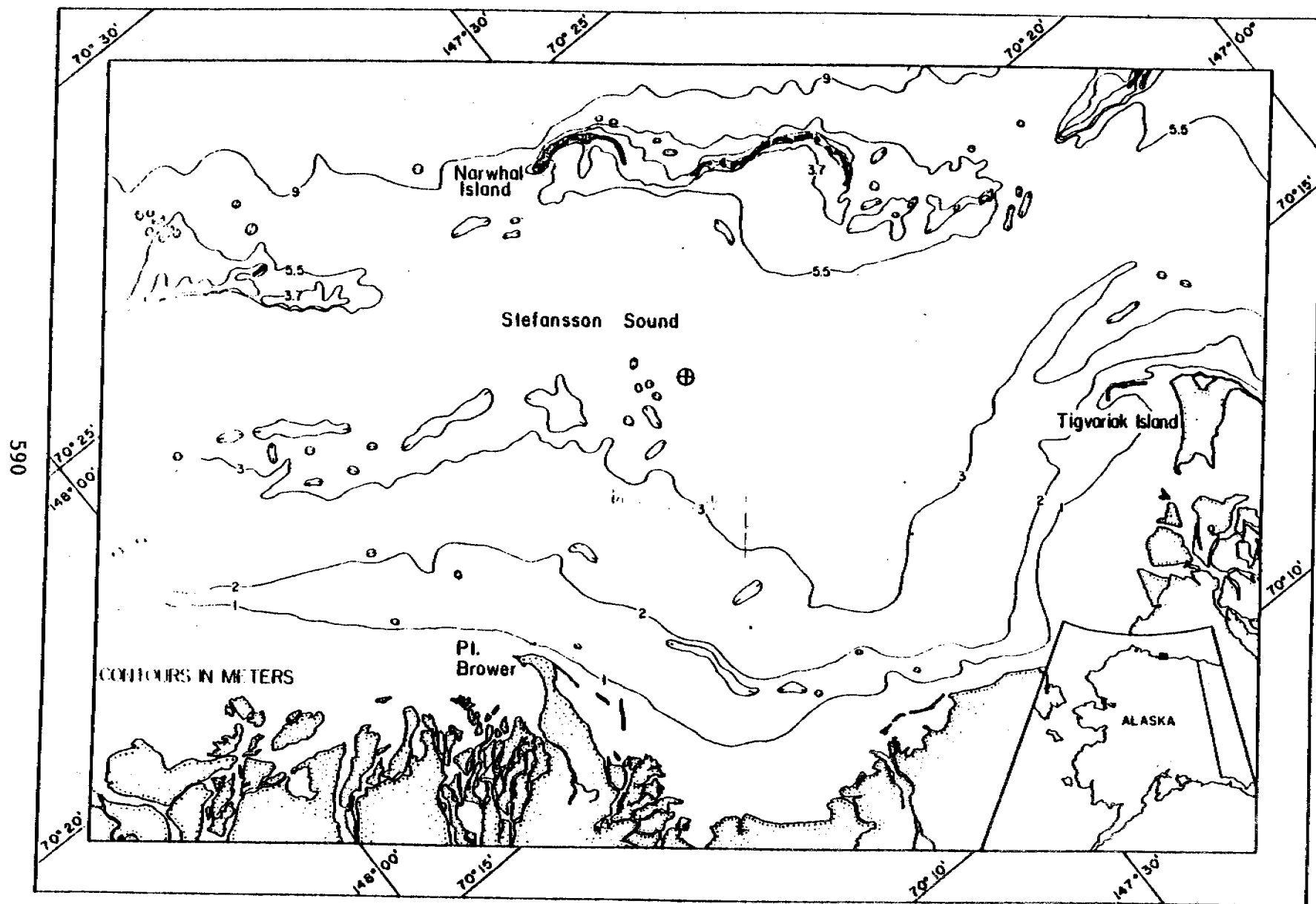


Figure 3. Stefansson Sound Boulder Patch station location.

# STEFANSSON SOUND BOULDER PATCH

WATER DEPTH = 0.10m

METER DEPTH = 4.02m

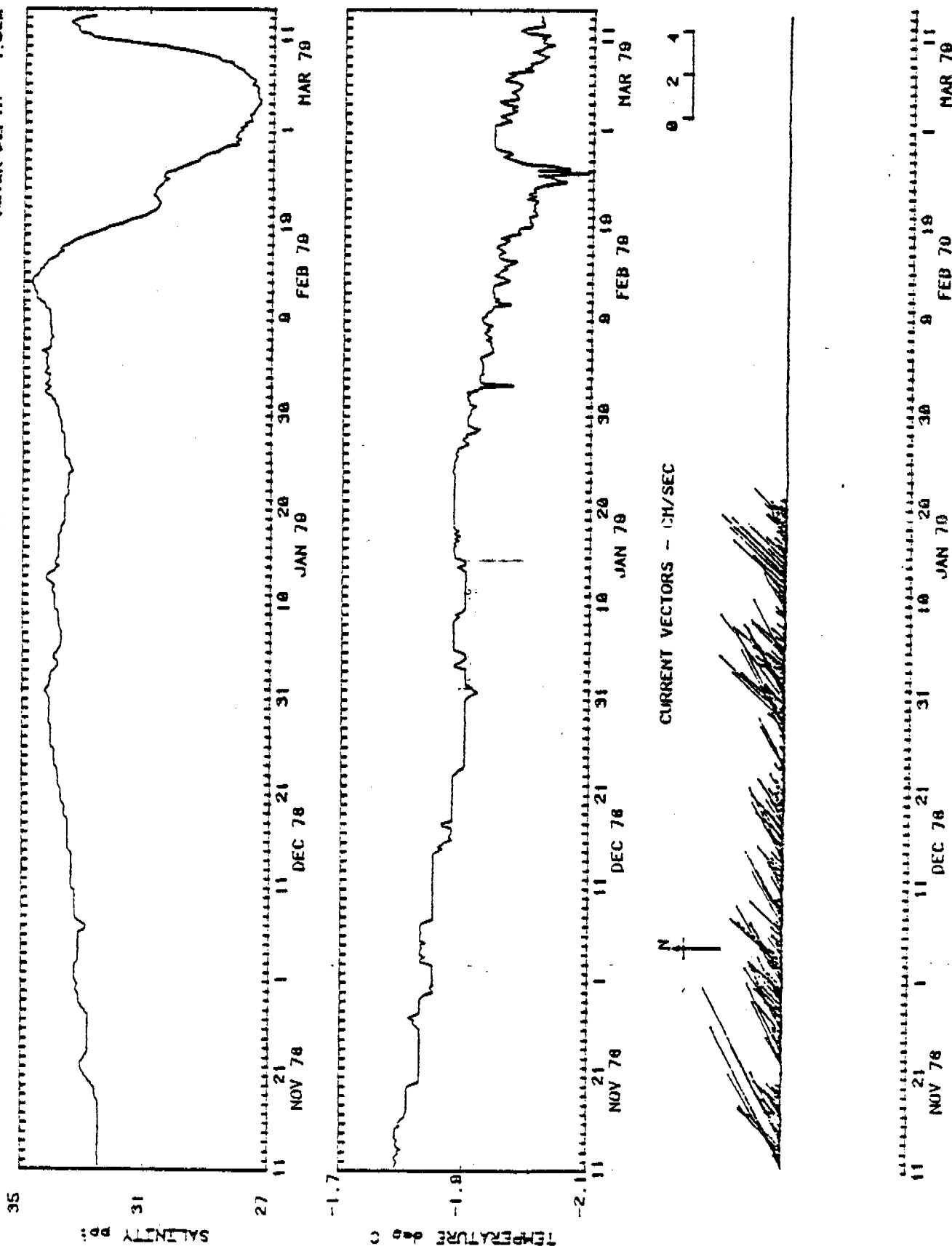


Figure 4. Salinity, temperature and current record from Stefansson Sound boulder patch at 4.02 m for November 1978 to November 1979.

# STEFANSSON SOUND BOULDER PATCH

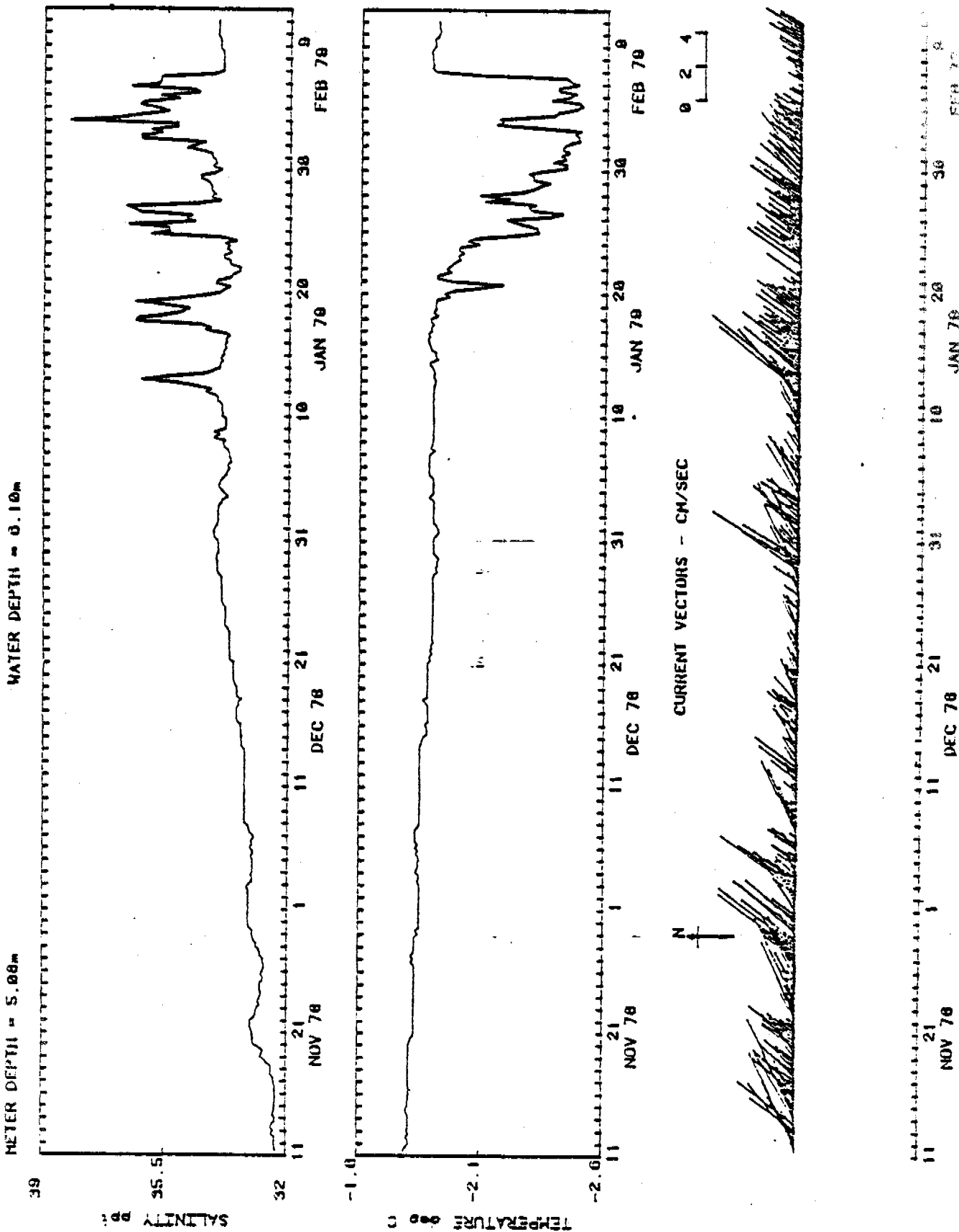


Figure 5. Salinity, temperature and current record from Stefansson Sound boulder patch at 5.08m depth from November 1978 to February 1979



# 0.5 KM. NORTH OF BROWNLOW POINT

WATER DEPTH = 7.32m

METER DEPTH = 5.24m

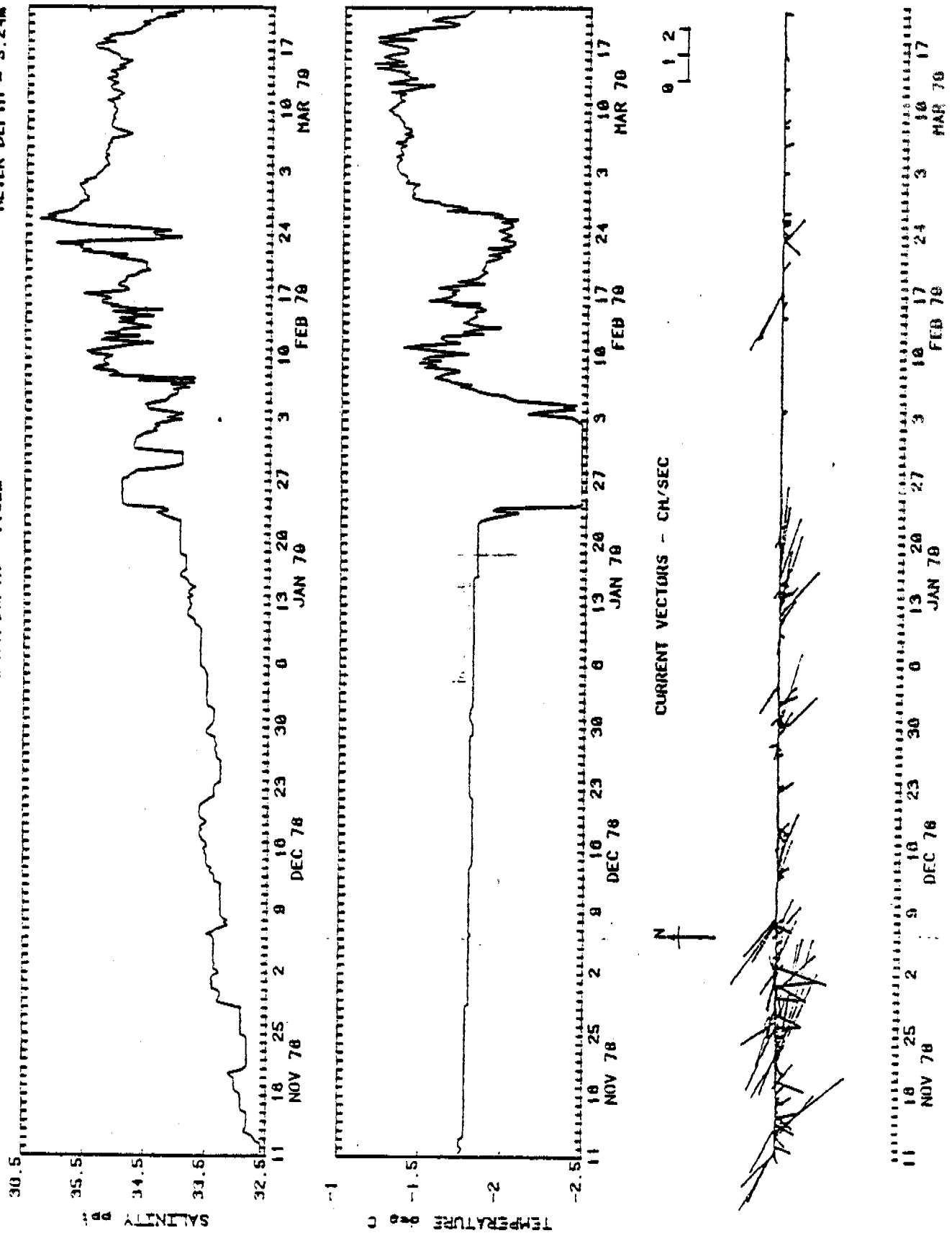
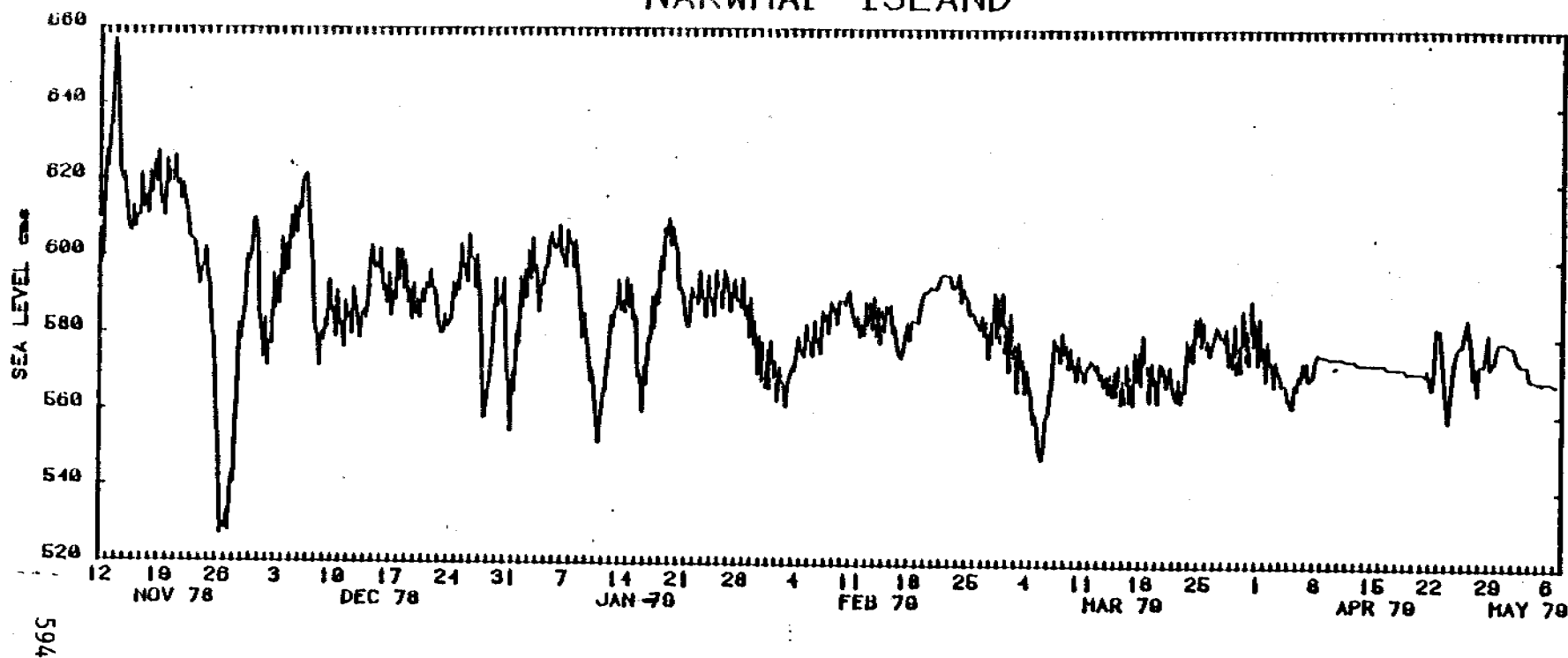


Figure 6. Salinity, temperature and current records for a mooring 0.5km north of Brownlow Point.

# NARWHAL ISLAND



765  
Figure 7. Narwhal Island sea level record for period 12 November 1978 to 7 May 1979.

# STEFANSSON SOUND BOULDER PATCH

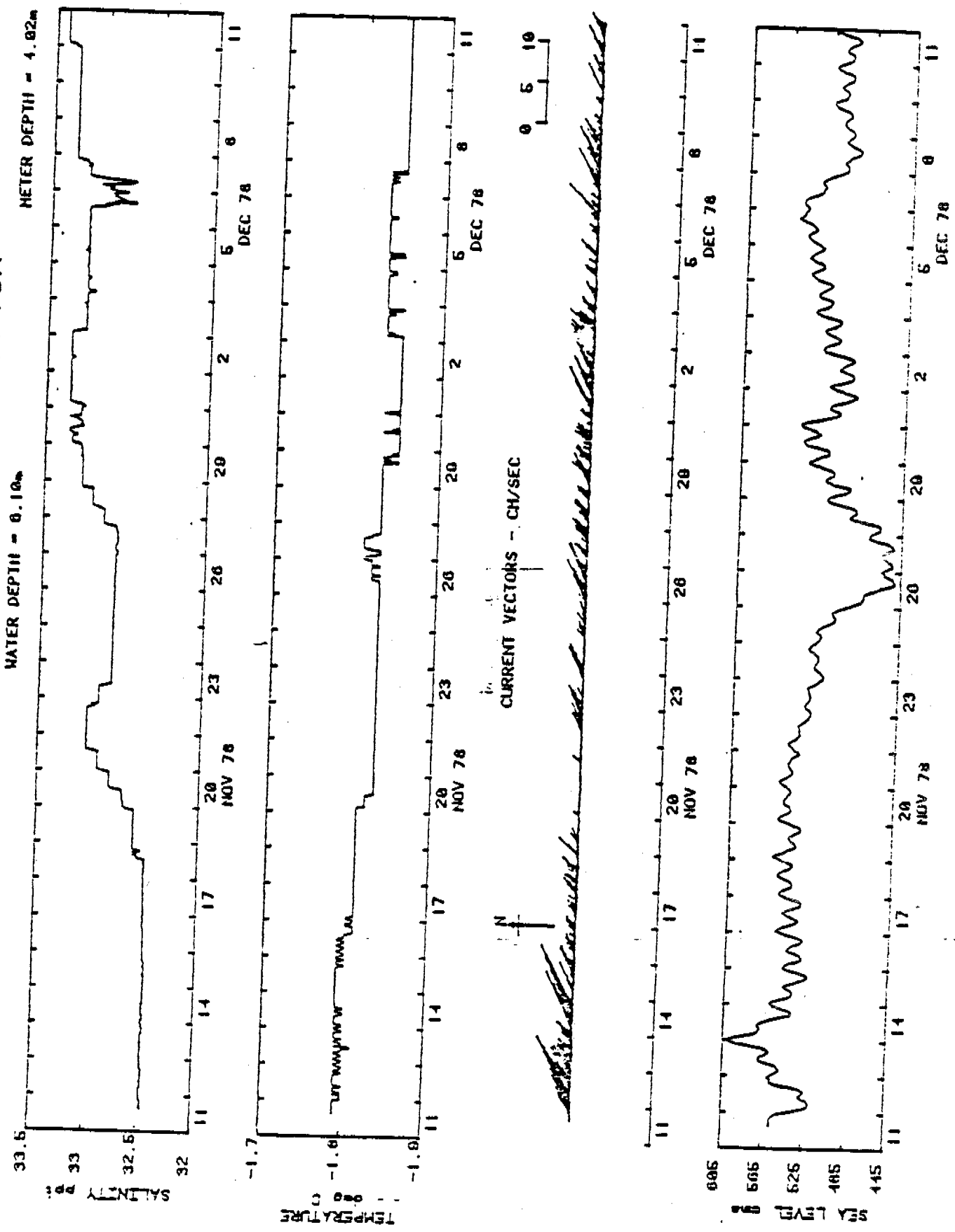
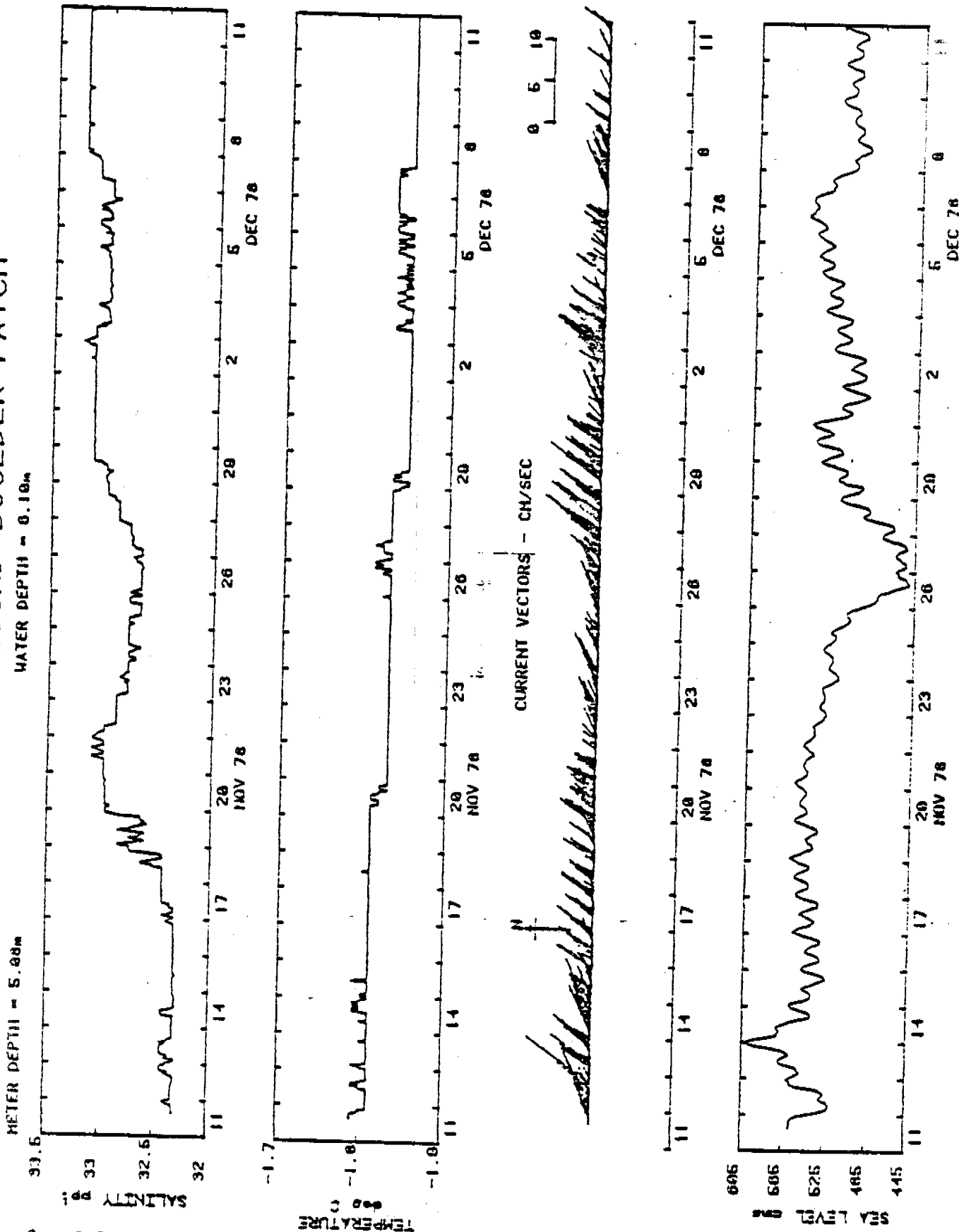


Figure 8. Salinity, temperature, current records and sea level for Stefansson Sound at 4 m depth for period 11 November to 11 December 1978.

# STEFANSSON SOUND BOULDER PATCH



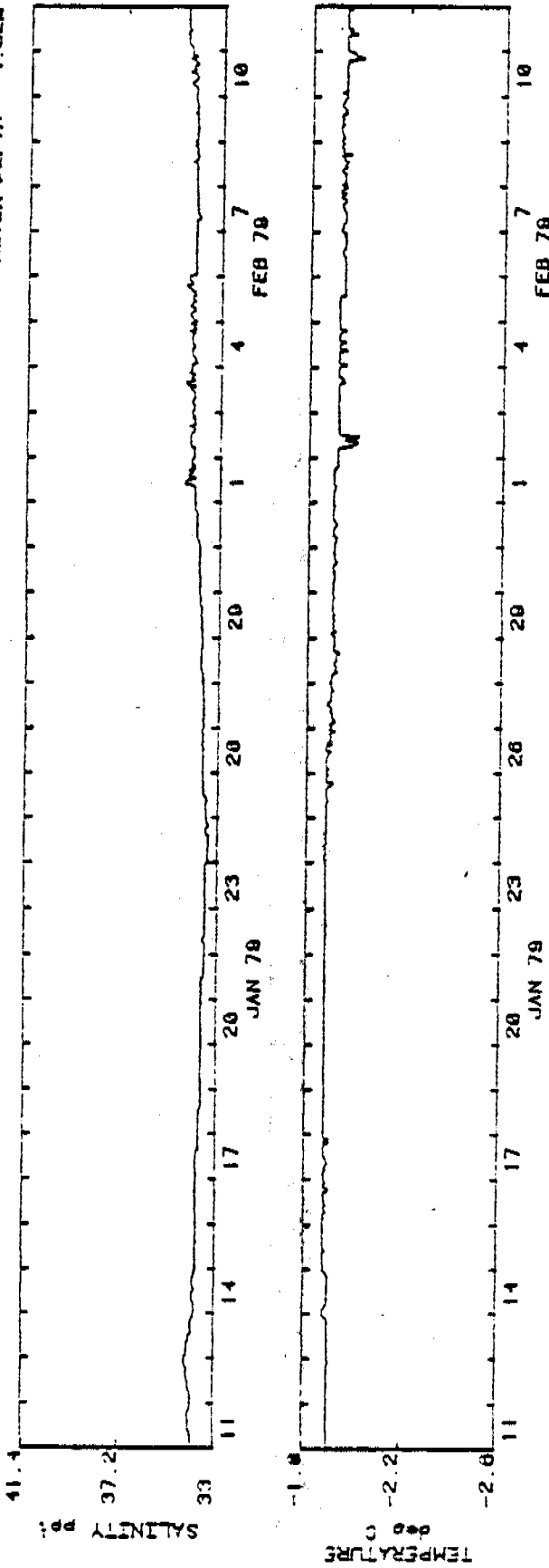
596

Figure 9. Salinity, temperature, current records and sea level for Stefansson Sound at 5.0 m depth for period 11 November to 11 December 1978.

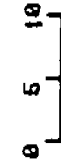
# STEFANSSON SOUND BOULDER PATCH

WATER DEPTH = 0.10m

METER DEPTH = 4.02m



CURRENT VECTORS - CM/SEC



# NARWHAL ISLAND

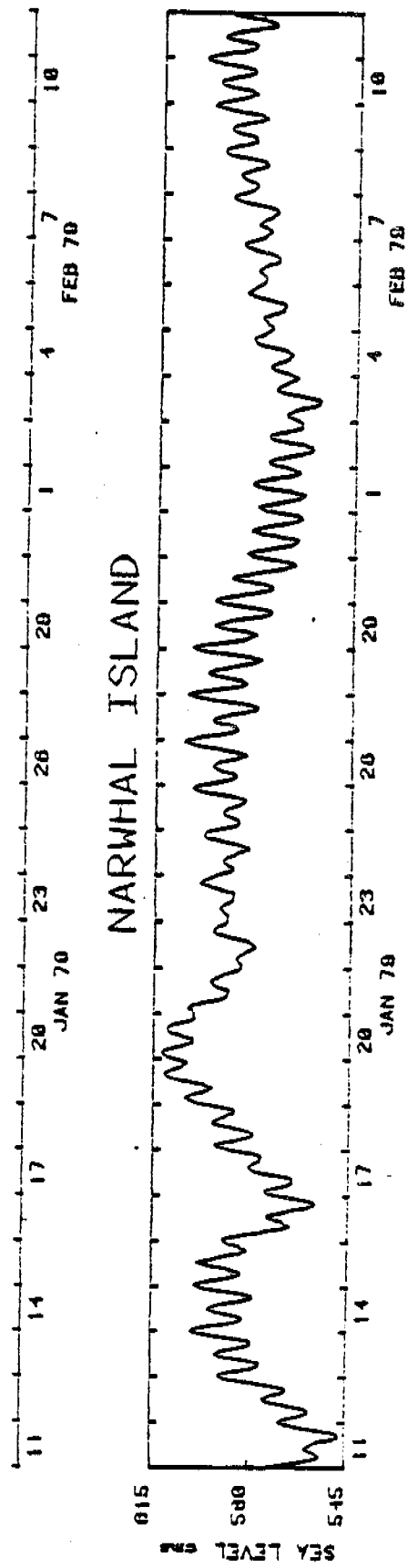
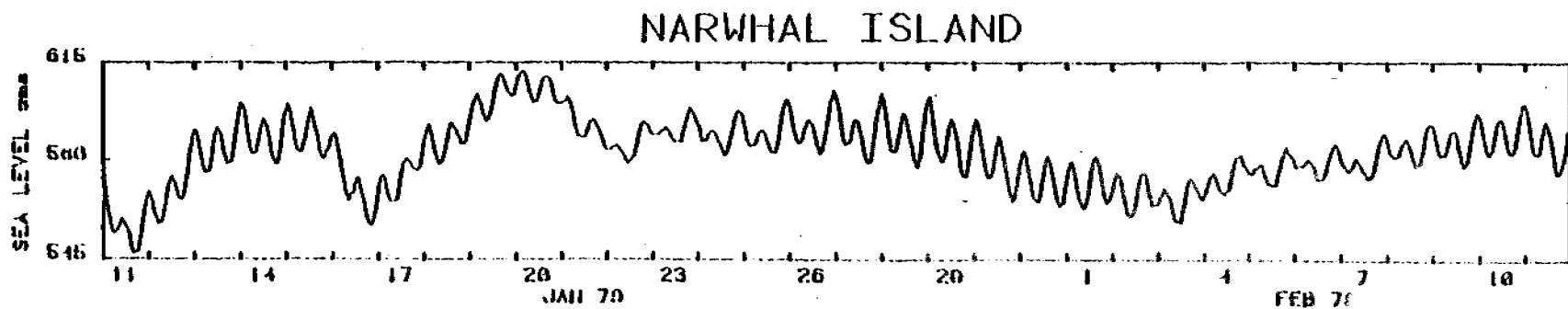
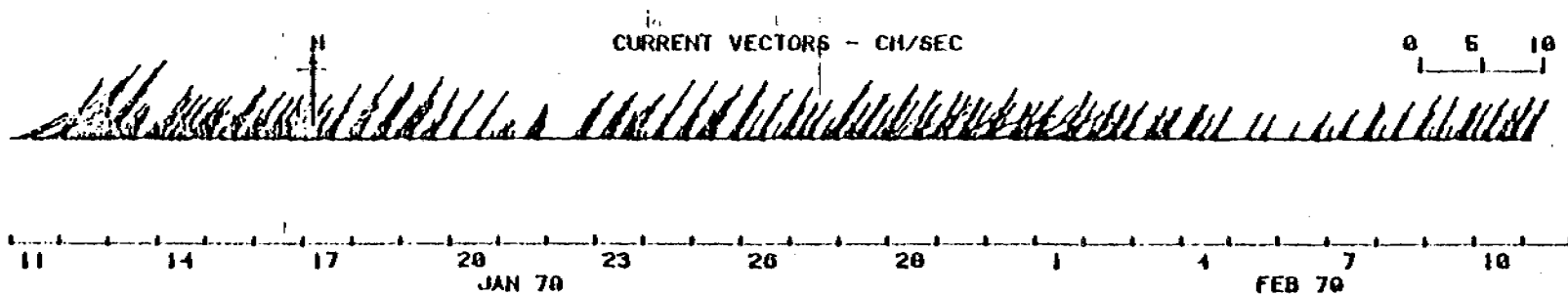
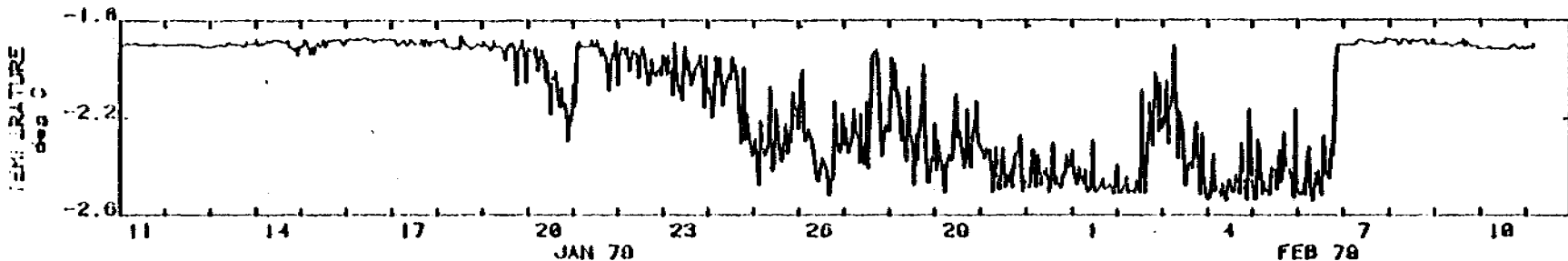
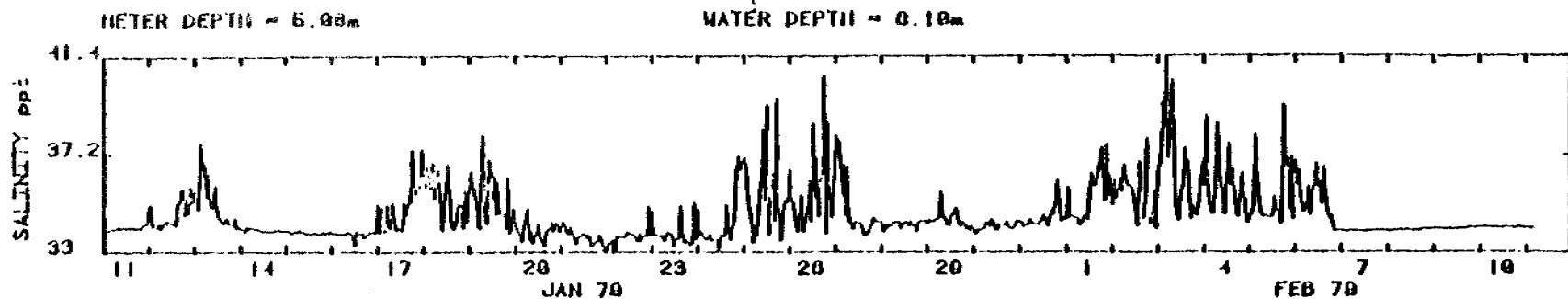


Figure 10. Salinity, temperature and current records for Stefansson Sound at 4 m depth and sea level record for Narwhal Island for period 11 December 1978 to 11 January 1979.

# STEFANSSON SOUND BOULDER PATCH

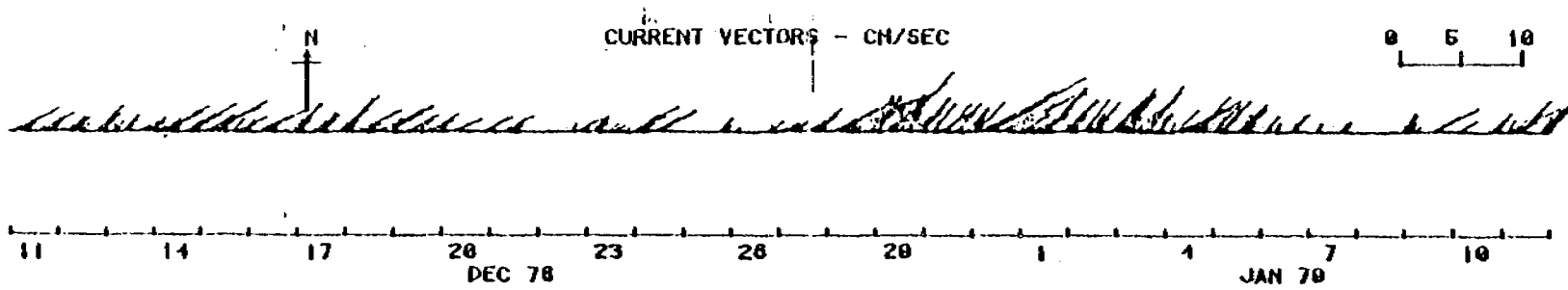
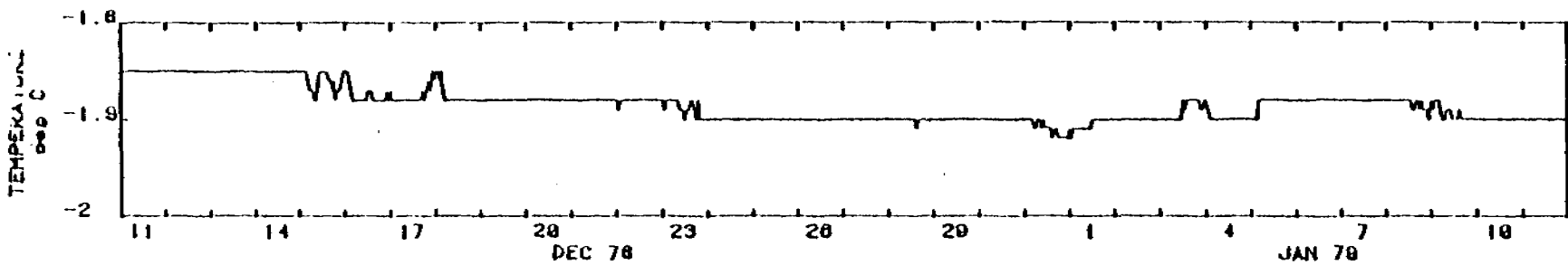
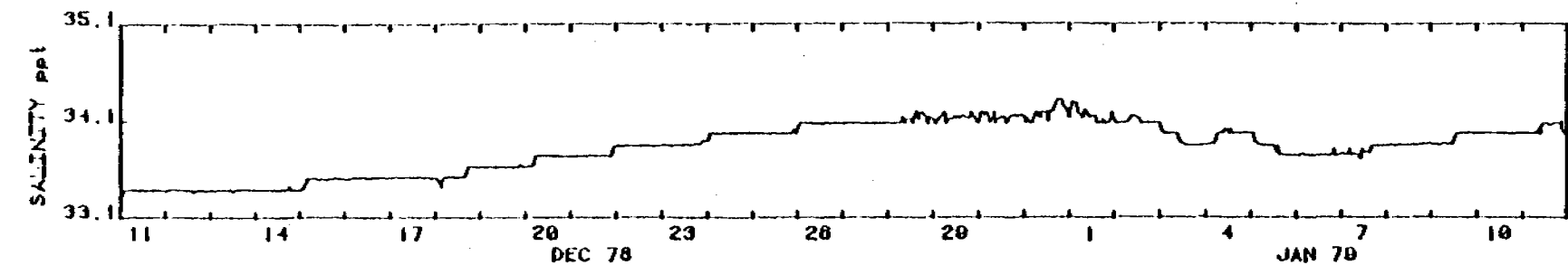


598 Figure 11. Salinity, temperature and current records for Stefansson Sound at 5 m and sea level for Narwhal Island for period 11 December 1978 to 11 January 1979.

# STEFANSSON SOUND BOULDER PATCH

WATER DEPTH = 0.10m

METER DEPTH = 4.02m



## NARWHAL ISLAND

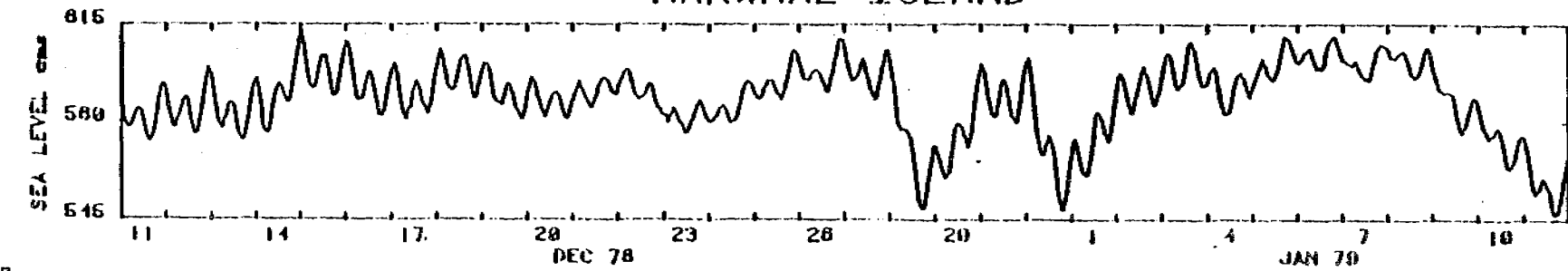


Figure 12. Salinity, temperature and current record for Stefansson Sound at 4 m depth and Narwhal Island and sea level record for period 11 January 1979 to 11 February 1979

## STEFANSSON SOUND BOULDER PATCH

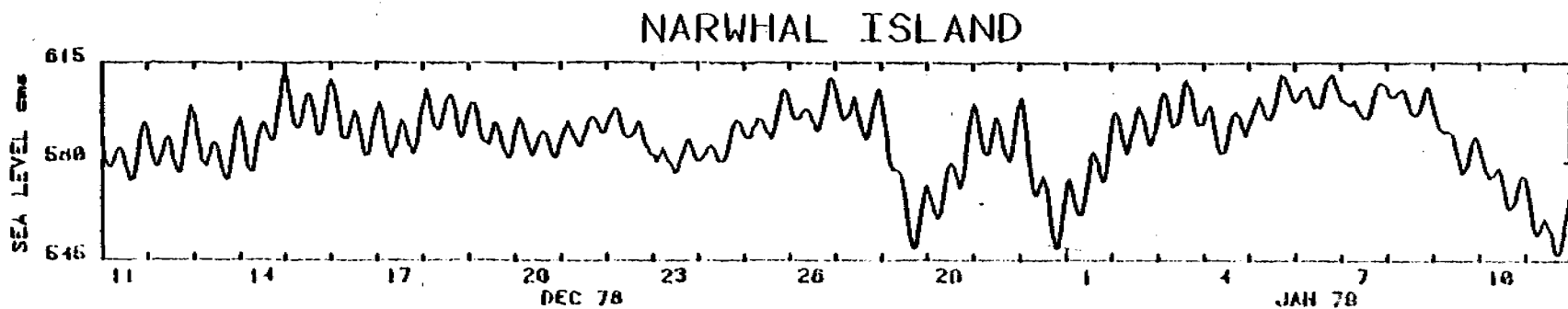
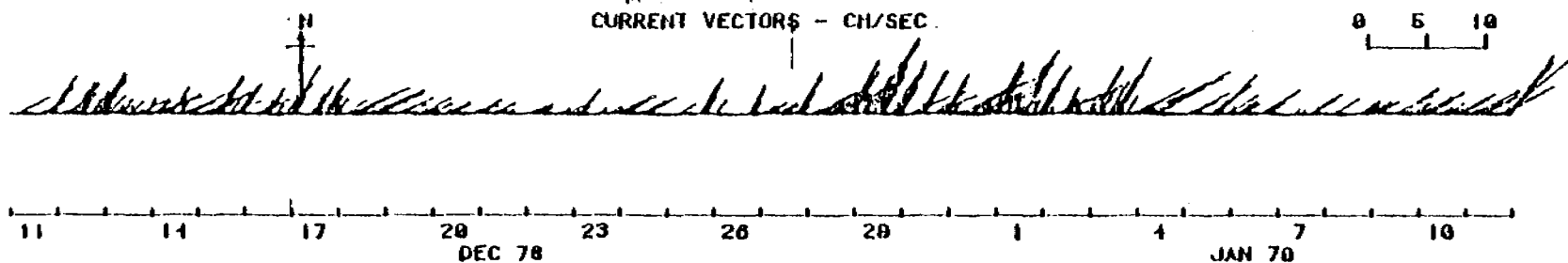
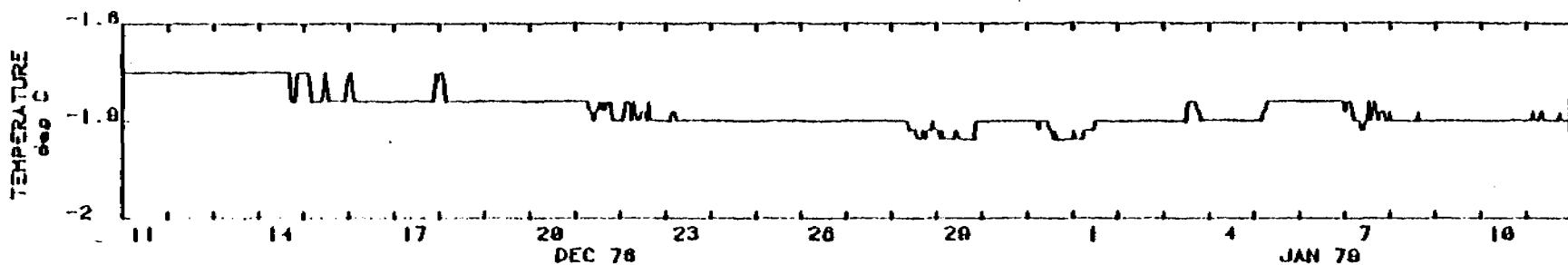
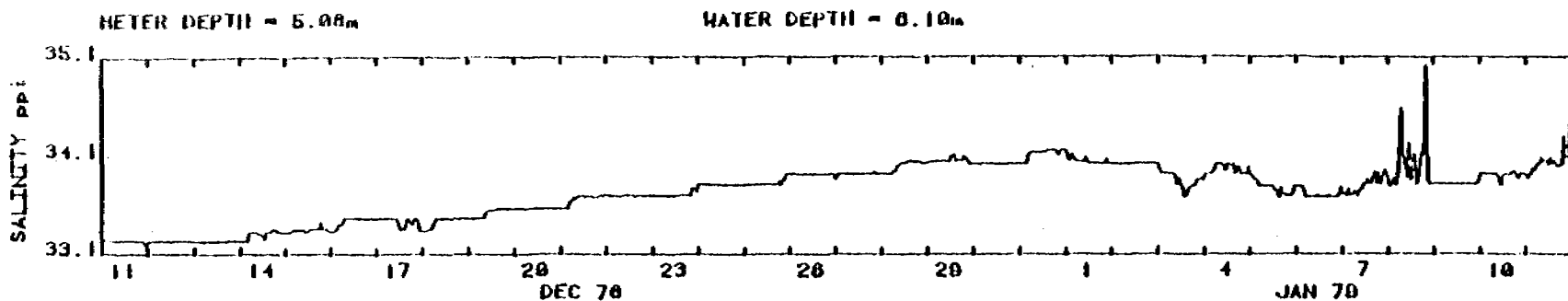


Figure 13. Salinity, temperature and current record for Stefansson Sound at 5m depth and Narwhal Island sea level record for period 11 January 1979 to 11 February 1979.

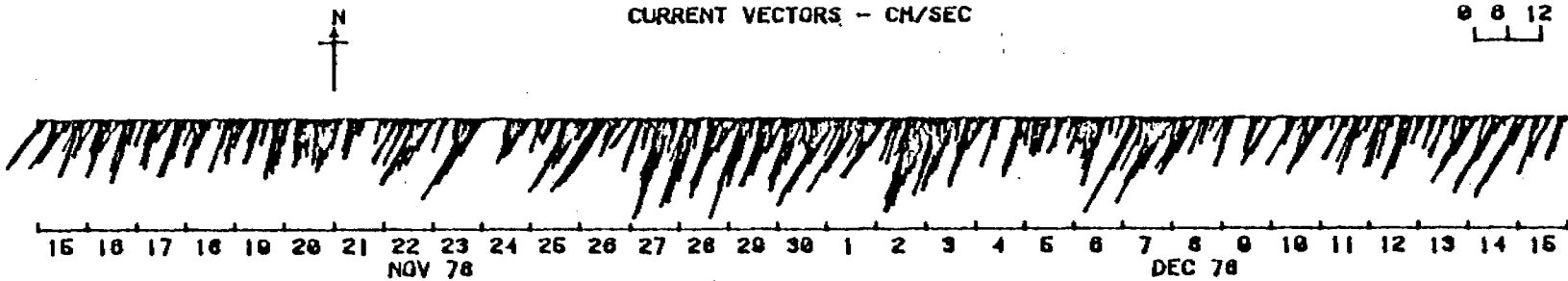


# STEFANSSON SOUND BOULDER PATCH

WATER DEPTH = 8.10m

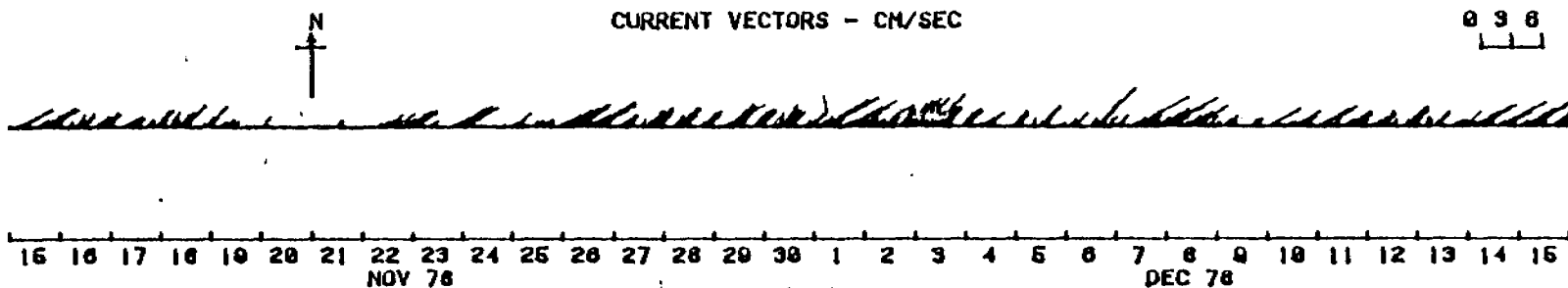
CURRENT VECTORS - CM/SEC

0 8 12



CURRENT VECTORS - CM/SEC

0 3 6



CURRENT VECTORS - CM/SEC

0 3 6

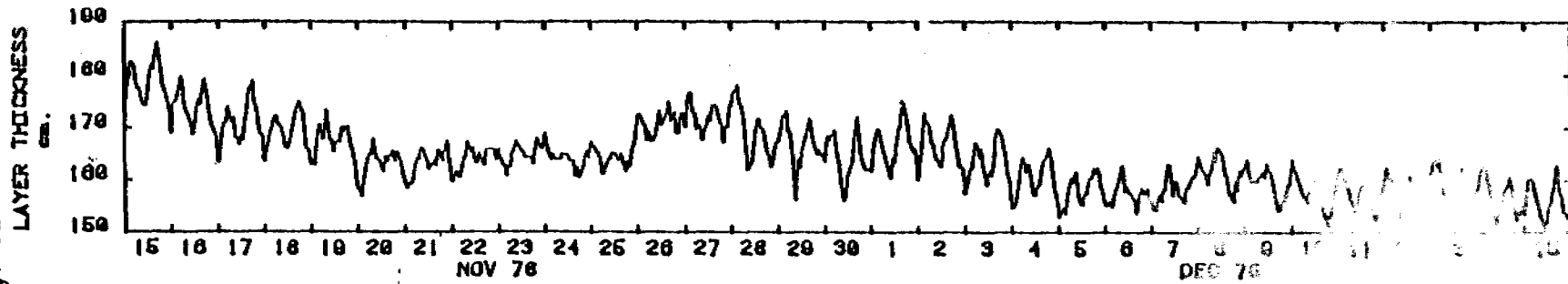
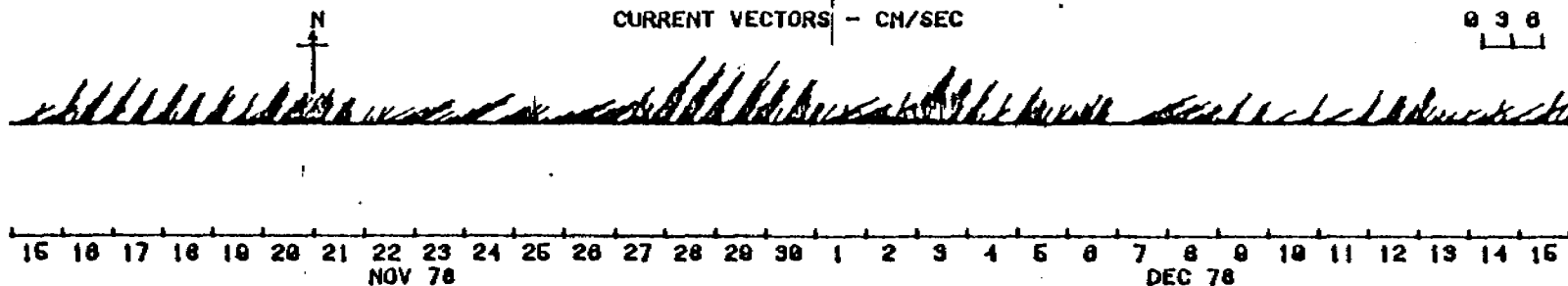


Figure 14. Current vectors from 4 and 5m depth and computed for a hypothetical upper layer on the basis of mass conservation.

